JOHANNES GUTENBERG UNIVERSITÄT MAINZ

PSMA inhibitor-based radiopharmaceuticals for diagnosis and therapy of prostate cancer

Dissertation

zur Erlangung des Grades eines

„doctor rerum naturalium (Dr. rer. nat.)“

der Fachbereiche

08 - Physik, Mathematik und Informatik,

09 - Chemie, Pharmazie und Geowissenschaften,

10 - Biologie,

Universitätsmedizin

der Johannes Gutenberg-Universität Mainz

vorgelegt von

Tilmann Grus

geboren in Wiesbaden

Mainz, Januar 2022

Max-Planck Graduate Center
mit der Johannes Gutenberg-Universität

Dekan:

Erster Berichterstatter:

Zweiter Berichterstatter:

Tag der mündlichen Prüfung: 23. März 2022

Die vorliegende Arbeit wurde unter der Betreuung von X.X. in der Zeit von September 2018 bis Januar 2022 am Institut für Kernchemie / Department Chemie- Standort TRIGA der Johannes Gutenberg-Universität Mainz angefertigt.

„I hereby declare that I wrote the dissertation submitted without any unauthorized external assistance and used only sources acknowledged in the work. All textual passages which are appropriated verbatim or paraphrased from published and unpublished texts as well as all information obtained from oral sources are duly indicated and listed in accordance with bibliographical rules. In carrying out this research, I complied with the rules of standard scientific practice as formulated in the statutes of Johannes Gutenberg-University Mainz to insure standard scientific practice."

Tilmann Grus

Mainz, Januar 2022

Abstract

Prostate cancer (PCa) is the second most common diagnosed cancer type among men worldwide. In relation to death rate, it is on the fifth place of all cancer types worldwide. When it is diagnosed early, the chances of cure are very good with a 5-year survival rate of 98%. Patients with advanced cancer often develop metastases, reducing the chances of cure drastically. Thus, an early diagnosis and therapy is crucial for an appropriate medical care.

The prostate-specific membrane antigen (PSMA) is a membrane-bound glycoprotein, which shows only a low expression in the healthy prostate but can be overexpressed up to 1000-fold by prostate cancer cells. Additionally, the expression correlates with the progress of the disease enabling classification of the stage of the disease. The discovery and exploration of PSMA led to an improvement of the patients care. Today, PSMA is used as target structure for the targeted diagnosis and therapy of prostate cancer and related metastases.

PSMA gained particular interest in the field of radiopharmacy. Here, addressing PSMA enables an early imaging and diagnosis of prostate cancer in the positron emission tomography (PET) or single-photon emission computed tomography (SPECT), even before morphological chances can be seen in computed tomography (CT) or magnetic resonance imaging (MRI). Besides this, PSMA enables the targeted enrichment of therapeutic radiopharmaceuticals. Many sensitive and highly potent PSMA radiopharmaceuticals were developed in the last years. Especially known among these are [^{68}Ga]Ga-PSMA-11 for PET, which is already approved by the FDA and [^{177}Lu]Lu-PSMA-617 for therapy of PCa.

Despite the research already conducted and the clinically established radiopharmaceuticals, in PSMA-based diagnosis and therapy of PCa there are still fields and problems that need to be improved or solved. Examples are the unwanted off-target accumulation of PSMA ligands or the targeted drug delivery. The aim of this work is the development of novel PSMA ligands, improvement of already existing ligands and the provision of solutions and applications for the existing problems of the PSMA imaging and therapy. For this purpose, new designed radiopharmaceutical compounds were synthesized, radiolabelled with diagnostic and/or therapeutic radionuclides, evaluated regarding their *in vitro* properties and in part evaluated regarding *in vivo* behaviour.

The first section of this work sets its focus on the use of the hybrid chelators DATA^{5m} and AAZTA^{5} as radiolabelling moiety. Here, different PSMA inhibitors were functionalised with the hybrid chelators. The DATA^{5m}-based compounds DATA^{5m}.SA.KuE and DATA^{5m}.PSMA-617 were evaluated regarding their radiolabelling properties with gallium-68. In followed up *in vitro* binding affinity studies the PSMA binding behaviour of the two compounds were examined. AAZTA^{5}.SA.KuE, which was synthesised and

evaluated radiochemically in previous studies, was also included. In animal studies, the potential of [^{68}Ga]Ga-DATA^{5m}.SA.KuE as diagnostic radiopharmaceutical and [^{44}Sc]Sc-/[^{177}Lu]Lu-AAZTA^{5}.SA.KuE as theranostic PSMA ligand were proven, as they show better kidney clearance than [^{68}Ga]Ga-PSMA-11, for example.

The second part deals with the problem of the PSMA-based therapy of PCa related bone metastases, since PSMA expression in bone metastases can be very heterogeneous. This makes the therapy with normal PSMA ligands more difficult. To solve this problem, the compound DOTA-L-Lys(SA.Pam)-PSMA-617 was developed in this work. Beside a PSMA target vector, the compound contains an additional bisphosphonate structure as targeting unit. The bisphosphonate enables the enrichment in bone areas with increased metabolism, as it is found in bone metastases. This enables the enrichment in PCa related bone metastases via two independent mechanisms. After synthesis, the novel compound was successfully radiolabelled with the therapeutic nuclide lutetium-177 and it showed a high *in vitro* PSMA and bone binding potential. In *in vivo* studies with tumour-bearing mice, it showed promising enrichment in the tumour as well as in the bone. This makes [^{177}Lu]Lu-DOTA-L-Lys(SA.Pam)-PSMA-617 to an interesting compound for therapy of PCa related bone metastases.

In the third part of this work, two drug delivery systems were developed, which enable the targeted transport of drugs to the prostate cancer cells via a PSMA targeting unit. For this purpose, BisHD-*hb*PG polymers were functionalised with a SA.KuE target vector and formed into liposomes. An additional ^{18}F-label enables the evaluation of the *in vivo* behaviour of the PSMA liposomes in PET measurements. In this work, the functionalisation of the polymers with the PSMA inhibitor, the radiolabelling and the liposome formation were established successfully. The *in vivo* examinations are pending. As second delivery system, a small molecule drug delivery conjugate (SMDC) was synthesized and evaluated. The cytotoxic drug MMAE was conjugated via the enzymatically cleavable linker valine-citrulline and squaric acid to the PSMA targeting unit 617.KuE. *In vitro* examinations showed that the novel compound is able to transport the drug via PSMA targeting to the cancer cell and MMAE is released via degradation of the valine-citrulline linker. Nevertheless, the cytotoxicity of the compound is lower than the cytotoxicity of free MMAE and the PSMA affinity is not that good than that of PSMA-617. Animal studies displayed that the application of the novel compound can inhibit tumour growth. Here, optimisation of the structure is necessary to increase affinity and cytotoxicity.

The last part of this work deals with the optimisation of the lysine-urea-glutamate (KuE) structure, which is the targeting vector of the most common PSMA radiopharmaceuticals. It is literature-known that the structure lysine-glutamate-urea-glutamate (K-EuE) provides better pharmacological properties. Thus, both target vectors were conjugated to squaric acid and were evaluated regarding *in*

vivo binding to PSMA along with the targeting unit of PSMA-617, KuE.617. All three structures had comparable affinities. Additionally, the influence of chelators on binding affinity should be examined. For this, each targeting unit was conjugated to the chelators DATA^{5m}, AAZTA^{5} and DO2AGA and the PSMA affinity as determined. Here, it was particularly noticeable that the addition of a chelator led to a general degrease of affinity. This was especially evident with the targeting unit SA.K-EuE. It was shown that the SA.K-EuE targeting unit is not suitable for conjugation with chelators. The superiority of K-EuE over KuE as it is described in literature could not be confirmed for squaric acid-based compounds. Although the affinities of the chelator conjugated SA.KuE and 617.KuE got also lower but only to a lesser extent. Additionally, no clear trend could be observed which chelator or which targeting unit had the better affinity. This seems to be dependent of the respective combination. In further studies, spacer moieties should be introduced between chelator and targeting unit to evaluate if a further distance between the two units can reduce the affinity degreasing influence of the chelator.

Zusammenfassung

Prostatakrebs (PCa) ist die zweithäufigste diagnostizierte Krebsart unter Männern weltweit. Bezogen auf die Sterblichkeitsrate liegt Prostatakrebs auf Platz fünf aller weltweit vorkommenden Krebsarten. Bei frühzeitiger Diagnose sind die Heilungschancen mit einer 5-jahres-Überlebensrate von 98 % sehr gut. Patienten mit fortgeschrittenen Prostatakrebs entwickeln häufig Metastasen und die Heilungschancen sinken drastisch. Aus diesem Grund ist eine frühzeitige Diagnose und Therapie essentiell.

Das Prostataspezifische Antigen (PSMA) ist ein membrangebundenes Glykoprotein, dass in der gesunden Prostata nur in einem sehr geringen Maße auftritt, aber von Prostatakrebszellen bis zu 1000-fach überexprimiert sein kann. Ebenso korreliert die Expression mit dem Verlauf der Krankheit, was eine Einschätzung des Krankeitsstadiums erlaubt. Die Entdeckung und Erforschung dieses membrangebundenen Proteins führte zu einer deutlichen Verbesserung der Patientenversorgung. So wird das PSMA heute als Targetstruktur zur zielgerichteten Diagnose und Therapie von Prostatakrebs und den entsprechenden Metastasen eingesetzt.

Besonderes Interesse erlangte PSMA im Bereich der Radiopharmazie. Hier ermöglicht die Adressierung von PSMA die frühzeitige Bildgebung und Diagnose von Prostatakrebs in der Positronen-Emissions-Tomographie (PET) oder Einzelphotonen-Emissionscomputertomographie (SPECT), noch bevor morphologische Veränderungen in der Computertomographie (CT) oder Magnetresonanztomographie (MRT) sichtbar werden. Daneben ermöglicht PSMA die zielgerichtete Anreicherung von therapeutischen Radiopharmaka. Viele sensitive und hoch potente PSMA Radiopharmaka wurden in den letzten Jahren entwickelt. Besonders bekannt sind hierunter das durch die FDA zugelassene [^{68}Ga]Ga-PSMA-11 für die PET und [^{177}Lu]Lu-PSMA-617 für die Therapie von PCa.

Trotz der bereits erfolgten Forschung und bereits klinisch etablierten Radiopharmaka, gibt es immer noch Bereiche und Probleme in der Diagnose und Therapie von PCa mit Hilfe von PSMA, die es zu optimieren, beziehungsweise zu lösen gilt. Hier ist zum Beispiel die ungewollte off-target Anreicherung von PSMA Liganden oder auch der gezielte Wirkstofftransport zu nennen. Das Ziel dieser Arbeit ist die Entwicklung neuer PSMA Liganden, Verbesserung bereits existierender PSMA Liganden und die Bereitstellung von Lösungsansätzen und Anwendungen für bestehende Probleme der PSMA Bildgebung und Therapie. Dazu werden neu designte radiopharmazeutische Verbindungen synthetisiert, mit diagnostischen und/oder therapeutischen Radionukliden radioaktiv markiert und diese hinsichtlich ihrer *in vitro* Eigenschaften und zum Teil auch hinsichtlich ihrer *in vivo* Eigenschaften untersucht.

Der erste Abschnitt dieser Arbeit legt seinen Fokus auf die Verwendung der Hybridchelatoren DATA^{5m} und AAZTA^{5} als Radiomarkierungseinheit. Hierbei wurden verschiedene PSMA-Inhibitoren mit den Hybridchelatoren funktionalisiert. Die DATA^{5m} basierten Verbindungen DATA^{5m}.SA.KuE und DATA^{5m}.PSMA-617 wurden hierbei hinsichtlich ihrer Radiomarkierungseigenschaften mit Gallium-68 untersucht. In folgenden *in vitro* Bindungsaffinitätsstudien wurden die beiden Verbindungen und die schon in voran gegangenen Arbeiten synthetisierte und radiochemisch untersuchte Verbindung AAZTA^{5}.SA.KuE hinsichtlich hier PSMA Bindungseigenschaften untersucht. In Tierstudien konnte das Potential von [^{68}Ga]Ga-DATA^{5m}.SA.KuE als diagnostisches Radiopharmakon und [^{44}Sc]Sc-/[^{177}Lu]Lu-AAZTA^{5}.SA.KuE als theranostischer PSMA-Ligand gezeigt werden, die zum Beispiel bessere Nierenausscheidung aufwiesen, als [^{68}Ga]Ga-PSMA-11.

Der zweite Abschnitt befasst sich mit der Problematik der PSMA-basierten Therapie von PCa-bedingten Knochenmetastasen, da diese in ihrer PSMA Expression sehr heterogen sein können. Dies erschwert die Therapie mit reinen PSMA-Liganden. Zur Lösung dieses Problems, wurde in dieser Arbeit die Verbindung DOTA-L-Lys(SA.Pam)-PSMA-617 hergestellt. Sie besitzt neben einem PSMA Targetvektor auch eine Bisphosphonatstruktur als Targetvektor. Die Bisphosphonateineit ermöglicht die Anreicherung Knochenbereichen mit erhöhtem Stoffwechsel, wie er in Knochenmetastasen zu finden ist. So kann eine Anreicherung über zwei unterschiedliche Mechanismen erfolgen. Die entwickelte Verbindung wurde nach Synthese erfolgreich radiochemisch mit dem therapeutischn Nuklid Lutetium-177 markiert und zeigte *in vitro* hohes PSMA- und Knochenbindungspotential. *In vivo* Studien in tumortragenden Mäusen zeigten sowohl eine vielversprechende Anreicherung im Tumor, als auch im Knochenbereich, was [^{177}Lu]Lu-DOTA-L-Lys(SA.Pam)-PSMA-617 zu einer Interessanten Verbindung für die Therapie von PCa-bedingten Knochenmetastasen macht.

Im dritten Teil dieser Arbeit wurden zwei Wirkstofftransportsysteme entwickelt, die es ermöglichen über einen PSMA-Targetvektor Wirkstoffe gezielt zur Prostatakrebszelle zu transportieren. Dazu wurden BisHD-*hb*PG-Polymere mit dem SA.KuE-Targetvektor funktionalisiert und zu Liposomen verarbeitet. Ein zusätzliches ^{18}F-Label ermöglicht die Untersuchung des *in vivo* Verhaltens der PSMA-Liposome in PET Messungen. In dieser Arbeit konnte die Funktionalisierung der Polymere mit dem PSMA Inhibitor, die Radiomarkierung und die Liposomsynthese erfolgreich etabliert werden. Die *in vivo* Untersuchungen stehen noch aus. Als zweites Wirkstofftransportsystem wurde ein *Small molecule drug delivery Konjugat* (SMDC) synthetisiert und evaluiert. Dazu wurde das Zytostatikum MMAE über den enzymatisch spaltbaren Linker Valin-Citrullin und über Quadratsäure an den PSMA-Targetvektor 617.KuE gekoppelt. *In vitro* Untersuchungen zeigten, dass die neue Verbindung gezielt über PSMA transportiert wird und auch die MMAE Freisetzung gezielt über den Valin-Citrullin-Linker erfolgt, allerdings ist die Zytotoxizität geringer, als die des freien MMAEs und auch die PSMA-Affinität ist deutlich schlechter, als die von PSMA-617. Tierstudien zeigten, dass die Applikation der Verbindung

das Tumorwachstum inhibieren kann. Hier ist eine Optimierung der Struktur nötig zur Erhöhung der Affinität und Zytotoxizität.

Der vierte Abschnitt behandelt die Optimierung der Lysin-Harnstoff-Glutamat (KuE) Struktur, die als Targetvektor in den gängigsten PSMA-Radiopharmaka vorkommt. Es ist Literaturbekannt, dass die Struktur Lysin-Glutamat-Harnstoff-Glutamat (K-EuE) bessere pharmakologische Eigenschaften aufweist. Daher wurden beide Targetvektoren an Quadratsäure gekoppelt und zusammen mit der Targetingeinheit von PSMA-617, 617.KuE hinsichtlich der *in vitro* Bindung an PSMA untersucht. Alle drei Strukturen wiesen ähnliche Affinitäten auf. Des Weiteren sollte der Einfluss von Chelatoren auf die Bindungsaffinität untersucht werden. Dazu wurde an jede der drei Targetingeinheiten die Chelatoren $DATA^{5m}$, $AAZTA^{5}$ und DO2AGA gekoppelt und ebenfalls die PSMA-Affinität bestimmt. Hier viel besonders auf, dass sich durch die Anbringung eines Chelators generell die Affinität verschlechtert. Dies war besonders deutlich bei SA.K-EuE. Es wurde gezeigt, dass der SA.K-EuE Targetvektor nicht geeignet ist für die Konjugation an Chelatoren. Die, in der Literatur benannte, Überlegenheit von K-EuE gegenüber KuE konnte für Quadratsäure-basierte Verbindungen nicht bestätigt werden. Zwar verschlechterten sich die Affinitäten auch beim Anbringen eines Chelators an SA.KuE und 617.KuE, allerdings nur in einem geringen Maße. Hier war außerdem kein eindeutiger Trend zu erkennen, welcher Chelator oder welche Targeteinheit die besten Affinitäten ermöglicht. Dies scheint abhängig von der jeweiligen Kombination zu sein. In weiteren Studien sollte ein Spacer zwischen Chelator und Targetingeinheit gebracht werden, um zu untersuchen, ob so der Einfluss des Chelators auf die Affinität reduziert werden kann.

Table of Content

1. Introduction 1

1.1 Positron emission tomography (PET) 1

1.1.1. Function of PET 2

1.2 Diagnostic radionuclides 7

1.2.1 Gallium-68 9

1.2.2 Scandium-44 12

1.2.3 Fluorine-18 13

1.3 Endoradiotherapy and therapeutic nuclides 13

1.3.1 Lutetium-177 15

1.4 Radiolabelling chemistry 17

1.4.1 Chelatorsystems 17

1.4.2 Radiofluorination 23

1.5 Squaric acid as conjugation agent 27

1.6 Prostate cancer 28

1.6.1 Prostate-specific membrane antigen (PSMA) 29

1.7 Bisphosphonates 34

1.8 Small molecule drug conjugates 36

1.9 Liposomes 38

2. Objectives 41

2.1 Project A: Hybrid chelator conjugated PSMA inhibitors 42

2.2 Project B: Prostate cancer and related bone metastases 44

2.3 Project C: PSMA inhibitor conjugated drug delivery systems 44

2.4 Project D: PSMA inhibitor structure optimisation 45

2.5 Author contribution to the research project 46

3. References 47

4. Manuscripts 65

4.1 Project A: Hybrid chelator conjugated PSMA inhibitors 67

4.1.1 Hybrid Chelator-Based PSMA Radiopharmaceuticals: Translational Apporach 69

4.1.2 [^{68}Ga]Ga-DATA^{5m}-PSMA-617 as diagnostic kit-based counterpart for [^{177}Lu]Lu-PSMA-617 99

4.2 Project B: Prostate cancer and related bone metastases 117

4.2.1 DOTA conjugate of Bisphosphonate and PSMA-inhibitor: .....
A promising combination for therapy of prostate cancer related bone metastases 119

4.3 Project C: PSMA inhibitor conjugated drug delivery systems 147

4.3.1 ^{18}F-labeled, PSMA-specific liposomes: promising and PET-traceable tool .....
for future targeted drug delivery in the treatment of prostate cancer 149

4.3.2 Old drug, new delivery strategy: MMAE repacked 199

4.4 Project D: PSMA inhibitor structure optimisation 223

4.4.1 Comparison of the binding affinity of squaramide containing .....
lysine-urea-glutamate- and glutamate-urea-glutamate-based PSMA inhibitors 225

5. Conclusion 253

5.1 Project A: Hybrid chelator conjugated PSMA inhibitors 254

5.2 Project B: Prostate cancer and related bone metastases 256

5.3 Project C: PSMA inhibitor conjugated drug delivery systems 258

5.4 Project D: PSMA inhibitor structure optimisation 261

5.5 References in the conclusion 262

6. Appendix 265

6.1 List of abbreviations 265

6.2 List of publications 268

6.3 Acknowledgment 269

6.4 Eidesstattliche Erklärung 270

6.5. Curriculum Vitae 271

1. Introduction

Our society is ageing. Although younger people can develop cancer, the chance of developing cancer increases significantly with the age.[1] For example, in the US one of two men and one of three women will be diagnosed with cancer in their lifetime.[2] This shows the importance of diagnosis and therapy of cancer in medicine. An early diagnosis is just as important as a therapy that is optimally suited and adapted to the patient.

When radioactivity was discovered in 1896 by Henri Becquerel, no one could have imagined the contribution it could make to modern medicine nowadays.[3]

First imaging techniques became possible through the discovery of the X-rays by Roentgen in 1895, even before the discovery of radioactivity itself.[4] Radioactivity gained a lot of attention and many methods and techniques were developed to use radioactivity for medical applications. This includes the development of the tracer principle by de Hevesy in 1923 or the first evaluation of the human blood flow using radioactivity by Blumgart and colleagues in 1927.[5,6]

With diagnostic application areas, such as positon emission tomography (PET) or single-photon emission computed tomography (SPECT) and the therapeutic use of radionuclides, nuclear medicine is an important field in modern patient care.[7]

1.1 Positron emission tomography (PET)

The development of non-invasive imaging techniques has contributed to a considerable improvement in the diagnosis and monitoring of diseases. A differentiation is made between structural imaging and functional imaging. Probably the best known are computed tomography (CT), magnetic resonance imaging (MRI) and ultrasound. All three of these procedures belong to structural imaging and allow the visualisation of the morphological structure of the body.[4] This can be used to identify morphological changes associated with a disease. However, many diseases often do not show any morphological changes or develop them in later stages of the disease. This is where functional imaging techniques show an advantage.[7] Nuclear medical imaging procedures such as positon emission tomography (PET) or single photon emission computed tomography (SPECT) can be used to visualise metabolic processes in the body. For example, cancer can be diagnosed based on its increased metabolism compared to healthy cells before it becomes morphologically visible in structural imaging or before the first symptoms appear.[10] If both methods (PET/CT, PET/MRI or SPECT/CT) are combined, meaningful images can be generated and an exact localisation of the tumour or the location of the disturbed metabolism is possible.[14]

In 2015, 62% of the annual nuclear medicine imaging examinations in Germany were carried out using SPECT or SPECT/CT and 24% using PET and PET/CT.[8] Although PET has a better resolution and sensitivity, it is much more cost-intensive than SPECT.[9]

In PET, the patient receives an injection of a radioactively labelled compound. Depending on the type of compound, it participates in the metabolism and can be localised in the body via the resulting γ-radiation.[10] The injected compound is dosed in such a way that it participates in the metabolism without influencing it (tracer principle).[11]

One major application belongs to the field of oncology. In Germany, the radiopharmaceutical [^{18}F]FDG (2-deoxy-2-[^{18}F]fluoro-D-glucose) is mainly used for this purpose. In 2013, 95% of PET examinations were carried out with [^{18}F]FDG.[12] In recent years, however, the number of available radiopharmaceuticals has increased due to constant research and further development.

1.1.1. Function of PET

The basis of PET is the decay of β^+-emitters. These nuclides are proton rich, which makes them instable. They stabilise themselves by conversion of a proton into a neutron (equation 1a). During this process, a positron (e^+) and an electron neutrino (ν_e) are emitted. This leads to a decrease of the atomic number (Z) and the increase of the neutron number (N) by one. The mass number (A) remains constant (equation 1b).[13]

$$\text{a)}\quad {}^{1}_{1}\mathrm{p} \rightarrow {}^{1}_{0}\mathrm{n} + \mathrm{e}^{+} + \nu_{\mathrm{e}} + \mathrm{Q}$$

$$\text{b)}\quad {}^{\mathrm{A}}_{\mathrm{Z}}\mathrm{X}_{\mathrm{N}} \rightarrow {}^{\mathrm{A}}_{\mathrm{Z}-1}\mathrm{X}_{\mathrm{N}+1} + \mathrm{e}^{+} + \nu_{\mathrm{e}} + \mathrm{Q}$$

Equation 1: Formulation of the β^+-conversion.

As the mother nuclide stabilises during the β^+-conversion, kinetic energy Q is released. This is transferred to the particles that are created during the conversion. These are the daughter nuclide, and the two emitted particles, the positron e^+ and the electron-neutrino ν_e The kinetic distributed statistically between the three particles and limited to a maximum energy Q_β^{max}, which is characteristic for a certain nuclide. This energy is normally in the range of 20 keV and few MeV.[13] The energy distribution to each of the three particles is shown in equation 2.

$$\mathrm{Q}_{\beta}^{\max} = \mathrm{E}_{\text{daughter nuclide}} + \mathrm{E}_{\text{positron}} + \mathrm{E}_{\text{electron-neutrino}}$$

Equation 2: Distribution of the conversion energy.

Normally, just a little amount of energy is distributed to the daughter nuclide (recoil energy). The large amount is divided between e^+ and ν_e. Due to the statistical distribution between both particles, a continuous energy spectrum can be found.[13]

The emitted proton covers a certain distance. Along the way, it interacts with the surrounding matter and loses kinetic energy through inelastic collisions, ionisation or production of free radicals. The range of the positron depends on the energy and the surrounding matter.[14] For example, a positron with an energy of 1 MeV covers a distance of about 3 m in air and in aluminium it has a range of only 1.5 mm.[13] Its lifetime is about 400 to 500 ps.[14] When the positron has reached an energy of about 5 to 10 eV and hits an electron, annihilation occurs in which the complete mass of the positron and the electron is converted in energy of 1.02 MeV according to $E=mc^2$. The complete process, starting from β^+-conversation until annihilation is shown in figure 1.

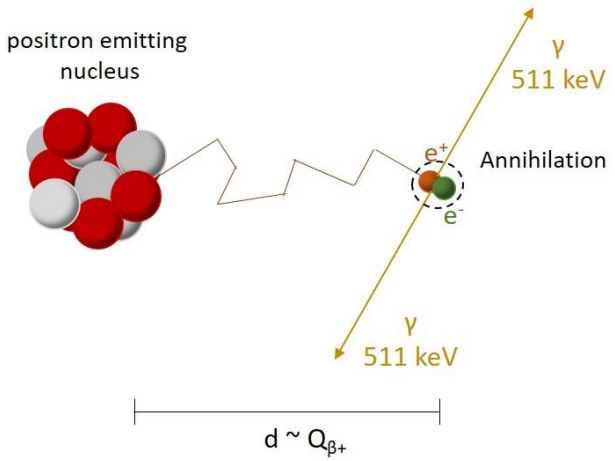

Figure 1: Illustration of the β^+-decay, the travel distance of the positron, which is proportional to the β^+ energy, and the subsequent annihilation with the emission of two γ-quants with an angular distribution of 180° and 511 keV each. Figure based on Ganguly et al.[14]

A differentiation is made between direct annihilation and positronium formation. In direct annihilation, all the energy is emitted directly in the form of photons. Here again, a distinction is made between different types of annihilation, where two-quantum annihilation and three-quantum annihilation are the most common.[14,15] Both types are shown in figure 2.

How many gamma rays are emitted depends on the spin orientation of the positron and the electron. If there is an antiparallel alignment, two protons with an energy of 511 keV each are emitted with an angle of 180°, which can differ by a few milliradians if the system was not at absolute rest during annihilation.[15] With parallel alignment of the spins, three photons are emitted with different angles and energy distribution.[15] The probability of either two- or three-quantum annihilation depends on the quantum states and the ratio of the cross sections, which is 1/372 (two-quantum state/three-quantum state).[15]

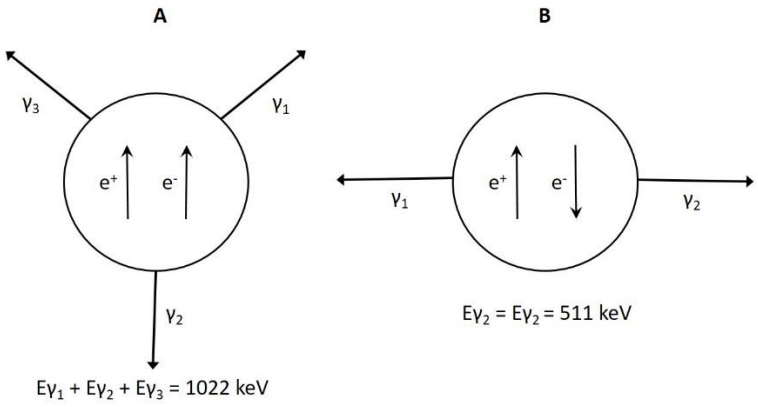

Figure 2: Three-quantum annihilation (A) and two-quantum annihilation (B) and their energy distribution. Figure based on Ache.[15]

If the positron reaches a kinetic energy level of less than 100 eV other possibilities besides the free annihilation can occur. This could be an interaction with matter, which can result in either ionisation (equation 3a) or electronic excitation (equation 3b). In addition, the positron can combine with a shell electron to form a positronium(PS, equation 3c).[13]

$$\text{a)}\quad e^+ + M \rightarrow e^+ + M^+ + e^-$$
$$\text{b)}\quad e^+ + M \rightarrow e^+ + M^*$$
$$\text{c)}\quad e^+ + M \rightarrow PS + M^+$$

Equation 3: Interaction possibilities of a positron with a kinetic energy lower 100 eV. a) ionisation; b) electronic excitation; c) formation of a positronium (Ps).[13]

The positronium can be seen as a hydrogen analogue in which the proton has been replaced by the positron.[13] The formation of the positronium is described by the *ore gap* theory.[16] This theory states that the positronium formation can only occur in a narrowly defined energy window, the so called ore gap. Above this energy value, the already discussed interaction with matter occurs and below this value the energy to form a positronium is too low. The ore gap lays between the first excited state of M and (V-6.8) eV, where V describes the ionisation potential of the electron and 6.8 eV represents the binding energy of the positronium.[13,17] As with free annihilation, the positronium can occur as a state with antiparallel spin (singlet-Ps, para-Ps), as well as state with parallel spin (triplet-Ps, ortho-Ps). The ratio of both states is 1:3 (p:o). The para-positronium has a lifetime of around $1.25*10^{-10}$ s and annihilates under emission of two gamma rays with 511 keV each and an angle of 180°. The characteristic of this positronium is that it always annihilates at exactly the same angle and with exactly the same energy distribution is used in PET as the fundamental measurement principle. In comparison, the ortho-positronium shows a longer lifespan of around $1.4*10^{-7}$ s and annihilates under the emission of three γ-quants with a variable energy distribution and angle.[13,15]

As already discussed, based on the measurement principle, only the para-positronium is suitable for PET, but the longer lasting ortho-positronium converts into the para-positronium its lifetime due to the influence of magnetic fields, which can be caused by surrounding ions. As a result, annihilation of the para-positronium occurs significantly more frequently than annihilation of the ortho-positronium despite the initial ortho-positronium formation rate of 75%.[13,15,16,18]

To localise the site of accumulation of the radiotracer in the patient, the so-called coincidence measurement is used.[19] The patient is positioned in a ring-shaped detector system. If in a defined period two gamma rays with an energy of 511 keV each are registered at opposite points of the detector, it is registered as true event and used to calculate a 3D picture. The point of annihilation is located on the imaginary line between both measurement points of the detector, the so called *line of response* (LOR).[19] Coincidence measurement is based on two assumptions that do not fully apply in reality, which leads to a lack of precision. On the one hand, it is assumed that the positron was travelling in a straight line. However, due to the different energies of the isotopes, no exact line can be defined. Additionally, the actual decay of the isotope does not occur on the LOR but only the annihilation of the emitted positron. The second assumption is that the angular distribution of the gamma rays is exact 180°. This distribution can vary slightly.[19,20] Modern PET devices have a resolution of 3-5 mm.[21] Coincidence measurement is also the reason for the superior sensitivity of PET in contrast to SPECT. PET also does not require collimators, while the gamma cameras used in SPECT require such collimators.[19,22] Figure 3 shows the principle of a PET measurement.

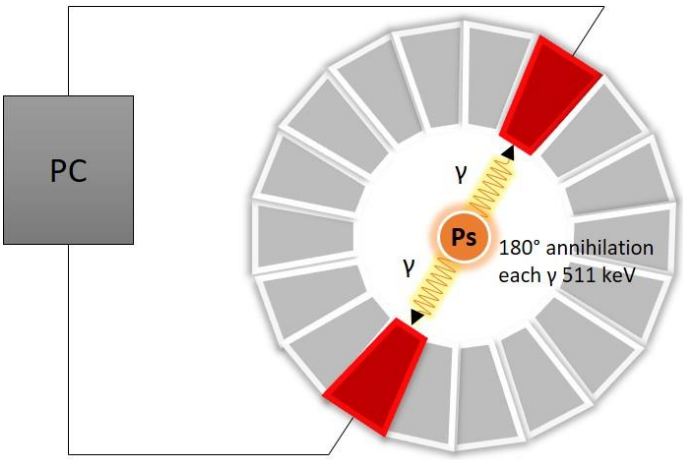

Figure 3: Schematic illustration of the annihilation of a positronium (Ps) and the subsequent coincidence measurement in the PET detector ring. Coincidence measurement is also possible after direct two-quant annihilation. Figure based on Piel et al.[21]

PET detector rings are only able to detect 1% of all annihilations processes. This is due to the limited axial field of view and the absence of an ideal detector material.[23,24] Beside the true registered events, there are two additional events which can be detected as coincidence event (figure 4). Randoms are two photons coming from two different annihilation events but are randomly registered

simultaneously at two opposite points of the detector. Coincidence events as result of scattering are called scatters. Randoms as well as scatters must be excluded from the measurement to get a correct PET image.[20,22,24]

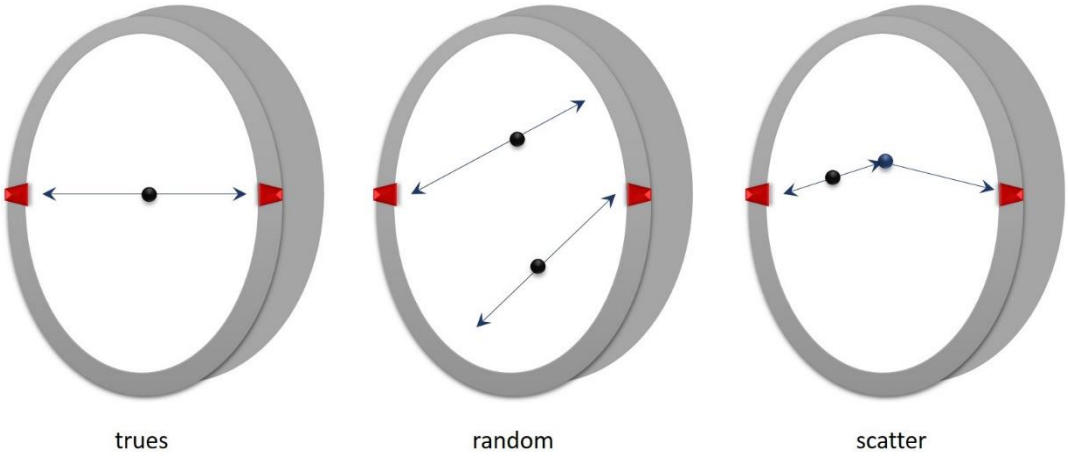

Figure 4: Annihilation events that can be registered in the coincidence measurement. Trues arise from the measurement of the two photons that originate from an annihilation event and run on an LOR. They are the events that are to be measured. Randoms arise when two photons from two different annihilation processes are randomly detected by two opposite detector elements. Scatters occur when a photon is scattered.

Modern PET cameras, as shown in figure 3, are ring-shaped scintillation detectors arranged around the patient and divided into blocks. These blocks consist of several scintillation crystals coupled to a photomultiplier. If a photon hits such a crystal, a light flash (also in form of a photon) is generated and the photomultiplier transforms this photon into an electrical signal, which is registered by the PC.[19,25]

The selection of the scintillation material is crucial for the performance of the detector. Some important aspects have to be considered to get a detector, which detects a high number of incoming gamma rays. Detection of all gamma rays is impossible due to physical boundaries. At the moment, there did not exist a perfect detector material. All state-of-the-art detector materials are a compromise of all important factors.[20] The most important aspect is the stopping power. Stopping power describes the ability of the material to slow down an incoming gamma rays, so it can be detected. This can be achieved through high density and high atomic numbers. Spatial resolution is also important. The better the spatial resolution, the better the exact place of annihilation can be determined. This can be achieved by using smaller crystals, but has higher costs as a consequence. A good energy resolution enables a good filtration of scattered coincidence events and a short cool down and processing time of the detector allows the registration of more photons in one time unit. If the scintillator has a high light output, more crystals can be coupled to one multiplier.[22,24–27]

While the NaI(Tl) detector is the tool of choice for general gamma ray detection because of its properties and is also very well suited for SPECT, it is not optimal for PET because it does not ensures

good detection for higher γ-energies than 200 keV, as occur in PET with 511 keV.[25] In the seventies, bismuth germanate crystals (BGO, Bi_4GeO_{12}) were introduced and represented the PET standard for a long period of time until it was replaced by more efficient cerium-doped orthosilicates like gadolinium orthosilicate (GSO, Gd_2SiO_5:Ce) or lutetium oxyorthosilicate (LSO, Lu_2SiO_3:Ce).[19,22,25,27] Table 1 shows an overview of some physical properties of the mentioned scintillation materials.

Table 1: Physical properties of some PET detector materials. Data taken from Ziegler.[22]

	NaI	**BGO**	**GSO**	**LSO**
Density (g/cm^3)	3.7	7.1	6.7	7.4
Effective Z	51	75	59	65
Photons (MeV)	41000	9000	8000	26000
Scintillation time (ns)	230	300	60	40

1.2 Diagnostic radionuclides

There are many known radioactive isotopes but only few are suitable for PET imaging due to the operating principle of PET. Most important limiting factor is the conversion mode of the radioactive isotope. Since the measurement principle consists of the detection of gamma rays generated during annihilation of a positron and an electron only isotopes undergoing β^+-conversion can be used. Additionally, some more factors for choice of a nuclide have to be considered. Table 2 shows a selection of the most important PET nuclides and their properties.

Table 2: Common PET-nuclides and their properties. Data taken from Qaim[28], Costa et al[29], Filosofov et al[30], Holland et al[31] and Yoshinaga et al[32].

nuclide	**$t_{1/2}$**	**$E_{\beta+ max}$ (MeV)**	**β^+-conversion**	**production**
^{15}O	2.0 min	1.73	99.9%	^{15}N(p,n)^{15}O (cyclotron)
^{13}N	10.0 min	1.20	100%	^{16}O(p,α)^{13}N (cyclotron)
^{11}C	20.4 min	0.96	99.8%	e.g. ^{14}N(p,α)^{11}C (cyclotron)
^{18}F	110 min	0.63	97%	^{18}O(p,n)^{18}F (cyclotron)
^{124}I	4.2 d	2.13	22%	e.g. ^{124}Te(p,n)^{124}I (cyclotron)
^{68}Ga	67.7 min	1.90	89%	^{68}Ge/^{68}Ga-generator
^{89}Zr	78.4 h	0.90	22.7%	^{89}Y(p,n)^{89}Zr (cyclotron)
^{44}Sc	3.93 h	1.47	94%	^{44}Ca(p,n)^{44}Sc (cyclotron) ^{44}Ti/^{44}Sc-generator
^{82}Rb	1.27 min	3.15	21.2%	^{82}Sr/^{82}Rb-generator

As described, only proton rich β^+ emitters are suitable for PET. Important to consider is the concurrence process of the β^+ conversion, the electron capture (EC). Electron capture describes the process of the capture of an electron into the nucleus and its conversion together with a proton into a neutron (equation 4).[13]

$$\text{a)} \quad {}^{1}_{1}\mathrm{p} + e^{-} \rightarrow {}^{1}_{0}\mathrm{n} + \nu_{\mathrm{e}} + \mathrm{Q}$$

$$\text{b)} \quad {}^{\mathrm{A}}_{\mathrm{Z}}\mathrm{X}_{\mathrm{N}} \rightarrow {}_{\mathrm{Z}-1}{}^{\mathrm{A}}\mathrm{X}_{\mathrm{N}+1} + \nu_{\mathrm{e}} + \mathrm{Q}$$

Equation 4: Formulation of the electron capture process.

During this process, no positron is released and thus it is not suitable for PET and the isotope which is selected should have a high β^+ conversion percentage and a low EC percentage.

Another important point is the maximum β^+ energy of the nuclide. This is the maximum energy that can be transferred to the positron and is proportional to the average travel distance of the positron until annihilation occurs. The further its range, the lower is the resolution of the PET image. Therefore, the nuclide of choice should have a low maximum β^+ energy.[33]

A factor to consider is the half-life ($t_{1/2}$). Two points are important here. First, the half-life has to match the biological behaviour of the lead structure. A good example in this context are antibodies in the immuno-PET. Antibodies show comparatively slow pharmacokinetics and thus longer half-lives are required. Commonly used short-lived nuclides like fluorine-18 ($t_{1/2}$ = 109.8 min) or gallium-68 ($t_{1/2}$ = 67.7 min) are not suitable in this context. They are normally used for the so-called small molecules. For antibody labelling longer-lived nuclides like zirconium-89 ($t_{1/2}$ = 78.4 h) or iodine-124 ($t_{1/2}$ = 4.2 d) are used.[34–37] Radionuclides with a very short half-life like oxygen-15 ($t_{1/2}$ = 2.0 min) or nitrogen-13 ($t_{1/2}$ = 9.9 min) show to short half-lives even for easy tracer syntheses. They are only used as simple compounds like $[^{15}O]H_2O$ or $[^{13}N]NH_3$.[38–40]

Another important aspect to consider in terms of half-life is the time that passes from production to application. After production of the nuclide, the synthesis of the desired radiopharmaceutical takes place, followed by purification and quality control. It is important to develop fast procedures to keep the time as short as possible. Optimally the injection should be done three half-lives after the production to allow a good imaging result.[38]

Next, the specific activity A_s has to be noted, The specific activity is defined as amount of radioactive isotope in the probe related to the complete amount of the element and is given as Bq/g.[41] The specific activity should be as high as possible to gain isotopically pure compounds and is influenced by the production of the nuclide. There are three different possible states. Is the nuclide complete pure, it is named *carrier-free* (c.f.). This state can only be achieved with artificially produced elements, such as

technetium, since contamination with other isotopes cannot be prevented in the case of natural elements. Such isotopes are called *no carrier added* (n.c.a.) isotopes. If an isotope of the same element is added during the production or cannot be separated, the received isotope is called *carrier added* (c.a.). This can be the case, if adsorption of the desired isotope at the vessel wall has to be prevent. By adding such a carrier, the specific activity decreases significantly.[38,42]

Another aspect is the availability.[29] Due to the radioactive properties, PET nuclides cannot be purchased and stored in advance. They have to be produced for each application, so the availability is directly connected to the production. There are three production routes for radionuclides. Some nuclides, including the most prominent PET nuclide fluorine-18 or carbon-11 can be produced via a cyclotron. Such cyclotrons are expensive in acquisition and maintenance, thus cyclotrons are only found in big nuclear medical facilities. Due to their longer half-life, some nuclides, such as fluorine-18, can be transported from the cyclotron site to local nuclear medicine units. In addition, there are reactor produced nuclides.[43] Another cheaper and simpler alternative and thus also feasible for practising nuclear medicine physicians is the availability of nuclides via radionuclide generator (see 1.2.1). Such generators are cheaper and handy than cyclotrons and reactors.[44,45] The most prominent diagnostic radionuclide technetium-99m (SPECT) is available via a ^{99}Mo/^{99m}Tc generator.[46] The development of the ^{68}Ge/^{68}Ga generator in the last decades led to an erratic development of ^{68}Ga-based radiopharmaceuticals.[44,47,48]

1.2.1 Gallium-68

The circumstance that gallium-68 ($t_{1/2}$ = 68 min) is available via generator system and its physical properties made it a popular PET nuclide.[49,50] It converts with 89% by β^+ conversion to zinc-68 (see equation 5). Its maximum β^+ energy is 1.90 MeV and its average energy is 0.74 MeV.[50]

$$^{68}_{31}\mathrm{Ga}_{37} \rightarrow {}^{68}_{30}\mathrm{Zn}_{38} + \mathrm{e}^+ + \nu_\mathrm{e} + \mathrm{Q}$$

Equation 5: β^+-conversion of gallium-68.

Gallium has the atomic number 31 and is part of group 13 (IUPAC nomenclature) of the periodic table of elements, also called third main group, boron group or earth metal group.

In aqueous solution, gallium-68 exits in the oxidation number +3. The cation shows a pk_a value of 2.6 and an ion radius of 47-62 pm.[51] Important to keep in mind is that free hydrated Ga(III) is only stable in acidic medium, thus radiolabelling has to be carried out under acidic conditions. At higher pH values $Ga(OH)_3$ and at even higher pH values $[Ga(OH)_4]^-$ is formed.[50,51] Following the HSAB principle by Pearson[52], gallium is a hard lewis acid and forms stable complexes with hard bases. In the complexation

chemistry mainly ligands with oxygen- or nitrogen atoms are used for complexation of gallium. 6-fold coordinated gallium complexes are the most thermodynamically stable and mostly used ones. In those complexes, a pseudo-octahedral coordination is found. Besides the coordination number of 6, also 3-,4- and 5-fold coordinated complexes are known.

In the complex chemistry of gallium-68, attention must be paid to the fact that the gallium ion Ga(III) is similar to Fe(III). Both have the same charge, similar ion radii, similar ionisation potentials and both prefer a coordination number of six. It must therefore be ensured that the gallium-68 complex is more stable than the corresponding iron complex and the work should be as iron-free as possible. *In vivo*, the serum protein transferrin, which is responsible for iron transport in the body, has two iron-binding sites with high gallium(III) affinity. Possible PET gallium-68 complexes must be more stable than the corresponding ^{68}Ga-transferrin complex to avoid transchelation.[50,51,53,54]

Gallium-68 is obtained using a ^{68}Ge/^{68}Ga radionuclide generator. The principle of this generator system is as following: The long-lived mother nuclide is fixed on an inorganic (e.g. TiO_2) or organic matrix. The mother nuclide converts into the shorter-lived daughter nuclide and an equilibrium arises after a defined time which correlates with the half-life of the daughter nuclide. The daughter can be eluted from the matrix while the mother remains and decays further, thus producing new daughter nuclide. It is important that daughter and mother differ chemically, making an efficient separation possible. There are two different types of radiochemical equilibrium. In secular equilibrium, the half-life of the mother is significantly longer than that of the daughter ($t_{1/2,\ daughter} << t_{1/2,\ mother}$) and the activity of the mother nuclide does not decrease measurably while many half-lives of the daughter pass. A secular equilibrium is found at a half-life ratio of 1:100. After reaching the equilibrium, the activity of both nuclides remain the same. The ^{68}Ge/^{68}Ga radionuclide generator is an example for such an equilibrium. The other kind is the transient equilibrium. Here, the mother also shows a longer half-life than the daughter, but with a ratio less than 1:100 ($t_{1/2,\ daughter} < t_{1/2,\ mother} < 100\ t_{1/2,\ daughter}$). In this case, the conversion of the mother is not negligible any more. In contrast to the secular equilibrium, after reaching the state of equilibrium, the activities of both nuclides are not equal. The activity of the daughter exceeds the activity of the mother nuclide. The ^{99}Mo/^{99m}Tc generator is an example for a transient equilibrium.[13,50,55]

In case of the ^{68}Ge/^{68}Ga radionuclide generator the mother nuclide germanium-68 is produced by irradiation of a gallium target (e.g. Ga_2O_3 or Ga_4Ni) via the (p, 2n) nuclear reaction using a cyclotron. High current cyclotrons are required. The production of germanium-68 by nuclear fission is also possible but the yield is lower.[55] After purification, germanium-68 is fixed on the matrix and is ready for use as generator. It converts by EC with a half-life of 270.8 d to gallium-68. The elution of gallium-68 is usually done with a dilute hydrochloric acid solution. The equilibrium is reached after ~14 hours. In

clinical routine the generators are eluted much more frequently, since 90% of the maximum of the activity of gallium-68 is generated after about three half-lives (3 hours).[47,48,50,55] Because of the long half-life of the mother nuclide germanium-68 the generator can be used at least one year.[44]

Theoretically, it is possible to use the eluted gallium-68 directly for synthesis of radiotracers. Practically there are some points to consider. During the lifetime of a generator, there is a potentially increasing germanium-68 breakthrough. This is a problem because of the long half-life of germanium-68. The generator can also carry some impurities like iron(III) or the conversion product zinc-68 or titan, a component of the matrix. Additionally, due to the elution with a hydrochloride acid solution, the proton concentration is very high and this can produce problems during the labelling procedure.[48,56] So-called post-processing methods enable the separation of these unwanted impurities so that gallium-68 can be obtained in pure form. There are three common forms of post-processing. The simples tone is the fractionating. The eluate is collected in small fractions and only the fractions with the highest activity are used. This is no direct purification but only a concentration of activity, because about two third of the activity is contained in 1 to 2 mL of the eluate. Though this process impurities such as Zn(II) or Fe(III) are not chemically separated but there is less present due to the smaller volume.[57–59]

Another technique is the use of anion exchange cartridges. The eluate is transferred in another vessel containing a higher HCl concentration, so that at the end the gallium is dissolved in a 5.5 M HCl solution. At these conditions gallium is present as $[^{68}Ga]GaCl_4^-$ and can be adsorbed on a strong anion exchange cartridge. Water flushes the gallium-68 from the exchanger, which can than be used for labelling. The ^{68}Ge-breakthrough is removed, but other impurities like zinc and iron remain in the solution.[47,60,61]

The third and most effective method is the use of cation exchange cartridges. The eluate is flushed directly through a cation exchanger and the gallium-68 is fixed. Afterwards, it is washed with an acetone/HCl-solution. This washing step removes all metallic impurities. The pure gallium-68 is then eluted from the cartridge using another acetone/HCl-solution and used for radiolabelling. This technique yields 97% of the eluted gallium within 4 minutes in a purified form.[47,56,59] To avoid the use of acetone in pre-clinical and clinical applications, variants of the cation exchange-based post-processing were developed. Ethanolic or saline containing solutions are used here instead of acetone.[56,62]

The development of radionuclide generators enables the availability of nuclides for diagnosis and therapy even without the presence of large-scale equipment such as a cyclotron. Additionally, an elaborate purification of the medically usable daughter nuclides is avoided. Thus the interest in the

development of novel generator systems and generator-based radiopharmaceuticals has increased remarkably in the last decades.[55]

1.2.2 Scandium-44

Scandium-44 is another radionuclide, which is suitable for PET. With 3.97 h, it has a longer half-life than gallium-68. This enables PET imaging of tracers with longer pharmacokinetic properties, as well as the transportation to other facilities.[63] Besides the suitable half-life there are additional physical properties, making scandium-44 a promising PET nuclide. It converts with a percentage of 94.3% via β^+ conversion into calcium-44 (see equation 6). The maximum β^+ energy is 1.47 MeV, whereby the emitted positron shows an average energy of 0.63 MeV.[64,65]

$$^{44}_{21}\mathrm{Sc}_{23} \rightarrow {}^{44}_{20}\mathrm{Ca}_{24} + \mathrm{e}^+ + \nu_\mathrm{e} + \mathrm{Q}$$

Equation 6: β^+-conversion of scandium-44.

In aqueous solution, scandium-44 is present as a trivalent cation. Just like gallium-68 it is categorized as a hard lewis acid and forms stable complexes with hard bases such as oxygen or nitrogen. There are known coordination numbers ranging from 6 to 8, while 8 is the preferred one.[66] In application, scandium is often coordinated by the chelator DOTA (1,4,7,10-tetraazacyclo-dodecane-1,4,7,10-tetraacetic acid), with which it forms stable complexes.[63,64,66–69]

There are two common production routes for scandium-44. One option is that it can be obtained via a ^{44}Ti/^{44}Sc generator. Titan-44 converts via EC with a half-life of 60.6 years into scandium-44.[70] Titan-44 itself can be produced via the ^{45}Sc(p,2n)^{44}Ti nuclear reaction. Also nuclear fission of vanadium or chrome targets is possible.[55] After irradiation and separation of titan-44, it can be fixed on an anion exchange cartridge. The scandium can be eluted with an oxalic acid/HCl-solution from the generator matrix.[30] As with the gallium-68 generator, this is an example for a generator with secular equilibrium.[70] The disadvantage is the availability of the generator. The production of titan-44 is very elaborate due to the small cross section of the ^{45}Sc(p,2n)^{44}Ti reaction and the resulting need of a long irradiation time.[71] Thus, the direct production of scandium-44 using a cyclotron is quite more popular.[63] The scandium is produced using the ^{44}Ca(p,n)^{44}Sc reaction with a proton energy of 8-13 MeV. Normally [^{44}Ca]$CaCO_3$ or natural Calcium is used as target material.[72,73]

Scandium is chemically quite similar to the therapeutic nuclide lutetium-177 despite a somewhat smaller ion radius. Therefore scandium-44 is suitable as diagnostic counterpart for lutetium-177 in theranostic approaches.[74,75] In terms of theranostic usage, the therapeutic nuclide scandium-47 is also an interesting counterpart to scandium-44, because of the identical chemical properties.[76,77]

1.2.3 Fluorine-18

The most prominent PET nuclide is fluorine-18. Its half-life of 109.6 min, the maximum β^+ energy of 0.63 MeV, its 97% β^+ conversion and its chemical properties are well suited for use as PET nuclide.[28,78,79] Equation 7 shows the β^+ conversion of fluorine-18.

$$^{18}_{9}\mathrm{F}_9 \rightarrow {}^{18}_{8}\mathrm{O}_{19} + \mathrm{e}^+ + \nu_\mathrm{e} + \mathrm{Q}$$

Equation 7: β^+-conversion of fluorine-18.

Because of its comparatively long half-life with 109.6 min, the synthesis of complex tracers, their purification and quality control are possible while at the same time enough activity is left to perform longer *in vivo* examinations. The half-life additionally enables the transport of fluorine-18 or ^{18}F-labeled tracers to facilities without a cyclotron.[80] The low β^+ energy results in a low range (< 2.4 mm) of the positron and therefore in a good resolution of the PET image.[81]

The production of fluorine-18 is cyclotron-based. More than 20 different production routes are known in which different flourine-18 species are obtained and which can be used in different radiolabelling strategies (see 1.4.2.). The most common method is the nuclear reaction ^{18}O(p,n)^{18}F. Water that has been enriched with oxygen-18 ([^{18}O]H_2O) is irradiated with protons in an energy range of 16 → 3 MeV yielding n.c.a. fluorine-18. It is obtained as fluorine anion in aqueous solution ([^{18}F]F^-_{aq}) and can be used for nucleophilic radiofluorination reactions. This nuclear reaction leads to specific activities of $10^4 – 10^5$ Ci/mmol. If fluorine-18 is needed for electrophilic radiofluorination, it is usually produced via the nuclear reaction ^{20}Ne(d,α)^{18}F (deuteron energy range 14 → 0 MeV). Neon gas is used as target and fluorine-18 is obtained as [^{18}F]F_2 gas. To avoid an adsorption of [^{18}F]F_2 at the target wall, the addition of [^{nat}F]F_2 gas is required. Therefore it can only be obtained as c.a. [^{18}F]F_2 gas with a specific activity of 1-10 Ci/mmol, which is significant lower than that of fluorine-18 produced via ^{18}O(p,n)^{18}F nuclear reaction.[28,78,79]

The most prominent ^{18}F-tracer is [^{18}F]FDG. It is used in PET imaging regarding neurological, oncological and cardiological questions. With 90% it is most commonly used in oncology.[82]

1.3 Endoradiotherapy and therapeutic nuclides

Besides the diagnostic area, radioactivity can also be used in therapy. The most common method is the therapy with an external photon or particle beam. To keep the radiation dose that reaches the tumour as large as possible, while keeping the unwanted radiation of healthy tissue as small as possible, a precise knowledge of geometry and localisation of the tumour is required.[83,84] In contrast

to that, endoradiotherapy (ERT) is similar to PET. Radionuclides are attached to molecules that accumulate in the target tissue and enable a high specificity and selectivity of the radiation. ERT also enables the therapy of patients with multicentral or multifocal tumours or metastases which can't be completely treated by normal radiation beam.[83]

Nowadays chemotherapy is the tool of choice in cancer treatment and shows some advantages in contrast to extern beam radiation therapy and ERT, but also disadvantages, which can not to be neglected. Especially the side effects can be severe and thus allow only the therapy of patients with a certain health condition. The principle of ERT and the precise irradiation of the cancer cells significantly reduces the side effects in comparison to chemotherapy.[84]

The mechanism of action of ERT is based ionisation caused by radiation of the emitted nuclides. While β^+ emitters are used in PET, β^- , α and auger electron emitters are used in ERT.[84–86] The aim of the therapy is the damage of the DNA of the cancer cells and the following induction of apoptosis or similar mechanisms, which ultimately results in the death of the cancer cell. There are two ways a damage of the DNA can be obtained. On the one hand, ionising radiation can interact directly with DNA and cause single-strand breaks. On the other hand, the ionising radiation can lead to the formation of free radicals, which then interact with the DNA and lead to its damage.[85] There are many different DNA damages, which are recognised and repaired by special repair mechanisms with varying degrees of ease and thus also lead to cell death in different degrees of success. Single-strand breaks or DNA base damage can be recognised more easily than double-strand breaks or multiply damaged sites.[85,87]

The severity of the damage to the radiated cell depends on the absorbed dose of energy, which is transferred from the irradiation to the cell. The higher this so-called linear energy transfer (LET) is, the more the cell is damaged and the more likely double-strand breaks and the death of the cell occur.[84] α particles show the highest LET, followed by β^- particles.[88] There are two more effects which are important for a high effectiveness of ERT. Based on the chosen radionuclide, the range of the radiation is longer than the diameter of one cell. Thus, cancer cells which have not internalised or bound the radioligand are also irradiated (cross-fire effect). Additionally, the radiation-induced bystander effect causes cells to behave as if they had been irradiated, even though they were not exposed to radiation. This may be due to the fact that they are in the direct vicinity of irradiated cells and are induced by signal factors. However, the exact mechanism of the bystander effect is not yet known.[89,90]

Similar to PET, there are some parameters of the nuclide which have to be considered during the choice of the ERT nuclide. Table 3 shows a selection of possible ERT nuclides and their physical properties.

Table 3: some common ERT-nuclides and their properties. Data taken from Zalutsky[86], Zalutsky et al[91], Qin et al[92], Qaim[93] and Apostolidis et al.[94]

Nuclide	Type	$t_{1/2}$	$E_{Average}$	Mean range	production
^{131}I	short range β$^-$	8.1 d	182 keV	910 µm	^{130}Te(n,γ)^{131m,g}Te -> ^{131}I
^{177}Lu	short range β$^-$	6.7 d	133 keV	670 µm	^{176}Lu(n,γ)^{177}Lu ^{176}Yb(n,γ)^{177}Yb -> ^{177}Lu
^{186}Re	medium range β$^-$	3.8 d	362 keV	1800 µm	^{185}Re(n,γ)^{186}Re
^{153}Sm	medium range β$^-$	1.9 d	229 keV	1200 µm	^{152}Sm(n,γ)^{153}Sm
^{90}Y	long range β$^-$	2.7 d	935 keV	3900 µm	^{89}Y(n,γ)^{90}Y ^{90}Sr/^{90}Y-generator
^{225}Ac	α	10.0 d	5.74 MeV	40-100 µm	e.g. ^{226}Ra(p,2n)^{225}Ac
^{211}At	α	7.21h	5.87 MeV	50 µm	^{209}Bi(α,2n)^{211}At

Very important parameters are the energy of the emitted radiation, the type of radiation and the range. These must be chosen dependent on the size of the tumour.[95] α emitters have the largest LET (ca. 80-100 keV/µm), but only a short range (40-100 µm). β$^-$ emitters vary in their energy and range but generally have a greater range (0.05-12 mm), but smaller LET (ca. 0.2 keV/µm) than α emitter. Auger emitter have a high LET (1-23 keV/µm) but a very short range (few nm).[88,96] Larger tumours should be treated with β$^-$ emitters of greater range, while for smaller tumours or its residues after surgical removal β$^-$ emitters with lower energy or α emitters can be considered. Therefore, it is important to know the dimensions of the tumour before therapy. Previous PET examination can provide information.[84–86,88,95,96] To get the maximum dose of radiation at the target tissue it is important to choose a nuclide with a half-life which matches the pharmacokinetics of the therapeutic agent. With regard to the half-life, the same considerations as with PET are important.[95] Additionally, the availability and the costs of the nuclide have to be considered.[95]

1.3.1 Lutetium-177

Lutetium-177 is one of the most prominent radioisotopes used for ERT. This is due to the very well suited physical properties for ERT of the lanthanide and due its easy production with high specific yields at a lot of facilities worldwide.[97] Lutetium-177 converts to hafnium-177 with a half-life of 6.7 d via β$^-$ conversion (equation 8).

$$^{177}_{71}\mathrm{Lu}_{106} \rightarrow {}^{177}_{72}\mathrm{Hf}_{105} + \mathrm{e}^- + \bar{\nu}_\mathrm{e} + \mathrm{Q}$$

Equation 8: Conversion of lutetium-177 in hafnium-177.

The conversion takes place at 76% with a maximum energy of $E_{\beta(max)}$ = 0.497 MeV to the ground state hafnium-177, at 9.7% to the first excited state ($E_{\beta(max)}$ = 0.384 MeV) and at 12% to the third excited state ($E_{\beta(max)}$ = 0.176 MeV). The second excited state is negligible. The excited states converts to the ground state through γ emission. Here the gamma lines with energies of 208 keV (11%) and 113 keV (6.6%) are interesting due to their possibility to be used in SPECT imaging. Because of that fact, the *in vivo* behaviour of ^{177}Lu-labeled compounds can be monitored by SPECT imaging .[98,99]

Lutetium-177 has a range of 670 µm in tissue. Thereby, it is perfectly suitable for therapy of smaller tumours and metastases. The low β^- energy and the low-energy photon emission result in a low radiation dose of patient, physician and radiochemist and also simplify the use of higher activities of lutetium-177. Additionally, the half-life of 6.7 days enables more complex synthesis as well as transport to other facilities.[98]

The production can be achieved by to different ways. Figure 5 shows an overview.

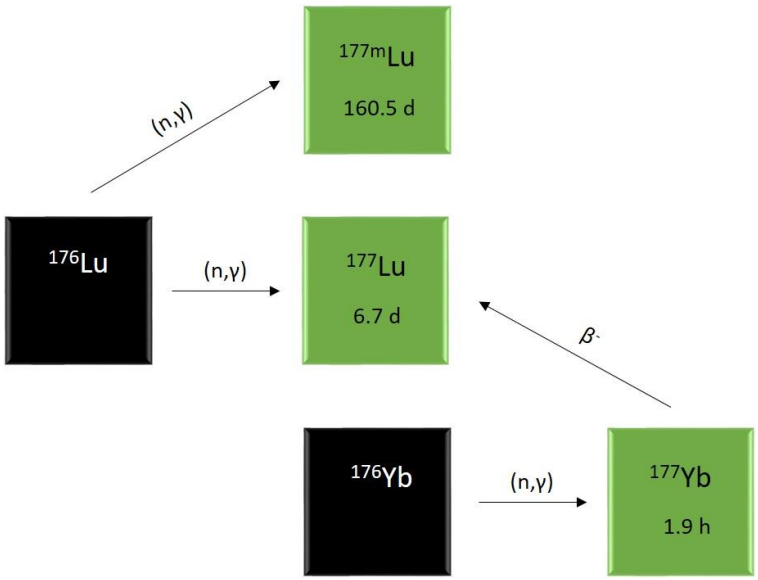

Figure 5: Production routes of lutetium-177.

The first production route is the nuclear reaction ^{176}Lu(n,γ)^{177}Lu. Natural or with lutetium-176 enriched Lu_2O_3 is used as target. This route is the simplest and cheapest one, but beside the desired luetitium-177, long-lived lutetium-177m is formed as side product as well. This has to be considered in terms of dosimetry and waste disposal. An alternative route is an indirect production route. Here, Yb_2O_3 is irradiated in a (n,γ) nuclear reaction and ytterbium-177 is produced. This converts to lutetium-177 with a half-life of 1.9 h. This leads to n.c.a. lutetium-177 and higher specific activities are achieved in contrast to the direct production route. Additionally, no lutetium-177m contaminant is present. The disadvantage is that the small amounts of lutetium-177 produced have to be separated from the target material and the irradiation yield is much lower than with direct production.[86,97,98,100]

There are also production routes using a cyclotron, these routes have no significance in routine application.[98]

Like the diagnostic nuclides gallium-68 as well as scandium-44, lutetium-177 prefers the oxidation state of +3. The hard lewis acid Lu(III) forms stable complexes with hard ligands like oxygen or nitrogen with coordination numbers of 6 to 9.[99]

1.4 Radiolabelling chemistry

The way a radionuclide is attached to the tracer depends on the type of nuclide. A difference is made here between organic nuclides, like fluorine-18 or carbon-11 and metallic nuclides like gallium-68 or lutetium-177. Organic nuclides can be inserted via a covalent bond, whereby with some isotopes, like carbon-11, one takes advantage of the fact that the element occurs in many biomolecules and it is simply to swap an atom for the radioactive isotope. Other organic nuclides, like fluorine-18, can only be introduced this way, as they only rarely occur in (bio)molecules. Analogies between existing units are used here (analogy tracer, see section 1.3.2.).[38] Metallic nuclides have to be bound in a different way. So-called chelators are bound covalently to the target vector and these chelators are forming a chelate complex with the radiometal. Generally in terms of analogy tracers and chelators it has to be noted that the introduction can influence the chemical, physical and pharmacological properties of the original biomolecule or the target vector.[101,102]

1.4.1 Chelatorsystems

As already mentioned, radio metals are introduced into the radiopharmaceutical via chelators. Figure 6 shows the general structure of a metal nuclide-based radiopharmaceutical.

Figure 6: General design of a radiotracer with a metalnuclide. Figure based on Fani et al.[103]

The three major units of such a radiotracer are the target vector, which is a pharmaceutical component that determines the biological localisation in the patient. This can be for example peptides, small

molecules, antibodies or fragments of antibodies. Secondly, a chelate moiety, which is responsible for complexation of the therapeutic or diagnostic radionuclide. And third, the linker unit can fulfil several tasks. First, it can act as a spacer to put space between the often-bulky chelator and the target vector to avoid steric influences. Furthermore, it can serve as a modulator of the pharmacokinetics of the radiotracer.[103] A very interesting and promising linker unit is squaric acid.[104] It can be introduced as squaramides and shows, beside an easy chemistry, positive features regarding pharmacokinetic properties. For further information, see section 1.5.

So-called bifunctional chelators (BFC) have enough functionalities (usually carboxyl groups) that bind to the target structure and at the same time enough functionalities remain for a stable complexation of the radiometal.[105] As an alternative, the backbone of the chelator can also be functionalised.[103]

There are some important criteria, which have to be considered during the selection of the BFC. It is important that the nuclide/chelator complex shows a high thermodynamic as well as a high kinetic stability. The thermodynamic stability is the strength of the binding/interaction of the donor atoms and the nuclide. The kinetic stability describes the stability against dissociation or transmetalation. The radionuclide must not leave the chelator inside the body. This would lead to the loss of the diagnostic or therapeutic effect and additionally, the nuclide can also have a toxic effect. The following points have to be addressed to get a stabile complexation: a) the size of the chelator have to match with the ion radius of the nuclide; b) the number and chemical properties of the donor atoms have to fit to the nuclide; c) the charge. Beside this, as described in section 1.1.1, there are natural complex former, like transferrin and attention has to be paid that the complexation of the nuclide in the BFC is more stable than the complexation of the natural complex former to avoid transchelation.[103,106,107]

Based on the structure of a chelator, there are to groups of chelators, acyclic and macrocyclic chelators. In general, macrocyclic chelators are thermodynamically more stable than acyclic chelators because of the high number of free rotatable bindings of the acyclic chelator. To form a chelate complex, an acyclic chelator must undergo a drastic change in its conformation. This leads to a higher decrease of entropy than it is the case for cyclic chelators, which already have a pre-oriented conformation due to their cyclic system and no large rotation of the bonds is possible (macrocyclic effect).[102,103,108] Acyclic chelators showing a low energy barrier to form chelate complexes, which enables a fast complexation at mild conditions. This has the advantage that sensitive molecules can be labelled. On the other hand, the low energy barrier also results in lower kinetic stability, which leads to rapid dissociation of the complex and thus low *in vivo* stability.[102,103] Due to the higher energy barrier macrocyclic chelators showing a significant higher kinetic stability, but require higher temperatures (60-95 °C) and longer reaction times to yield a quantitative labelling result which is a problem with sensitive molecules like

antibodies.[102] Based on the pre-oriented structure the number of complexable nuclides for some macrocyclic nuclides are smaller in contrast to acyclic chelators.[100]

1.4.1.1 Acyclic chelators

Acyclic chelators are open chain polydental ligands which contain donor atoms like nitrogen or oxygen and therefore suitable for complexation of metal ions. In 1974, this principle was used for the first time by Sundberg et al. to label proteins with indium-111. EDTA (ethylenediaminetetraacetic acid) was used as chelator.[103,109,110] Since then many different acyclic chelators were developed. An overview of some important acyclic chelators are shown in figure 7.

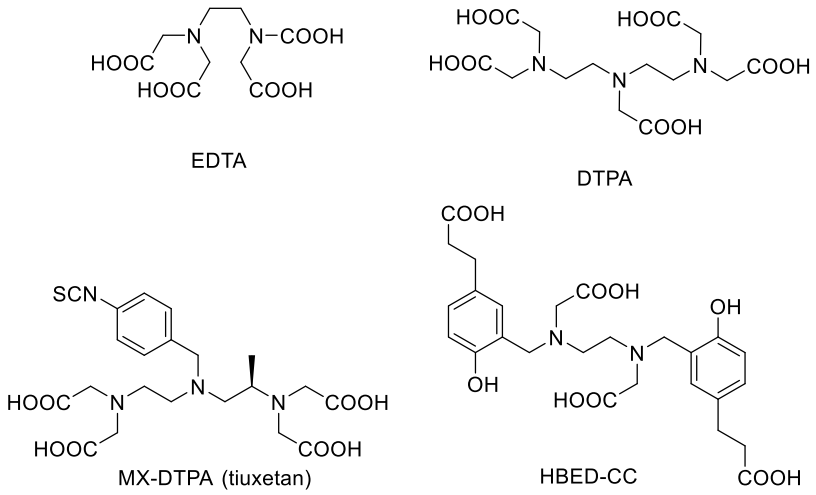

Figure 7: Structures of common acyclic chelators.

Since the complex stability of EDTA/Me(III) complexes has proven to be very unstable and thus not applicable *in vivo*, the chelator DTPA (diethylenetriaminepentaacetic acid) was developed.[111] DTPA can be labelled at mild conditions with a wide range of radiometals.[102] Therefore, it is one of the most used acyclic chelators and also finds clinical application. For example, the indium-111 labelled and FDA approved compound [^{111}In]In-DTPA-octreotide is used as SPECT-radiotracer for neuroendocrine tumours.[102,105] Due to the poor kinetic stability of DTPA, attempts have been made to improve the stability through derivatisation of the backbone. This modification leads to a more rigid form which also leads to a less loss of entropy compared to DTPA during the process of complexation and thus resulting in a higher kinetic stability.[103] This is how the bifunctional chelator MX-DTPA or also known as tiuxetan (1,4-methyl-benzyl isothiocyanate diethylenetriamine pentaacetic acid) was designed, which can be linked to a target vector via a isocyanate unit and which owns a more rigid scaffold due to the methylated backbone. This chelator was used for coupling to the CD-20 antibody Ibritumomab

and is used for imaging (indium-111) and for therapy (yttrium-90) under the FDA approved name Zevalin™.[103,112]

Another important representative of acyclic chelators is HBED (*N,N*'-Di(2-hydroxybenzyl)ethylenediamine-*N,N*'-diacetic acid). The phenolic unit enables not only the complexation of trivalent metals but also the complexation of metals like technetium or palladium.[113] HBED shows optimal labelling properties for gallium and also a high *in vivo* stability.[105] The bifunctional derivative HBED-CC (*N,N*'-bis-[2-hydroxy-5-(carboxyethyl)benzyl]ethylenediamine-*N,N*'-diacetic acid) has gained a lot of attention in recent years. HBED-CC was conjugated to a urea-based PSMA (prostate-specific membrane antigen) inhibitor and used for PET imaging of prostate cancer. Today, the so-called [^{68}Ga]Ga-PSMA-11 ([^{68}Ga]Ga-PSMA-HBED-CC) is state of art in PET imaging of prostate cancer and one of the most used tracers in this field.[114–116]

1.4.1.2 Macrocyclic chelators

Beside the acyclic chelators there is the group of macrocyclic chelators. Compared to acyclic chelators, they show higher thermodynamic stabilities, as well as a higher kinetic inertness, but require harsher labelling conditions and longer labelling reaction times.[102] There exist a variety of macrocyclic chelators. Some important bifunctional macrocyclic chelators are shown in figure 8.

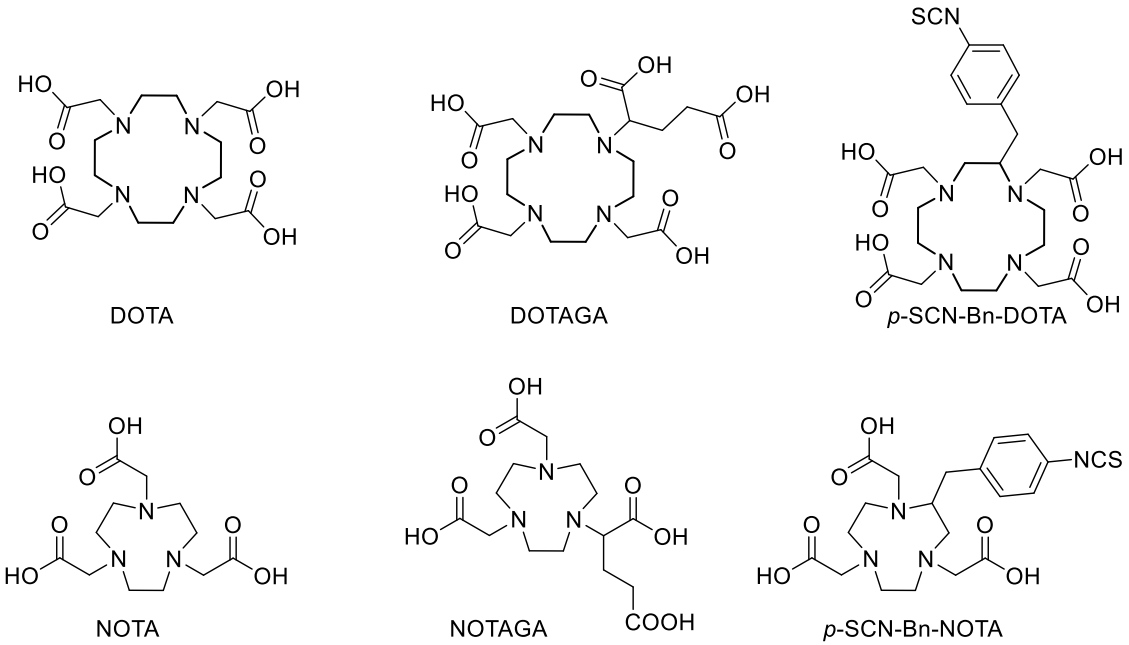

Figure 8: Structures of some common chelators and their bifunctional derivatives.

Among all, DOTA (1,4,7,10-tetraazacyclo-dodecane-1,4,7,10-tetraacetic acid) is the most important one in radiopharmacy. DOTA is based on a cyclene scaffold, whose nitrogen atoms were

functionalised.[103] DOTA complexes a variety of di- and trivalent metals stable. Beside the diagnostic nuclides like gallium-68, scandium-44 or indium-111, it can also be labelled with therapeutic nuclides like lutetium-177, actinium-225 or yttrium-90 and is therefore suitable for use in theranostic approaches.[102,111] For example, one can simply access the theranostic nuclide pairs yttrium-86 (PET) and yttrium-90 (ERT) or scandium-44 (PET) and scandium-47 (ERT) which all form stable complexes with DOTA.[77,117] DOTA can be functionalized using the carboxy groups. Although usually the four cyclic nitrogen atoms and three carboxy groups are sufficient donor atoms for the complexation of many metals, it can occur that the coordination is disturbed by the functionalisation. This problem may occur especially with higher lanthanides and lead to stability problems.[105] A solution of this problem can be the functionalisation of the backbone, such as the introduction of an additional glutaric acid as seen in DOTAGA (1,4,7,10-tetraazacyclododececane-1-glutaric acid-4,7,10-triacetic acid) or the functionalisation of the backbone with a *p*-Bn-NCS ester (*p*-SCN-Bn-DOTA). For both variants, an additional functional unit is available for functionalisation while all four carboxy groups of the cyclene scaffold are free for complexation.[102,105] A variety of DOTA derivatives are commercially available, making the DOTA chelator universally applicable. An example of the clinical use of DOTA conjugated radiopharmaceuticals is [^{68}Ga]Ga-DOTATOC. It is used for PET imaging of neuroendocrine tumours.[118] Another prominent example of DOTA-based radiopharmaceuticals is PSMA-617, which can be labelled with lutetium-177 or actinium-225 for therapy of prostate cancer.[119,120]

Another chelator is NOTA (1,4,7-triazacyclononane-1,4,7-triacetic acid). Due to its hexadental N_2O_3 structure the number of complexable nuclides is not that high than in comparison to DOTA. It is particularly well suited for gallium-67/68 and copper-64. Due to its size and donor atom number and the high *in vivo* stability NOTA is considered as optimal chelator for gallium-68.[102,105] In contrast to other macrocyclic chelators, NOTA can be labelled with gallium-68 at mild conditions.[105,121]

NOTA is not a BFC per se, since all functional groups for complexation of the nuclide (e.g. gallium-68) are needed. Here, analogous to DOTAGA, the functionalisation of the scaffolding offers a solution. NODAGA (1,4,7-triazacyclononane,1-glutaric acid-4,7-acetic acid) or *p*-SCN-Bn-NOTA provide an additional functional group and are BFCs.[102] Both NODAGA and *p*-SCN-Bn-NOTA are among the most important BFC derivatives of NOTA.[105]

In the area of PET nuclides, both gallium-68 as well as scandium-44 form stable complexes with the important chelators NOTA and DOTA. Here however, it can be observed that the ^{68}Ga-NOTA complex is more stable than the ^{68}Ga-DOTA complex and in contrast to this, the ^{44}Sc-DOTA complex is again more stable than the ^{44}Sc-NOTA. The reason is the number of donor atoms of each chelator and the preferred coordination number of the metal nuclide. NOTA provides six donor atoms and gallium

prefers the coordination number of six. In contrast, DOTA has eight donors, which can be used completely to complex scandium-44. Scandium-44 prefers the coordination number 8.[66]

1.4.1.3 Hybrid chelators

A third class of chelators are the hybridic chelators (figure 9) which combine the strong chelator/metal interaction and the kinetic stability of macrocyclic chelators with the fast labelling kinetic under mild conditions of acyclic chelators. The combination of the advantages of both chelator classes are achieved through the combination of structural features of both chelator types. Hybrid chelators have a cyclic component as well as an acyclic part.[105,122,123] The heptadentale chelator AAZTA (1,4-bis (carboxymethyl)-6-[bis(carboxymethyl)]amino-6-methylperhydro-1,4-diazepine) matches this concept. AAZTA consists of a perhydro-diazepine scaffold with two cyclic amines and an exocyclic amine, which can act as donor atoms for labelling. A functionalisation of the amines with carboxy groups provides further donor atoms.[124,125]

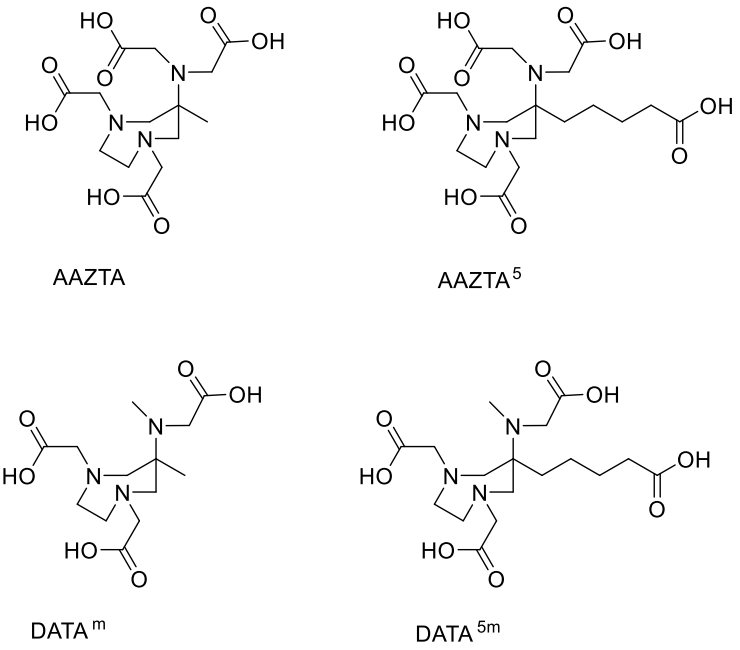

Figure 9: Structure of the hybrid chelators AAZTA and DATA^{m} and their BFC derivatives AAZTA^{5} and DATA^{5m}.

AAZTA was originally developed as Gd(III) chelator for MRI, but also shows good labelling properties with transition metals like scandium-44 or lanthanides like lutetium-177 and can be therefore used as chelator in ERT and PET applications.[126–128] To connect AAZTA to target vectors, the bifunctional version AAZTA^{5} (1,4-bis-(carboxylmethyl)-6-[bis-(carboxymethyl)-amino-6-pentanoic-acid]-perhydro-1,4-diazepine) was developed.[128] Known in literature are currently AAZTA conjugates with peptidic target

vectors such as AAZTA^5-TOC for neuroendocrine tumours[128], with small molecules like FAP inhibitors (AAZTA^5.SA.FAPi)[129] and antibody conjugates such as AAZTA^5-SA-bevacizumab[125].

At low pH values, which are present e.g. during gallium-68 labelling, AAZTA shows a pseudo-axial conformation AAZTA, which makes gallium-68 complexation more difficult. Additionally, three different [^{68}Ga]Ga-AAZTA species with varying stability are observed.[130,131] For this reason, the AAZTA structure was optimized for an optimal gallium-68 labelling and stability. This is how the hexadental DATA^m (1,4-bis(carboxymethyl)-6-[amino(methyl) carboxymethyl]methylperhydro-1,4-diazepine) was developed, showing optimal labelling properties at mild conditions and short reaction times in combination with very good complex stabilities with gallium-68.[130,132,133] Both DATA^m as well as its bifunctional version DATA^{5m} (1,4-bis(carboxymethyl)-6-pentanoic acid[amino(methyl) carboxymethyl] perhydro-1,4-diazepine) form a stable octahedral complex with their N_3O_3 structure with gallium-68.[134] This favourable conditions enable the labelling of sensitive molecules such as antibody conjugates. The chelator DATA can also be used in kit type labelling strategies enable a simplified application and handeling.[123,135] There are known DATA based radiopharmaceuticals which are already clinical examined. These include the somatostatin agonist [^{68}Ga]Ga-DATATOC[122,123] and the FAP inhibitor [^{68}Ga]Ga-DATA^{5m}.SA.FAPi[136].

1.4.2 Radiofluorination

Fluorine-18 can be introduced into an organic molecule covalently. While carbon-11 can be introduced as radioactive label through the exchange of an existing carbon atom of the compound, however, fluorine rarely occurs in biomolecules, thus this method is not often applicable. Therefore, fluorine-18 is inserted through the exchange of other atoms or groups of the molecule. Here, some analogies are used. Possible exchange candidates are, for example, hydrogen atoms or hydroxyl groups due to their behaviour as bioisoster to fluorine.[137-139] Hydrogen is a possibility because of the similar van der Waals radii (hydrogen: 1.20 Å; fluorine: 1.35 Å), whereas the binding energy of the carbon to the fluorine is stronger than to hydrogen (H-C: 98 kcal/mol; F-C: 112 kcal/mol).[81] The exchange of hydroxyl groups against a fluorine is another attractive variant and it is possible due to the similar electronic properties. Both act as electron pair donors and both have similar carbon bond lengths (C-F: 1.39 Å; C-OH: 1.43 Å).[38,81,137–139]

It should be kept in mind that the introduction of fluorine has an influence on the physicochemical as well as on the pharmacological properties of the tracer, since, for example, the electronegativity of fluorine can have an influence on the charge distribution of the molecule, if a hydrogen atom is replaced by fluorine.[38,138,139]

In general, a distinction is made between three different radiofluorination methods. They are described below.

1.4.2.1. Nucleophilic radiofluorination

Nucleophilic radiofluorination is the most common method in radiopharmaceutical chemistry. N.c.a. $[^{18}F]F^-$ is introduced via a second order nucleophilic substitution (S_N2) into the labelling precursor. Common leaving groups for these reactions are sulfonic esters, such as triflate, nosylate or tosylate, but also halogens, such as iodine or bromine. It is obvious that fluorine, which is also a good leaving group, is not used as a leaving group in radiofluorination, as otherwise the specific activity is lowered.[78,140] Another aspect which has to be considered while using the S_N2 mechanism is the Walden inversion. With stereospecific compounds, it comes to an inversion of the conformation. For example, this must be considered when using this reaction during the synthesis of $[^{18}F]$FDG.[141]

$[^{18}F]F^-$ is obtained in an aqueous solution after production. In this aqueous form it is not suitable to use in a nucleophilic reaction due to the fact that $[^{18}F]F^-$ forms hydrogen bonds with the water, degreasing the nucleophilicity drastically. The $[^{18}F]F^-_{aq}$ has to be purified and cleaned from all traces of water prior usage. This step is called azeotropic drying. Fluorine-18 is trapped on an anion exchange cartridge and water is removed. To elute $[^{18}F]F^-$ from the cartridge, a solution of acetonitrile, a cryptand and a base is used.[79,81]

Suitable bases are salts with soft cations such as K^+ or Cs^+. This leads to a weak ion pair, which can be separated easily. The base is added, for example, as oxalate or carbonate and is also used to prevent the formation of HF. The aminopolyether Kryptofix® 2.2.2 (4,7,13,16,21,24-Hexaoxa-1,10-diazabicyclo[8.8.8]-hexacosane) is normally used as cryptand. Tetraalkylammonium carbonate is also possible. This phase transfer catalyst has the task to trap the cation and leads to the formation of a strong nucleophilic $[^{18}F]F^-$ anion.[79]

The mixture eluted from the exchanger is dried to dryness and completely freed from water by a repeated azeotropic distillation using acetonitrile. Thereupon, the desired solvent can be added and the radiofluorination can be started. As solvents, dipolar aprotic solvents like DMSO, DMF or acetonitrile are possible, because of their solvatisation of the cation, but no interaction with the fluoride.[79,81,140,141]

As already mentioned, the most prominent example of ^{18}F-tracer which is obtained by nucleophilic radiofluorination is $[^{18}F]$FDG. Acetyl-protected mannose triflate is used here as the reactant. The triflate is the leaving group and after Walden inversion the acetyl protected $[^{18}F]$FDG is formed. Hydrolysis is used for deprotection and the ready to use $[^{18}F]$FDG is obtained.[142]

1.4.2.2. Electrophilic adiofluorination

Electrophilic c.a. $[^{18}F]F_2$ which is used for electrophilic radiofluorination is produced in a cyclotron. Since, as already described, inactive carrier has to be added, the specific activity is significant lower in contrast to nucleophilic $[^{18}F]F^-$. Only one fluorine of $[^{18}F]F_2$ is a fluorine-18 isotope, thus the maximum radiochemical yield is 50% in such reactions. $[^{18}F]F_2$ is very reactive and less selective. Some methods are developed to transform $[^{18}F]F_2$ in less reactive and more selective fluorinating agents. For example, $[^{18}F]F_2$ can passed through a sodium acetate column to obtain [^{18}F]acetylhypofluoride. Other examples for mild fluorinating agents are fluorosulfonamides and xenon difluoride.[79–81,140,143]

The first synthesis of [^{18}F]FDG in 1976 was a electrophilic synthesis route.[144] Despite a lot of improvements of this synthesis route, today [^{18}F]FDG is not produced via a electrophilic route anymore due to the disadvantages in comparison to the nucleophilic radiofluorination (specific activity, yield and side products).[38,142,144] Clinically applied compounds that are produced by electrophilic fluorination are for example [^{18}F]F-DOPA for dopaminergic imaging.[81,145]

1.4.2.3. Radiofluorination with prosthetic groups

Another method for fluorine-18 labelling is the labelling via a prosthetic group. It can be considered especially for labelling of sensitive biomolecules, such as antibodies, proteins or peptides.[81] This molecules are not resistant against the harsh conditions which are required for the previous described methods due to sensitive structure elements such as disulphide bridges or H-acidic units.[143] To label such molecules indirect labelling strategies with so-called prosthetic groups are possible. These are small units which can be labelled with fluorine-18 fast and in high yields using a direct fluorination method. These units can be introduced in the sensitive molecule using simple reactions such as alkylation or amidation. It is important to notice that prosthetic groups can also influence the pharmacologic properties. Therefore, it makes sense to use the existing structures. So, if a molecule which should be fluorinated using an indirect method, carries an alkyl chain, it is useful to exchange this alkyl chain against a radiofluorinated version. Is the molecule a peptide, for example, it is possible to use the primary amine of a lysine side chain for the introduction of the prosthetic group.[81,140,143,146]

An important prosthetic group is [^{18}F]Fluoroethyl tosylate ([^{18}F]FETos). It is used in the synthesis of the clinical used O-2-[^{18}F]fluoroethyl-L-tyrosine ([^{18}F]FET).[140,147] [^{18}F]FETos can be prepared easy, fast and in high yields.[38] Automated procedures are also known and established.[148]

Another established method for the introduction of prosthetic groups is the use of the copper(I)-catalysed huisgen 1,3-dipolar cycloaddition (CuAAC) and is also called click chemistry.[149,150] This term was introduced 2001 by Kolb et al and refers to a category of organic synthetic reactions that allow to

synthesize compounds fast, under easy conditions, without further elaborate purification and in high yields.[151] The click chemistry is not only of great interest in the field of radiopharmaceutical chemistry of great interest, but today also no longer indispensable in the general field of drug development.[150,152]

During the copper(I) catalysed huisgen 1,3-dipolar cycloaddition an azide reacts with an alkyne forming a 1,2,3-triazol (Figure 10).[149] Following this principle, the molecule to be labelled can be functionalised with an azide or an alkyne. The prosthetic group than carries the complimentary structure element and can be "clicked" to the molecule after a successful direct radiofluorination.

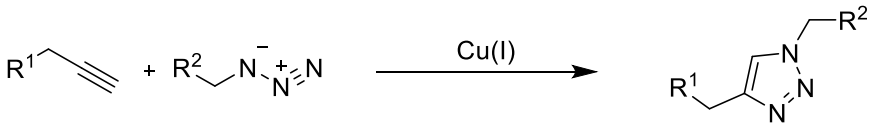

Figure 10: copper(I)-catalyzed 1,3-dipolar cycloaddition.

While the uncatalysed cycloaddition of an alkyne and an azide is not part of the click chemistry due to long reaction times, high temperatures are required and because no pure product is obtained (a mixture of 1,5- and 1,4-substituted triazoles are achieved), the copper catalysis leads to a fast, regioselective reaction under mild conditions.[149] Additionally, the reaction can be carried out in a lot of different solvents as well as in a wide pH range (4-12) and in presence of a lot of different functional groups.[153,154] Copper(II)-salts, such as $CuSO_4$ are possible as catalysts. It is reduced in situ to copper(I). As reduction agent sodium ascorbate has been established. Copper(I) salts can also be used directly, but the formation of side products can occur.[153]

Figure 11 shows the mechanism of the CuAAC containing two copper atoms proposed by Worrell et al.[155] In the first part of the catalytic circle, one copper atom coordinate the alkyne, forming an σ-bound copper acetylide with a π-bound to the other copper atom (I). This compound coordinates the azide (II). This is followed by a nucleophilic attack of the terminal nitrogen atom of the azide on the β-carbon atom of the alkine, forming a C-N bond (III). Then the ring formation and protonation follows leading to the 1,2,3-triazole (IV).[155]

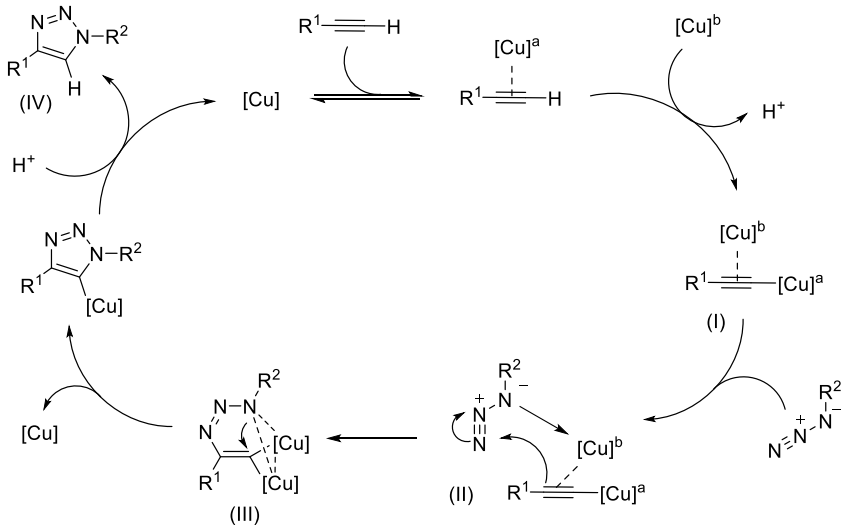

Figure 11: Proposed CuAAC mechanism according to Worrell et al.[155]

A disadvantage of the CuAAC is the fact that the copper has to be fully removed after the synthesis prior to patient application.[156,157] It should also be noted again that the formed triazole could have influence on the pharmacological properties of the tracer.

To avoid the usage of the cytotoxic copper, the strain-promoted-alkyne-azide-cycloaddition (SPAAC) was developed. Here stained alkynes, such as dibenzocyclooctynes are used.[150,158] The usage of such stained alkynes pushes the alkyne into a conformation that favours the cycloaddition due to a degreased activation energy. The triazole is formed without the use of a copper catalyst.[159]

1.5 Squaric acid as conjugation agent

Squaric acid (SA, 3-4-dihydroxycyclobut-3-ene-1,2-dione) is a very interesting and versatile tool in chemistry. Due to its properties, it gained interest in a board field of chemistry and it is used for example in drug development[160], as chelating agent[161] or in organocatalysis[162].

Squaric acid got its name because of its nearly squaric structure and it shows an aromatic character, since it is planar and the Hückel-rule (4n+2 π electrons, n=0) is applicable.[104] Due to this aromaticity, the dianion is highly mesomeric stabilised.[104,163] It is a strong acid with pka values of pk_{a1} = 0.5-1.2 and pk_{a2} = 2.2-3.5.[104]

Squaric acid is also increasingly used as linker molecule in the conjugation chemistry of carbohydrates[104] or polymers[164]. Here, the chemical and physical properties are used for a simple conjugation. Normally, the esters of squaric acid are used as educt and are conjugated with amines.[104] Squaric acid can undergo a pH controlled asymmetric amidation with amines (figure 12). [104,165–167]

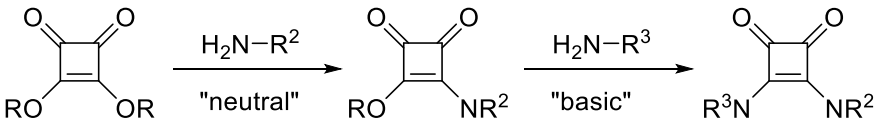

Figure 12: Asymmetric amidation of squaric acid.

First, under neutral pH conditions, the first amidation occurs and a monoamide is formed due to the increase of aromatic stability by addition of the amine. The second amidation can take place, when the pH value is increased. More basic conditions result in a deprotonated form of the monoamide. This deprotonation makes the nucleophilic attack of a second amine on the remaining ester group of the monoamide possible. Finally, a stable square bisamide is formed.[165,167–169] The monoamide can be isolated and stored after the first reaction, which allows the exchange of the amine for the second amidation and therefore the asymmetric amidation.[104,169] Amines are the only functional group that can be used for this type of amidation of squaric esters. This enables a simplified synthesis of conjugates, which only carrying one amine. No dimerization or side reactions with other nucleophilic groups occur and no elaborated protecting group chemistry and harsh deprotection is required as it is the case for many other standard amide formation reactions.[104,125] Thus, also sensitive biomolecules, such as antibodies can be conjugated.[125,165,170] Additionally since amines are often already a part of biomolecules, there is no need for a synthetically introduction.[167]

1.6 Prostate cancer

Cancer is one of the leading causes of death worldwide. While in many developing countries cancer is the second leading cause of death behind cardiovascular diseases, it is the leading cause in most industrialised countries.[171] The incidence and mortality of cancer is increasing worldwide. The reasons are manifold. The rising world population and the ageing society play a role, as well as socio-economic trends.[172] Among cancer, prostate cancer (PCa) is the second most common diagnosed cancer and at number five of cancer related deaths in 2020 worldwide.[172] Although, two third of men who die from prostate cancer are older than 75, in studies of autopsies of persons died of other death causes, in the age group 50 to 59, more than 20% of people with prostate cancer were found.[173]

The abrupt rise of prostate cancer case numbers in the 1990s was due to the introduction of the PSA test. PSA (prostate specific antigen) is an enzyme which is expressed in the prostate and elaborated PSA levels indicate PCa and it is therefore used as tumour marker for PCa.[172] Today, the PSA test is not recommended for symptom free men for early detection since an elaborate PSA level doesn‘t necessarily indicate a pathological disorder of the prostate (false-positive) and the over diagnosis of symptom free prostate cancer often leads to physic and psychic stressful treatment without the cancer

ever becoming clinically significant for the patient. Nevertheless, an early diagnosis leads to a 5-year survival rate of around 98%.[174] The advantages and disadvantages of a PSA test for early diagnosis of prostate cancer must therefore be well weighed.[173,175,176] The classical rectal examination is still a reliable preventive check-up method.[177]

1.6.1 Prostate-specific membrane antigen (PSMA)

The prostate-specific membrane antigen (PSMA) is a zinc dependent glutamate carboxypeptidase II (GCPII) and consists of 750 amino acids with a mass of about 100 kDa.[178,179] The type II membrane glycoprotein is membrane-bound and has a intracellular area with 18 amino acids, a transmembrane area containing the amino acids 19-43 and an extracellular area, which makes up the largest part of PSMA with more than 700 amino acids.[179,180]

Besides the prostate, PSMA expression is also found in some other tissues like kidney, small intestine or the nervous system.[178] Currently, the exact physiological function of PSMA in all the named tissues is not exactly known. There are only two known functions of PSMA as *N*-acetyl-L-aspartyl-L-glutamate peptidase (NAALDase) and folate hydrolase (see figure 13). In each case glutamate is split off from *N*-acetyl-aspartyl-glutamate (NAAG) or folic acid-(poly)-γ-glutamate respectively.[113,178]

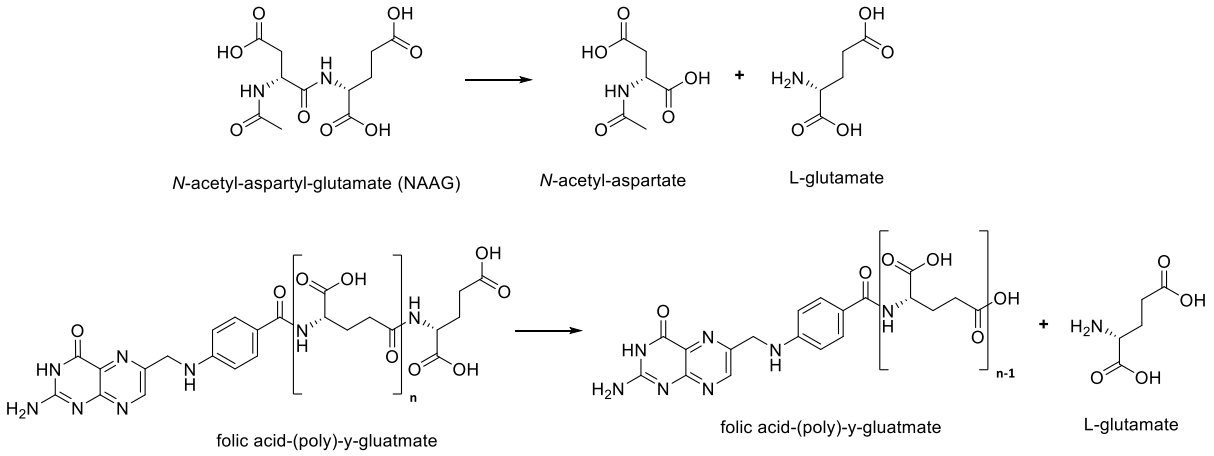

Figure 13: Currently known enzymatic activities of PSMA.

While PSMA is expressed in the healthy prostate only at low degrees, it is highly overexpressed in prostate cancer, reaching 100 to 1000 times of the normal value.[181,182] This can be seen in over 90% of all PCa patients.[183] The reason for this high overexpression in PCa is unknown.[184] The expression degree is also dependent on the stage of the disease and therefore can be used for determination of the severity of the disease as well as for monitoring of the therapy process.[180] The PSMA substrate complex

is internalized into the cell after binding of the substrate. This enables a trapping of the substrate and thus the radiopharmaceutical inside the PCa cell.[181,182,185]

Patients with PCa can develop bone metastases.[186] For patients with late stage PCa the metastasis of bone even affects 90%.[187] The presence of bone metastases has a negative effect on the healing chances. Only 30% of patients with PCa related bone metastases still live after 5 years.[183]

The binding pocket of PSMA with its active centre is well investigated.[188] The extracellular area of PSMA is divided into a protease domain, an apical domain and a C-terminal domain. The binding pocket and the active site are composed of amino acids from all three domains.[189] A schematic overview is shown in figure 14.

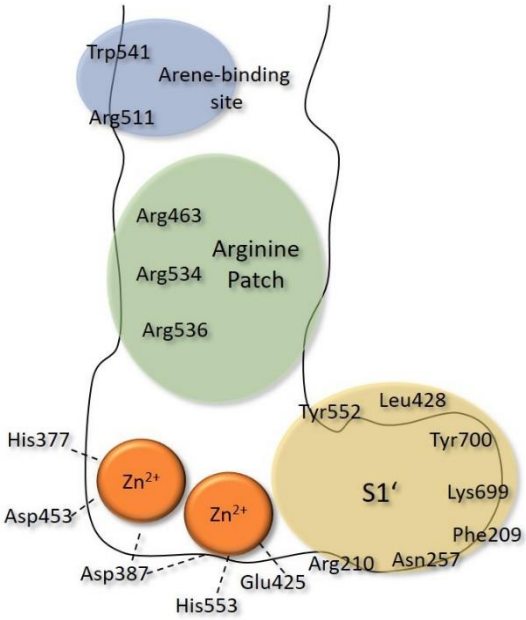

Figure 14: Schematic illustration of the PSMA binding pocket. Figure was designed based on the information of [188-190].

The binding pocket is funnel-shaped with a diameter of 20 Å and a depth of around 20 Å. The pocket generally consists of five areas. The active site is localized at the end of the funnel. The centre of the active site are two zinc ions, which are responsible for the enzymatic activity. Both zinc ions are tetrahedral coordinated by His553 and Glu425 or His377 and Asp453 respectively and bridged by Asp387. If there is no substrate in the binding pocket, then both zinc ions are coordinating a hydroxide anion. Next to the active site, the pharmacophore S1‘ pocket is localized. This pocket has a side of about 8 x 8 x 8 Å and is mainly responsible for the selectivity, specificity and affinity of PSMA towards potential substrates or inhibitors. To address this pocket is crucial for high binding affinities. It has a high affinity towards glutamate and glutamate like structures, which can also be seen in natural substrates. Glutamate structures are bound in this pocket via different ionic interactions as well as

hydrogen bonds. The side chain of Arg210 and the hydroxy groups of Tyr552 and Tyr700, interacting with the α-carboxylate group of glutamate, are worth mentioning. Additionally, the γ-carboxylate group of glutamate forms a hydrogen bond with the amide group Asn257 and a salt bridge with the side chain amine of Lys69. Van der Waals interactions are also important for the glutamate selectivity. Here, the side chains of Phe209 and Leu428 are crucial. The active site and the S1‘ pocket cover about 8 Å of the complete binding pocket. The remaining 12 Å are known as non-pharmacophore site and this area is very variable concerning selectivity and conformation and thus accepts a variety of different structure types of the substrate or an inhibitor. In this area there are two structural characteristics of PSMA, which can increase affinity if these characteristics are addressed by the substrate or inhibitor. The so-called arginine patch is a positive charged area, defined by the side chains of Arg534, Arg536 and Arg463. Thus, substrates or inhibitors with high affinity contain in position P1 negative charges. The entrance funnel of the binding pocket has an open and a closed conformation. While the conformation has no influence on enzyme activity, the open conformation exposes a binding area (Arg463, Arg511 and Trp541) for aromatic units. The aromatic unit can interact with the side chains of Arg511 and Trp541 with π-interactions. Addressing this area increases the affinity significantly.[188–190]

The overexpression of PSMA in PCa cells and the internalisation makes PSMA an interesting target for diagnosis and therapy of PCa. Beside antibodies and their fragments, small molecule inhibitors are possible targeting vectors.[185,191]

Small molecule inhibitors are targeting vectors, which are small compounds with a low molecular mass. Due to the well-known binding pocket, it is possible to adjust the inhibitor structure so that the inhibitor fits perfect into the pocket and obtain a high affinity. Some structural aspects are to be considered due to the described PSMA structure. To receive high affinities, position P1' should be a glutamate group that can interact optimally with the S1' pocket. In order to serve as inhibitor and not as a substrate, the small molecule have to carry a unit that addresses the zinc groups but can’t be split by the enzyme. Negative units such as carboxyl groups and aromatic units of the inhibitor structure located in the area of the entrance funnel can, in the right position, increase the affinity through interactions with the arginine patch or the aromatic binding unit respectively.

The first developed PSMA inhibitors were based on a phosphonate scaffold (figure 15).[192] The phosphonate unit isn’t cleavable by the active site but coordinates the zinc ions. However, they were not developed for the treatment or imaging of PCa, but for the treatment of neurodegenerative diseases, as NAAG is a neurotransmitter in the central nervous system.[192] Among this developed novel PSMA inhibitors, 2-phosponomethyl pentanedioic acid (2-PMPA) is still today one of the most potent PSMA inhibitors and still used *in vivo* and *in vitro* examinations as blocking agent for control

experiments.[185] Additionally, the affinity these compounds already show that even the exchange of glutamate against the structural similar aspartate leads to a decrease of affinity.[192]

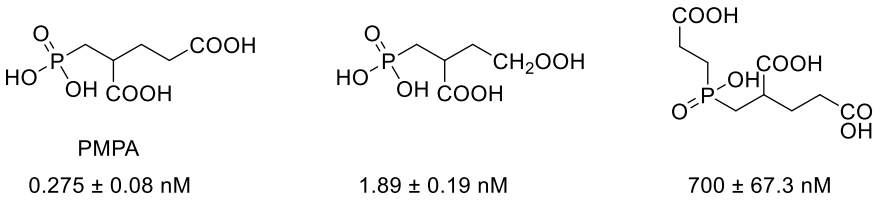

Figure 15: First PSMA inhibitors based on a phosphonate scaffold.[192]

Despite further development of the phosphonate-based inhibitors[193,194] and first clinical studies[195] they no longer have great significance today.[185] Due to the difficult synthesis and handling of this phosphonate-based compounds, Kozikowski et al. replaced the phosphonate against an urea unit. Urea units show the same inhibitory capabilities but the synthesis is easier.[196] The structure activity relationship evaluations of Kozikowski et al showed also that a urea-based inhibitor should carry beside a glutamate group an additional group with carboxyl functionality to increase the affinity.[196] These urea-glutamate based inhibitors have become established nowadays and are most often found in the form of lysine-urea-glutamate (KuE, figure 16A).[185,191,197] While the glutamate terminus remain free for binding the S1‘ pocket, the lysine side chain can be used for further functionalisation, e.g. the conjugation to a chelator. Glutamate-urea-glutamate (EuE, figure 16B) is another common urea-based inhibitor.[185,198,199] It was shown that an additional conjugation of a glutamate carboxyl group of EuE with the amino group of lysine (K-EuE, figure 16C) has a positive influence on e.g. affinity, internalisation and clearance properties. This is due to additional carboxyl group of lysine is modulating the hydrophilicity.[199,200]

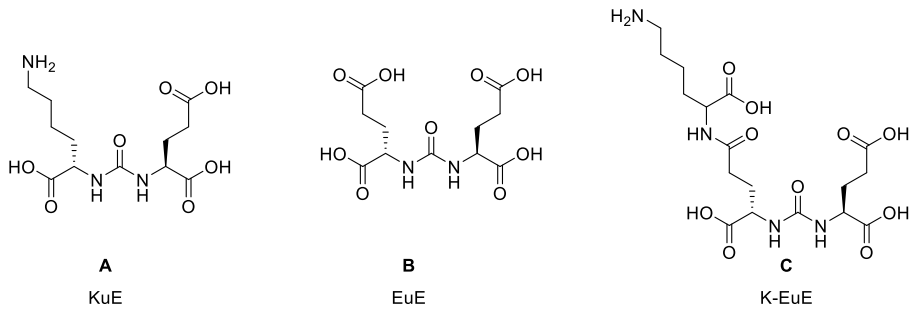

Figure 16: Common urea-based PSMA inhibitors. A: lysine-urea-glutamate; B: glutamate-urea-glutamate; C: lysine-glutamate-urea-glutamate.

Since the introduction of urea-glutamate based inhibitors, a wide variety of PSMA radiopharmaceuticals were developed and tested. Figure 17 shows an overview of some important urea-based PSMA inhibitors.

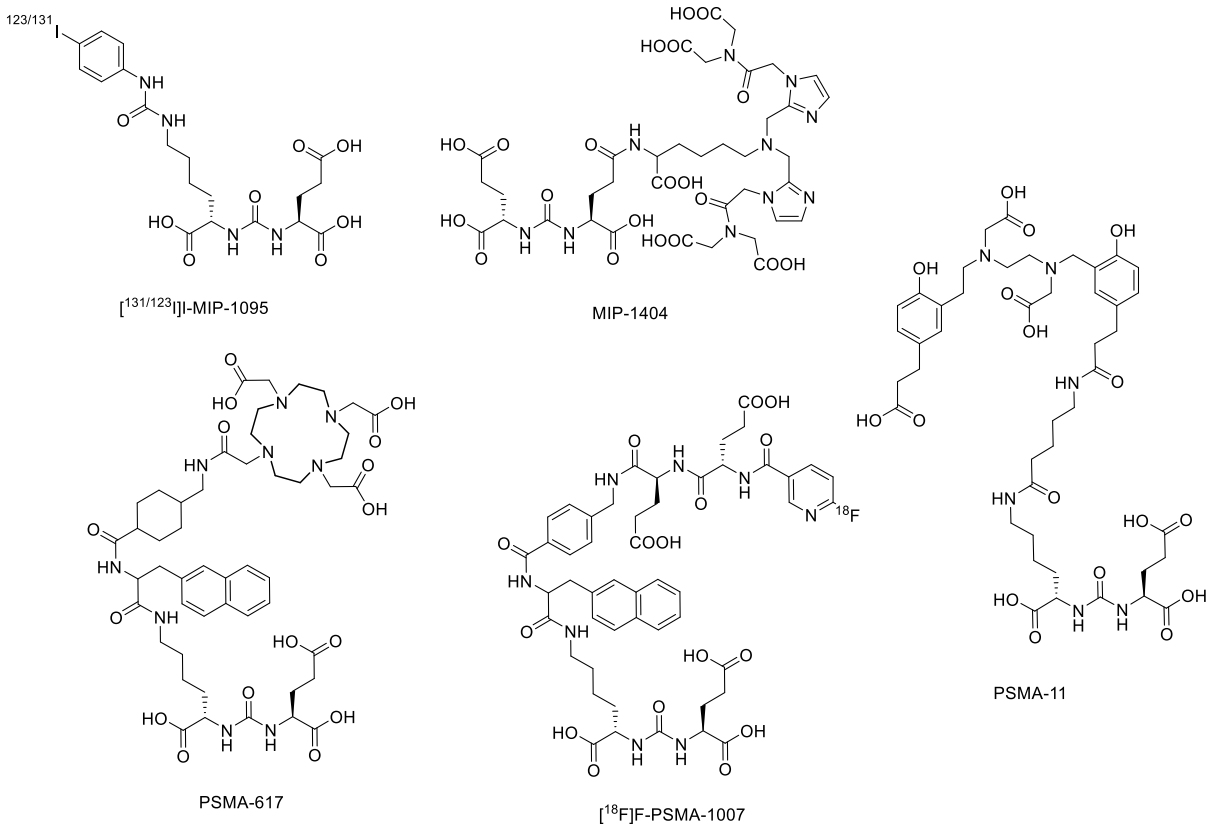

Figure 17: Some common PSMA radiopharmaceuticals.

One of the first urea-based inhibitors in clinical use for imaging of PCa was the iodine-123 labelled KuE derivative MIP-1095. MIP-1095 was also labelled with the therapy nuclide iodine-131 and the first ERT with a urea-based PSMA inhibitor was carried out.[184,201–203] [^{99m}Tc]Tc-MIP-1404 is the first PSMA technetium ligand which is investigated in a phase 3 clinical study.[184,199,204] The most prominent and most used diagnostic PSMA radiopharmaceutical is [^{68}Ga]Ga-PSMA-11.[184,197] Here, KuE is linked via a hexyl linker to the HBED-CC chelator. The HBED-CC chelator contains aromatic units which participate in the ligand-enzyme interaction and thus increase the affinity. [^{68}Ga]Ga-PSMA-11 shows a fast pharmacokinetic and a very good tumour-to-background ratio.[115,184,205,206] A number of clinical studies prove the great benefit of [^{68}Ga]Ga-PSMA-11.[207–210] In 2020, [^{68}Ga]Ga-PSMA-11 was officially approved by the FDA.[211] The most prominent PSMA ligand in terms of therapeutic approaches PSMA-617. The KuE unit is linked to the chelator DOTA and the linking unit is optimally adjusted to the binding pocket with regard to pharmacokinetic properties. Thus, for example, the linker contains a naphthyl unit for binding to the aromatic unit of PSMA.[197,212,213] The [^{177}Lu]Lu-PSMA-617 therapy of PCa and especially the therapy of its final stage the metastatic castration-resistant prostate cancer was also investigated in several studies.[214] A phase 3 clinical trial, the so-called VISION study, was finished mid-2021 and recommends the approval as standard care for patients with advanced PSMA-positive metastatic castration-resistant prostate cancer, due to a prolonged progression-free survival of patients.[120]

Besides the application of PSMA-167 with the β^--emitter lutetium-177, applications with the α-emitter actinium-225 are also known.[215,216] Based on the structure of PSMA-617, PSMA-1007 was developed. PSMA-1007 is a potent PSMA inhibitor for labelling with fluorine-18 and provides a cyclotron-based alternative to the generator-based [^{68}Ga]Ga-PSMA-11.[217,218]

1.7 Bisphosphonates

Diseases such as osteoporosis, bone metastases or Paget's disease are associated with an increased bone degradation through an enhanced osteoclast activity.[219,220] For more than 40 years, bisphosphonates are used as therapeutic agent for such illnesses. The usage of bisphosphonates is based on two properties of the bisphosphonates. First, bisphosphonates show a high affinity towards hydroxyapatite (HAP), the main component of the inorganic bone matrix and second, bisphosphonates show an inhibitory effect towards osteoclast activity.[219]

Structurally, bisphosphonates are derivatives of pyrophosphate, in which both phosphate groups are connected via a carbon atom.[221] Figure 18 shows the general structure of bisphosphonates.

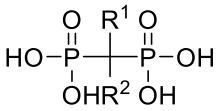

Figure 18: Basic structure of bisphosphonates.

The human bone consists to 9% of water, to 22% of an organic matrix and to 69% of an inorganic mineral matrix.[222] The inorganic matrix again consists mainly of calcium and phosphate ions which forms the crystalline structure hydroxyapatite (HAP, $Ca_{10}(PO_4)_6(OH_2)_2$) are responsible for the stability of the bone along with collagen.[223] Because of the deprotonated oxygen atoms of the phosphate groups bisphosphonates are able to coordinate calcium ions bidental. This coordination is responsible for the high affinity towards hydroxyapatite.[219] While the phosphate groups are indispensable for HAP binding, the rests R^1 and R^2 are variable. However, it should be noted that even small modifications of the rest groups can have a significant influence on the chemical, biological and therapeutic properties.[221] Today, most of the common used bisphosphonates contain a hydroxyl group in the position of R^2 because it was shown that achieve a tridental complexation of the calcium ions leading to a better HAP affinity in contrast to bisphosphonates without a hydroxyl group.[219,224] R^1 can be used for a further functionalisation. This led to a development of a variety of different bisphosphonates in the last decades. It was also shown that if the bisphosphonate carries a nitrogen or an amine in the rest R^1 the antiresorptive effect and the inhibition of osteoclasts are increased by a factor of 10 to 10.000.[220] These results are the consequence of years of research and continuous development. While

bisphosphonates of the first generation contain no nitrogen and, in some cases, not even a hydroxyl group, bisphosphonates of the second and third generation contain at least one nitrogen. The second generation in combination with an alkyl chain and the third generation contains a nitrogen containing ring system.[220,225] Examples of all three generations are shown in figure 19.

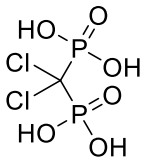

clodronate (1. generation)

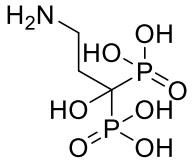

pamidronate (2. generation)

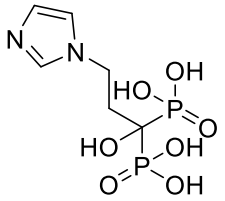

zoledronate (3. generation)

Figure 19: Bisphosphonates of the three generations.

The structural analogy of the bisphosphonates towards pyrophosphate is also the reason for the antiresorptive effect.[226] The significant better inhibition of osteoclasts of nitrogen-containing bisphosphonates is due to different mechanisms of action of both types of bisphosphonates. After a bisphosphonate is bound to HAP, it is dissolved in the acidic surrounding of the osteoclast and is endocytosed. The further influence of the bisphosphonate now depends on the type of bisphosphonate. Bisphosphonates without nitrogen are build inside adenosine triphosphate (ATP), the energy supplier of a cell, due to its similarities with pyrophosphate. Since the P-C-P bond of the bisphosphonates is, in contrast to the P-O-P bound of pyrophosphates, not cleavable through cellular mechanisms, apoptosis is initiated. Nitrogen containing bisphosphonates inhibit the farnesyl pyrophosphate synthase (FFPS) leading to the stop of the mevalonate pathway. This has impacts on the construction of the cytoskeleton, like the break of action rings or influence of the vesicular transport inside the osteoclast. Further complex biochemical mechanisms lead to the apoptosis of the osteoclast.[220,224,226]

Bisphosphonates are not only established in the conventional therapy, but also interesting in the field of nuclear medicine as targeting vector for therapeutic and diagnostic approaches. Bisphosphonates can be used for diagnosis and therapy of bone metastases. Due to the increased metabolic activity, bone metastases lead to an enhanced bone remodelling which is accompanied with an increased uncover of HAP to which bisphosphonates bind more than to healthy bone tissue.[227]

First bisphosphonates used in nuclear medicine were simple bisphosphonates which complex a radionuclide but also offered enough free binding sites for complexation of calcium containing HAP.[219] In SPECT technetium-99m labelled compounds such as [^{99m}Tc]Tc-MDP ([^{99m}Tc]Tc-methylenediphosphonate) and [^{99m}Tc]Tc-HMDP ([^{99m}Tc]Tc-hydroxymethylenediphosphonate) are used (figure 20).[219,228] Radiopharmaceuticals such as [^{153}Sm]Sm-EDTMP ([^{153}Sm]Sm-

ethylenediaminetetramethylene phosphonic acid), are leading to a reduction of pain of 62-84% in patients with bone metastasis are known for therapy.[228,229]

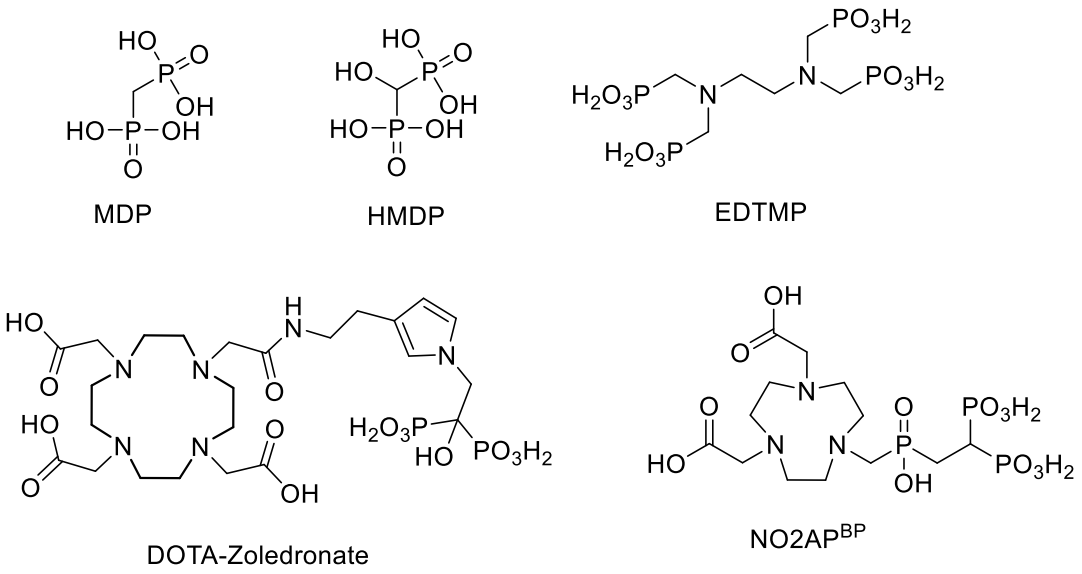

Figure 20: bisphosphonates for use in nuclear medicine.

A further development of these bisphosphonate tracers are bisphosphonates functionalized with a chelator. In these cases, all functional groups of the bisphosphonate remains free for HAP coordination, increasing the affinity.[230] Examples for such bisphosphonates are NO2AP^{BP} and DOTA-Zoledronate (Figure 20). While DOTA-Zoledronate contains a DOTA chelator and can be used for diagnosis as well as therapy, NO2AP^{BP} carries a NOTA chelator for gallium-68 labelling.[231–233]

1.8 Small molecule drug conjugates

Small molecule drug conjugates (SMDC) are understood to be molecules which consists of a therapeutic unit, e.g. a cytostatic drug, a cleavable linking unit and a small molecule as targeting vector. The aim is to transport the non-selective cytostatic drug with the help of a tumour specific targeting vector to the desired enrichment site, where it is released by the linker which is cleavable under special conditions. The affinity of the targeting vector leads to a highly selective accumulation in the target tissue and is accumulated much less in healthy tissue.[234,235] This means that the cytostatic drug no longer has to be applied systematically, which can reduce side effects.[236]

SMDCs are a further development of antibody drug conjugates (ADC).[237] In contrast to ADCs, the usage of small molecules as target vectors have some advantages. They are cheaper and can be produced with a higher efficiency, show no immunological side effects and show better pharmacokinetic properties.[237,238]

About one of three clinical used ADCs containing the cytostatic drug monomethyl auristatin E (MMAE).[239] The cytotoxic effect of MMAE is based on the inhibition of the tubulin depolymerisation and shows an average IC_{50} value of 3.2 ± 0.51 nM. This is 10 to 100 times more potent than doxorubicin (average IC_{50} value of 631 nM) in average.[240,241] Beside ADC-based MMAE conjugates, some SMDC-based MMAE conjugates are also known. MMAE is linked to the targeting system via the enzymatically cleavable linker valine-citrulline in many of this conjugates.[242] One example of such a conjugate is the der ADC Brentuximab vedotin (figure 21). Here, MMAE is linked to a CD-30 antibody using the dipeptide valine-citrulline, a *p*-amino benzyloxycarbonyl (PABC) spacer and a maleimidecaproyl structure. This ADC is approved for the therapy of CD30-expressing peripheral T-cell lymphomas since 2018.[243–245]

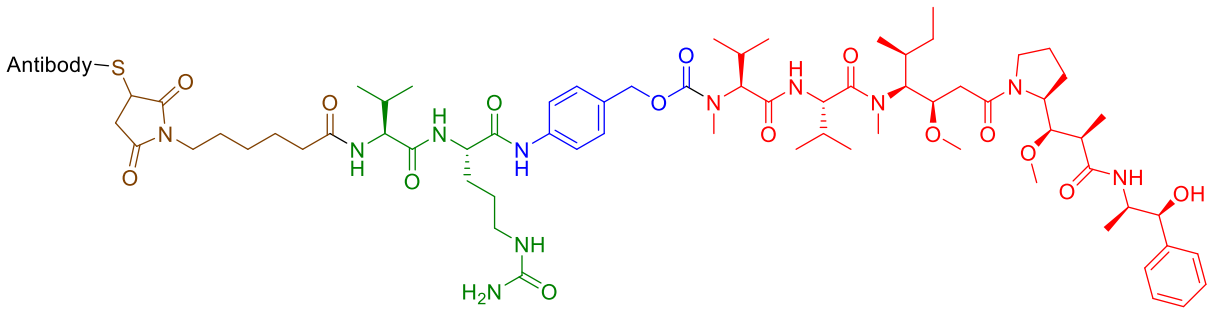

Figure 21: Sturcture of the MMAE-based and valine-citrulline linked ADC Brentuximab-Vedotin. Black: Antibody; brown: maleimidocaproyl spacer; green: valine-citrulline linker; *p*-amino benzyloxycarbonyl (PABC) spacer; red: MMAE.

Once the conjugate is bound to the target, it is internalized via clathrin-mediated endocytosis. In the cell it is incorporated into a lysosomal vesicle in that a high concentration of proteolytic enzymes are found. One of these enzymes is cathepsin B that recognise valine-citrulline as substrate and cleaves the amide bounding between the citrulline unit and the PABC spacer. The terminal PABC is not stable under these conditions and a 1,6-elimination takes place, which releases, beside PABC degradation products, the free MMAE. This can now unfold its cytotoxic effect in the cell.[242,246]

Besides enzymatically cleavable linkers such as valine-citrulline, there are other classes of cleavable linkers. Acid-labile linker, like hydrazones are hydrolysed in the acidic environment of endosomes and lysosomes while they are stable in the pH neutral blood. Disulfid linker are stable in the blood under physiological conditions, but they are reduced and cleaved by glutathione (GSH) in the cytoplasm.[247,248]

1.9 Liposomes

Liposomes represent a different kind of drug delivery system. The first liposome was approved as drug delivery system in 1995 by the FDA.[249] Liposomes are modelled on the cell membrane of natural cells and consist mainly of phospholipids.[250] Phospholipids are amphiphilic structures with a hydrophilic head and a hydrophobic tail and glycerol as scaffold. Two of the hydroxyl groups of the glycerol are functionalized with fatty acids and form the hydrophobic tail area. The fatty acids vary in length and number of unsaturated bonds. The third hydroxyl group of glycerol is functionalized with a phosphate group. This in turn can be connected to various terminal head groups, depending on the type of phospholipid. A lot of different head groups are known, including amines, such as choline, alcohols like glycerol or amino acids like serine.[251] Because of the amphiphilic character, phospholipids form a lipid bilayer in aqueous solutions which then in turn create a spherical vesicle, the liposome (figure 22). The bilayer encloses an aqueous area. Here, the phospholipids align themselves so that the hydrophobic tails form the inner part of the bilayer and the hydrophilic head groups are directed outwards towards the aqueous environment and the aqueous core. The size of a liposome can vary from 30 nm up to micrometres.[250,252] Liposomes are suitable as transport system of different classes of drugs. Hydrophobic agents can be integrated inside the bilayer, while hydrophilic agents and other classes such as DNA or proteins can be transported inside the aqueous area.[252,253]

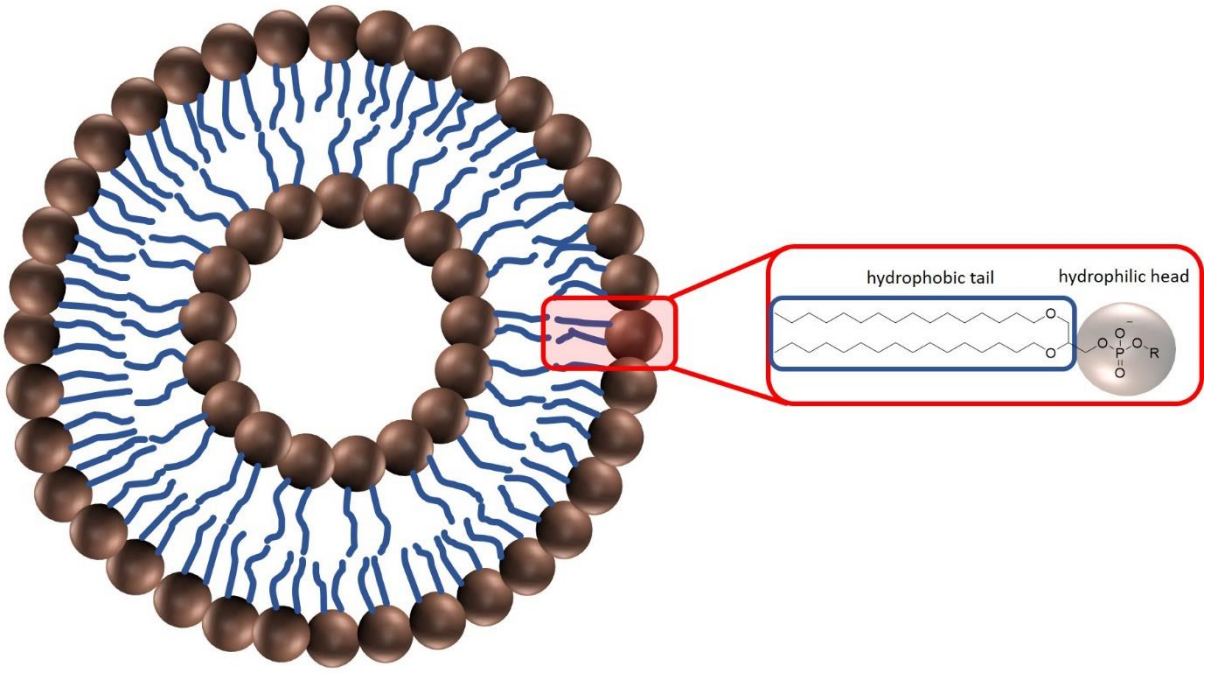

Figure 22: Basic structure of a liposome.

Some important parameters that have to be considered during liposome composition are the size, permeability, stability and charge. The size has a great influence on the pharmacokinetics and the

uptake in excretory organs. Liposomes with a size bigger than 5.5 nm are not taken up by the kidneys leading to an increased blood circulation. Liposomes with sizes between 50 and 100 nm are taken up by the liver.[254]

The permeability of liposomes is determined by the so-called transition temperature of phospholipids (T_C) and is dependent on the length and saturation of the fatty acids and the head group. If the surrounding temperature is lower than the transition temperature the liposome is stated in the so-called gel phase. In this phase the permeability and fluidity are low. If the temperature is higher than the die T_C, the liposome is stated in a fluid state with a high permeability, which can lead to a loss of the loaded drug. Thus, the transition temperature of liposomes for *in vivo* application should be above body temperature, so that no therapeutic payload is lost bevor internalisation.[255,256]

Liposomes show a natural flip-flop effect, which can causes unwanted loss of payload. The introduction of cholesterol into the membrane is stabilising the liposomes. It is important to use a defined definition, because cholesterol is stabilising the liposomes, but also has an influence on the size.[256]

Regarding the time of blood circulation to additional factors have to be considered. Classical liposomes interact and adsorb blood circulating proteins leading to an increased excretion.[249] Liposomes consists of natural occurring phospholipids and thus are biodegradable and non-toxic.[250,256] Nevertheless, liposomes are recognised by the so-called mononuclear phagocyte system (MPS). This leads to an fast excretion via liver and spleen.[257] Polyethylene glycol (PEG) chains or other hydrophilic polymer chains which are integrated to the outer sphere of liposome structure, reduce this interactions and increase the blood circulation time.[249] For a further functionalisation of the liposome, for example with a target vector, a lot of different further shielding units with additional linking able functionalities with increased circulation times are developed.[258] One example are hyperbranched polymers. These are often hyperbranched polyglycerols (hbPG).[259,260]

2. Objectives

Since several years, novel urea-based PSMA inhibitors gain great interest in nuclear medicine and oncology. Radioactive labelled PSMA ligands, such as [^{68}Ga]Ga-PSMA-11 or [^{177}Lu]Lu-PSMA-617, lead to an improvement in diagnosis and therapy of prostate cancer and can thus lead to an improved medical care of patients with prostate cancer.[261]

There are some PSMA ligands which are already approved or are recommended to be approved.[120,211] Such compounds, like PSMA-617 or PSMA-11 already show good results in clinical routine, but still displays some disadvantages. One example is PSMA-617 which is recommended by a multicentre study for routine application for treatment of patients with late stage prostate cancer and recommended for FDA approval[120], but nevertheless, besides the desired tumour uptake, it also shows undesired increased uptake in other tissues like the salivary glands.[262] This side effect leads to an unwanted irradiation and destruction of these tissues.[262] Additionally, there are other unsolved challenges, which cannot be solved by the actual existing compounds or research. Some of these challenges are addressed in this dissertation. For example, the development of suitable drug delivery systems for a targeted delivery of cytotoxic drugs to the prostate cancer cell or the therapy of bone metastases, which can be difficult to treat with the known PSMA ligands due to a heterogeneous PSMA expression. Here, for all of these problems, no suitable systems or applications could be established in the past. Further developments and new combinations of different approaches could lead to an increased medical care of prostate cancer patients.

The present work focuses on the development, improvement and novel applications of urea-glutamate-based PSMA inhibitors for the diagnosis and therapy of prostate cancer to improve the care of patients with prostate cancer. One major part deals with the use of the squaric acid conjugated PSMA inhibitor KuE (SA.KuE). The use of SA.KuE as linking unit was introduced by Nils Engelbogen in his dissertation[263] and further developed by Lukas Greifenstein.[121,264,265] In this work, the use of SA.KuE is further developed and evaluated.

This work is divided into four main sections addressing different aspects of the project. In each subproject of this dissertation, a different aspect of the optimisation or new development of PSMA radiopharmaceuticals is discussed. These problems are addressed in form of publications and manuscripts. They should contribute to solve the still open problems and issues in the field of PSMA imaging and PSMA-based therapy as discussed above. An overview of the main projects is shown in figure 23. The objectives of the individual projects are described below.

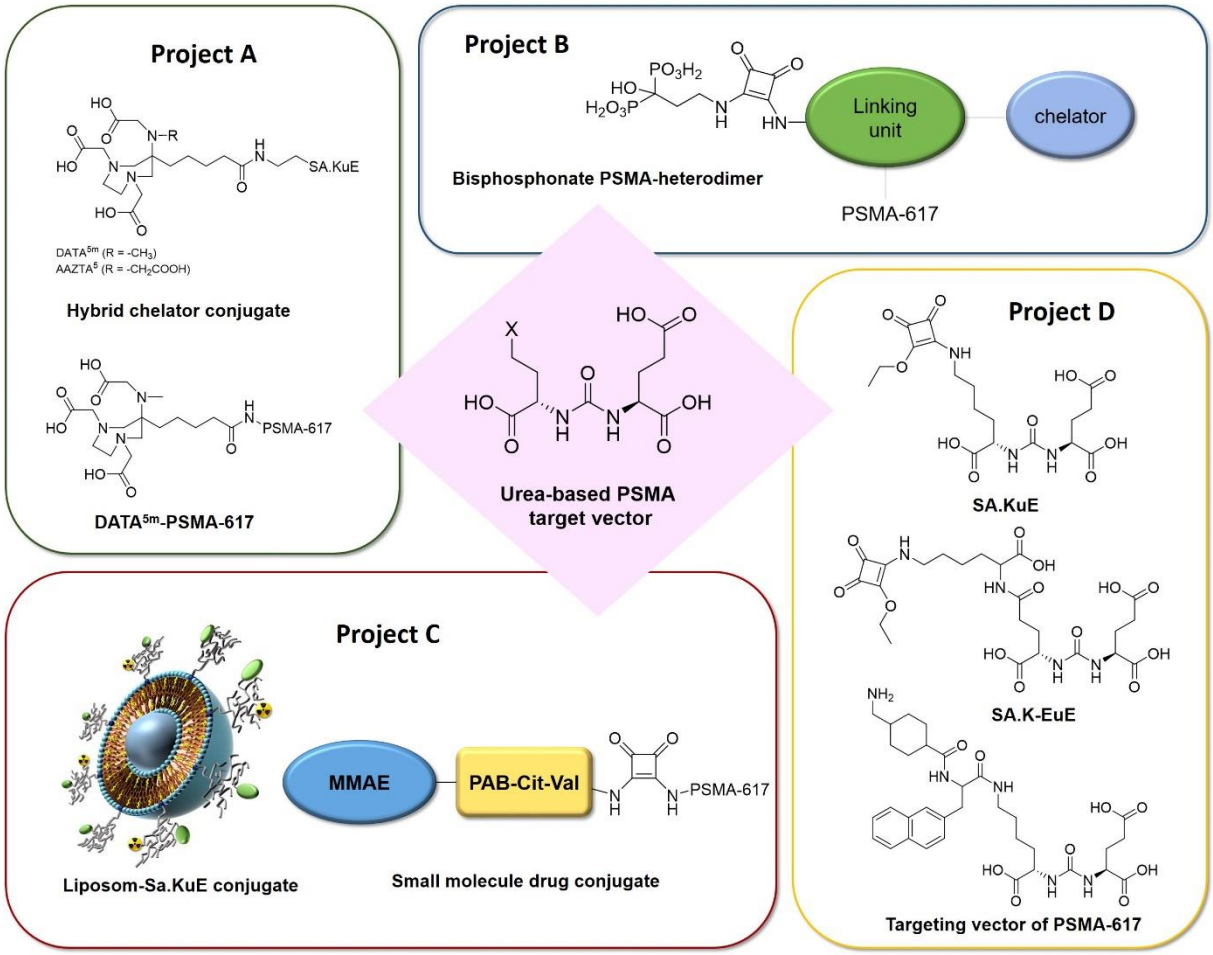

Figure 23: Graphic overview of the four main projects.

2.1 Project A: Hybrid chelator conjugated PSMA inhibitors

The first project is about the synthesis and evaluation of hybrid chelator conjugated PSMA inhibitors. Hybrid chelators are chelators that combine structure elements of acyclic as well as macrocyclic chelators and thus combine the advantages of both types. Thus, hybrid chelators can be labelled with radionuclides fast and under mild conditions and show high complex stabilities. These properties of the hybrid chelators enable a kit-type approach, as it is common with ^{99m}Tc-radiopharmaceuticals[266] and thus enable an easier clinical routine.

In the first publication *Hybrid chelator-based PSMA-radiopharmaceuticals: translational approach* belonging to this project, the hybridic chelator DATA^{5m} is conjugated via a squaramide (SA) linker unit to the PSMA inhibitor KuE (lysine-urea-glutamate). This enables a kit-like labelling approach of a PSMA radiopharmaceutical. In a previous work, this inhibitor moiety was already linked to macroyclic chelators, such as DOTAGA or NODAGA, via squaric acid and the resulting compound DOTAGA.SA.KuE

was already evaluated *in vitro* and *in vivo*. In that study the compound was comparable to the clinical relevant compounds PSMA-11 und PSMA-617.[121]

The conjugation of the chelator unit and the inhibition moiety via squaric acid is carried out in an asymmetric amidation reaction. An additional aim of this study is to show that this type of synthesis is faster and easier than the elaborated resin-based synthesis of PSMA-617, yielding a compound with comparable *in vitro* and *in vivo* potential.

After the synthesis of DATA^{5m}.SA.KuE, the radiolabelling properties with gallium-68 and the *in vitro* and *in vivo* behaviour are evaluated. Due to the structure of DATA^{5m} it can only be labelled with the diagnostic radionuclide gallium-68.

Along with DATA^{5m}.SA.KuE, AAZTA^{5}.SA.KuE is also evaluated *in vitro* and *in vivo*. AAZTA^{5} is also a hybrid chelator that can be labelled with diagnostic radionuclides, such as scandium-44, and therapeutic nuclides, such as lutetium-177 and thus can be used in theranostic approaches. The synthesis and radiochemical evaluation of AAZTA^{5}.SA.KuE with scandium-44 and lutetium-177 was already carried out in a previous work.[265]

For the *in vitro* evaluation of both compounds, the binding affinities were determined in a competitive binding assay and the internalisation ratios were determined in PSMA-positive LNCaP cells and compared with [^{68}Ga]Ga-PSMA-11. The tumour accumulation and the general organ distribution were determined in PSMA-positive LNCaP tumour carrying Balb/c nude mice and compared with [^{68}Ga]Ga-PSMA-11.

[^{177}Lu]Lu-PSMA-617 contains the macrocyclic chelator DOTA and is the most prominent representative of therapeutic used PSMA inhibitors. For previous diagnosis, dose calculations and therapy progress monitoring it is normally combined with the diagnostic PSMA radiopharmaceutical [^{68}Ga]Ga-PSMA-11, which, however, has a different linker structure than PSMA-617. In the second manuscript of this project, *[^{68}Ga]Ga-DATA^{5m}-PSMA-617 as novel diagnostic kit-based counterpart for [^{177}Lu]Lu-PSMA-617,* a DATA^{5m} chelator should replace the DOTA chelator of PSMA-617. With [^{68}Ga]Ga-DATA^{5m}-PSMA-617 a compound as diagnostic counterpart to [^{177}Lu]Lu-PSMA-617 is presented that should keep the same pharmacokinetic properties by using the same linking unit. The synthesized DATA^{5m}-PSMA-617 is evaluated regarding radiolabelling properties with gallium-68, lipophilicity and *in vitro* binding affinity. Evaluation of the *in vivo* pharmacokinetic properties are planned and are currently being conducted. It is compared with [^{68}Ga]Ga-PSMA-617. The results of radiolabelling and binding affinity are compared to a previous study of J-P. Sinnes[267].

2.2 Project B: Prostate cancer and related bone metastases

90% of all men with prostate cancer in a late stage will develop PCa related bone metastases.[268] Bone metastases reduce the live quality and are a negative indicator for the survival chances of the patient.[269] Although these bone metastases are caused by prostate cancer, it is possible that they lose PSMA expression during the progression of the disease.[186] This complicates the treatment of the metastases with the common PSMA radiopharmaceuticals, such as [^{177}Lu]Lu-PSMA-617. Because of the high affinity towards the inorganic bone material HAP, bisphosphonates were established as targeting vector for pathologic changes of the bone with increased bone metabolism, as they can be found at bone metastases.[219]

The aim of this project (manuscript named *DOTA conjugate of bisphosphonate and PSMA-inhibitor: A promising combination for therapy of prostate cancer related bone metastases)* is to develop a compound that carries both, a PSMA inhibitor as well as a bisphosphonate target vector, combining the advantages of PSMA targeting and bone targeting for therapy of primary tumours and especially therapy of PSMA expression heterogeneous PCa related bone metastases. Radiolabelling with lutetium-177 can be carried out using the additionally containing chelator DOTA. The HAP binding potential, as well as the *in vitro* PSMA binding affinity are to be tested. This should be followed by an *ex vivo* biodistribution study with LNCaP tumour-bearing Balb/c mice. In this study, the tumour and bone accumulation should be evaluated.

2.3 Project C: PSMA inhibitor conjugated drug delivery systems

An important concept in oncology is the transport of drugs with so-called drug delivery systems. This principle shifts away from the systemic application of drugs to the targeted transport to the place where they are supposed to show the effect.[234] This enables the application of higher doses, reduces side effects due to the decreased accumulation in healthy tissue and can bypass bad bioavailability of some drugs.[236,270]

In project C, the development of two different PSMA inhibitor-based drug delivery systems for the targeted transport of drugs to the prostate cancer is presented. One method to transport a drug can be the inclusion of the drug into liposomes. Liposomes are stable in the blood system and are only opened in the tumour cell, where the drug is then released. In this work (manuscript with the name *^{18}F-labeled, PSMA-specific liposomes: promising and PET-traceable tool for future targeted drug delivery in the treatment of prostate cancer*), hyperbranched polyglycerols with hydrophobic alkyl chain anchors (BisHD-*hb*PG), functionalised via a copper(I)-catalysed huisgen 1,3-dipolar cycloaddition with the azide functionalized PSMA inhibitor SA.KuE (EuK.SA.Azide) are presented. Additionally, a

functionalisation and radiolabelling with [^{18}F]F-TEG-Azide is carried out. After both functionalisation steps, the liposome should be formed with cholesterol and DOPC. To obtain liposomes with a defined size, they are separated via an extrusions process and the liposomes with one defined size are collected. Thus, liposomes are synthesized which are transported direct to the prostate cancer cell via the PSMA targeting vector KuE where the drug, e.g. a cytostatic drug, is released and can affect the cancer cell. Fluorine-18 labelling can be used to evaluate the *in vivo* behaviour in PET measurements. The use of the hyperbranched polyglycerols is to shield the liposome and increase the resistance to the mononuclear phagocyte system, leading to an increased blood circulation time. The radiolabelling of the PSMA inhibitor containing BisHD-*hb*PG polymers and the followed-up liposome formation should be compared with the radiolabelling and liposome formation of the PSMA inhibitor free BisHD-*hb*PG polymers.

The second manuscript (*old drug, new delivery strategy: MMAE repacked*) of this project describes the development of a small molecule drug delivery system. Here, the cytotoxic drug MMAE, which is too potent for the systematic application, should be conjugated via a cleavable linker to the targeting structure of PSMA-617. For conjugation the simplified synthesis of squaric acid conjugation chemistry should be used. Several types of cancer, including prostate cancer, show a high expression of the lysosomal protease cathepsin B, a valine-citrulline unit is used as cleavable linker, since it is a substrate of cathepsin B. Thus, a SMDC conjugate should be developed, in which the drug MMAE can be delivered in a targeted transport via the PSMA-617 targeting unit to the prostate cancer cell. Here, it will be internalised and MMAE will be released through the lysosomal cathepsin B mediated cleavage of the valine-citrulline linker. After the successful synthesis of the compound, the *in vitro* PSMA binding affinity as well as the *in vitro* cytotoxicity will be determined. The potential of the cleavable linker is evaluated in an enzyme-based cleavage assay. The toxicity should be further determined in healthy NOD-SCID mice and the therapeutic effect should be evaluated PSMA-positive LNCaP tumour-bearing NOD-SCID mice.

2.4 Project D: PSMA inhibitor structure optimisation

The most used urea-based PSMA inhibitor is KuE. Some studies indicating that the use of K-EuE instead of KuE leads to an improvement of the PSMA radiopharmaceuticals, for example regarding higher PSMA binding affinity or tumour-to-organ ratios.[199,200]

In this project and in the manuscript c*omparison of the binding affinity of squaramide containing lysine-urea-glutamate- and glutamate-urea-glutamate-based PSMA inhibitors*, different KuE and K-EuE-based PSMA inhibitors should be synthesized. The conjugation of the inhibitor structures to the

chelator moiety is performed by squaric acid-based conjugation, since the introduced squaramide should act as aromatic unit and should increase the affinity. Three different chelators should be used for functionalisation. The two hybrid chelators $DATA^{5m}$ and $AAZTA^{5}$ are supposed to be investigated as well as the DOTA derivative DO2AGA, which has in one position an amine group instead of a carboxyl group, allowing further functionalisation via sqauric acid. For comparison with a common and frequently used reference compound, the DOTA chelator of PSMA-617 should be replaced by the three chelators and these compounds should be investigated. The *in vitro* binding affinity is determined in a competitive radioligand binding assay and the binding affinities of each compound were compared among each other and compared to the targeting units without a chelator to determine the binding potential of each targeting unit as well as the influence of the chelator towards affinity.

2.5 Author contribution to the research project

This dissertation and research project consist of different publications and manuscripts to which different authors have contributed. The author of this dissertation, Tilmann Grus, carried out literature research of already literature known PSMA radiopharmaceuticals and their potency and usability. He identified possibilities and concepts to optimise the existing literature-known compounds and he also investigated concepts to overcome the still existing and literature-known problems in this research field as discussed above. Tilmann Grus designed compounds to realise these concepts and developed suitable organic chemical synthesis routes and carried out these syntheses. Accordingly, the author of this dissertation synthesized and worked on many more compounds in the organic chemical laboratory, than discussed in this work, since some are not synthetically accessible and some didn't show suitable properties in follow-up studies. Furthermore, T. Grus was main responsible for all in this work described radiochemical studies. He designed, planned, and carried out the radiochemical evaluations and the followed data analysis and interpretation.

He was involved in the design of the *in vivo* and *ex vivo* animal studies and was also involved in some of those, in which he assisted in. Tilmann Grus also carried out the interpretation of the final results of the experiments and wrote the manuscripts.

The contribution of T. Grus to the individual publications and manuscripts varies and some of the above mentioned contributions were done in some publications or manuscripts in close collaboration with other authors. A detailed contribution description to each publication and manuscript can be found in front of the corresponding publication or manuscript.

3. References

(1) White, M. C.; Holman, D. M.; Boehm, J. E.; Peipins, L. A.; Grossmann, M.; Henley, S. J. Age and Caner Risk: A Potentially Modifiable Relationship. *Am J Prev Med* **2014**, *46* (3 Suppl 1), S7-15.

(2) Siegel, R. L.; Miller, K. D.; Fuchs, H. E.; Jemal, A. Cancer Statistics, 2021. *CA. Cancer J. Clin.* **2021**, *71* (1), 7–33.

(3) Jönsson, B.-A. Henri Becquerel's Discovery of Radioactivity - 125 Years Later. *Phys. Medica* **2021**, *87*, 144–146.

(4) Donya, M.; Radford, M.; ElGuindy, A.; Firmin, D.; Yacoub, M. H. Radiation in Medicine: Origins, Risks and Aspirations. *Glob. Cardiol. Sci. Pract.* **2014**, *2014* (4), 437-348.

(5) Budinger, T. F.; Jones, T. 1.01 History of Nuclear Medicine and Molecular Imaging. In *Comprehensive Biomedical Physics, Volume 1: Nuclear Medicine and Molecular Imaging,* 1st Edition*;* Budinger, T. F., Brahme, A., Eds.; Elsevier B.V.: Amsterdam, Oxford, Waltham, 2014; Vol. 1, pp. 1-37.

(6) Stöcklin, G.; Qaim, S. M.; Rösch, F. The Impact of Radioactivity on Medicine. *Radiochim. Acta* **1995**, *70–71* (Supplement), 249–272.

(7) Hacker, M.; Beyer, T.; Baum, R. P.; Kalemis, A.; Lammertsma, A. A.; Lewington, V.; Talbot, J. N.; Verzijlbergen, F. Nuclear Medicine Innovations Help (Drive) Healthcare (Benefits). *Eur. J. Nucl. Med. Mol. Imaging* **2015**, *42* (2), 173–175.

(8) Hellwig, D.; Marienhagen, J.; Menhart, K.; Grosse, J. Nuklearmedizin in Deutschland. *Nuklearmedizin.* **2017**, *56* (2), 55–68.

(9) Rahmim, A.; Zaidi, H. PET versus SPECT: Strengths, Limitations and Challenges. *Nucl. Med. Commun.* **2008**, *29* (3), 193–207.

(10) Phelps, M. E. Positron Emission Tomography Provides Molecular Imaging of Biological Processes. *Proc. Natl. Acad. Sci. U. S. A.* **2000**, *97* (16), 9226–9233.

(11) Niese, S. George de Hevesy (1885-1966), Founder of Radioanalytical Chemistry. *Czech. J. Phys.* **2006**, *56* (SUPPL. 4), D3–D11.

(12) Kotzerke, J.; Oehme, L.; Grosse, J.; Hellwig, D.; Arbeitsausschuss PET der DGN. Positronenemissionstomographie 2013 in Deutschland. *Nuklearmedizin* **2015**, *54* (02), 53–59.

(13) Rösch, F. *Nuclear - and Radiochemistry. Volume 1: Introduction,* 1st Edition; De Gruyter Graduate: Berlin, Boston; 2014.

(14) Ganguly, B. N.; Mondal, N. N.; Nandy, M.; Roesch, F. Some Physical Aspects of Positron Annihilation Tomography: A Critical Review. *J. Radioanal. Nucl. Chem.* **2009**, *279* (2), 685–698.

(15) Ache, H. J. Chemistry of the Positron and of Positronium. *Angew. Chemie Int. Ed. English* **1972**, *11* (3), 179–199.

(16) Tao, S. J. The Formation of Positronium in Molecular Substances. *Appl. Phys.* **1976**, *10 (1)*, 67–79.

(17) Berko, S.; Pendleton, H. N. Positronium. *Ann. Rev. Nucl. Part. Sci.* **1980**, *30*, 543–581.

(18) Brandt, W.; Berko, S.; Walker, W. W. Positronium Decay in Molecular Substances. *Phys. Rev.* **1960**, *120* (4), 1289–1295.

(19) Fahey, F. H. Positron Emission Instrumentation. *Radiol. Clin. North Am.* **2001**, *39* (5), 919–929.

(20) Beyer, T. Physik/Technik. In *PET/CT-Atlas,* 2nd Edition; Mohnike, W., Hör, G., Schelbert, H., Eds.; Springer-Verlag Berlin Heidelberg New York: Berlin Heidelberg, 2011; pp 7–34.

(21) Piel, M.; Vernaleken, I.; Rösch, F. Positron Emission Tomography in CNS Drug Discovery and Drug Monitoring. *J. Med. Chem.* **2014**, *57* (22), 9232–9258.

(22) Ziegler, S. I. Positron Emission Tomography: Principles, Technology, and Recent Developments. *Nucl. Phys. A* **2005**, *752*, 679c-687c.

(23) Cherry, S. R.; Badawai, R. D.; Karp, J. S.; Moses, W. W.; Price, P.; Jones, T. Total-Body Imaging: Transforming the Role of Positron Emission Tomography. *Sci. Transl. Med.* **2017**, *9* (381), eaaf6169.

(24) Levin, C. S. Primer on Molecular Imaging Technology. *Eur. J. Nucl. Med. Mol. Imaging* **2005**, *32* (Suppl. 2), S325–S345.

(25) Melcher, C. L. Scintillation Crystals for PET. *J. Nucl. Med.* **2000**, *41* (6), 1051–1055.

(26) Teräs, M.; Tolvanen, T.; Johansson, J. J.; Williams, J. J.; Knuuti, J. Performance of the New Generation of Whole-Body PET/CT Scanners: Discovery STE and Discovery VCT. *Eur. J. Nucl. Med. Mol. Imaging* **2007**, *34* (10), 1683–1692.

(27) Lewellen, T. K. Recent Developments in PET Detector Technology. *Phys Med Biol* **2008**, *53* (17), R287–R317.

(28) Qaim, S. M. Cyclotron Prodcution of Medical Radionuclides. In *Handbook of Nuclear Chemistry,* 2nd Edition; Vértes, A., Nagy, S., Klencsár, Z., Lovas, R. G., Rösch, F., Eds.; Springer: Boston, MA, 2011; Vol. 4, pp 1903–1933.

(29) Costa, P.; Metello, L.; Alves, F.; Duarte Naia, M. Cyclotron Production of Unconventional Radionuclides for PET Imaging: The Example of Titanium-45 and Its Applications. *Instruments* **2018**, *2* (2), 8.

(30) Filosofov, D. V.; Loktionova, N. S.; Rösch, F. A ^{44}Ti/^{44}Sc Radionuclide Generator for Potential Application of ^{44}Sc-Based PET-Radiopharmaceuticals. *Radiochim. Acta* **2010**, *98* (3), 149–156.

(31) Holland, J. P.; Williamson, M. J.; Lewis, J. S. Unconventional Nuclides for Radiopharmaceuticals. *Mol. Imaging* **2010**, *9* (1), 1–20.

(32) Yoshinaga, K.; Klein, R.; Tamaki, N. Generator-Produced Rubidium-82 Positron Emission Tomography Myocardial Perfusion Imaging-From Basic Aspects to Clinical Applications. *J. Cardiol.* **2010**, *55* (2), 163–173.

(33) Jodal, L.; Le Loirec, C.; Champion, C. Positron Range in PET Imaging: An Alternative Approach for Assessing and Correcting the Blurring. *Phys. Med. Biol.* **2012**, *57* (12), 3931–3943.

(34) Wei, W.; Rosenkrans, Z. T.; Liu, J.; Huang, G.; Luo, Q.; Cai, W. ImmunoPET : Concept , Design , and Applications. *Chem. Rev.* **2020**, *120* (8), 3787–3851.

(35) Zhang, Y.; Hong, H.; Cai, W. PET Tracers Based on Zirconium-89. *Curr Radiopharm* **2011**, *4* (2), 131–139.

(36) Reddy, S.; Robinson, M. ImmunoPET In Cancer Models. *Semin Nucl Med* **2010**, *40* (3), 182–189.

(37) Deri, M. A.; Zeglis, B. M.; Francesconi, L. C.; Lewis, J. S. PET Imaging with ^{89}Zr: From Radiochemistry to the Clinic. *Nucl Med Biol* **2013**, *40* (1), 3–14.

(38) Rösch, F.; Piel, M. Radiochemie/Tracer. In *PET/CT-Atlas,* 2nd Edition; Mohnike, W., Hör, G., Schelbert, H., Eds.; Springer-Verlag Berlin Heidelberg New York: Berlin Heidelberg, 2011; pp 35–72.

(39) Bom, M. J.; Van Diemen, P. A.; Driessen, R. S.; Everaars, H.; Schumacher, S. P.; Wijmenga, J. T.; Raijmakers, P. G.; Van De Ven, P. M.; Lammertsma, A. A.; Van Rossum, A. C.; Knuuti, J.; Danad, I.; Knaapen, P. Prognostic Value of [^{15}O]H_2O Positron Emission Tomography-Derived Global and Regional Myocardial Perfusion. *Eur. Heart J. Cardiovasc. Imaging* **2020**, *21* (7), 777–786.

(40) Albano, D.; Giubbini, R.; Bertagna, F. ^{13}N-NH_3 PET/CT in Oncological Disease. *Jpn. J. Radiol.* **2019**, *37* (12), 799–807.

(41) Coenen, H. H.; Gee, A. D.; Adam, M.; Antoni, G.; Cutler, C. S.; Fujibayashi, Y.; Jeong, J. M.; Mach, R. H.; Mindt, T. L.; Pike, V. W.; Windhorst, A. D. Consensus Nomenclature Rules for Radiopharmaceutical Chemistry — Setting the Record Straight. *Nucl. Med. Biol.* **2017**, *55*, v–xi.

(42) De Goeij, J. J. M.; Bonardi, M. L. How Do We Define the Concepts Specific Activity, Radioactive Concentration, Carrier, Carrier-Free and No-Carrier-Added? *J. Radioanal. Nucl. Chem.* **2005**, *263*, 13–18.

(43) Schlyer, D. J. Production of Radionuclides in Accelerators. In *Handbook of Radiopharamceuticals: Radiochemistry and Applications,* 1st Edition; Welch, M. J., Redvanly, C. S., Eds.; John Wiley & Sons Ltd: Chichester, 2003; pp 1–70.

(44) Dash, A.; Chakravarty, R. Radionuclide Generators: The Prospect of Availing PET Radiotracers to Meet Current Clinical Needs and Future Research Demands. *Am. J. Nucl. Med. Mol. Imaging* **2019**, *9* (1), 30–66.

(45) Vorster, M.; Maes, A.; Van Dewiele, C.; Sathekge, M. Gallium-68: A Systematic Review of Its Nononcological Applications. *Nucl. Med. Commun.* **2013**, *34* (9), 834–854.

(46) Duatti, A. Review on ^{99m}Tc Radiopharmaceuticals with Emphasis on New Advancements. *Nucl. Med. Biol.* **2021**, *92*, 202–216.

(47) Roesch, F.; J. Riss, P. The Renaissance of the ^{68}Ge/^{68}Ga Radionuclide Generator Initiates New Developments in ^{68}Ga Radiopharmaceutical Chemistry. *Curr. Top. Med. Chem.* **2012**, *10* (16), 1633–1668.

(48) Rösch, F. Past, Present and Future of ^{68}Ge/^{68}Ga Generators. *Appl. Radiat. Isot.* **2013**, *76*, 24–30.

(49) Sanchez-Crespo, A. Comparison of Gallium-68 and Fluorine-18 Imaging Characteristics in Positron Emission Tomography. *Appl. Radiat. Isot.* **2013**, *76*, 55–62.

(50) Maeke, H. R.; Andre, J. P. ^{68}Ga-PET Radiopharmacy: A Generator-Based Alternative to ^{18}F-Radiopharmacy. In *PET-Chemistry - The Driving Force in Molecular Imaging. Ernst Schering Research Foundation Workshop, vol. 64,* 1st Edition; Schubiger, P. A., Lehmann, L., Friebe, M., Eds.; Springer-Verlag Berlin Heidelberg New York: Berlin Heidelberg, 2007; pp 215–242.

(51) Wadas, Thaddeus, J.; Wong, E. H.; Weisman, G. R.; Anderson, C. J. Coordinating Radiometals of Copper, Gallium, Indium, Yttrium and Zirconium for PET and SPECT Imaging of Disease. *Chem Rev.* **2010**, *110* (5), 2858–2902.

(52) Pearson, R. C. Hard and Soft Acids and Base. *J. Am. Chem. Soc.* **1963**, *85* (22), 3533–3539.

(53) Reichert, D. E.; Lewis, J. S.; Anderson, C. J. Metal Complexes as Diagnostic Tools. *Coord. Chem. Rev.* **1999**, *184* (1), 3–66.

(54) Anderson, C. J.; Welch, M. J. Radiometal-Labeled Agents (Non-Technetium) for Diagnostic Imaging. *Chem. Rev.* **1999**, *99* (9), 2219–2234.

(55) Rösch, F.; Knapp, F. F. Radionuclide Generators. In *Handbook of Nuclear Chemistry,* 2nd Edition; Vértes, A., Nagy, S., Klencsár, Z., Lovas, R., Rösch, F., Eds.; Springer: Boston, MA, 2011;Vol. 4, pp 1935–1976.

(56) Seemann, J.; Eppard, E.; Waldron, B. P.; Ross, T. L.; Roesch, F. Cation Exchange-Based Post-Processing of ^{68}Ga-Eluate: A Comparison of Three Solvent Systems for Labelling of DOTATOC, NO2AP^{BP} and DATA^{m}. *Appl. Radiat. Isot.* **2015**, *98*, 54–59.

(57) Breeman, W. A. P.; De Blois, E.; Sze Chan, H.; Konijnenberg, M.; Kwekkeboom, D. J.; Krenning, E. P. ^{68}Ga-Labeled DOTA-Peptides and ^{68}Ga-Labeled Radiopharmaceuticals for Positron Emission Tomography: Current Status of Research, Clinical Applications, and Future Perspectives. *Semin. Nucl. Med.* **2011**, *41* (4), 314–321.

(58) Breeman, W. A. P.; De Jong, M.; De Blois, E.; Bernard, B. F.; Konijnenberg, M.; Krenning, E. P. Radiolabelling DOTA-Peptides with ^{68}Ga. *Eur. J. Nucl. Med. Mol. Imaging* **2005**, *32* (4), 478–485.

(59) Zhernosekov, K. P.; Filosofov, D. V.; Baum, R. P.; Aschoff, P.; Bihl, H.; Razbash, A. A.; Jahn, M.; Jennewein, M.; Rösch, F. Processing of Generator-Produced ^{68}Ga for Medical Application. *J. Nucl. Med.* **2007**, *48* (10), 1741–1748.

(60) Meyer, G. J.; Mäcke, H.; Schuhmacher, J.; Knapp, W. H.; Hofmann, M. ^{68}Ga-Labelled DOTA-Derivatised Peptide Ligands. *Eur. J. Nucl. Med. Mol. Imaging* **2004**, *31* (8), 1097–1104.

(61) Loktionova, N. S.; Belozub, A. N.; Filosofov, D. V.; Zhernosekov, K. P.; Wagner, T.; Türler, A.; Rösch, F. Improved Column-Based Radiochemical Processing of the Generator Produced ^{68}Ga. *Appl. Radiat. Isot.* **2011**, *69* (7), 942–946.

(62) Eppard, E.; Wuttke, M.; Nicodemus, P. L.; Rösch, F. Ethanol-Based Post-Processing of Generator-Derived ^{68}Ga Toward Kit-Type Preparation of ^{68}Ga-Radiopharmaceuticals. *J. Nucl. Med.* **2014**, *55* (6), 1023–1028.

(63) Hernandez, R.; Valdovinos, H. F.; Yang, Y.; Chakravarty, R.; Hong, H.; Barnhart, T. E.; Cai, W. Sc: An Attractive Isotope for Peptide-Based PET Imaging. *Mol. Pharm.* **2014**, *11*, 2954–2961.

(64) Pruszyński, M.; Majkowska-Pilip, A.; Loktionova, N. S.; Eppard, E.; Roesch, F. Radiolabeling of DOTATOC with the Long-Lived Positron Emitter ^{44}Sc. *Appl. Radiat. Isot.* **2012**, *70* (6), 974–979.

(65) Ferguson, S.; Jans, H. S.; Wuest, M.; Riauka, T.; Wuest, F. Comparison of Scandium-44g with Other PET Radionuclides in Pre-Clinical PET Phantom Imaging. *EJNMMI Phys.* **2019**, *6*, 23.

(66) Domnanich, K. A.; Müller, C.; Farkas, R.; Schmid, R. M.; Ponsard, B.; Schibli, R.; Türler, A.; van der Meulen, N. P. ^{44}Sc for Labeling of DOTA- and NODAGA-Functionalized Peptides: Preclinical in vitro and in vivo Investigations. *EJNMMI Radiopharm. Chem.* **2017**, *1*, 8.

(67) Umbricht, C. A.; Benešová, M.; Schmid, R. M.; Türler, A.; Schibli, R.; van der Meulen, N. P.; Müller, C. ^{44}Sc-PSMA-617 for Radiotheragnostics in Tandem with ^{177}Lu-PSMA-617—Preclinical Investigations in Comparison with ^{68}Ga-PSMA-11 and ^{68}Ga-PSMA-617. *EJNMMI Res.* **2017**, *7*, 9.

(68) Eppard, E.; de la Fuente, A.; Benešová, M.; Khawar, A.; Bundschuh, R. A.; Gärtner, F. C.; Kreppel, B.; Kopka, K.; Essler, M.; Rösch, F. Clinical Translation and First In-Human Use of [^{44}Sc]Sc-PSMA-617 for PET Imaging of Metastasized Castrate-Resistant Prostate Cancer. *Theranostics* **2017**, *7* (18), 4359–4369.

(69) Eppard, E.; de la Fuente, A.; Mohr, N.; Allmeroth, M.; Zentel, R.; Miederer, M.; Pektor, S.; Rösch, F. Labeling of DOTA-Conjugated HPMA-Based Polymers with Trivalent Metallic Radionuclides for Molecular Imaging. *EJNMMI Res.* **2018**, *8*, 16.

(70) Roesch, F. Scandium-44: Benefits of a Long-Lived PET Radionuclide Available from the ^{44}Ti/^{44}Sc Generator System. *Curr. Radiopharm.* **2012**, *5* (3), 187–201.

(71) Krajewski, S.; Cydzik, I.; Abbas, K.; Bulgheroni, A.; Simonelli, F.; Holzwarth, U.; Bilewicz, A. Cyclotron Production of ^{44}Sc for Clinical Application. *Radiochim. Acta* **2013**, *101* (5), 333–338.

(72) van der Meulen, N. P.; Bunka, M.; Domnanich, K. A.; Müller, C.; Haller, S.; Vermeulen, C.; Türler, A.; Schibli, R. Cyclotron Production of ^{44}Sc: From Bench to Bedside. *Nucl. Med. Biol.* **2015**, *42* (9), 745–751.

(73) van der Meulen, N. P.; Hasler, R.; Talip, Z.; Grundler, P. V.; Favaretto, C.; Umbricht, C. A.; Müller, C.; Dellepiane, G.; Carzaniga, T. S.; Braccini, S. Developments toward the Implementation of ^{44}Sc Production at a Medical Cyclotron. *Molecules* **2020**, *25* (20), 4706.

(74) Majkowska-Pilip, A.; Bilewicz, A. Macrocyclic Complexes of Scandium Radionuclides as Precursors for Diagnostic and Therapeutic Radiopharmaceuticals. *J. Inorg. Biochem.* **2011**, *105* (2), 313–320.

(75) Mikolajczak, R.; Huclier-Markai, S.; Alliot, C.; Haddad, F.; Szikra, D.; Forgacs, V.; Garnuszek, P. Production of Scandium Radionuclides for Theranostic Applications: Towards Standardization of Quality Requirements. *EJNMMI Radiopharm. Chem.* **2021**, *6*, 19.

(76) Müller, C.; Domnanich, K. A.; Umbricht, C. A.; Van Der Meulen, N. P. Scandium and Terbium Radionuclides for Radiotheranostics: Current State of Development towards Clinical Application. *Br. J. Radiol.* **2018**, *91* (1091), 20180074.

(77) Müller, C.; Bunka, M.; Haller, S.; Köster, U.; Groehn, V.; Bernhardt, P.; Van Der Meulen, N.; Türler, A.; Schibli, R. Promising Prospects for ^{44}Sc-/^{47}Sc-Based Theragnostics: Application of ^{47}Sc for Radionuclide Tumor Therapy in Mice. *J. Nucl. Med.* **2014**, *55* (10), 1658–1664.

(78) Banister, S.; Roeda, D.; Dolle, F.; Kassiou, M. Fluorine-18 Chemistry for PET: A Concise Introduction. *Curr. Radiopharm.* **2010**, *3* (2), 68–80.

(79) Coenen, H. H. Fluorine-18 Labeling Methodes: Features and Possibilities of Basic Reactions. In *PET-Chemistry - The Driving Force in Molecular Imaging,* 1. Editon; Schubiger, P. A., Lehmann, L., Friebe, M., Eds.; Springer-Verlag Berlin Heidelberg New York: Berlin Heidelberg New York, 2007; pp 15–50.

(80) Ametamey, S. M.; Honer, M.; Schubiger, P. A. Molecular Imaging with PET. *Chem. Rev.* **2008**, *108* (5), 1501–1516.

(81) Jacobson, O.; Kiesewetter, D. O.; Chen, X. Fluorine-18 Radiochemistry, Labeling Strategies and Synthetic Routes. *Bioconjug. Chem.* **2015**, *26* (1), 1–18.

(82) Hoh, C. K. Clinical Use of FDG PET. *Nucl. Med. Biol.* **2007**, *34* (7), 737–742.

(83) Rösch, F. Radiolanthanides in Endoradiotherapy: An Overview. *Radiochim. Acta* **2007**, *95* (6), 303–311.

(84) Zoller, F.; Eisenhut, M.; Haberkorn, U.; Mier, W. Endoradiotherapy in Cancer Treatment - Basic Concepts and Future Trends. *Eur. J. Pharmacol.* **2009**, *625* (1–3), 55–62.

(85) Kassis, A. I. Therapeutic Radionuclides. *Semin Nucl Med* **2008**, *38* (5), 358–366.

(86) Zalutsky, M. R. Radionuclide Therapy. In *Handbook of Nuclear Chemistry*, 2nd Edition; Vértes, A., Nagy, S., Klencsár, Z., Lovas, R. G., Rösch, F., Eds.; Springer: Boston, MA, 2011; Vol. 4, pp 2179–2209.

(87) Mavragani, I. V.; Nikitaki, Z.; Kalospyros, S. A.; Georgakilas, A. G. Ionizing Radiation and Complex DNA Damage: From Prediction to Detection Challenges and Biological Significance. *Cancers.* **2019**, *11* (11), 1789.

(88) Kassis, A. I.; Adelstein, S. J. Radiobiologic Principles in Radionuclide Therapy. *J. Nucl. Med.* **2005**, *46* (1 suppl.), 4S-12S.

(89) Haberkorn, U.; Giesel, F.; Morgenstern, A.; Kratochwil, C. The Future of Radioligand Therapy: α, β, or Both? *J. Nucl. Med.* **2017**, *58* (7), 1017–1018.

(90) Brady, D.; O'Sullivan, J. M.; Prise, K. M. What Is the Role of the Bystander Response in Radionuclide Therapies? *Front. Oncol.* **2013**, *3* (August), 215.

(91) Zalutsky, M.; Vaidyanathan, G. Astatine-211-Labeled Radiotherapeutics An Emerging Approach to Targeted Alpha-Particle Radiotherapy. *Curr. Pharm. Des.* **2005**, *6* (14), 1433–1455.

(92) Qin, Y.; Imobersteg, S.; Blanc, A.; Frank, S.; Schibli, R.; Béhé, M. P.; Grzmil, M. Evaluation of Actinium-225 Labeled Minigastrin Analogue [^{225}Ac]Ac-DOTA-PP-F11N for Targeted Alpha Particle Therapy. *Pharmaceutics* **2020**, *12* (11), 1088.

(93) Qaim, S. M. Therapeutic Radionuclides and Nuclear Data. *Radiochim. Acta* **2001**, *89* (4–5), 297–302.

(94) Apostolidis, C.; Molinet, R.; McGinley, J.; Abbas, K.; Möllenbeck, J.; Morgenstern, A. Cyclotron Production of Ac-225 for Targeted Alpha Therapy. *Appl. Radiat. Isot.* **2005**, *62* (3), 383–387.

(95) Cutler, C. S.; Hennkens, H. M.; Sisay, N.; Huclier-Markai, S.; Jurisson, S. S. Radiometals for Combined Imaging and Therapy. *Chem. Rev.* **2013**, *113* (2), 858–883.

(96) Ku, A.; Facca, V. J.; Cai, Z.; Reilly, R. M. Auger Electrons for Cancer Therapy – a Review. *EJNMMI Radiopharm. Chem.* **2019**, *4*, 27.

(97) Banerjee, S.; Pillai, M. R. A.; Knapp, F. F. Lutetium-177 Therapeutic Radiopharmaceuticals: Linking Chemistry, Radiochemistry, and Practical Applications. *Chem. Rev.* **2015**, *115* (8), 2934–2974.

(98) Dash, A.; Pillai, M. R. A.; Knapp, F. F. Production of ^{177}Lu for Targeted Radionuclide Therapy: Available Options. *Nucl. Med. Mol. Imaging (2010).* **2015**, *49* (2), 85–107.

(99) Banerjee, S.; Pillai, M. R. A.; Knapp, F. F. Lutetium-177 Therapeutic Radiopharmaceuticals: Linking Chemistry, Radiochemistry, and Practical Applications. *Chem. Rev.* **2015**, *115* (8), 2934–2974.

(100) Pillai, M. R. A.; Chakraborty, S.; Das, T.; Venkatesh, M.; Ramamoorthy, N. Production Logistics of ^{177}Lu for Radionuclide Therapy. *Appl. Radiat. Isot.* **2003**, *59* (2–3), 109–118.

(101) Hao, G.; N Singh, A.; Liu, W.; Sun, X. PET with Non-Standard Nuclides. *Curr. Top. Med. Chem.* **2010**, *10* (11), 1096–1112.

(102) Price, E. W.; Orvig, C. Matching Chelators to Radiometals for Radiopharmaceuticals. *Chem. Soc. Rev.* **2014**, *43*, 260–290.

(103) Fani, M.; Good, S.; Maecke, H. R. Radiometals (Non-Tc, Non-Re) and Bifunctional Labeling Chemistry. In *Handbook of Nuclear Chemistry*, 2nd Edition; Vértes, A., Nagy, S., Klencsár, Z., Lovas, R. G., Rösch, F., Eds.; Springer: Boston, MA, 2011; Vol. 4, pp 2143–2178.

(104) Wurm, F. R.; Klok, H. A. Be Squared: Expanding the Horizon of Squaric Acid-Mediated Conjugations. *Chem. Soc. Rev.* **2013**, *42* (21), 8220–8236.

(105) Spang, P.; Herrmann, C.; Roesch, F. Bifunctional Gallium-68 Chelators: Past, Present, and Future. *Semin. Nucl. Med.* **2016**, *46* (5), 373–394.

(106) Liu, S. Bifunctional Coupling Agents for Radiolabeling of Biomolecules and Target-Specific Delivery of Metallic Radionuclides. *Adv Drug Deliv Rev* **2008**, *6023* (12), 1347–1370.

(107) Brechbiel, Martin, W. Bifunctional Chelates for Metal Nuclides. *Q J Nucl Med Mol Imaging* **2008**, *52* (2), 166–173.

(108) Hancock, R. D. Chelate Ring Size and Metal Ion Selection: The Basis of Selectivity for Metal Ions in Open-Chain Ligands and Macrocycles. *J. Chem. Educ.* **1992**, *69* (8), 615–621.

(109) Sundberg, M. W.; Meares, C. F.; Goodwin, D. A.; Diamanti, C. I. Chelating Agents for the Binding of Metal Ions to Macromolecules. *Nature* **1974**, *250*, 587–588.

(110) Sundberg, M. W.; Meares, C. F.; Goodwin, D. A.; Diamanti, C. I. Selective Binding of Metal Ions to Macromolecules Using Bifunctional Analogs of EDTA. *J. Med. Chem.* **1974**, *17* (12), 1304–1307.

(111) Sarko, D.; Eisenhut, M.; Haberkorn, U.; Mier, W. Bifunctional Chelators in the Design and Application of Radiopharmaceuticals for Oncological Diseases. *Curr. Med. Chem.* **2012**, *19* (17), 2667–2688.

(112) Chinn, P.; Braslawsky, G.; White, C.; Hanna, N. Antibody Therapy of Non-Hodgkin's B-Cell Lymphoma. *Cancer Immunol. Immunother.* **2003**, *52* (5), 257–280.

(113) Pillai, M. R. A.; Nanabala, R.; Joy, A.; Sasikumar, A.; Russ Knapp, F. F. Radiolabeled Enzyme Inhibitors and Binding Agents Targeting PSMA: Effective Theranostic Tools for Imaging and Therapy of Prostate Cancer. *Nucl. Med. Biol.* **2016**, *43* (11), 692–720.

(114) Eder, M.; Neels, O.; Müller, M.; Bauder-Wüst, U.; Remde, Y.; Schäfer, M.; Hennrich, U.; Eisenhut, M.; Afshar-Oromieh, A.; Haberkorn, U.; Kopka, K. Novel Preclinical and Radiopharmaceutical Aspects of [^{68}Ga]Ga-PSMA-HBED-CC: A New PET Tracer for Imaging of Prostate Cancer. *Pharmaceuticals* **2014**, *7* (7), 779–796.

(115) Eder, M.; Schäfer, M.; Bauder-Wüst, U.; Hull, W. E.; Wängler, C.; Mier, W.; Haberkorn, U.; Eisenhut, M. ^{68}Ga-Complex Lipophilicity and the Targeting Property of a Urea-Based PSMA Inhibitor for PET Imaging. *Bioconjug. Chem.* **2012**, *23* (4), 688–697.

(116) Grunert, M.; Eberhardt, N.; Prasad, V.; Beer, A. J. Nuclear Medical Diagnostics and Treatment of Prostate Cancer: Who Needs PSMA-PET Imaging and When? Is There a Need for PSMA Therapy? *J. fur Urol. und Urogynakologie* **2021**, *28* (2), 58–72.

(117) Nayak, T. K.; Brechbiel, Martin, W. ^{86}Y Based PET Radiopharmaceuticals: Radiochemistry and Biological Applications. *Med Chem* **2011**, *7* (5), 380–388.

(118) Graham, M. M.; Gu, X.; Ginader, T.; Breheny, P.; Sunderland, J. J. ^{68}Ga-DOTATOC Imaging of Neuroendocrine Tumors: A Systematic Review and Metaanalysis. *J. Nucl. Med.* **2017**, *58* (9), 1452–1458.

(119) Sathekge, M.; Bruchertseifer, F.; Knoesen, O.; Reyneke, F.; Lawal, I.; Lengana, T.; Davis, C.; Mahapane, J.; Corbett, C.; Vorster, M.; Morgenstern, A. ^{225}Ac-PSMA-617 in Chemotherapy-Naive Patients with Advanced Prostate Cancer: A Pilot Study. *Eur. J. Nucl. Med. Mol. Imaging* **2019**, *46*, 129–138.

(120) Sartor, O.; de Bono, J.; Chi, K. N.; Fizazi, K.; Herrmann, K.; Rahbar, K.; Tagawa, S. T.; Nordquist, L. T.; Vaishampayan, N.; El-Haddad, G.; Park, C. H.; Beer, T. M.; Armour, A.; Pérez-Contreras, W. J.; DeSilvio, M.; Kpamegan, E.; Gericke, G.; Messmann, R. A.; Morris, M. J.; Krause, B. J. Lutetium-177–PSMA-617 for Metastatic Castration-Resistant Prostate Cancer. *N. Engl. J. Med.* **2021**, *385* (12), 1091–1103.

(121) Greifenstein, L.; Engelbogen, N.; Lahnif, H.; Sinnes, J.-P.; Bergmann, R.; Bachmann, M.; Rösch, F. Synthesis, Labeling and Preclinical Evaluation of a Squaric Acid Containing PSMA-inhibitor Labeled with ^{68}Ga – a Comparison with PSMA-11 and PSMA-617. *ChemMedChem* **2020**, *15* (8), 695–704.

(122) Yadav, D.; Ballal, S.; Yadav, M. P.; Tripathi, M.; Roesch, F.; Bal, C. Evaluation of [^{68}Ga]Ga-DATA-

TOC for Imaging of Neuroendocrine Tumours: Comparison with [^{68}Ga]Ga-DOTA-NOC PET/CT. *Eur. J. Nucl. Med. Mol. Imaging* **2020**, *47* (4), 860–869.

(123) Sinnes, J. P.; Nagel, J.; Waldron, B. P.; Maina, T.; Nock, B. A.; Bergmann, R. K.; Ullrich, M.; Pietzsch, J.; Bachmann, M.; Baum, R. P.; Rösch, F. Instant Kit Preparation of ^{68}Ga-Radiopharmaceuticals via the Hybrid Chelator DATA: Clinical Translation of [^{68}Ga]Ga-DATA-TOC. *EJNMMI Res.* **2019**, *9*, 48.

(124) Waldron, B. P.; Parker, D.; Burchardt, C.; Yufit, D. S.; Zimny, M.; Roesch, F. Structure and Stability of Hexadentate Complexes of Ligands Based on AAZTA for Efficient PET Labelling with Gallium-68. *Chem. Commun.* **2013**, *49* (6), 579–581.

(125) Klasen, B.; Moon, E. S.; Rösch, F. AAZTA^5-Squaramide Ester Competing with DOTA-, DTPA- and CHX-A-DTPA-Analogues: Promising Tool for ^{177}Lu-Labeling of Monoclonal Antibodies under Mild Conditions. *Nucl. Med. Biol.* **2021**, *96–97*, 80–93.

(126) Aime, S.; Calabi, L.; Cavallotti, C.; Gianolio, E.; Giovenzana, G. B.; Losi, P.; Maiocchi, A.; Palmisano, G.; Sisti, M. [Gd-AAZTA]-: A New Structural Entry for an Improved Generation of MRI Contrast Agents. *Inorg. Chem.* **2004**, *43* (24), 7588–7590.

(127) Nagy, G.; Szikra, D.; Trencsényi, G.; Fekete, A.; Garai, I.; Giani, A. M.; Negri, R.; Masciocchi, N.; Maiocchi, A.; Uggeri, F.; Tóth, I.; Aime, S.; Giovenzana, G. B.; Baranyai, Z. AAZTA: An Ideal Chelating Agent for the Development of ^{44}Sc PET Imaging Agents. *Angew. Chemie - Int. Ed.* **2017**, *56* (8), 2118–2122.

(128) Sinnes, J.; Nagel, J.; Rösch, F. AAZTA^5/AAZTA^5-TOC: Synthesis and Radiochemical Evaluation with ^{68}Ga, ^{44}Sc and ^{177}Lu. *EJNMMI Radiopharm Chem.* **2019**, *4*, 18.

(129) Moon, E. S.; Rymenant, Y. Van; Battan, S.; Loose, J. De; Bracke, A.; Van Der Veken, P.; De Meester, I.; Rösch, F. In vitro Evaluation of the Squaramide-Conjugated Fibroblast Activation Protein Inhibitor-Based Agents AAZTA^5.SA.FAPi and DOTA.SA.FAPi. *moleules* **2021**, *26* (12), 3482.

(130) Waldron, B. P.; Parker, D.; Burchardt, C.; Yufit, D. S.; Zimny, M.; Roesch, F. Structure and Stability of Hexadentate Complexes of Ligands Based on AAZTA for Efficient PET Labelling with Gallium-68. *Chem. Commun.* **2013**, *49* (6), 579–581.

(131) Parker, D.; Waldron, B. P.; Yufit, D. S. Crystallographic and Solution NMR Structural Analyses of Four Hexacoordinated Gallium(Iii) Complexes Based on Ligands Derived from 6-Amino-Perhydro-1,4-Diazepine. *Dalt. Trans.* **2013**, *42* (22), 8001–8008.

(132) Farkas, E.; Nagel, J.; Waldron, B. P.; Parker, D.; Tóth, I.; Brücher, E.; Rösch, F.; Baranyai, Z. Equilibrium, Kinetic and Structural Properties of Gallium(III) and Some Divalent Metal Complexes Formed with the New DATA^m and DATA^{5m} Ligands. *Chem. Eur. J.* **2017**, *23* (43), 10358–10371.

(133) Seemann, J.; Waldron, B. P.; Roesch, F.; Parker, D. Approaching “kit-Type” Labelling with ^{68}Ga: The DATA Chelators. *ChemMedChem* **2015**, *10* (6), 1019–1026.

(134) Farkas, E.; Nagel, J.; Waldron, B. P.; Parker, D.; Tóth, I.; Brücher, E.; Rösch, F.; Baranyai, Z. Equilibrium, Kinetic and Structural Properties of Gallium(III) and Some Divalent Metal Complexes Formed with the New DATA^m and DATA^{5m} Ligands. *Chem. Eur. J.* **2017**, *23* (43), 10358–10371.

(135) Seemann, J.; Waldron, B.; Parker, D.; Roesch, F. DATATOC: A Novel Conjugate for Kit-Type ^{68}Ga Labelling of TOC at Ambient Temperature. *EJNMMI Radiopharm. Chem.* **2017**, *1*, 4.

(136) Kreppel, B.; Gaertner, F. C.; Marinova, M.; Attenberger, U.; Meisenheimer, M.; Toma, M.;

Kristiansen, G.; Feldmann, G.; Moon, E. S.; Roesch, F.; Van Der Veken, P.; Essler, M. [^{68}Ga]Ga-DATA^{5m}.SA.FAPi PET/CT: Specific Tracer-Uptake in Focal Nodular Hyperplasia and Potential Role in Liver Tumor Imaging. *Nuklearmedizin* **2020**, *59* (05), 387–389.

(137) Ross, T. L.; Wester, H. J. ^{18}F: Labeling Chemistry and Labeled Compounds. In *Handbook of Nuclear Chemistry,* 2nd Edition; Vértes, A., Nagy, S., Klencsár, Z., Lovas, R. G., Rösch, F., Eds.; Springer: Boston, MA, 2011; Vol. 4, pp 2021–2071.

(138) Park, B. K.; Kitteringham, N. R.; O'Neill, P. M. Metabolism of Fluorine-Containing Drugs. *Annu. Rev. Pharmacol. Toxicol.* **2001**, *41*, 443–470.

(139) Hagmann, W. K. The Many Roles for Fluorine in Medicinal Chemistry. *J. Med. Chem.* **2008**, *51* (15), 4359–4369.

(140) Schirrmacher, R.; Wängler, C.; Schirrmacher, E. Fluorine-18 Radiochemistry: Theory and Practice. In *Munich Molecular Imaging Handbook Series - Pharmaceutical Radiochemistry (I),* 1st Edition; Wester, H. J., Ed.; SCINTOMICS: Fürstenfeldbruck, 2010; pp 5–74.

(141) Mason, N. S.; Mathis, Chester, A. Radiohalogens for PET Imaging. In *Positron Emission Tomography*, 1st Edition; Bailey, D. L., Townsend, D. W., Valk, P. E., Maisey, M. N., Eds.; Springer: London, 2005; pp 203–222.

(142) Yu, S. Review of ^{18}F-FDG Synthesis and Quality Control. *Biomed. Imaging Interv. J.* **2006**, *2* (4), e57.

(143) Jacobson, O.; Chen, X. PET Designated Flouride-18 Production and Chemistry. *Curr Top Med Chem* **2010**, *10* (11), 1048–1059.

(144) Fowler, J. S.; Ido, T. Initial and Subsequent Approach for the Synthesis of ^{18}FDG. *Semin. Nucl. Med.* **2002**, *32* (1), 6–12.

(145) Forsback, S.; Eskola, O.; Haaparanta, M.; Bergman, J.; Solin, O. Electrophilic Synthesis of 6-[^{18}F]Fluoro-L-DOPA using Post-Target Produced [^{18}F]F_2. *Radiochim. Acta* **2008**, *96* (12), 845–848.

(146) Wester, H. J.; Schottelius, M. Fluorine-18 Labeling of Peptides and Proteins. In *PET-Chemistry - The Driving Force in Molecular Imaging. Ernst Schering Foundation Workshop, vol 64,* 1st Edition; Schubiger, P., Lehmann, L., Friebe, M., Eds.; Springer-Verlag Berlin Heidelberg New York: Berlin Heidelberg, 2007; pp 79–111.

(147) Schirrmacher, R.; Wängler, B.; Bailey, J.; Bernard-Gauthier, V.; Schirrmacher, E.; Wängler, C. Small Prosthetic Groups in ^{18}F-Radiochemistry: Useful Auxiliaries for the Design of ^{18}F-PET Tracers. *Semin. Nucl. Med.* **2017**, *47* (5), 474–492.

(148) Kniess, T.; Laube, M.; Brust, P.; Steinbach, J. 2-[^{18}F]Fluoroethyl Tosylate-a Versatile Tool for Building ^{18}F-Based Radiotracers for Positron Emission Tomography. *Medchemcomm* **2015**, *6* (10), 1714–1754.

(149) Wangler, C.; Schirrmacher, R.; Bartenstein, P.; Wangler, B. Click-Chemistry Reactions in Radiopharmaceutical Chemistry: Fast & Easy Introduction of Radiolabels into Biomolecules for In Vivo Imaging. *Curr. Med. Chem.* **2010**, *17* (11), 1092–1116.

(150) Kettenbach, K.; Schieferstein, H.; Ross, T. L. ^{18}F-Labeling Using Click Cycloadditions. *Biomed Res. Int.* **2014**, *2014*, 361329.

(151) Kolb, H. C.; Finn, M. G.; Sharpless, K. B. Click Chemistry: Diverse Chemical Function from a Few Good Reactions. *Angew. Chemie - Int. Ed.* **2001**, *40* (11), 2004–2021.

(152) Thirumurugan, P.; Matosiuk, D.; Jozwiak, K. Click Chemistry for Drug Development and Diverse Chemical-Biology Applications. *Chem. Rev.* **2013**, *113* (7), 4905–4979.

(153) Rostovtsev, V. V.; Green, L. G.; Fokin, V. V.; Sharpless, K. B. A Stepwise Huisgen Cycloaddition Process: Copper(I)-Catalyzed Regioselective "Ligation" of Azides and Terminal Alkynes. *Angew. Chemie - Int. Ed.* **2002**, *41* (14), 2596–2599.

(154) Bock, V. D.; Hiemstra, H.; Van Maarseveen, J. H. Cu I-Catalyzed Alkyne-Azide "Click" Cycloadditions from a Mechanistic and Synthetic Perspective. *European J. Org. Chem.* **2006**, *2006* (1), 51–68.

(155) Worrell, B. T.; Malik, J. A.; Fokin, V. V. Direct Evidence of a Dinuclear Copper Intermediate in Cu(I)- Catalyzed Azide–Alkyne Cycloadditions. *Science.* **2013**, *340* (6131), 457–460.

(156) Agard, N. J.; Baskin, J. M.; Prescher, J. A.; Lo, A.; Bertozzi, C. R. A Comparative Study of Bioorthogonal Reactions with Azides. *ACS Chem. Biol.* **2006**, *1* (10), 644–648.

(157) Gaetke, L. M.; Chow-Johnson, H. S.; Chow, C. K. Copper: Toxicological Relevance and Mechanisms. *Arch Toxicol* **2014**, *88* (11), 1929–1938.

(158) Jewett, J. C.; Sletten, E. M.; Bertozzi, C. R. Rapid Cu-Free Click Chemistry with Readily Synthesized Biarylazacyclooctynones. *J. Am. Chem. Soc.* **2010**, *132* (11), 3688–3690.

(159) Ess, D. H.; Jones, G. O.; Houk, K. N. Transition States of Strain-Promoted Metal-Free Click Chemistry: 1,3-Dipolar Cycloadditions of Phenyl Azide and Cyclooctynes. *Org. Lett.* **2008**, *10* (8), 1633–1636.

(160) Agnew-Francis, K. A.; Williams, C. M. Squaramides as Bioisosteres in Contemporary Drug Design. *Chem. Rev.* **2020**, *120* (20), 11616–11650.

(161) Seleem, H. S.; Ramadan, A. A. T.; Taha, A.; Eid, M. F.; Samy, F. The Complexation of a Novel Squaric Bis(Thiosemicarbazone); 3,4-Bis{[(Aminothioxomethyl)Amino]Azamethylene}cyclobut-Ene-1,2-Diol. *Spectrochim. Acta - Part A Mol. Biomol. Spectrosc.* **2011**, *78* (3), 1097–1104.

(162) Bae, H. Y.; Song, C. E. Unprecedented Hydrophobic Amplification in Noncovalent Organocatalysis "on Water": Hydrophobic Chiral Squaramide Catalyzed Michael Addition of Malonates to Nitroalkenes. *ACS Catal.* **2015**, *5* (6), 3613–3619.

(163) Prohens, R.; Portell, A.; Font-Bardia, M.; Bauzá, A.; Frontera, A. Experimental and Theoretical Study of Aromaticity Effects in the Solid State Architecture on Squaric Acid Derivatives. *Cryst. Growth Des.* **2014**, *14* (5), 2578–2587.

(164) Huppertsberg, A.; Kaps, L.; Zhong, Z.; Schmitt, S.; Stickdorn, J.; Deswarte, K.; Combes, F.; Czysch, C.; Vrieze, J. De; Kasmi, S.; Choteschovsky, N.; Klefenz, A.; Medina-Montano, C.; Winterwerber, P.; Chen, C.; Bros, M.; Lienenklaus, S.; Sanders, N. N.; Koynov, K.; Schuppan, D.; Lambrecht, B. N.; David, S. A.; Geest, B. G. De; Nuhn, L. Squaric Ester-Based, PH-Degradable Nanogels: Modular Nanocarriers for Safe, Systemic Administration of Toll-like Receptor 7/8 Agonistic Immune Modulators. *J. Am. Chem. Soc.* **2021**, *143* (26), 9872–9883.

(165) Tietze, L. F.; Arlt, M.; Beller, M.; Glüsenkamp, K.; Jahdeb, E.; Rajewskyb, M. F. Squaric Acid Diethyl Ester: A New Coupling Reagent for the Formation of Drug Biopolymer Conjugates. Synthesis of Squaric Acid Ester Amides and Diamides. *Anticancer Agents* **1991**, *124* (5), 1215–1221.

(166) Lim, N. C.; Morton, M. D.; Jenkins, H. A.; Brückner, C. Squaric Acid N-Hydroxylamides: Synthesis, Structure, and Properties of Vinylogous Hydroxamic Acid Analogues. *J. Org. Chem.* **2003**, *68* (24), 9233–9241.

(167) Grus, T.; Lahnif, H.; Klasen, B.; Moon, E.-S.; Greifenstein, L.; Roesch, F. Squaric Acid-Based Radiopharmaceuticals for Tumor Imaging and Therapy. *Bioconjug. Chem.* **2021**, *32* (7), 1223–1231.

(168) Quiñonero, D.; Frontera, A.; Ballester, P.; Deyà, P. M. A Theoretical Study of Aromaticity in Squaramide and Oxocarbons. *Tetrahedron Lett.* **2000**, *41* (12), 2001–2005.

(169) Dingels, C.; Wurm, F.; Wagner, M.; Klok, H. A.; Frey, H. Squaric Acid Mediated Chemoselective PEGylation of Proteins: Reactivity of Single-Step-Activated α-Amino Poly(Ethylene Glycol)s. *Chem. - A Eur. J.* **2012**, *18* (52), 16828–16835.

(170) Berg, E.; Gill, H.; Marik, J.; Ogasawara, A.; Williams, S.; van Dongen, G.; Danielle, V.; Cherry, S. R.; Tarantal, A. F. Total-Body PET and Highly Stable Chelators Together Enable Meaningful ^{89}Zr-Antibody PET Studies up to 30 Days After Injection. *J. Nucl. Med.* **2020**, *61* (3), 453–460.

(171) Bray, F.; Laversanne, M.; Weiderpass, E.; Soerjomataram, I. The Ever-Increasing Importance of Cancer as a Leading Cause of Premature Death Worldwide. *Cancer* **2021**, *127* (16), 3029–3030.

(172) Sung, H.; Ferlay, J.; Siegel, R. L.; Laversanne, M.; Soerjomataram, I.; Jemal, A.; Bray, F. Global Cancer Statistics 2020: GLOBOCAN Estimates of Incidence and Mortality Worldwide for 36 Cancers in 185 Countries. *CA. Cancer J. Clin.* **2021**, *71* (3), 209–249.

(173) Grossman, D. C.; Curry, S. J.; Owens, D. K.; Bibbins-Domingo, K.; Caughey, A. B.; Davidson, K. W.; Doubeni, C. A.; Ebell, M.; Epling, J. W.; Kemper, A. R.; Krist, A. H.; Kubik, M.; Seth Landefeld, C.; Mangione, C. M.; Silverstein, M.; Simon, M. A.; Siu, A. L.; Tseng, C. W. Screening for Prostate Cancer US Preventive Services Task Force Recommendation Statement. *JAMA - J. Am. Med. Assoc.* **2018**, *319* (18), 1901–1913.

(174) Rawla, P. Epidemiology of Prostate Cancer. *World J Oncol* **2019**, *10* (2), 63–89.

(175) Sohn, E. Diagnostic Dilemma. *Nature* **2015**, *528*, S120–S122.

(176) Tikkinen, K. A. O.; Dahm, P.; Lytvyn, L.; Heen, A. F.; Vernooij, R. W. M.; Siemieniuk, R. A. C.; Wheeler, R.; Vaughan, B.; Fobuzi, A. C.; Blanker, M. H.; Junod, N.; Sommer, J.; Stirnemann, J.; Yoshimura, M.; Auer, R.; MacDonald, H.; Guyatt, G.; Vandvik, P. O.; Agoritsas, T. Prostate Cancer Screening with Prostate-Specific Antigen (PSA) Test: A Clinical Practice Guideline. *BMJ* **2018**, *362,* k3581.

(177) Cabarkapa, S.; Perera, M.; McGrath, S.; Lawrentschuk, N. Prostate Cancer Screening with Prostate-Specific Antigen: A Guide to the Guidelines. *Prostate Int.* **2016**, *4* (4), 125–129.

(178) Barinka, C.; Rojas, C.; Slusher, B.; Pomper, M. Glutamate Carboxypeptidase II in Diagnosis and Treatment of Neurologic Disorders and Prostate Cancer. *Curr Med Chem.* **2012**, *19* (6), 856–870.

(179) Ghosh, A.; Heston, W. D. W. Tumor Target Prostate Specific Membrane Antigen (PSMA) and Its Regulation in Prostate Cancer. *J. Cell. Biochem.* **2004**, *91* (3), 528–539.

(180) Perner, S.; Hofer, M. D.; Kim, R.; Shah, R. B.; Li, H.; Möller, P.; Hautmann, R. E.; Gschwend, J. E.; Kuefer, R.; Rubin, M. A. Prostate-Specific Membrane Antigen Expression as a Predictor of Prostate Cancer Progression. *Hum. Pathol.* **2007**, *38* (5), 696–701.

(181) Haberkorn, U.; Eder, M.; Kopka, K.; Babich, J. W.; Eisenhut, M. New Strategies in Prostate Cancer: Prostate-Specific Membrane Antigen (PSMA) Ligands for Diagnosis and Therapy. *Clin. Cancer Res.* **2016**, *22* (1), 9–15.

(182) Donin, N. M.; Reiter, R. E. Why Targeting PSMA Is a Game Changer in the Management of Prostate Cancer. *J. Nucl. Med.* **2018**, *59* (2), 177–182.

(183) Parsi, M.; Desai, M. H.; Desai, D.; Singhal, S.; Khandwala, P. M.; Potdar, R. R. PSMA: A Game Changer in the Diagnosis and Treatment of Advanced Prostate Cancer. *Med. Oncol.* **2021**, *38* (8), 89.

(184) Rahbar, K.; Afshar-Oromieh, A.; Jadvar, H.; Ahmadzadehfar, H. PSMA Theranostics: Current Status and Future Directions. *Mol. Imaging* **2018**, *17*, 1536012118776068.

(185) Fakiri, M. El; Geis, N. M.; Ayada, N.; Eder, M.; Eder, A. C. PSMA-Targeting Radiopharmaceuticals for Prostate Cancer Therapy: Recent Developments and Future Perspectives. *Cancers* **2021**, *13* (16), 3967.

(186) Silver, D. A.; Pellicer, I.; Fair, W. R.; Heston, W. D. W.; Cordon-Cardo, C. Prostate-Specific Membrane Antigen Expression in Normal and Mailgant Human Tissues. *Clin. Cancer Rersearch* **1997**, *3* (1), 81–85.

(187) Thomas, T. S.; Pachynski, R. K. Treatment of Advanced Prostate Cancer. *Mo. Med.* **2018**, *115* (2), 156–161.

(188) Pavlicek, J.; Ptacek, J.; Barinka, C. Glutamate Carboxypeptidase II: An Overview of Structural Studies and Their Importance for Structure-Based Drug Design and Deciphering the Reaction Mechanism of the Enzyme. *Curr. Med. Chem.* **2012**, *19* (9), 1300–1309.

(189) Mesters, J. R.; Barinka, C.; Li, W.; Tsukamoto, T.; Majer, P.; Slusher, B. S.; Konvalinka, J.; Hilgenfeld, R. Structure of Glutamate Carboxypeptidase II, a Drug Target in Neuronal Damage and Prostate Cancer. *EMBO J.* **2006**, *25* (6), 1375–1384.

(190) Zhang, A. X.; Murelli, R. P.; Barinka, C.; Michel, J.; Cocleaza, A.; Jorgensen, W. L.; Lubkowski, J.; Spiegel, D. A. A Remote Arene-Binding Site on Prostate Specific Membrane Antigen Revealed by Antibody-Recruiting Small Molecules. *J. Am. Chem. Soc.* **2010**, *132* (36), 12711–12716.

(191) Czerwińska, M.; Bilewicz, A.; Kruszewski, M.; Wegierek-Ciuk, A.; Lankoff, A. Targeted Radionuclide Therapy of Prostate Cancer-from Basic Research to Clinical Perspectives. *Molecules* **2020**, *25* (7), 1743.

(192) Jackson, P. F.; Cole, D. C.; Slusher, B. S.; Stetz, S. L.; Ross, L. E.; Donzanti, B. A.; Trainor, D. A. Design, Synthesis, and Biological Activity of a Potent Inhibitor of the Neuropeptidase N-Acetylated α-Linked Acidic Dipeptidase. *J. Med. Chem.* **1996**, *39* (2), 619–622.

(193) Jackson, P. F.; Tays, K. L.; Maclin, K. M.; Ko, Y. S.; Li, W.; Vitharana, D.; Tsukamoto, T.; Stoermer, D.; Lu, X. C. M.; Wozniak, K.; Slusher, B. S. Design and Pharmacological Activity of Phosphinic Acid Based NAALADase Inhibitors. *J. Med. Chem.* **2001**, *44* (24), 4170–4175.

(194) Nan, F.; Bzdega, T.; Pshenichkin, S.; Wroblewski, J. T.; Wroblewska, B.; Neale, J. H.; Kozikowski, A. P. Dual Function Glutamate-Related Ligands: Discovery of a Novel, Potent Inhibitor of Glutamate Carboxypeptidase II Possessing MGluR3 Agonist Activity. *J. Med. Chem.* **2000**, *43* (5), 772–774.

(195) Behr, S. C.; Aggarwal, R.; VanBrocklin, H. F.; Flavell, R. R.; Gao, K.; Small, E. J.; Blecha, J.; Jivan, S.; Hope, T. A.; Simko, J. P.; Kurhanewicz, J.; Noworolski, S. M.; Korn, N. J.; De Los Santos, R.; Cooperberg, M. R.; Carroll, P. R.; Nguyen, H. G.; Greene, K. L.; Langton-Webster, B.; Berkman, C. E.; Seo, Y. Phase I Study of CTT1057, an ^{18}F-Labeled Imaging Agent with Phosphoramidate Core Targeting Prostate-Specific Membrane Antigen in Prostate Cancer. *J. Nucl. Med.* **2019**, *60* (7), 910–916.

(196) Kozikowski, A. P.; Nan, F.; Conti, P.; Zhang, J.; Ramadan, E.; Bzdega, T.; Wroblewska, B.; Neale, J. H.; Pshenichkin, S.; Wroblewski, J. T. Design of Remarkably Simple, yet Potent Urea-Based Inhibitors of Glutamate Carboxypeptidase II (NAALADase). *J. Med. Chem* **2001**, *44* (3), 298–301.

(197) Kopka, K.; Benešová, M.; Bařinka, C.; Haberkorn, U.; Babich, J. Glu-Ureido-Based Inhibitors of Prostate-Specific Membrane Antigen: Lessons Learned during the Development of a Novel Class of Low-Molecular-Weight Theranostic Radiotracers. *J. Nucl. Med.* **2017**, *58* (Suppl 2), 17S-26S.

(198) Kularatne, S. A.; Zhou, Z.; Yang, J.; Post, C. B.; Low, P. S. Design, Synthesis, and Preclinical Evaluation of Prostate-Specific Membrane Antigen Targeted ^{99m}Tc-Radioimaging Agents. *Mol. Pharm.* **2009**, *6* (3), 790–800.

(199) Hillier, S. M.; Maresca, K. P.; Lu, G.; Merkin, R. D.; Marquis, J. C.; Zimmerman, C. N.; Eckelman, W. C.; Joyal, J. L.; Babich, J. W. ^{99m}Tc-Labeled Small-Molecule Inhibitors of Prostate-Specific Membrane Antigen for Molecular Imaging of Prostate Cancer. *J. Nucl. Med.* **2013**, *54* (8), 1369–1376.

(200) Robu, S.; Schmidt, A.; Eiber, M.; Schottelius, M.; Günther, T.; Hooshyar Yousefi, B.; Schwaiger, M.; Wester, H. J. Synthesis and Preclinical Evaluation of Novel ^{18}F-Labeled Glu-Urea-Glu-Based PSMA Inhibitors for Prostate Cancer Imaging: A Comparison with ^{18}F-DCFPyl and ^{18}F-PSMA-1007. *EJNMMI Res.* **2018**, *8*, 30.

(201) Zechmann, C. M.; Afshar-Oromieh, A.; Armor, T.; Stubbs, J. B.; Mier, W.; Hadaschik, B.; Joyal, J.; Kopka, K.; Debus, J.; Babich, J. W.; Haberkorn, U. Radiation Dosimetry and First Therapy Results with a ^{124}I/ ^{131}I-Labeled Small Molecule (MIP-1095) Targeting PSMA for Prostate Cancer Therapy. *Eur. J. Nucl. Med. Mol. Imaging* **2014**, *41* (7), 1280–1292.

(202) Maresca, K. P.; Hillier, S. M.; Femia, F. J.; Keith, D.; Barone, C.; Joyal, J. L.; Zimmerman, C. N.; Kozikowski, A. P.; Barrett, J. A.; Eckelman, W. C.; Babich, J. W. A Series of Halogenated Heterodimeric Inhibitors of Prostate Specific Membrane Antigen (PSMA) as Radiolabeled Probes for Targeting Prostate Cancer. *J. Med. Chem.* **2009**, *52* (2), 347–357.

(203) Barrett, J. A.; Coleman, R. E.; Goldsmith, S. J.; Vallabhajosula, S.; Petry, N. A.; Cho, S.; Armor, T.; Stubbs, J. B.; Maresca, K. P.; Stabin, M. G.; Joyal, J. L.; Eckelman, W. C.; Babich, J. W. First-in-Man Evaluation of 2 High-Affinity PSMA-Avid Small Molecules for Imaging Prostate Cancer. *J. Nucl. Med.* **2013**, *54* (3), 380–387.

(204) Schmidkonz, C.; Hollweg, C.; Beck, M.; Reinfelder, J.; Goetz, T. I.; Sanders, J. C.; Schmidt, D.; Prante, O.; Bäuerle, T.; Cavallaro, A.; Uder, M.; Wullich, B.; Goebell, P.; Kuwert, T.; Ritt, P. ^{99m}Tc-MIP-1404-SPECT/CT for the Detection of PSMA-Positive Lesions in 225 Patients with Biochemical Recurrence of Prostate Cancer. *Prostate* **2018**, *78* (1), 54–63.

(205) Afshar-Oromieh, A.; Malcher, A.; Eder, M.; Eisenhut, M.; Linhart, H. G.; Hadaschik, B. A.; Holland-Letz, T.; Giesel, F. L.; Kratochwil, C.; Haufe, S.; Haberkorn, U.; Zechmann, C. M. PET Imaging with a [^{68}Ga]Gallium-Labelled PSMA Ligand for the Diagnosis of Prostate Cancer: Biodistribution in Humans and First Evaluation of Tumour Lesions. *Eur. J. Nucl. Med. Mol. Imaging* **2013**, *40* (4), 486–495.

(206) Bois, F.; Noirot, C.; Dietemann, S.; Mainta, I. C.; Zilli, T.; Garibotto, V.; Walter, M. A. [^{68}Ga]Ga-PSMA-11 in Prostate Cancer: A Comprehensive Review. *Am. J. Nucl. Med. Mol. Imaging* **2020**, *10* (6), 349–374.

(207) Afshar-Oromieh, A.; Avtzi, E.; Giesel, F. L.; Holland-Letz, T.; Linhart, H. G.; Eder, M.; Eisenhut, M.; Boxler, S.; Hadaschik, B. A.; Kratochwil, C.; Weichert, W.; Kopka, K.; Debus, J.; Haberkorn, U. The Diagnostic Value of PET/CT Imaging with the ^{68}Ga-Labelled PSMA Ligand HBED-CC in the Diagnosis of Recurrent Prostate Cancer. *Eur. J. Nucl. Med. Mol. Imaging* **2015**, *42* (2), 197–209.

(208) Afshar-Oromieh, A.; Holland-Letz, T.; Giesel, F. L.; Kratochwil, C.; Mier, W.; Haufe, S.; Debus, N.; Eder, M.; Eisenhut, M.; Schäfer, M.; Neels, O.; Hohenfellner, M.; Kopka, K.; Kauczor, H. U.; Debus, J.; Haberkorn, U. Diagnostic Performance of ^{68}Ga-PSMA-11 (HBED-CC) PET/CT in Patients with Recurrent Prostate Cancer: Evaluation in 1007 Patients. *Eur. J. Nucl. Med. Mol. Imaging* **2017**, *44* (8), 1258–1268.

(209) Eiber, M.; Maurer, T.; Souvatzoglou, M.; Beer, A. J.; Ruffani, A.; Haller, B.; Graner, F. P.; Kübler, H.; Haberhorn, U.; Eisenhut, M.; Wester, H. J.; Gschwend, J. E.; Schwaiger, M. Evaluation of

Hybrid ^{68}Ga-PSMA Ligand PET/CT in 248 Patients with Biochemical Recurrence after Radical Prostatectomy. *J. Nucl. Med.* **2015**, *56* (5), 668–674.

(210) Schwenck, J.; Rempp, H.; Reischl, G.; Kruck, S.; Stenzl, A.; Nikolaou, K.; Pfannenberg, C.; la Fougère, C. Comparison of ^{68}Ga-Labelled PSMA-11 and ^{11}C-Choline in the Detection of Prostate Cancer Metastases by PET/CT. *Eur. J. Nucl. Med. Mol. Imaging* **2017**, *44*, 92–101.

(211) FDA Approves First PSMA-Targeted PET Imaging Drug for Men with Prostate Cancer https://www.fda.gov/News-Events/Press-Announcements/Fda-Approves-First-Psma-Targeted-Pet-Imaging-Drug-Men-Prostate-Cancer (Accessed 08. Nov. 2021).

(212) Benešová, M.; Schäfer, M.; Bauder-Wüst, U.; Afshar-Oromieh, A.; Kratochwil, C.; Mier, W.; Haberkorn, U.; Kopka, K.; Eder, M. Preclinical Evaluation of a Tailor-Made DOTA-Conjugated PSMA Inhibitor with Optimized Linker Moiety for Imaging and Endoradiotherapy of Prostate Cancer. *J. Nucl. Med.* **2015**, *56* (6), 914–920.

(213) Benešová, M.; Bauder-Wüst, U.; Schäfer, M.; Klika, K. D.; Mier, W.; Haberkorn, U.; Kopka, K.; Eder, M. Linker Modification Strategies to Control the Prostate-Specific Membrane Antigen (PSMA)-Targeting and Pharmacokinetic Properties of DOTA-Conjugated PSMA Inhibitors. *J. Med. Chem.* **2016**, *59* (5), 1761–1775.

(214) Sun, M.; Niaz, M. O.; Nelson, A.; Skafida, M.; Niaz, M. J. Review of ^{177}Lu-PSMA-617 in Patients With Metastatic Castration-Resistant Prostate Cancer. *Cureus* **2020**, *12* (6), 10–17.

(215) Rosar, F.; Krause, J.; Bartholomä, M.; Maus, S.; Stemler, T.; Hierlmeier, I.; Linxweiler, J.; Ezziddin, S.; Khreish, F. Efficacy and Safety of [^{225}Ac]Ac-PSMA-617 Augmented [^{177}Lu]Lu-PSMA-617 Radioligand Therapy in Patients with Highly Advanced mCRPC with Poor Prognosis. *Pharmaceutics* **2020**, *13* (5), 722.

(216) Sathekge, M.; Bruchertseifer, F.; Knoesen, O.; Reyneke, F.; Lawal, I.; Lengana, T.; Davis, C.; Mahapane, J.; Corbett, C.; Vorster, M.; Morgenstern, A. ^{225}Ac-PSMA-617 in Chemotherapy-Naive Patients with Advanced Prostate Cancer: A Pilot Study. *Eur. J. Nucl. Med. Mol. Imaging* **2019**, *46*, 129–138.

(217) Cardinale, J.; Schäfer, M.; Benešová, M.; Bauder-Wüst, U.; Leotta, K.; Eder, M.; Neels, O. C.; Haberkorn, U.; Giesel, F. L.; Kopka, K. Preclinical Evaluation of ^{18}F-PSMA-1007, a New Prostate-Specific Membrane Antigen Ligand for Prostate Cancer Imaging. *J. Nucl. Med.* **2017**, *58* (3), 425–431.

(218) Awenat, S.; Piccardo, A.; Carvoeiras, P.; Signore, G.; Giovanella, L.; Prior, J. O.; Treglia, G. Diagnostic Role of ^{18}F-PSMA-1007 PET/CT in Prostate Cancer Staging: A Systematic Review. *Diagnostics* **2021**, *11* (3), 552.

(219) Palma, E.; Correia, J. D. G.; Campello, M. P. C.; Santos, I. Bisphosphonates as Radionuclide Carriers for Imaging or Systemic Therapy. *Mol. Biosyst.* **2011**, *7* (11), 2950–2966.

(220) Drake, M. T.; Clarke, B. L.; Khosla, S. Bisphosphonates: Mechanism of Action and Role in Clinical Practice. *Mayo Clin Proc* **2008**, *83* (9), 1032–1045.

(221) Fleisch, H. Development of Bisphosphonates. *Breast Cancer Res.* **2002**, *4*, 30.

(222) Kattimani, V. S.; Kondaka, S.; Lingamaneni, K. P. Hydroxyapatite–-Past, Present, and Future in Bone Regeneration. *Bone Tissue Regen. Insights* **2016**, *7*, 9–19.

(223) Florencio-Silva, R.; Sasso, G. R. D. S.; Sasso-Cerri, E.; Simões, M. J.; Cerri, P. S. Biology of Bone Tissue: Structure, Function, and Factors That Influence Bone Cells. *Biomed Res. Int.* **2015**, *2015*, 421746.

(224) Papapoulos, S. E. Bisphosphonates: How Do They Work? *Best Pract. Res. Clin. Endocrinol. Metab.* **2008**, *22* (5), 831–847.

(225) Santos, J. C. B.; De Melo, J. A.; Maheshwari, S.; De Medeiros, W. M. T. Q.; De Medeiros, W. M. T. Q.; Oliveira, J. W. D. F.; Moreno, C. J.; Amzel, L. M.; Gabelli, S. B.; Silva, M. S. Bisphosphonate-Based Molecules as Potential New Antiparasitic Drugs. *Molecules* **2020**, *25* (11), 2602.

(226) Rogers, M. J.; Gordon, S.; Benford, H. L.; Luckman, S. P. Cellular and Molecular Mechanisms of Action of Bisphosphonates. *Cancer* **2000**, *88* (12), 2961–2978.

(227) Lin, J. H. Bisphosphonates: A Review of Their Pharmacokinetic Properties. *Bone* **1996**, *18* (2), 75–85.

(228) Ogawa, K.; Ishizaki, A. Well-Designed Bone-Seeking Radiolabeled Compounds for Diagnosis and Therapy of Bone Metastases. *Biomed Res. Int.* **2015**, *2015*, 676053.

(229) Paes, F. M.; Serafini, A. N. Systemic Metabolic Radiopharmaceutical Therapy in the Treatment of Metastatic Bone Pain. *Semin. Nucl. Med.* **2010**, *40* (2), 89–104.

(230) Ogawa, K.; Mukai, T.; Inoue, Y.; Ono, M.; Saji, H. Development of a Novel ^{99m}Tc-Chelate-Conjugated Bisphosphonate with High Affinity for Bone as a Bone Scintigraphic Agent. *J. Nucl. Med.* **2006**, *47* (12), 2042–2047.

(231) Pfannkuchen, N.; Meckel, M.; Bergmann, R.; Bachmann, M.; Bal, C.; Sathekge, M.; Mohnike, W.; Baum, R. P.; Rösch, F. Novel Radiolabeled Bisphosphonates for PET Diagnosis and Endoradiotherapy of Bone Metastases. *Pharmaceuticals* **2017**, *10* (2), 45.

(232) Holub, J.; Meckel, M.; Kubíček, V.; Rösch, F.; Hermann, P. Gallium(III) Complexes of NOTA-Bis (Phosphonate) Conjugates as PET Radiotracers for Bone Imaging. *Contrast Media Mol. Imaging* **2015**, *10* (2), 122–134.

(233) Meckel, M.; Bergmann, R.; Miederer, M.; Roesch, F. Bone Targeting Compounds for Radiotherapy and Imaging: *Me(III)-DOTA Conjugates of Bisphosphonic Acid, Pamidronic Acid and Zoledronic Acid. *EJNMMI Radiopharm. Chem.* **2017**, *1*, 14.

(234) Casi, G.; Neri, D. Antibody-Drug Conjugates and Small Molecule-Drug Conjugates: Opportunities and Challenges for the Development of Selective Anticancer Cytotoxic Agents. *J. Med. Chem.* **2015**, *58* (22), 8751–8761.

(235) Drago, J. Z.; Modi, S.; Chandarlapaty, S. Unlocking the Potential of Antibody–Drug Conjugates for Cancer Therapy. *Nat. Rev. Clin. Oncol.* **2021**, *18* (6), 327–344.

(236) Jahangirian, H.; Kalantari, K.; Izadiyan, Z.; Rafiee-Moghaddam, R.; Shameli, K.; Webster, T. J. A Review of Small Molecules and Drug Delivery Applications Using Gold and Iron Nanoparticles. *Int. J. Nanomedicine* **2019**, *14*, 1633–1657.

(237) Krall, N.; Scheuermann, J.; Neri, D. Small Targeted Cytotoxics: Current State and Promises from DNA-Encoded Chemical Libraries. *Angew. Chemie - Int. Ed.* **2013**, *52* (5), 1384–1402.

(238) Wang, X.; Shirke, A.; Walker, E.; Sun, R.; Ramamurthy, G.; Wang, J.; Shan, L.; Mangadlao, J.; Dong, Z.; Li, J.; Wang, Z.; Schluchter, M.; Luo, D.; Wang, Y.; Stauffer, S.; Brady-Kalnay, S.; Hoimes, C.; Lee, Z.; Basilion, J. P. Small Molecule-Based Prodrug Targeting Prostate Specific Membrane Antigen for the Treatment of Prostate Cancer. *Cancers.* **2021**, *13* (3), 417.

(239) Wang, Y.; Liu, L.; Fan, S.; Xiao, D.; Xie, F.; Li, W.; Zhong, W.; Zhou, X. Antibody-Drug Conjugate Using Ionized CYS-Linker-MMAE as the Potent Payload Shows Optimal Therapeutic Safety. *Cancers.* **2020**, *12* (3), 744.

(240) Qi, R.; Wang, Y.; Bruno, P. M.; Xiao, H.; Yingjie, Y.; Li, T.; Lauffer, S.; Wei, W.; Chen, Q.; Kang, X.;

Song, H.; Yang, X.; Huang, X.; Detappe, A.; Matulonis, U.; Pepin, D.; Hemann, M. T.; Birrer, M. J.; Ghoroghchian, P. P. Nanoparticle Conjugates of a Highly Potent Toxin Enhance Safety and Circumvent Platinum Resistance in Ovarian Cancer. *Nat. Commun.* **2017**, *8*, 2166.

(241) Doronina, S. O.; Toki, B. E.; Torgov, M. Y.; Mendelsohn, B. A.; Cerveny, C. G.; Chace, D. F.; DeBlanc, R. L.; Gearing, R. P.; Bovee, T. D.; Siegall, C. B.; Francisco, J. A.; Wahl, A. F.; Meyer, D. L.; Senter, P. D. Development of Potent Monoclonal Antibody Auristatin Conjugates for Cancer Therapy. *Nat. Biotechnol.* **2003**, *21* (7), 778–784.

(242) Jain, N.; Smith, S. W.; Ghone, S.; Tomczuk, B. Current ADC Linker Chemistry. *Pharm. Res.* **2015**, *32* (11), 3526–3540.

(243) Richardson, N. C.; Kasamon, Y. L.; Chen, H.; de Claro, R. A.; Ye, J.; Blumenthal, G. M.; Farrell, A. T.; Pazdur, R. FDA Approval Summary: Brentuximab Vedotin in First-Line Treatment of Peripheral T-Cell Lymphoma. *Oncologist* **2019**, *24* (5), 180–187.

(244) Donato, E. M.; Fernández-Zarzoso, M.; Hueso, J. A.; de la Rubia, J. Brentuximab Vedotin in Hodgkin Lymphoma and Anaplastic Large-Cell Lymphoma: An Evidence-Based Review. *Onco. Targets. Ther.* **2018**, *11*, 4583–4590.

(245) Liu-Kreyche, P.; Shen, H.; Marino, A. M.; Iyer, R. A.; Humphreys, W. G.; Lai, Y. Lysosomal P-Gp-MDR1 Confers Drug Resistance of Brentuximab Vedotin and Its Cytotoxic Payload Monomethyl Auristatin E in Tumor Cells. *Front. Pharmacol.* **2019**, *10*, 749.

(246) Katz, J.; Janik, J. E.; Anas, Y. Brentuximab Vedotin (SGN-35). *Clin. Cancer Res.* **2011**, *17* (20), 6428–6436.

(247) Nolting, B. Linker Technologies for Antibody-Drug Conjugates. In *Antibody-Drug Conjugates - Methodes in Molecular Biology (Methods and Protocols), vol. 1045,* 1st Edition; Ducry, L., Ed.; Humana Press, Totowa, NJ, 2013; vol. 1045, pp 71–100.

(248) Lu, J.; Jiang, F.; Lu, A.; Zhang, G. Linkers Having a Crucial Role in Antibody–Drug Conjugates. *Int. J. Mol. Sci.* **2016**, *17* (4), 561.

(249) Zylberberg, C.; Matosevic, S. Pharmaceutical Liposomal Drug Delivery: A Review of New Delivery Systems and a Look at the Regulatory Landscape. *Drug Deliv.* **2016**, *23* (9), 3319–3329.

(250) Akbarzadeh, A.; Rezaei-sadabady, R.; Davaran, S.; Joo, S. W.; Zarghami, N. Liposome: Classification , Preparation , and Applications. *Nanoscale Res. Lett.* **2013**, *8*, 102.

(251) Drescher, S.; van Hoogevest, P. The Phospholipid Research Center: Current Research in Phospholipids and Their Use in Drug Delivery. *Pharmaceutics* **2020**, *12* (12), 1235.

(252) Sercombe, L.; Veerati, T.; Moheimani, F.; Wu, S. Y.; Sood, A. K.; Hua, S. Advances and Challenges of Liposome Assisted Drug Delivery. *Front. Pharmacol.* **2015**, *6*, 286.

(253) Monteiro, N.; Martins, A.; Reis, R. L.; Neves, N. M. Liposomes in Tissue Engineering and Regenerative Medicine. *J. R. Soc. Interface* **2014**, *11* (101), 20140459.

(254) Ernsting, M. J.; Murakami, M.; Roy, A.; Li, S.-D. Factors Controlling the Pharmacokinetics, Biodistribution and Intratumoral Penetration of Nanoparticles. *J Control Release* **2013**, *172* (3), 782–794.

(255) Beltrán-Gracia, E.; López-Camacho, A.; Higuera-Ciapara, I.; Velázquez-Fernández, J. B.; Vallejo-Cardona, A. A. Nanomedicine Review: Clinical Developments in Liposomal Applications. *Cancer Nanotechnol.* **2019**, *10*, 11.

(256) Pattni, B. S.; Chupin, V. V.; Torchilin, V. P. New Developments in Liposomal Drug Delivery. *Chem. Rev.* **2015**, *115* (19), 10938–10966.

(257) Allen, T. M.; Cullis, P. R. Liposomal Drug Delivery Systems: From Concept to Clinical Applications. *Adv. Drug Deliv. Rev.* **2013**, *65* (1), 36–48.

(258) Owens, D. E.; Peppas, N. A. Opsonization, Biodistribution, and Pharmacokinetics of Polymeric Nanoparticles. *Int. J. Pharm.* **2006**, *307* (1), 93–102.

(259) Wilms, D.; Stiriba, S.; Frey, H. Hyperbranched Polyglycerols: From the Controlled Synthesis of Biocompatible Polyether Polyols to Multipurpose Applications. *Acc. Chem. Res.* **2010**, *43* (1), 129–141.

(260) Wagener, K.; Worm, M.; Pektor, S.; Schinnerer, M.; Thiermann, R.; Miederer, M.; Frey, H.; Rösch, F. Comparison of Linear and Hyperbranched Polyether Lipids for Liposome Shielding by ^{18}F-Radiolabeling and Positron Emission Tomography. *Biomacromolecules* **2018**, *19* (7), 2506–2516.

(261) Cuccurullo, V.; Di Stasio, G. D.; Mansi, L. Nuclear Medicine in Prostate Cancer: A New Era for Radiotracers. *World J. Nucl. Med.* **2018**, *17* (2), 70–78.

(262) Tönnesmann, R.; Meyer, P. T.; Eder, M.; Baranski, A. C. [^{177}Lu]Lu-PSMA-617 Salivary Gland Uptake Characterized by Quantitative in Vitro Autoradiography. *Pharmaceuticals* **2019**, *12* (1), 18.

(263) Engelbogen, N. Quadratsäurediester als Brücke zwischen Chelatoren und Biomolekülen in der Radiopharmazie : Synthese und Evaluierung von Radiopharmaka zur Diagnose von Leberfibrose sowie zur Diagnose und Therapie von Tumorerkrankungen. *Dissertation - Johannes Gutenberg-Universität Mainz* **2017**.

(264) Greifenstein, L. Synthesis, Radiolabeling and in vitro and in vivo Evaluation of different Chelator Systems with ^{44}Sc, ^{64}Cu, ^{68}Ga and ^{177}Lu. *Dissertation - Johannes Gutenberg-Universität Mainz* **2019**.

(265) Greifenstein, L.; Grus, T.; Nagel, J.; Sinnes, J. P.; Rösch, F. Synthesis and Labeling of a Squaric Acid Containing PSMA-Inhibitor Coupled to AAZTA^5 for Versatile Labeling with ^{44}Sc, ^{64}Cu, ^{68}Ga and ^{177}Lu. *Appl. Radiat. Isot.* **2020**, *156*, 108867.

(266) Papagiannopoulou, D. Technetium-99m Radiochemistry for Pharmaceutical Applications. *J. Label. Compd. Radiopharm.* **2017**, *60* (11), 502–520.

(267) Sinnes, J.-P. Synthese und radiochemische Evaluierung von Chelatoren für milde Markierungen mit ^{68}Ga, ^{44}Sc Und ^{177}Lu sowie in vitro- Und in vivo- Evaluierung von deren TOC- und PSMA-Derivaten. *Dissertation. - Johannes Gutenberg-University Mainz* **2018**.

(268) Larson, S. R.; Zhang, X.; Dumpit, R.; Coleman, I.; Lakely, B.; Roudier, M.; Higano, C. S.; True, L. D.; Lange, P. H.; Montgomery, B.; Corey, E.; Nelson, P. S.; Vessella, R. L.; Morrissey, C. Characterization of Osteoblastic and Osteolytic Proteins in Prostate Cancer Bone Metastases. *Prostate* **2013**, *73* (9), 932–940.

(269) Ahmadzadehfar, H.; Matern, R.; Baum, R. P.; Seifert, R.; Kessel, K.; Bögemann, M.; Kratochwil, C.; Rathke, H.; Ilhan, H.; Svirydenka, H.; Sathekge, M.; Kabasakal, L.; Yordanova, A.; Garcia-Perez, F. O.; Kairemo, K.; Maharaj, M.; Paez, D.; Virgolini, I.; Rahbar, K. The Impact of the Extent of the Bone Involvement on Overall Survival and Toxicity in MCRPC Patients Receiving [^{177}Lu]Lu-PSMA-617: A WARMTH Multicentre Study. *Eur. J. Nucl. Med. Mol. Imaging* **2021**, *48* (12), 4067–4076.

(270) Yan, L.; Shen, J.; Wang, J.; Yang, X.; Dong, S.; Lu, S. Nanoparticle-Based Drug Delivery System: A Patient-Friendly Chemotherapy for Oncology. *Dose-Response* **2020**, *18* (3), 1559325820936161.

4. Manuscripts

This work is based on different publications and manuscripts. An overview of the manuscript can be found below. A brief summary and the author contributions to each publication or manuscript can be found in front of each publication/manuscript.

4.1 Project A: Hybrid chelator conjugated PSMA inhibitors

4.1.1 Hybrid chelator-based PSMA-radiopharmaceuticals: translational approach

X.X. *, Tilmann Grus*, X.X., X.X., X.X. and X.X.

*Authors contributed equally

Published in *Molecules* 2021, *26*, 6332

4.1.2 [^{68}Ga]Ga-DATA^{5m}-PSMA-617 as diagnostic kit-based counterpart for [^{177}Lu]Lu-PSMA-617

Tilmann Grus, X.X. and X.X.

In preparation for submission

4.2 Project B: Prostate cancer and related bone metastases

4.2.1 DOTA conjugate of bisphosphonate and PSMA inhibitor: A promising combination for therapy of prostate cancer related bone metastases.

Tilmann Grus, X.X., X.X., X.X. and X.X.

Submitted to Frontiers in Nuclear Medicine - Radiopharmacy and Radiochemistry

4.3 Project C: PSMA inhibitor conjugated drug delivery systems

4.3.1 ^{18}F-labeled, PSMA-specific liposomes: promising and PET-traceable tool for future targeted drug delivery in the treatment of prostate cancer.

X.X. [*], Tilmann Grus[*], X.X. [*], X.X. and X.X.

*Authors contributed equally

In preparation for submission

4.3.2 Old drug, new delivery strategy: MMAE repacked

X.X., Tilmann Grus, X.X. and X.X.

In preparation for submission.

4.4 Project D: PSMA inhibitor structure optimisation

4.4.1 Comparison of the binding affinity of squaramide containing lysine-urea-glutamate- and glutamate-urea-glutamate-based PSMA inhibitors

Tilmann Grus, X.X., X.X. and X.X.

In preparation for submission

4.1 Project A: Hybrid chelator conjugated PSMA inhibitors

Hybrid Chelator-Based PSMA Radiopharmaceuticals: Translational Apporach

X.X.*, Tilmann Grus*, X.X., X.X., X.X. and X.X.

*Authors contributed equally

Published in *Molecules* 2021, *26*, 6332

Summary

PSMA is a promising target for diagnosis and therapy of prostate cancer. There are already several PSMA ligands known and applied in nuclear medicine.[1] Nevertheless, these PSMA ligands are still not perfect. For example, [^{177}Lu]Lu-PSMA-617 displays unwanted accumulation in healthy tissues such as kidney or salivary glands.[2] This is dose limiting and can lead to severe side effects. A previous study already indicated that the novel squaric acid based KuE target vector (SA.KuE) shows similar or even better properties.[3]

Another aim is the development of hybrid chelator conjugated PSMA ligands. Hybrid chelators, such as DATA^{5m} or AAZTA^{5} can be radiolabelled fast and under mild conditions, which enables a kit-type application of hybrid chelator containing compounds. Kit-type applications simplify the radiosynthesis.[4] The fresh prepared nuclide just has to be added to the kit vial and after brief shaking, the radiopharmaceutical is ready for use without further purification. Such kit applications are already known in technetium-99m chemistry where they are used as standard for simplification of clinical application.[5] Several studies prove that DATA^{5m} is suitable for kit applications.[4,6]

DATA^{5m}.SA.KuE was synthesized and showed good radiolabelling properties and stabilities with gallium-68. *In vitro* and *in vivo* behaviour was evaluated along with scandium-44 and lutetitium-177 labelled AAZTA^{5}.SA.KuE. Synthesis and radiolabelling was evaluated in a previous study.[7] Both compounds showed two times lower *in vitro* PSMA binding affinity in comparison to PSMA-11, but internalisation ratio and tumour uptake was comparable. The sqauric acid containing compounds displayed a lower kidney uptake. This shows that these compounds have favourable kidney clearance properties, reducing radiation exposure of the kidney. This is especially important regarding therapy with [^{177}Lu]Lu-AAZTA^{5}.SA.KuE, since higher amounts of activity are used in therapy. The study showed that [^{68}Ga]Ga-DATA^{5m}.SA.KuE as well as the theranostic pair [^{44}Sc]Sc-AAZTA^{5}.SA.KuE and [^{177}Lu]Lu-AAZTA^{5}.SA.KuE are promising novel PSMA ligands for future diagnosis and therapy of prostate cancer.

Autor contributions:

Project conception was made by **T. Grus** X.X., X.X. and X.X. Organic synthesis and radiochemical synthesis, *in vivo* stability and evaluation of the radiochemical data was done by **T. Grus** X.X. was responsible for LNCaP cell cultivation, *in vitro* binding affinity assay and internalisation studies and for their data analysis. **T.Grus**, X.X. and X.X. performed the animal studies. X.X. performed the data analysis of the animal studies. **T.Grus** and X.X. wrote and edited the manuscript. All authors reviewed the manuscript. The project was supervised by X.X. and X.X.

References in the summary

(1) Kopka, K.; Benešová, M.; Bařinka, C.; Haberkorn, U.; Babich, J. Glu-Ureido-Based Inhibitors of Prostate-Specific Membrane Antigen: Lessons Learned during the Development of a Novel Class of Low-Molecular-Weight Theranostic Radiotracers. *J. Nucl. Med.* **2017**, *58* (Suppl 2), 17S-26S.

(2) Rupp, N. J.; Umbricht, C. A.; Pizzuto, D. A.; Lenggenhager, D.; Töpfer, A.; Müller, J.; Muehlematter, U. J.; Ferraro, D. A.; Messerli, M.; Morand, G. B.; Huber, G. F.; Eberli, D.; Schibli, R.; Müller, C.; Burger, I. A. First Clinicopathologic Evidence of a Non-PSMA-Related Uptake Mechanism for ^{68}Ga-PSMA-11 in Salivary Glands. *J. Nucl. Med.* **2019**, *60* (9), 1270–1276.

(3) Greifenstein, L.; Engelbogen, N.; Lahnif, H.; Sinnes, J.-P.; Bergmann, R.; Bachmann, M.; Rösch, F. Synthesis, Labeling and Preclinical Evaluation of a Squaric Acid Containing PSMA Inhibitor Labeled with ^{68}Ga: A Comparison with PSMA-11 and PSMA-617. *ChemMedChem* **2020**, *15* (8), 695–704.

(4) Seemann, J.; Waldron, B.; Parker, D.; Roesch, F. DATATOC: A Novel Conjugate for Kit-Type ^{68}Ga Labelling of TOC at Ambient Temperature. *EJNMMI Radiopharm. Chem.* **2017**, *1*, 4.

(5) Papagiannopoulou, D. Technetium-99m Radiochemistry for Pharmaceutical Applications. *J. Label. Compd. Radiopharm.* **2017**, *60* (11), 502–520.

(6) Seemann, J.; Waldron, B. P.; Roesch, F.; Parker, D. Approaching "kit-Type" Labelling with ^{68}Ga: The DATA Chelators. *ChemMedChem* **2015**, *10* (6), 1019–1026.

(7) Greifenstein, L.; Grus, T.; Nagel, J.; Sinnes, J. P.; Rösch, F. Synthesis and Labeling of a Squaric Acid Containing PSMA-Inhibitor Coupled to AAZTA^5 for Versatile Labeling with ^{44}Sc, ^{64}Cu, ^{68}Ga and ^{177}Lu. *Appl. Radiat. Isot.* **2020**, *156*, 108867.

Abstract

Background: Prostate-specific membrane antigen (PSMA) has been extensively studied in the last decade. It became a promising biological target in the diagnosis and therapy of PSMA-expressing cancer diseases. Although there are several radiolabeled PSMA inhibitors available, the search for new compounds with improved pharmacokinetic properties and simplified synthesis is still ongoing. In this study, we developed PSMA ligands with two different hybrid chelators and a modified linker. Both compounds have displayed a promising pharmacokinetic profile.

Methods: DATA^{5m}.SA.KuE and AAZTA^{5}.SA.KuE were synthesized. DATA^{5m}.SA.KuE was labeled with gallium-68 and radiochemical yields of various amounts of precursor at different temperatures were determined. Complex stability in phosphate-buffered saline (PBS) and human serum (HS) was examined at 37 °C. Binding affinity and internalization ratio were determined in i*n vitro* assays using PSMA-positive LNCaP cells. Tumor accumulation and biodistribution were evaluated *in vivo* and *ex vivo* using an LNCaP Balb/c nude mouse model. All experiments were conducted with PSMA-11 as reference.

Results: DATA^{5m}.SA.KuE was synthesized successfully. AAZTA^{5}.SA.KuE was synthesized and labeled according to the literature. Radiolabeling of DATA^{5m}.SA.KuE with gallium-68 was performed in ammonium acetate buffer (1 M, pH 5.5). High radiochemical yields (>98%) were obtained with 5 nmol at 70 °C, 15 nmol at 50 °C, and 60 nmol (50 µg) at room temperature. [^{68}Ga]Ga-DATA^{5m}.SA.KuE was stable in human serum as well as in PBS after 120 min. PSMA binding affinities of AAZTA^{5}.SA.KuE and DATA^{5m}.SA.KuE were in the nanomolar range. PSMA-specific internalization ratio was comparable to PSMA-11. *In vivo* and *ex vivo* studies of [^{177}Lu]Lu-AAZTA^{5}.SA.KuE, [^{44}Sc]Sc-AAZTA^{5}.SA.KuE and [^{68}Ga]Ga-DATA^{5m}.SA.KuE displayed specific accumulation in the tumor along with fast clearance and reduced off-target uptake.

Conclusions: Both KuE-conjugates showed promising properties especially *in vivo* allowing for translational theranostic use.

Keywords: prostate specific membrane antigen PSMA; hybrid chelator; radionuclide diagnosis and therapy

1. Introduction

Prostate-specific membrane antigen (PSMA) has become a very popular target in the diagnosis and treatment of prostate cancer in the last decade. PSMA is a glycoprotein with several functions originating from its glutamate-carboxypeptidase activity. In the central nervous system, PSMA acts as NAALADase, which cleaves the glutamate moiety from the neurotransmitter N-acetyl aspartyl glutamate. However, in the proximal small intestine, this enzyme, called folate hydrolase FOLH1, releases glutamate residues from poly-glutamated folate.[1,2] Besides these physiological functions, PSMA seems to play an important role in prostate carcinogenesis since it is highly expressed in prostate tumor cells. This expression correlates with the aggressiveness and invasiveness of the tumor[3–5], and is a major reason for choosing PSMA as a molecular target in the management of prostate cancer (PCa).

Prostate cancer is the second most common cancer among men and the fifth leading cause of death worldwide.[6,7] However, early detection of PC in a localized stage can significantly reduce its mortality, leading to a 5-year survival rate of more than 90%.[8] In contrast, late-stage tumors are aggressive and almost resistant to available therapies. Metastatic castration-resistant prostate cancer (mCRPC) is one of the most aggressive forms of prostate cancer, with poor outcomes and restricted therapy options.[9] One of the most promising approaches herein is PSMA-targeted radioligand diagnosis and therapy. The unique characteristics of PSMA as a molecular target in combination with the small-molecule PSMA inhibitors as target vectors paved the way for the development of highly sensitive radiopharmaceuticals like the PET radioligand [^{68}Ga]Ga-PSMA-11 and its therapeutic counterpart [^{177}Lu]Lu-PSMA-617.[10,11]

One of the challenges in designing appropriate PSMA inhibitors for theranostic use is balancing the reduction of off-target accumulation in order to minimize the exposure and irradiation of excretory organs and other tissues where physiological PSMA expression is known, such as the salivary glands and the kidneys[12–15], with the development of PSMA ligands which can be easily synthesized and effectively labeled. To address some of these concerns, we developed AAZTA^{5}.SA.KuE and DATA^{5m}.SA.KuE.

Like all PSMA ligands, the herein described PSMA radiopharmaceuticals consist of three parts: chelator, linker moiety, and a KuE-based PSMA-targeting vector.

The chelator is responsible for the introduction of the radionuclide. In this study, the bifunctional hybrid chelators DATA^{5m} (6-pentanoic acid-6-aminoperhydro-1,4-diazapine-triacetate) and AAZTA^{5} (6-pentanoic acid-6-aminoperhydro-1,4-diazepine tetra-acetic acid) are used (Figure 1). With regard to radiometals, hybrid chelators combine the positive complexation properties of acyclic chelators, such as fast complexation kinetics at mild temperatures, with the advantages of cyclic chelators, such as

prolonged complex stability.[16,17] In these structures, the two tertiary diazepine amines provide the cyclic component for complexation. Another amine outside the perhydro-1,4-diazepine backbone provides another complexation unit (acyclic component). The remaining complexation sites are provided by carboxy groups alkylated to the amines.[16,18–20]

AAZTA[5] shows ideal labeling properties for transition metals, such as scandium as well as for lanthanides, e.g., gadolinium and lutetium. Thus, AAZTA[5] is suitable as a chelator for diagnostic use (e.g., scandium-44), as well as for therapeutic applications (e.g., lutetium-177).[17,21,22]

The DATA[5m] chelator has optimal labeling properties at mild conditions for the generator-based PET nuclide gallium-68. Furthermore, the AAZTA and DATA chelators are also suitable for instant kit-labeling applications with e.g., lutetium-177 and gallium-68.[17,23]

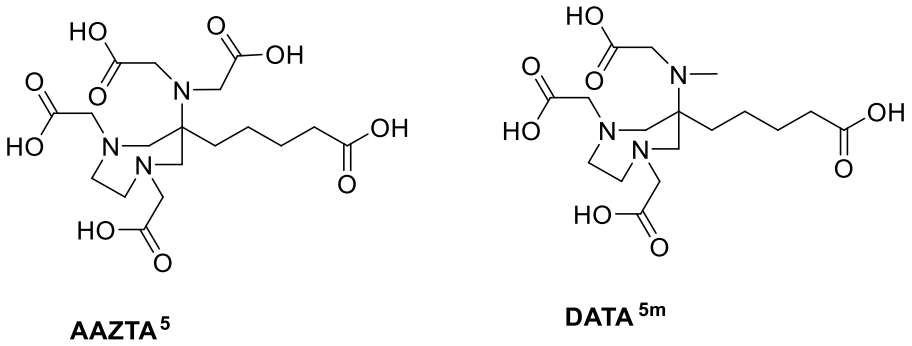

Figure 1: *Bifunctional derivatives of the hybrid chelators AAZTA[5] and DATA[5m].*

Lysine-urea-glutamate (KuE) has been established as a PSMA inhibitor. KuE consists of lysine and glutamate which are both linked to each other via a urea unit. KuE is based on the natural PSMA-substrate NAAG, but cannot be cleaved by the enzyme.[10] Both PSMA-617 and PSMA-11 carry this structural unit as the PSMA-binding entity.[24]

The third structural element found in PSMA radiopharmaceuticals is the linker moiety, connecting the chelator to the urea-based target vector. In addition to the function of coupling, these linkers are usually designed to improve the pharmacokinetics of the compounds.[10] These moieties can interact with the aromatic-binding region of the PSMA binding pocket, leading to an increase in the affinity of the PSMA ligand.[25] The coupling of KuE is achieved via the side-chain amine of the lysine. Usually, amide coupling reactions are used for this purpose. Alternatively, conjugation can be achieved by using square acid diethyl esters (SADE). This group allows two amines to be selectively coupled via asymmetric amidation, forming a squaramide. This simplifies the synthesis in so far as, for example, no protective group chemistry is required, as is the case with standard amide couplings. The coupling reaction is selective with amines only and by controlling the amidation of both squaric acid esters via

pH.[17,26–29] The control of the asymmetric amidation via the pH value can be explained by the different aromaticity and thus the different mesomeric stabilities of the individual intermediates at the different pH values (Figure 2).[30–32]

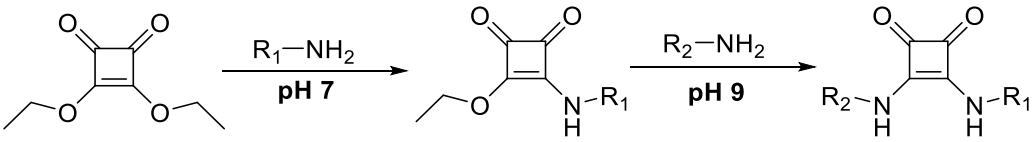

Figure 2: Asymmetric amidation of SADE with different amines. The reactions are driven by change in aromaticity of the different intermediates.

With regard to PSMA radiopharmaceuticals, the use of squaric acid shows another advantage. Squaric acid has an aromatic character and can therefore interact with the aromatic binding region in the PSMA binding pocket resulting in an increased affinity. Greifenstein et al. recently demonstrated that a squaramide containing DOTAGA-KuE derivative is comparable to the standard compounds PSMA-617 and PSMA-11 in terms of *in vitro* binding affinity, tumor accumulation, and *in vivo* kinetics.[28]

2. Results

2.1. Organic synthesis

2.1.1. Synthesis of AAZTA[5].SA.KuE was according to literature.[17]

The synthesis of the DATA chelator is based on the synthesis described by Farkas et al. [16] and Greifenstein et al. [17] It was synthesized according to Figure 3.

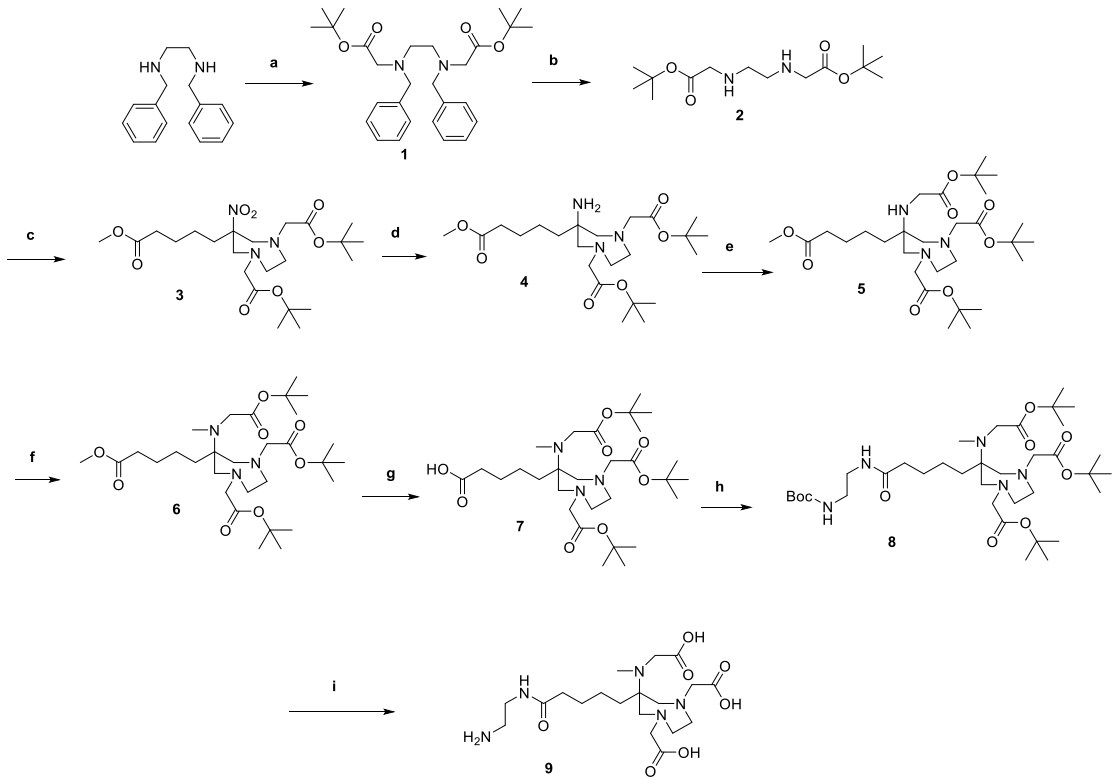

Figure 3: Synthesis of DATA^{5m}: (a) tert-butyl bromoacetate, Na_2CO_3, ACN, 96%; (b) Pd/C, EtOH, formic acid, H_2, 98%; (c) paraformaldehyde, 2-nitrocyclohexanone, MeOH, 77%; (d) Raney®-Nickel, EtOH, H_2, 72%; (e) *tert*-butyl bromoacetate, DIPEA, MeCN, 62%; (f) Formalin (37%), AcOH, $NaBH_4$, ACN, 74%; (g) LiOH, dioxane/H_2O, 84%; (h) tertbutyl(2aminoethyl)carbamate, HATU, DIPEA, ACN, 94%; (i) TFA/DCM, 1:1.

N,N'-dibenzylethyldiamines were first reacted with *tert*-butyl bromoacetate to give the di-alkylated compound **1**. The benzyl protecting groups were then removed by reduction. The diazepane **3** was formed by a double Mannich reaction. For this purpose, 2-nitrocyclohexanone was used, the ring of which was opened using the anion exchanger Amberlyst® A21. In the following Mannich reaction, this ring-opened intermediate reacted with **2** to form the desired diazepane **3**.

After reduction of the nitro group (**4**), *tert*-butyl bromoacetate was added in an undercurrent to give the mono-alkylated compound **5**. The secondary amine of **5** was then methylated in a reductive amination. This led to the protected chelator DATA^{5m} **6**. In order to functionalize **6** with the target vector, however, it was necessary to introduce an ethylenediamine bridge. For this purpose, the methyl ester of **6** was saponified using lithium hydroxide (compound **7**) and the mono Boc-protected ethylenediamine was linked via an amide coupling to get **8**. After an acidic deprotection compound **9** could be conjugated to the target vector using squaric acid.

The PSMA inhibitor lysine-urea-glutamate (KuE) was synthesized and coupled to 3,4-dibutoxycyclobut-3-en-1,2-dione (SADE) according to Figure 4.

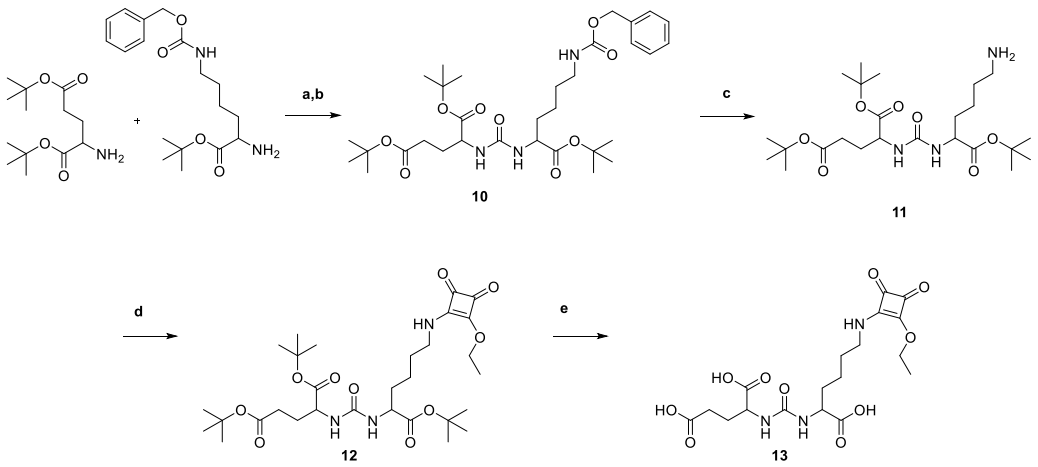

Figure 4: *Synthesis of the PSMA inhibitor lysine-urea-glutamate-squaric acid monoester: (a) N(ε)-benzoyloxycarbonyl-L-lysine, triphosgene, triethylamine DCM, 0 °C; (b) L-glutamic acid di-*tert*-butyl ester hydrochloride, triethylamine, DCM, 41%; (c) Pd/C, MeOH, H_2, 96%; (d) 3,4-dibutoxycyclobut-3-en-1,2-dione, 0.5 M phosphate buffer pH 7, ethyl acetate, 77%; (e) TFA/DCM, 1:1, 83%.*

For the introduction of the urea unit, the amino group of the protected lysine was transformed into an isocyanate using triphosgene. The isocyanate was then reacted with *tert*-butyl protected glutamate and the protected PSMA inhibitor lysine-urea-glutamate **10** was obtained and followed by reductive deportation of the lysine side chain, yielding **11**. This compound was then coupled to SADE in phosphate buffer at pH 7. Acidic deprotection of the protected compound **12** led to the couplable PSMA inhibitor lysine-urea-glutamate-squaric acid monoester **13** (KuE.SAME).

The free primary amine of DATA^{5m} (**9**) was then coupled to the free coupling side of KuE.SAME (**13**) in 0.5 M phosphate buffer at pH 9 to obtain the final compound DATA^{5m}.SA.KuE (**14**) (Figure 5).

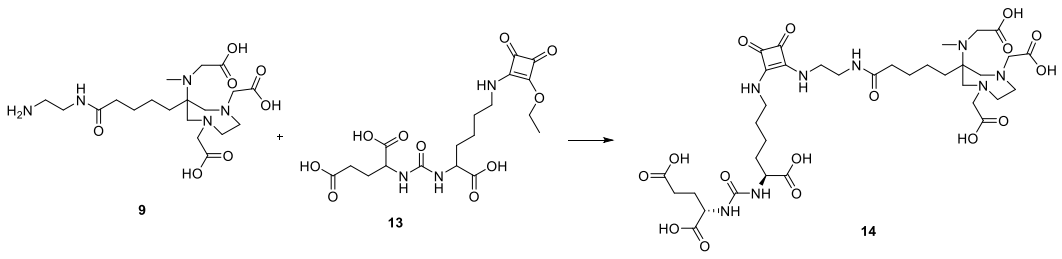

Figure 5: Synthesis of DATA^{5m}.SA.KuE (**14**) 0.5 M phosphate buffer pH 9, 10%.

2.1.2. Radiolabelling

Radiolabelling of AAZTA^5.SA.KuE with scandium-44 and lutetium-177 was performed according to the literature.[17]

DATA^{5m}.SA.KuE was radiolabeled with gallium-68 in ammonium acetate buffer (1 M, pH 5.5), varying amounts of precursor (5 nmol to 60 nmol), and different temperatures (room temperature to 70 °C).

Labeling was carried out in triplicate with 30–50 MBq of gallium-68. Figure 6A shows the kinetic studies of the gallium-68-radiolabeling of DATA^{5m}.SA.KuE. The lower the quantity of precursor used, the higher the temperature required to obtain quantitative radiochemical yields (RCY). Labeling of 10 nmol at 50 °C only achieved a RCY of 56% after 15 minutes. The increase to 15 nmol at 50 °C results in quantitative RCY (> 99%). The increase of temperature even allowed the quantitative labeling (> 99% RCY) of 5 nmol. Furthermore, 50 µg (60 nmol) can be radiolabeled in yields of over 99% with gallium-68 even at room temperature. The high radiochemical yield and high purity of [^{68}Ga]Ga-DATA^{5m}.SA.KuE was confirmed by radio-HPLC (Figure 6B).

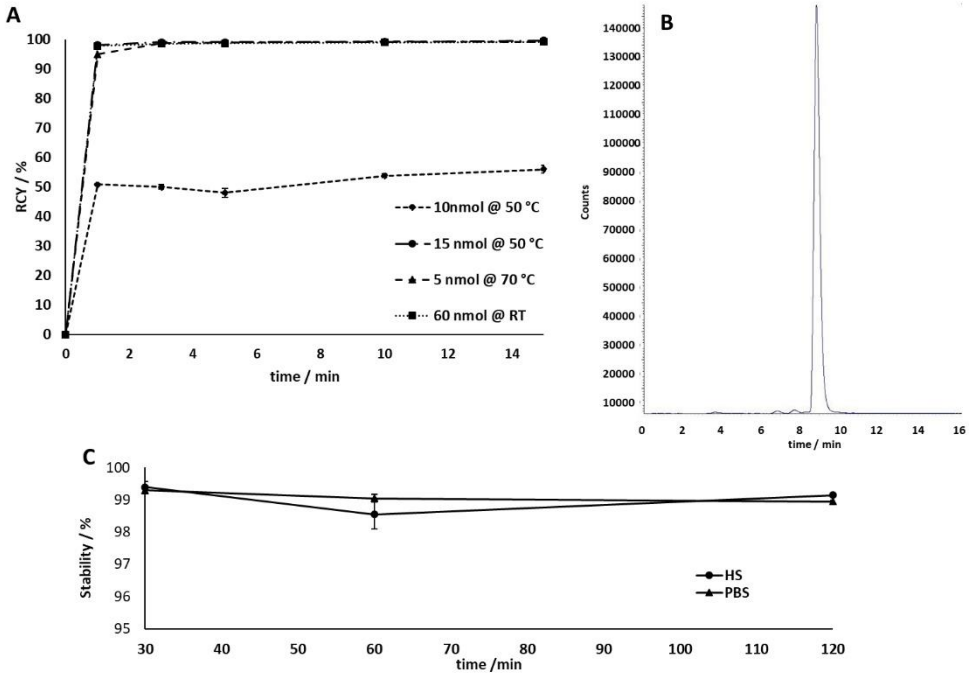

Figure 6: ***(A)*** Kinetic studies of ^{68}Ga-radiolabeling of DATA^{5m}.SA.KuE for various amounts of precursor and different temperatures. Labeling of 15 nmol at 50 °C, 5 nmol at 70 °C and 60 nmol at RT resulting in quantitative RCYs after one minute. Radiolabeling of 10 nmol at 50 °C results in a RCY of 56% after 15 minutes. (**B)** Radio-HPLC of [^{68}Ga]Ga-DATA^{5m}.SA.KuE. t_R (free gallium-68) = 2.0 min; t_R ([^{68}Ga]Ga-DATA^{5m}.SA.KuE) = 8.8 min. Radio-HPLC confirmed purity and high RCY of [^{68}Ga]Ga-DATA^{5m}.SA.KuE. (**C**) Stability studies for [^{68}Ga] Ga-DATA^{5m}.SA.KuE complex in human serum (HS) and phosphate buffered saline (PBS) of intact conjugate at different time points.

Studies of the complex stability were performed in human serum (HS) and phosphate buffered saline (PBS). In both media, [^{68}Ga]Ga-DATA^{5m}.SA.KuE showed a stability of >98% over a period of 120 minutes (Figure 6C).

2.2. In vitro Studies

2.2.1. PSMA Binding Affinity

The PSMA binding affinity of DATA^{5m}.SA.KuE and AAZTA^{5}.SA.KuE, as well as PSMA-11, was determined in a competitive radioligand assay using PSMA-positive LNCaP cells that were incubated with 0.75 nM [^{68}Ga]Ga-PSMA-10 in the presence of 12 increasing concentrations of the non-labeled SA-conjugated compounds. The measured radioactivity values were plotted against the concentrations of the SA conjugates (Figure 7). IC_{50} values were determined using GraphPad Prism 9 (Table 1). AAZTA^{5}.SA.KuE and DATA^{5m}.SA.KuE showed similar binding affinities while PSMA-11 seems to have two-fold higher affinity *in vitro*.

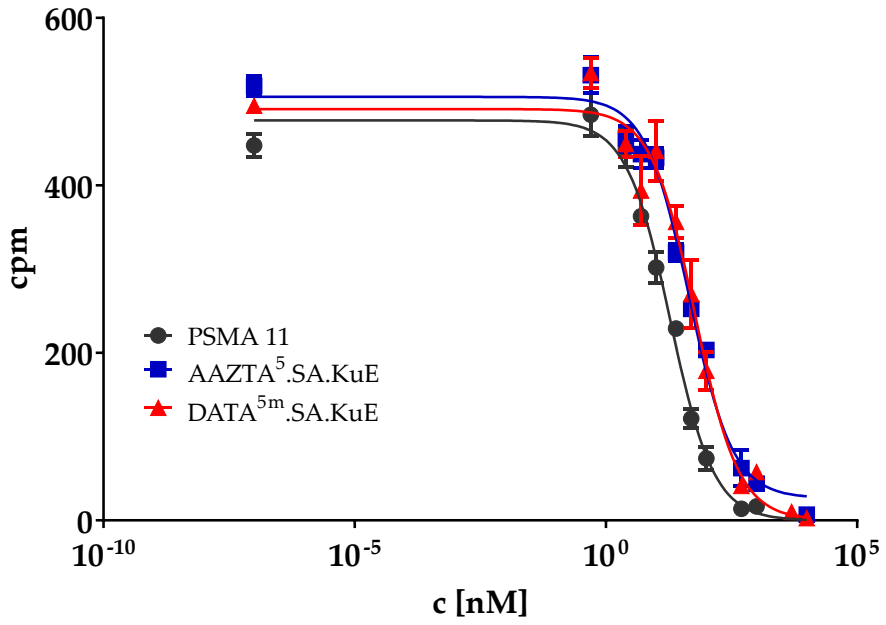

Figure 7: Inhibition curve of AAZTA^{5}.SA.KuE, DATA^{5m}.SA.KuE and PSMA-11. cpm: counts per minute.

Table 1: IC_{50} values of the investigated compounds. Data represented as mean ± SD (n = 3).

Compound	IC_{50} [nM]
DATA^{5m}.SA.KuE	51.1 ± 5.5
AAZTA^{5}.SA.KuE	52.1 ± 4.0
PSMA-11	26.2 ± 2.4

2.2.2. Internalization Ratio

PSMA ligands are internalized upon binding to PSMA, probably via clathrin-mediated endocytosis.[33,34] To determine the PSMA-specific cellular uptake of the developed PSMA ligands, we measured both the surface-bound and internalized radioactivity in PSMA-positive LNCaP cells at four different conditions; at 37 °C with and without blocking with the potent PSMA inhibitor PMPA (2-Phosphonomethyl pentanedioic acid) [35–37], and at 4 °C with and without blocking with PMPA. Results are plotted in Figure 8. [^{68}Ga]Ga-DATA^{5m}.SA.KuE displayed the highest internalization ratio 6.6 ± 0.6%, whereas the uptake fractions of [^{44}Sc]Sc-AAZTA^{5}.SA.KuE and [^{68}Ga]Ga-PSMA-11 were slightly lower (4.8% and 5.2%, respectively). PSMA-specific uptake was mainly reduced at 4 °C.

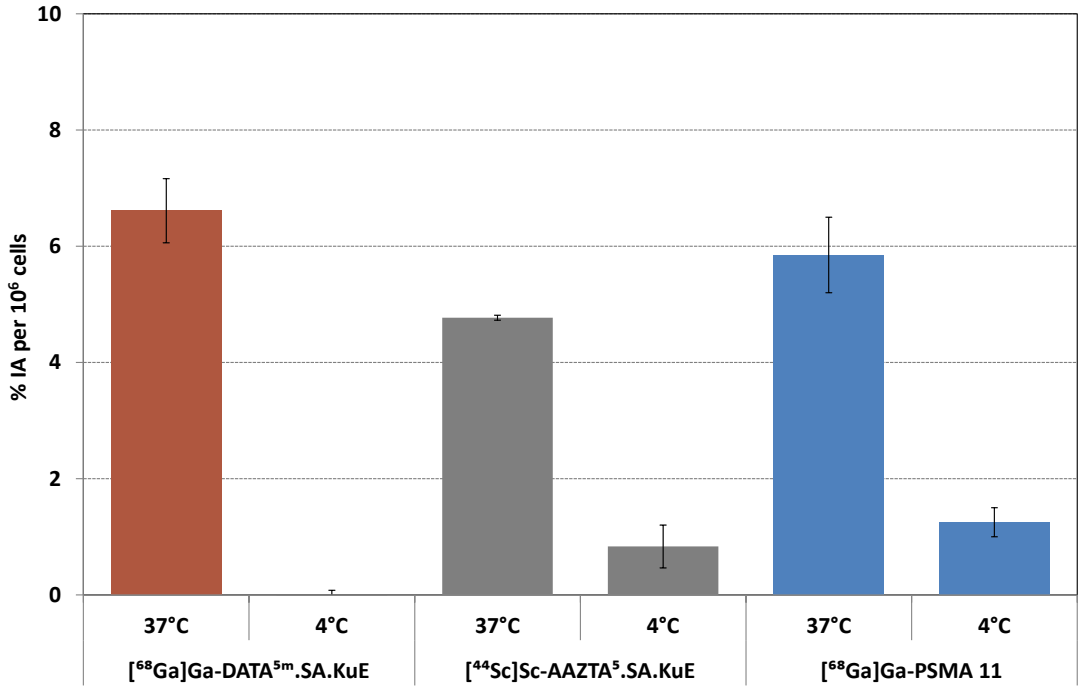

Figure 8: Internalization ratio of [^{68}Ga]Ga-DATA^{5m}.SA.KuE and [^{44}Sc]Sc-AAZTA^{5}.SA.KuE with [^{68}Ga]Ga-PSMA-11 as reference; % injected dose per 10^6 LNCaP cells.

2.3. Animal studies

In order to evaluate the *in vivo* behavior of the SA.KuE conjugates, an LNCaP-xenograft model was used. Labeling of AAZTA^{5}.SA.KuE with the different nuclides scandium-44 and lutetium-177 seemed to have no impact on the pharmacokinetic properties of the conjugates, since there were no significant differences observed in the biodistribution data (Figure 9). Tumor accumulation values of all four compounds were similar, 3.92 ± 0.50% ID/g, 5.41 ± 0.83% ID/g, 4.43 ± 0.56% ID/g and 5.52 ± 0.75% ID/g for [^{44}Sc]Sc-AAZTA^{5}.SA.KuE, [^{177}Lu]Lu-AAZTA^{5}.SA.KuE, [^{68}Ga]Ga-DATA^{5m}.SA.KuE and [^{68}Ga]Ga-PSMA-11 respectively. The higher kidney uptake of [^{68}Ga]Ga-PSMA-11 (73.39 ± 18.77% ID/g) is

noteworthy compared to the uptake of the SA.KuE conjugates (20.69 ± 7.24% ID/g, 22.70 ± 0.90% ID/g, 13.63 ± 6.81% ID/g for [^{44}Sc]Sc-AAZTA^{5m}.SA.KuE, [^{177}Lu]Lu-AAZTA^{5m}.SA.KuE and [^{68}Ga]Ga-DATA^{5}.SA.KuE respectively). Both tumor and kidney uptake of [^{68}Ga]Ga-DATA^{5}.SA.KuE were found to be PSMA-specific, since they could be blocked by co-injection of PMPA as seen in Figure 10.

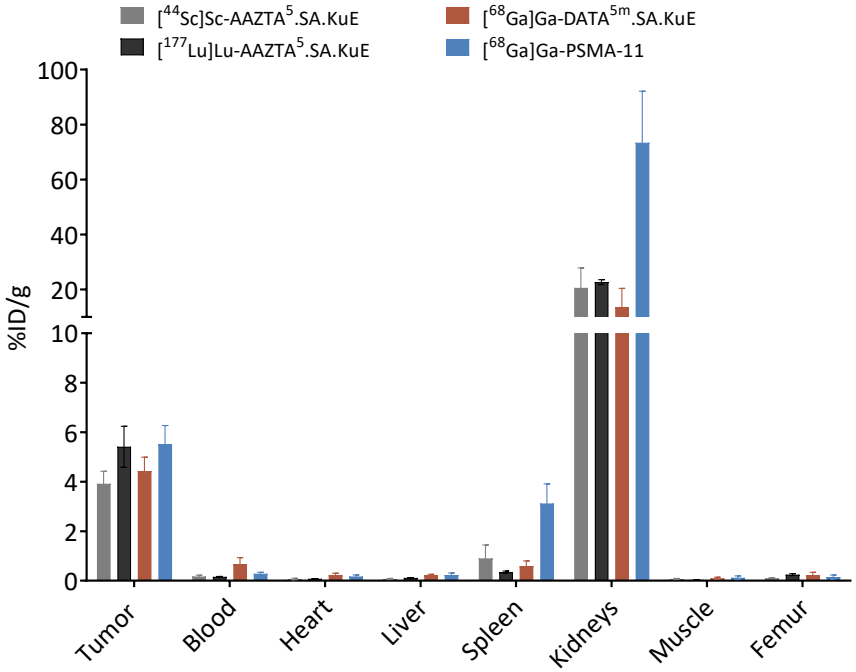

Figure 9: Ex vivo biodistribution data of [^{44}Sc]Sc-AAZTA^{5}.SA.KuE, [^{177}Lu]Lu-AAZTA^{5}.SA.KuE, [^{68}Ga]Ga-DATA^{5m}.SA.KuE and [^{68}Ga]Ga-PSMA-11 in LNCaP tumor-bearing Balb/c nude mice 1 h p.i. %ID/g: % injected dose per gram. Values are mean ± SD.

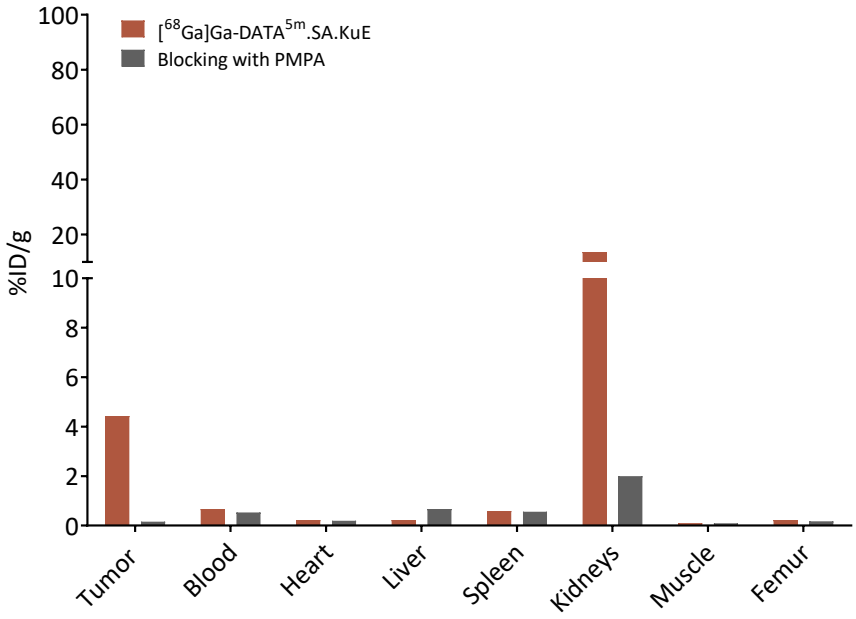

Figure 10: Ex vivo biodistribution of [^{68}Ga]Ga-DATA^{5m}.SA.KuE compared to organ accumulation after co-injection with an access PMPA.

To further understand the pharmacokinetics of the developed PSMA ligands, we performed µPET-scans with the same xenograft model (Figure 11). Tumor accumulation of all three compounds was very similar. The kidney uptake of [^{68}Ga]Ga-DATA^{5}.SA.KuE was remarkably lower than the reference compound [^{68}Ga]Ga-PSMA-11. This finding correlates with the results obtained from the time–activity curves of both compounds (Figure 12). Herein, the radioactivity concentration of [^{68}Ga]Ga-DATA^{5m}.SA.KuE decreased continuously 10 min p.i. while the concentration in the tumor remained constant. However, the radioactivity concentration of [^{68}Ga]Ga-PSMA-11 remained at a higher level during the period of the scan. As demonstrated in the µPET scans, uptake in the tumor as well as in the kidney was PSMA-specific. After co-injection of PMPA, almost no radioactivity could be detected (Figure 11).

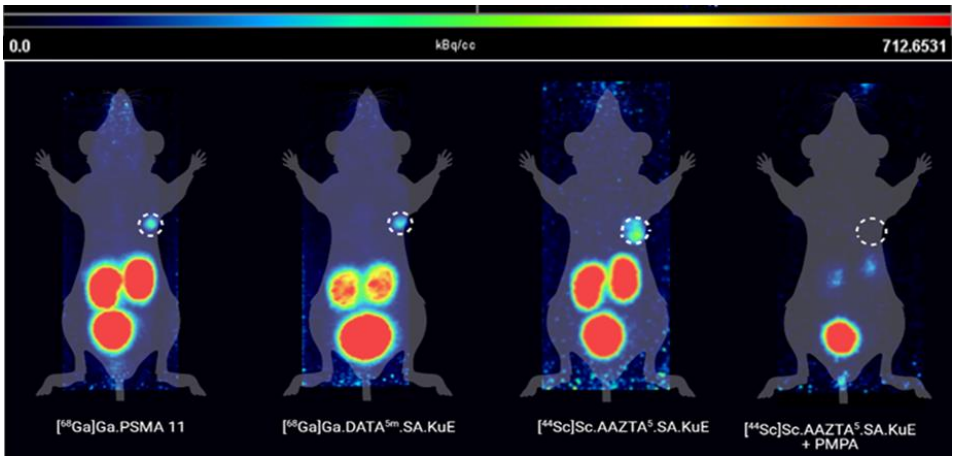

Figure 11: Maximum intensity projections of µPET scans 1 h p.i. of (**a**) [^{68}Ga]Ga-PSMA-11, (**b**) [^{68}Ga]Ga-DATA^{5m}.SA.KuE, (**c**) [^{44}Sc]Sc-AAZTA^{5}.SA.KuE and (**d**) co-injection of [^{44}Sc]Sc-AZTA^{5}.SA.KuE and PMPA (tumor circled).

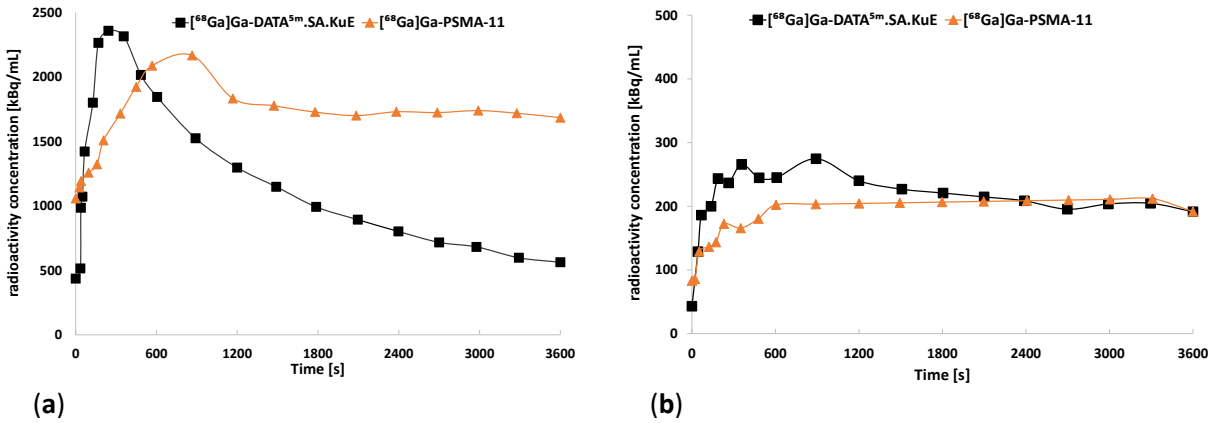

Figure 12: Time–activity curves of the uptake of [^{68}Ga]Ga-DATA^{5m}.SA.KuE and [^{68}Ga]Ga-PSMA-11 in the kidneys (**a**) and the tumor (**b**) over the total period of the µPET scan.

3. Discussion

The discovery of PSMA as molecular target in the diagnosis and therapy of prostate cancer, as well as the application of radiolabeled PSMA inhibitors, have revolutionized the management of this disease resulting in a significant improvement especially in staging and assessment of prostate cancer.[38] Although several PSMA ligands have been developed over the last decades, the search for novel tracers with optimized pharmacokinetic properties particularly for therapeutic purposes is still present, since some of the clinically used PSMA radioligand therapeutics e.g., [^{225}Ac]Ac-PSMA-617 display some severe side effects, like xerostomia.[12,13,39]

To determine the effect of the chelator on the PSMA binding affinity and the internalization ratio of PSMA ligands, we synthesized two PSMA inhibitors with different hybrid chelators. In the cell-based assays, both DATA^{5m}.SA.KuE and AAZTA^{5}.SA.KuE showed similar binding affinity and internalization ratios, indicating that an exchange of DATA^{5m} against AAZTA^{5} had no impact on either the binding affinity or on the internalization ratio in PSMA-positive LNCaP cells. These findings correlate with the results published by Sinnes et al., who investigated the influence of the exchange of DOTA chelator in DOTA-PSMA-617 against AAZTA^{5}. Both DOTA-PSMA-617 and AAZTA^{5}-PSMA-617 displayed similar *in vitro* binding affinities and internalization ratios in LNCaP cells.[40] However, the reported binding affinities and internalization ratios of AATA^{5}-PSMA-617 and DOTA-PSMA-617 were higher than those of the SA.KuE conjugates. In particular, [^{44}Sc]Sc-PSMA-617 seems to display high PSMA-binding affinity as published by several groups.[41,42] Since PSMA-617 was not commercially available at the time this study was performed, PSMA-11 was used as reference.

However, PSMA-11 displayed also higher binding affinity *in vitro* which could be due to the better interaction with the PSMA binding pocket. In contrast, the internalization ratio of PSMA-11 was similar to these of the SA.KuE-conjugates. Interestingly, the investigated internalization fraction of [^{68}Ga]Ga-PSMA-11 was noticeably lower compared to the ratio described in literature [42,43] which could be due to differences in study design and setup. The PSMA-specificity of binding and uptake in LNCaP cells and LNCaP tumors could be demonstrated for all herein investigated PSMA-inhibitors by blocking PSMA receptors with the potent inhibitor PMPA.

In order to evaluate the pharmacokinetic behavior of our compounds and to compare them with PSMA-11, we performed animal studies using an LNCaP xenograft model.

AAZTA^{5}.SA.KuE was labeled with the positron emitter scandium-44 and β^--emitterlutetium-177. Both radiotracers displayed similar biodistribution data, indicating that both isotopes do not impact the pharmacokinetic properties of the PSMA radioligand. This result makes this pair ideal for theranostic use. In addition, [^{68}Ga]Ga-DATA^{5m}.SA.KuE equally showed a promising biodistribution profile and a

good imaging contrast. Surprisingly, although PSMA-11 showed a two-fold higher binding affinity *in vitro*, tumor accumulation was similar to the SA.KuE-conjugates. Furthermore, the kidney uptake of [^{68}Ga]Ga-PSMA-11 was significantly higher than the SA.KuE-conjugated compounds. [^{68}Ga]Ga-DATA^{5m}.SA.KuE, [^{44}Sc]Sc-AAZTA^{5}.SA.KuE and [^{177}Lu]Lu-AAZTA^{5}.SA.KuE. Thus, these compounds seem to display a rapid renal clearance along with a good tumor accumulation. However, the tumor uptake of the SA.KuE conjugates was lower than that of the gallium-68 and lutetium-177 labeled PSMA-617 radioligands.[10,11] Ghiani et al. recently described a novel scandium-44 labeled PSMA radioligand with even higher tumor accumulation than the PSMA-617 counterpart.[41] Nevertheless, a direct comparison between the presented results and those reported by other groups is not possible because of the differences in xenograft models and experimental setups.

4. Materials and Methods

4.1. General

All chemicals were purchased from Sigma-Aldrich, Merck, Fluka, AlfaAesar, VWR, AcrosOrganics, TCI, Iris Biotech and Fisher Scientific and used without purification. Dry solvents were obtained from Merck and VWR, deuterated solvents for NMR spectra from Deutero. Thin layer chromatography was performed with silica gel 60 F254 coated aluminum plates from Merck. Evaluation was carried out by fluorescence extinction at λ = 254 nm and staining with potassium permanganate. The radio TLCs were evaluated using a CR-35 Bio test imager (Elysia-Raytest, Belgium)) from Raytest and the AIDA software (Elysia-Raytest, Belgium). The ^{1}H and ^{13}C NMR measurements were performed on an Avance III HD 300 spectrometer (Bruker Corporation, Billerica, MA, USA) (300 MHz, 5mm BBFO sample head with z-gradient and ATM and BACS 60 sample changer), an Avance II 400 (Bruker Corporation, Billerica, MA, USA) (400 MHz, 5 mm BBFO sample head with z-Gradient and ATM and SampleXPress 60 sample changer), and an Avance III 600 spectrometer (Bruker Corporation, Billerica, MA,USA) (600 MHz, 5mm TCI CryoProbe sample head with z-Gradient and ATM and SampleXPress Lite 16 sample changer). The LC/MS measurements were performed on an Agilent Technologies 1220 Infinity LC system coupled to an Agilent Technologies 6130B Single Quadrupole LC/MS system. Semi-preparative HPLC purification was performed on a 7000 series Hitachi LaChrom (Hitachi, Chiyoda, Japan).

4.2. Organic Synthesis

DATA^{5m} was synthesized according to the procedure described by Farkas et al.[16] and Greifenstein et al.[17]

N,N'-Dibenzyl-*N,N'*-di-(tert-butylacetate)-ethylendiamine (**1**)

N,N'-dibenzylethylendiamine (2.90 mL, 3.00 g, 12.50 mmol) and sodium carbonate (5.10 g, 48.70 mmol) were dissolved in acetonitrile (50 mL) and stirred for 30 min at room temperature. *Tert*-butyl bromoacetate (3.60 mL, 4.60 g, 23.70 mmol) in acetonitrile (10 mL) was added dropwise at room temperature. The reaction mixture was stirred overnight at 90 °C and filtered. The solvent was evaporated under reduced pressure. The product was purified by column chromatography (hexane/ethyl acetate; 6:1, R_f = 0.37) and obtained as a colorless solid (5.73 g, 12.2 mmol, 96%).

^{1}H-NMR (400 MHz, $CDCl_3$): δ [ppm] = 7.34–7.21 (m, 10H), 3.78 (s, 4H), 3.26 (s, 4H), 2.82 (s, 4H), 1.44 (s, 18H).

^{13}C-NMR (400 MHz, CDCl3): δ [ppm] = 171.03, 139.18, 129.05, 128.30, 127.10, 80.86, 58.39, 55.27, 51.73, 28.24.

MS (ESI$^+$): 469.4 $[M + H]^+$, calculated for $C_{28}H_{40}N_2O_4$: 468.30 $[M]^+$.

N,N'-di-(*tert*-butylacetate)-ethylendiamine (**2**)

Product **1** (2.3 g; 5.60 mmol) was dissolved in abs ethanol (15 mL) and formic acid (0.43 mL, 0.52 g, 11.0 mmol). To this solution palladium on activated carbon (416 mg, 16% wt) was added and the solution was saturated, kept and stirred overnight with hydrogen. Pd/C was filtered over celite and the solvent was evaporated under reduced pressure. The product (1.58 mg, 5.5 mmol, 98%) was used without further purification.

MS (ESI$^+$): 289.3 $[M + H]^+$, calculated for $C_{14}H_{28}N_2O_4$: 288.36 $[M]^+$.

1,4-Di(*tert*-butylacetate)-6-methyl-6-nitroperhydro-1,4-diazepane (**3**)

2-Nitrocyclohexanone (1.70 g, 12 mmol) and Amberlyst® A21 (2 mass equivalents) were dissolved in methanol (30 ml) and stirred at 90 °C for 1 h. Paraformaldehyde (1.30 g, 42.3 mmol) and Product (2) (3.50 g, 12 mmol) were added. The solution was heated overnight under reflux. The solvent was evaporated under reduced pressure. The product was purified by column chromatography (hexane/ethyl acetate; 2:1, R_f = 0.33) and obtained as a yellowish oil (4.52 g, 9.28 mmol, 77%).

^{1}H-NMR (400 MHz, $CDCl_3$): δ [ppm] = 3.65 (s, 3H), 3.60 (d, *J* = 14,6 Hz, 2H), 3.45 (d, *J* = 17,3 Hz, 2H), 3.30 (d, *J* = 17,3 Hz, 2H), 3.12 (d, *J* = 14,6 Hz, 2H), 2.84 (m, 4 H), 2.27 (t, 2H), 1.83 (m, 2H), 1.57 (m, 2H), 1.46 (s, 18H), 1.18 (m, 2H).

^{13}C-NMR (400 MHz, $CDCl_3$): δ [ppm] = 173.73, 170.92, 95.12, 81.31, 61.57, 61.18, 56.87, 51.68, 37.27, 33.71, 28.35, 24.82, 22.99.

MS (ESI^+): 488.3 $[M + H]^+$, calculated for $C_{23}H_{41}N_3O_8$: 487.29 $[M]^+$.

1,4-Di(*tert*-butylacetate)-6-methylpentanoate-6-amino-perhydro-1,4-diazepane (**4**)

Compound **3** (4.50 g, 9.30 mmol) was dissolved in abs. ethanol (40 mL). Raney® nickel was added and the solution was saturated, kept and stirred for four days with hydrogen at 40 °C. The nickel was filtered over celite and the solvent was evaporated under reduced pressure. Compound **4** (3.92 g, 8.60 mmol, 72%), was obtained as a greenish oil and used without further purification.

MS (ESI^+): 458.3 $[M + H]^+$, calculated for $C_{23}H_{43}N_3O_6$: 457.32 $[M]^+$.

1,4-Di(*tert*-butylacetate)-6-methylpentonate-6-amino-*tert*-butylacetate-perhydro-1,4-diazepane (**5**)

Compound **4** (1.30 g, 2.84 mmol) and *N,N*-diisopropylethylamine (483 µL, 367 mg, 2.84 mmol) were dissolved in dry acetonitrile (20 mL) and stirred for 20 min at room temperature. *Tert*-butyl bromoacetate (538 µL, 720 mg, 3.69 mmol) was added dropwise and stirred overnight at room temperature. The solvent was evaporated under reduced pressure. The product was purified by column chromatography (cyclohexane/ethyl acetate; 3:1 + 3% trimethylamine, R_f = 0.34) and obtained as a yellowish oil (1.01 g, 1.77 mmol, 62%).

^{1}H-NMR (400 MHz, $CDCl_3$): δ [ppm] = 3.65 (s, 3H), 3.29 (s, 4H), 3.21 (s, 2H), 2.83–2.60 (m, 8H), 2.30 (dd, *J* = 8.9, 6.3 Hz, 2H), 1.90 (s br, 1H), 1.62–1.54 (m, 2H), 1.46 (s, 9H), 1.44 (s, 18H), 1.32–1.23 (m, 4H).

MS (ESI^+): 572.4 $[M + H]^+$, calculated for $C_{29}H_{53}N_3O_8$: 571.38 $[M]^+$.

1,4-Di(*tert*-butylacetate)-6-methylpentonate-6-(amino(methyl)-*tert*-butylacetate)-perhydro-1,4 diazepane (**6**)

Compound **5** (1.00 g, 1.75 mmol), formalin solution (482 µL, 526 mg, 6.47 mmol), and acetic acid (300 µL, 315 mg, 5.25 mmol) were dissolved in dry acetonitrile (20 mL) and stirred at room temperature for 30 min. Sodium borhydride (200 mg, 5.29 mmol) was added portion-wise over 30 min. The reaction solution was stirred for 2 hours at room temperature. Water (25 mL) was added and extracted with chloroform (4 × 50 mL). The organic phase was separated and dried over sodium sulfate and evaporated under reduced pressure. The product was purified by column chromatography

(cyclohexane/ethyl acetate; 5:1 + 2% trimethylamine, R_f = 0.28) and obtained as colorless oil (0.76 g, 1.39 mmol, 74%).

^{1}H-NMR (400 MHz, $CDCl_3$): δ [ppm] = 3.65 (s, 3H), 3.42 (s, 2H), 3.32–3.18 (m, 4H), 2.93 (d, *J* = 14.0 Hz, 2H), 2.83–2.73 (m, 2H), 2.70–2.58 (m, 4H), 2.35−2.24 (m, 5H), 1.63–1.48 (m, 4H), 1.45 (s, 9H), 1.44 (s, 18H), 1.41–1.22 (m, 2H).

MS (ESI$^+$): 586.4 $[M + H]^+$, calculated for $C_{30}H_{55}N_3O_8$: 585.40 $[M]^+$.

1,4-Di(*tert*-butylacetate)-6-pentanoicacid-6-(amino(methyl)-*tert*-butylacetate)-perhydro-1,4-diazepane (**7**)

Compound **6** (0.75 g, 1.28 mmol) was dissolved in a 1,4-dioxane/water (2:1) mixture. Then, 1 M lithium hydroxide solution (1.92 mL, 1.92 mmol) was added and stirred for 7 days. After 2, 4, and 6 days 1 M lithium hydroxide solution (0.32 mL, 0.32 mmol) was added. 1,4-dioxane was evaporated under reduced pressure. The remaining water phase was extracted with chloroform (5 × 50 mL). The organic phase was washed with 1 M sodium hydrogen carbonate solution (25 mL) and brine (2 × 25 mL) and dried over sodium sulfate and evaporated under reduced pressure. The product (615 mg, 1.07 mmol, 84%) was obtained as a yellowish oil.

^{1}H-NMR (400 MHz, $CDCl_3$): δ [ppm] = 3.44 (s, 2H), 3.25 (d, *J* = 2.2 Hz, 4H), 2.93 (d, *J* = 14.0 Hz, 2H), 2.82–2.73 (m, 2H), 2.71–2.61 (m, 4H), 2.34 (t, *J* = 7.7 Hz, 2H), 2.27 (s, 3H), 1.65–1.51 (m, 4H), 1.45 (s, 18H), 1.44 (s, 9H), 1.43–1.21 (m, 2H).

^{13}C-NMR (400 MHz, $CDCl_3$): δ [ppm] = 178.46, 172.53, 170.98, 81.02, 80.44, 77.36, 62.86, 62.59, 62.48, 59.02, 54.21, 37.49, 36.92, 34.17, 28.37, 28.27, 25.71, 21.97.

MS (ESI$^+$): 572.4 $[M + H]^+$, calculated for $C_{29}H_{53}N_3O_8$: 571.38 $[M]^+$.

1,4-Di(*tert*-butylacetate)-6-((5-(2-((2-ethoxy-3,4-dioxocyclobut-1-en-1yl)amino-ethyl)amino)-5-oxopentyl)-6-(amino(methyl)-tert-butylacetate)-perhydro-1,4-diazepane (**8**)

Compound **7** (100 mg, 0.175 mmol), HATU (66.5 mg, 0.175 mmol), and DIPEA (90 µl, 69 mg, 0.525 mmol) were dissolved in dry acetonitrile (2 mL) and stirred for 15 min at room temperature. *Tert*-butyl(2-aminoethyl) carbamate (45 µL, 46 mg, 0.280 mmol) was added to the solution and stirred over night at room temperature. The solvent was evaporated under reduced pressure. The product was purified by column chromatography (dichloromethane/methanol; 20:1, R_f = 0.22) and obtained as a colorless oil (118.4 mg, 0.166 mmol, 94%).

^{1}H-NMR (400 MHz, $CDCl_3$): δ [ppm] = 6.34 (br, 1H), 5.26 (br, 1H), 3.60 (s, 4H), 3.38-3.34 (m, 2H), 3.26-3.24 (m, 2H), 3.21 (s, 4H), 2.96 (d, *J* = 14,1 Hz, 2H), 2.75-2.63 (m, 2H), 2.66-2.63 (m, 2H), 2.59 (d, *J* = 14,1 Hz, 2H), 2.19 (t, 2H), 1.62-1.53 (m, 4H), 1.43 (s, 18H), 1.42 (s, 27H), 1.28-1.20 (m, 2H).

^{13}C-NMR (400 MHz, $CDCl_3$): δ [ppm] = 174.38, 173.31, 172.80, 165.88, 82.85, 82.77, 63.44, 62.48, 62.05, 55.48, 54.47, 47.11, 40.81, 39.87, 35.55, 29.82, 28.53, 28.32, 28.14, 27.91, 26,17, 23.41.

MS (ESI$^+$): 714.5 $[M + H]^+$, calculated for $C_{36}H_{67}N_5O_9$: 713.49 $[M]^+$.

1,4-Di(acetate)-6-((5-(2-(aminoethyl)amino)-5-oxopentyl)-6-(amino(methyl)-acetate)-perhydro-1,4-diazepane (**9**)

Compound **8** (20 mg, 0.028 mmol) was dissolved in a solution of dichloromethane and triflouroacetic acid (2 mL, 1:1) and stirred over night at room temperature. The solvent was evaporated under reduced pressure and used without further purification.

MS (ESI$^+$): 446.2 $[M + H]^+$, calculated for $C_{19}H_{35}N_5O_7$: 445.25 $[M]^+$.

2-[3-(5-benzyloxycarbonylamino-1-tert-butoxycarbonyl-pentyl)-ureido]-pentanedioic acid di-*tert*-butyl ester (**10**)

Triphosgene (420 mg, 1.40 mmol) was dissolved in dichloromethane (5 mL) and cooled to 0 °C. A solution of N(ε)-benzoyloxycarbonyl-L-lysine (1.42 g, 3.80 mmol) and triethylamine (1.05 mL, 765 mg, 7.60 mmol) in dichloromethane (25 mL) was added dropwise over a period of 3 hours at 0 °C. The reaction mixture was stirred for 40 minutes and L-glutamic acid di-*tert*-butyl ester hydrochloride (1.13 g, 3.80 mmol) and triethylamine (1.05 mL, 765 mg, 7.60 mmol) in dichloromethane (20 mL) was added. The solution was stirred over night at room temperature. The solution was evaporated under reduced pressure. Ethyl acetate (25 mL) was added. The organic layer was washed with saturated $NaHCO_3$-solution (2 × 10 mL) and brine (2 × 10 ml), dried over sodium sulfate and evaporated under reduced pressure. The residue was purified by column chromatography (hexane/ethyl acetate; 20:1, R_f = 0.26) and the product was obtained as a colorless oil (357.6 mg, 0.58 mmol, 41%).

^{1}H-NMR (300 MHz, $CDCl_3$): δ [ppm] = 7.38–7.22 (m, 5H), 5.16 (d, *J* = 13.5 Hz, 1H), 5.09 (d, *J* = 3.2 Hz, 2H), 4.32 (dt, *J* = 7.5, 5.2 Hz, 2H), 3.16 (s, 2H), 2.40–2.15 (m, 2H), 1.93–1.68 (m, 2H), 1.43 (m, 29H).

^{13}C-NMR (300 MHz, $CDCl_3$): δ [ppm] = 172.54, 172.25, 172.15, 157.09, 156.61, 136.67, 128.47, 128.04, 128.01, 82.29, 81.84, 80.65, 77.24, 66.56, 53.38, 53.03, 40.63, 32.53, 31.52, 29.36, 28.28, 28.07, 28.00, 22.26.

MS (ESI$^+$): 622.4 $[M + H]^+$, 644.4 $[M + Na]^+$, calculated for $C_{32}H_{51}N_3O_9$: 621.36 $[M]^+$.

2-[3-(amino-1-tert-butoxycarbonyl-pentyl)-ureido]-pentanedioic acid di-*tert*-butyl ester (**11**)

Compound **10** (337.6 mg, 0.55 mmol) was dissolved in methanol (3 mL). To this, solution palladium on activated carbon (22 mg) was added and the solution was saturated, kept and stirred overnight with hydrogen. Pd/C was filtered over celite and the solvent was evaporated under reduced pressure. The product (260 mg, 0.53 mmol, 96%) was used without further purification.

^{1}H-NMR (300 MHz, $CDCl_3$): δ [ppm] = 5.48 (dd, *J* = 10.3, 8.1 Hz, 2H), 4.31 (dd, *J* = 5.7, 2.4 Hz, 2H), 2.77 (t, *J* = 6.6 Hz, 2H), 2.36–2.25 (m, 2H), 2.05 (ddd, *J* = 7.1, 5.9, 2.1 Hz, 1H), 1.92–1.68 (m, 2H), 1.44 (d, *J* = 7.1 Hz, 33H).

^{13}C-NMR (300 MHz, $CDCl_3$): δ [ppm] = 172.61, 172.47, 157.05, 82.07, 81.67, 80.55, 53.39, 52.99, 41.12, 32.40, 31.66, 31.43, 28.28, 28.08, 28.02, 22.20.

MS (ESI$^+$): 488.3 $[M + H]^+$, calculated for $C_{24}H_{45}N_3O_7$: 487.33 $[M]^+$.

2-[3-(2-(2-ethoxy-3,4-dioxo-cyclobut-1-en-1yl)amino-1-*tert*-butoxycarbonyl-pentyl)-ureido]-pentanedioic acid di-tert-butyl ester (**12**)

Compound **11** (260 mg, 0.53 mmol) was dissolved in 0.5 M phosphate buffer (pH 7, 2 mL), 3,4-dibutoxycyclobut-3-en-1,2-dione (82 µL, 95 mg, 0.53 mmol) was added and the pH was adjusted to 7. Ethyl acetate (1 mL) was added and stirred overnight. The solvent was then removed via lyophilization and ethyl acetate (2 mL) was added. The solution was then filtered and the solvent was removed under reduced pressure. The product (248 mg, 0.41 mmol, 77%) was obtained as a colorless oil and used without further purification.

^{1}H-NMR (300 MHz, $CDCl_3$): δ [ppm] = 4.78–4.73 (m, 2H), 4.13 (q, *J* = 7,1 Hz, 2H), 3.45 (d, *J* = 5,7 Hz, 2H), 2.36–2.32 (m, 2H), 2.06 (s, 4H), 1.74–1.55 (m, 2H), 1.52–1.43 (m, 27H), 1.27 (t, *J* = 7,1 Hz, 2H).

^{13}C-NMR (300 MHz, $CDCl_3$): δ [ppm] = 189.09, 172.22, 157.27, 124.41, 125.10, 77.35, 77.03, 76.71, 70.07, 53.20, 44.39, 31.59, 28.00, 21.93, 21.07, 14.20.

MS (ESI$^+$): 612,4 $[M + H]^+$, calculated for $C_{30}H_{49}N_3O_{10}$: 611,34 [M].

2-[3-(2-(2-ethoxy-3,4-dioxo-cyclobut-1-en-1yl)amino-1-carboxy-pentyl)-ureido]-pentanedioic acid (**13**)

Compound **12** (50 mg, 0.082 mmol) was stirred with a mixture of dichloromethane and trifluoracetic acid (2 mL, 1:1) at room temperature for 2 hours. The solvent was evaporated under reduced pressure. The product was obtained as a colorless oil (30.2 mg, 0.068 mmol, 83%) and used without further purification.

^{1}H-NMR (300 MHz, D_2O): δ [ppm] = 4.75–4.65 (m, 2H), 4.30 – 4.12 (m, 2H), 3.59 (dt, *J* = 23,5 Hz, 6,6 Hz, 1H), 3.48 (t, *J* = 6,6 Hz, 1H) 2.49 (t, *J* = 7,3 Hz, 2H), 2.16 (dtd, *J* = 15,3 Hz, 7,4 Hz, 5,2 Hz, 1H), 2.04–1.90 (m, 1H) 1.86–1.75 (m, 2H), 1.73 – 1.46 (m, 3H), 1.41 (dt, *J* = 7,1 Hz, 3,6 Hz, 5H).

^{13}C-NMR (300 MHz, D_2O): δ [ppm] = 188.86, 182.94, 177.13, 176.95, 176.05, 173.15, 159.08, 70.41, 52.91, 52.48, 30.26, 29.91, 28.86, 26.15, 21.59, 14.95.

MS (ESI$^+$): 444,2 $[M + H]^+$, calculated for $C_{18}H_{25}N_3O_{10}$: 443,15 $[M]^+$.

DATA^{5m}.SA.KuE (**14**)

Compound **9** (30 mg, 0.067 mmol) and compound **13** (42 mg, 0.095 mmol) were dissolved in 0.5 M phosphate buffer (pH 9, 1 mL). The pH was adjusted to **9** and stirred for two days at room temperature. The crude product was purified by HPLC (column: LiChrospher 100 RP18 EC (250 x 10 mm) 5 µ, flow rate: 5 mL/min, H2O/MeCN + 0.1% TFA, 9 to 15% MeCN in 20 min, Rt = 10.1 min) to obtain DATA^{5m}.SA.KuE as a white powder (5.26 mg, 0.0062 mmol, 10%).

MS (ESI$^+$): 843.3 $[M + H]^+$, 422.2 $[M + 2H]^{2+}$, 441.2 $[M + K + H]^{2+}$, calculated for $C_{35}H_{54}N_8O_{16}$: 842.37 $[M]^+$.

4.3. Radiolabelling

For radiochemical evaluation, gallium-68 was eluted from a ^{68}Ge/^{68}Ga-generator (ITG Graching, Munich, Germany) and purified manually with ethanol-based post-processing to separate iron, zinc, and germanium impurities.[44]

Radiolabelling was performed in 0.4 mL 1 M ammonium acetate buffer at pH 5.5. Reactions were carried out with different amounts of precursor (5, 10, 15, 60 nmol) and at different temperatures (RT, 50 °C, and 70 °C) with 30–50 MBq gallium-68. The pH was controlled at the start and after the labeling. For reaction control, radio-TLC (TLC Silica gel 60 F_{254} Merck) and citrate buffer pH 4 as mobile phase and radio-HPLC using an analytical HPLC 7000 series Hitachi LaChrom (Column: Merck Chromolith®

RP-18e, linear gradient of 5–95% MeCN (+0.1% TFA)/95–5% Water (+0.1% TFA) in 10 min). TLCs were measured in a TLC imager CR-35 Bio Test-Imager (Elysia-Raytest, Belgium) with the analysis software AIDA (Elysia-Raytest, Belgium).

Radiolabeling of AAZTA^5.SA.KuE with scandium-44 and lutetium-177 was performed according to the literature [17].

4.4. In vitro stability studies

Complex stability studies were performed in human serum (HS, human male AB plasma, USA origin, Sigma Aldrich) and phosphate buffered saline (Sigma Aldrich). First, 8–10 MBq of the labeled compound were added to 0.5 mL of the media. Afterwards, 30, 60, and 120 min aliquots were taken to evaluate the radiochemical stability. The percentage of complexed gallium-68, which corresponds to the percentage of *in vitro* radiochemical stability, was determined via radio-TLC. The studies were carried out in triplicate.

4.5. In vitro binding affinity

PSMA binding affinity was determined according to the literature.[45] LNCaP-cells (purchased from Sigma-Aldrich) were cultured in RPMI 1640 (Thermo Fisher Scientific) supplemented with 10% fetal bovine serum (Thermo Fisher Scientific), 100 µg/ml streptomycin, and 100 units/ml penicillin at 37 °C in 5% CO_2 in a humidified atmosphere. The medium was changed approximately every 3 days. Cells in exponential phase of growth were harvested by a 5 min treatment with a 0.05% trypsin–0.02% EDTA solution and neutralized with serum-containing medium prior to counting.

10^5 LNCaP cells per well were applied in MultiScreen$_{HTS}$ DV Filter Plates (Merck Millipore) and incubated with 0.75 nM [^{68}Ga]Ga-PSMA-10 in the presence of 12 increasing concentrations of the non-labeled SA-conjugated compounds. After incubation at room temperature for 45 min, cells bound on the filter plates were washed several times with ice-cold PBS to remove free radioactivity. The cell-bound activity was determined by punching out the filters and transferring them into individual tubes for measurement in a γ-counter (2480 WIZARD^2 Automatic Gamma Counter, PerkinElmer). Data were analyzed in GraphPad Prism 9 using nonlinear regression. Experiments were replicated 4-times.

4.6. Internalization Ratio

Internalization ratio was determined according to the literature.[45,46] Prior to seeding cells, 24-well plates were coated with 0.1% poly-L-lysine (Sigma-Aldrich) in PBS for 20 min at room temperature. Subsequently, 10^5 LNCaP cells in 1 mL RPMI 1640 Medium were added in each well and incubated for 24 h at 37 °C. Then, 250 µL of the ^{68}Ga-labeled compounds in Opti-MEM™ I Reduced Serum (ThermoFisher) were added to each well to a final concentration of 30 nM. The plates were then incubated for 45 min at 4 °C and 37 °C respectively either with or without adding PMPA (Sigma-Aldrich) to a final concentration of 500 µM. The supernatant was removed and the cells were washed several times with ice-cold PBS. Afterwards, cells were incubated twice with 50 mM glycine buffer pH 2.8 for 5 min to remove the surface-bound radioactivity. In order to determine the internalized fraction of the compounds, cells were lysed by incubation with 0.3 M NaOH for 10 min.

4.7. Animal studies

Six- to eight-week-old male BALB/cAnNRj (Janvier Labs) were inoculated subcutaneously with 5×10^6 LNCaP cells in 200 µL 1:1 (v/v) Matrigel/PBS (Corning®). *In vivo* and *ex vivo* experiments are conducted after tumors reached a volume of approximately 100 mm^3.

LNCaP-xenografts were anesthetized with 2% isoflurane prior to i.v. injection of 0.5 nmol of the radiolabeled compounds. The specific activities of the tracers were approximately 10 MBq/nmol, 6 MBq/nmol, and 15 MBq/nmol of gallium-68-labeled compounds, [^{44}Sc]Sc-AAZTA^5.SA.KuE and [^{177}Lu]Lu-AAZTA^5.SA.KuE, respectively. For blocking experiments, mice were co-injected with 1.5 µmol PMPA/mouse.

Biodistribution studies. The number of animals used in this study was: [^{68}Ga]Ga-DATA^{5m}.SA.KuE n = 5; [^{44}Sc]Sc-AAZTA^5.SA.KuE n = 2; [^{177}Lu]Lu-AAZTA^5.SA.KuE n = 2; [^{68}Ga]Ga-PSMA-11 n = 2; [^{44}Sc]Sc-AAZTA^5.SA.KuE + PMPA n = 1. Animals were sacrificed 1 h p.i. Organs of interest were collected and weighed. The radioactivity was measured and calculated as a decay-corrected percentage of the injected dose per gram of tissue mass %ID/g.

MicroPET-imaging. After i.v. injection of the labeled compounds, anesthetized mice (one mouse for each group) were placed in the prone position in a nanoScan® PET/MR (Mediso). MRI measurements were performed followed by a static PET scan with the nanoScan PET/MRI (Mediso, Budapest,

Hungary). PET data were reconstructed with Teratomo 3D (four iterations, six subsets, voxel size 0.4 mm), co-registered to the MR, and analyzed with Pmod software (version 3.6) (PMOD Technologies LLC, Zürich, Switzerland) Material Map for co-registration of the PET scan; 3D Gradient Echo External Averaging (GRE-EXT), Multi Field of View (FOV); slice thickness, 0.6 mm; TE, 2 ms; TR, 15 ms; flip angle, 25 deg.

5. Conclusion

In summary, the synthesized hybrid chelator-based PSMAradiopharmaceuticals DATA^{5m}.SA.KuE and AAZTA^{5}.SA.KuE could be labeled at mild conditions with high radiochemical yields. The stability of the labeled compounds in PBS and human serum was demonstrated. Both SA.KuE conjugates displayed good PSMA binding affinities in LNCaP cells along with good internalization ratios. Additionally, [^{68}Ga]Ga-DATA^{5m}.SA.KuE, [^{44}Sc]Sc-AAZTA^{5}.SA.KuE, and [^{177}Lu]Lu-AAZTA^{5}.SA.KuE showed similar *in vivo* behavior, suggesting that the exchange of either the chelator or the nuclide does not impact the pharmacokinetic of the investigated compounds. This finding renders [^{44}Sc]Sc-AAZTA^{5}.SA.KuE and [^{177}Lu]Lu-AAZTA^{5}.SA.KuE an interesting pair for theranostic application. Tumor accumulation of the tested PSMA radioligands was similar to that of [^{68}Ga]Ga-PSMA-11, although lower than the value reported in literature for PSMA-617. The decreased kidney uptake of the SA.KuE conjugates is noteworthy, which could be a major benefit in reducing irradiation of the kidneys, resulting in lower nephrotoxicity and improved tolerability.

Author Contributions: Conceptualization, X.X., X.X., T.G. and X.X.; methodology, X.X. T.G., X.X. and X.X.; software, X.X. T.G. and X.X.; validation, X.X. and T.G., formal analysis, X.X. and T.G.; investigation, X.X. and T.G.; data curation, X.X. and T.G.; writing—original draft preparation, X.X. and T.G.; writing—review and editing, X.X., T.G., X.X., X.X., X.X. and X.X.; supervision, X.X. and X.X. All authors have read and agreed to the published version of the manuscript.

Funding: This research received no external funding

Institutional Review Board Statement: The study was conducted according to the guidelines of the Declaration of Helsinki, and approved by the Ethics Committee of the state of Rhineland Palatinate according to §8 Abs. 1 Tierschutzgesetz, Landesuntersuchungsamt (23 177-07 G 15-1-033).

Informed Consent Statement: Not applicable

Data Availability Statement: The data presented in this study are available on request from the corresponding author.

Acknowledgments: The authors thank the Max Planck Graduate Center Mainz (MPGC) for supporting Tilmann Grus and X.X. The authors gratefully acknowledge X.X. for supporting X.X. The authors thank ITG Munich for supplying lutetium-177 and gallium-68-generators.

Conflicts of Interest: The authors declare no conflict of interest

Sample Availability: Not available

References

1. Chang, S.S.; Heston, W.D.W. The clinical role of prostate-specific membrane antigen (PSMA). *Urol Oncol*. **2002**, *7* (1), 7–12.

2. Chang, S.S.; Bander, N.H.; Heston, W.D.W. Biology of PSMA as a Diagnostic and Therapeutic Target. In *Management of Prostate Cancer, Current Clinical Urology,* 2nd Edition, Klein, E.A. eds.; Humana Press: Totowa, New Jersey, NJ, USA, **2004**; pp. 609–630.

3. Gourni, E.; Henriksen, G.; Gamez, P.; Caballero, A.B. Metal-based PSMA radioligands. *Molecules.* **2017**, *22* (4), 523.

4. Silver, D.A.; Pellicer, I.; Fair, W.R.; Heston, W.D.; Cordon-Cardo, C. Prostate-specific membrane antigen expression in normal and malignant human tissues. Clin. *Cancer Res*. 1997, *3* (1), 81-85.

5. Perner, S.; Hofer, M.D.; Kim, R.; Shah, R.B.; Li, H.; Möller, P.; Hautmann, R.E.; Gschwend, J.E.; Kuefer, R.; Rubin, M.A. Prostate-specific membrane antigen expression as a predictor of prostate cancer progression. *Hum. Pathol*. **2007**, *38* (5), 696–701.

6. Prostate cancer statistics, World Cancer Research Fund International. Available online: https://www.wcrf.org/dietandcancer/prostate-cancer-statistics/ (accessed on 19 May 2021).

7. Ferlay, J.; Colombet, M.; Soerjomataram, I.; Mathers, C.; Parkin, D.M.; Piñeros, M.; Znaor, A.; Bray, F. Estimating the global cancer incidence and mortality in 2018: GLOBOCAN sources and methods*. Int, J. Cancer*. **2019**, *144* (8), 1941–1953.

8. Rawla, P. Epidemiology of Prostate Cancer. *World. J. Oncol*. **2019**, *10* (2), 63–89.

9. Kirby, M.; Hirst, C.; Crawford, E.D. Characterising the castration-resistant prostate cancer population: A systematic review. *Int, J. Clin. Pract*. **2011**, *65* (11), 1180–1192.

10. Kopka, K.; Benešová, M.; Bařinka, C.; Haberkorn, U.; Babich, J. Glu-ureido-based inhibitors of prostate-specific membrane antigen: Lessons learned during the development of a novel class of low-molecular-weight theranostic radiotracers; *J. Nucl Med*. **2017**, *58* (Supplement 2), 17S–26S.

11. Benešová, M.; Schäfer, M.; Bauder-Wüst, U.; Afshar-Oromieh, A.; Kratochwil, C.; Mier, W.; Haberkorn, U.; Kopka, K.; Eder, M. Preclinical evaluation of a tailor-made DOTA-conjugated PSMA

inhibitor with optimized linker moiety for imaging and endoradiotherapy of prostate cancer. *J. Nucl Med*. **2015**, *56* (6), 914–920.

12. Valstar, M.H.; de Bakker, B.S.; Steenbakkers, R.J.H.M.; de Jong, K.H.; Smit, L.A.; Klein Nulent, T.J.W.; van Es, R.J.J.; Hofland, I.; de Keizer, B.; Jasperse, B.; Balm, A.J.M.; van der Schaaf, A.; Langendijk, J.A.; Smeele, L.E.; Vogel, V.V. The tubarial salivary glands: A potential new organ at risk for radiotherapy. *Radiother Oncol*. **2021**, *154*, 292–298.

13. Rupp, N.J.; Umbricht, C.A.; Pizzuto, D.A.; Lenggenhager, D.; Töpfer, A.; Müller, J.; Muehlematter, U.J.; Ferraro, D.A.; Messerli, M.; Morand, G.B.; Huber, G.F.; Eberli, D.; Schibli, R.; Müller, C.; Burger, I.A. First clinicopathologic evidence of a non-PSMA-related uptake mechanism for ^{68}Ga-PSMA-11 in salivary glands. *J. Nucl Med*. **2019**, *60* (9), 1270–1276.

14. Afshar-Oromieh, A.; Malcher, A.; Eder, M.; Eisenhut, M.; Linhart, H.G.; Hadaschik, B.A.; H. -L., T.; Giesel, F.L.; Kratochwil, C.; Haufe, S.; Haberkorn, U.; Zechmann, C.M. PET imaging with a [^{68}Ga]Gallium-labelled PSMA ligand for the diagnosis of prostate cancer: Biodistribution in humans and first evaluation of tumour lesions. *Eur J. Nucl Med. Mol. Imaging* **2013**, *40*, 486–495.

15. Hofman, M.S.; Hicks, R.J.; Maurer, T.; Eiber, M. Prostate-specific membrane antigen PET: Clinical utility in prostate cancer, normal patterns, pearls, and pitfalls. *Radiographics.* **2018**, *38* (1), 200–217.

16. Farkas, E.; Nagel, J.; Waldron, B.P.; Parker, D.; Tóth, I.; Brücher, E.; Rösch, F.; Baranyai, Z. Equilibrium, Kinetic and Structural Properties of Gallium(III) and Some Divalent Metal Complexes Formed with the New DATA^{m} and DATA^{5m} Ligands. *Chem*. *Eur*. *J.* **2017**, *23* (43), 10358–10371.

17. Greifenstein, L.; Grus, T.; Nagel, J.; Sinnes, J.P.; Rösch, F. Synthesis and labeling of a squaric acid containing PSMA-inhibitor coupled to AAZTA^{5} for versatile labeling with ^{44}Sc, ^{64}Cu, ^{68}Ga and ^{177}Lu. *Appl. Radiat Isot*. **2020**, *156,*108867.

18. Baranyai, Z.; Uggeri, F.; Giovenzana, G.B.; Bényei, A.; Brücher, E.; Aime, S. Equilibrium and kinetic properties of the lanthanoids(III) and various divalent metal complexes of the heptadentate ligand AAZTA*. Chem. Eur. J*. **2009**, *15* (7), 1696–1705.

19. Seemann, J.; Waldron, B.P.; Roesch, F.; Parker, D. Approaching "kit-type" labelling with ^{68}Ga: The DATA chelators. *Chem. Med. Chem.* **2015**, *10* (6), 1019–1026.

20. Waldron, B.P.; Parker, D.; Burchardt, C.; Yufit, D.S.; Zimny, M.; Roesch, F. Structure and stability of hexadentate complexes of ligands based on AAZTA for efficient PET labelling with gallium-68. *Chem. Comm*. **2013**, *49*, 579–581.

21. Nagy, G.; Szikra, D.D.; Trencsényi, G.; Fekete, A.; Garai, I.; Giani, A.M.; Negri, R.; Masciocchi, N.; Maiocchi, A.; Uggeri, F.; Tóth, I.; Aime, S.; Giovenzana, G.B.; Baranyai, Z. AAZTA: An Ideal Chelating Agent for the Development of ^{44}Sc PET Imaging Agents. *Angew. Chem. Int. Ed*. *Engl*. **2017**, *56* (8), 2118–2122.

22. Aime, S.; Calabi, L.; Cavallotti, C.; Gianolio, E.; Giovenzana, G.B.; Losi, P.; Maiocchi, A.; Palmisano, G.; Sisti, M. [Gd-AAZTA]$^{-}$: A new structural entry for an improved generation of MRI contrast agents. *Inorg. Chem*. **2004**, *43* (24), 7588–7590.

23. Tsionou, M.I.; Knapp, C.E.; Foley, C.A.; Munteanu, C.R.; Cakebread, A.; Imberti, C.; Eykyn, T.R.; Young, J.D.; Paterson, B.M.; Blower, P.J.; Ma, M.T. Comparison of macrocyclic and acyclic chelators for gallium-68 radiolabelling. *RSC Adv*. **2017**, *7*, 49586–49599.

24. Benešová, M.; Bauder-Wüst, U.; Schäfer, M.; Klika, K.D.; Mier, W.; Haberkorn, U.; Kopka, K.; Eder, M. Linker Modification Strategies to Control the Prostate-Specific Membrane Antigen (PSMA)-Targeting and Pharmacokinetic Properties of DOTA-Conjugated PSMA Inhibitors. *J. Med. Chem*. **2016**, *59* (5), 1761–1775.

25. Zhang, A.X.; Murelli, R.P.; Barinka, C.; Michel, J.; Cocleaza, A.; Jorgensen, W.L.; Lubkowski, J.; Spiegel, D.A. A Remote arene-binding site on prostate specific membrane antigen revealed by antibody-recruiting small molecules. *J. Am. Chem Soc*. **2010**, *132* (36), 12711–12716.

26. Tietze, L.F.; Arlt, M.; Beller, M.; Gliisenkampb, K.; Jahdeb, E.; Rajewskyb, M.F.; Glüsenkamp, K.-H.; Jähde, E.; Rajewsky, M.F. Squaric Acid Diethyl Ester: A New Coupling Reagent for the Formation of Drug Biopolymer Conjugates. Synthesis of Squaric Acid Ester Amides and Diamides. *Chem Ber*. **1991**, *124* (5), 1215–1221.

27. Wurm, F.R.; Klok, H.A. Be squared: Expanding the horizon of squaric acid-mediated conjugations. *Chem Soc. Rev*. **2013**, *42* (21), 8220–8236.

28. Greifenstein, L.; Engelbogen, N.; Lahnif, H.; Sinnes, .J.-P.; Bergmann, R.; Bachmann, M.; Rösch, F. Synthesis, Labeling and Preclinical Evaluation of a Squaric Acid Containing PSMA Inhibitor Labeled with ^{68}Ga: A Comparison with PSMA-11 and PSMA-617. *Chem. Med. Chem* **2020**, *15* (8), 695–704.

29. Grus, T.; Lahnif, H.; Klasen, B.; Moon, E.-S.; Greifenstein, L.; Roesch, F. Squaric Acid-Based Radiopharmaceuticals for Tumor Imaging and Therapy. *Bioconjug Chem*. **2021**, *32* (7), 1223–1231.

30. Prohens, R.; Portell, A.; Font-Bardia, M.; Bauzá, A.; Frontera, A. Experimental and theoretical study of aromaticity effects in the solid state architecture on squaric acid derivatives. *Cryst Growth Des*. **2014**, *14* (5), 2578–2587.

31. Quiñonero, D.; Frontera, A.; Ballester, P.; Deyà, P.M. A theoretical study of aromaticity in squaramide and oxocarbons. *Tetrahedron Lett*. **2000**, *41* (12), 2001–2005.

32. Dingels, C.; Wurm, F.; Wagner, M.; Klok, H.A.; Frey, H. Squaric acid mediated chemoselective PEGylation of proteins: Reactivity of single-step-activated α-amino poly(ethylene glycol)s. *Chem*. *Eur*. *J*. **2012**, *18* (52), 16828–16835.

33. Liu, H.; Rajasekaran, A.K.; Moy, P.; Xia, Y.; Kim, S.; Navarro, V.; Rahmati, R.; Bander, N.H. Constitutive and Antibody-induced Internalization of Prostate-specific Membrane Antigen. *Cancer Res*. **1998**, *58* (18), 4055–4060.

34. Winter, G.; Vogt, A.; Jiménez-Franco, L.D.; Rinscheid, A.; Yousefzadeh-Nowshahr, E.; Solbach, C.; Beer, A.J.; Glatting, G.; Kletting, P. Modelling the internalisation process of prostate cancer cells for PSMA-specific ligands. *Nucl Med. Biol*. **2019**, 72–73, 20–25.

35. Jackson, P. F.; Tays, K. L.; Maclin, K. M.; Ko, Y. S.; Vitharana D.; Tsukamoto, T.; Stoermer, D. Lu, X. C.; Wozniak, K.; Slusher, B.S. Design and Pharmacological Activity of Phosphinic Acid Based NAALADase Inhibitors. *J. Med. Chem*. **2001**, *44* (24), 4170–4175.

36. Jackson, P.F.; Cole, C.D.; Slusher, B.S.; Stetz, S.L.; Ross, L. E.; Donzanti, B. A.; Trainor, D. A. Design, Synthesis, and Biological Activity of a Potent Inhibitor of the Neuropeptidase N-Acetylated α-Linked Acidic Dipeptidase. *J. Med. Chem*. **1996**, *39* (2), 619–622.

37. Rais, R.; Rojas, C.; Wozniak, K.; Wu, Y.; Zhao, M.; Tsukamoto, T.; Rudek, M.A.; Slusher, B.S. Bioanalytical method for evaluating the pharmacokinetics of the GCP-II inhibitor 2-phosphonomethyl pentanedioic acid (2-PMPA). *J. Pharm Biomed. Anal*. **2014**, *88*, 162–169.

38. Killock, D. PSMA PET–CT improves staging. *Nat. Rev. Clin*. Oncol. **2020**, *17*, 337.

39. Langbein, T.; Chaussé, G.; Baum, R.P. Salivary gland toxicity of PSMA radioligand therapy: Relevance and preventive strategies. *J. Nucl Med*. **2018**, *59* (8), 1172–1173.

40. Sinnes, J.-P.; Bauder-Wüst, U.; Schäfer, M.; Moon, E.S.; Kopka, K.; Rösch, F. ^{68}Ga, ^{44}Sc and ^{177}Lu-labeled AAZTA^{5}-PSMA-617: Synthesis, radiolabeling, stability and cell binding compared to DOTA-PSMA-617 analogues. *EJNMMI Radiopharm. Chem*. **2020**, *5*, 28.

41. Ghiani, S.; Hawala, I.; Szikra, D.; Trencsényi, G.; Baranyai, Z.; Nagy, G.; Vágner, A.; Stefania, R.; Pandey, S.; Maiocchi, A. Synthesis, radiolabeling, and pre-clinical evaluation of [^{44}Sc]Sc-AAZTA conjugate PSMA inhibitor, a new tracer for high-efficiency imaging of prostate cancer. *Eur J. Nucl Med. Mol. Imaging***. 2021**, *48*, 2351–2362.

42. Eppard, E.; de la Fuente, A.; Benešová, M.; Khawar, A.; Bundschuh, R.A.; Gärtner, F.C.; Kreppel, B.; Kopka, K.; Essler, M.; Rösch, F. Clinical translation and first in-human use of [^{44}Sc]Sc-PSMA-617 for PET imaging of metastasized castrate-resistant prostate cancer. *Theranostics* **2017**, *7* (18), 4359–4369.

43. Schäfer, M.; Bauder-Wust, U.; Leotta, K. A dimerized urea-based inhibitor of the prostate-specific membrane antigen for ^{68}Ga-PET imaging of prostate cancer. *EJNMMI Res.* **2012**, *2*, 23.

44. Eppard, E.; Wuttke, M.; Nicodemus, P.L.; Rösch, F. Ethanol-based post-processing of generator-derived ^{68}Ga Toward kit-type preparation of ^{68}Ga-radiopharmaceuticals. *J. Nucl Med*. **2014**, *55* (6), 1023–1028.

45. Eder, M.; Schäfer, M.; Bauder-Wüst, U.; Hull, W.E.; Wängler, C.; Mier, W.; Haberkorn, U.; Eisenhut, M. ^{68}Ga-complex lipophilicity and the targeting property of a urea-based PSMA inhibitor for PET imaging. *Bioconjug Chem*. **2012**, *23* (4), 688–697.

46. Askoxylakis, V.; Mier, W.; Zitzmann, S.; Ehemann, V.; Zhang, J.; Krämer, S.; Beck, C.; Schwab, M.; Eisenhut, M.; Haberkorn, U. Characterization and development of a peptide (p160) with affinity for neuroblastoma cells. *J. Nucl Med*. **2006**, *47* (6), 981–988.

[^{68}Ga]Ga-DATA^{5m}-PSMA-617 as diagnostic kit-based counterpart for [^{177}Lu]Lu-PSMA-617

Tilmann Grus, X.X. and X.X.

In preparation for submission

Summary

[^{177}Lu]Lu-PSMA-617 is one of the most used therapeutic PSMA radiopharmaceutical. For diagnosis and therapy control it is very often combined with [^{68}Ga]Ga-PSMA-11.[1] Both compounds contain a KuE unit as target vector, but vary in linker and chelator and thus also vary in pharmacological properties.[2] In this project, the DOTA chelator of PSMA-617 was replaced by the hybrid chelator DATA^{5m} to enable the radiolabelling under mild conditions and make PSMA-617 accessible for kit labelling approaches. Additionally, the combination of [^{68}Ga]Ga-DATA^{5m}-PSMA-617 and [^{177}Lu]Lu-(DOTA)-PSMA-617 enables the use in clinical routine of a theranostic compound pair for diagnosis and therapy of prostate cancer with the same pharmacophore unit and exactly the same pharmacokinetic properties.

After a resin-based synthesis of the novel compound, the eligibility to radiolabel DATA^{5m}-PSMA-617 fast and under mild conditions with gallium-68 and complex stabilities in PBS, NaCl and human serum were demonstrated. Thus, a kit-type application is possible.

The lipophilicity of [^{68}Ga]Ga-DATA^{5m}-PSMA-617 was higher than the lipophilicities of PSMA-617 and PSMA-11 (-1.69 ± 0.12 vs. -2.00[3] vs. -2.91 ± 0.06[4]). Since only the chelator is different in DATA^{5m}-PSMA-617 and (DOTA)-PSMA-617, the chelator seems to have a high impact on the lipophilicity. The lipophilicity itself has an influence on pharmacokinetic properties.

The *in vitro* binding affinity of [^{68}Ga]Ga-DATA^{5m}-PSMA-617 also vary significant from [^{68}Ga]Ga-(DOTA)-PSMA-617. With 92.1 ± 11.7 nM the IC_{50} value of the novel compound showed a 6-fold lower affinity in contrast to [^{68}Ga]Ga-(DOTA)-PSMA-617 (15.9 ± 5.1 nM[5]). The different chelator and the different lipophilicity can also cause this variation, since a different lipophilicity can lead to different binding conditions inside the binding pocket of PSMA.

In a comparison to a previous study[6], in which radiolabelling an affinity were evaluated, the results of the previous study could not be verified.

Autor contributions

T. Grus and X.X. planned the study. **T. Grus** performed organic synthesis, radiolabelling synthesis, *in vivo* stability, lipophilicity studies and analysed the data. X.X. was in charge of the LNCaP cells, the *in vitro* binding affinity and the evaluation of the obtained data. **T. Grus** wrote the manuscript. X.X. supervised the project.

References in the summary

(1) Wichmann, C. W.; Ackermann, U.; Poniger, S.; Young, K.; Nguyen, B.; Chan, G.; Sachinidis, J.; Scott, A. M. Automated Radiosynthesis of [^{68}Ga]Ga-PSMA-11 and [^{177}Lu]Lu-PSMA-617 on the IPHASE MultiSyn Module for Clinical Applications. *J. Label. Compd. Radiopharm.* **2021**, *64* (3), 140–146.

(2) Kopka, K.; Benešová, M.; Bařinka, C.; Haberkorn, U.; Babich, J. Glu-Ureido-Based Inhibitors of Prostate-Specific Membrane Antigen: Lessons Learned during the Development of a Novel Class of Low-Molecular-Weight Theranostic Radiotracers. *J. Nucl. Med.* **2017**, *58* (Suppl 2), 17S-26S.

(3) Benešová, M.; Schäfer, M.; Bauder-Wüst, U.; Afshar-Oromieh, A.; Kratochwil, C.; Mier, W.; Haberkorn, U.; Kopka, K.; Eder, M. Preclinical Evaluation of a Tailor-Made DOTA-Conjugated PSMA Inhibitor with Optimized Linker Moiety for Imaging and Endoradiotherapy of Prostate Cancer. *J. Nucl. Med.* **2015**, *56* (6), 914–920.

(4) Baranski, A. C.; Schäfer, M.; Bauder-Wüst, U.; Roscher, M.; Schmidt, J.; Stenau, E.; Simpfendörfer, T.; Teber, D.; Maier-Hein, L.; Hadaschik, B.; Haberkorn, U.; Eder, M.; Kopka, K. PSMA-11–Derived Dual-Labeled PSMA Inhibitors for Preoperative PET Imaging and Precise Fluorescence-Guided Surgery of Prostate Cancer. *J. Nucl. Med.* **2018**, *59* (4), 639–645.

(5) Greifenstein, L.; Engelbogen, N.; Lahnif, H.; Sinnes, J.-P.; Bergmann, R.; Bachmann, M.; Rösch, F. Synthesis, Labeling and Preclinical Evaluation of a Squaric Acid Containing PSMA Inhibitor Labeled with ^{68}Ga: A Comparison with PSMA-11 and PSMA-617. *ChemMedChem* **2020**, *15* (8), 695–704.

(6) Sinnes, J.-P. Synthese Und radiochemische evaluierung von Chelatoren für milde Markierungen mit ^{68}Ga, ^{44}Sc Und ^{177}Lu sowie *in vitro*- Und *in vivo*- Evaluierung von deren TOC- Und PSMA-Derivaten. *Dissertation. - Johannes Gutenberg-University Mainz* **2018**.

Abstract

Background: With high new case and death rates every year, prostate cancer (PCa) plays an important role within the field of cancer. PSMA (prostate-specific membrane antigen), a membrane-bound glycoprotein which is highly overexpressed in PCa, is an important target for radiopharmaceuticals for diagnosis and therapy of prostate cancer. A prominent representative of the therapeutically applied radiopharmaceuticals is [^{177}Lu]Lu-PSMA-617. It is often combined with the PET radiopharmaceutical [^{68}Ga]Ga-PSMA-11, which can be used for diagnosis and therapy progress control. In this work, we present a diagnostic PSMA radioligand. This radioligand contains a DATA^{5m} chelator, which can be labelled in a kit type labelling approach with gallium-68 and would therefore allow the simple supply of [^{68}Ga]Ga-PSMA-PET tracer. To maintain the same pharmacokinetic properties, the same linking and targeting unit is used as it is present in [^{177}Lu]Lu-PSMA-617.

Methods: DATA^{5m}-PSMA-617 was synthesized and radiolabelled with gallium-68. Different buffer systems, temperatures and amounts of precursor were evaluated. *In vitro* complex stability was determined in human serum (HS), phosphate buffered saline (PBS) and NaCl. The lipophilicity was determined by evaluating the distribution of the compound in a mixture of n-octanol and PBS. The IC_{50} value was evaluated in a competitive radioligand binding assay with PSMA-positive LNCaP cells and [^{68}Ga]Ga-PSMA-10 as reference.

Results: Best radiolabelling results were achieved in a 1 M ammonium acetate pH 5.5 buffer system and 50 nmol precursor at room temperature. The final product [^{68}Ga]Ga-DATA^{5m}-PSMA-617 showed a purity of over 99% without a purification step. The compound was stable in HS, PBS and NaCl for at least 90 min. With a $logD_{7.4}$ value of -1.69 ± 0.12 [^{68}Ga]Ga-DATA^{5m}-PSMA-617 showed a higher lipophilicity in contrast to [^{177}Lu]Lu-PSMA-617 and [^{68}Ga]Ga-PSMA-11. The affinity of DATA^{5m}-PSMA-617 towards PSMA was determined with a value of 92.1 ± 11.7 nM. Thus, the affinity aws 3.5-fold and 6-fold lower than the affinities of PSMA-11 and PSMA-617, respectively.

Conclusion: The kit-labelling ability of DATA^{5m}-PSMA-617 with gallium-68 was proven. Due to the differences of lipophilicity and in vitro PSMA binding affinity, the structure of DATA^{5m}-PSMA-617 should be optimised so that it has more similar properties to [^{177}Lu]Lu-PSMA-617.

Keywords: PSMA, DATA, PSMA-617, gallium-68, theranostics.

Introduction

With the increase in life expectancy in recent decades, the number of age-related diseases, such as cancer, is also increasing.[1] Among cancer, prostate cancer (PCa) plays an important role due to its high number of new cases and deaths.[2,3] The discovery of the membrane-bound glycoprotein PSMA (prostate-specific membrane antigen) and research on its association with prostate cancer opened up a completely new method for diagnosing and treating this type of cancer.

PSMA is a membrane-bound and zinc-dependent glutamate carboxypeptidase II (GCPII) whose physiological function in the prostate is largely unknown.[4] It is almost absent in the healthy prostate, whereas it is strongly overexpressed in PCa.[5] In addition to the localisation of the tumour, PSMA can also be used to classify the progress of the disease and monitor therapy as its expression correlates with the progression of the disease.[6]

For successful diagnosis and therapy using radioactivity, the radionuclide must dock with high specificity and selectivity at the PSMA-target. The use of PSMA ligands, which fits perfect in the PSMA binding pocket enables this. In recent years, small molecule PSMA inhibitors consisting of a glutamate-urea scaffold have become established as PSMA ligands.[7–10]

The most prominent and promising PSMA radiopharmaceutical for prostate cancer is PSMA-617, a small molecule PSMA inhibitor consisting of lysine and glutamate linked by a urea bond.[11,12] The PSMA inhibitor is linked to the DOTA chelator, allowing labelling with a variety of nuclides, such as the diagnostic nuclide ^{68}Ga or ^{44}Sc, as well as the therapeutic nuclides ^{177}Lu and ^{225}Ac.[12–14] PSMA inhibitor and chelator are conjugated via a linker that increases the affinity and selectivity of the molecule towards PSMA. The recently completed worldwide VISION study with over 1000 patients recommends the inclusion of [^{177}Lu]Lu-PSMA-617 as standard therapy.[15]

Prior to therapy with [^{177}Lu]Lu-PSMA-617, the patient's PSMA status is classified.[16] Several PSMA diagnostics are currently clinically established for this purpose. These include, for example, [^{18}F]F-PSMA-1007[17,18], [^{18}F]F-DCFBC[19], [^{18}F]F-DCFPyL[20,21], [^{68}Ga]Ga-PSMA-11[22,23], [^{68}Ga]Ga-PSMA-617[12] or [^{68}Ga]Ga-PSMA-I&T[24]. All compounds differ only slightly in their pharmacokinetics and properties.[25]

The most common combination in theranostics is [^{68}Ga]Ga-PSMA-11 (Figure 1A) and [^{177}Lu]Lu-PSMA-617 (Figure 1B).[15,26–30] Compared to the ^{18}F-containing diagnostics, the ^{68}Ga compounds have the advantage that the ^{68}Ga is more easily available via ^{68}Ge/^{68}Ga-generators if no expensive and maintenance-intensive cyclotron is available for ^{18}F production.

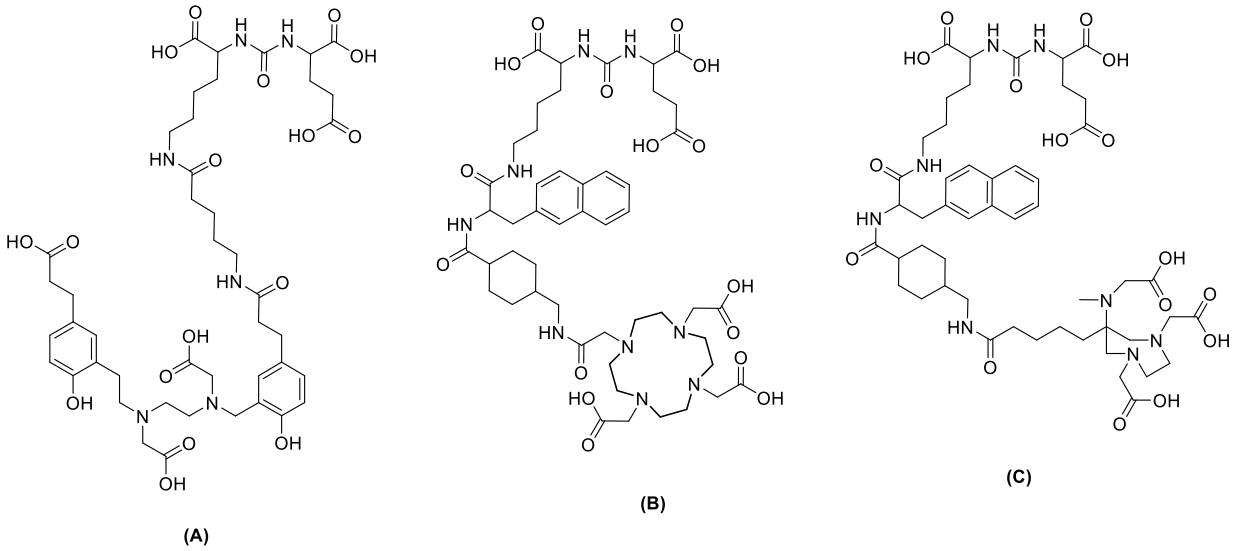

Figure 1.: Chemical structure of (A) PSMA-11, (B) (DOTA)-PSMA-617 and (C) DATA^{5m}-PSMA-617

The most commonly used chelator in metallic PSMA radiopharmaceuticals is DOTA or its derivative DOTAGA. They are found, for example, in PSMA-617 (DOTA)[12] or in PSMA-I&T (DOTAGA)[24]. These macrocyclic chelators enclose the radionuclide in a cage and exhibit high thermodynamic and kinetic stability, but have a high kinetic energy barrier, which requires high temperatures for labelling.[31,32] The HBED-CC chelator used in PSMA-11 is an acyclic chelator that allows lower labelling temperatures but has low chelator-metal stability.[23,31,32]

The use of a hybrid chelators, such as DATA^{5m}, can be an alternative for macrocyclic and acyclic chelators. Hybrid chelators combine the rapid complexation properties of acyclic chelators and the complex stability of macrozyclic chelators.[33–35] DATA^{5m} is an optimal chelator for ^{68}Ga, as it quantitatively complexes ^{68}Ga in one minute at room temperature and is therefore well suited for use in radiolabelling "instant-kit" sets as known for many ^{99m}Tc compounds.[36] The kit-labelling process of DATA-containing compounds has already been described several times and its suitability has been proven.[36–39]

Coupled with a PSMA inhibitor, this would allow the possibility of simple and rapid supply of a PSMA diagnostic for PSMA PET/CT via kit labelling. The DATA^{5m}-PSMA radiopharmaceutical is using the same linker and target vector unit like PSMA-617. This is done in order to ensure the same biodistribution properties and behaviour for both, the diagnostic DATA^{5m}-based PSMA radiopharmaceutical and the therapeutic (DOTA)-PSMA-617. This allows a theranostic application.

To investigate the applicability of such a DATA^{5m}-PSMA inhibitor, in this work the linker and PSMA inhibitor moiety of PSMA-617 was coupled to DATA^{5m} (Figure 1C) and investigated with regard to its labelling properties with ^{68}Ga and its *in vitro* and *in vivo* behaviour. J.-P. Sinnes already evaluated the

radiochemical properties and affinity of DATA^{5m}-PSMA-617 in his doctoral thesis.[40] This study also aims to verify the reproducibility of these results and is conducting further lipophilicity and *in vivo* studies.

Results

Organic synthesis of DATA^{5m}-PSMA-617

The unconjugated and protected prochelator DATA^{5m}-3^{t}Bu was synthesized according to a procedure described by Seemann et al.[39] and Lahnif et al.[41] The KuE target vector unit in combination with the corresponding linker unit, which is also present in the literature-known PSMA-617, was synthesised via a solid-phase synthesis as described by Benešová et al.[11,12]

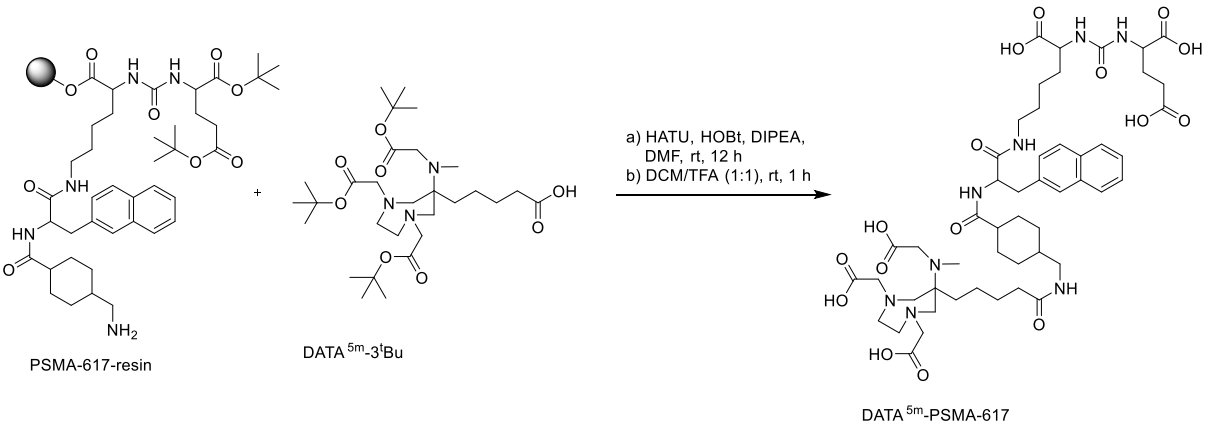

Figure 2: Synthesis of DATA^{5m}-PSMA-617

Figure 2 shows the conjugation of the chelator unit and the target vector-linker motif. The free carboxyl group of DATA^{5m}-3^{t}Bu was conjugated to the free amino function of the resin using a standard peptide coupling protocol. The conjugated, protected and resin-bound DATA^{5m}-3^{t}Bu-PSMA-617 was then treated with a mixture of dichloromethane (DCM) and trifluoroacetic acid (TFA) (1:1) to deprotect and cleave the compound from the resin. The final compound DATA^{5m}-PSMA-617 was obtained after successful HPLC purification.

Radiolabelling and radiochemical evaluation of [^{68}Ga]Ga-DATA^{5m}-PSMA-617

To find the best conditions for the radiolabelling of DATA^{5m}-PSMA-617 different buffer systems, amounts of precursor and labelling temperatures were evaluated. Figure 3 shows the labelling kinetics of the different conditions.

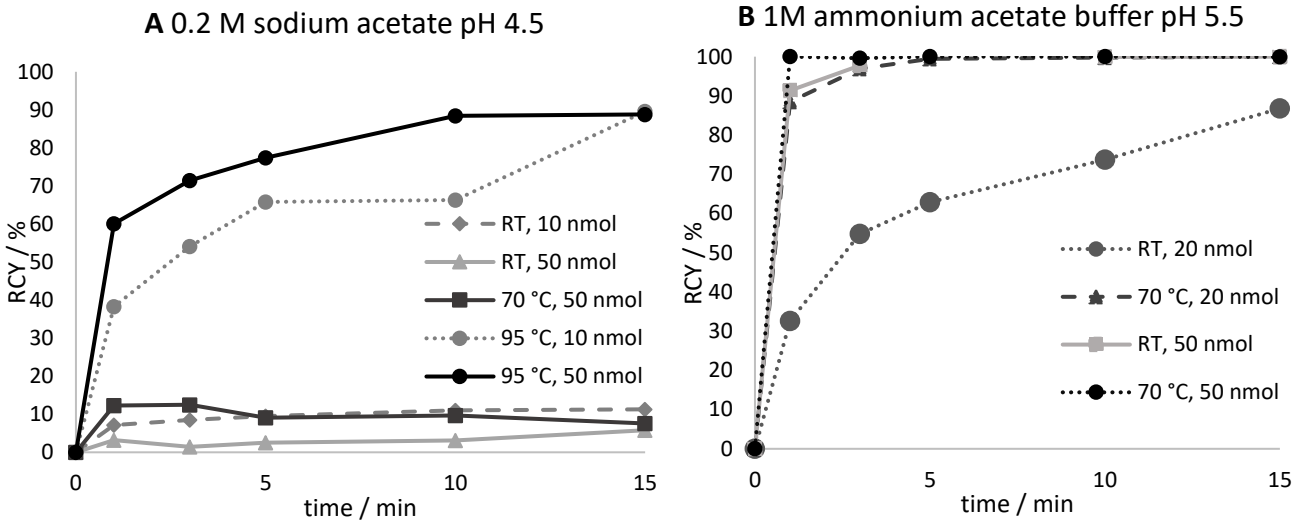

Figure 3: Kinetic studies of 68Ga-labelling of DATA^{5m}-PSMA-617 for different buffer systems, amounts of precoursor and temperatures.

The performed experiments showed that the radiochemical yield (RCY) of the radiolabelling of DATA^{5m}-PSMA-617 was highly dependent on pH value, temperature and amount of precursor. The pH value was controlled before and after labelling studies. First, the reaction was carried out in 0.2 M sodium acetate buffer with a pH value of 4.5 (figure 3A). At room temperature for both evaluated amounts of precursor (10 and 50 nmol) no higher labelling yields than 15% and 10% respectively could be achieved. An increase of temperature to 70 °C was not accompanied by an increase in yield. At a temperature of 95°C, DATA^{5m}-PSMA-617 can be labelled with a yield of nearly 90% after 15 min for amounts of 10 nmol (89% RCY) and 50 nmol (88% RCY) of the precursor. To achieve a better RCY the buffer system was changed. The next experiments were carried out in a 1M ammonium acetate buffer pH 5.5 (figure 3B). In this buffer system higher yields are obtained. At room temperature, a RCY of 86% was obtained with 20 nmol after 15 min and quantitative yields are reached with 50 nmol after 10 min, where after 3 min a RCY of 97% was already achieved. Elevated temperatures, such as 70 °C led to an even faster labelling kinetics. 20 nmol reached quantitative labelling after 3 min and 50 nmol after 1 min. The radiochemical purity was determined by radio-HPLC. After labelling, [^{68}Ga]Ga-DATA^{5m}-PSMA-617 showed a purity of 99.1% (See figure 4).

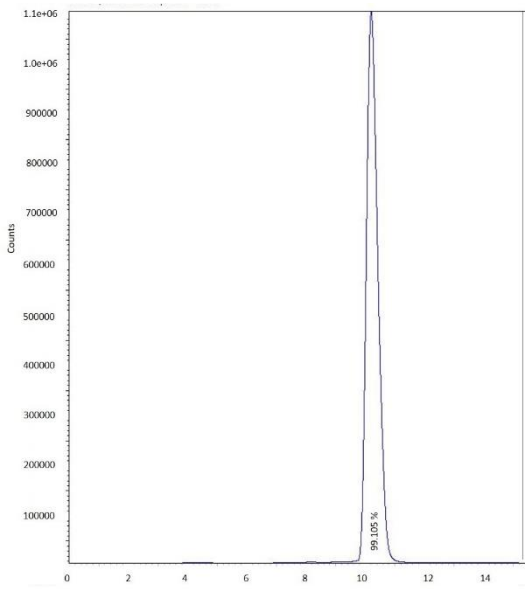

Figure 4: Radio-HPLC of [^{68}Ga]Ga-DATA-PSMA617 shows a purity of 99.1%.(Conditions: Luna 5u C18(2) 100A – 5µ 250x4.6mm 1ml/min; 5% to 95% B in 15 min. (A: Water + 0.1% TFA; B: MeCN + 0.1% TFA))

To investigate the *in vivo* stability of the [^{68}Ga]Ga-DATA^{5m}-PSMA-617 complex, it was incubated for 90 min at 37 °C in human serum (HS), phosphate buffered saline (PBS) and NaCl. [^{68}Ga]Ga-DATA^{5m}-PSMA-617 was completely stable in all three media for at least 90 minutes.

The lipophilicity of [^{68}Ga]Ga-DATA^{5m}-PSMA-617 was determined by evaluate the distribution of [^{68}Ga]Ga-DATA^{5m}-PSMA-617 in n-octanol and water. The compound showed a lipophilicity ($LogD_{7.4}$ value) of -1.69 ± 0.17.

In vitro affinity assay

In a competitive radioligand assay with PSMA-positive LNCaP cells, the binding affinity of DATA^{5m}-PSMA-617 was determined and compared to the affinity of the frequently used standard PET PSMA radiopharmaceutical PSMA-11. PSMA-11 served as reference to compare DATA^{5m}-PSMA-617 with a ^{68}Ga-labelled PET PSMA-radiopharmaceutical. In addition, a comparison is made with PSMA-617 to evaluate the influence of the DATA^{5m} chelator. The Affinities are shown in table 1. DATA^{5m}-PSMA-617 showed a 3.5-fold lower affinity than PSMA-11 and even a 6-fold lower affinity in contrast to PSMA-617.

Table 1: in vitro affinities of DATA^{5m}-PSMA-617, PSMA-11 and PSMA-617. *Data taken from Greifenstein et al.[42]

Compound	IC_{50}
DATA^{5m}-PSMA-617	92.1 ± 11.7 nM
PSMA-11*	26.2 ± 2.4 nM
PSMA-617*	15.9 ± 5.1 nM

Discussion

The DOTA-based PSMA-617 is one of the most known radiopharmaceuticals for therapy of prostate cancer. As diagnostic radiopharmaceutical, [^{68}Ga]Ga-PSMA-11 is usually used, but differs in its targeting unit from PSMA-617. In this work, we present a possible diagnostic counterpart to PSMA-617, which contains the same targeting unit, which should provide the same pharmacological properties. Furthermore, it contains a DATA^{5m} chelator and thus is suitable for kit-type radiolabelling.[36–39]

The synthesis of both parts of the compound, the protected and couple able DATA^{5m} chelator as well as the PSMA-617-resin was straight forward. The coupling of both components in a simple amide coupling reaction was easy and resulted in a high yield (87%) of DATA^{5m}-PSMA-617 after HPLC purification.

Radiolabelling of DATA^{5m}-PSMA-617 with gallium-68 was only successful in a buffer system with a pH value of pH 5.5. Here, quantitative radiochemical yields were obtained for 50 nmol at room temperature. Lower amounts of precursor require higher temperatures. Radio-HPLC and radio-TLC analysis proved quantitative yields and radio-HPLC also showed a purity of over 99%. Thus, no free gallium-68 or side product was present and it was not necessary to purify the compound after labelling, for example via cartridges. Labelling at a pH of 4.5 didn't achieve high yields. This finding is in accordance to the results of other publications, which have shown that the optimal pH value for ^{68}Ga-labelling of different DATA chelators is at pH 5.[36] However, it had also been shown that the DATA chelator can be labelled in pH ranges from 4 to 7.[37,39] In this study, the actual pH value was determined prior to labelling and after labelling and didn't show any significant change during the labelling reaction. Thus, a decrease or increase in the pH value can't be the reason for the low labelling yield and shows that here the optimum pH value is above 5, too.

The stability of [^{68}Ga]Ga-DATA^{5m}-PSMA-617 was evaluated in HS, PBS and NaCl. No loss of complexation was observed in 90 min. All complexes remained 100% stable.

In this study optimal radiolabelling conditions could be found for DATA^{5m}-PSMA-617. However, the parameters for optimal labelling found by Sinnes in his study could not be reproduced.[40] This could be due to different generator systems.

Further novel lipophilicity studies were carried out. With an $logD_{7.4}$ value of -1.69 ± 0.12, [^{68}Ga]Ga-DATA^{5m}-PSMA-617 showed an lower hydrophilicity than PSMA-617 (-2.00[12]) and [^{68}Ga]Ga-PSMA-11 (-2.91 ± 0.06[43]). The comparison of the lipophilicities of DATA^{5m}-PSMA-617 and (DOTA)-PSMA-617 showed that the chelator has a high impact on the overall lipophilicity of the molecule. Although structurally, DATA and DOTA are not very different, the small variation seems to have an impact on lipophilicity. Here, especially the number of nitrogen atoms is interesting. DOTA contains one more nitrogen than DATA and nitrogen atoms are known to have an influence on the lipophilicity by reduce the $logD_{7.4}$ value making it more hydrophilic.[44] This effect seems to be also relevant in this case. A higher lipophilicity can have influence on the pharmacokinetics such as excretion, plasma protein binding and blood clearance.[45] [^{68}Ga]Ga-DATA^{5m}-PSMA-617 could be adjusted to the hydrophilicity of the DOTA compound by adding PEG chains, which adding oxygen atoms to the molecule and lead to a reduced lipophilicity. Since, J-P. Sinnes did not carried out lipophilicity measurements, a comparison is not possible.

The exchange of DOTA against DATA had a significant high influence on the binding affinity towards PSMA. With a value of 92.1 ± 11.7 nM the affinity of DATA^{5m}-PSMA-617 was 6-fold lower than the affinity of PSMA-617 (15.9 ± 5.1 nM) and 3.5-fold lower than the affinity of PSMA-11 (26.2 ± 2.4 nM).[42] Since the targeting and linker unit are the same in both molecules, this significant difference have to be based on the different chelator. Since the different chelators seems to have different influences on the lipophilicity, this could lead to changed binding properties in the PSMA binding pocket.

All in all, DATA chelator seems not to be as well suited for *in vitro* PSMA binding as the DOTA chelator does. This fact can also be seen in previous published articles of DATA^{5m}- and DOTA-based PSMA radiopharmaceuticals.[41,42] DOTAGA (1,4,7,10-tetraazacyclododececane,1-glutaric acid-4,7,10-triacetic acid) chelator, a derivative of DOTA, conjugated to the PSMA targeting unit SA.KuE showed a similar affinity (17.6 ± 5.1 nM) towards PSMA like PSMA-617.[42] In contrast to that, if the same PSMA targeting vector SA.KuE is conjugated to DATA^{5m}, the final compound DATA^{5m}.SA.KuE showed an IC_{50} value of 51.1 ± 5.5 nM and thus a significant lower affinity than the DOTA conjugate.[41] J.-P. Sinnes investigated the affinity of DATA^{5m}-PSMA-617 as part of his doctoral thesis.[40] With a value of 21.5 ± 1.15 nM[40], he found a significantly better IC_{50} value than found in the present study. This can only be attributed to different experimental protocols and differences in handling and can therefore not be used here as a comparison with the reference compounds. In this study, all compounds were evaluated in the same assay, which enables comparability.

Animal studies to evaluate the tumour accumulation of [^{68}Ga]Ga-DATA^{5m}-PSMA-617 and the comparison to [^{177}Lu]Lu-PSMA-617 are being carried out at the radiochemical studies laboratory, INRASTES NCSR "Demokritos" in Athens, Greece. Unfortunately, the results are pending.

Conclusion

The aim of this work was the development of a dignostic counterpart to [^{177}Lu]Lu-PSMA-617 with exact the same pharmacological properties. This would enable a theranostic application. The diagnostic compound DATA^{5m}-PSMA-617 contains a DATA chelator instead of the DOTA chelator, which is found in PSMA-617. The use of this hybridic chelator enables a kit-typle labelling.

It was possible to radiolabel DATA^{5m}-PSMA-617 with gallium-68 fast and under mild conditions. This proves the suitability of the compound for kit application. [^{68}Ga]Ga-DATA^{5m}-PSMA-617 showed a higher lipophilicity. This could have an influence on *in vitro* PSMA binding affinity, since the DATA compound showed a lower affinity than the DOTA derivative. To use [^{68}Ga]Ga-DATA^{5m}-PSMA-617 as diagnostic counterpart to [^{177}Lu]Lu-PSMA-617 the structure should be optimised to obtain a compound with more similar lipophilicity and binding properties, such as [^{177}Lu]Lu-PSMA-617. This could be achieved through adding lipophilicity influencing spacer, such as PEG groups.

The results of the previous study of J-P. Sinnes[40] are different than the results found in this study. This could be due to differencies in the assay protocol and the conduction of the assay. Since Sinnes already found IC_{50} values of DATA^{5m}-PSMA-617 similar to PSMA-617, the novel compound [^{68}Ga]Ga-DATA^{5m}-PSMA-617 also seems to be a promising novel diagnostic compound as counterpart to the therapeutic [^{177}Lu]Lu-PSMA-617. The ongoing animal studies are required to evaluate the *in vivo* potential of [^{68}Ga]Ga-DATA^{5m}-PSMA-617.

Methods and Materials

General

All chemicals were purchased from Sigma-Aldrich, Merck, Fluka, AlfaAesar, VWR, AcrosOrganics, TCI, Iris Biotech and Fisher Scientific and used without further purification. Dry solvents were obtained from Merck, deuterated from Deutero. Silica gel 60 F254 coated aluminum plates from Merck were used for thin layer chromatography (TLC). TLCs were evaluated by fluorescence extinction at λ=254 nm or potassium permanganate staining. The ^{1}H and ^{13}C NMR measurements were performed on An Avance II 400 spectrometer (400 MHz, 5mm BBFO sample head with z-Gradient and ATM and

SampleXPress 60 sample changer) from Bruker were used for ^{1}H and ^{13}C NMR measurements. An Agilent Technologies 1220 Infinity LC system coupled to an Agilent Technologies 6130B Single Quadrupole LC/MS system were used for LC-MS measurements. For semi-preparative HPLC purification a 7000 series Hitachi LaChrom HPLC were used. A CR-35 Bio test imager from Raytest and the AIDA (Raytest) software were used for evaluation of Radio-TLCs.

Organic synthesis

Synthesis of DATA^{5m}(tBu)$_3$ was carried out as described by Seemann et al.[39] and Lahnif et al.[41] The solid phase based synthesis of the PSMA-617-resin was carried out as described by Benešová et al.[11,12]

DATA^{5m}(tBu)$_3$-PSMA-617-resin

DATA^{5m}(*t*Bu)$_3$ (150 mg, 0.26 mmol), HATU (133 mg, 0.352 mmol), HOBt (102 mg, 0.753 mmol) and DIPEA (129 µL, 0.753 mmol) were dissolved in DMF (3 mL) and stirred for 30 min. The PSMA-617-resin was left to soak in DMF (2 mL) for 30 min. The resin was then added to the remaining mixture and stirred overnight. The solid phase was washed with DMF (3 x 5 mL) and DCM (3 x 5 mL) and used in the next step without further purification.

DATA^{5m}-PSMA-617

The DATA^{5m}(*t*Bu)$_3$-PSMA-617-resin was dissolved in a mixture of TFA and DCM (1:1, 5 mL) and stirred for 30 min. The solution was separated from the solid phase and the procedure was repeated once. The combined TFA/DCM solution was evaporated under reduced pressure and the crude product was purified by semi-preparative HPLC (column: LiChrospher 100 RP18 EC (250 x 10 mm) 5 µ, flow rate: 5 mL/min, H_2O/MeCN + 0.1% TFA, 26% MeCN isocratic, t_R = 15.8 min). The product was obtained as white solid (14.6 mg, 0.0014 mmol, 87%)

MS (ESI$^+$): 521.4 1/2[M+H]$^+$, 1043.4 [M+2H]$^+$, calculated for $C_{50}H_{72}N_8O_{16}$: 1041.2 [M]$^+$

Radiolabelling

The ^{68}Ga for ^{68}Ga radiolabelling was obtained from a ^{68}Ge/^{68}Ga-generator from ITG München, Germany). Prior to labelling, the gallium-68 was purified using the ethanol-based cationic post processing method first described by Eppard et al.[46]

For radiolabelling, the purified ^{68}Ga (30-50 MBq) was dissolved in the buffer to be evaluated and the desired amount of precursor (10 nmol, 20 nmol or 48 nmol) was added. The solution was stirred for 15 min at different temperatures (RT, 70 °C and 95 °C). Aliquots were taken after 1, 3, 5, 10 and 15 min to determine the RCY by radio-TLC or radio-HPLC. For Radio-TLC (TLC Silica gel 60 F254 Merck) citrate buffer (pH 4) was used as mobile phase and radio-HPLC was carried out using an analytical HPLC 7000 series Hitachi LaChrom (Column: Merck Chromolith® RP-18e, 5-95% MeCN (+0,1% TFA)/ 95-5% Water (+0,1% TFA) in 10 min).

In vitro stability studies

3-5 MBq of the labelled compound was incubated in 0.5 mL of human serum (HS, human male AB plasma, USA origin, Sigma Aldrich), saline and phosphate buffered saline (PBS) to investigate the *in vitro* complex stability of the radiolabelled compound. Aliquots were taken after 30, 60 and 90 min and were analysed by radio-TLC.

Lipophilicity determination

To determine the $LogD_{7.4}$ value the labelling solution was adjusted to pH 7. 2 MBq of the labelling solution were mixed with a final volume of 700 µL PBS and 700 µL n-octanol. The solution was shaken at 1500 U/min for 2 min. After centrifugation for another 2 min 300 µL of each phase was transferred into a new Eppendorf vial and 3 µL were pipetted on a TLC blade. This was repeated twice. For the repetition, the vial with the higher activity was used. The TLC blade was analysed via a phosphor imager and the $logD_{7.4}$ value was calculated based on the measured counts on the TLC blade.

***In vitro* binding affinity**

The *in vitro* binding affinity was determined by a competitive radioligand PSMA binding assay published by Benešová et al.[12] In RPMI 1650 (Thermo Fisher Scientific) PSMA-positive LNCaP-cells (Sigma-Aldrich) were cultured at 37°C in 5% CO_2 in the presence of 100 units/ml penicillin and 100 µg/ml streptomycin. The cells were incubated for 45 min with 0.75 nM [^{68}Ga]Ga-PSMA-10 and different concentrations of DATA^{5m}-PSMA-617. The cells were washed with PBS and the probes were analysed in a γ-counter (2480 WIZARD^2 Automatic Gamma Counter, PerkinElmer). The IC_{50} value was obtained after nonlinear regression of the data with GraphPad Prism 9.

Acknowledgment

The authors thank the Max Planck Graduate Center Mainz (MPGC) for supporting Tilmann Grus. The authors acknowledge X.X. for supporting X.X.

References

(1) Smetana, K.; Lacina, L.; Szabo, P.; Dvoánková, B.; Broŝ, P.; Ŝedo, A. Ageing as an Important Risk Factor for Cancer. *Anticancer Res.* **2016**, *36* (10), 5009–5017.

(2) Ferlay, J.; Colombet, M.; Soerjomataram, I.; Parkin, D. M.; Piñeros, M.; Znaor, A.; Bray, F. Cancer Statistics for the Year 2020: An Overview. *Int. J. Cancer* **2021**, *149* (4), 778–789.

(3) American Cancer Society. *American Cancer Society. Cancer Facts & Figures 2021. Atlanta: American Cancer Society; 2021*; 2021.

(4) Barinka, C.; Rojas, C.; Slusher, B.; Pomper, M. Glutamate Carboxypeptidase II in Diagnosis and Treatment of Neurologic Disorders and Prostate Cancer. *Curr Med Chem.* **2012**, *19* (6), 856–870.

(5) Czarniecki, M.; Mena, E.; Lindenberg, L.; Cacko, M.; Harmon, S.; Radtke, J. P.; Giesel, F.; Turkbey, B.; Choyke, P. L. Keeping up with the Prostate-Specific Membrane Antigens (PSMAs): An Introduction to a New Class of Positron Emission Tomography (PET) Imaging Agents. *Transl. Androl. Urol.* **2018**, *7* (5), 831–843.

(6) Bostwick, D. G.; Pacelli, A.; Blute, M.; Roche, P.; Murphy, G. P. Prostate Specific Membrane Antigen Expression in Prostatic Intraepithelial Neoplasia and Adenocarcinoma: A Study of 184 Cases. *Cancer* **1998**, *82* (11), 2256–2261.

(7) Kopka, K.; Benešová, M.; Bařinka, C.; Haberkorn, U.; Babich, J. Glu-Ureido-Based Inhibitors of Prostate-Specific Membrane Antigen: Lessons Learned during the Development of a Novel Class of Low-Molecular-Weight Theranostic Radiotracers. *J. Nucl. Med.* **2017**, *58* (Suppl 2), 17S-26S.

(8) Lütje, S.; Heskamp, S.; Cornelissen, A. S.; Poeppel, T. D.; van den Broek, S. A. M. W.; Rosenbaum-Krumme, S.; Bockisch, A.; Gotthardt, M.; Rijpkema, M.; Boerman, O. C. PSMA Ligands for Radionuclide Imaging and Therapy of Prostate Cancer: Clinical Status. *Theranostics* **2015**, *5* (12), 1388–1401.

(9) Rahbar, K.; Afshar-Oromieh, A.; Jadvar, H.; Ahmadzadehfar, H. PSMA Theranostics: Current Status and Future Directions. *Mol. Imaging* **2018**, *17*, 1536012118776068.

(10) Pillai, M. R. A.; Nanabala, R.; Joy, A.; Sasikumar, A.; Russ Knapp, F. F. Radiolabeled Enzyme Inhibitors and Binding Agents Targeting PSMA: Effective Theranostic Tools for Imaging and Therapy of Prostate Cancer. *Nucl. Med. Biol.* **2016**, *43* (11), 692–720.

(11) Benešová, M.; Bauder-Wüst, U.; Schäfer, M.; Klika, K. D.; Mier, W.; Haberkorn, U.; Kopka, K.; Eder, M. Linker Modification Strategies to Control the Prostate-Specific Membrane Antigen (PSMA)-Targeting and Pharmacokinetic Properties of DOTA-Conjugated PSMA Inhibitors. *J. Med. Chem.* **2016**, *59* (5), 1761–1775.

(12) Benešová, M.; Schäfer, M.; Bauder-Wüst, U.; Afshar-Oromieh, A.; Kratochwil, C.; Mier, W.; Haberkorn, U.; Kopka, K.; Eder, M. Preclinical Evaluation of a Tailor-Made DOTA-Conjugated PSMA Inhibitor with Optimized Linker Moiety for Imaging and Endoradiotherapy of Prostate Cancer. *J. Nucl. Med.* **2015**, *56* (6), 914–920.

(13) Umbricht, C. A.; Benešová, M.; Schmid, R. M.; Türler, A.; Schibli, R.; van der Meulen, N. P.; Müller, C. ^{44}Sc-PSMA-617 for Radiotheragnostics in Tandem with ^{177}Lu-PSMA-617—Preclinical Investigations in Comparison with ^{68}Ga-PSMA-11 and ^{68}Ga-PSMA-617. *EJNMMI Res.* **2017**, *7*, 9.

(14) Rosar, F.; Krause, J.; Bartholomä, M.; Maus, S.; Stemler, T.; Hierlmeier, I.; Linxweiler, J.; Ezziddin, S.; Khreish, F. Efficacy and Safety of [^{225}Ac]Ac-PSMA-617 Augmented [^{177}Lu]Lu-PSMA-617 Radioligand Therapy in Patients with Highly Advanced Mcrpc with Poor Prognosis. *Pharmaceutics* **2020**, *13* (5), 722.

(15) Sartor, O.; de Bono, J.; Chi, K. N.; Fizazi, K.; Herrmann, K.; Rahbar, K.; Tagawa, S. T.; Nordquist, L. T.; Vaishampayan, N.; El-Haddad, G.; Park, C. H.; Beer, T. M.; Armour, A.; Pérez-Contreras, W. J.; DeSilvio, M.; Kpamegan, E.; Gericke, G.; Messmann, R. A.; Morris, M. J.; Krause, B. J. Lutetium-177–PSMA-617 for Metastatic Castration-Resistant Prostate Cancer. *N. Engl. J. Med.* **2021**, *385* (12), 1091–1103.

(16) Fendler, W.; Kratochwil, C.; Ahmadzadehfar, H.; Rahbar, K.; Baum, R.; Schmidt, M.; Pfestroff, A.; Lützen, U.; Prasad, V.; Heinzel, A.; Heuschkel, M.; Ruf, J.; Bartenstein, P.; Krause, B. Therapie Mit ^{177}Lu-PSMA-617, Dosimetrie Und Nachsorge Beim Metastasierten Kastrationsresistenten Prostatakarzinom. *Nuklearmedizin* **2016**, *55* (03), 123–128.

(17) Cardinale, J.; Schäfer, M.; Benešová, M.; Bauder-Wüst, U.; Leotta, K.; Eder, M.; Neels, O. C.; Haberkorn, U.; Giesel, F. L.; Kopka, K. Preclinical Evaluation of ^{18}F-PSMA-1007, a New Prostate-Specific Membrane Antigen Ligand for Prostate Cancer Imaging. *J. Nucl. Med.* **2017**, *58* (3), 425–431.

(18) Awenat, S.; Piccardo, A.; Carvoeiras, P.; Signore, G.; Giovanella, L.; Prior, J. O.; Treglia, G. Diagnostic Role of ^{18}F-PSMA-1007 PET/CT in Prostate Cancer Staging: A Systematic Review. *Diagnostics* **2021**, *11* (3), 552.

(19) Mease, R. C.; Dusich, C. L.; Foss, C. A.; Ravert, H. T.; Dannals, R. F.; Seidel, J.; Prideaux, A.; Fox, J. J.; Sgouros, G.; Kozikowski, A. P.; Pomper, M. G. N-[N-[(S)-1,3-Dicarboxypropyl]Carbamoyl]-4-[^{18}F]Fluorobenzyl-L- Cysteine, [^{18}F]DCFBC: A New Imaging Probe for Prostate Cancer. *Clin. Cancer Res.* **2008**, *14* (10), 3036–3043.

(20) Rousseau, E.; Wilson, D.; Lacroix-Poisson, F.; Krauze, A.; Chi, K.; Gleave, M.; McKenzie, M.; Tyldesley, S.; Larry Goldenberg, S.; Bénard, F. A Prospective Study on ^{18}F-DCFPYL PSMA PET/CT Imaging in Biochemical Recurrence of Prostate Cancer. *J. Nucl. Med.* **2019**, *60* (11), 1587–1593.

(21) Szabo, Z.; Mena, E.; Rowe, S. P.; Plyku, D.; Nidal, R.; Eisenberger, M. A.; Antonarakis, E. S.; Fan, H.; Dannals, R. F.; Chen, Y.; Mease, R. C.; Vranesic, M.; Bhatnagar, A.; Sgouros, G.; Cho, S. Y.; Pomper, M. G. Initial Evaluation of [^{18}F]DCFPyL for Prostate-Specific Membrane Antigen (PSMA)-Targeted PET Imaging of Prostate Cancer. *Mol Imaging Biol.* **2015**, *17* (4), 565–574.

(22) Eder, M.; Schäfer, M.; Bauder-Wüst, U.; Hull, W. E.; Wängler, C.; Mier, W.; Haberkorn, U.; Eisenhut, M. ^{68}Ga-Complex Lipophilicity and the Targeting Property of a Urea-Based PSMA Inhibitor for PET Imaging. *Bioconjug. Chem.* **2012**, *23* (4), 688–697.

(23) Eder, M.; Neels, O.; Müller, M.; Bauder-Wüst, U.; Remde, Y.; Schäfer, M.; Hennrich, U.; Eisenhut, M.; Afshar-Oromieh, A.; Haberkorn, U.; Kopka, K. Novel Preclinical and Radiopharmaceutical Aspects of [^{68}Ga]Ga-PSMA-HBED-CC: A New PET Tracer for Imaging of Prostate Cancer. *Pharmaceuticals* **2014**, *7* (7), 779–796.

(24) Weineisen, M.; Schottelius, M.; Simecek, J.; Baum, R. P.; Yildiz, A.; Beykan, S.; Kulkarni, H. R.; Lassmann, M.; Klette, I.; Eiber, M.; Schwaiger, M.; Wester, H. J. ^{68}Ga-and ^{177}Lu-Labeled PSMA i and T: Optimization of a PSMA-Targeted Theranostic Concept and First Proof-of-Concept Human Studies. *J. Nucl. Med.* **2015**, *56* (8), 1169–1176.

(25) Fendler, W. P.; Eiber, M.; Beheshti, M.; Bomanji, J.; Ceci, F.; Cho, S.; Giesel, F.; Haberkorn, U.; Hope, T. A.; Kopka, K.; Krause, B. J.; Mottaghy, F. M.; Schöder, H.; Sunderland, J.; Wan, S.; Wester, H. J.; Fanti, S.; Herrmann, K. ^{68}Ga-PSMA PET/CT: Joint EANM and SNMMI Procedure Guideline for Prostate Cancer Imaging: Version 1.0. *Eur. J. Nucl. Med. Mol. Imaging* **2017**, *44* (6), 1014–1024.

(26) Hofmann, M. S.; Emmett, L.; Sandhu, S.; Iravani, A.; Joshua, A. M.; Goh, J. C.; Tan, T. H.; Krikwood, I. D.; Ng, S.; Francis, R. J.; Gedye, C.; Rutherford, N. K.; Weickhardt, A.; Scott, A. M.; Lee, S.-T.; M., K. E.; Azad, A. A.; Zhang, A. Y. [^{177}Lu]Lu-PSMA-617 versus Cabazitaxel in Patients with Metastatic Castration-Resistant Prostate Cancer (TheraP): A Randomised, Open-Label, Phase 2 Trial. *Lancet* **2021**, *297* (10276), 797–804.

(27) Das, T.; Guleria, M.; Parab, A.; Kale, C.; Shah, H.; Sarma, H. D.; Lele, V. R.; Banerjee, S. Clinical Translation of ^{177}Lu-Labeled PSMA-617: Initial Experience in Prostate Cancer Patients. *Nucl. Med. Biol.* **2016**, *43* (5), 296–302.

(28) Rosar, F.; Kochems, N.; Bartholomä, M.; Maus, S.; Stemler, T.; Linxweiler, J.; Khreish, F.; Ezziddin, S. Renal Safety of [^{177}Lu]Lu-PSMA-617 Radioligand Therapy in Patients with Compromised Baseline Kidney Function. *Cancers.* **2021**, *13* (12), 3095.

(29) Yordanova, A.; Becker, A.; Eppard, E.; Kürpig, S.; Fisang, C.; Feldmann, G.; Essler, M.; Ahmadzadehfar, H. The Impact of Repeated Cycles of Radioligand Therapy Using [^{177}Lu]Lu-PSMA-617 on Renal Function in Patients with Hormone Refractory Metastatic Prostate Cancer. *Eur. J. Nucl. Med. Mol. Imaging* **2017**, *44* (9), 1473–1479.

(30) Wichmann, C. W.; Ackermann, U.; Poniger, S.; Young, K.; Nguyen, B.; Chan, G.; Sachinidis, J.; Scott, A. M. Automated Radiosynthesis of [^{68}Ga]Ga-PSMA-11 and [^{177}Lu]Lu-PSMA-617 on the IPHASE MultiSyn Module for Clinical Applications. *J. Label. Compd. Radiopharm.* **2021**, *64* (3), 140–146.

(31) Price, E. W.; Orvig, C. Matching Chelators to Radiometals for Radiopharmaceuticals. *Chem. Soc. Rev.* **2014**, *43*, 260–290.

(32) Tsionou, M. I.; Knapp, C. E.; Foley, C. A.; Munteanu, C. R.; Cakebread, A.; Imberti, C.; Eykyn, T. R.; Young, J. D.; Paterson, B. M.; Blower, P. J.; Ma, M. T. Comparison of Macrocyclic and Acyclic Chelators for Gallium-68 Radiolabelling. *RSC Adv.* **2017**, *7* (78), 49586–49599.

(33) Spang, P.; Herrmann, C.; Roesch, F. Bifunctional Gallium-68 Chelators: Past, Present, and Future. *Semin. Nucl. Med.* **2016**, *46* (5), 373–394.

(34) Waldron, B. P.; Parker, D.; Burchardt, C.; Yufit, D. S.; Zimny, M.; Roesch, F. Structure and Stability of Hexadentate Complexes of Ligands Based on AAZTA for Efficient PET Labelling with Gallium-68. *Chem. Commun.* **2013**, *49* (6), 579–581.

(35) Farkas, E.; Nagel, J.; Waldron, B. P.; Parker, D.; Tóth, I.; Brücher, E.; Rösch, F.; Baranyai, Z. Equilibrium, Kinetic and Structural Properties of Gallium(III) and Some Divalent Metal Complexes Formed with the New DATA^{m} and DATA^{5m} Ligands. *Chem. Eur. J.* **2017**, *23* (43), 10358–10371.

(36) Seemann, J.; Waldron, B. P.; Roesch, F.; Parker, D. Approaching “kit-Type” Labelling with ^{68}Ga: The DATA Chelators. *ChemMedChem* **2015**, *10* (6), 1019–1026.

(37) Sinnes, J. P.; Nagel, J.; Waldron, B. P.; Maina, T.; Nock, B. A.; Bergmann, R. K.; Ullrich, M.; Pietzsch, J.; Bachmann, M.; Baum, R. P.; Rösch, F. Instant Kit Preparation of ^{68}Ga-Radiopharmaceuticals via the Hybrid Chelator DATA: Clinical Translation of [^{68}Ga]Ga-DATA-TOC. *EJNMMI Res.* **2019**, *9*, 48.

(38) Nock, B. A.; Kaloudi, A.; Nagel, J.; Sinnes, J.-P.; Roesch, F.; Maina, T. Novel Bifunctional DATA

Chelator for Quick Access to Site-Directed PET ^{68}Ga-Radiotracers: Preclinical Proof-of-Principle with [Tyr3]Octreotide. *Dalt. Trans.* **2017**, *46* (42), 14584–14590.

(39) Seemann, J.; Waldron, B.; Parker, D.; Roesch, F. DATATOC: A Novel Conjugate for Kit-Type ^{68}Ga Labelling of TOC at Ambient Temperature. *EJNMMI Radiopharm. Chem.* **2017**, *1*, 4.

(40) Sinnes, J.-P. Synthese und radiochemische Evaluierung von Chelatoren für milde Markierungen mit ^{68}Ga, ^{44}Sc Und ^{177}Lu Sowie *in vitro*- und *in vivo*- Evaluierung von deren TOC- Und PSMA-Derivaten. *Dissertation. - Johannes Gutenberg-University Mainz* **2018**.

(41) Lahnif, H.; Grus, T.; Pektor, S.; Greifenstein, L.; Schreckenberger, M.; Rösch, F. Hybrid Chelator-Based PSMA Radiopharmaceuticals: Translational Approach. *Molecules* **2021**, *26* (21), 6332.

(42) Greifenstein, L.; Engelbogen, N.; Lahnif, H.; Sinnes, J.-P.; Bergmann, R.; Bachmann, M.; Rösch, F. Synthesis, Labeling and Preclinical Evaluation of a Squaric Acid Containing PSMA Inhibitor Labeled with ^{68}Ga: A Comparison with PSMA-11 and PSMA-617. *ChemMedChem* **2020**, *15* (8), 695–704.

(43) Baranski, A. C.; Schäfer, M.; Bauder-Wüst, U.; Roscher, M.; Schmidt, J.; Stenau, E.; Simpfendörfer, T.; Teber, D.; Maier-Hein, L.; Hadaschik, B.; Haberkorn, U.; Eder, M.; Kopka, K. PSMA-11–Derived Dual-Labeled PSMA Inhibitors for Preoperative PET Imaging and Precise Fluorescence-Guided Surgery of Prostate Cancer. *J. Nucl. Med.* **2018**, *59* (4), 639–645.

(44) Linton, M. A.; Burke, B. J.; Johnson, T. W.; Ninkovic, S.; Gajiwala, K. S.; Richardson, P.; Le, P. T. Effect of Water Solvation on the Lipophilicity of Isomeric Pyrimidine-Carboxamides. *Bioorganic Med. Chem.* **2015**, *23* (13), 3408–3413.

(45) Robu, S.; Schmidt, A.; Eiber, M.; Schottelius, M.; Günther, T.; Hooshyar Yousefi, B.; Schwaiger, M.; Wester, H. J. Synthesis and Preclinical Evaluation of Novel ^{18}F-Labeled Glu-Urea-Glu-Based PSMA Inhibitors for Prostate Cancer Imaging: A Comparison with ^{18}F-DCFPyl and ^{18}F-PSMA-1007. *EJNMMI Res.* **2018**, *8*, 30.

(46) Eppard, E.; Wuttke, M.; Nicodemus, P. L.; Rösch, F. Ethanol-Based Post-Processing of Generator-Derived ^{68}Ga Toward Kit-Type Preparation of ^{68}Ga-Radiopharmaceuticals. *J. Nucl. Med.* **2014**, *55* (6), 1023–1028.

4.2 Project B: Prostate cancer and related bone metastases

DOTA conjugate of Bisphosphonate and PSMA-inhibitor: A promising combination for therapy of prostate cancer related bone metastases

Tilmann Grus, X.X., X.X., X.X. and X.X.'

Submitted to Frontiers in Nuclear Medicine - Radiopharmacy and Radiochemistry

Summary

Developing of bone metastases is a serious problem for patients with prostate cancer.[1] It is often difficult to conduct appropriate therapy of bone metastases with the state-of-art PSMA radiopharmaceutical [^{177}Lu]Lu-PSMA-617, since PSMA expression can vary or completely be missing in bone metastases.[2–4] Other approaches for a successful deposition of therapeutic radioactivity, besides the use of PSMA target vectors have to be found.

In this manuscript, a novel heterodimeric compound is presented which enables bone targeting via two different mechanisms and thus enables therapy of bone metastases independently of a high PSMA expression. This compound is composed of the PSMA inhibitor structure of PSMA-617, which can be used for enrichment in bone metastases based on PSMA, but also consists of the bisphosphonate pamidronate. Bisphosphonates show high affinity towards hydroxyapatite, the inorganic matrix of bones and bind to bone regions with high metabolism rate, as also found in bone metastases.[5,6] A DOTA chelator for metal nuclide radiolabelling is also part of the molecule.

After the 15 step synthesis of the novel DOTA-L-Lys(SA.Pam)-PSMA-617 the radiochemical properties, as well as the *in vitro* affinity towards both targets were evaluated. The compound was labelled in less than 15 min with lutetium-177 yielding radiochemical yields of more than 90%. The formed complex was stable in several media (PBS, NaCl, human serum) for at least 14 days. [^{177}Lu]Lu-DOTA-L-Lys(SA.Pam)-PSMA-617 showed very good HAP binding properties, while [^{177}Lu]Lu-PSMA-617 was not able to bind to HAP. PSMA binding affinity of the heterodimer was worse than the PSMA affinity of [^{177}Lu]Lu-PSMA-617 and also the literature known *in vivo* tumour accumulation of [^{177}Lu]Lu-PSMA-617[7] is better than the tumour accumulation found for [^{177}Lu]Lu-DOTA-L-Lys(SA.Pam)-PSMA-617 in *ex vivo* biodistribution studies in tumour bearing mice. Bone uptake is not known for [^{177}Lu]Lu-PSMA-617, but due to the bisphosphonate structure the novel compound showed a bone uptake, which is comparable to other literature known bisphosphonates.[8]

This study showed that [^{177}Lu]Lu-DOTA-L-Lys(SA.Pam)-PSMA-617 is a promising candidate for therapy of PCa related bone metastases with low or unknown PSMA expression. In such cases the dual targeting mechanism of the novel compound could superior to the single targeting mechanism of [^{177}Lu]Lu-PSMA-617. This needs to be further investigated in additional studies with mice with bone metastases and in initial human applications.

Autor contributions:

T. Grus, X.X. and X.X. planned the study. **T. Grus** performed organic synthesis, radiolabelling synthesis, *in vivo* stability, lipophilicity studies, HAP binding studies and the analysis of the obtained data. X.X. was responsible for LNCaP cell cultivation and *in vitro* binding affinity assay and its evaluation. Animal studies were performed by **T.Grus**, X.X. and X.X. X.X. performed the data analysis of the animal studies. **T. Grus** and X.X. wrote the manuscript. All authors reviewed the manuscript. The project was supervised by X.X. and X.X.

References in the summary

(1) Thomas, T. S.; Pachynski, R. K. Treatment of Advanced Prostate Cancer. *Mo. Med.* **2018**, *115* (2), 156–161.

(2) Acar, E.; Bekis, R.; Polack, B. Comparison of Bone Uptake in Bone Scan and Ga-68 PSMA PET/CT Images in Patients with Prostate Cancer. *Curr. Med. Imaging Rev* **2019**, *15* (6), 589–594.

(3) Silver, D. A.; Pellicer, I.; Fair, W. R.; Heston, W. D.; Cordon-Cardo, C. Prostate-Specific Membrane Antigen Expression in Normal and Malignant Human Tissues. *Clin. Cancer Res.* **1997**, *3* (1), 81-85.

(4) Ahmadzadehfar, H.; Matern, R.; Baum, R. P.; Seifert, R.; Kessel, K.; Bögemann, M.; Kratochwil, C.; Rathke, H.; Ilhan, H.; Svirydenka, H.; Sathekge, M.; Kabasakal, L.; Yordanova, A.; Garcia-Perez, F. O.; Kairemo, K.; Maharaj, M.; Paez, D.; Virgolini, I.; Rahbar, K. The Impact of the Extent of the Bone Involvement on Overall Survival and Toxicity in MCRPC Patients Receiving [^{177}Lu]Lu-PSMA-617: A WARMTH Multicentre Study. *Eur. J. Nucl. Med. Mol. Imaging* **2021**, *48* (12), 4067–4076.

(5) Lin, J. H. Bisphosphonates: A Review of Their Pharmacokinetic Properties. *Bone* **1996**, *18* (2), 75–85.

(6) Palma, E.; Correia, J. D. G.; Campello, M. P. C.; Santos, I. Bisphosphonates as Radionuclide Carriers for Imaging or Systemic Therapy. *Mol. Biosyst.* **2011**, *7* (11), 2950–2966.

(7) Benešová, M.; Schäfer, M.; Bauder-Wüst, U.; Afshar-Oromieh, A.; Kratochwil, C.; Mier, W.; Haberkorn, U.; Kopka, K.; Eder, M. Preclinical Evaluation of a Tailor-Made DOTA-Conjugated PSMA Inhibitor with Optimized Linker Moiety for Imaging and Endoradiotherapy of Prostate Cancer. *J. Nucl. Med.* **2015**, *56* (6), 914–920.

(8) Meckel, M.; Bergmann, R.; Miederer, M.; Roesch, F. Bone Targeting Compounds for Radiotherapy and Imaging: *Me(III)-DOTA Conjugates of Bisphosphonic Acid, Pamidronic Acid and Zoledronic Acid. *EJNMMI Radiopharm. Chem.* **2017**, *1*, 14.

Abstract

Background: Prostate cancer (PCa) is one of the most common cancer types worldwide. 90% of men with late stage PCa will develop bone metastases. Since the expression level of PSMA (prostate-specific membrane antigen) in bone metastases can vary significantly, a compound is being searched for which accumulates in bone metastases independently of PSMA level. With DOTA-L-Lys(SA.Pam)-PSMA-617, we present in this paper a compound that, in addition to a PSMA inhibitor as a target vector, also contains a bisphosphonate that is established as a bone tracer and thus combines the advantages of PSMA targeting and bone targeting. This is a class of small molecules combining targeting of two different targets with the potential advantages for treatment of biologically heterogeneous bone metastasis from prostate cancer. The molecule can be labelled with ^{177}Lu via the DOTA chelator and used for the therapy of PCa-related bone metastases.

Methods: DOTA-L-Lys(SA.Pam)-PSMA-617 was synthesized in a 15 step synthesis and radiolabelled in 1 M ammonium acetate buffer pH 5.5 at 95 °C. Different amounts of precursor were evaluated. Complex stability was evaluated in three different media (HS, PBS and NaCl). The $logD_{7.4}$ value was evaluated via the determination of the equilibrium distribution in a PBS/n-octanol mixture. A hydroxyapatite binding assay was used to evaluate the potential binding of the compound to bone metastases. *In vitro* affinity was determined in a competitive binding assay and K_i value was evaluated. To evaluate the binding potential in mice, *ex vivo* biodistribution studies were carried out in LNCaP tumour-bearing Balb/c mice.

Results: [^{177}Lu]Lu-labelling of DOTA-L-Lys(SA.Pam)-PSMA-617 showed quantitative RCY within 10 minutes and a high complex stability over a period of 14 days. The lipophilicity of the labelled compound was similar to the lipophilicity of the reference compound [^{177}Lu]Lu-PSMA-617 (-2.29 ± 0.12% vs. -2.23 ± 0.20) and showed an excellent and selective HAP binding of 98.2 ± 0.11%. With a K_i of 42.3 ± 7.7 nM the PSMA binding affinity was lower in comparison to [^{177}Lu]Lu-PSMA-617. First *ex vivo* biodistribution studies with LNCaP tumour-bearing Balb/c mice showed a PSMA dependent tumour accumulation of 4.2 ± 0.7%ID/g and a femur accumulation of 3.4 ± 0.4%ID/g. High tumour-to-blood and bone-to-blood-ratios (210 and 170) were also achieved.

Conclusions: [^{177}Lu]Lu-DOTA-L-Lys(SA.Pam)-PSMA-617 is a promising compound for theranostic of PCa related bone metastases. Accumulation on the bone metastases via two mechanisms also enables the treatment of bone metastases that show little or no PSMA expression.

Keywords: PSMA, Bisphosphonate, Pamidronate, Bone metastases, prostate cancer, Lutetium-177

Introduction

Prostate cancer (PCa) is one of the most commonly diagnosed cancer diseases in the world and one of the leading causes of cancer-related deaths worldwide.[1] The 5-year survival rate for early diagnosed and localised PCa is 98%. However, if metastases have already formed, the rate decreases to 30%.[2]

The introduction of prostate-specific membrane antigen (PSMA) as a molecular target has revolutionised the diagnosis and treatment of PCa. In recent years, there has been a rapid increase in new radiopharmaceuticals for diagnosis and targeted radionuclide therapy of PCa.[3,4] Particularly small molecule-based PSMA ligands have received a lot of attention.[5,6] The type II transmembrane glycoprotein PSMA or glutamate carboxypeptidase II (GCPII) consists of 750 amino acids and is located in the cell membrane of prostate epithelial cells. Usually, PSMA expression is upregulated in PCa and correlates with the aggressiveness of the disease.[7] Apart from PCa, PSMA is physiologically expressed only in few normal tissues, such as the kidney and the salivary glands.[8] Upon binding of a substrate to PSMA, internalisation occurs. With regard to therapy, a targeted and irreversible uptake of the therapeutic nuclide into the PCa cell is thus possible.[9]

The most commonly used PSMA inhibitors are based on urea derivatives. The currently most promising PET-PSMA radiopharmaceutical is PSMA-11, which can be labelled with ^{68}Ga. [11] PSMA-617, labelled with ^{177}Lu ([^{177}Lu]Lu-PSMA-617, Lu-PSMA) is the most important therapeutic compound until now.[8,12,13] The results of the clinical phase III study have just been published. The so-called VISION study demonstrated a good tolerability of the [^{177}Lu]Lu-PSMA-617 therapy along with an increase in the overall survival rate. Hence, introduction of [^{177}Lu]Lu-PSMA-617 as standard treatment is recommended.[14]

Most men with advanced PCa develop bone metastases.[15] This affects about 90% of men with late stage PCa.[16] The presence of bone metastases is a negative indicator for the survival of the patient. The WARMTH study has shown that the overall survival rate of patients with bone metastases treated with [^{177}Lu]Lu-PSMA-617 is lower than when the overall survival rate of patients without bone metastases.[17] Independently of this, bone metastases cause a significant reduction in quality of life due to, e.g., pain and pathological fractures or compression of the spinal cord and nerve roots or the displacement of red bone marrow, which appears especially in advanced PCa.[18]

While metastasis in bone tissue can be osteoblastic, osteolytic or mixed forms, PCa-related metastases are usually osteblastic.[19,20] In both cases, the hydroxyapatite (HAP), the mineral material of the bone, is uncovered due to the increased metabolism and bone remodelling.[21,22]
Over the last 40 years, bisphosphonates have become established as drugs for various bone diseases.[23] The efficacy of these pyrophosphate derivatives is based on a high affinity to HAP, which is due to the

chelation of the calcium ions of HAP.[24] Bisphosphonates, such as MDP (methylene diphosphonate) or EDTMP (ethylenediamine tetra(methylene phosphonic acid)), are acyclic phosphonic acids that can both complex a radionuclide and adsorb to HAP, enabling diagnosis or therapy via the radioactivity of the nuclide.[25] [^{153}Sm]Sm-EDTMP is used, for example, for reduction of bone metastases-induced pain.[26] In addition, there are bisphosphonates that are functionalised with a chelator that enables the radiolabelling. These include compounds such as BPAMP[27] or the most promising [^{177}Lu]Lu-DOTA^{ZOL}.[28,29]

One of the first clinically investigated nitrogen-containing bisphosphonate is pamidronate (Pam). The conjugation of Pam to squaric acid (SA) not only allows an easy and rapid conjugation with other moieties, such as chelators,[30] but also supports the antiresorptive effect of the bisphosphonate due to the presence of an amine component at this position.[31,32] This is also the case, for example, with the highly potent bisphosphonate zolendronate.[28,29,31] Unpublished data indicate that SA.Pam has a higher bone uptake than, for example, DOTA^{ZOL}.

Prostate cancer can vary widely in the expression of PSMA. It is known that primary tumours and especially metastases can be PSMA-negative.[33–37] This can also be the case for bone metastases.[35,36] Here, it was shown that there is a high correlation between bone metabolic activity and cancer-related PSMA expression in bone lesions at early stages of the disease, implying that bone metastases have significantly higher PSMA expression at early stages. In later stages, this correlation is increasingly absent or there is a greater deviation, which implies a lower PSMA expression in bone metastases.[38] The reasons for this heterogeneous expression are manifold and many effects can play a role. These can be the complex biochemical and pathobiological processes due to genetically and non-genetically induced differentiation types of the tumour and the metastases in the progress of the disease.[16,36,39,40] Another influence can be, for example, the type of therapy.[41]

It was found that low average PSMA expression in metastases is associated with a shorter overall survival rate.[40] At the moment, it is not yet clear whether patients with low PSMA-levels benefit from a therapy with lutetium-177 labelled PSMA-617.[40]

Therefore, there is a need for a compound that can accumulate at PCa-related bone metastases also independently of PSMA-level. In terms of imaging, different pairs of PSMA PET-tracers and bone scan agents have been studied in the past with varying results in their performance.[38,41–46] For example, a study by Rowe et al showed that the PSMA inhibitor [^{18}F]F-DCFPyl detected more bone lesions than the bisphosphonate [^{99m}Tc]Tc-MDP and Na^{18}F, which also have a high affinity towards HAP.[43] In another study by Uprimmy et al [^{18}F]NaF outperformed [^{68}Ga]Ga-PSMA-11 by finding more bone lesions.[45]

The combination of the advantages of PSMA targeting and bone targeting in one compound would reduce the complexity of the treatment, enables additional expression-independent therapy of bone metastases and thus would be favourable. In this way, bone metastases can be treated via two mechanisms, the possible PSMA expression and the imbalanced metabolic mechanism of the bone cells. In this study, we developed a chimeric compound containing the highly affine PSMA inhibitor KuE on the one side and a bisphosphonate drug (pamidronate, Pam) on the other side. Both targeting moieties are coupled to the DOTA chelator and can therefore be used for endoradiotherapy with e.g. ^{177}Lu. Furthermore, we used the PSMA-617 linker for coupling the KuE unit to DOTA, since it has been proven that this linker plays an important role in enhancing the PSMA binding affinity.[8] Moreover, pamidronate was coupled to DOTA via squaramide, which has also shown a positive impact in terms of simplified synthesis and improved pharmacokinetics.[47]

Results

Organic synthesis of DOTA-L-Lys(SA.Pam)-PSMA-617

The synthesis of DOTA-L-Lys(SA.Pam)-PSMA-617 was divided into three parts. First the solid-phase based synthesis route of the PSMA-617 motif (**6**) based on the synthetic route developed by Benešová et al.[8,12] (figure 1). The bisphosphonate-based target vector (**8**) unit was synthesized in a two-step synthesis (figure 2). Both target vectors were then combined in a third synthesis step using lysine as a linking bridge and functionalised with a DOTA chelator for radiolabelling (figure 3).

The eight-step solid-phase synthesis of the PSMA-617-backbone (figure 1) started from L-lysine which is bound to a Wang-resin. In the first step, an isocyanate was generated by adding triphosgene to bis(*tert*-butyl)-L-glutamate, which was then added to the Fmoc-deprotected lysine-resin to generate the KuE unit of the PSMA inhibitor. To add the PSMA-617-linker unit, the alloc protecting group of the side chain amine of **1** was removed by reduction. This was followed by addition of the amino acids 3-(2-napthyl)-L-alanine and 4-aminomethylcyclohecxane-OH (4-Amc-OH) to the side chain amine of lysine, using a standardised solid-phase based peptide synthesis protocol with HATU (1-[Bis(dimethylamino)methylene]-1H-1,2,3-triazolo[4,5-b]pyridinium 3-oxide hexafluorophosphate) as coupling reagent. The final solid-phase bound and protected PSMA-617-target vector motif (**5**) was obtained. The Fmoc protecting group of the aminomethylcyclohexane group was removed for further functionalisation.

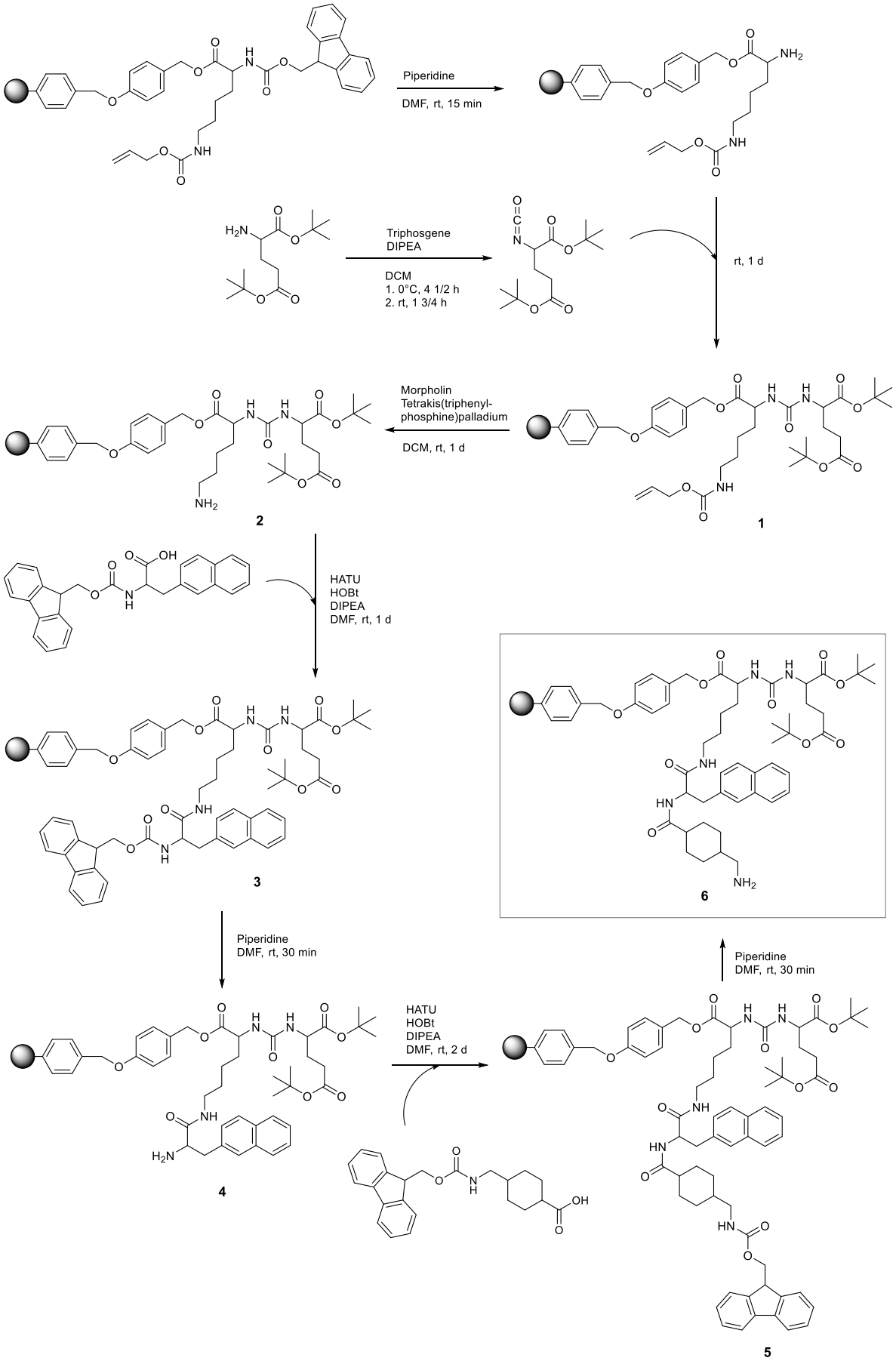

Figure 1: synthesis scheme of the resin bound PSMA-617 backbone.

The second target vector, the squaric acid conjugated bisphosphonate pamidronate (**8**) was synthesized in a two-step synthesis with an overall yield of 28% (figure 2). According to literature, β-Alanine was transformed into pamidronate (**7**) using phosphorus acid and phosphorus trichloride.[48] This was followed by an asymmetric amidation to conjugate the amine of the bisphosphonate to the squaric acid ester.

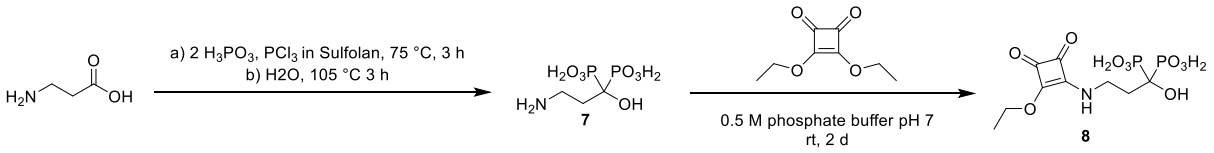

Figure 2: synthesis scheme of the pamidronate target vector (8)

The final part of the synthesis was the conjugation of the two target vectors **6** and **8** and the DOTA-chelator using lysine as bridging unit (figure 3). First, protected lysine was conjugated to the free amine of the resin bound compound **6**. After Fmoc deprotection, DOTA-Tris(*tert*-butyl ester) was conjugated. Both steps were carried out with HATU as reagent for amide formation. This reaction led to the complete protected and resin bound compound **11**. This compound was completely deprotected under acidic conditions and removed from the solid phase. In the further process of the reaction, protective groups are no longer necessary, as the following asymmetric amidation is highly selective for amines. Compound **12** was purified via semi preparative HPLC resulting in a yield of 4% after the amide formation steps. Finally, the second target vector Pam.SA (**8**) was added - this was done via the asymmetric amidation of the squaric acid monoester and the free amine of compound **12**. Due to poor solubility of the bisphosphonate **8** in organic solvents, this reaction was carried out in aqueous phosphate buffer at a pH value of 9. The final compound **13** was purified via semi-preparative HPLC with a yield of 84%. The entire compound DOTA-L-Lys(SA.Pam)-PSMA-617 was prepared in 15 steps with a total yield of 1%.

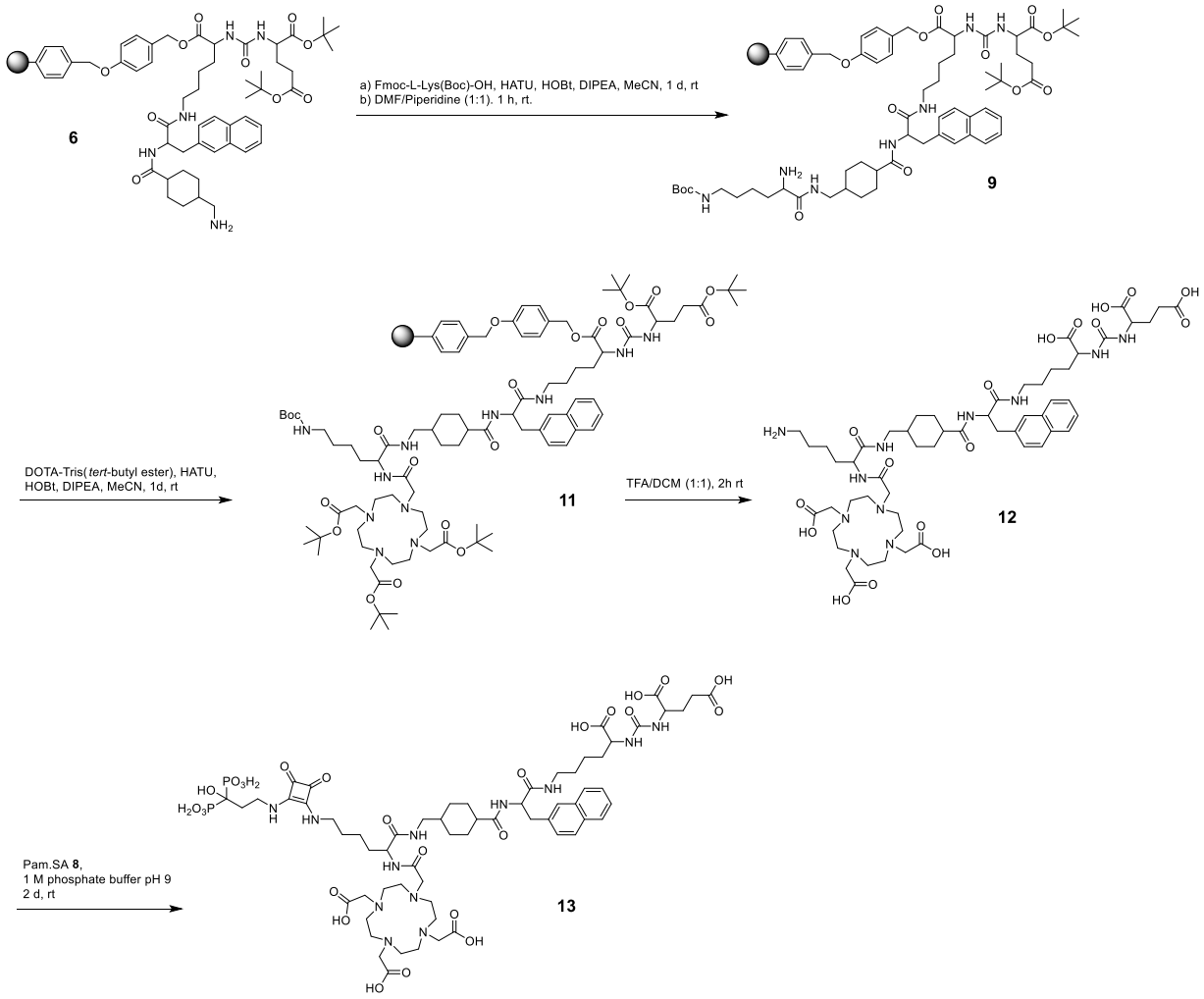

Figure 3: synthesis scheme of DOTA-L-Lys(SA.Pam)-PSMA-617 (**13**)

Radiochemical evaluation with lutetium-177

Radiolabelling of compound **13** with Lu-177 was carried out at 95°C in 1 mL of ammonium acetate buffer (1 M, pH 5.5). The radiochemical yield (RCY) as a function of precursor amount (5 to 30 nmol) was evaluated and illustrated in figure 4.

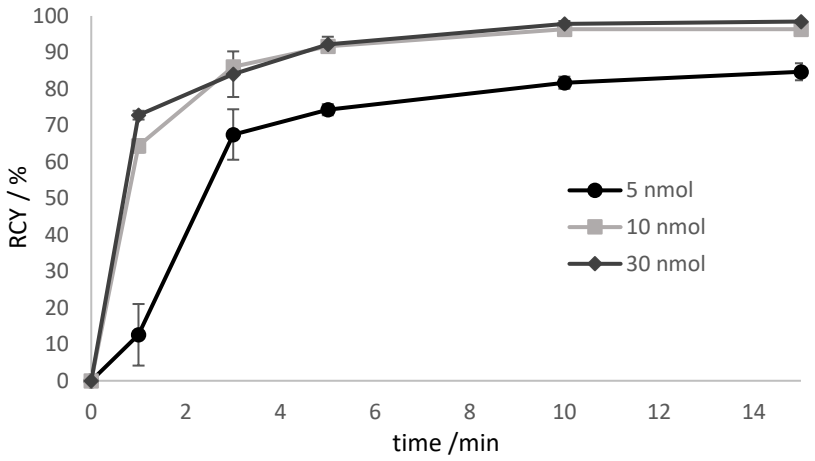

Figure 4: labelling kinetics of [^{177}Lu]Lu-13 for various amounts of precursor at 95 °C in 1 M ammonium acetate buffer pH 5.5 at 95 °C. Precoursor amounts of > 10 nmol resulting in RCYs of > 96% after 10 min.

For substance amounts higher than 10 nmol, radiochemical yields of over 90% were already achieved after 5 min. The RCY was almost quantitative after 10 min. In contrast, with a substance quantity of 5 nmol, the RCY obtained after 5 min was of only 75%. In the further progress of the reaction, the yield increased to 85%, but then stagnated there indicating that the labelling kinetics are depending on the amount of the precursor. RCY and radiochemical purity were analysed by radio-TLC and radio-HPLC. On radio-TLC the labelled compound [^{177}Lu]Lu-**13** showed a R_f of 0.0, while free unlabelled [^{177}Lu]Lu^{3+} showed a R_f of 0.8 – 1 in citrate buffer as mobile phase. On analytical radio-HPLC, the compound had a retention time (t_R) of 9.8 min.

Since the stability of the ligand-chelator conjugate is crucial for a translational use, complex stability studies were carried out different media (phosphate buffered saline (PBS), isotonic saline (NaCl) and human serum (HS)). Results are shown in figure 5.

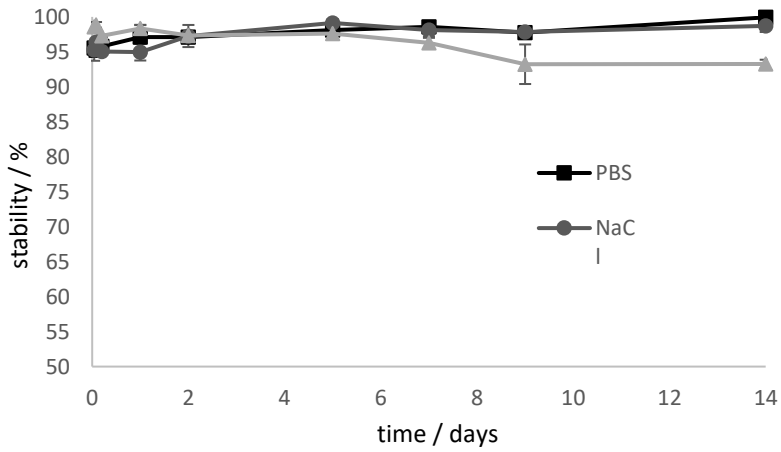

Figure 5: Stability studies of [^{177}Lu]Lu-**13** in different media for 14 d. [^{177}Lu]Lu-**13** is stable in PBS and NaCl. The stability in HS decreases to 93% after 9 days.

In PBS and saline, [^{177}Lu]Lu-**13** showed > 98% intact conjugate even after 14 days. Stability in human serum decreases slightly. However, after 9 d, 93% were still intact. Stability was preserved and even after 14 days the stability in HS was still at 93%.

The lipophilicity of the compound was determined via the equilibrium distribution in a mixture of n-octanol and PBS using the shake flask method. Log$D_{7.4}$ values of [^{177}Lu]Lu-**13** and the reference compound [^{177}Lu]Lu-PSMA-617 are shown in table 1. The lipophilicity of the lutetium-labelled compound **13** was similar to the lipophilicity of [^{177}Lu]Lu-PSMA-617.

Table 1: experimentally determined log$D_{7.4}$ values of [^{177}Lu]Lu-**13** and the reference [^{177}Lu]Lu-PSMA-617

Compound	**log$D_{7.4}$ (n-octanol/PBS)**
[^{177}Lu]Lu-**13**	- 2.29 ± 0.12
[^{177}Lu]Lu-PSMA-617	- 2.23 ± 0.20

Binding studies on hydroxyapatite (HAP)

The Ca-containing hydroxyapatite is found in mammal bones.[49] Crystalline HAP is therefore suitable as a model compound to investigate the accumulation potential of bisphosphonates to the bone structure or bone metastases *in vitro*. Figure 6 shows the enrichment of [^{177}Lu]Lu-**13**, [^{177}Lu]Lu-PSMA-617 and free [^{177}Lu]Lu to HAP in comparison to the enrichment of [^{177}Lu]Lu-**13** and free [^{177}Lu]Lu^{3+} to HAP previously blocked with pamidronate.

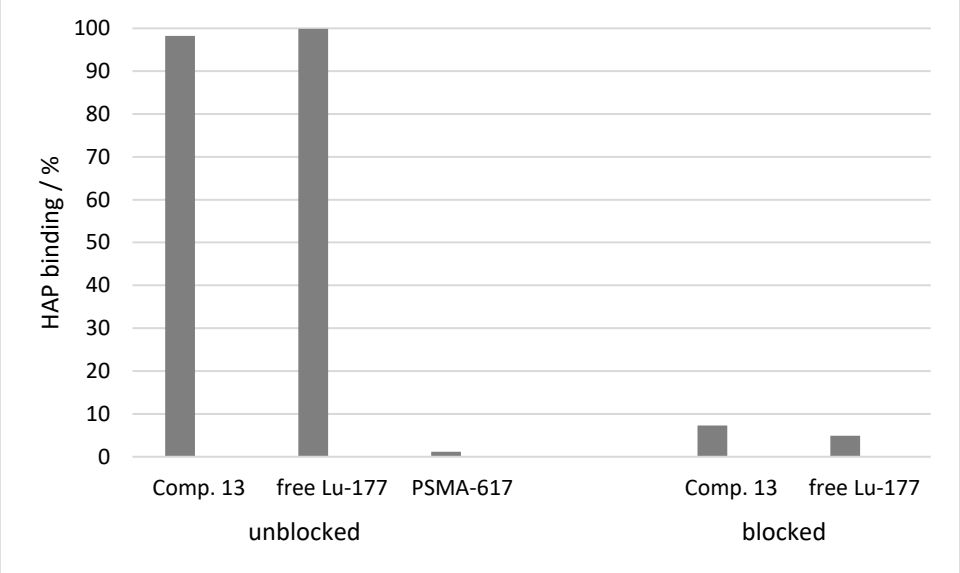

Figure 6: Percent enrichment of [^{177}Lu]Lu-**13** (98.2 ± 0.11%), [^{177}Lu]Lu-PSMA-617 (1.20 ± 0.30%) and free [^{177}Lu]Lu^{3+} (99.89 ± 0.02%) to HAP in comparison to the percent enrichment of [^{177}Lu]Lu-**13** (7.31 ± 1.08%) and free [^{177}Lu]Lu^{3+} (4.89 ± 0.51%) to HAP previously blocked with pamidronate.

Uncomplexed lutetium cation [^{177}Lu]Lu^{3+} is known for its high affinity towards HAP.[49] Therefore, it was used as positive sample. In this study, it showed a HAP-binding of 99.89 ± 0.02%. [^{177}Lu]Lu-**13** also showed also a nearly complete enrichment at the HAP surface (98.2 ± 0.11%), comparable to the free lutetium cation. In contrast, [^{177}Lu]Lu-PSMA-617 displayed no notable binding (1.20 ± 0.30%). To evaluate the selectivity of binding, HAP was blocked with an excess of pamidronate prior to incubation with the test compounds. The binding of [^{177}Lu]Lu-**13** (7.31 ± 1.08%) as well as [^{177}Lu]Lu^{3+} (4.89 ± 0.51%) decreased significantly, indicating a specific binding to the calcium ions of the apatite structure.

In vitro affinity assay

In a further step, we evaluated the PSMA binding affinity of compound **13** in a competitive radioligand assay and compared the calculated K_i value to the inhibition constant values of compound **12** to evaluate the influence of the SA.Pam unit and to PSMA-617 as seen in table 2. Compound **13** showed good binding affinity similar to that of [^{nat}Lu]Lu-**13**, thus indicating that radionuclide complexation does not have any impact on PSMA-binding. However, the bisphosphonate-free PSMA tracer DOTA-L-Lys-PSMA-617 (compound **12**) displayed 2-fold higher binding potency than the pamidronate-PSMA conjugates, indicating an influence of the SA.Pam unit. In addition, the binding affinity of the reference compound PSMA-617 in this assay was also higher than in comparison to compound **13**. Compound **12** showed a 2.5-fold lower affinity in contrast to PSMA-617.

Table 2: inhibition constant values of PSMA ligands. Values are mean ±SD. *IC_{50} values can be found at Greifenstein et al.[47]

Compound	**K_i [nM]**
compound **13**	52.6 ± 3.5
[^{nat}Lu]Lu-**13**	42.3 ± 7.7
compound **12** (DOTA-L-Lys-PSMA-617)	19.7 ± 3.3
PSMA-617*	6.9 ± 1.3

ex vivo studies

Biodistribution studies of [^{177}Lu]Lu-**13** were performed using LNCaP tumour-bearing Balb/c mice. The accumulation of the ^{177}Lu-labelled tracer in several organs was determined and illustrated in figure 7. Although the accumulation of the tracer in both tumour and femur were similar (4.2 ± 0.7%ID/g and 3.4 ± 0.4%ID/g respectively), the bone-uptake was, in contrast to tumour-uptake, not PSMA-specific since it could not be blocked by the PSMA inhibitor PMPA (2-(Phosphonomethyl)pentanedioic acid). Additionally, [^{177}Lu]Lu-**13** showed the highest accumulation in the kidneys 16.5 ±2.1%ID/g, which seems to be PSMA-specific because it could be reduced by co-injection of PMPA. In contrast, the

uptake in the liver as well as in the spleen was PSMA-unspecific. Noteworthy is the high tumour-to-blood and bone-to-blood ratios (210 and 170 respectively) resulting from a minimal accumulation in the blood.

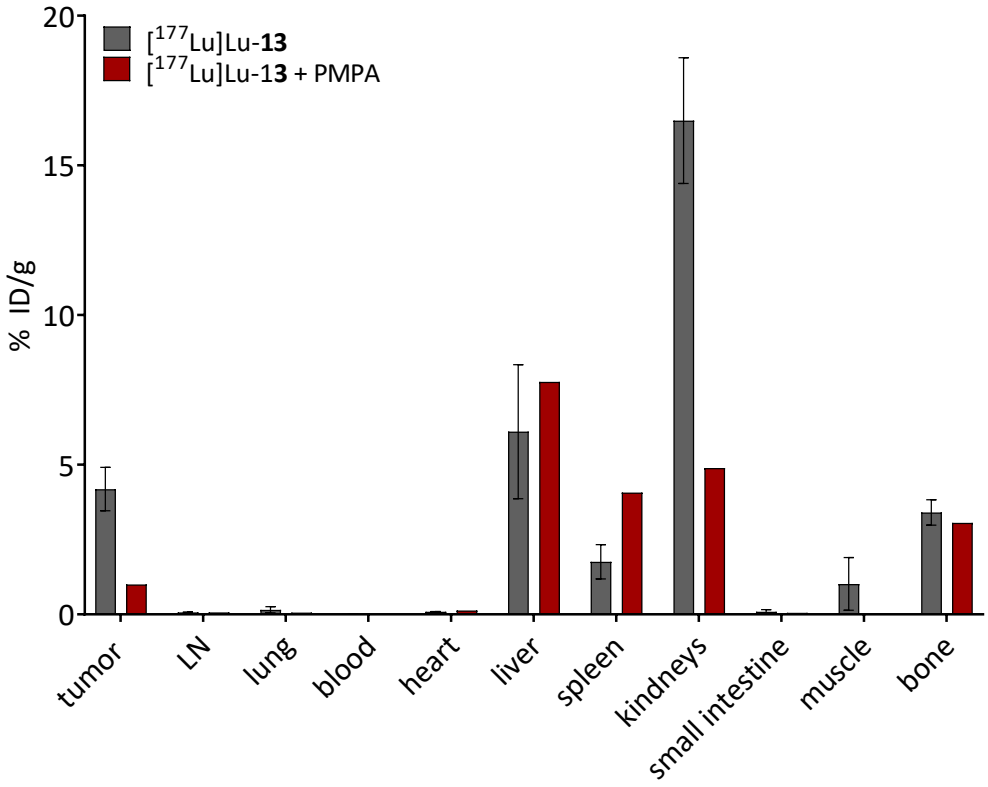

Figure 7: biodistribution of 0.5 nmol [^{177}Lu]Lu-**13** at 24 h p.i. (n=3). PSMA-selectivity was assessed by co-injection of 1,5 mol PMPA. Data are % injected dose per gram tissue.

Discussion

Due to the heterogeneity in PSMA-expression of many bone metastases, the dual-targeting strategy could be an advantageous approach in the treatment of prostate cancer-related bone metastases. A new heterodimeric compound containing a PSMA inhibitor target vector, a bisphosphonate drug and a DOTA chelator was developed and evaluated regarding radiolabelling, lipophilicity, HAP binding, *in vitro* affinity towards PSMA and *ex vivo* kinetic properties.

The compound DOTA-L-Lys(SA.Pam)-PSMA-617 (**13**) was prepared in 15 steps with a total yield of 1%.

Radiolabelling of **13** with ^{177}Lu showed a fast and quantitative RCY after 10 min with quantities over 10 nmol. The ^{177}Lu-labelled compound was stable (< 98%) in PBS and saline for 14 days and in HS for 5 days, releasing 7% of the ^{177}Lu until day 9 and remaining stable even after 14 days (93%). Thus, the complexation of the therapeutic nuclide seems to be stable even after two weeks. Due to the long half-

life of ^{177}Lu (7 days), it is also possible to store the labelled compound for a short time before injection, for example, for the treatment of several patients with one batch of tracer. The most suitable medium here is isotonic saline, which could also serve as injection medium. Moreover, the high stability of [^{177}Lu]Lu-**13** in HS makes it unlikely that ^{177}Lu will be released during the circulation time in the blood. The experimentally determined $logD_{7.4}$ value as a measure of lipophilicity is almost identical to the value of [^{177}Lu]Lu-PSMA-617, which serves as reference, indicating the hydrophile character of both compounds.

An aqueous suspension of crystalline HAP was used as a bone tissue model to test the HAP binding potency of the novel compound. The adsorption of [^{177}Lu]Lu-**13** to HAP was almost quantitative. It is nearly identical to the adsorption shown by free $^{177}Lu^{3+}$. Uncomplexed $^{177}Lu^{3+}$ is known for its high HAP affinity and correspondingly strong accumulation in bone tissue.[50] Compared to other literature-known DOTA conjugated bisphosphonates, e.g. $DOTAM^{PAM}$ (92.2 ± 2.7%), $DOTAM^{ZOL}$ (92.7 ± 1.3%) or BPAPD (83.0 ± 0.8%), [^{177}Lu]Lu-**13** showed an even better adsorption.[51]

By blocking of HAP with an excess of pamidronate prior to addition of [^{177}Lu]Lu-**13** or [^{177}Lu]Lu^{3+}, no significant adsorption was observed. This proves that the selective binding of [^{177}Lu]Lu-**13** to HAP is due to the adsorption of the SA.Pam unit at the calcified HAP surface. As expected, [^{177}Lu]Lu-PSMA-617 showed no notable binding to HAP. This shows that, in contrast to [^{177}Lu]Lu-**13**, [^{177}Lu]Lu-PSMA-617 can only accumulate in bone metastases via one mechanism, namely PSMA-binding.

In addition to HAP adsorption, [^{nat}Lu]Lu-**13** displayed a PSMA binding affinity in the nanomolar range. The complexation of the radiometal had no impact on the binding potency, since the K_i values of both complexed and uncomplexed conjugates were similar (42.3 ± 7.7 nM and 52.6 ± 3.5 nM for [^{nat}Lu]Lu-**13** and **13** respectively). However, the bisphosphonate-free compound **13** showed 2-fold higher binding potency revealing that the coupling of pamidronate affects the interaction of the tracer with the PSMA binding pocket, possibly through changes in the conformation of the molecule.

Biodistribution studies were conducted in LNCaP tumour-bearing mice in order to better characterize the translational potential of the dual-targeting properties of [^{177}Lu]Lu-**13.** In terms of PSMA-specific accumulation, [^{177}Lu]Lu-**13** showed good PSMA-specific tumour accumulation 4.2 ± 0.7%ID/g, which could be reduced by blocking the PSMA receptors with the potent PSMA inhibitor PMPA. According to literature the tumour-uptake of [^{177}Lu]Lu-PSMA-617 seems to be significantly higher 11.2 ± 4.17%ID/g.[8] However, this could be due to the higher binding affinity of this tracer K_i= 6.9 ± 1.3 nM vs. 42.3 ± 7.7 nM for [^{nat}Lu]Lu-**13**. Nevertheless, [^{177}Lu]Lu-PSMA-617 did not display any binding to HAP as discussed above, thus accumulation in PSMA negative bone metastases is supposed to be minimal since bone-uptake is depending on PSMA-expression. In contrast, [^{177}Lu]Lu-**13**

showed bone accumulation in the same range as tumour accumulation. This could not be blocked by PMPA suggesting that bone uptake is solely resulting from HAP binding. As already discussed, compound **13** can therefore be used in contrast to PSMA-617 for the therapy of PSMA negative bone metastases, since it can also accumulate at the metastases via the increased bone metabolism. Compared to the results published by Meckel et al, [^{177}Lu]Lu-**13** showed similar bone uptake as [^{177}Lu]Lu-DOTA^{ZOL} (3.4 ± 0.4%ID/g and 3.2 ± 0.4%ID/g respectively).[51] However, kidney accumulation of [^{177}Lu]Lu-**13** was higher than [^{177}Lu]Lu-DOTA^{ZOL} (16.5 ± 2.1%ID/g vs. 1,3 ± 0.1%ID/g[51] respectively). This could be due to the existence of PSMA receptors in the kidneys as known from literature.[36] Furthermore, the uptake in the liver and the spleen seems to be PSMA-independent, since no blocking effects were observed. The reason has yet to be found, as increased liver uptake is not known here for either bisphosphonates or PSMA-617. Nevertheless, target-to-background ratio of [^{177}Lu]Lu-**13**, 24h after injection, was remarkably high (tumour-to-blood-ratio, 210; bone-to-blood ratio, 170) revealing the promising potential of this compound. Especially with regard to the conjugated DOTA-chelator, which is a versatile chelator not only used in complexing the therapeutic β^- nuclide Lu-177, which is evaluated in this study, but is also applicable with other clinically relevant nuclides used in diagnosis by PET (e.g. ^{68}Ga or ^{44}Sc) or SPECT (e.g. ^{111}In or ^{67}Ga). Furthermore, the use of compound **13** in combination with α-emitters (e.g. ^{225}Ac or ^{213}Bi) would be interesting for the treatment of bone metastases in close distance to the bone marrow due to the short range of these nuclides.

Conclusion

In this work, a novel chimeric compound for therapy of prostate cancer related bone metastases was designed and successfully synthesized. Key structure elements of the novel compound are the following. First, the well-known and established PSMA inhibitor KuE in combination with the PSMA-617 linker unit enables high affinity towards PSMA. Second, the bisphosphonate pamidronate as HAP target vector shows high bone accumulation. It is conjugated via SA unit, which allows easy conjugation chemistry as well as increase of the antiresorptive effect of the bisphosphonate. Finally, the DOTA chelator allows the labelling with a wide range of diagnostic and therapeutic radiometals.

DOTA-L-Lys(SA.Pam)-PSMA-617 shows both excellent labelling properties and very good and selective HAP binding, which is superior to other DOTA-conjugated bisphosphonate compounds. The *in vitro* PSMA affinity is lower than that of PSMA-617, which can be ascribed to an influence of the Pam.SA group. Nevertheless, the compound shows both PSMA-dependent tumour uptake and PSMA-independent and pamidronate driven uptake into bone tissue and a remarkably high tumour-to-blood as well as bone-to-blood-ratio after 24 h.

The available results show that the new compound might be suited for the therapy of PCa-related bone metastases. Despite the lower affinity and in vivo uptake compared to [^{177}Lu]Lu-PSMA-617, the new compound could contribute significantly to the therapy of bone metastases by exploiting the heterodimeric dual-targeting mechanism and thereby increasing avidity as discussed above. This is particularly the case when PSMA expression in metastases is low or absent and therapy with [^{177}Lu]Lu-PSMA-617 or other PSMA-based therapeutics is not possible. In addition, it enables a simpler therapeutic approach. Likewise, PSMA-negative metastases cannot be "overlooked". The possibility to target via both target vectors with a single theranostic radiotracer could improve patient management. Although the compound in the first studies is a promising compound for theranostics of PCa related bone metastases, further investigation and optimisation is needed to improve the radiotracer.

Materials and Methods

General

All chemicals were purchased from Sigma-Aldrich, Merck, Fluka, AlfaAesar, VWR, AcrosOrganics, TCI, Iris Biotech and Fisher Scientific and used without purification. Dry solvents were obtained from Merck and VWR, deuterated solvents for NMR spectra from Deutero. PSMA-617 was purchased from Hycultec. Thin layer chromatography was performed with silica gel 60 F254 coated aluminum plates from Merck. Evaluation was carried out by fluorescence extinction at λ=254 nm and staining with potassium permanganate. The radio TLCs were evaluated using a CR-35 Bio test imager from Raytest and the AIDA (Raytest) software. The ^{1}H and ^{13}C NMR measurements were performed on an Avance III HD 300 spectrometer (300 MHz, 5mm BBFO sample head with z-gradient and ATM and BACS 60 sample changer), an Avance II 400 spectrometer (400 MHz, 5mm BBFO sample head with z-Gradient and ATM and SampleXPress 60 sample changer) and an Avance III 600 spectrometer (600 MHz, 5mm TCI CryoProbe sample head with z-Gradient and ATM and SampleXPress Lite 16 sample changer) from Bruker. The LC/MS measurements were performed on an Agilent Technologies 1220 Infinity LC system coupled to an Agilent Technologies 6130B Single Quadrupole LC/MS system. Semi-preparative HPLC purification was performed on a 7000 series Hitachi LaChrom and the respectively mentioned conditions and column. For radiolabelling experiments n.c.a. [^{177}Lu]$LuCl_3$ in 0.04 M HCl (ITM, Garching, Germany) was used.

Organic synthesis

Solid phase synthesis of the PSMA ligand (PSMA-167-resin)

The synthesis of the glutamate-urea-lysine binding motif and the linker of the PSMA-617 backbone was carried out following the established solid phase peptide chemistry as described by Benešová et al. with slight adjustments to the reaction procedures.[8,12]

Bis(*tert*-butyl)-L-glutamate-hydrochloride (4.5 g, 15.21 mmol) and DIPEA (7.98 g, 10.5 mL, 61.74 mmol) were dissolved in dry dichloromethane (200 mL) and cooled to 0 °C. Triphosgene (1.56 g, 5.26 mmol) in dichloromethane (30 mL) were added dropwise over a period of 4.5 h. After the complete addition, the solution was stirred for an additional hour.

The Fmoc protecting group of Fmoc-L-Lysine(Alloc)-Wang resin (1.65 g, 1.5 mmol, 0.9 mmol/g) was removed by stirring it in a piperidine/DMF (1:1) solution for 15 minutes followed by a washing step with dichloromethane.

The deprotected L-lysine(Alloc)-Wang resin was added to the previous prepared solution and stirred over night at room temperature. The resin (compound **1**) was washed with dichloromethane (15 mL) and used without further purification.

Tetrakis(triphenylphosphin)palladium (516.0 mg, 0.45 mmol) und morpholine (3.92 g, 3.92 mL, 45.00 mmol) were dissolved in dichloromethane (12 mL) and added to compound **1**. The solution was stirred for 1 d under exclusion of light. Afterwards it was washed with dichloromethane (15 mL), a 1% DIPEA solution in DMF (3 x 13 mL) and a sodium diethyldithiocarbamat trihydrate solution (15 mg/mL) in DMF (9 x 10.5 mL x 5 minutes), resulting in compound **2**, the resin-immobilized and Alloc-deprotected glutamate-urea-lysine conjugate.

Fmoc-3-(2-naphthyl)-L-alanine (1.75 g, 4.00 mmol), HATU (1.52 g, 4.00 mmol), HOBt (540 mg, 4.00 mmol) and DIPEA (780 mg, 1.02 mL, 6.03 mmol) were dissolved in dry DMF (10 mL) and added to the resin. The solution was stirred overnight and then washed with DMF (10 mL) and dichloromethane (10 mL).

To remove the Fmoc-group, the resin (compound **3**) was stirred in a piperidine/DMF (1:1, 3 x 11 mL) solution for 10 minutes each and washed with DMF (10 mL) and dichloromethane (10 mL), resulting in compound **4**.

Fmoc-4-Amc-OH (1.52 g, 4 mmol), HATU (1.52 g, 4.00 mmol), HOBt (540 mg, 4.00 mmol) and DIPEA (780 mg, 1.02 mL, 6.03 mmol) were dissolved in dry DMF (10 mL) and added to the resin (compound **4**).

The solution was stirred for two days and then washed with DMF (10 mL) and dichloromethane (10 mL).

To remove the Fmoc-group from compound **5**, it was stirred in a piperidine/DMF (1:1, 11 mL) solution for 10 minutes each and washed with DMF (10 mL) and dichloromethane (10 mL), leading to the final resin bound PSMA-617 backbone (**6**).

*Pamidronate (**7**, Pam)*

β-Alanine (1.5 g, 0.017 mol) and phosphorus acid (2.76 g, 0.034 mol) were dissolved in Sulfolane (5.5 mL) and cooled to 0 °C. Phosphorus trichloride (4.62 g, 2.95 mL, 0.034 mmol) was added dropwise. The solution was stirred for 3 h at 75 °C. Water (15 mL) was added and stirred for 12 h at 100°C. Ethanol (15 mL) was added and the product (**7**, 1.48 g, 0.006 mol, 37%) was obtained as yellow solid after crystallisation at 0°C for 3 days.

^{1}H-NMR (300 MHz, D_2O) δ [ppm] = 3.34 (t, *J* = 7.1 Hz, 2H), 2.31 (tt, *J* = 13.7, 7.1 Hz, 2H).

^{13}C-NMR (400 MHz, D_2O): δ [ppm] = 72.58, 36.14, 30.54.

^{31}P-NMR (121.5 MHz, D_2O) δ [ppm] = 17.58 (s, 2P).

MS (ESI^+): 236.0 $[M+H]^+$, calculated for $C_3H_{11}NO_7P_2$: 235.07 $[M]^+$.

*Pamidronate-squaric acid ethylester (**8**, SA.Pam)*

Pamidronate (500 mg, 2.13 mmol) was dissolved in phosphate buffer (0.5 M, pH 7, 5 mL). 3,4-Diethoxycyclobut-3-ene-1,2-dione (squaric acid diethylester, SADE, 542 mg, 468 µL, 3.2 mmol) was added and the mixture was stirred for 2 days at room temperature. Ethanol (3 mL) was added for crystallisation. The mixture was allowed to stand for 3 days in the freezer to complete crystallisation. The white precipitation was washed with cold ethanol and compound **8** (0.58 g, 1.62 mol, 76%) was obtained as white solid.

^{1}H-NMR (400 MHz, D_2O) δ [ppm] = 4.79-4.62 (m, 2H), 3.31 (t, *J* = 6.6 Hz, 2H), 2.32-2.15 (m, 2H) 1.42 (dt, *J* = 11.7, 7.2 Hz, 3H).

^{31}P-NMR (162 MHz, D_2O) δ [ppm] = 17,92 (s), 2.26 (s).

MS (ESI^+): 360.0 $[M+H]^+$,720.0 2$[M+H]^+$, 763.0 2$[M+Na]^+$, calculated for $C_9H_{15}NO_{10}P_2$: 359.16 $[M]^+$.

*Fmoc-L-Lys(Boc)-PSMA-617-resin (**9**)*

Fmoc-L-Lys(Boc)-OH (506 mg, 0.0011 mmol), HATU (415 mg, 0.0011 mg, HOBt (146 mg, 0.0011 mmol) and DIPEA (277 µl, 211 mg, 0.00162 mmol) were dissolved in acetonitrile (4 mL) and stirred for 30 min. The PSMA-617-resin (300 mg, 0.0027 mmol, 0.09 mmol/g) was added and the mixture was stirred for one day at room temperature. The resin was washed with acetonitrile (10 mL) and dichloromethane (10 mL) and used in the next step.

*L-Lys(Boc)-PSMA-617-resin (**10**)*

The Fmoc-L-Lys(Boc)-PSMA-617-resin (**9**) was stirred for one hour in a mixture of DMF and Piperidine (1:1, 6 mL). The Fmoc deprotected resin was washed with DMF (10 mL) and dichloromethane (10 mL) and used in the next step without further purification.

*DOTA(tBu)$_3$-L-Lys(Boc)-PSMA-617-resin (**11**)*

DOTA-Tris(*tert*-butyl ester) (310 mg, 0.54 µmol), HATU 308 mg, 0.00081 mmol), HOBt (110 mg, 0.00081 mmol) and DIPEA (184 µL, 140 mg, 0.0011 mmol) were dissolved in acetonitrile (4 mL) and stirred for 30 min. L-Lys(Boc)-PSMA-617-resin (**10**, 461 mg, 0.00027 mmol, 0.9 mmol/g) was added and the mixture was stirred for one day at room temperature. The resin was washed with acetonitrile (10 mL) and dichloromethane (10 mL) and used in the next step without further purification.

*DOTA-L-Lys-PSMA-617 (**12**)*

DOTA(tBu)$_3$-L-Lys(Boc)-PSMA-617-resin (**11,** 536 mg, 0.00027 mmol, 0.9 mmol/g) was stirred in a solution of TFA and dichloromethane (1:1, 4 mL) for 2 hours. The TFA/dichloromethane solution was evaporated under reduced pressure and the product (**12**, 10.6 mg, 0.0091 mmol, 4%) was obtained as a colourless powder after semi-preparative HPLC purification (column: LiChrospher 100 RP18 EC (250 x 10 mm) 5 µ, flow rate: 5 mL/min, H_2O/MeCN + 0.1% TFA, 25% MeCN isocratic, t_R = 10.3 min).

MS (ESI$^+$): 1172.5 $[M+2H]^+$,585.9 1/2$[M+2H]^+$, 391.0 1/3$[M+2H]^+$, calculated for $C_{55}H_{83}N_{11}O_{17}$: 1170.33 $[M]^+$

*DOTA-L-Lys(SA.Pam)-PSMA-617 (**13**)*

Compound **12** (10 mg, 0.0085 mmol) and compound **8** (16 mg, 0.043 mmol) were dissolved in phosphate buffer (0.5 M, pH 9, 1mL) and stirred for 2 days. The product (**13**, 10.56 mg, 0.0071 mmol,

84%) was obtained as a colourless powder after semi-preparative HPLC purification (column: LiChrospher 100 RP18 EC (250 x 10 mm) 5 µ, flow rate: 5 mL/min, H_2O/MeCN + 0.1% TFA, 23% to 28% MeCN in 20 min, t_R = 8.2 min).

MS (ESI^+): 511.3 1/3[M+H+2Na]$^+$, 520.0 [1/3M+2K]$^+$, 781.0 1/2[M+2K]$^+$, calculated for $C_{62}H_{92}N_{12}O_{26}P_2$: 1483.42 [M]$^+$

Radiolabelling of DOTA-L-Lys(SA.Pam)-PSMA-617 with Lutetium-177 ([^{177}Lu]Lu-13)

For radiolabelling experiments n.c.a. [^{177}Lu]$LuCl_3$ in 0.04 M HCl (ITG, Garching, Germany) was used.

Radiolabelling was performed in 1 mL 1 M ammonium acetate buffer at pH 5.5. Reactions were carried out with different amounts of precursor (5, 10, 30 nmol) and at 95 °C with 40 – 50 MBq n.c.a. lutetium-177. Radio-TLC (TLC Silica gel 60 F254 Merck) and citrate buffer (pH 4) as mobile phase and radio-HPLC using an analytical HPLC 7000 series Hitachi LaChrom (Column: Merck Chromolith® RP-18e, 5-95% MeCN (+0,1% TFA)/ 95-5% Water (+0,1% TFA) in 10 min) was used for reaction control. TLC´s were measured in TLC imager CR-35 Bio Test-Imager from Elysia-Raytest (Straubenhardt, Germany) with AIDA software.

In vitro stability studies

Complex stability studies were carried out in human serum (HS, human male AB plasma, USA origin, Sigma Aldrich) and phosphate buffered saline (Sigma Aldrich). 5 MBq of the radioactive compound were incubated in 0.5 mL of the media for 14 d. After several time points (1h, 2h, 5h, 1d, 2d, 5d, 7d, 9d and 14d), aliquots were taken out to evaluate the radiochemical stability. Experiments were carried out as triplicate.

Lipophilicity determination

Using the shake flask method, the $logD_{7.4}$ value of the compound was determined. The labelling solution was adjusted to pH 7.4 and 5 MBq were diluted in 700 µl n-octanol and 700 µl PBS. It was shaken for 2 min at 1500 U/min and then centrifuged. 400 µl of the n-octanol phase and 400 µl of the PBS phase were each transferred to a new Eppendorf tube. 3-6 µl were then pipetted on a TLC plate and analysed via phosphor imager. $LogD_{7.4}$ value was calculated by determining the ratio of the activities of the two phases. This procedure was repeated twice more with the respective phase with higher activity, so that three coefficients were obtained and the mean value was calculated.

Binding studies of ^{177}Lu-labelled compound on hydroxyapatite (HAP)

Hydroxyapatite (20 mg) was incubated in saline (1 mL) for 24 h. 50 µl of the labelled [^{177}Lu]Lu-**13** (5 MBq) and respectively [^{177}Lu]Lu-PSMA-617 (5 MBq) was added. The suspension was vortexed for 20 s and incubated for 1 h at room temperature. The samples were passed through a filter (CHROMAFIL® Xtra PTFE-45/13) and the supernatant was washed with water (500 µL). The radioactivity of the liquids and the HAP-containing supernatant were measured with a curiemeter (Aktivimeter Isomed 2010 MED Nuklear-Medizintechnik Dresden GmbH). The binding of [^{177}Lu]Lu-**13** and [^{177}Lu]Lu-PSMA-617 was determined as percent of activity absorbed to HAP. Free Lu-177 was examined as a positive probe analogously.

For blocking experiments, Hydroxyapatite (20 mg) was incubated in saline (1 mL) with pamidronate (100 mg) and evaluated with [^{177}Lu]Lu-**13** and free Lu-177 as described above.

***In vitro* binding affinity**

Cold [^{nat}Lu]Lu complexes were synthesized by shaking a mixture of **13** (371 µL of a 1 mg/ml solution, 250 nmol) and $LuCl_3$ (129 µL of a 1 mg /mL solution, 375 nmol; metal to ligand ratio 1.5 to 1) in 1 M ammonium acetate buffer at 95 °C for 2 hours. Complexation was monitored by ESI-LC/MS.

Based on the protocol published by Benešová et al. the PSMA binding affinity was determined in a competitive radioligand assay.[8] PSMA-positive LNCaP-cells (purchased from Sigma-Aldrich) were cultured in RPMI 1640 (Thermo Fisher Scientific) supplemented with 10% fetal bovine serum (Thermo Fisher Scientific), 100 µg/ml streptomycin, and 100 units/ml penicillin at 37°C in 5% CO_2. These cells were incubated for 45 min with rising concentrations of the test compounds in the presence of 0.75 nM [^{68}Ga]Ga-PSMA-10. Free radioactivity was removed by several washing steps with ice-cold PBS. Probes were measured in a γ-counter (2480 WIZARD^2 Automatic Gamma Counter, PerkinElmer). Obtained data were analyzed in GraphPad Prism 9 using nonlinear regression.

Animal studies

All animal experiments were approved by the ethical committee of the state of Rhineland Palatinate (according to §8 Abs. 1 Tierschutzgesetz, Landesuntersuchungsamt) and performed in accordance with relevant federal laws and institutional guide-lines approval Nr. 23 177-07/G 21-1-022.

6- to 8-week-old male BALB/cAnNRj (Janvier Labs) were inoculated subcutaneously with $5x10^6$ LNCaP cells in 200 µL 1:1 (v/v) Matrigel/PBS (Corning®). Experiments are conducted after the tumour has reached a volume of approximately 100 cm^3.

LNCaP xenografts were anesthetized with 2% isoflurane prior to i.v. injection of 0.5 nmol of [^{177}Lu]Lu-**13**. The specific activity was approximately 3 MBq/nmol. PSMA-selectivity was investigated by co-injection of 1.5 µmol PMPA/mouse.

Animals were sacrificed 24 h p.i. Organs were collected and weighed. The radioactivity was measured and calculated as decay-corrected percentage of the injected dose per gram of tissue mass %ID/g.

Acknowledgment

The authors would like to thank ITM (Graching, Germany) for providing n.c.a. Lutetium-177. The also authors thank the Max Planck Graduate Center Mainz (MPGC) for supporting Tilmann Grus. The authors gratefully acknowledge X.X. for supporting X.X.

References

(1) Ferlay, J.; Colombet, M.; Soerjomataram, I.; Parkin, D. M.; Piñeros, M.; Znaor, A.; Bray, F. Cancer Statistics for the Year 2020: An Overview. *Int. J. Cancer* **2021**, *149* (4), 778–789.

(2) American Cancer Society. *American Cancer Society. Cancer Facts & Figures 2021. Atlanta: American Cancer Society; 2021*; 2021.

(3) Donin, N. M.; Reiter, R. E. Why Targeting PSMA Is a Game Changer in the Management of Prostate Cancer. *J. Nucl. Med.* **2018**, *59* (2), 177–182.

(4) Rahbar, K.; Afshar-Oromieh, A.; Jadvar, H.; Ahmadzadehfar, H. PSMA Theranostics: Current Status and Future Directions. *Mol. Imaging* **2018**, *17*, 1536012118776068.

(5) Rowe, S. P.; Gorin, M. A.; Pomper, M. G. Imaging of Prostate-Specific Membrane Antigen with Small-Molecule PET Radiotracers: From the Bench to Advanced Clinical Applications. *Annu. Rev. Med.* **2019**, *70*, 461–477.

(6) Kopka, K.; Benešová, M.; Bařinka, C.; Haberkorn, U.; Babich, J. Glu-Ureido-Based Inhibitors of Prostate-Specific Membrane Antigen: Lessons Learned during the Development of a Novel Class of Low-Molecular-Weight Theranostic Radiotracers. *J. Nucl. Med.* **2017**, *58* (Suppl 2), 17S-26S.

(7) Hoffmann, M. A.; Miederer, M.; Wieler, H. J.; Ruf, C.; Jakobs, F. M.; Schreckenberger, M. Diagnostic Performance of ^{68}Gallium-PSMA-11 PET/CT to Detect Significant Prostate Cancer and Comparison with ^{18}FEC PET/CT. *Oncotarget* **2017**, *8* (67), 111073–111083.

(8) Benešová, M.; Schäfer, M.; Bauder-Wüst, U.; Afshar-Oromieh, A.; Kratochwil, C.; Mier, W.; Haberkorn, U.; Kopka, K.; Eder, M. Preclinical Evaluation of a Tailor-Made DOTA-Conjugated PSMA Inhibitor with Optimized Linker Moiety for Imaging and Endoradiotherapy of Prostate

Cancer. *J. Nucl. Med.* **2015**, *56* (6), 914–920.

(9) Haberkorn, U.; Eder, M.; Kopka, K.; Babich, J. W.; Eisenhut, M. New Strategies in Prostate Cancer: Prostate-Specific Membrane Antigen (PSMA) Ligands for Diagnosis and Therapy. *Clin. Cancer Res.* **2016**, *22* (1), 9–15.

(10) Khawar, A.; Eppard, E.; Roesch, F.; Ahmadzadehfar, H.; Kürpig, S.; Meisenheimer, M.; Gaertner, F. C.; Essler, M.; Bundschuh, R. A. Preliminary Results of Biodistribution and Dosimetric Analysis of [^{68}Ga]Ga-DOTA ZOL : A New Zoledronate-Based Bisphosphonate for PET/CT Diagnosis of Bone Diseases. *Ann. Nucl. Med.* **2019**, *33* (6), 404–413.

(11) Eder, M.; Eisenhut, M.; Babich, J.; Haberkorn, U. PSMA as a Target for Radiolabelled Small Molecules. *Eur. J. Nucl. Med. Mol. Imaging* **2013**, *40* (6), 819–823.

(12) Benešová, M.; Bauder-Wüst, U.; Schäfer, M.; Klika, K. D.; Mier, W.; Haberkorn, U.; Kopka, K.; Eder, M. Linker Modification Strategies to Control the Prostate-Specific Membrane Antigen (PSMA)-Targeting and Pharmacokinetic Properties of DOTA-Conjugated PSMA Inhibitors. *J. Med. Chem.* **2016**, *59* (5), 1761–1775.

(13) Rahbar, K.; Ahmadzadehfar, H.; Kratochwil, C.; Haberkorn, U.; Schafers, M.; Essler, M.; Baum, R. P.; Kulkarni, H. R.; Schmidt, M.; Drzezga, A.; Bartenstein, P.; Pfestroff, A.; Luster, M.; Lutzen, U.; Marx, M.; Prasad, V.; Brenner, W.; Heinzel, A.; Mottaghy, F. M.; Ruf, J.; Meyer, P. T.; Heuschkel, M.; Eveslage, M.; Bögemann, M.; Fendler, W. P.; Krause, B. J. German Multicenter Study Investigating ^{177}Lu-PSMA-617 Radioligand Therapy in Advanced Prostate Cancer Patients. *J. Nucl. Med.* **2017**, *58* (1), 85–90.

(14) Sartor, O.; de Bono, J.; Chi, K. N.; Fizazi, K.; Herrmann, K.; Rahbar, K.; Tagawa, S. T.; Nordquist, L. T.; Vaishampayan, N.; El-Haddad, G.; Park, C. H.; Beer, T. M.; Armour, A.; Pérez-Contreras, W. J.; DeSilvio, M.; Kpamegan, E.; Gericke, G.; Messmann, R. A.; Morris, M. J.; Krause, B. J. Lutetium-177–PSMA-617 for Metastatic Castration-Resistant Prostate Cancer. *N. Engl. J. Med.* **2021**, *385* (12), 1091–1103.

(15) Thomas, T. S.; Pachynski, R. K. Treatment of Advanced Prostate Cancer. *Mo. Med.* **2018**, *115* (2), 156–161.

(16) Larson, S. R.; Zhang, X.; Dumpit, R.; Coleman, I.; Lakely, B.; Roudier, M.; Higano, C. S.; True, L. D.; Lange, P. H.; Montgomery, B.; Corey, E.; Nelson, P. S.; Vessella, R. L.; Morrissey, C. Characterization of Osteoblastic and Osteolytic Proteins in Prostate Cancer Bone Metastases. *Prostate* **2013**, *73* (9), 932–940.

(17) Ahmadzadehfar, H.; Matern, R.; Baum, R. P.; Seifert, R.; Kessel, K.; Bögemann, M.; Kratochwil, C.; Rathke, H.; Ilhan, H.; Svirydenka, H.; Sathekge, M.; Kabasakal, L.; Yordanova, A.; Garcia-Perez, F. O.; Kairemo, K.; Maharaj, M.; Paez, D.; Virgolini, I.; Rahbar, K. The Impact of the Extent of the Bone Involvement on Overall Survival and Toxicity in MCRPC Patients Receiving [^{177}Lu]Lu-PSMA-617: A WARMTH Multicentre Study. *Eur. J. Nucl. Med. Mol. Imaging* **2021**, *48* (12), 4067–4076.

(18) Sartor, O.; Hoskin, P.; Bruland, Ø. S. Targeted Radio-Nuclide Therapy of Skeletal Metastases. *Cancer Treat. Rev.* **2013**, *39* (1), 18–26.

(19) Fang, J.; Xu, Q. Differences of Osteoblastic Bone Metastases and Osteolytic Bone Metastases in Clinical Features and Molecular Characteristics. *Clin. Transl. Oncol.* **2015**, *17* (3), 173–179.

(20) Saad, Fred; Gleason, Donald M.; Murray, Robin; Tchekmedyian, Simon; Venner, Peter; Lacome, Louis; Chin, Joseph L.; Vinholes, Jeferson J.; Goas, J. Allen; Chen, B. A Randomized, Placebo-Controlled Trial of Zoledronic Acid in Patients with Hormone-Refractory Metastatic Prostate Carcinoma. *J. Natl. Cancer Inst.* **2002**, *94* (19), 1458–1468.

(21) Wong, S. K.; Mohamad, N. V.; Giaze, T. R.; Chin, K. Y.; Mohamed, N.; Ima-Nirwana, S. Prostate Cancer and Bone Metastases: The Underlying Mechanisms. *Int. J. Mol. Sci.* **2019**, *20* (10), 2587.

(22) Lin, J. H. Bisphosphonates: A Review of Their Pharmacokinetic Properties. *Bone* **1996**, *18* (2), 75–85.

(23) Fleisch, H. Development of Bisphosphonates. *Breast Cancer Res.* **2002**, *4*, 30.

(24) Palma, E.; Correia, J. D. G.; Campello, M. P. C.; Santos, I. Bisphosphonates as Radionuclide Carriers for Imaging or Systemic Therapy. *Mol. Biosyst.* **2011**, *7* (11), 2950–2966.

(25) Ogawa, K.; Ishizaki, A. Well-Designed Bone-Seeking Radiolabeled Compounds for Diagnosis and Therapy of Bone Metastases. *Biomed Res. Int.* **2015**, *2015*, 676053.

(26) Eary, Janet, F.; Collins, Carolyn; Stabin, Michael; Vernon, Cheryl; Petersdorf, Steve; Baker, Melissa; Hartnett, S.; Ferency, S.; Addison, S. J.; Appelbaum, F.; Gordon, E. E. Samarium-153-EDTMP Biodistribution and Estimation. *J. Nucl. Med.* **1993**, *34* (7), 1031–1036.

(27) Meckel, M.; Nauth, A.; Timpe, J.; Zhernosekov, K.; Puranik, A. D.; Baum, R. P.; Roesch, F. Development of a [^{177}Lu]BPAMD Labeling Kit and an Automated Synthesis Module for Routine Bone Targeted Endoradiotherapy. *Cancer Biother. Radiopharm.* **2015**, *30* (2), 94–99.

(28) Khawar, A.; Eppard, E.; Roesch, F.; Ahmadzadehfar, H.; Kürpig, S.; Meisenheimer, M.; Gaertner, F. C.; Essler, M.; Bundschuh, R. A. Biodistribution and Post-Therapy Dosimetric Analysis of [^{177}Lu]Lu-DOTA^{ZOL} in Patients with Osteoblastic Metastases: First Results. *EJNMMI Res.* **2019**, *9*, 102.

(29) Kreppel, B.; Gaertner, F. C.; Ahmadzadehfar, H.; Khawar, A.; Roesch, F.; Kuerpig, S.; Meisenheimer, M.; Essler, M.; Bundschuh, R. A. [^{177}Lu]Lu-DOTA-Zoledronate Therapy – First Application in a Patient with Primary Osseous Metastatic Bronchial Carcinoma. *Nuklearmedizin* **2020**, *59* (3), 281–283.

(30) Grus, T.; Lahnif, H.; Klasen, B.; Moon, E.-S.; Greifenstein, L.; Roesch, F. Squaric Acid-Based Radiopharmaceuticals for Tumor Imaging and Therapy. *Bioconjug. Chem.* **2021**, *32* (7), 1223–1231.

(31) Meisenheimer, M.; Kürpig, S.; Essler, M.; Eppard, E. DOTA-ZOL: A Promising Tool in Diagnosis and Palliative Therapy of Bone Metastasis-Challenges and Critical Points in Implementation into Clinical Routine. *Molecules* **2020**, *25* (13), 2988.

(32) Van Beek, E.; Löwik, C.; Que, I.; Papapoulos, S. Dissociation of Binding and Antiresorptive Properties of Hydroxybisphosphonates by Substitution of the Hydroxyl with an Amino Group. *J. Bone Miner. Res.* **1996**, *11* (10), 1492–1497.

(33) Hyväkkä, A.; Virtanen, V.; Kemppainen, J.; Grönroos, T. J.; Minn, H.; Sundvall, M. More than Meets the Eye: Scientific Rationale behind Molecular Imaging and Therapeutic Targeting of Prostate-Specific Membrane Antigen (PSMA) in Metastatic Prostate Cancer and Beyond. *Cancers.* **2021**, *13* (9), 2244.

(34) Mannweiler, S.; Amersdorfer, P.; Trajanoski, S.; Terrett, J. A.; King, D.; Mehes, G. Heterogeneity of Prostate-Specific Membrane Antigen (PSMA) Expression in Prostate Carcinoma with Distant Metastasis. *Pathol. Oncol. Res.* **2009**, *15* (2), 167–172.

(35) Acar, E.; Bekis, R.; Polack, B. Comparison of Bone Uptake in Bone Scan and Ga-68 PSMA PET/CT Images in Patients with Prostate Cancer. *Curr. Med. Imaging Rev* **2019**, *15* (6), 589–594.

(36) Silver, D. A.; Pellicer, I.; Fair, W. R.; Heston, W. D. W.; Cordon-Cardo, C. Prostate-Specific Membrane Antigen Expression in Normal and Mailgant Human Tissues. *Clin. Cancer Rersearch*

1997, *3* (1), 81–85.

(37) Ravi Kumar, A. S.; Hofman, M. S. Mechanistic Insights for Optimizing PSMA Radioligand Therapy. *Clin. Cancer Res.* **2020**, *26* (12), 2774–2776.

(38) Harmon, S. A.; Mena, E.; Shih, J. H.; Adler, S.; McKinney, Y.; Bergvall, E.; Mehralivand, S.; Sowalsky, A. G.; Couvillon, A.; Madan, R. A.; Gulley, J. L.; Eary, J.; Mease, R. C.; Pomper, M. G.; Dahut, W. L.; Turkbey, B.; Lindenberg, L.; Choyke, P. L. A Comparison of Prostate Cancer Bone Metastases on ^{18}F-Sodium Fluoride and Prostate Specific Membrane Antigen (^{18}F-PSMA) PET/CT: Discordant Uptake in the Same Lesion. *Oncotarget* **2018**, *9* (102), 37676–37688.

(39) Roudier, M. P.; True, L. D.; Higano, C. S.; Vesselle, H.; Ellis, W.; Lange, P.; Vessella, R. L. Phenotypic Heterogeneity of End-Stage Prostate Carcinoma Metastatic to Bone. *Hum. Pathol.* **2003**, *34* (7), 646–653.

(40) Seifert, R.; Seitzer, K.; Herrmann, K.; Kessel, K.; Schäfers, M.; Kleesiek, J.; Weckesser, M.; Boegemann, M.; Rahbar, K. Analysis of PSMA Expression and Outcome in Patients with Advanced Prostate Cancer Receiving ^{177}Lu-PSMA-617 Radioligand Therapy. *Theranostics* **2020**, *10* (17), 7812–7820.

(41) Harmon, S. A.; Bergvall, E.; Mena, E.; Shih, J. H.; Adler, S.; McKinney, Y.; Mehralivand, S.; Citrin, D. E.; Couvillon, A.; Madan, R. A.; Gulley, J. L.; Mease, R. C.; Jacobs, P. M.; Pomper, M. G.; Turkbey, B.; Choyke, P. L.; Lindenberg, M. L. A Prospective Comparison of ^{18}F-Sodium Fluoride PET/CT and PSMA-Targeted ^{18}F-DCFBC PET/CT in Metastatic Prostate Cancer. *J. Nucl. Med.* **2018**, *59* (11), 1665–1671.

(42) Pyka, T.; Okamoto, S.; Dahlbender, M.; Tauber, R.; Retz, M.; Heck, M.; Tamaki, N.; Schwaiger, M.; Maurer, T.; Eiber, M. Comparison of Bone Scintigraphy and ^{68}Ga-PSMA PET for Skeletal Staging in Prostate Cancer. *Eur. J. Nucl. Med. Mol. Imaging* **2016**, *43* (12), 2114–2121.

(43) Rowe, S. P.; Mana-Ay, M.; Javadi, M. S.; Szabo, Z.; Leal, J. P.; Pomper, M. G.; Pienta, K. J.; Ross, A. E.; Gorin, M. A. PSMA-Based Detection of Prostate Cancer Bone Lesions with ^{18}F-DCFPyL PET/CT: A Sensitive Alternative to ^{99m}Tc-MDP Bone Scan and Na^{18}F PET/CT? *Clin. Genitourin. Cancer* **2016**, *14* (1), e115–e118.

(44) Rowe, S. P.; Macura, K. J.; Mena, E.; Blackford, A. L.; Nadal, R.; Antonarakis, E. S.; Eisenberger, M.; Carducci, M.; Fan, H.; Dannals, R. F.; Chen, Y.; Mease, R. C.; Szabo, Z.; Pomper, M. G.; Cho, S. Y. PSMA-Based [^{18}F]DCFPyL PET/CT Is Superior to Conventional Imaging for Lesion Detection in Patients with Metastatic Prostate Cancer. *Mol. Imaging Biol.* **2016**, *18* (3), 411–419.

(45) Uprimny, C.; Svirydenka, A.; Fritz, J.; Kroiss, A. S.; Nilica, B.; Decristoforo, C.; Haubner, R.; von Guggenberg, E.; Buxbaum, S.; Horninger, W.; Virgolini, I. J. Comparison of [^{68}Ga]Ga-PSMA-11 PET/CT with [^{18}F]NaF PET/CT in the Evaluation of Bone Metastases in Metastatic Prostate Cancer Patients Prior to Radionuclide Therapy. *Eur. J. Nucl. Med. Mol. Imaging* **2018**, *45* (11), 1873–1883.

(46) Janssen, J. C.; Meißner, S.; Woythal, N.; Prasad, V.; Brenner, W.; Diederichs, G.; Hamm, B.; Makowski, M. R. Comparison of Hybrid ^{68}Ga-PSMA-PET/CT and ^{99m}Tc-DPD-SPECT/CT for the Detection of Bone Metastases in Prostate Cancer Patients: Additional Value of Morphologic Information from Low Dose CT. *Eur. Radiol.* **2018**, *28* (2), 610–619.

(47) Greifenstein, L.; Engelbogen, N.; Lahnif, H.; Sinnes, J.-P.; Bergmann, R.; Bachmann, M.; Rösch, F. Synthesis, Labeling and Preclinical Evaluation of a Squaric Acid Containing PSMA Inhibitor Labeled with ^{68}Ga: A Comparison with PSMA-11 and PSMA-617. *ChemMedChem* **2020**, *15* (8), 695–704.

(48) Kovacs, R.; Grün, A.; Nemeth, O.; Garadnay, S.; Greiner, I.; Keglevich, G. The Synthesis of

Pamidronic Derivatives in Different Solvents: An Optimization and a Mechanistic Study. *Heteroat. Chem.* **2014**, *25* (3), 186–193.

(49) Cawthray, J. F.; Creagh, A. L.; Haynes, C. A.; Orvig, C. Ion Exchange in Hydroxyapatite with Lanthanides. *Inorg. Chem.* **2015**, *54* (4), 1440–1445.

(50) Breeman, W. A. P.; Van der Wansem, K.; Bernard, B. F.; Van Gameren, A.; Erion, J. L.; Visser, T. J.; Krenning, E. P.; De Jong, M. The Addition of DTPA to[^{177}Lu-DOTA0, Tyr3]Octreotate Prior to Administration Reduces Rat Skeleton Uptake of Radioactivity. *Eur. J. Nucl. Med. Mol. Imaging* **2003**, *30* (2), 312–315.

(51) Meckel, M.; Bergmann, R.; Miederer, M.; Roesch, F. Bone Targeting Compounds for Radiotherapy and Imaging: *Me(III)-DOTA Conjugates of Bisphosphonic Acid, Pamidronic Acid and Zoledronic Acid. *EJNMMI Radiopharm. Chem.* **2017**, *1*, 14.

4.3 Project C: PSMA inhibitor conjugated drug delivery systems

^{18}F-labeled, PSMA-specific liposomes: promising and PET-traceable tool for future targeted drug delivery in the treatment of prostate cancer

X.X., Tilmann Grus, X.X., X.X. and X.X.

In preparation for submission

Summary

The packaging of drugs in liposomes is a well known method of transportation of drugs.[1] The use of liposomes as nanocarrier has some advantages. For example, side effects can be reduced and bioavailability can be increased.[2]

In this study, a liposome-based drug transport system should be developed. The liposomes are functionalized with the squaric acid conjugated and urea-based PSMA inhibitor KuE. This PSMA inhibitor allows the targeted transport of cytotoxic drug carrying liposomes to prostate cancer cells. A fluorine-18 labelled unit is also conjugated to the liposomes to evaluate the *in vivo* behaviour of the novel liposomes. In this study, surface of the liposomes are coated with hyperbranched polyglycerols with hydrophobic alkyl chain anchors (BisHD-*hb*PG). This coating enables a stealth effect which allow an improved blood circulation due to the increased resistance against the mononuclear phagocyte system.[3]

After synthesis of the BisHD-*hb*PG block copolymers and their functionalisation with alkyne groups, the polymers were functionalized with the azide carrying SA.KuE PSMA target vector via CuAAC.

The radiolabelling and the liposome formation of the PSMA inhibitor containing polymers should be compared with the non-PSMA conjugated polymers. In the next step the ^{18}F-radiolabel [^{18}F]F-TEG-N_3 was synthesized by an automated synthesis modul (RCY = 53%) and was also conjugated to the polymers via CuAAC by hand. This conjugation was conducted with a quantitative radiochemical yield.

With the freshly prepared ^{18}F-labeled polymers, liposome formation was conducted via thin film hydration under addition of DOPC and cholesterol. Extrusion through membranes with defined pore size was carried out to obtain small uniform unilamellar liposomes. The final liposomes were purified via a size exclusion chromatography column. The complete synthesis of the liposomes, starting with the radiolabelling was done in 82 min for the KuE functionalised liposomes (RCY = 25%) and in 75 min for the not functionalised liposomes (RCY = 14%). The analysis of the size of the liposomes was performed via dynamic light scattering and showed diameters of 157.5 nm for the simple liposomes and 199.1 nm for the KuE conjugated version. Both liposomes show favourable sizes, since it is literature known that liposomes with sizes of 100 to 200 nm showed the most effectively tumour uptake.[4,5] Thus the KuE containing liposomes could be a promising drug delivery system for transportation of drugs to the prostate cancer cell. Drug loading and releasing experiments and *in vivo* evaluation need to be done in future.

Author contributions

The study was planned by X.X., **T. Grus** and X.X. Organic synthesis and characterisation of the functionalized polymer was done by X.X. Organic synthesis of the clickable PSMA target vector was done by **T. Grus**. Functionalisation and purification the polymer with the PSMA target vector was carried out by **T. Grus** and X.X. **T.Grus**, X.X. and X.X. were responsible for the characterisation of the functionalised polymer. **T. Grus** and X.X. carried out the radiochemical synthesis and evaluation and were in charge for Liposome formation and purification. **T. Grus**, X.X. and X.X. wrote the manuscript. All authors reviewed the manuscript. The project was supervised X.X. and X.X.

References of the summary

(1) Sercombe, L.; Veerati, T.; Moheimani, F.; Wu, S. Y.; Sood, A. K.; Hua, S. Advances and Challenges of Liposome Assisted Drug Delivery. *Front. Pharmacol.* **2015**, *6* (DEC), 286.

(2) Yan, L.; Shen, J.; Wang, J.; Yang, X.; Dong, S.; Lu, S. Nanoparticle-Based Drug Delivery System: A Patient-Friendly Chemotherapy for Oncology. *Dose-Response* **2020**, *18* (3), 1559325820936161.

(3) Wagener, K.; Worm, M.; Pektor, S.; Schinnerer, M.; Thiermann, R.; Miederer, M.; Frey, H.; Rösch, F. Comparison of Linear and Hyperbranched Polyether Lipids for Liposome Shielding by ^{18}F-Radiolabeling and Positron Emission Tomography. *Biomacromolecules* **2018**, *19* (7), 2506–2516.

(4) Ernsting, M. J.; Murakami, M.; Roy, A.; Li, S.-D. Factors Controlling the Pharmacokinetics, Biodistribution and Intratumoral Penetration of Nanoparticles. *J Control Release* **2013**, *172* (3), 782–794.

(5) Liu, D.; Mori, A.; Huang, L. Role of Liposome Size and RES Blockade in Controlling Biodistribution and Tumor Uptake of GM1-Containing Liposomes. *BBA - Biomembr.* **1992**, *1104* (1), 95–101.

Abstract

Inhibitors of the prostate-specific membrane antigen (PSMA) belong to one of the most important substance classes in nuclear medicine. L-lysine-urea-L-glutamate (KuE) represents a key motif in recent diagnostics and therapeutic radiopharmaceuticals targeting the PSMA. Multifunctional polyether structures play a crucial role in shielding liposomes from degradation in the blood stream due to their stealth effect. In this work alkyne-functionalized hyperbranched polyglycerols (*hb*PG) with a long hydrophobic alkyl chain anchor (BisHD) were synthesized and consecutively modified with an azide-bearing, squaramide coupled PSMA inhibitor (KuE.SA.Azide) *via* Cu(I)-catalyzed alkyne-azide cycloaddition (CuAAC). Subsequent radiolabeling *via* similar reaction of [^{18}F]F-TEG-Azide with residual alkyne-groups followed by liposomal preparation led to a promising system for future targeted drug delivery in the treatment of prostate cancer that can be pre-evaluated *in vitro* and *in vivo via* positron emission tomography (PET).

Introduction

Among men, prostate cancer is the most common cancer in industrialized countries and the fifth leading cause of cancer death worldwide.[1,2] However, with early detection, there are good treatment options leading to a five-year survival rate of more than 90%.[2,3] The prostate specific membrane antigen (PSMA) is associated with the diagnosis of prostate cancer. This membrane-bound glycoprotein belongs to the group of carboxypeptidases, which cleaves off C-terminal glutamate and for example catalyzes the hydrolysis of *N*-acetylaspartylglutamate to *N*-acetylaspartate. It is rarely found in healthy tissues but shows overexpression in prostate cancer cells.[4,5] For this reason, a variety of radiopharmaceutical drugs based on longer peptides, antibodies and small molecules targeting PSMA have been used for the diagnosis and treatment of prostate cancer.[6,7] These compounds have similar structures to *N*-acetylaspartyl glutamate with a C-terminal glutamate to address the glutamate recognition domain of PSMA.[8] Furthermore, the glutamate moiety must be attached to another non-cleavable group to prevent cleavage by PSMA *in vivo*. The presence of an aromatic moiety in the linker region significantly improves the affinity of the radiopharmaceutical by addressing an aromatic binding moiety in the binding pocket of the PSMA.[9] A variety of PSMA inhibitors are urea-based, such as the most important PSMA radiopharmaceuticals PSMA-11 and PSMA-617.[8,10,11] The lead structure of these molecules is a L-lysine-urea-L-glutamate (KuE) motif that resembles the structure of *N*-acetylaspartyl glutamate and is not cleavable by PSMA.

The use of squaric acid diethyl ester (3,4-Diethoxycyclobut-3-ene-1,2-dione; SADE) as coupling reagent provides a unique strategy for conjugation of target vectors, linker units and other molecules. It is already widely used in the coupling of biomolecules for preparation of e.g. carbohydrate- or protein-polymer-conjugates.[12]

The application of SADE simplifies the synthetic process. For example, no protective groups or further coupling reagents are required. There are also no by-products that need to be removed.

The two ester groups react selectively with amines under mild conditions.[13] The amidation can be carried out asymmetrically *via* pH control, since formation of the monoamide in the first step leads to reduced reactivity. By increasing the pH value, deprotonation occurs, whereby the aromatic stabilization of the monoamide is lost and the second amidation can take place.[14–16] This prevents dimerization and enables asymmetric amidation with high selectivity and high yields.

Squaric acid shows a high acidity (pK_{a1} = 0.5-1.2; pK_{a2} = 2.2-3.5) and due to Hückel rule ([4n + 2] π-electrons, n = 0) for aromatic systems, it represents an aromatic unit.[17,18] In PSMA-specific radiopharamceuticals, squaric acid thus provides a moiety that interacts with the aromatic binding site in the binding pocket leading to increased affinity.[19,20]

The problem with small molecules, however, is their rapid excretion by the kidney and the associated short retention in the blood. In order to increase the circulation time, a variety of approaches have been pursued in recent decades.[21-22] One possible approach is to use drug delivery systems such as liposomes.[23,24] Liposomes are vesicular structures that mimic a biomembrane. They typically consist of amphiphilic phospholipids and are often additionally stabilized using cholesterol. The problem with these systems is that they are easily recognized by macrophages of the mononuclear phagocyte system (MPS) due to their size, which leads to increased uptake in the liver and spleen.[23,25-26] To increase the circulation time in the blood, the stealth effect of PEGylated systems is used. Polyethylene glycol chains are attached to the surface of the liposomes to shield them from macrophages.[27,28] PEG has been the "gold standard" for creating stealth liposomes for years.[29] In recent years, however, antibody-mediated immune responses have been increasingly observed.[30] In addition, functional groups for further functionalization are missing because methoxy PEG (mPEG) is commonly used. A promising alternative is the highly biocompatible and water-soluble hyperbranched polyglycerol (*hb*PG).[31] Hyperbranched polyglycerol has a large number of hydroxyl groups, which allows functionalization with targeting vectors, radiolabels or targeting ligands for direct drug delivery.[32] Wagener *et al*. investigated and compared liposome shielding *in vivo via* PET using ^{18}F-labeled, linear and hyperbranched polyether lipids. They observed comparably high stability and prolonged blood circulation of all investigated structures with differences in spleen accumulation mainly due to the different liposomal sizes.[33] Furthermore, very recently, they analogously prepared and investigated either fluorescence- or radiolabeled liposomes being functionalized with trimannose moieties for active targeting of dendritic cells (DCs). Compared to non-functionalized liposomes, the trimannosylated analogues provided significantly increased uptake in the spleen and liver, presumably due to the presence of DCs.[34] Hofmann *et al.* introduced different strategies to synthesize a variety of linear-hyperbranched polyether lipids. For this purpose, cholesterol or dialkyl-based anchors with different chain length are directly used as initiators in an anionic ring opening polymerization (AROP) of various epoxide monomers. This procedure enables a variety of polyether architectures with an adjustable number of hydroxyl groups.[35] Furthermore, a study showed the stability of liposomes depending on the used anchor structure. Anchor structures with an alkyl chain between 18-20 methylene units showed an inherently higher stability of the liposomal membrane compared to cholesterol.[36]

The cyclotron-produced positron emitter fluorine-18 provides several advantageous properties for radiolabeling and *in vivo* evaluation of liposomal structures *via* PET. Although it belongs to the shorter-lived radionuclides, its half-life of 109.7 min is longer than that of many other commonly used PET-isotopes (such as ^{68}Ga, ^{11}C, ^{13}N, ^{15}O) allowing for more time-consuming synthesis and making it suitable not only for imaging of small molecules but also larger systems with prolonged circulation such as

peptides, polymers and liposomes.[37,38] Furthermore, the almost exclusive β^+-decay (96.9%) of fluorine 18 produces low energy positrons ($E_{\beta+,max}$ = 635 keV) ensuring a high spatial PET-resolution.[39] In contrast to radiometals, fluorine-18 is typically covalently bound to the respective molecule. Therefore, utilization of larger chelating structures that may impair liposome preparation or affect the shielding properties of the liposomal surface, is not required. Application of a structurally compliant, ^{18}F-labeled synthon such as the frequently used 1-Azido-2-(2-(2-[^{18}F]fluoroethoxy)ethoxy)ethane ([^{18}F]F-TEG-N_3) enables indirect radiolabeling of the hyperbranched polyether construct without significantly affecting its chemical and biological properties.[33,34,40,41]

In the present study the initial steps included synthesis of both an alkyne-functionalized hyperbranched polyglycerol with a long hydrophobic alkyl chain anchor and an azide-bearing squaramide coupled KuE-derivative. In the next step the corresponding KuE-functionalized polyether lipid was formed *via* CuAAC. Subsequently, the previously synthesized precursor 2-(2-(2-Azidoethoxy)ethoxy)ethyl-*p*-toluenesulfonate (Ts-TEG-N_3) was ^{18}F-labeled using a custom-built semiautomatic modular system. A second copper(I)-catalyzed click-reaction between the resulting [^{18}F]F-TEG-N_3 and residual alkyne groups of the polyether led to the desired radiolabeled lipid. In the final step, the corresponding liposomes were prepared *via* thin film hydration method using DOPC and cholesterol as additives and liposomal size was adjusted by repeated extrusion. SEC purification finally resulted in ^{18}F-labeled, KuE-functionalized, *hb*PG-shielded liposomes representing a promising system for future drug delivery in the treatment of prostate cancer that can be traced and pre-evaluated *in vivo via* PET.

Experimental part

Terminology

The amphiphilic block copolymer based on the hydrophobic initiator 1,2-bis-*n*-hexadecyl glyceryl ether (BisHD-OH) and the monomer ethoxyethyl glycidyl ether (EEGE) to synthesize the protected macroinitiator is named BisHD-P(EEGE). After cleavage of the acetal protecting groups the resulting linear poly(glycerol) (*lin*PG) is named BisHD-*lin*PG. After the slow monomer addition (SMA) with the monomer glycidol the resulting hyperbranched polyglycerol (*hb*PG) polymer is named BisHD-*hb*PG. The precursor 2-(2-(2-Azidoethoxy)ethoxy)ethyl-*p*-toluenesulfonate is named Ts-TEG-N_3 and the ^{18}F-labeled click-synthon 1-Azido-2-(2-(2-[^{18}F]fluoroethoxy)ethoxy)ethane is named [^{18}F]F-TEG-N_3. The PSMA-inhibitor 2-(3-(5-Amino-1-carboxy-pentyl)ureido)pentanedioic acid (L-lysine-urea-L-glutamate) is named KuE.SA. The KuE.SA-functionalized BisHD-*hb*PG is named BisHD-*hb*PG-KuE.SA.

Instrumentation and Materials

^{1}H NMR (300 MHz), ^{13}C NMR (75 MHz) and 2D spectra were recorded on a Bruker Avance III HD 300 (5 mm BBFO-Probe with z-Gradient and ATM). ^{1}H NMR (400 MHz), ^{13}C NMR (100 MHz) and 2D spectra were measured on a Bruker Avance II 400 MHz (5 mm BBFO-Probe Z-gradient and ATM, SampleXPress 60 auto sampler). ^{1}H NMR (600 MHz), ^{13}C NMR (151 MHz) and 2D spectra were measured on a Bruker Avance III 600 MHz (5 mm TCI-CryoProbe Z-gradient and ATM, SampleXPress lite 16 sampler).The chemical shifts were internally referred to residual proton signals of the deuterated solvent. The NMR spectra were analyzed *via* MestReNova v11.0 software.

Mass spectrometry was measured *via* Agilent Technologies 1220 Infinity LC system coupled to an Agilent Technologies 6130 Single Quadrupole LC/MS system. HPLC purification and analysis was performed using a Merck LaChrom system with Hitachi L7100 pump and L7400 UV-detector and the respectively mentioned column and conditions. Spin Filtration was carried out using Pall Microsep Advance centrifugal filters (MWCO = 1000 g/mol).

Size exclusion chromatography (SEC) for the synthesized polymers was performed at 50 °C in *N,N*-dimethylformamide (with 1 g/L lithium bromide added) as eluent on an Agilent 1,100 Series equipped with Polymer Standards Service (PSS) HEMA columns with 300/100/40 Å porosity and a RI detector. The determination of the molecular weights was determined by a calibration with poly(ethylene glycol) standards by PSS.

During radiosynthesis, activity of the samples was measured using a PC-based dose calibrator (ISOMED 2010, Nuklear Medizintechnik Dresden GmbH). Radio thin layer chromatography (radio-TLC) was performed using Merck Silica 60 F_{254} TLC plates; and ethylacetate:hexane (1:1) as mobile phase. Radio-TLC results were analyzed *via* image plate scanner (CR35-Bio, Elysia Raytest) and AIDA Image Analysis software (Elysia Raytest).

Dynamic light scattering (DLS) was measured using a Malvern Zetasizer Nano ZS. The cell holder was equipped with a Peltier-controlled thermostat. The samples were prepared with a concentration of 1 µL per 1 mL of PBS buffer solution from Sigma Aldrich (dilution 1:1000) and measured at a laser wavelength of 633 nm and a scattering angle of 173°. All samples were measured at a constant temperature of 25 °C. Measurements were performed in disposable polystyrene cuvettes from the company Brand. The analysis was carried out using Malvern Zetasizer Software 7.11 from Macromedia.

All solvents and reagents were purchased generally from the suppliers Acros Organics, Tokyo Chemical Industry (TCI), Sigma-Aldrich, Fluka, Fisher Scientific, Alfa Aesar, IRIS Biotech and VWR and were used as received unless otherwise stated. Deuterated solvents were purchased from Deutero GmbH. Dialysis membranes (regenerated cellulose, MWCO = 500 g/mol and MWCO = 1000 g/mol) were

purchased from Orange Scientific. EEGE was synthesized according to literature.[42] Glycidol was stirred over CaH_2 and freshly distilled before use. Dry *N*-methylpyrrolidone (NMP) was stored over molecular sieve before use.

Aqueous [^{18}F]fluoride was produced *via* proton-irradiation of enriched [^{18}O]H_2O using a PETtrace 700S cyclotron (GE Healthcare).

Organic synthesis procedure

Synthesis of the hydrophobic alkyl chain anchor (BisHD-OH)

BisHD-OH was synthesized as described in literature.[43] More details are in the supporting information (SI-Scheme 1, SI-figure 1).

Synthesis of BisHD-linPG macroinitiator

The synthesis was carried out according to literature.[44]

The synthesis is described for BisHD-*lin*PG_{22} as a representative example.

1,2-bis-*n*-hexadecyl glyceryl ether (BisHD-OH) (2.00 g, 3.70 mmol, 1 eq.) and CsOH mono hydrate (0.56 mg, 3.33 mmol, 0.9 eq.) was placed in a dry Schlenk flask and dissolved in benzene (10 mL). The solution was stirred at 60 °C for at least 30 min and dried in vacuo overnight to remove moisture. Dry Dioxan (50 mL) was added and after 20 min EEGE (11.89 g, 81.34 mmol, 12.01 mL, 22 eq.) *via* syringe. The solution was stirred at 80 °C for 6 d. The solvent was removed in vacuo. The polymer was dissolved again in methanol (50 mL) and 4 g of an acidic ion exchange resin (Dowex 50WX8) was added to the polymer solution to cleave the acetal protecting groups of BisHD-P(EEGE). The solution was stirred and heated to 50 °C overnight. Afterwards, the resin was removed by filtration and the solvent was removed partly in vacuo. The crude polymer was precipitated twice in cold diethyl ether. The resulting block copolymer was dried in vacuo. The polymer was isolated as a brownish resin in a yield of 90%.

^{1}H NMR (400 MHz, DMSO-d_6) δ [ppm] = 4.78 – 4.25 (m, 15H, OH), 3.67 – 3.13 (m, 123H, CH_2-O and CH_2-CH-O), 1.48 – 1.43 (m, 4H, CH_2-CH_2-O), 1.35 – 1.05 (m, 52H, CH_2), 0.85 (t, J = 6.8 Hz, 6H, CH_3-CH_2).

Synthesis of BisHD-hbPG

The synthesis was carried out according to literature.[44]

Hypergrafting of glycidol is described for the macroinitiator BisHD-*lin*PG_{22} as a representative example.

The macroinitiator BisHD-*lin*PG_{22} (0.20 g, 0.10 mmol, 1 eq.) was placed in a Schlenk flask, dissolved in benzene (3 mL) and dried in vacuo overnight. BisHD-*lin*PG_{22} was again dissolved in benzene (2 mL) and CsOH mono hydrate (33.58 mg, 0.20 mmol, 2 eq., equates to a degree of deprotonation of 10% of hydroxyl groups) was added. The solution was stirred at 60 °C for at least 1 hour and dried in vacuo overnight to remove moisture. The macroinitiator was dissolved in *N*-methylpyrrolidone (NMP) (1 mL) and a solution of glycidol (0.59 mg, 7.90 mmol, 0.51 mL, 40 eq.) (5%) in NMP was added to the initiator solution over a time period of 16 h (0.5 mL/h) at 100 °C. The solution was stirred for additional 2 h to ensure complete conversion of glycidol. Subsequently, the solvent was removed under reduced pressure and the crude product was dialyzed for 16 h against methanol (MWCO = 1000 g/mol). The solvent was removed under reduced pressure and the product was dried in vacuo. The polymer was isolated in a yield of 60%.

^{1}H NMR (400 MHz, pyridine-d_5) δ [ppm] = 6.58 – 5.80 (m, 74H, OH), 4.44 – 3.45 (m, 380H, CH_2-O and CH_2-CH-O), 1.73 – 1.60 (s, 4H, CH_2-CH_2-O), 1.44 – 1.20 (m, 52H, CH_2), 0.88 (t, J = 6.5 Hz, 6H, CH_3-CH_2).

Functionalization of BisHD-hbPG with propargyl bromide

The functionalization is described for BisHD-*hb*PG_{74} as representative example.

BisHD-*hb*PG_{74} (0.70 g, 0.12 mmol, 1 eq.) was placed in a Schlenk flask and dissolved in dimethylformamide (DMF) (15 mL). The solution was cooled to 0 °C and sodium hydride (19.6 mg, 0.82 mmol, 7 eq.) was added. The solution was stirred for 1 h at 0 °C to ensure complete deprotonation. Subsequently, propargyl bromide (0.52 mL, 0.46 mmol, 4 eq.) (80 wt% in toluene) was added and the mixture was allowed to slowly reach room temperature. The solution was stirred at room temperature for 2 days. Afterwards, water (2 mL) was added and the solvent was removed under reduced pressure. The crude product was dialyzed against methanol (MWCO = 500 g/mol) for 24 h. The solvent was removed under reduced pressure and the product was dried in vacuo overnight. The alkyne-functionalized polymer was isolated in a yield of 75%.

^{1}H NMR (400 MHz, pyridine-d_5) δ [ppm] = 6.61 – 5.86 (s, 67H, OH), 4.73 – 4.49 (s, 4H, OCH_2-CCH), 4.46 – 3.48 (m, 383H, CH_2-O and CH_2-CH-O), 1.74 – 1.60 (m, 4H, CH_2-CH_2-O), 1.49 – 1.17 (s, 52H, CH_2), 0.88 (t, J = 6.8 Hz, 6H, CH_3-CH_2).

Synthesis of KuE.SA.N_3

Synthesis of the squaramide functionalized PSMA inhibitor KuE.SA was carried out according to the already published procedure.[20]

Synthesis of 2-(3-(5-Amino-1-carboxy-pentyl)ureido)pentanedioic acid (L-lysine-urea-L-glutamate (KuE)

H-Glu(*t*Bu)-O*t*Bu (0.9 g, 3 mmol) and DIPEA (2 mL, 12 mmol) were dissolved in dry dichloromethane (150 mL). The solution was cooled to 0 °C and triphosgene (300 mg, 1 mmol) was added over a period of 4 h. The solution was then stirred for 1 h at room temperature. The H-Lys(Boc)-2CT-polystyrene solid phase (0.78 mmol/g, 390 mg, 0.3 mmol) was added to the reaction solution and stirred for additional 16 h at room temperature. The solid phase was filtered and washed with dichloromethane. The product was cleaved from the solid phase with TFA (3 x 7 mL, 10 min, RT) and purified by semi-preparative HPLC (column: Phenomenex Luna C18 (250 x 10 mm) 10 µ, flow rate: 5 mL/min, H_2O/MeCN + 0.1% TFA, 0-5% MeCN in 20 min, t_R = 9.0 min). KuE was obtained as a colorless oil (67.9 mg, 0.21 mmol, 71%).

^{1}H-NMR (300 MHz, D_2O) δ [ppm] = 4.22 (ddd, *J* = 12.4, 9.0, 5.0 Hz, 2H, HOOC-C*H*-NH-CO), 2.98 (t, *J* = 7.5 Hz, 2H, NH_2-CH_2), 2.50 (t, *J* = 7.3 Hz, 2H, HOOC-CH_2-CH_2), 2.16 (dtd, *J* = 14.9, 7.5, 5.1 Hz, 1H, HOOC-CH_2-CH_2), 2.00 – 1.76 (m, 2H, HOOC-CH_2-CH_2, NH_2-$(CH_2)_3$-CH_2), 1.76 – 1.60 (m, 3H, NH_2-CH_2-CH_2, NH_2-$(CH_2)_3$-CH_2), 1.55 – 1.22 (m, 2H, NH_2-$(CH_2)_2$-CH_2)).

MS (ESI$^+$): 320.1 $[M+H]^+$, calculated for $C_{12}H_{21}N_3O_7$: 319.14 $[M]^+$.

Synthesis of 2-(3-(1-Carboxy-5-((2-ethoxy-3,4-dioxocyclobut-1-en-1-yl)amino)pentyl)ureido)-pentanedioic acid (KuE.SA)

KuE (10 mg, 31.3 µmol) was dissolved in 0.5 M phosphate buffer (pH 7; 250 µL). To this solution 3,4-diethoxycyclobut-3-ene-1,2-dione (5.3 mg, 4.6 µL, 31.3 µmol) was added. The pH was adjusted to pH 7 using 1 M NaOH. The solution was shaken for 16 h. The product KuE.SA was purified by semi-preparative HPLC (column: Phenomenex Luna C18 (250 x 10 mm) 10 µ, flow rate: 5 mL/min, H_2O/MeCN + 0.1% TFA, 12-30% MeCN in 20 min, t_R = 10.0 min) and obtained as a colorless solid (27.8 mg, 62.7 µmol, 23%).

^{1}H-NMR (300 MHz, D_2O) δ [ppm] = 4.75 – 4.65 (m, 2H, HOOC-C*H*-NH-CO), 4.30 – 4.12 (m, 2H, O-CH_2-CH_3), 3.59 (dt, *J* = 23.5 Hz, 6.6 Hz, 1H, NH-CH_2), 3.48 (t, *J* = 6.6 Hz, 1H, NH-CH_2) 2.49 (t, *J* = 7.3 Hz, 2H, HOOC-CH_2-CH_2), 2.16 (dtd, *J* = 15.3 Hz, 7.4 Hz, 5.2 Hz,1H, HOOC-CH_2-CH_2), 2.04 – 1.90 (m, 1H, HOOC-

CH_2-C*H*$_2$) 1.86 – 1.75 (m, 2H, NH-$(CH_2)_3$-C*H*$_2$), 1.73 – 1.46 (m, 2H, NH-CH_2-C*H*$_2$), 1.41 (dt, *J* = 7.1 Hz, 3.6 Hz, 5H, NH-$(CH_2)_2$-C*H*$_2$, O-CH_2-C*H*$_3$).

^{13}C-NMR (300 MHz, D_2O) δ [ppm] = 188.86 (NH-C-*C*O), 182.94 (O-C-*C*O), 177.13 (HOO*C*-CH-$(CH_2)_2$-COOH), 176.95 (HOO*C*-CH_2-CH_2), 176.05 (NH-C=*C*-O), 173.15 (NH-*C*=C-O), 159.08 (NH-*C*O-NH), 70.41 (O-*C*H_3-CH_2), 52.91 (HOOC-*C*H-NH (Lys)), 52.48 (HOOC-*C*H-NH (Glu)), 44.03 ((NH-CH_2-*C*H_2)), 30.26 (NH-*C*H_2), 29.91 (HOOC-*C*H_2-CH_2), 28.86 (NH-$(CH_2)_3$-*C*H_2), 26.15 (HOOC-CH_2-*C*H_2), 21.59 (NH-$(CH_2)_2$-*C*H_2), 14.95 (O-CH_3-*C*H_2).

MS (ESI$^+$): 444.2 $[M+H]^+$, calculated for $C_{18}H_{25}N_3O_{10}$: 443.15 $[M]^+$.

Synthesis of 2-Azidoethylamine

2-Bromoethylamine hydrobromide (1 g, 4.9 mmol) and sodium azide (952 mg, 14.6 mmol) were dissolved in water (15 mL) and stirred overnight at 75 °C. The reaction mixture was cooled to 0 °C and potassium hydroxide (1.2 g, 21.4 mmol) was added. The product was extracted from the aqueous solution with diethyl ether (3 x 20 mL). The organic layer was evaporated under reduced pressure and 2-Azidoethylamine was obtained as colorless oil (372 mg, 4.3 mmol, 87%).

^{1}H-NMR (300 MHz, chloroform-*d*$_3$) δ [ppm] = 3.37 (t, *J* = 5.7 Hz, 2H, C*H*$_2$-NH_2), 2.92 – 2.84 (m, 2H, N_3-C*H*$_2$), 1.42 (s, 2H, -N*H*$_2$).

^{13}C-NMR (300 MHz, chloroform-*d*$_3$) δ [ppm] = 54.50 (*C*H_2-N_3), 41.47 (*C*H_2-NH_2).

MS (ESI$^+$): 87.1 $[M+H]^+$ calculated for $C_2H_6N_4$: 86.06 $[M]^+$.

Synthesis of 2-(3-(5-((2-((2-azidoethyl)amino)-3,4-dioxocyclobut-1-en-1-yl)amino)-1-carboxypentyl)ureido)-pentanedioic acid (KuE.SA.N$_3$*)*

2-Azidoethylamine (40 mg, 0.46 µmol) and KuE.SA (6 mg, 13.5 µmol) were dissolved in 0.5 M phosphate buffer (pH 9, 300 µL) and the pH was readjusted to pH 9 with 1 M NaOH solution. The reaction mixture was shaken overnight and the product (6 mg, 12.4 µmol, 92%) was obtained as a colorless oil after semi-preparative HPLC purification (column: Phenomenex Luna C18 (250 x 10 mm) 10 µ, flow rate: 5 mL/min, H_2O/MeCN + 0.1% TFA, 10-40% MeCN in 20 min, t_R = 8.2 min).

^{1}H-NMR (400 MHz, D_2O) δ [ppm] = 4.25 (dd, *J* = 9.1, 5.1 Hz, 1H, HOOC-C*H*-Glu), 4.19 (dd, *J* = 8.8, 4.9 Hz, 1H, HOOC-C*H*-Lys), 3.55 – 3.49 (m, 2H, NH-C*H*$_2$-CH_2-N_3), 3.17 (t, *J* = 5.5 Hz, 1H, C*H*$_2$-N_3), 2.50 (t, *J* = 7.3 Hz, 2H, HOOC-C*H*$_2$), 2.17 (dq, *J* = 12.5 Hz, 7.3 Hz, 1H, NH-CH_2-C*H*$_2$), 2.00 – 1.89 (m, 1H, NH-C*H*$_2$-CH_2),

1.85 (p, *J* = 7.9 Hz, 7.2 Hz, 1H, HOOC-CH_2-C*H*$_2$), 1.73 (dt, *J* = 13.7 Hz, 6.9 Hz, 1H, HOOC-CH_2-C*H*$_2$), 1.64 (p, *J* = 7.3 Hz, 6.4 Hz, 2H, NH-$(CH_2)_3$-C*H*$_2$), 1.45 (q, *J* = 8.4 Hz, 2H, NH-$(CH_2)_2$-C*H*$_2$).

^{13}C-NMR (400 MHz, D_2O) δ [ppm] = 177.26 (SA.*C*=O), 176.86 (HOO*C*-CH_2-CH_2), 176.10 (2C, HOO*C*-CH), 159.15 (NH-*C*O-NH), 117.66 (, NH-C-*C*-NH), 114,80 (NH-*C*-C-NH), 53.06 (HOOC-*C*H-Lys), 52.47 (HOOC-*C*H-Glu), 51.45 (*C*H_2-N_3), 43.50 (NH-*C*H_2-CH_2-N_3), 30.37 (NH-$(CH_2)_3$-*C*H_2), 29.87 (HOOC-*C*H_2), 29.36 (NH-CH_2-*C*H_2), 26.07 (HOOC-CH_2-*C*H_2), 21.62 (NH-$(CH_2)_2$-*C*H_2).

MS (ESI$^+$): 484.4 $[M+H]^+$, 506.2 $[M+Na]^+$, calculated for $C_{18}H_{25}N_7O_9$: 483.17 $[M]^+$.

Synthesis of the KuE.SA.triazolyl-BisHD-hbPG

KuE.SA-functionalization of BisHD-*hb*PG *via* CuAAC was performed according to a modified protocol by Yamamoto *et al.*[45] The synthesis is described for KuE.SA-triazolyl-BisHD-*hb*PG_{74} as representative example.

Alkyne-BisHD-*hb*PG_{674} (23 mg, 3.8 µmol, ca. 7 alkyne-groups per polymer) was dissolved in PBS (1 mL). KuE.SA.N_3 (4.6 mg, 9.5 µmol) in PBS (1 mL), DMSO (36 µL), *N,N,N′,N′′,N*′′-pentamethyldiethylenetriamine and PMDETA (1 µL, 3.8 µmol) were added. The mixture was heated to 45 °C and CuBr (5.4 µL of a 1 mg/mL solution in DMSO; 5.4 µg, 0.038 µmol) was added and stirred at 45 °C and under argon atmosphere for 16 h. Purification was carried out by spin filtration. The solution was transferred into a centrifuge tube (Pall Microsep Advance 1K) and centrifuged for 30 min (4696 *g*). The concentrate was dissolved in water (1 mL) and centrifuged again for 15 min (4696 *g*). This washing step was repeated 7 times. In the last step the concentrate was centrifuged (4696 *g*) for 1 h. Lyophilisation gave the product as brownish solid (24.2 mg).

Synthesis of the precursor 2-(2-(2-Azidoethoxy)ethoxy)ethyl-p-toluenesulfonate (Ts-TEG-N_3)

Ts-TEG-N_3 was synthesized as described in literature.[40]

Radiosynthesis of 1-Azido-2-(2-(2-[^{18}F]fluoroethoxy)ethoxy)ethane ([^{18}F]F-TEG-N_3)

Radiolabeling of the precursor Ts-TEG-N_3 and subsequent purification to produce [^{18}F]F-TEG-N_3 was performed *via* semiautomatic custom modular system using cyclotron-produced [^{18}F]fluoride according to the procedure already reported in literature.[40]

[^{18}F]fluoride was first trapped on a preconditioned (10 mL 1 M K_2CO_3 solution, 10 mL Milli-Q water, 20 mL air) Sep-Pak QMA light cartridge (Waters) and subsequently eluted into a reaction vial using a mixture of 1 M K_2CO_3 solution (15 µL, 15 µmol), Kryptofix® 222 (15 mg, 40 µmol) and acetonitrile (1 mL). Azeotropic removal of residual water was achieved *via* evaporation of the solvent under reduced pressure and helium flow at 80 °C. After cooling to 40 °C, a solution of Ts-TEG-N_3 (10.0 mg, 30.4 µmol) in acetonitrile (1 mL) was added and the reaction vial was heated to 90 °C for 10 min. After completion of the radiolabeling reaction, the mixture was cooled down again to 40 °C and MeCN/H_2O (1:1) (1 mL) was added. The resulting solution of crude compound was subsequently purified *via* semipreparative HPLC (column: Phenomenex Luna C18 semipreparative (250 x 10 mm) 10 µ, flow rate: 3 mL/min, MeCN/H_2O 1:1, t_R = 8.0 min). The collected product fraction was diluted by Milli-Q water (35 mL) and passed through a preconditioned (10 mL acetonitrile, 10 mL Milli-Q water, 20 mL air) Lichrolut EN cartridge (Merck). Subsequently, the cartridge was dried with a stream of helium and eluted with anhydrous diethylether (1.5 mL) into a vial equipped with a stirring bar and a septum. Evaporation of the solvent under reduced pressure and helium flow (10 mL/min) at 40 °C led to the product ([^{18}F]F-TEG-N_3) with a decay corrected radiochemical yield of 53%.

Synthesis of ([^{18}F]F-TEG-triazolyl)(KuE-SA-triazolyl)-BisHD-hbPG

^{18}F-labeling of the KuE-SA-triazolyl-BisHD-*hb*PG *via* copper(I)-catalyzed azide-alkyne cycloaddition (CuAAC) was performed similarly to the method already published.[33] The synthesis is described for ([^{18}F]F-TEG-triazolyl)-(KuE-SA-triazolyl)-BisHD-*hb*PG_{63} as representative example.

In detail, a solution of KuE-SA-triazolyl-BisHD-*hb*PG_{63} (3.1 mg, 0.56 µmol) in 1 mL PBS was added to a vial containing a layer of [^{18}F]F-TEG-N_3 and a stirring bar. Successively, 12.5 µL DMSO, 15 µL 1 M $CuSO_4$ solution (15 µmol) and 25 µL 2.4 M sodium ascorbate in PBS (60 µmol) were added and the resulting mixture was heated to 70 °C for 15 min while stirring. Completion of the reaction was confirmed *via* radio-TLC (radiolabeled product: R_f = 0, [^{18}F]F-TEG-N_3: R_f = 0.8-0.9). Subsequently, the solution was passed through preconditioned (0.8 mL 1 M HCl, 5 mL H_2O, 0.8 mL 1 M NaOH, 5 mL H_2O, 10 mL air) Chelex 100 chelating resin (600 mg, Bio-Rad) to remove catalytic copper. The cartridge was flushed with 1.5 mL abs. ethanol and the eluate was combined with the first aqueous flow-through yielding a solution of purified, $^{18}F^-$labeled polyether lipid with a decay corrected radiochemical yield of 73%.

Synthesis of ([^{18}F]F-TEG-triazolyl)-BisHD-hbPG

^{18}F-labeling of the non-KuE-functionalized, alkyne-bearing BisHD-hbPG (3.5 mg, 0.65 µmol) was accomplished via CuAAC analogously to the synthesis of ([^{18}F]F-TEG-triazolyl)(KuE-SA-triazolyl)-BisHD-hbPG resulting in a decay-corrected radiochemical yield of 81%.

Liposome formation

^{18}F-labeled, KuE-functionalized liposomes were prepared *via* thin film hydration and automatic extrusion similar to the method already published in literature.[33,34]

1,2-dioleoyl-*sn*-glycero-3-phosphocholine (DOPC, 241 µL, 20 mg/mL in ethanol, 6.13 µmol, 55 mol%) and cholesterol (246 µL, 7 mg/mL in ethanol, 4.46 µmol, 40 mol%) were added to the obtained aqueous-ethanolic solution of the ^{18}F-labeled polyether lipid ([^{18}F]F-TEG-triazolyl)(KuE-SA-triazolyl)-BisHD-hbPG (0.56 µmol, 5 mol%)**.** The solvents were removed under reduced pressure *via* rotary evaporator providing a thin oily layer. Addition of 0.8 mL PBS and subsequent ultrasonication for 10 min at 50 °C led to a turbid yellow suspension. To obtain uniform liposomes of small size, the suspension was extruded automatically through polycarbonate membranes of different pore sizes (400 nm, 100 nm and 50 nm, 21 times each) *via* custom-built extrusion device equipped with a LiposoFast extruder unit (AVESTIN Europe GmbH). In order to separate smaller components and structures, the resulting liposomes were finally purified *via* fractionated size exclusion chromatography (SEC) using Sephacryl S-400 HR resin (Cytiva, 4 mL in a 6 mL SPE tube) and PBS as mobile phase (0.5 mL per fraction). The radiolabeled KuE-functionalized liposomes eluted in fractions 3-5 as a slightly turbid suspension with a decay-corrected radiochemical yield of 25%.

Results and discussion

Polymer synthesis and characterization

The amphiphilic block copolymer BisHD-*hb*PG was synthesized in a multi-step procedure.

Synthesis of the hydrophobic BisHD-OH anchor

The hydrophobic anchor structure BisHD-OH was synthesized as initiator for the anionic ring opening polymerization (AROP) of epoxides. The initiator was prepared in a straightforward two-step synthesis based on a procedure of Stauch *et al.*, performing a Williamson etherification and using 1-*O*-benzyl

glycerol and hexadecyl bromide, followed by hydrogenation to remove the benzyl protecting group.[43] In the past, two other hydrophobic anchors 1,2-bis-*n*-icosanyl glyceryl ether (BisID-OH) with longer and 1,2-bis-*n*-octadecyl glyceryl ether (BisOD-OH) with shorter alkyl chain lengths of the anchor structures were also used for the AROP.[44] In a study of Gleue *et al*., the influence of the length of the amphiphilic anchors on the stability of the liposome membrane and the exchange between liposome membrane and cell membrane was investigated.[36] Due to the good stability of BisHD-OH, this anchor was used as an initiator for our structures.

Synthesis of BisHD-linPG macroinitiator

In the first reaction step a BisHD-P(EEGE) precursor polymer was synthesized *via* AROP with ethoxy ethyl glycidyl ether (EEGE). For the polymerization of EEGE the BisHD-OH was first deprotonated with cesium hydroxide monohydrate and dried in vacuo overnight to remove any moisture. Cesium hydroxide monohydrate was used as base for the deprotonation to ensure a good reactivity for the polymerization due to the formation of a dissociated ion pair.[46,47] The resulting initiator salt was dissolved in dioxane and the AROP of EEGE was performed under slightly reduced pressure and at elevated temperatures (80 °C) for 6 days. High temperatures were necessary to enable a polymerization clearly above the melting point of the initiator and to increase the overall reactivity. The polymerization of EEGE leads to linear structures (PEEGE) with acetal-protected hydroxyl groups, which can be released upon acidic treatment according to literature.[48] The resulting linear polyglycerol (BisHD-*lin*PG) structure exhibits numerous hydroxyl groups and can therefore be used as a macroinitiator to prepare the hyperbranched polyglycerol (*hb*PG) block (scheme 1).

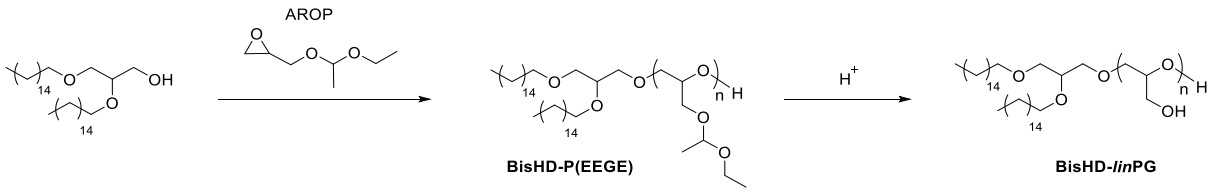

Scheme 1: Synthesis route for the macroinitiator BisHD-P(EEGE) and cleavage of the protecting acetal groups resulting in BisHD-linPG.

Synthesis of BisHD-hbPG

BisHD-*lin*PG was used for "hypergrafting" of glycidol *via* slow monomer addition (SMA) technique to obtain the BisHD-*hb*PG polyether lipids. For the synthesis, the free hydroxyl groups of the BisHD-*lin*PG macroinitiator were deprotonated using cesium hydroxide monohydrate and dried overnight to remove any moisture. The initiator salt was dissolved in *N*-methyl-2-pyrrolidone (NMP) to guarantee

a good solubility of the macroinitiator and the resulting BisHD-*hb*PG. The monomer glycidol was added *via* SMA approach over a time period of 16 h to obtain well-defined BisHD-*hb*PG (scheme 2).

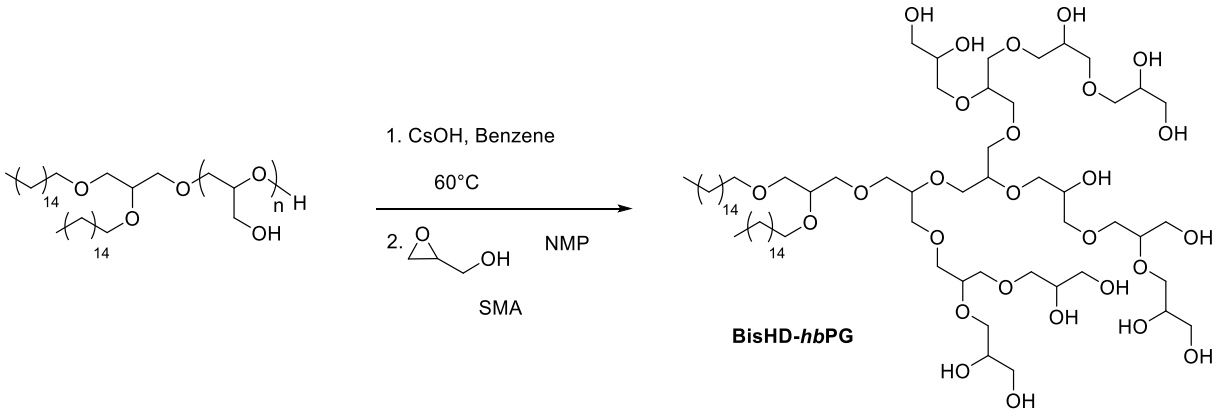

Scheme 2: Synthesis route for BisHD-hbPG via slow monomer addition (SMA) of glycidol.

The key characterization data of BisHD-P(EEGE), BisHD-*lin*PG and BisHD-*hb*PG are summarized in table 1.

Table 1: Characterization data of the precursor BisHD-P(EEGE), the macroinitiator BisHD-linPG and the block copolymer BisHD-hbPG.

Sample	M_n $^{NMR\ a}$ (g·mol^{-1})	M_n $^{SEC\ b}$ (g·mol^{-1})	Đ ^{b}
BisHD-P(EEGE)$_{22}$	3750	2230	1.06
BisHD-linPG$_{22}$	2170	1990	1.07
BisHD-hbPG$_{74}$	6010	3830	1.26

[a] Obtained from ^{1}H NMR spectroscopy. [b] Determined via SEC (RI, DMF, PEG standards).

AROP of BisHD and EEGE yielded the macroinitiator BisHD-P(EEGE), which was obtained with 22 EEGE units and a molecular weight (M_n) of 3750 g·mol^{-1} with a low dispersity ($Đ$=1.06). The BisHD-*lin*PG had a lower molecular weight of 2170 g·mol^{-1}, because of the acidic cleavage of the acetal groups. After the SMA with glycidol the BisHD-*hb*PG was obtained with 74 glycidol units and a molecular weight of 6010 g·mol^{-1}. The dispersity ($Đ$=1.26) is quiet good for this kind of "hypergrafting" reaction. The molecular weights determined *via* SEC are deviating from the results determined *via* ^{1}H NMR, due to the applied PEG standards in the calibration and the varying hydrodynamic volume (V_h), especially for the BisHD-*hb*PG polymer compared to PEG.

An overlay of the monomodal SEC traces of the precursor BisHD-P(EEGE), the macroinitiator BisHD-*lin*PG and the amphiphilic block copolymer BisHD-*hb*PG is shown in figure 1. An expected slight shift to a lower molecular weight is observed between the SEC trace before (blue) and after cleavage of the

protecting groups (green). Furthermore, a shift to a higher molecular weight due to the changing V_h of the hyperbranched block copolymer can be observed (red).

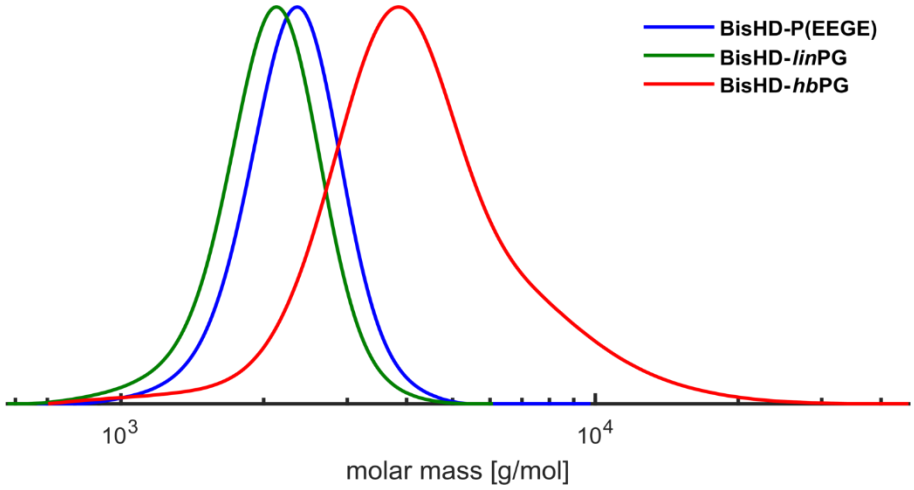

Figure 1: SEC traces (RI detector, DMF, PEG standards) of the precursor BisHD-P(EEGE), the macroinitiator BisHD-*lin*PG and the block copolymer BisHD-*hb*PG.

The ^{1}H NMR spectra of BisHD-P(EEGE) and the spectra of BisHD-*lin*PG after the deprotection are shown in SI-Figure 2 and SI-Figure 3. The acetal protecting groups could be completely cleaved off. The ^{1}H NMR spectra of BisHD-*hb*PG$_{74}$ is shown in figure 2 with assigned signals.

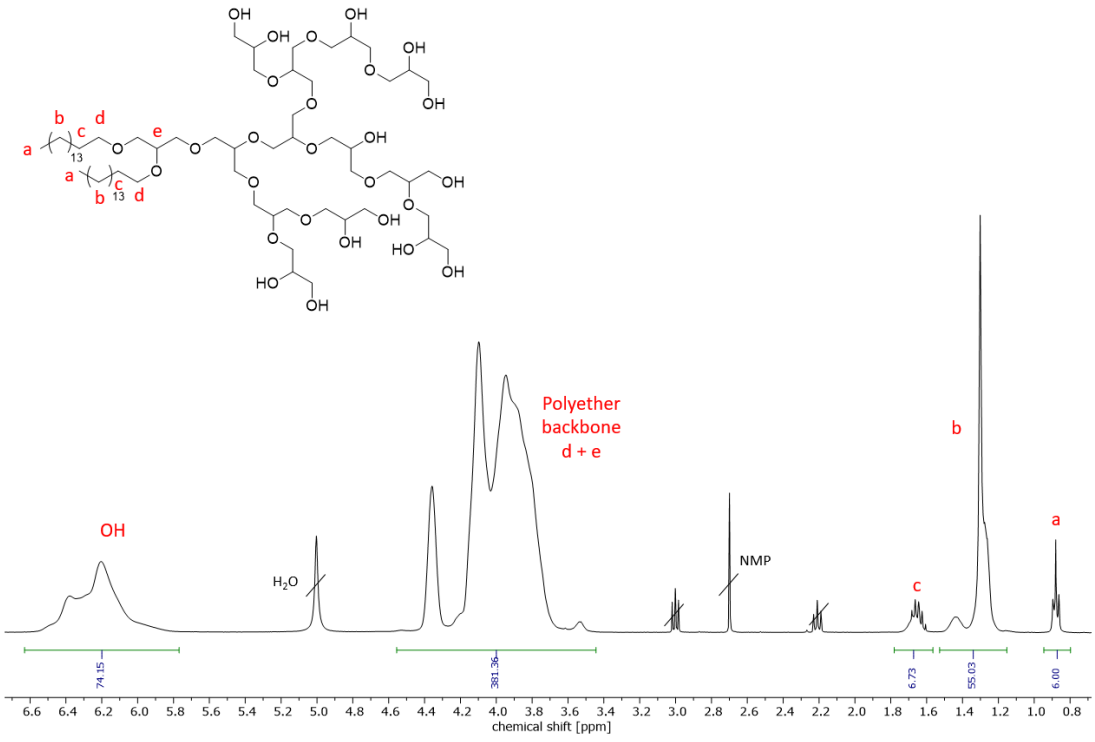

Figure 2: ^{1}H NMR spectrum (400 MHz, pyridine-d_5) of BisHD-*hb*PG$_{74}$ (entry 3, table 1).

Post-polymerization modification

The amphiphilic BisHD-*hb*PG block copolymer was functionalized with propargyl bromide to attach alkyne-moieties. The alkyne-groups enables a copper(I)-catalyzed azide alkyne cycloaddition (CuAAC) with azide-bearing molecules. This reaction is known from literature and was adapted for the synthesized amphiphilic block copolymer.[40] For the functionalization, the hydroxyl groups of BisHD-*hb*PG were deprotonated using sodium hydride (NaH). The degree of functionalization was controlled *via* the amount of applied propargyl bromide. The successful functionalization was proven *via* NMR spectroscopy. The characteristic resonances for the propargyl group could be assigned *via* ^{1}H NMR spectrum (figure 3) and ^{1}H, ^{13}C-HSQC NMR spectrum (SI-Figure 6). The number of alkyne groups cannot be accurately determined by integrating the signals in the ^{1}H NMR spectrum. The characteristic NMR signals of the alkyne group are strongly broadened in deuterated pyridine. However, from the decrease in the number of protons of the hydroxyl group from 74 to 67 protons, it can be concluded that an average of 7 alkyne groups per polymer are bound for further functionalization.

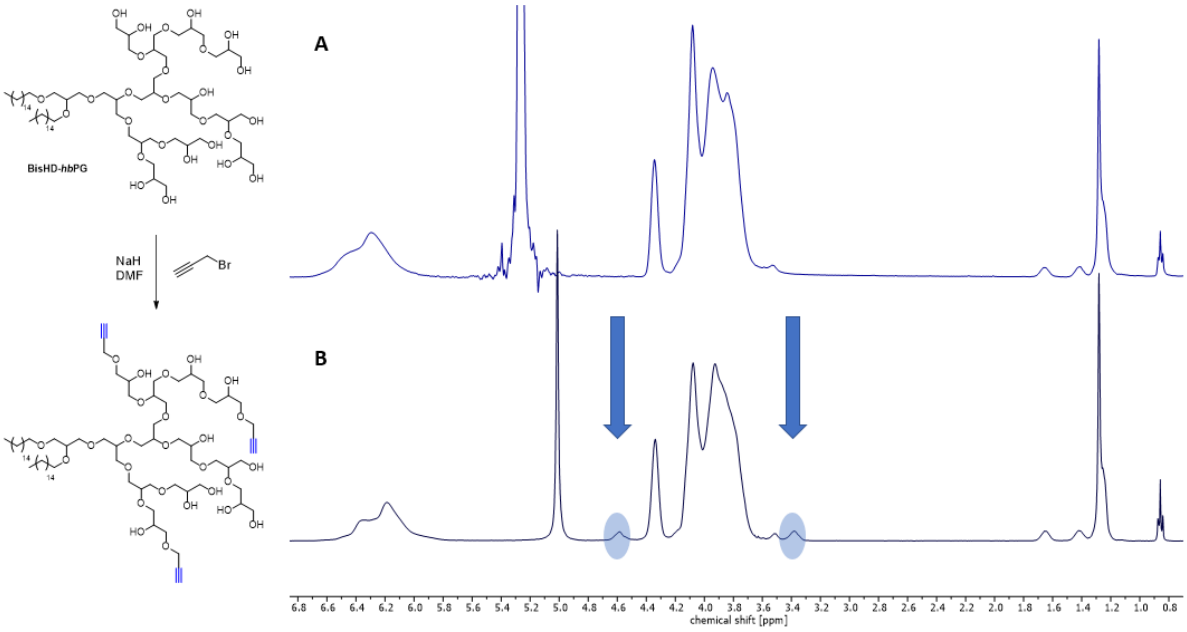

Figure 3: ^{1}H NMR spectra (400 MHz, pyridine-d_5) of BisHD-hbPG$_{74}$ (**A**, top) and BisHD-hbPG$_{74}$-alkyne (**B**, bottom). The appearing signals for the propargyl group are emphasized in blue.

In table 2 the characteristics of BisHD-*hb*PG before and after functionalization with propargyl bromide is summarized.

Table 2: Characterization data of the BisHD-hbPG and BisHD-hbPG-alkyne.

Sample	M_n NMR [a] (g·mol^{-1})	M_n SEC [b] (g·mol^{-1})	Đ [b]	Alkyne moieties[b]
BisHD-hbPG$_{74}$	6010	3830	1.26	
BisHD-hbPG$_{74}$-alkyne	6500	4470	1.22	7

[a] Obtained from ^{1}H NMR spectroscopy. [b] Determined via SEC (RI, DMF, PEG standards).

SEC measurements reveal moderate size distribution for the functionalized BisHD-*hb*PG-alkyne polymer. Moreover, the successful attachment of alkyne-moieties to BisHD-*hb*PG is proven due to the shift of the SEC trace to lower elution volume translating to higher molecular weight (figure 4). Polydispersity decreases minimally after functionalization due to purification by dialysis.

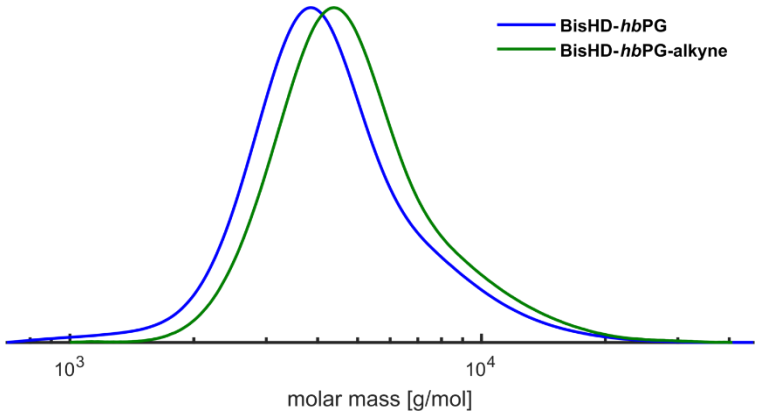

Figure 4: SEC traces (RI detector, DMF, PEG standards) of BisHD-hbPG before (blue) and after functionalization (green) with propargyl bromide.

Synthesis of the PSMA inhibitor and functionalization of the hyperbranched polyether lipid

Synthesis of the azide-functionalized PSMA inhibitor KuE.SA.N$_3$

Synthesis of the actual PSMA inhibitor L-lysine-urea-L-glutamate (KuE) was adopted from the procedure described by Greifenstein *et al.*[20] In the first step, slow addition of triphosgene to a cooled solution of twice *tert*-butyl protected L-glutamic acid and DIPEA led to the corresponding isocyanate, which was directly reacted with Nε-Boc-protected L-lysine bound to a chlorotrityl polystyrene resin (scheme 3). Nucleophilic attack of the partially positively charged isocyanate-carbon by the α-nitrogen of lysine resulted in the solid phase-bound, urea coupled and protected amino acids. Simultaneous cleavage and deprotection using TFA followed by HPLC purification finally provided the desired product KuE with a yield of 71%.

Subsequently, the squaric acid moiety was introduced using SADE at pH 7 *via* formation of the corresponding monoamide (scheme 3). In this step, a severe pH control using a buffered medium is required to prevent further amidation and therefore KuE-dimerization, which occurs at more basic

conditions. The HPLC-purified KuE.SA was obtained with a yield of 23%. The rather moderate yield does not reflect low formation of the product (as confirmed *via* LC/MS), but is mainly attributed to a loss during HPLC purification.

The next step finally included azide-functionalization *via* second amidation of the squaric acid monoamide at pH 9 using 2-azidoethylamine (scheme 3). The azide-bearing precursor was previously synthesized starting from 2-bromoethylamine hydrobromide by means of sodium azide and potassium hydroxide. After HPLC purification, the desired clickable PSMA inhibitor KuE.SA.N_3 was finally obtained with a yield of 86%.

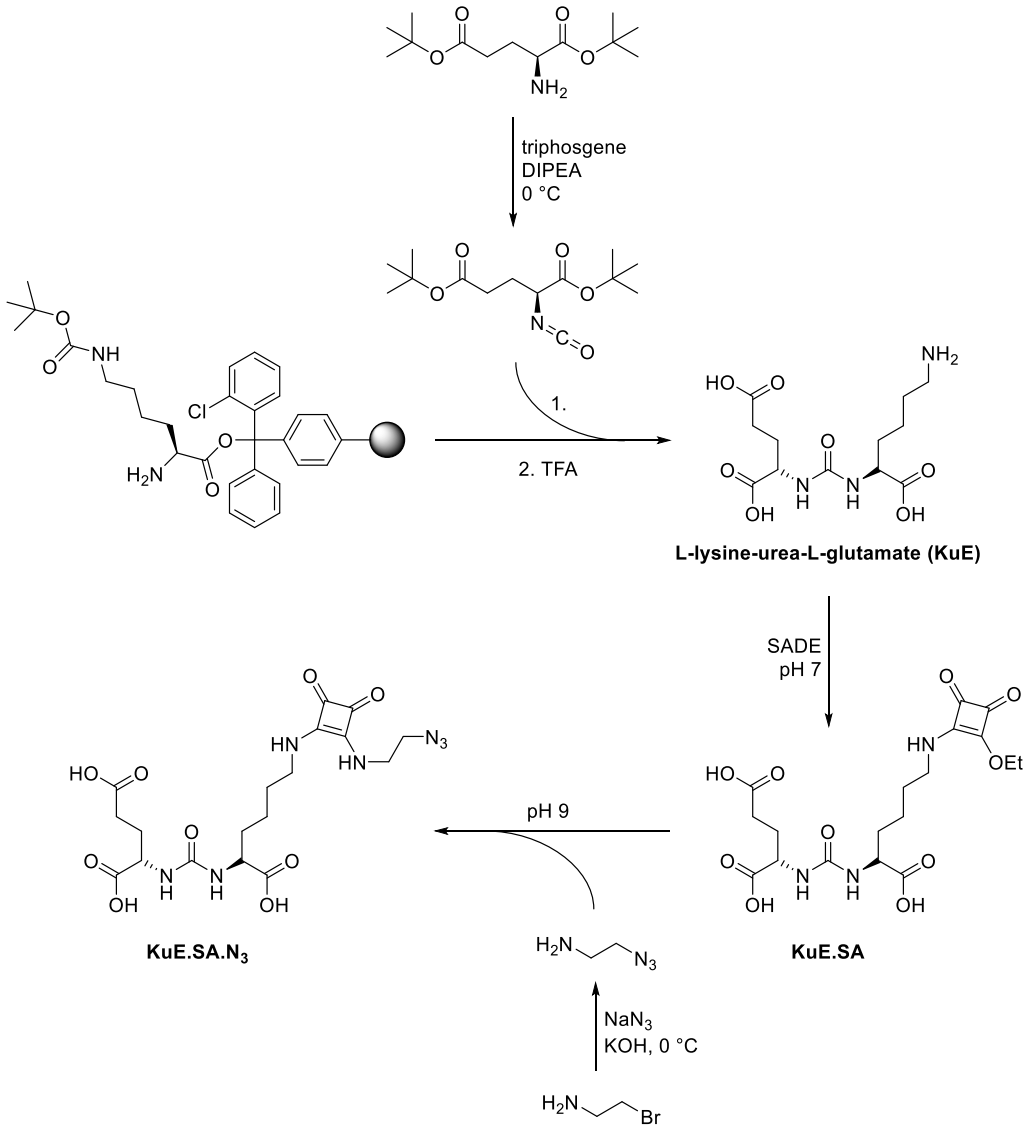

Scheme 3: Synthesis of the PSMA inhibitor L-lysine-urea-L-glutamate (KuE) and subsequent azide-functionalization *via* formation of the corresponding squaric acid diamide.

KuE.SA-functionalization of alkyne-bearing BisHD-hbPG

In order to ensure specific binding to PSMA expressing cancer of the later prepared liposomal system, the alkyne-bearing hyperbranched polyether lipid was functionalized with KuE.SA *via* CuAAC, also named click-reaction (scheme 4). This modification was achieved similarly to the method Wagener *et al.* used for preparation of trimannosylated lipids.[34] Therefore, BisHD-*hb*PG-alkyne was reacted with the previously synthesized KuE.SA.N_3 using copper(I) bromide and PMDETA as base. The base PMDETA is added to promote the formation of the copper acetylide intermediate.[49] Subsequent coordination of the azide leads to the formation of a six-membered metallacycle, which in turn is then converted to the triazolyl-connected product through ring contraction and protonolytic cleavage of the catalyst. To ensure sufficient functionalization of the polyether lipid with the PSMA inhibitor on the one hand and to leave binding sites unoccupied for subsequent radiolabeling on the other hand, 2.5 equivalents KuE.SA.N_3 were used. Purification of the product for removal of small reaction components and unbound reactant was achieved via spin filtration (MWCO = 1000 g/mol).

To verify the successful binding of KuE.SA.N_3 to the polymer using CuAAC, NMR spectra were prepared. In the ^{1}H and ^{13}C spectra, only very weak characteristic signals could be detected. Reasons for this are on the one hand the large molecular weight of the polymer compared to the molecular weight of the attached group, many signals overlap with the signals of the polymer and the deuterated solvent pyridine has an additional strong shielding effect. However, by ^{1}H, ^{13}C HSQC analysis, the successful binding could be confirmed. The spectra can be taken from the supporting information (SI-figures 14-18). Furthermore, a decrease in the protons of the alkyne groups on the polymer was observed and the KuE.SA functionalized liposomes showed fluorescence in the DLS later on, further confirming the successful functionalization.

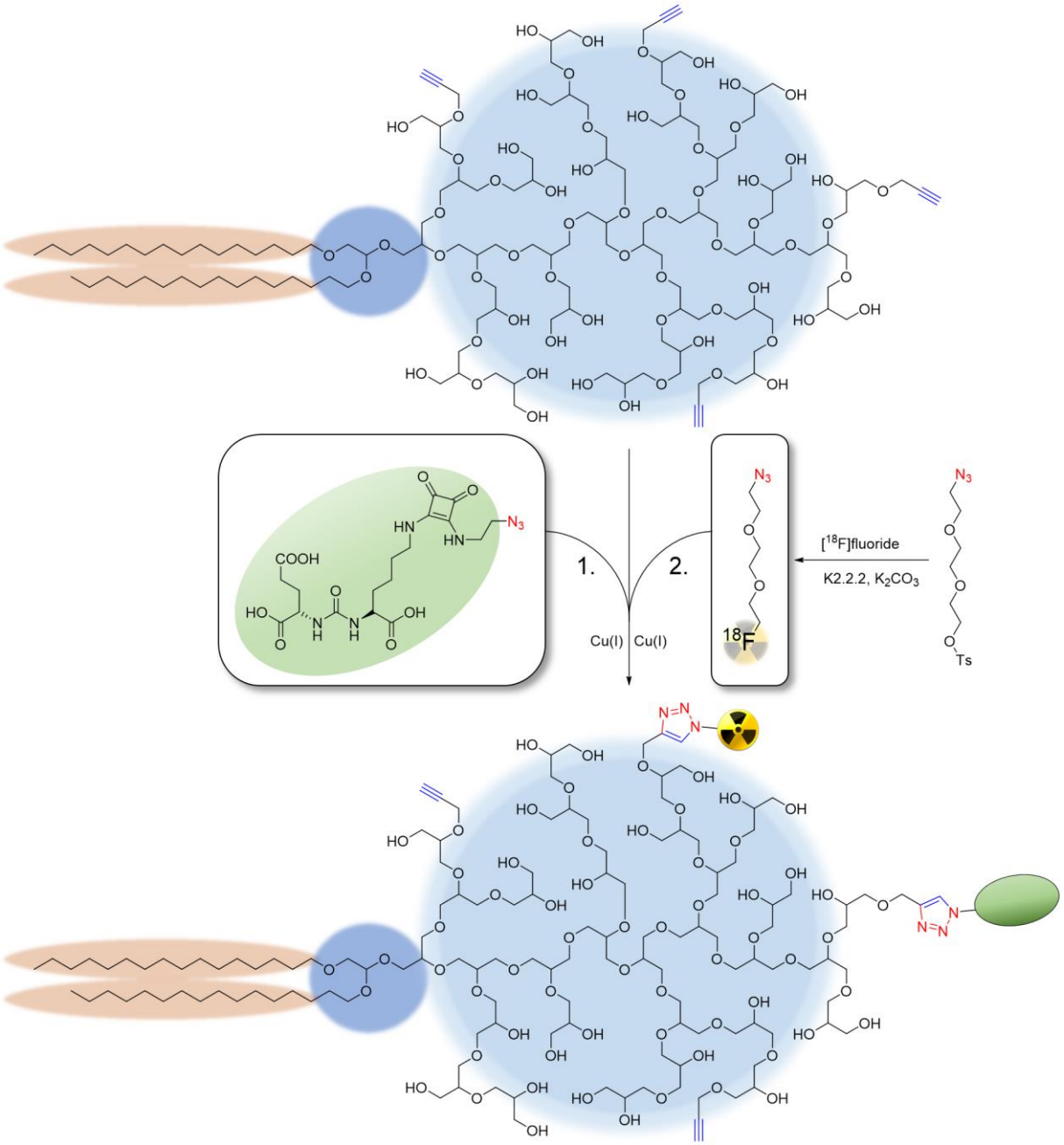

Scheme 4: Consecutive KuE.SA-functionalization and ^{18}F-labeling of the alkyne-bearing hyperbranched polyether lipid BisHD-hbPG using CuAAC.

Radiosynthesis

Radiosynthesis first included nucleophilic ^{18}F-labeling of the prior synthesized click-synthon Ts-TEG-N_3 according to the procedure of previous reports.[33,34,40] In this step a semiautomatic custom-built modular system was used significantly simplifying and accelerating the synthesis and minimizing radiation exposure to the experimentalist. Cyclotron produced [^{18}F]fluoride was first separated from target [^{18}O]water via trapping on a quaternary methyl ammonium (QMA) anion exchange cartridge and subsequently eluted using a mixture of aqueous K_2CO_3, [2.2.2]cryptand (Kryptofix® 222) and

acetonitrile. The aminopolyether Kryptofix® 222 serves as phase transfer catalysator enhancing fluoride-nucleophilicity and -solubility in organic solvents via complexation of the potassium counter ion.[50,51] Since hydrated [^{18}F]fluoride is strongly inactivated for nucleophilic reactions, complete removal of residual water plays a crucial role and was realized via azeotropic evaporation of the solvent. Nucleophilic substitution of the added precursor Ts-TEG-N_3 was achieved within 10 min at 90 °C. Further processing of the crude product consecutively included HPLC purification, dilution, polymer-based solid phase extraction using diethylether as eluent and evaporation of the solvent. The whole procedure lasted 100 min and therefore slightly less than one half-life of the radionuclide. The ^{18}F-labeled click synthon [^{18}F]F-TEG-N_3 was obtained with a decay corrected radiochemical yield of 53%.

As shown in scheme 4, residual unoccupied alkyne groups were used for radiolabeling of the KuE.SA-functionalized BisHD-*hb*PG via repeated CuAAC using previously synthesized [^{18}F]F-TEG-N_3. Therefore, the polyether lipid was combined with the radiolabeled synthon and the click reaction was initiated via addition of copper(II) sulfate and sodium ascorbate analogously to the KuE-functionalization described above. In this case, an elevated temperature of 70 °C was used to accelerate the conversion of reactants. As determined via radio-TLC (figure 5), completion of the reaction could be confirmed already after 15 min as indicated by almost quantitative radiochemical yield (98.8%). To separate cytotoxic copper, the reaction mixture was subsequently passed through a Chelex 100 chelating resin. A distinct blue layer at the very top of the cartridge indicated successful removal of the catalytic metal ion. Furthermore, Wagener *et al*. confirmed the efficiency of this method via the absence of precipitated copper sulfide after addition of sodium sulfide to the purified solution.[33] For maximum product recovery, the resin was additionally flushed with ethanol resulting in an aqueous-ethanolic solution of radiolabeled polyether lipid. In the case of BisHD-*hb*PG-KuE.SA, total duration of this synthesis step accounted for 32 min and the ^{18}F-labeled analogue could be obtained with a decay corrected radiochemical yield of 73%. For comparison, non-KuE-modified BisHD-*hb*PG was radiolabeled analogously (81% RCY, 45 min).

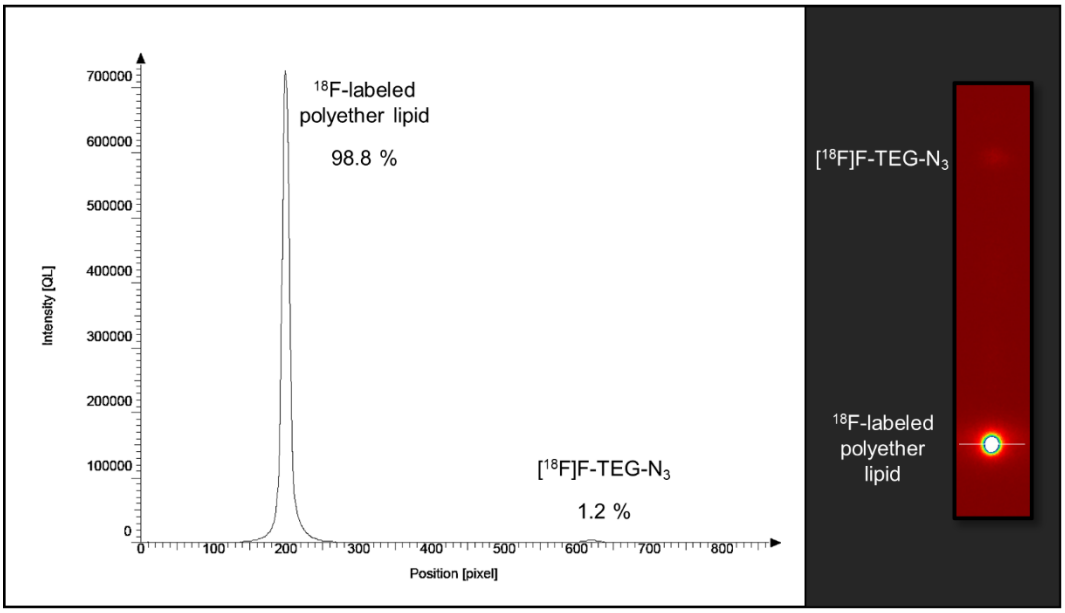

Figure 5: Radio-TLC image (right) and analyzed TLC chromatogram (left) showing the ^{18}F-labeling (CuAAC) results of ([^{18}F]F-TEG-triazolyl)-BisHD-*hb*PG-KuE.SA after 15 min at 70 °C (solid phase: silica gel, mobile phase: ethylacetate:hexane 1:1; ^{18}F-labeled polyether lipid: R_f = 0, [^{18}F]F-TEG-N_3: R_f = 0.8-0.9). The chromatogram position of 200 pixels indicates the TLC-baseline.

Liposome Formation and Characterization

As already mentioned, liposomes are typically prepared using amphiphilic phospholipids containing of a hydrophylic "head" and two hydrophobic "tails". Upon contact with polar solvents (e.g. water), these molecules spontaneously arrange themselves to form mono- and bilayers as well as spheric structures such as micelles or vesicular liposomes. In this study we used DOPC as structure-defining component. This zwitterionic phospholipid has a low gel-fluid phase transition temperature of approx. -22 °C and therefore enables preparation of fluid-state liposomes at room temperature.[52,53] For further stabilization, we additionally used cholesterol, which occupies free space of the bilayer and therefore decreases the flexibility and mobility of surrounding fluid-phase lipids leading to an increased mechanical rigidity, decreased water permeability and reduced aggregation-tendency of the liposomal system.[54–58] Ethanolic solutions of these two components (55 mol% DOPC, 40 mol% cholesterol) were blended with the previously ^{18}F-labeled, KuE-functionalized BisHD-*hb*PG (5 mol%) and liposome preparation via thin film hydration was achieved according to the procedure described by Wagener *et al*.[33,34] Therefore, removal of the solvents under reduced pressure using a rotary evaporator led to a thin oily layer of the different constituents. Subsequently, large multilamellar vesicles of hetereogeneous size distribution were formed via hydration using PBS and ultrasonication. In order to obtain small uniform unilamellar liposomes, the suspension was extruded repeatedly through polycarbonate membranes of different pore sizes (400, 100 and 50 nm) using a custom-built automatic

extrusion device. In contrast to manually driven extrusion, the applied device ensures constant speed and pressure leading to reproducible and narrow size distribution while minimizing the radiation exposure to the experimentalist.[33] Removal of smaller components like unassembled lipids and micelles was achieved via fractionated SEC (SI-figure 19) resulting in a purified suspension of ^{18}F-labeled, KuE-functionalized and *hb*PG shielded liposomes with a decay corrected radiochemical yield of 25%. Duration of the entire procedure accounted for 82 min. For comparison, ^{18}F-labeled but non-KuE-functionalized liposomes were prepared analogously (14% RCY, 75 min). After complete decay of the activity, the size of both KuE.SA-bearing and non-KuE-functionalized liposomes was measured via DLS (SI-table 1, SI-figure 20-22. The BisHD-*hb*PG-alkyne liposomes indicated a diameter of 157.5 nm, for the analogous KuE.SA-bearing liposomes a higher value of 199.1 nm was measured. The significant difference in size may result from the measurement, as the sample of functionalized liposomes exhibits fluorescence, which may distort the measurement result. For this reason, the PDIs of the measured samples also differ (SI-table 1). Since preparation, processing and extrusion was carried out analogously for both systems, the difference in size is presumably based on an increased steric demand due to KuE.SA-functionalization of the polyether lipid. Additionally, it may also be partly influenced by the measurement itself, as the sample of functionalized liposomes exhibits fluorescence, which may distort the DLS-results. The liposomal size plays a crucial role for the pharmacological behavior *in vivo*. Ideally, the hydrodynamic diameter should on the one hand be large enough to prevent interaction with hepatocytes and thus filtration through the liver, which occurs up to a particle size of 50-100 nm.[59] On the other hand, it should not exceed 300 nm to avoid an increased accumulation in the spleen.[60] Furthermore, (non-functionalized) liposomes with sizes ranging from 100 to 200 nm were reported to take advantage of tumour permeability most effectively resulting in optimal target uptake.[59,61] The dimensions of both liposomal systems described herein meet these requirements and were comparable to the values of similar vesicles reported in the literature.[34] The liposomes containing KuE.SA-functionalized BisHD-*hb*PG therefore represent promising tools for targeted drug delivery in the treatment of PSMA-expressing prostate cancer. Furthermore, utilization of the ^{18}F-labeled vesicles should ensure *in vivo* evaluation of the pharmacokinetics via PET in future follow-up studies.

Conclusion

In this study, the synthesis of an alkyne-functionalized hyperbranched polyglycerol with a long hydrophobic alkyl chain anchor (BisHD-*hb*PG) via AROP on the one hand and of a squaramide coupled PSMA inhibitor (KuE.SA) on the other hand is described. To combine these two structures, Cu(I)-catalyzed alkyne-azide cycloaddition (CuAAC) was used. For this purpose, BisHD-*hb*PG was functionalized with alkyne groups and the PSMA inhibitor was modified with an azide group. In a

second CuAAC the BisHD-*hb*PG-KuE.SA polymers were radiolabeled with a previously synthesized ^{18}F-labeled precursor. To obtain PSMA-specific drug delivery systems with a prolonged circulation behavior in the blood stream, liposomes were formed via thin film hydration method. The syntheses and radiolabeling were straightforward and achieved high yields. By combining the KuE.SA functionalized liposomes and the radiolabeling with fluorine-18, a promising system for future targeted drug delivery in the treatment of prostate cancer was introduced. This enables prostate cancer-targeted delivery of liposome-entrapped therapeutics and pre-evaluation of liposome behavior *in vitro* and *in vivo* via positron emission tomography (PET).

Acknowledgment

We thank X.X. for technical assistance, X.X. for SEC measurements, X.X. and X.X. for production and provision of fluorine-18. X.X. and X.X. thank the X.X. for financial support. T.G. thanks the MPGC (Max Planck Graduate Center) for financial support.

References

(1) Torre, L. A.; Bray, F.; Siegel, R. L.; Ferlay, J.; Lortet-Tieulent, J.; Jemal, A. Global Cancer Statistics, 2012. *CA. Cancer J. Clin.* **2015**, *65* (2), 87–108.

(2) Sung, H.; Ferlay, J.; Siegel, R. L.; Laversanne, M.; Soerjomataram, I.; Jemal, A.; Bray, F. Global Cancer Statistics 2020: GLOBOCAN Estimates of Incidence and Mortality Worldwide for 36 Cancers in 185 Countries. *CA. Cancer J. Clin.* **2021**, *71* (3), 209–249.

(3) Rawla, P. Epidemiology of Prostate Cancer. *World J. Oncol.* **2019**, *10* (2), 63–89.

(4) Perner, S.; Hofer, M. D.; Kim, R.; Shah, R. B.; Li, H.; Möller, P.; Hautmann, R. E.; Gschwend, J. E.; Kuefer, R.; Rubin, M. A. Prostate-Specific Membrane Antigen Expression as a Predictor of Prostate Cancer Progression. *Hum. Pathol.* **2007**, *38* (5), 696–701.

(5) Silver, D. A.; Pellicer, I.; Fair, W. R.; Heston, W. D.; Cordon-Cardo, C. Prostate-Specific Membrane Antigen Expression in Normal and Malignant Human Tissues. *Clin. Cancer Res.* **1997**, *3* (1), 81-85.

(6) Okarvi, S. M. Recent Developments of Prostate-Specific Membrane Antigen (PSMA)-Specific Radiopharmaceuticals for Precise Imaging and Therapy of Prostate Cancer: An Overview. *Clin. Transl. Imaging* **2019**, *7* (3), 189–208.

(7) Wester, H. J.; Schottelius, M. PSMA-Targeted Radiopharmaceuticals for Imaging and Therapy. *Semin. Nucl. Med.* **2019**, *49* (4), 302–312.

(8) Pillai, M. R. A.; Nanabala, R.; Joy, A.; Sasikumar, A.; Russ Knapp, F. F. Radiolabeled Enzyme Inhibitors and Binding Agents Targeting PSMA: Effective Theranostic Tools for Imaging and Therapy of Prostate Cancer. *Nucl. Med. Biol.* **2016**, *43* (11), 692–720.

(9) Kopka, K.; Benešová, M.; Bařinka, C.; Haberkorn, U.; Babich, J. Glu-Ureido-Based Inhibitors of

Prostate-Specific Membrane Antigen: Lessons Learned during the Development of a Novel Class of Low-Molecular-Weight Theranostic Radiotracers. *J. Nucl. Med.* **2017**, *58* (Suppl 2), 17S-26S.

(10) Benešová, M.; Schäfer, M.; Bauder-Wüst, U.; Afshar-Oromieh, A.; Kratochwil, C.; Mier, W.; Haberkorn, U.; Kopka, K.; Eder, M. Preclinical Evaluation of a Tailor-Made DOTA-Conjugated PSMA Inhibitor with Optimized Linker Moiety for Imaging and Endoradiotherapy of Prostate Cancer. *J. Nucl. Med.* **2015**, *56* (6), 914–920.

(11) Kozikowski, A. P.; Zhang, J.; Nan, F.; Petukhov, P. A.; Grajkowska, E.; Wroblewski, J. T.; Yamamoto, T.; Bzdega, T.; Wroblewska, B.; Neale, J. H. Synthesis of Urea-Based Inhibitors as Active Site Probes of Glutamate Carboxypeptidase II: Efficacy as Analgesic Agents. *J. Med. Chem.* **2004**, *47* (7), 1729–1738.

(12) Wurm, F. R.; Klok, H. A. Be Squared: Expanding the Horizon of Squaric Acid-Mediated Conjugations. *Chem. Soc. Rev.* **2013**, *42* (21), 8220–8236.

(13) Tietze, L. F.; Arlt, M.; Beller, M.; Glüsenkamp, K.-H.; Jähde, E.; Rajewsky, M. F. Squaric Acid Diethyl Ester: A New Coupling Reagent for the Formation of Drug Biopolymer Conjugates. Synthesis of Squaric Acid Ester Amides and Diamides. *Chem. Ber.* **1991**, *124* (5), 1215–1221.

(14) Dingels, C.; Wurm, F.; Wagner, M.; Klok, H. A.; Frey, H. Squaric Acid Mediated Chemoselective PEGylation of Proteins: Reactivity of Single-Step-Activated α-Amino Poly(Ethylene Glycol)s. *Chem. - A Eur. J.* **2012**, *18* (52), 16828–16835.

(15) Quiñonero, D.; Frontera, A.; Ballester, P.; Deyà, P. M. A Theoretical Study of Aromaticity in Squaramide and Oxocarbons. *Tetrahedron Lett.* **2000**, *41* (12), 2001–2005.

(16) Prohens, R.; Portell, A.; Font-Bardia, M.; Bauzá, A.; Frontera, A. Experimental and Theoretical Study of Aromaticity Effects in the Solid State Architecture on Squaric Acid Derivatives. *Cryst. Growth Des.* **2014**, *14* (5), 2578–2587.

(17) Semmingsen, D. The Structure of Squaric Acid (3,4-Dihydroxy-3-Cyclobutene-1,2-Dione). *Tetrahedron Lett.* **1973**, *11*, 807–808.

(18) West, R.; Powell, D. L. New Aromatic Anions. III. Molecular Orbital Calculations on Oxygenated Anions. *J. Am. Chem. Soc.* **1963**, *85* (17), 2577–2579.

(19) Zhang, A. X.; Murelli, R. P.; Barinka, C.; Michel, J.; Cocleaza, A.; Jorgensen, W. L.; Lubkowski, J.; Spiegel, D. A. A Remote Arene-Binding Site on Prostate Specific Membrane Antigen Revealed by Antibody-Recruiting Small Molecules. *J. Am. Chem. Soc.* **2010**, *132* (36), 12711–12716.

(20) Greifenstein, L.; Engelbogen, N.; Lahnif, H.; Sinnes, J. P. J.-P.; Bergmann, R.; Bachmann, M.; Rösch, F. Synthesis, Labeling and Preclinical Evaluation of a Squaric Acid Containing PSMA Inhibitor Labeled with ^{68}Ga: A Comparison with PSMA-11 and PSMA-617. *ChemMedChem* **2020**, *15* (8), 695–704.

(21) Wicki, A.; Witzigmann, D.; Balasubramanian, V.; Huwyler, J. Nanomedicine in Cancer Therapy: Challenges, Opportunities, and Clinical Applications. *J. Control. Release* **2015**, *200*, 138–157.

(22) Shi, J.; Kantoff, P. W.; Wooster, R.; Farokhzad, O. C. Cancer Nanomedicine: Progress, Challenges and Opportunities. *Nat. Rev. Cancer* **2017**, *17*, 20–37.

(23) Allen, T. M.; Cullis, P. R. Liposomal Drug Delivery Systems: From Concept to Clinical Applications. *Adv. Drug Deliv. Rev.* **2013**, *65* (1), 36–48.

(24) Pattni, B. S.; Chupin, V. V.; Torchilin, V. P. New Developments in Liposomal Drug Delivery. *Chem. Rev.* **2015**, *115* (19), 10938–10966.

(25) Akbarzadeh, A.; Rezaei-sadabady, R.; Davaran, S.; Joo, S. W.; Zarghami, N. Liposome:

Classification, Preparation, and Applications. *Nanoscale Res. Lett.* **2013**, *8* (1), 102.

(26) Ishida, T.; Harashima, H.; Kiwada, H. Liposome Clearance. *Biosci. Rep.* **2002**, *22* (2), 197–224.

(27) Herzberger, J.; Niederer, K.; Pohlit, H.; Seiwert, J.; Worm, M.; Wurm, F. R.; Frey, H. Polymerization of Ethylene Oxide, Propylene Oxide, and Other Alkylene Oxides: Synthesis, Novel Polymer Architectures, and Bioconjugation. *Chem. Rev.* **2016**, 116 (*4*), 2170-2243.

(28) Veronese, F. M.; Pasut, G. PEGylation, Successful Approach to Drug Delivery. *Drug Discov. Today* **2005**, *10* (21), 1451–1458.

(29) Immordino, M. L.; Dosio, F.; Cattel, L. Stealth Liposomes: Review of the Basic Science, Rationale, and Clinical Applications, Existing and Potential. *Int. J. Nanomedicine* **2006**, *1* (3), 297–315.

(30) Huckaby, J. T.; Jacobs, T. M.; Li, Z.; Perna, R. J.; Wang, A.; Nicely, N. I.; Lai, S. K. Structure of an Anti-PEG Antibody Reveals an Open Ring That Captures Highly Flexible PEG Polymers. *Commun. Chem.* **2020**, *3*, 124.

(31) Wilms, D.; Stiriba, S.; Frey, H. Hyperbranched Polyglycerols: From the Controlled Synthesis of Biocompatible Polyether Polyols to Multipurpose Applications. *Acc. Chem. Res.* **2010**, *43* (1), 129–141.

(32) Kasza, G.; Kali, G.; Domján, A.; Petho, L.; Szarka, G.; Iván, B. Synthesis of Well-Defined Phthalimide Monofunctional Hyperbranched Polyglycerols and Its Transformation to Various Conjugation Relevant Functionalities. *Macromolecules* **2017**, *50* (8), 3078–3088.

(33) Wagener, K.; Worm, M.; Pektor, S.; Schinnerer, M.; Thiermann, R.; Miederer, M.; Frey, H.; Rösch, F. Comparison of Linear and Hyperbranched Polyether Lipids for Liposome Shielding by ^{18}F-Radiolabeling and Positron Emission Tomography. *Biomacromolecules* **2018**, *19* (7), 2506–2516.

(34) Wagener, K.; Bros, M.; Krumb, M.; Langhanki, J.; Pektor, S.; Worm, M.; Schinnerer, M.; Montermann, E.; Miederer, M.; Frey, H.; Opatz, T.; Rösch, F. Targeting of Immune Cells with Trimannosylated Liposomes. *Adv. Ther.* **2020**, *3* (6), 1900185.

(35) Hofmann, A. M.; Wurm, F.; Huhn, E.; Nawroth, T.; Langguth, P.; Frey, H. Hyperbranched Polyglycerol-Based Lipids via Oxyanionic Polymerization: Toward Multifunctional Stealth Liposomes. *Biomacromolecules* **2010**, *11* (3), 568–574.

(36) Gleue, L.; Schupp, J.; Zimmer, N.; Becker, E.; Frey, H.; Tuettenberg, A.; Helm, M. Stability of Alkyl Chain-Mediated Lipid Anchoring in Liposomal Membranes. *Cells* **2020**, *9* (10), 2213.

(37) Jacobson, O.; Kiesewetter, D. O.; Chen, X. Fluorine-18 Radiochemistry, Labeling Strategies and Synthetic Routes. *Bioconjug. Chem.* **2015**, *26* (1), 1–18.

(38) Cole, E.; Stewart, M.; Littich, R.; Hoareau, R.; Scott, P. Radiosyntheses Using Fluorine-18: The Art and Science of Late Stage Fluorination. *Curr. Top. Med. Chem.* **2014**, *14* (7), 875–900.

(39) Bé, M.-M.; Chisté, V.; Dulieu, C.; Chechev, V.; Kuzmenko, N.; Helmer, R.; Nichols, A.; Schönfeld, E.; Dersch, R. *Table of Radionuclides*; 2004; Vol. 1.

(40) Reibel, A. T.; Müller, S. S.; Pektor, S.; Bausbacher, N.; Miederer, M.; Frey, H.; Rösch, F. Fate of Linear and Branched Polyether-Lipids in Vivo in Comparison to Their Liposomal Formulations by ^{18}F-Radiolabeling and Positron Emission Tomography. *Biomacromolecules* **2015**, *16* (3), 842–851.

(41) Kettenbach, K.; Schieferstein, H.; Ross, T. L. ^{18}F-Labeling Using Click Cycloadditions. *Biomed Res. Int.* **2014**, *2014*, 361329.

(42) Fitton, A. O.; Hill, J.; Jane, D. E.; Millar, R. Synthesis of Simple Oxetanes Carrying Reactive 2-Substituents. *Synthesis (Stuttg).* **1987**, *1987* (12), 1140–1142.

(43) Stauch, O.; Uhlmann, T.; Fröhlich, M.; Thomann, R.; El-Badry, M.; Kim, Y. K.; Schubert, R. Mimicking a Cytoskeleton by Coupling Poly(N-Isopropylacrylamide) to the Inner Leaflet of Liposomal Membranes: Effects of Photopolymerization on Vesicle Shape and Polymer Architecture. *Biomacromolecules* **2002**, *3* (2), 324–332.

(44) Hofmann, A. M.; Wurm, F.; Frey, H. Rapid Access to Polyfunctional Lipids with Complex Architecture via Oxyanionic Ring-Opening Polymerization. *Macromolecules* **2011**, *44* (12), 4648–4657.

(45) Yamamoto, S.; Nakahama, S.; Yamaguchi, K. A Heterobifunctional Linker Bearing Azide-Reactive Alkyne and Thiol-Reactive Maleimide Connected with N-(2-Nitrobenzyl)Imide to Synthesize Photocleavable Diblock Copolymers. *Chem. Lett.* **2013**, *4* (8), 791–793.

(46) Brocas, A. L.; Mantzaridis, C.; Tunc, D.; Carlotti, S. Polyether Synthesis: From Activated or Metal-Free Anionic Ring-Opening Polymerization of Epoxides to Functionalization. *Prog. Polym. Sci.* **2013**, *38* (6), 845–873.

(47) Penczek, S.; Cypryk, M.; Duda, A.; Kubisa, P.; Słomkowski, S. Living Ring-Opening Polymerizations of Heterocyclic Monomers. *Prog. Polym. Sci.* **2007**, *32* (2), 247–282.

(48) Schömer, M.; Frey, H. Water-Soluble "Poly(Propylene Oxide)" by Random Copolymerization of Propylene Oxide with a Protected Glycidol Monomer. *Macromolecules* **2012**, *45* (7), 3039–3046.

(49) Binder, W. H.; Sachsenhofer, R. "Click" Chemistry in Polymer and Materials Science. *Macromol. Rapid Commun.* **2007**, *28* (1), 15–54.

(50) Lu, S.; Lepore, S. D.; Song, Y. L.; Mondal, D.; Cohn, P. C.; Bhunia, A. K.; Pike, V. W. Nucleophile Assisting Leaving Groups: A Strategy for Aliphatic ^{18}F-Fluorination. *J. Org. Chem.* **2009**, *74* (15), 5290–5296.

(51) Stewart, M. N.; Hockley, B. G.; Scott, P. J. H. Green Approaches to Late-Stage Fluorination: Radiosyntheses of ^{18}F-Labelled Radiopharmaceuticals in Ethanol and Water. *Chem. Commun.* **2015**, *51* (79), 14805–14808.

(52) Ladbrooke, B. D.; Chapman, D. Thermal Analysis of Lipids, Proteins and Biological Membranes a Review and Summary of Some Recent Studies. *Chem. Phys. Lipids* **1969**, *3* (4), 304–356.

(53) Siwak, D. R.; Tari, A. M.; Lopez-Berestein, G. Liposomal Antisense Oligonucleotides for Cancer Therapy. *Methods Enzymol.* **2004**, *387*, 241–253.

(54) Corvera, E.; Mouritsen, O. G.; Singer, M. A.; Zuckermann, M. J. The Permeability and the Effect of Acyl-Chain Length for Phospholipid Bilayers Containing Cholesterol: Theory and Experiment. *Biochim. Biophys. Acta - Biomembr.* **1992**, *1107* (2), 261–270.

(55) Needham, D.; Nunn, R. S. Elastic Deformation and Failure of Lipid Bilayer Membranes Containing Cholesterol. *Biophys. J.* **1990**, *58* (4), 997–1009.

(56) Demel, R. A.; De Kruyff, B. The Function of Sterols in Membranes. *Biochim. Biophys. Acta - Rev. Biomembr.* **1976**, *457* (2), 109–132.

(57) Virden, J. W.; Berg, J. C. NaCl-Induced Aggregation of Dipalmitoylphosphatidylglycerol Small Unilamellar Vesicles with Varying Amounts of Incorporated Cholesterol. *Langmuir* **1992**, *8* (6), 1532–1537.

(58) Bhattacharya, S.; Haldar, S. Interactions between Cholesterol and Lipids in Bilayer Membranes.

Role of Lipid Headgroup and Hydrocarbon Chain-Backbone Linkage. *Biochim. Biophys. Acta - Biomembr.* **2000**, *1467* (1), 39–53.

(59) Ernsting, M. J.; Murakami, M.; Roy, A.; Li, S. D. Factors Controlling the Pharmacokinetics, Biodistribution and Intratumoral Penetration of Nanoparticles. *J. Control. Release* **2013**, *172* (3), 782–794.

(60) Moghimi, S. M.; Hunter, A. C.; Murray, J. C. Long-Circulating and Target-Specific Nanoparticles: Theory to Practice. *Pharmacol. Rev.* **2001**, *53* (2), 283–318.

(61) Liu, D.; Mori, A.; Huang, L. Role of Liposome Size and RES Blockade in Controlling Biodistribution and Tumor Uptake of GM1-Containing Liposomes. *BBA - Biomembr.* **1992**, *1104* (1), 95–101.

Supporting Information

^{18}F-labeled, PSMA-specific liposomes: promising and PET-traceable tool for future targeted drug delivery in the treatment of prostate cancer

X.X., Tilmann Grus, X.X., X.X. and X.X.

Synthesis of the hydrophobic anchor structure

Synthesis of BisHD-OH

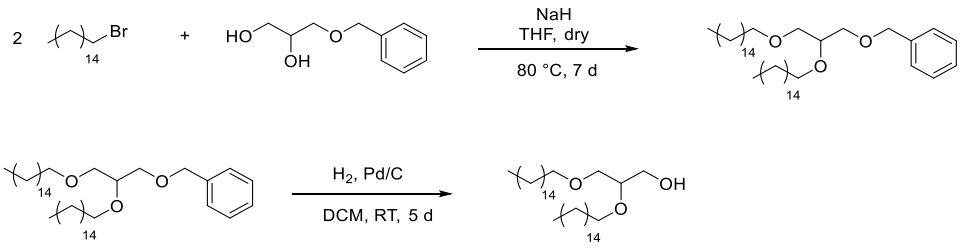

SI-scheme 1: Synthesis route of the hydrophobic anchor structure.

^{1}H NMR (400 MHz, Chloroform-*d*) δ (ppm) = 3.72 – 3.41 (m, 9H, C*H*$_2$-O and CH$_2$-C*H*-O), 1.61 – 1.49 (m, 4H, C*H*$_2$-CH$_2$-O), 1.25 (s, 52H, C*H*$_2$), 0.88 (t, *J* = 6.8 Hz, 6H, C*H*$_3$-CH$_2$).

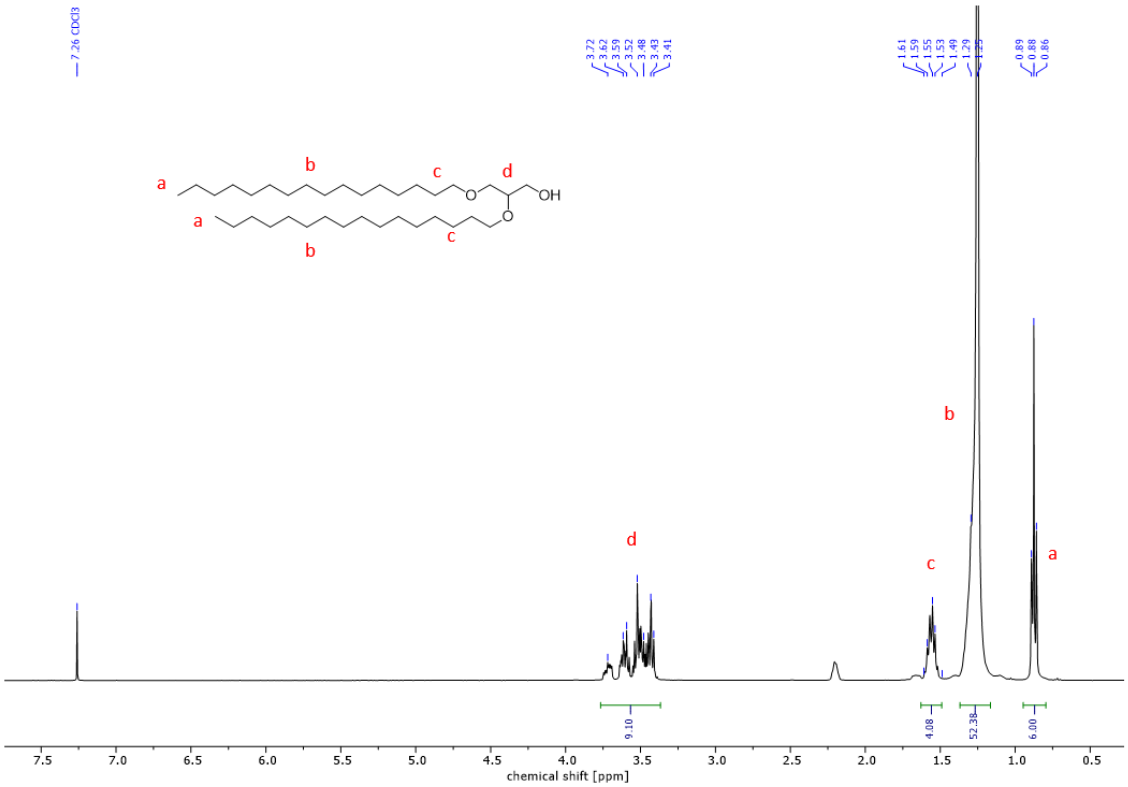

SI-figure 1: ^{1}H NMR spectrum (400 MHz, chloroform-d$_3$) of BisHD-OH.

Polymer synthesis and characterization

Synthesis of BisHD-linPG macroinitiator

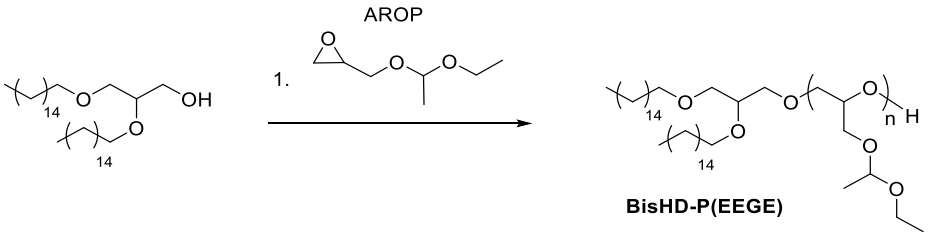

SI-Scheme 2: Synthesis route of BisHD-P(EEGE).

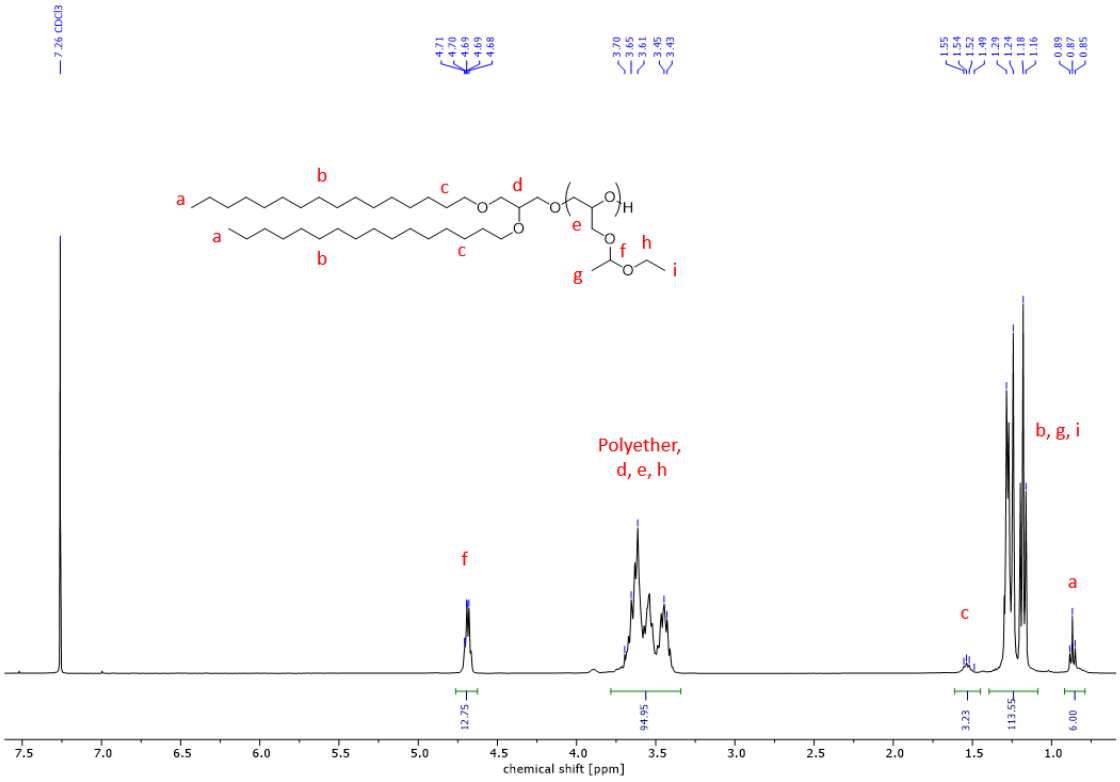

SI-figure 2: ^{1}H NMR spectrum (400 MHz, chloroform-d_3) of BisHD-P(EEGE).

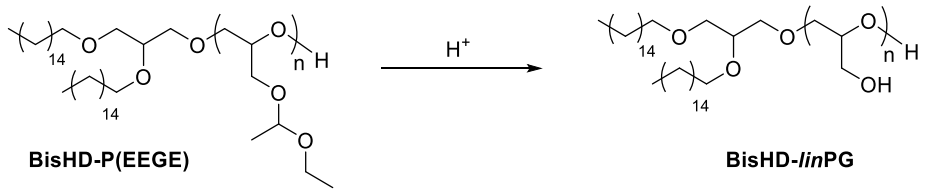

SI-scheme 3: Synthesis route of the macroinitiator BisHD-*lin*PG.

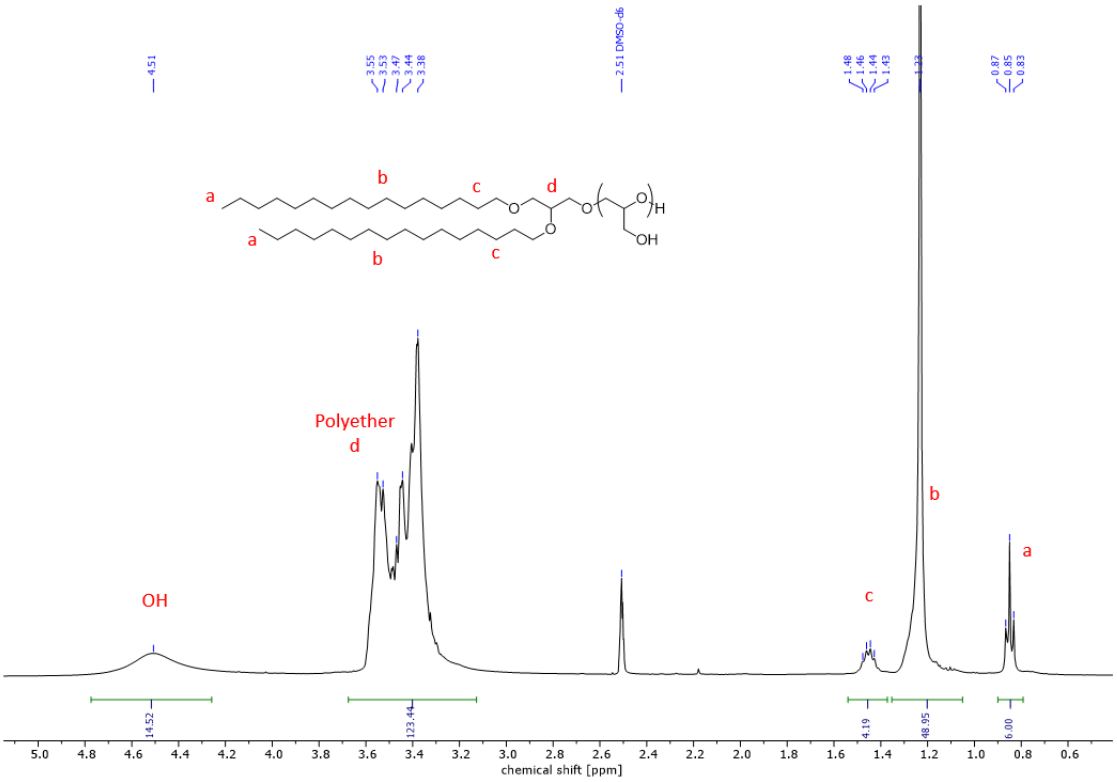

SI-figure 3: ^{1}H NMR spectrum (400 MHz, DMSO-d_6) of BisHD-*lin*PG.

Synthesis of BisHD-hbPG

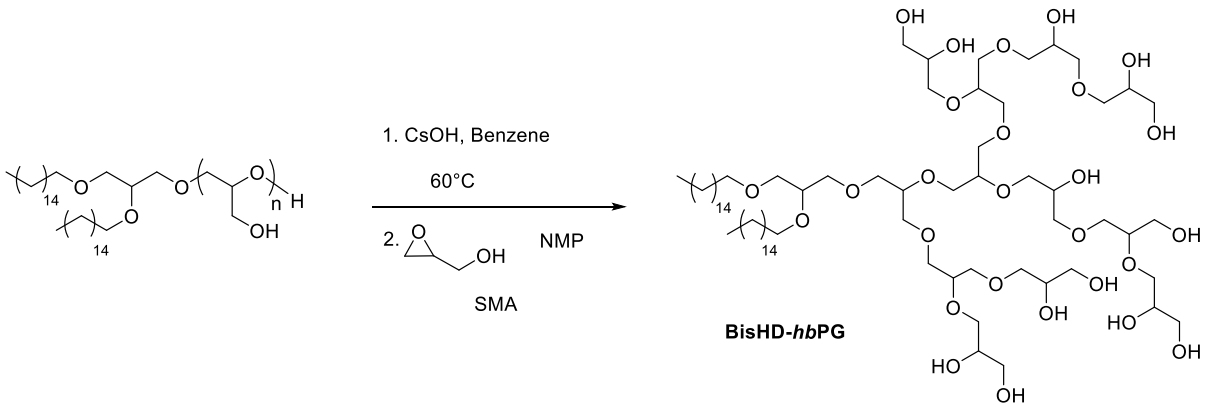

SI-Scheme 4: Synthesis route of BisHD-*hb*PG.

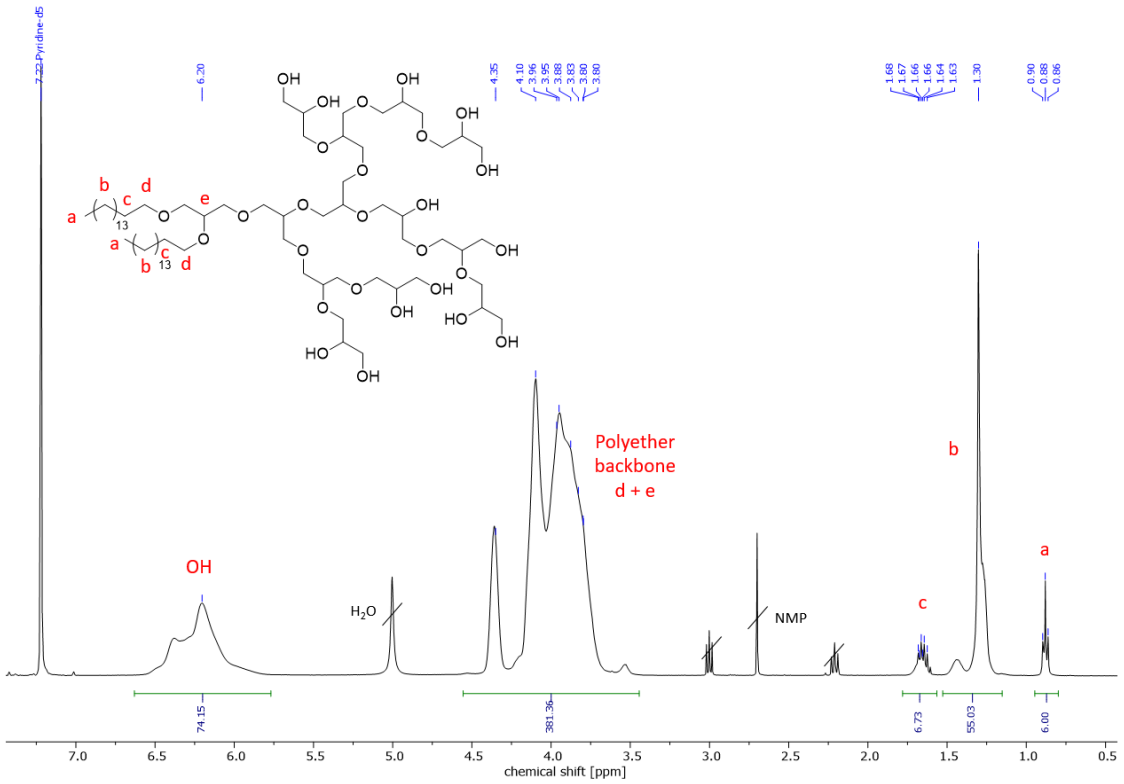

SI-figure 4: ^{1}H NMR spectrum (400 MHz, pyridine-d_5) of BisHD-*hb*PG.

Synthesis of BisHD-hbPG-alkyne

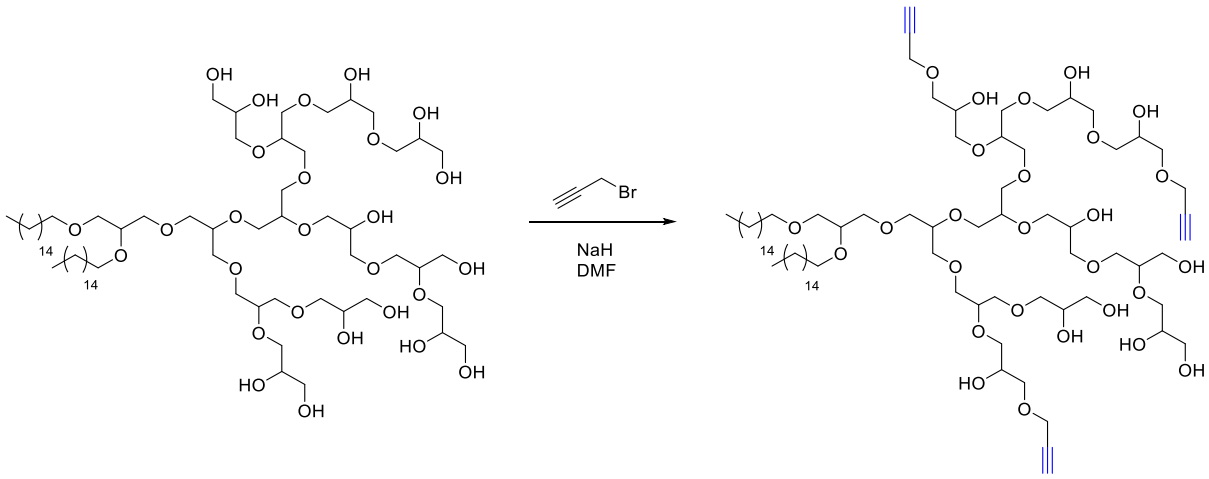

SI-scheme 5: Synthesis route of BisHD-*hb*PG-alkyne.

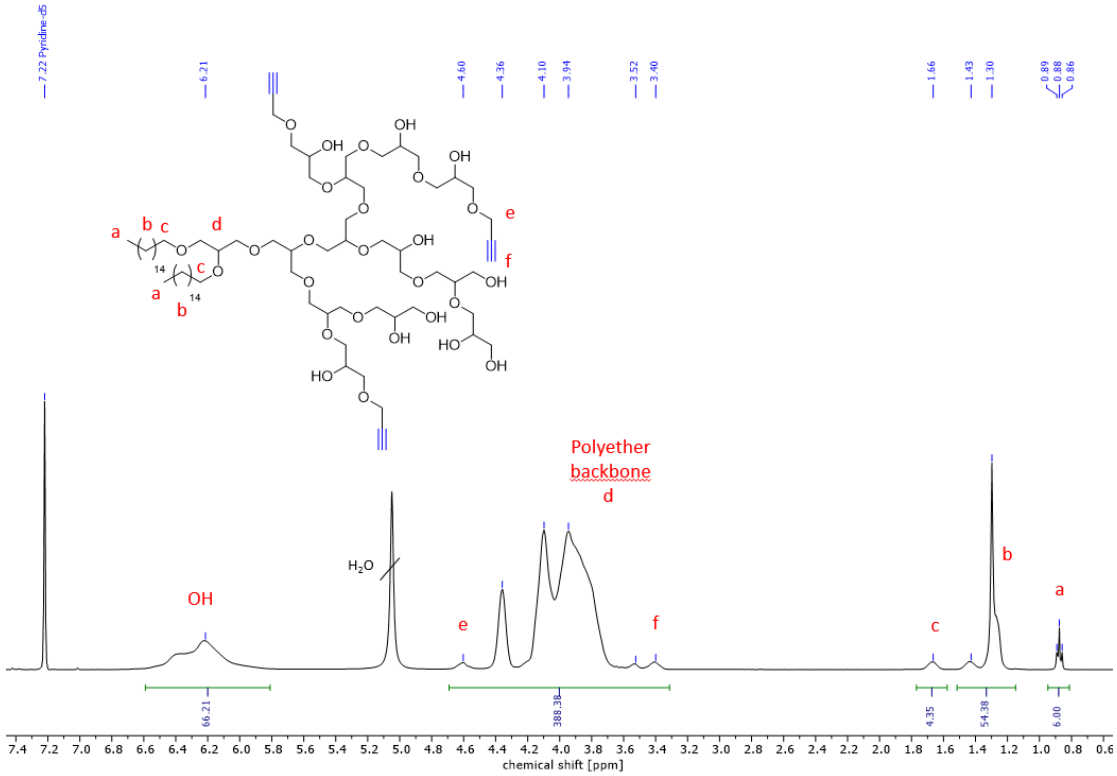

SI-figure 5: ^{1}H NMR spectrum (400 MHz, pyridine-d_5) of BisHD-*hb*PG-alkyne.

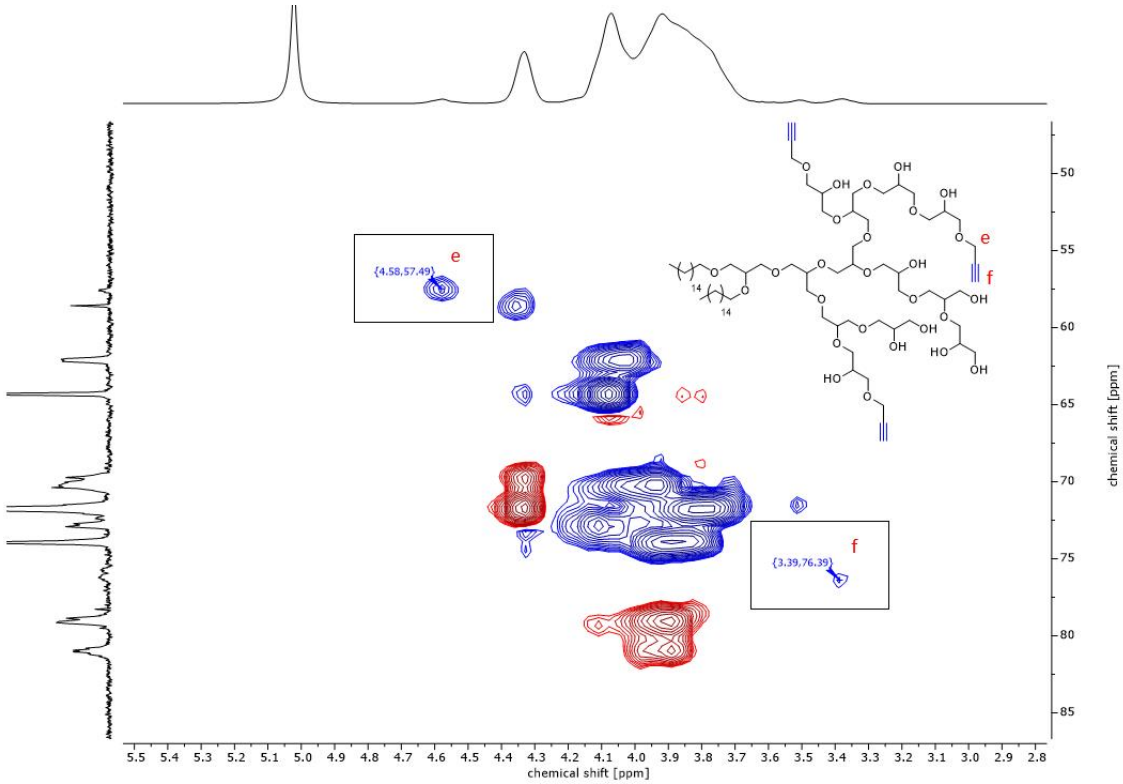

SI-figure 6: ^{1}H, ^{13}C HSQC NMR spectrum (400 MHz, pyridine-d_5) of BisHD-*hb*PG-alkyne.

Synthesis of KuE.SA.N_3

Synthesis of 2-(3-(5-Amino-1-carboxy-pentyl)ureido)pentanedioic acid (L-lysine-urea-L-glutamate (KuE)

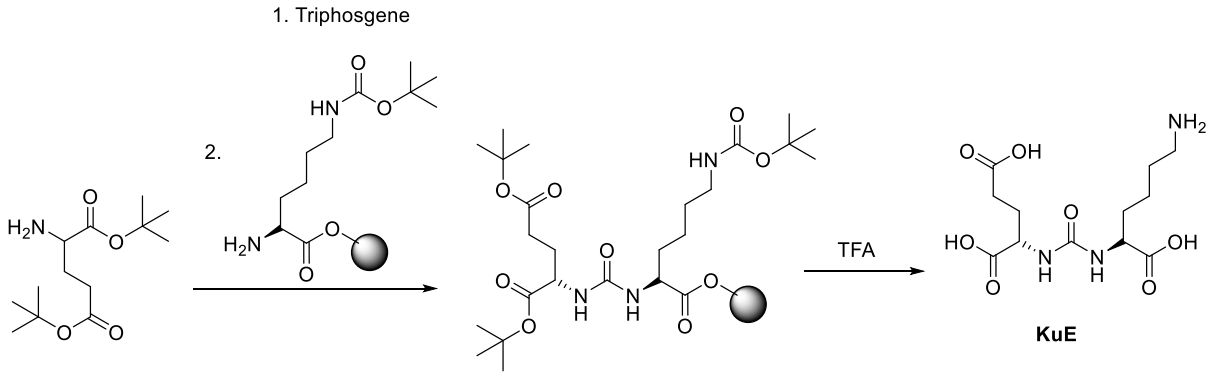

SI-scheme 6: Synthesis route of KuE.

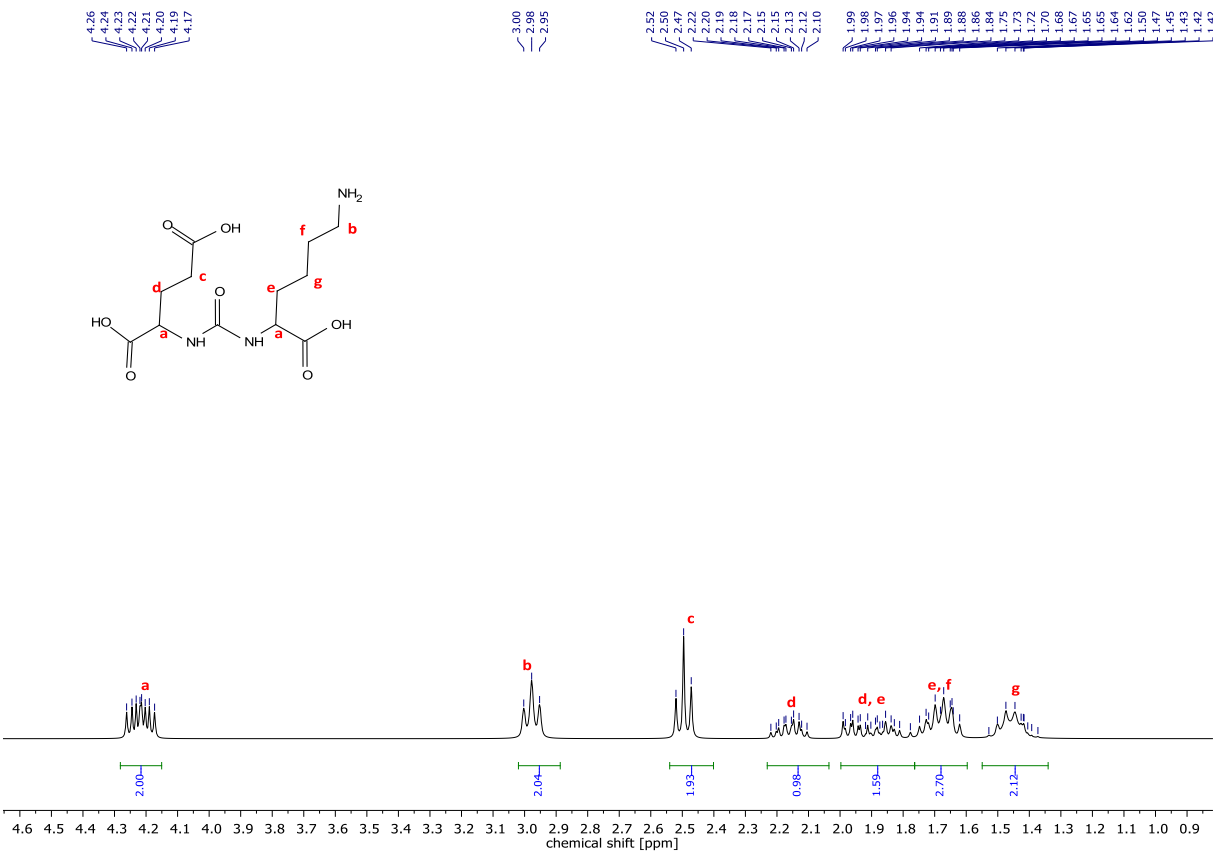

SI-figure 7: ^{1}H NMR spectra (300 MHz, D_2O) of KuE.

Synthesis of 2-(3-(1-Carboxy-5-((2-ethoxy-3,4-dioxocyclobut-1-en-1-yl)amino)pentyl)ureido)-pentanedioic acid (KuE.SA)

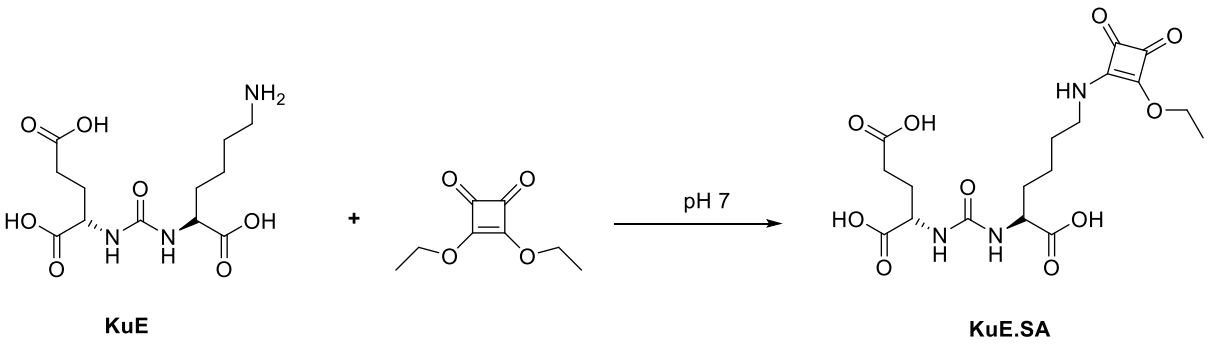

SI-scheme 7: Synthesis route of KuE.SA.

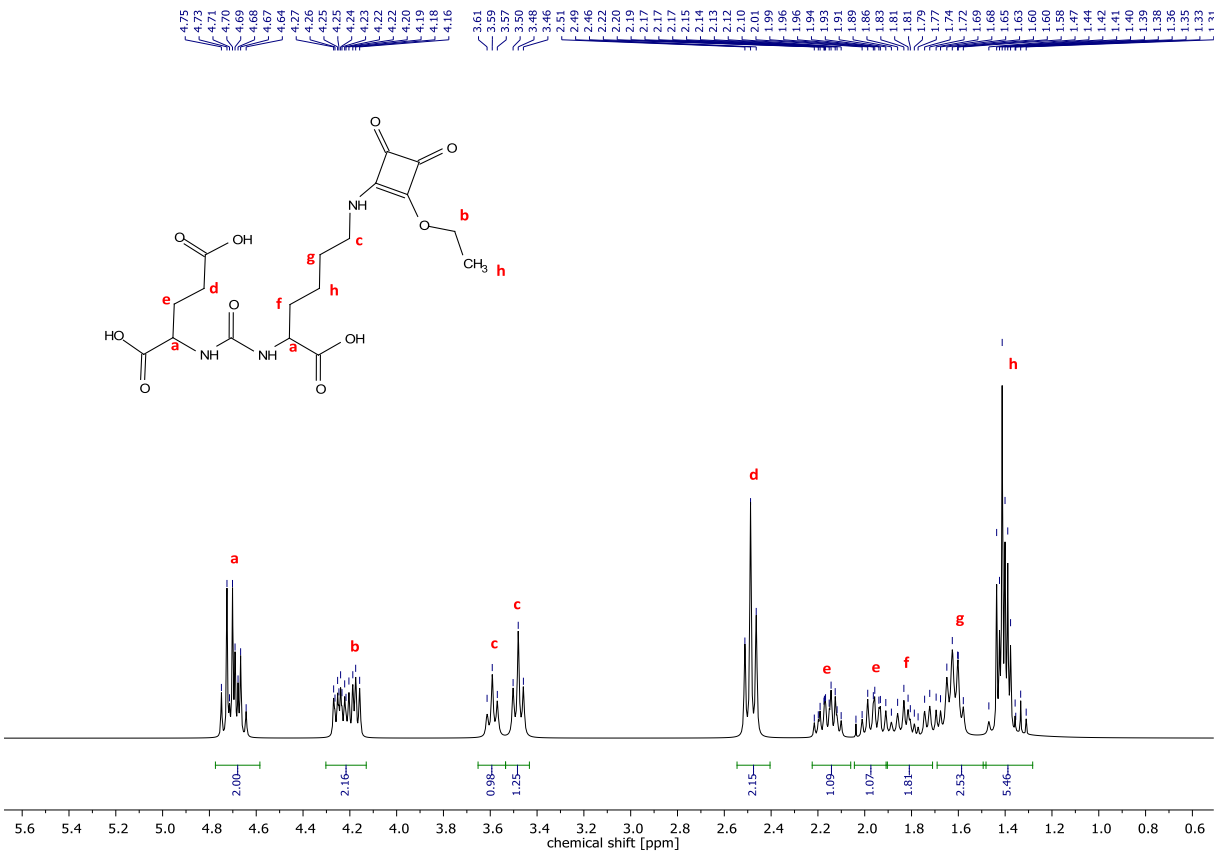

SI-figure 8: ^{1}H NMR spectrum (300 MHz, D_2O) of KuE.SA.

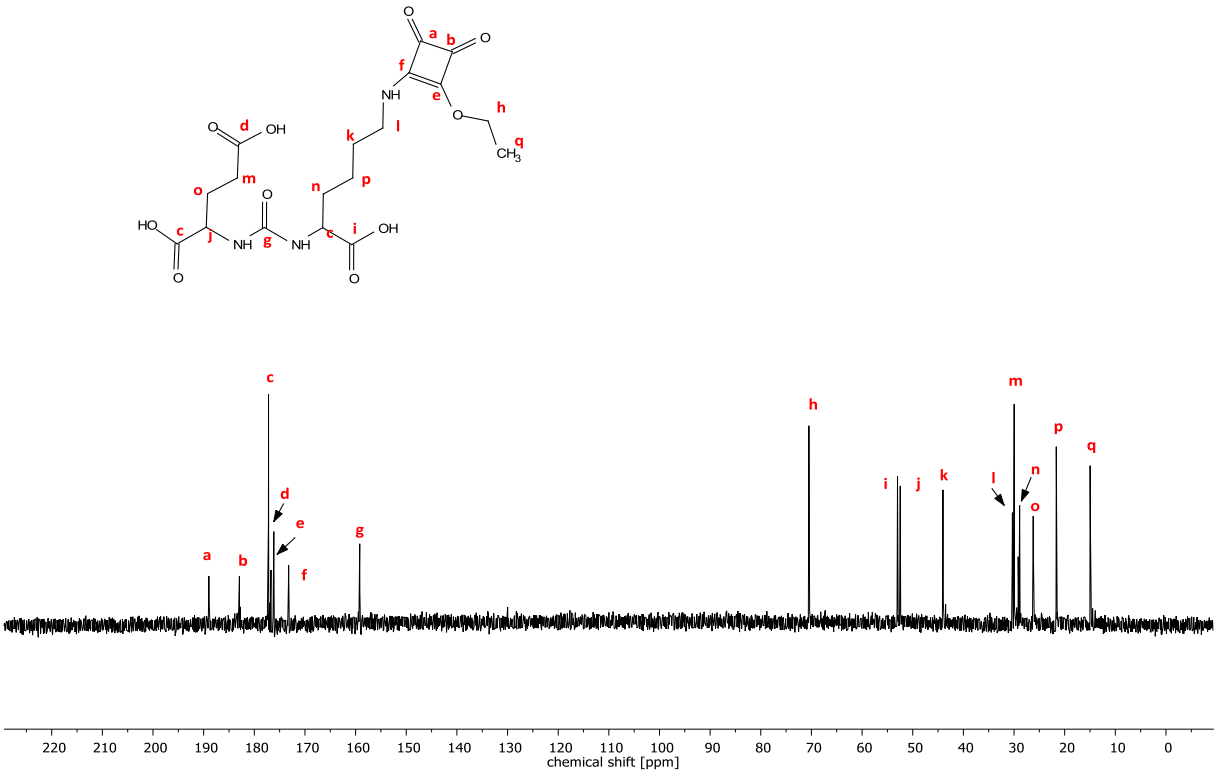

SI-figure 9: ^{13}C NMR spectrum (300 MHz, D_2O) of KuE.SA.

Synthesis of 2-Azidoethylamine

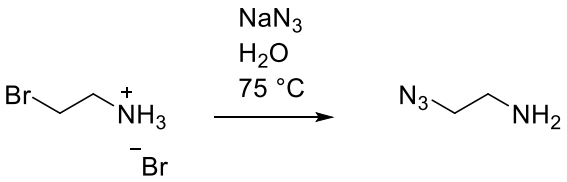

SI-scheme 8: Synthesis route of 2-Azidoethylamine.

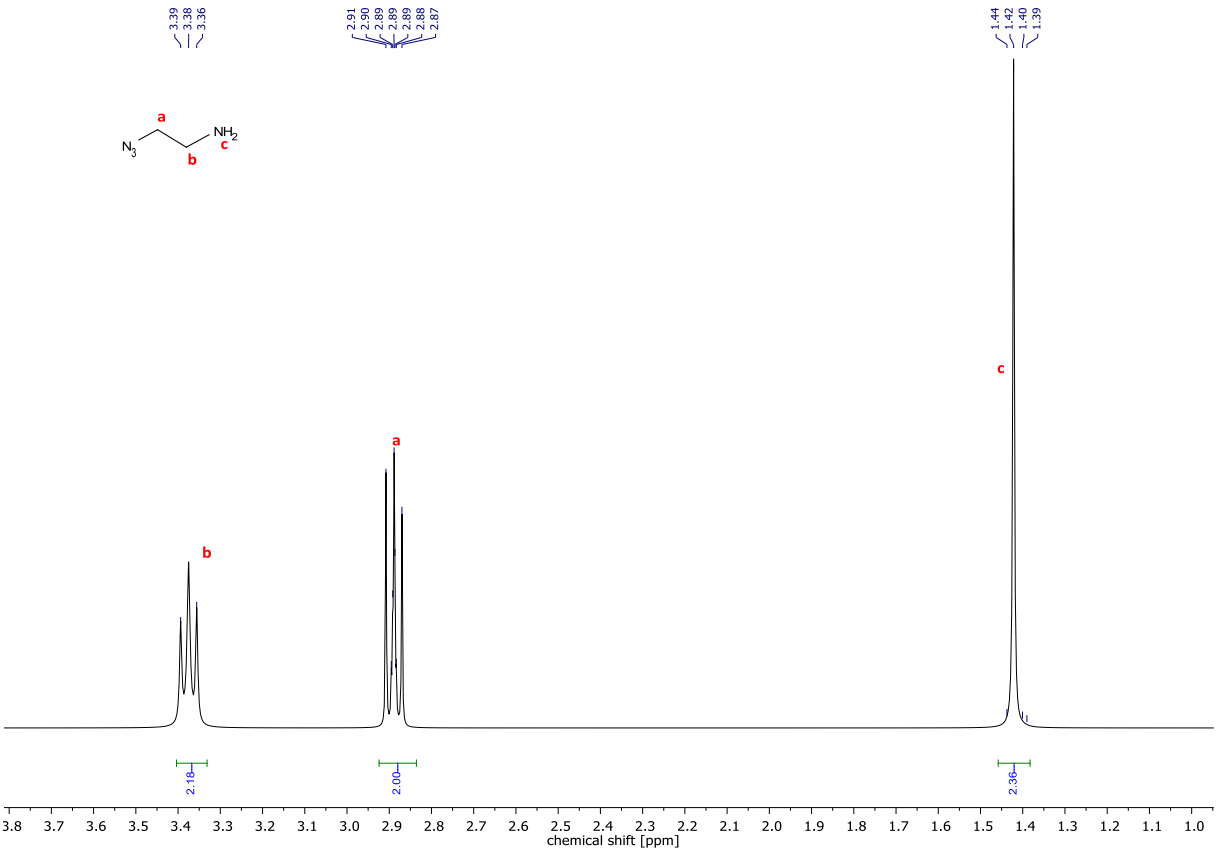

SI-figure 10: ^{1}H NMR spectrum (300 MHz, $CDCl_3$) of 2-Azidoethylamine.

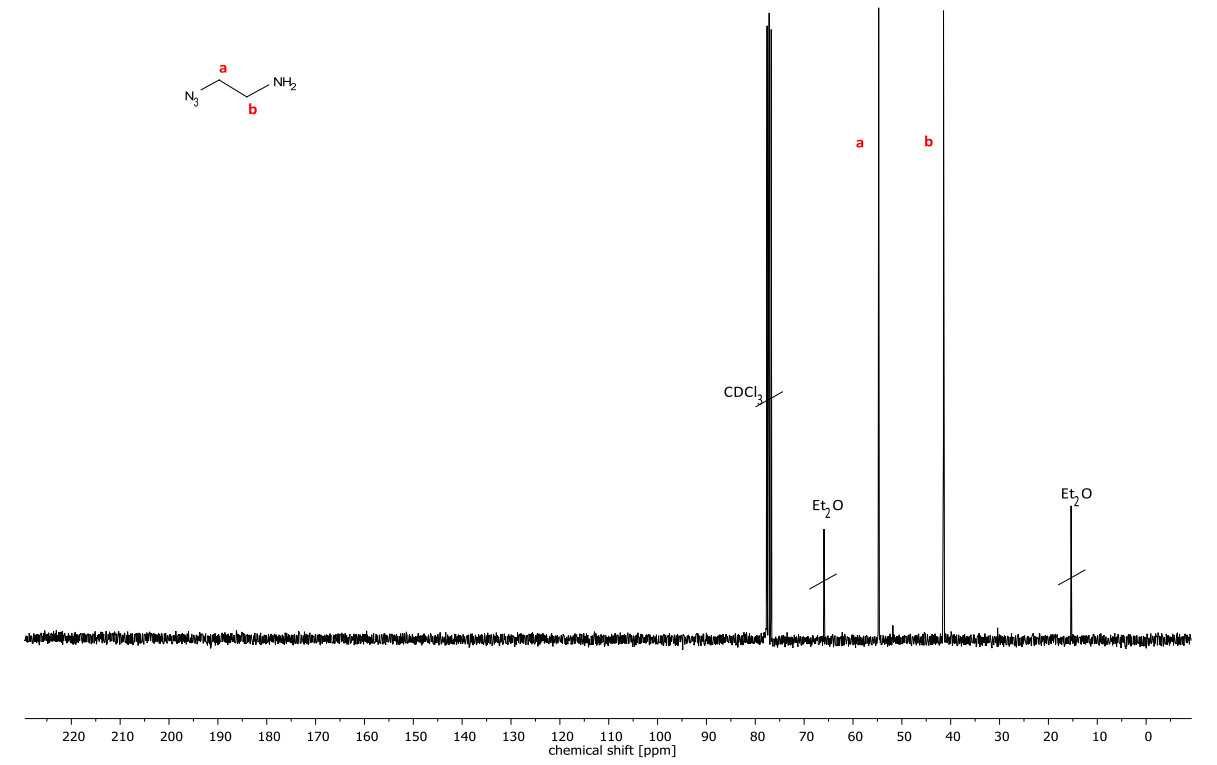

SI-figure 11: ^{13}C NMR spectrum (300 MHz, $CDCl_3$) of 2-Azidoethylamine.

Synthesis of 2-(3-(5-((2-((2-azidoethyl)amino)-3,4-dioxocyclobut-1-en-1-yl)amino)-1-carboxypentyl)ureido)pentanedioic acid (KuE.SA.N_3)

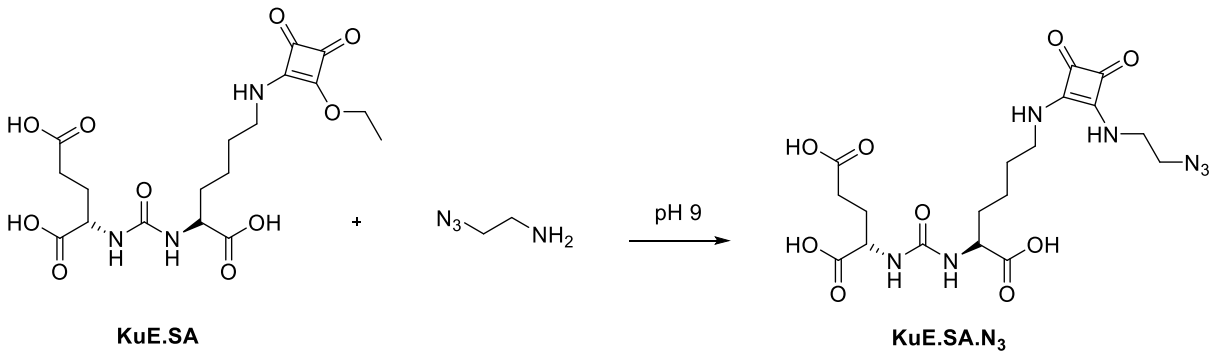

SI-scheme 9: Synthesis route of KuE.SA.N_3.

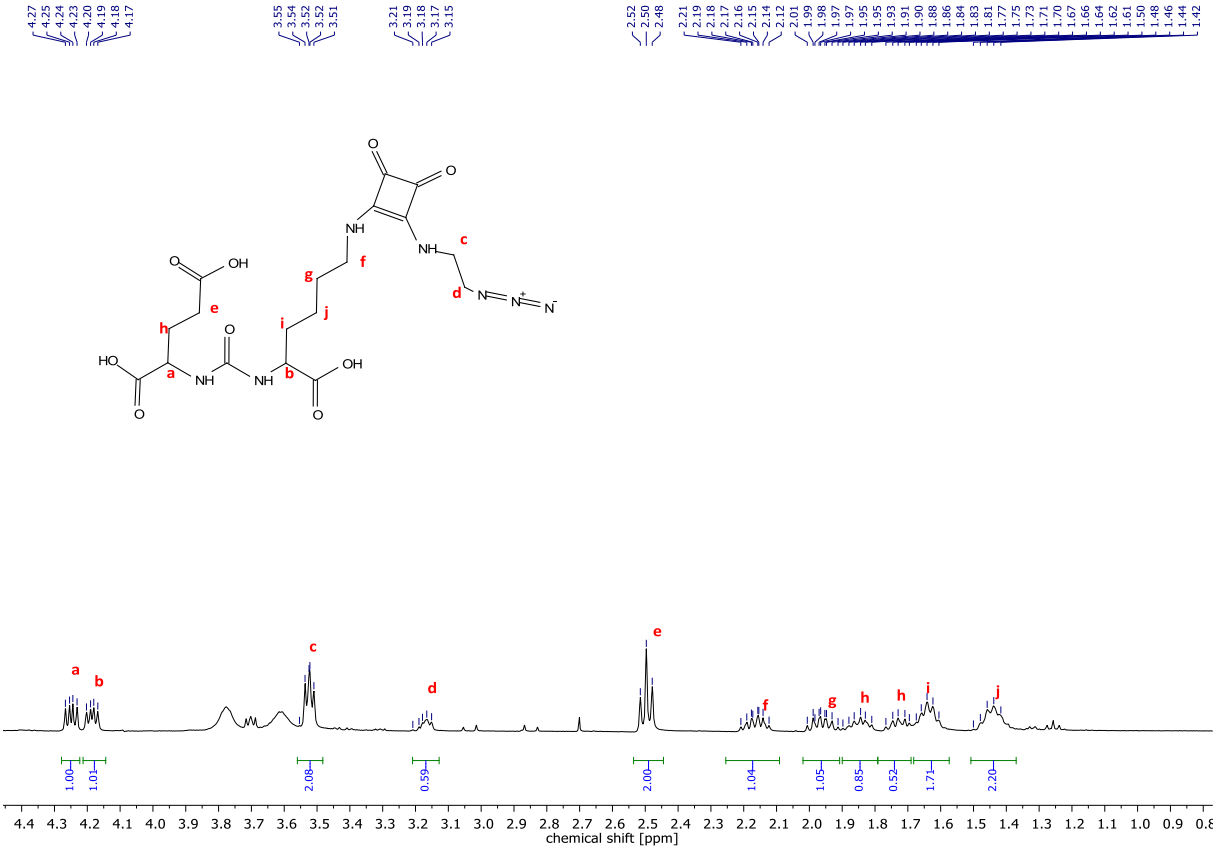

SI-figure 12: ^{1}H NMR spectrum (400 MHz, D_2O) of KuE.SA.N_3.

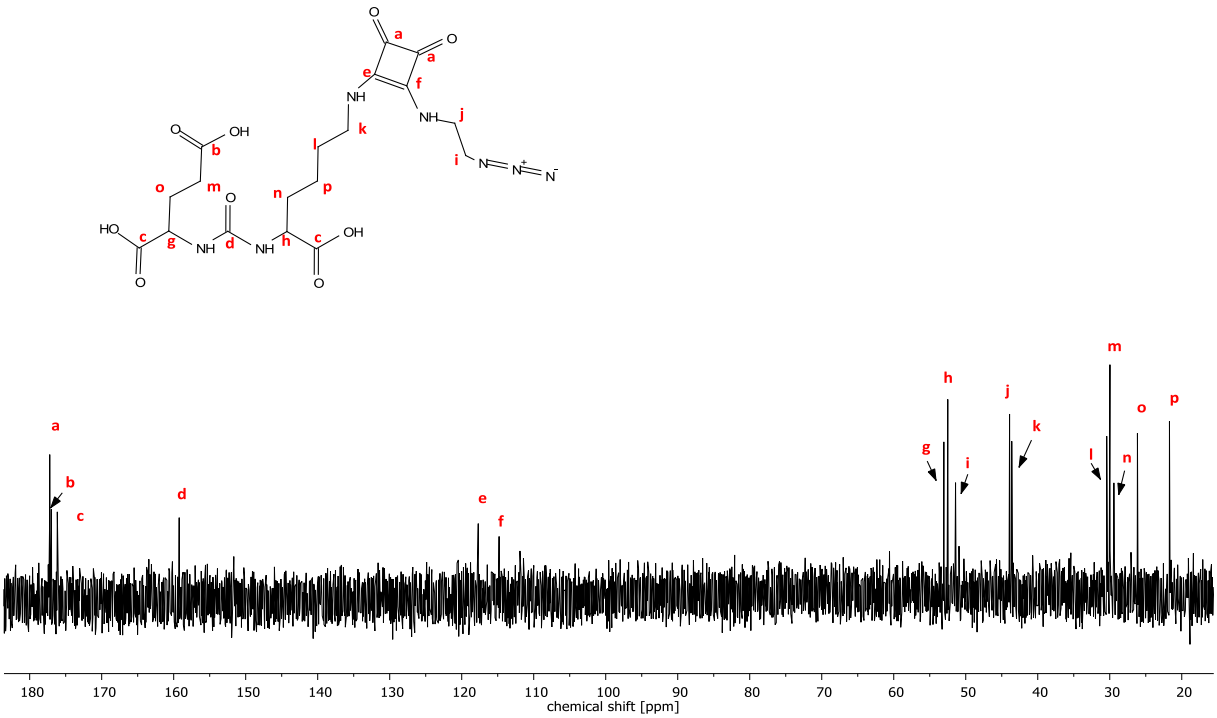

SI-figure 13: ^{13}C NMR spectrum (400 MHz, D_2O) of KuE.SA.N_3.

Synthesis of the KuE.SA.triazolyl-BisHD-hbPG

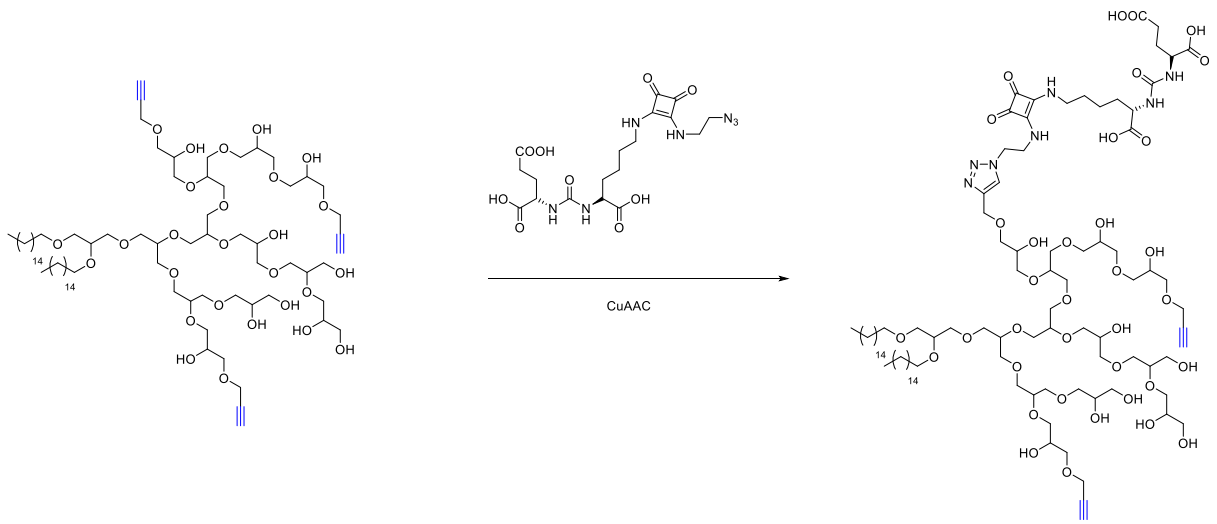

SI-scheme 10: Synthesis of the KuE.SA.triazolyl-BisHD-*hb*PG.

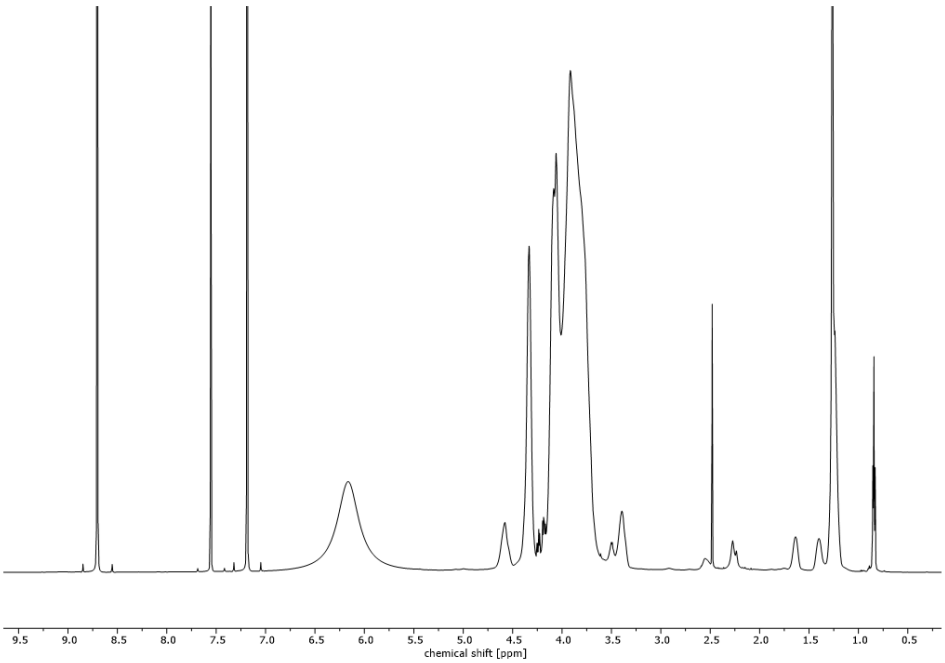

SI-Figure 14: ^{1}H NMR spectrum (600 MHz, pyridine-d_5) of the KuE.SA.triazolyl-BisHD-*hb*PG.

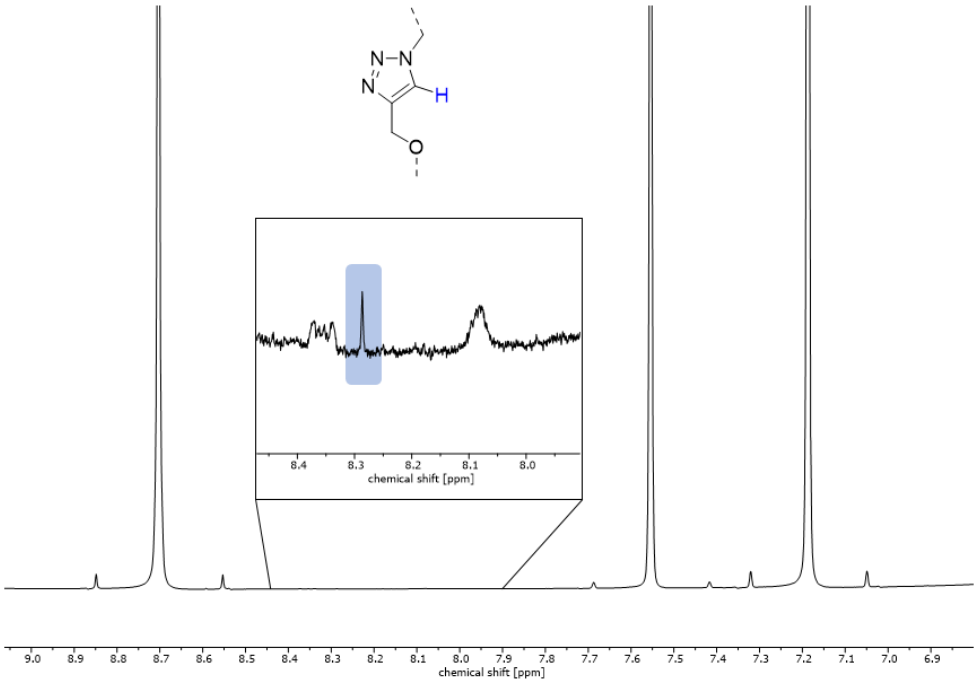

SI-figure 15: Zoom-in ^{1}H NMR spectrum (600 MHz, pyridine-d_5) of the KuE.SA.triazolyl-BisHD-*hb*PG.

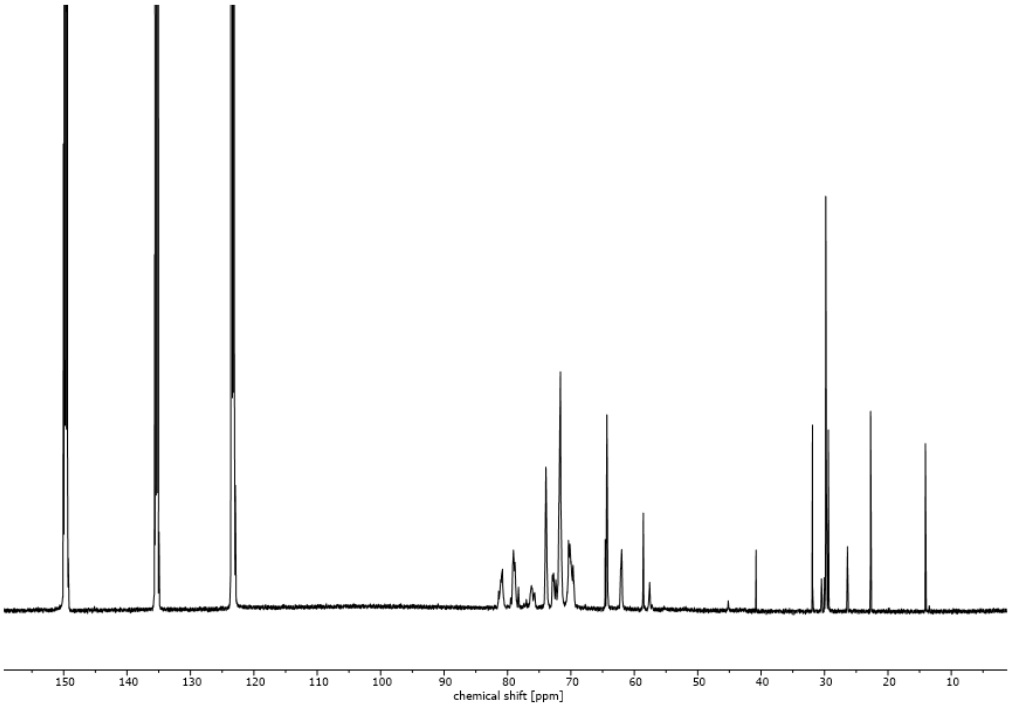

SI-figure 16: ^{13}C NMR spectrum (151 MHz, pyridine-d_5) of the KuE.SA.triazolyl-BisHD-*hb*PG.

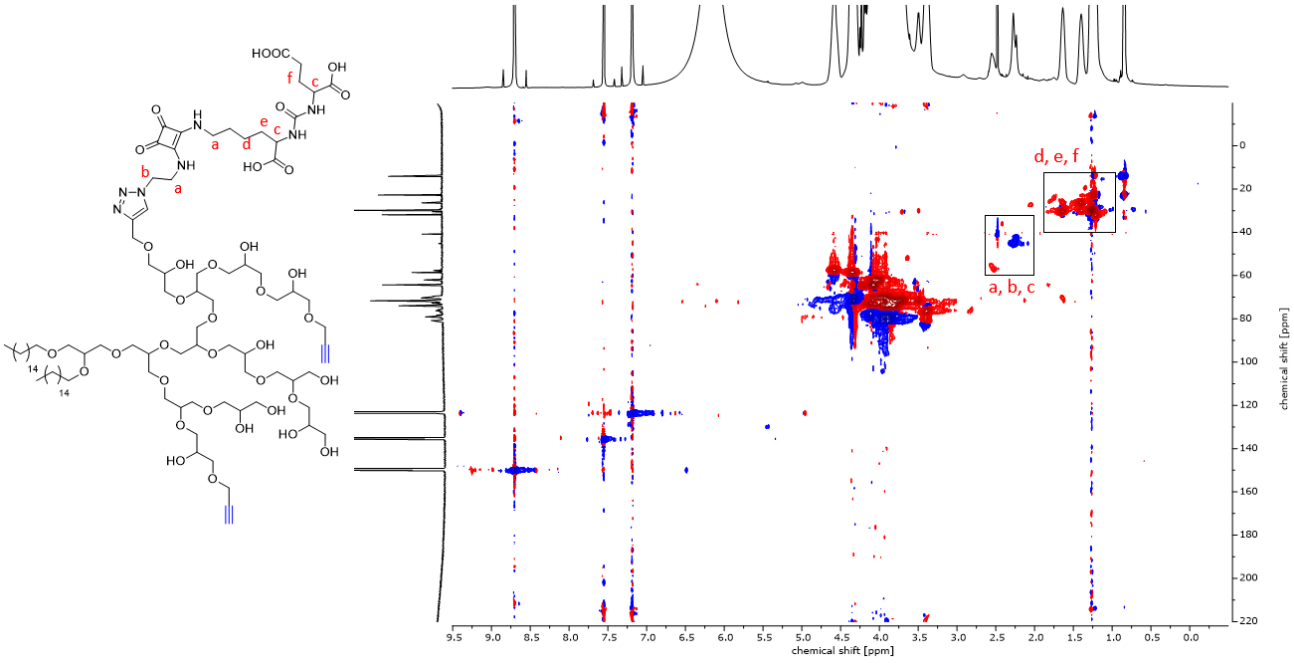

SI-figure 17: ^{1}H, ^{13}C HSQC NMR spectrum (600 MHz, pyridine-d_5) of the KuE.SA.triazolyl-BisHD-*hb*PG.

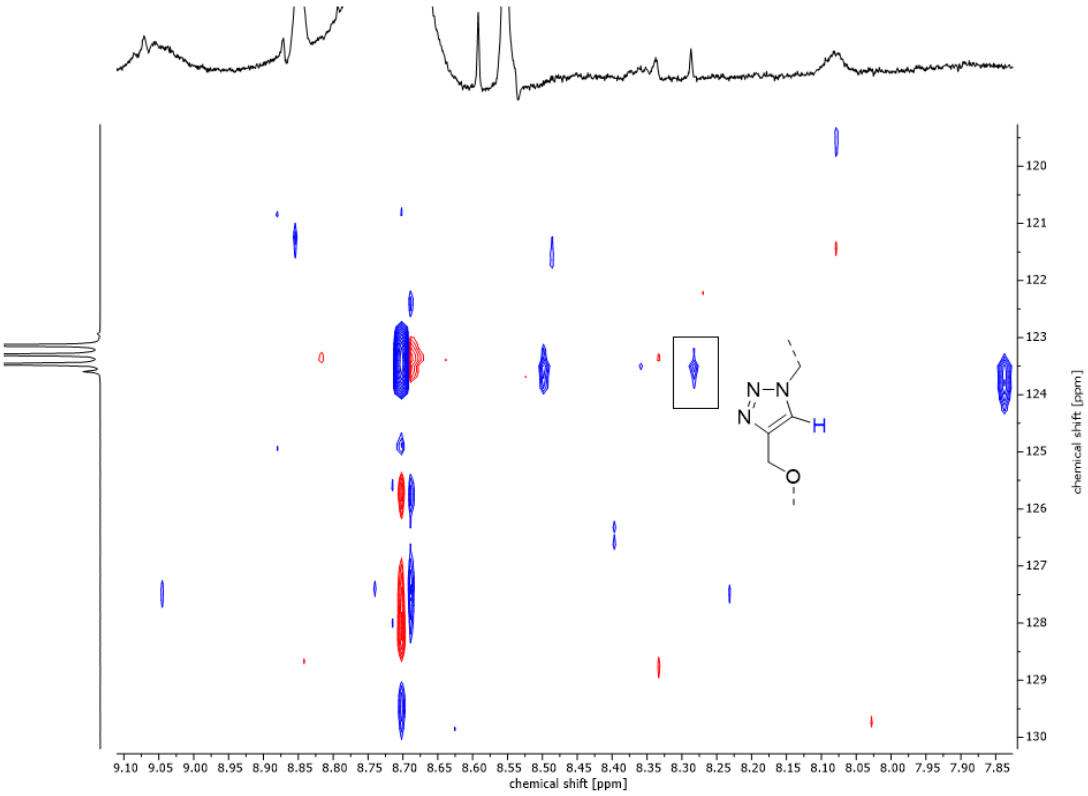

SI-figure 18: Zoom-in ^{1}H, ^{13}C HSQC NMR spectrum (600 MHz, pyridine-d_5) of the KuE.SA.triazolyl-BisHD-*hb*PG.

SEC elugram of the ^{18}F-labeled BisHD-hbPG-KuE.SA liposomes

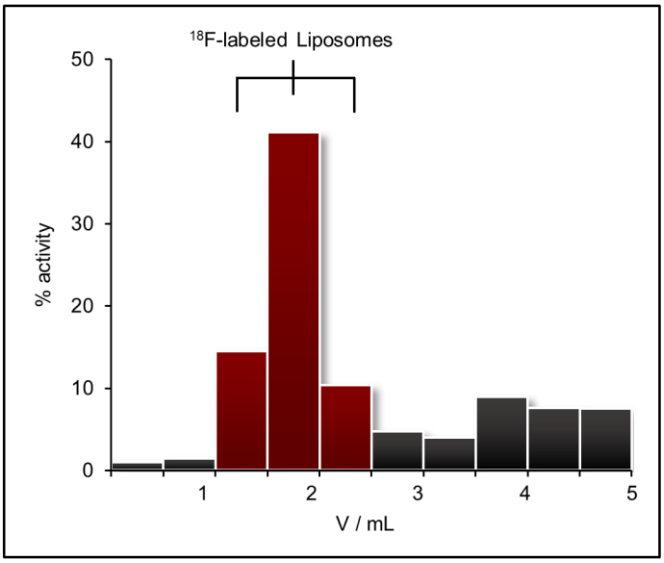

SI-figure 19: SEC elugram displaying the distribution of radioactivity in consecutive fractions of 0.5 mL PBS during purification of ^{18}F-labeled BisHD-*hb*PG-KuE.SA liposomes.

DLS measurement

SI-table 1: DLS measurement data of the liposomes BisHD-*hb*PG-alkyne and BisHD-*hb*PG-KuE.SA.

Sample	Z-Average [a]	Size [a]	Intensity [a]	PDI [a]
	d.nm	d.nm	%	
BisHD-hbPG-alkyne liposomes	144.9	157.5	100	0.071
BisHD-hbPG-KuE.SA liposomes	167.4	199.1	100	0.206

[a] Determined by DLS via Zetasizer.

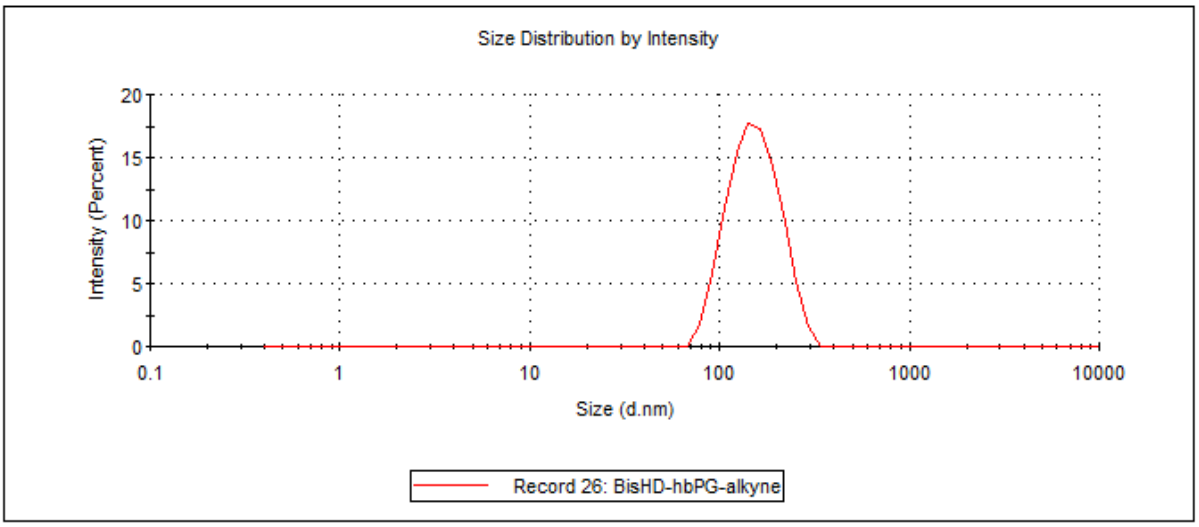

SI-figure 20: DLS measurement of the liposomes BisHD-*hb*PG-alkyne.

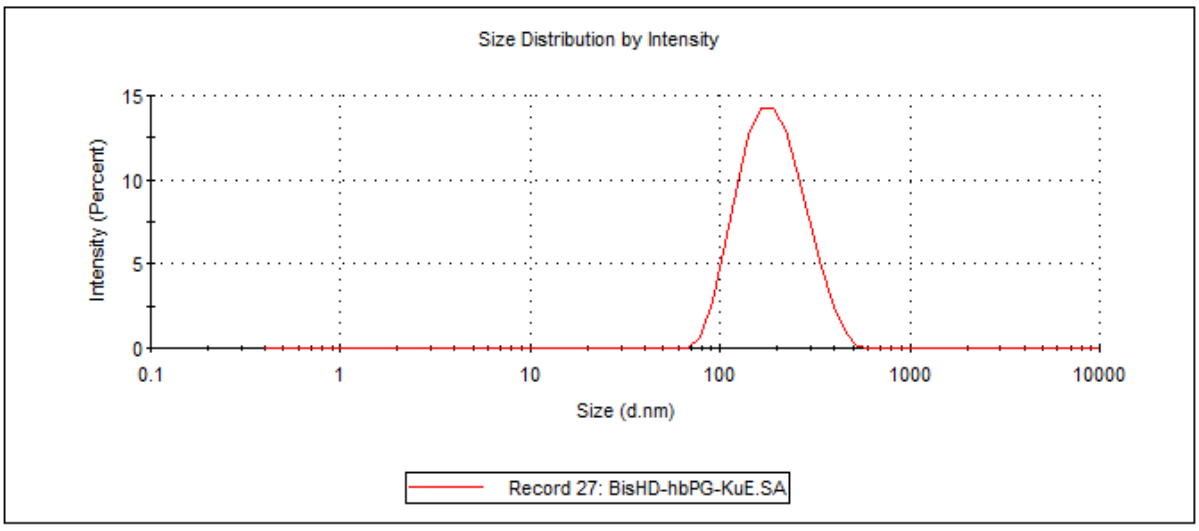

SI-figure 21: DLS measurement of the liposomes BisHD-*hb*PG-KuE.SA.

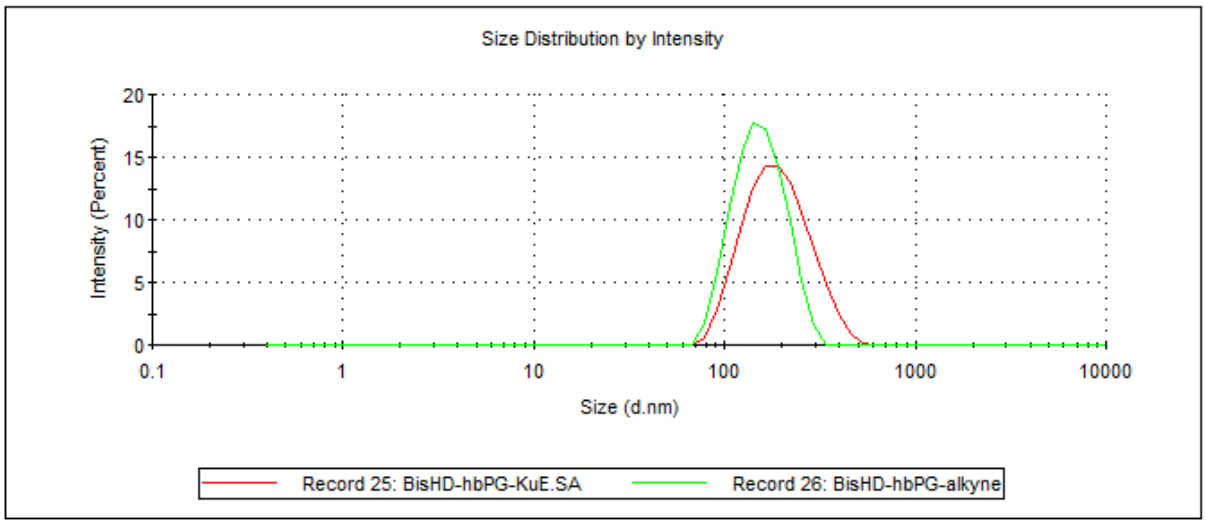

SI-figure 22: Overlay of the DLS measurements of the liposomes BisHD-*hb*PG-alkyne (green) and BisHD-*hb*PG-KuE.SA (red).

Old drug, new delivery strategy: MMAE repacked

X.X., Tilmann Grus, X.X. and X.X.

In preparation for submission

Summary

The targeted transport of a non-selective cytotoxic drug as a prodrug to the desired area of effect has several advantages, such as reduced side effects, in contrast to a systematic application.[1] One method to get such a targeted transport is the use of so-called small-molecule drug delivery conjugate (SMDC). In a SMDC the cytotoxic drug is conjugated to a cleavable linker and a target vector. The target vector is responsible for the targeted transport. After the SMDC reached the place of action, the drug is released through degradation of the cleavable linker under certain conditions.[2]

The aim of this project is the development of a SMDC for the targeted transport of the cytotoxic drug MMAE to prostate cancer cells. The targeting unit of PSMA-617 is conjugated via sqauric acid to the cleavable linker valine-citrulline (VC) and to MMAE. After the conjugate reached the cancer cell and got internalised, MMAE is released by the cleavage of Valine-citrulline by cathepsin B in the lysosomes. Thus, MMAE can affect the cancer cell and can induce apoptosis.

The *in vitro* and *in vivo* behaviour of the novel synthesized compound MMAE.VC.SA.617 was evaluated. Although the novel compound contained the same binding unit as PSMA-617, the binding affinity was lower than the binding affinity of PSMA-617. (21.5 ± 1.9 nM for PSMA-617 and 188.6 ± 24.7 nM for MMAE.VC.SA.617). This could be due to the high structural differences besides the targeting unit and the influence of the rest of the conjugate on the PMSA binding conformation. The *in vitro* cytotoxicity of MMAE.VC.SA.617 was also nearly ten times lower than the cytotoxicity of free MMAE. Nevertheless, PSMA blocking and cathepsin B blocking showed that the designed enrichment and release mechanism of the SMDC is functional. PSMA blocking led to a decreased cytotoxicity since no conjugate reached the cancer cell and blocking of cathepsin B also led to a decreased cytotoxicity because no MMAE was cleaved from the conjugate.

The novel SMDC was evaluated *in vivo* in prostate cancer tumour bearing mice. It was shown that MMAE.VC.SA.617 can inhibit tumour growth, but not tumour regression was observed. In comparison with free MMAE, the SMDC showed a higher drug tolerance.

All in all, MMAE.VC.SA.617 is a promising candidate for further drug delivery of MMAE to PCa cells. Nevertheless, the structure of the novel compound should be optimised to increase binding affinity, which could lead to a better availability and toxicity of MMAE inside the cancer cell.

Author contributions

The project was planned by X.X., **T. Grus**, X.X. and X.X. Organic synthesis was performed by **T. Grus**. Cell cultivation, *in vitro* binding affinity studies, immunofluorescence studies, cytotoxicity studies and the analysis of the obtained data was done by X.X. X.X. and X.X. planned the animal experiments. The animal studies were conducted by X.X. and data analysis of the animal studies was done by X.X. **T. Grus**, X.X. and X.X. wrote the manuscript. All authors reviewed the manuscript. The project was supervised by X.X.

References of the summary

(1) Jahangirian, H.; Kalantari, K.; Izadiyan, Z.; Rafiee-Moghaddam, R.; Shameli, K.; Webster, T. J. A Review of Small Molecules and Drug Delivery Applications Using Gold and Iron Nanoparticles. *Int. J. Nanomedicine* **2019**, *14*, 1633–1657.

(2) Casi, G.; Neri, D. Antibody-Drug Conjugates and Small Molecule-Drug Conjugates: Opportunities and Challenges for the Development of Selective Anticancer Cytotoxic Agents. *J. Med. Chem.* **2015**, *58* (22), 8751–8761.

Abstract

Background: Targeting therapy is a concept that has gained significant importance in the last years, especially in oncology. The severe dose-limiting side effects of chemotherapy necessitate the development of novel, efficient and tolerable therapy approaches. In this regard, PSMA has been well established as a molecular target for diagnosis as well as therapy of prostate cancer. Although most PSMA-targeting ligands are radiopharmaceuticals used in imaging or radioligand therapy, this article describes an evaluation of a PSMA targeting small molecule-drug conjugate, thus addressing a hitherto little-explored field.

Methods: PSMA binding affinity and cytotoxicity were determined *in vitro* using cell-based assays. Enzyme-specific cleavage of the active drug was quantified via an enzyme-based assay. Efficacy and tolerability *in vivo* were assessed using an LNCaP xenograft model.

Results: the binding affinity of the MMAE-conjugate was moderate compared to the drug-free PSMA ligand. Cytotoxicity *in vitro* was in the nanomolar range. Both binding and cytotoxicity were found to be PSMA-specific. Additionally, complete MMAE release could be reached after incubation with cathepsin B. *In vivo*, the MMAE-conjugate displayed good tolerability and dose-dependent inhibition of tumour growth.

Conclusion: the developed MMAE-conjugate showed good properties *in vitro* as well as *in vivo*. Nevertheless, further optimization is required to better exploit the translational potential of this compound.

Keywords: MMAE; PSMA; drug targeting; Small-molecule drug conjugates; prostate cancer

Introduction

Chemotherapy is one of the most important pillars in the treatment of cancer diseases. However, the toxicity of this approach, resulting from the unspecific interaction of cytotoxic drugs with healthy tissue, presents one of the major drawbacks of this cancer treatment.[1,2]

Targeted drug delivery was one of the strategies developed in the last decades to face these challenges. Antibody Drug-Conjugates (ADCs) thereby represented a breakthrough.[3,4] ADCs consist of a cytotoxic drug and an antibody with high affinity to its target. Both components are connected via a linker, mostly a cleavable linker. Since ADCs are supposed to be stable constructs, the cytotoxic payload is only released after binding to the target. Nevertheless, this approach seems to have some limitations and disadvantages such as long circulation time and therefore high exposure of healthy tissues, the reduced EPR effect due to low penetration of the large antibodies into tumour tissue and the expensive and sophisticated synthesis of these drug conjugates.[4–7] Small molecule drug conjugates (SMDCs) have been developed to tackle all these challenges. The low molecular weight of targeting vectors in SMDCs allows a circumventing of practically all the disadvantages mentioned above.

Prostate cancer is the most common cancer in men and the fifth-leading cause of cancer death worldwide.[8,9] In the management of prostate cancer, the prostate-specific membrane antigen (PSMA) has been validated as a reliable tumour-associated biomarker and target for diagnosis as well as for therapy of this disease.[10,11] PSMA is a membrane glycoprotein expressed on prostate tumour cells at significantly higher concentrations than on healthy tissue. Additionally, PSMA-expression correlates with the grade of metastasis and progression of the tumour, allowing a concise staging and therapy.[12–14]

In the last decade, several PSMA-targeting pharmaceuticals have been developed. Radionuclide-based PSMA ligands like [^{68}Ga]Ga-PSMA-11 and [^{177}Lu]Lu-PSMA-617 have played a significant role in the tremendous progress made in the diagnosis and therapy of prostate cancer.[15–18] Beyond the radionuclide therapy approach, PSMA-targeted drug conjugates have been also thoroughly investigated. Two PSMA-targeting ADCs, MLN2704 and PSMA-ADC have even entered clinical studies but failed due to side effects and lack of tolerability. These disappointing outcomes are probably resulting from the instability of the ADCs and the subsequent deconjugation as well as the long circulation time of these immunoconjugates.[19–21] Another promising approach to target PSMA was the use of small-molecule high affinity PSMA inhibitors as homing ligands. Several groups have reported positive results in preclinical studies, thus demonstrating the potential of SMDCs to circumvent the restrictions on tolerability, safety and efficacy of ADCs.[22–25]

Developing a small molecule drug conjugate requires a thorough design and the right choice of building components. The SMDC described in this study consists of three main modules. The targeting unit KuE-617 is a high affine PSMA inhibitor which is part of the clinically used radiopharmaceutical PSMA-617. This moiety is crucial in the design of targeted drug delivery systems, since it is responsible for delivering the cytotoxic payload to the desired "address". Obviously, this cytotoxic payload needs to be a highly potent drug mostly with a narrow therapeutic window and therefore not applicable as single drug. Herein we have chosen the potent antimitotic drug Monomethyl auristatin E (MMAE) which is part of several ADCs, such as the FDA-approved brentuximab vedotin (ADCETRIS™).[26] Besides these essential components, the linker plays a decisive role in the efficacy, stability and resulting tolerability of the whole SMDC. In our developed SMDC, we used a valine-citrulline linker to conjugate MMAE to KuE-617. This dipeptide belongs to the class of enzyme-cleavable linkers. It is cleaved by cathepsin B, which is a lysosomal protease overexpressed in various forms of cancer, including prostate cancer.[27,28]

Results

Organic synthesis

The synthesis of MMAE.VC.SA.617 was carried out in a fast and straightforward two-step synthesis. The commercially available compounds MMAE.VC and NH_2-PSMA-617 were used as starting components and were coupled using squaric acid diester as linking unit. The synthesis route is shown in figure 1.

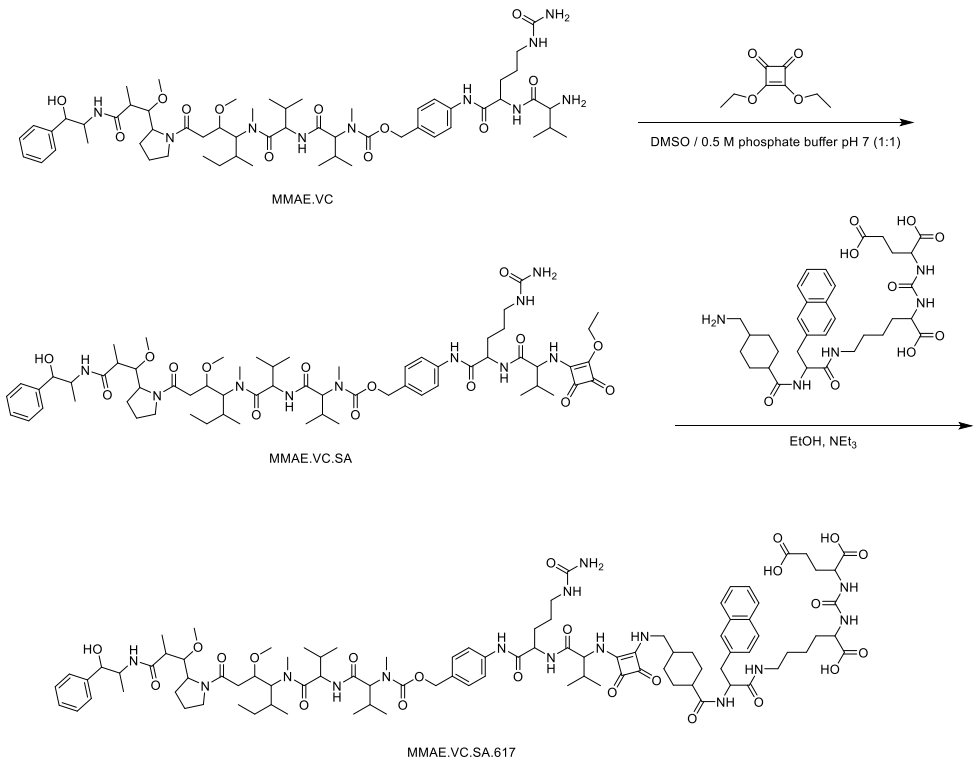

Figure 1: Synthesis of MMAE.VC.SA.617.

The use of the squaric acid diester as a coupling reagent is particularly suitable because of its ability to conjugate two amines quickly, selectively and under mild conditions.[29] This asymmetric amidation can be performed in both aqueous and organic media, which makes it very versatile. It is highly selective towards amines, making the use of protecting groups on other nucleophilic groups unnecessary. This coupling method is receiving more and more attention, ranging from the conjugation of bioconjugates and nanoparticles to use in radiopharmaceuticals[29–31]

In the first step the primary amine of the terminal valine of MMAE.VC was conjugated to squaric acid diethyl ester through an asymmetric amidation in an aqueous phosphate buffer at pH 7. To improve the solubility of MMAE.VC, DMSO was added. The reaction resulted in a quantitative conversion of MMAE.VC to MMAE.VC.SA. monitored by LC-MS. In the second step, MMAC.VC.SA as well as NH_2-PSMA-617 were dissolved in ethanol and in the presence of triethylamine, the second asymmetric amidation took place. MMAC.VC.SA.617 was isolated in a yield of 43% by semi-preparative HPLC purification.

Binding affinity

One of the most important characteristics of drug conjugates is the specific and strong interaction with the addressed target. In order to evaluate the binding potency of the MMAE-conjugate, we performed a competitive radioligand binding assay using PSMA-positive LNCaP cells. Furthermore, we determined the affinity of the drug-free KuE-617 in the same assay to get a better understanding of the effect of conjugation regarding the interaction within the PSMA binding pocket. The binding affinity of KuE-617 expressed as the IC_{50} value was in the same range as the clinically-used PSMA radiopharmaceutical PSMA-11 and PSMA-617. However, the insertion of MMAE resulted in a significant decrease in binding potency (table 1). It should be noted that the binding of MMAE.VC.SA.617 was demonstrated to be PSMA-specific since no binding occurs after co-incubation with the potent PSMA inhibitor PMPA (figure 2).

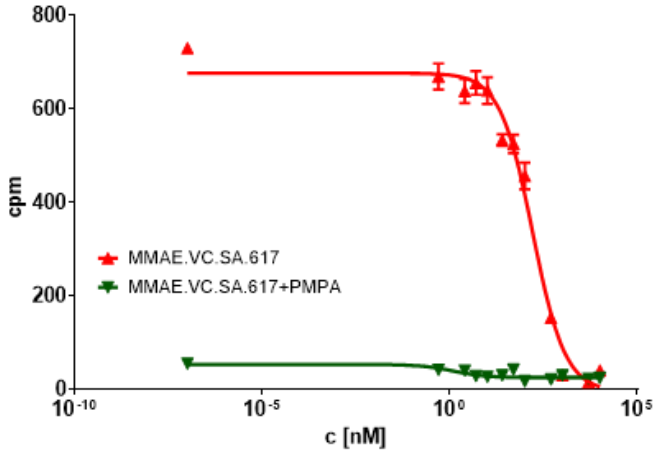

Figure 2: Concentration-inhibition curve of MMAE.VC.SA.617 compared to MMAE.VC.SA.617 + PMPA (n=3). cpm: counts per minute.

Table 1: binding potency of the PSMA-targeted compounds. Values are expressed as Mean ± SD.

compound	**IC_{50} [nM]**
PSMA-11	17.4 ± 1.6
PSMA 617	15.1 ± 3.8
KuE-617-linker	21.5 ± 1.9
MMAE.VC.SA.617	188.6 ± 24.7

In vitro cytotoxicity

CellTiter-Blue® Viability Assay

The cytotoxicity of MMAE.VC.SA.617 was evaluated *in vitro* using Celltiter-Blue®. The conjugation of MMAE to the KuE-617 linker resulting in the dimeric compound seems to affect *in vitro* cytotoxicity, since the IC_{50} value of the MMAE conjugate is approx. 10-times higher than the non-conjugated MMAE. Nevertheless, following the blockade of PSMA receptors by excess addition of PMPA, the cytotoxic effect of MMAE.VC.SA.617 decreased. Furthermore, co-incubation of the LNCaP cells with the cathepsin inhibitor E-64 led to a similar decrease in cytotoxicity. This is probably due to the inhibition of cathepsin B, which is responsible for cleavage of the valine-citrulline linker and thus the subsequent release of MMAE. Table 2 shows the results of the Celltiter-Blue® cytotoxic assay.

Table 2: IC_{50} values of the compounds tested in the Celltiter-Blue® cytotoxic assay. Values are mean ± SD.

compound	**IC_{50} [nM]**
MMAE	0.23 ± 0.06
MMAE.VC.SA.617	33.0 ± 4.9
MMAE.VC.SA.617 + PMPA	92.8 ± 8.3
MMAE:VC.SA.617 + E-64	84.4 ± 0.1

Immunofluorescence studies

To further evaluate the cytotoxic effect of MMAE compared to MMAE.VC.SA.617 we treated LNCaP cells for 24 h with either MMAE (figure 3b), MMAE.VC.SA.617 (figure 3c) and MMAE.VC.SA.617 plus PMPA (figure 3d) prior to co-staining with DAPI and α-tubulin antibody. Cells incubated with both MMAE and MMAE.VC.SA.617 showed a distinctive tubulin disruption resulting in a significant damage of the microtubule cytoskeleton. However, co-incubation with PMPA reduced the cytotoxic effect of MMAE.VC.SA.617 and therefore demonstrated the PSMA-selectivity of this SMDC.

a) Control

b) LNCaP + MMAE

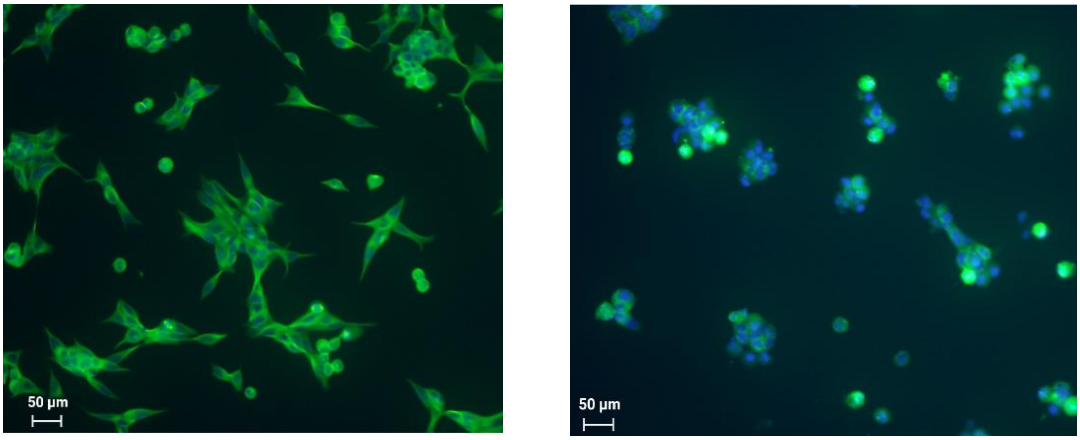

c) LNCaP + MMAE.VC.SA.617

d) LNCaP + MMAE.VC.SA.617 + PMPA

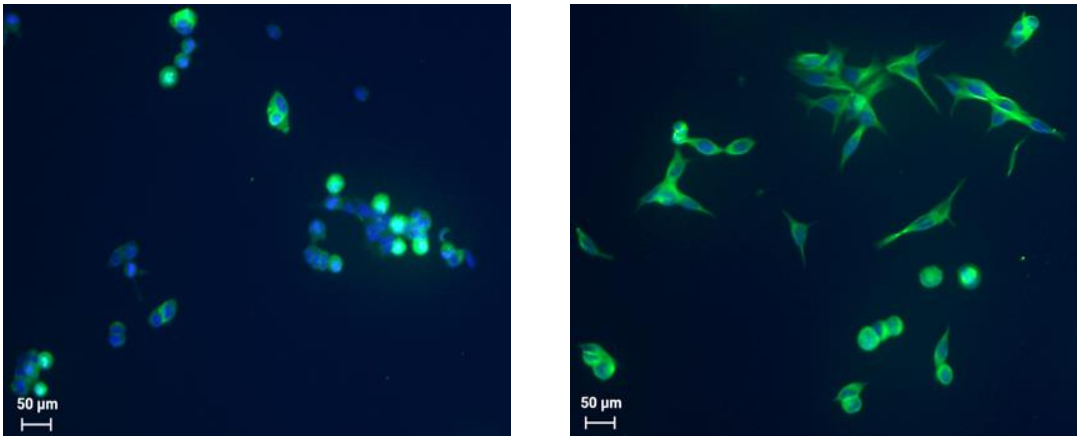

Figure 3: Immunofluorescent staining of α-tubulin (green) with Alexa fluor 488 α-tubulin antibody. Cell nuclei are counterstained with DAPI (blue). Images were taken at 20X magnification. LNCaP cells were used as control (a), incubated with either 1 nM MMAE (b), or 100 nM MMAE.VC.SA.617 (c). PSMA-specific effect was determined by co-incubation of 100 µM PMPA (d).

Cathepsin B cleavage assay

The cathepsin-specific cleavage of MMAE.VC.SA.617 was evaluated by incubating LNCaP cells at 37 °C with cathepsin B (figure 4a). A control experiment was conducted by determining the stability of MMA.VC.SA.617 in PBS (in the absence of cathepsin) (figure 4b). Aliquots were taken at different time points and analysed via liquid chromatography mass spectrometry LC/MS. The concentration of MMAE increased continuously after incubation with cathepsin B. Complete release from the drug conjugate was reached after approx. 20 min. In contrast, in the absence of cathepsin B, MMAE.VC.SA.617 remained almost stable.

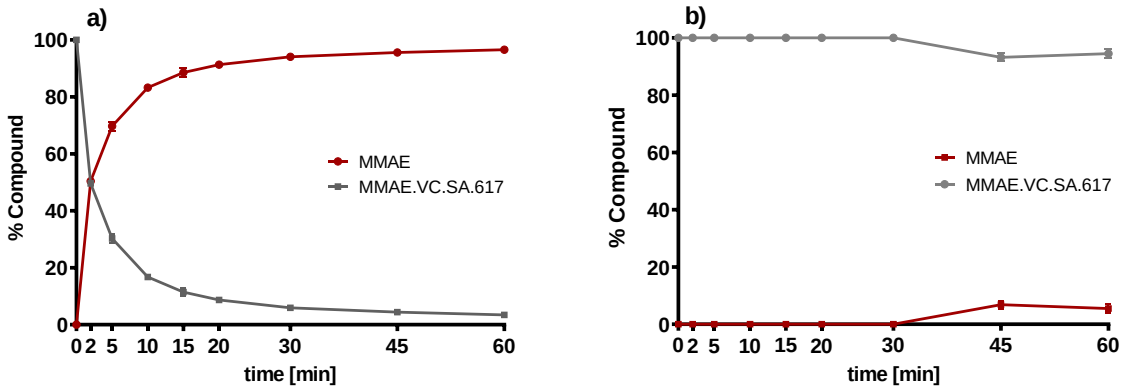

Figure 4: a) quantification of MMAE release after incubation with cathepsin B; b) control experiment: stability of MMAE.VC.SA.617 in PBS without incubation with cathepsin B.

Animal studies

In order to determine the pharmacological properties of MMAE.VC.SA.617 we inoculated LNCaP cells into NOD-SCID mice to generate a xenograft model. Prior to *in vivo* studies in tumour-bearing mice, we conducted a toxicological study in healthy NOD-SCID mice to determine the maximal tolerable dose of MMAE. Mice injected with 1 mg/Kg MMAE had to be euthanized 5 days post-injection due to massive body-weight loss (figure 5).

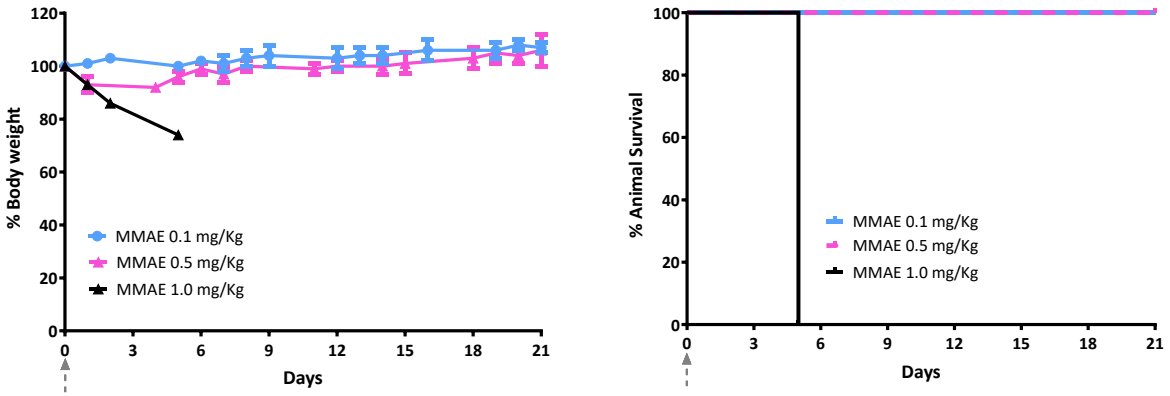

Figure 5: Body-weight change (left) and survival curve (right) of NOD-SCID mice after one i.v. injection of MMAE (n=3 mice per group).

Based on these findings, *in vivo* therapeutic efficacy studies were conducted with 3 different active drug concentrations of MMAE.VC.SA.617, namely 0.1 mg/kg, 0.5 mg/kg and 1.0 mg/kg. In the reference group, mice were injected with either 0.1 mg/kg or 0.5 mg/kg MMAE.

In the MMAE.VC.SA.617 group, mice injected with either 0.5 mg/kg or 1.0 mg/kg seemed to well tolerate the treatment since body weight remained almost constant and all mice survived until the end of the experiment. Surprisingly, in the 0.1 mg/kg MMAE.VC.SA.617 group only one mouse survived the treatment. In this group tumour volume increased continuously over time while in the group with the higher concentrations, treatment seemed to inhibit tumour growth resulting in a constant tumour volume. On the other hand, 4 mice injected with 0.5 mg/kg MMAE were sacrificed after the 5^{th} injection due to massive weight loss. Although one mouse survived and was cured after the 4^{th} injection, the treatment led to a weight loss of about 40% indicating the toxicity of therapy with this MMAE concentration. In contrast, all animals survived in the 0.1 mg/kg MMAE group. However, tumour volume remained constant so that tumour regression could not be observed. Figure 6 shows the results.

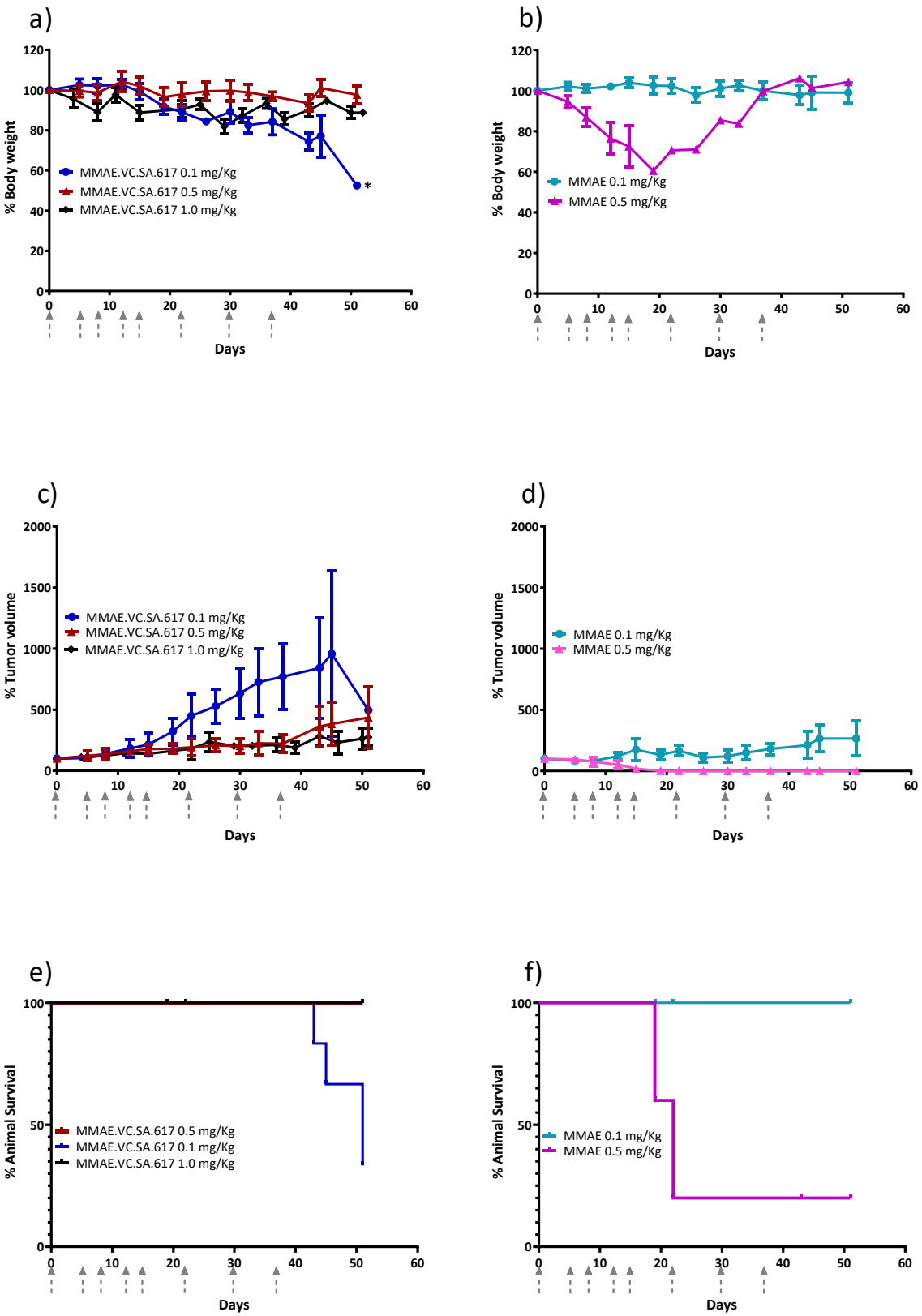

Figure 6: Antitumour effect and tolerability of MMAE and MMAE.VC.SA.617. a) body weight change of animals injected vial tail vain with different doses of MMAE.SA.617 and b) MMAE. Grey arrows indicate time of injection. b) + c) monitoring of tumour volume development of mice during and post treatment. Values are mean ± SD (n=5). e) + f) Kaplan-Meier survival curves.

Discussion

The development of strategies for selective drug delivery is one of the most important research fields in the fight against cancer. Herein we described a small-molecule drug conjugate consisting of the potent antimitotic drug MMAE and the high affinity PSMA inhibitor KuE-617. Both entities are linked via a valine-citrulline-PABC linker. The design, synthesis and subsequent *in vitro* and *in vivo* evaluation were performed in several steps.

The compound MMAE.VC.SA.617 was synthesized in a fast and straightforward 2-step synthesis. The two units of the compound, the drug-linker conjugate MMAE.VC and the PSMA-binding unit KuE-617, were conjugated via asymmetric amidation using a squaric acid linking unit. In the first step, squaric acid had to be added every second day, as it was observed via LC-MS to be consumed during the reaction. After 8 days, MMAE had been quantitatively converted. In this case, the amidation was carried out in an aqueous buffer solution, as the progress of the reaction is controlled by the pH value. However, since the MMAE conjugate did not dissolve completely in water, DMSO was added.

The second stage of the reaction was carried out in ethanol. In the organic medium, triethylamine was added as a base to enable the second asymmetric amidation of the squaric acid linker unit. The final compound MMAE.VC.SA.617 was obtained after semi-preparative HPLC purification.

The PSMA-binding affinities of MMAE.VC.SA.617 as well as of the drug-free conjugate KuE-617 were determined in a cell-based radioligand competitive assay. The IC_{50} value of KuE-617 was in the low nanomolar range, similar to the chelator-based PSMA radioligands PSMA-617 and PSMA-11 (21.5 ± 1.9 nM, 15.1 ± 3.8 nM and 17.4 ± 1.6 nM respectively). However, the insertion of MMAE led to a significant decrease in PSMA-binding affinity resulting in nearly 10-fold higher IC_{50} value than KuE-617 (188.6 ± 24.7 nM vs. 21.5 ± 1.9 nM) indicating that the conjugation of KuE-617 to MMAE had a negative impact on binding affinity of the PSMA inhibitor, probably due to changes in the conformation of the drug conjugate and its orientation within the PSMA binding pocket.

In the field of drug targeting, selecting a potent drug is as important as designing a high affinity targeting unit. The cytotoxic drug used herein is the tubulin inhibitor MMAE, which is already used in several ADCs.[26,32,33] To characterize the pharmacological properties of the MMAE-conjugate we determined its cytotoxicity using CellTiter-Blue®. This assay is based on the ability of viable cells to transform resazurin into the fluorescence-emitter resorufin. Thus, the fluorescence signal correlates with cell viability. The IC_{50} value of the single drug MMAE was as expected in the picomolar range whereas the cytotoxicity of MMAE.VC.SA.617 was about 100-fold lower (0.23 ± 0.06 nM vs. 33.0 ± 4.9 nM). This could be explained with the decreased lipophilicity of MMAE.VC.SA.617 and the associated reduction in its passive diffusion through the cell membrane. Another possible reason could

be an incomplete release of MMAE within tumour cells. Nevertheless, the PSMA-specific uptake of MMAE.VC.SA.617 could be demonstrated by blocking PSMA receptors using PMPA which leads to a 3-times lower cytotoxicity (92.8 ± 8.3 nM). Additionally, the inhibition of cathepsin B via co-incubation with E-64 and the resulting decrease in cytotoxicity proved the essential role that this enzyme plays in the cleavage of the valine-citrulline linker and the subsequent release of MMAE. This enzyme-dependent cleavage of the dipeptide linker is a crucial feature in targeted therapeutics, since the active drug should be released only after uptake in tumour cells.

In a further step, we tried to better characterize the cytotoxicity of MMAE.VC.SA.617 using immunofluorescence imaging. It is known that the antimitotic drug MMAE acts by inhibiting the α-tubulin polymerization. This could be proved with the conducted Immunofluorescence studies which showed a distinctive disturbance in tubulin formation of LNCaP cells incubated with either MMAE or MMAE.VC.SA.617 (figure 3b-c). The cytotoxic effect of MMAE.VC.SA.617 could be reduced by co-incubation with PMPA and thus blocking of PSMA receptors (figure 3d). These results were in accordance with the findings described above.

The targeted delivery of cytotoxic drugs to tumour cells requires not only binding to tumour-associated structures but also a specific release of the conjugated drug in tumour tissue. The SMDC described herein includes a valine-citrulline linker, which is one of the commonly used linkers in ADCs.[34–36] Valine-citrulline is cleaved by enzymes of the cathepsin-family, especially cathepsin B, which is highly expressed in tumour cells.[27,37] In order to verify the cathepsin-specific cleavage of MMAE.VC.SA.617, we quantified the ratio of MMAE over time in the presence or absence of cathepsin B (figure 4a-b). As expected, MMAE could be released completely after about 20 min of incubation with cathepsin B whereas MMAE.VC.SA.617 remained almost stable in PBS.

Based on the positive results obtained from the *in vitro* assays, we performed animal studies in order to characterize the *in vivo* profile of MMAE.VC.SA.617 in terms of antitumour effect and tolerability. Thereby, we used the single drug MMAE as our reference. According to the results from the toxicity study, we chose two different concentrations of MMAE.VC.SA.617: 0.65 mg/kg and 3.35 mg/kg which were equivalent to 0.1 mg/kg and 0.5 mg/kg MMAE respectively. Additionally, we decided to treat one group with 6.7 mg/kg MMAE.VC.SA.617 (equivalent to 1mg/kg MMAE). This MMAE concentration was found to be toxic in non-tumour-bearing NOD-SCID mice, since all animals died after only one injection of 1.0 mg/kg MMAE (figure 5). More specifically, in the 0.1 mg/kg MMAE group all animals survived until the end of the experiment. Although the treatment was well tolerated, the tumour volume remained constant so that no tumour regression could be observed even after eight injections. However, in the 0.1 mg/kg MMAE.VC.SA.617 the treatment even failed to inhibit tumour growth resulting in the death of 4 mice before the end of the experiment due to grave body weight loss and

large tumour volume. These unexpected results could be attributed to insufficient drug delivery into the tumour tissue. As concluded from *in vitro* studies the cytotoxicity of the MMAE conjugate was two-fold of magnitude lower than the single drug MMAE, which could have different reasons as explained above. This loss in cytotoxicity could not be compensated by the active PSMA-targeting since MMAE.VC.SA.617 displayed a moderate binding affinity. Despite these unexpected results in the 0.1 mg/kg MMAE.VC.SA.617 group, the tolerability of MMAE.VC.SA.617 in the two other concentrations 0.5 mg/kg and 1.0 mg/kg could be demonstrated (100% animal survival). Consequently, MMAE.VC.SA.617 seems to be stable in mouse blood, since no toxic side effects occurred in these groups even after 8 i.v. injections. Moreover, tumour growth could be effectively inhibited even though tumour regression did not occur. On the other hand, only one mouse survived in the 0.5 mg/kg MMAE group, indicating a higher toxicity compared to the treatment with SMDC.

In summary, the synthesized MMAE.VC.SA.617 was proved to be selective in terms of PSMA binding and cytotoxicity toward PSMA-positive LNCaP cells. The *in vitro* cleavage of the valine-citrulline linker by cathepsin B has also been demonstrated. Animal studies have shown a good tolerability of MMAE.VC.SA.617 even at high concentrations. Although the treatment with the SMDC could not lead to a complete regression, tumour growth could be inhibited in both the 0.5 mg/kg and 1.0 mg/kg groups.

With regard to these results, further optimization of the chemical structure of the MMAE-SMDC is required to improve the PSMA binding affinity and the cytotoxicity of the compound. Possible approaches would be on the one hand, the use of a target vector with a higher PSMA binding affinity than KuE-617, on the other hand the use of a different linker/ spacer either to enhance the lipophilicity of the molecule and thus the passive diffusion through the cell membrane or to avoid a possible interaction of MMAE with the targeting unit, which could lead to a change in the conformation of the SMDC and therefore to a disadvantageous orientation within the PSMA binding pocket.

Materials and Methods

General

Chemicals were purchased from Sigma-Aldrich, Merck, VWR, AcrosOrganics and TCI. MMAE.VC was purchased from Hycultec GmbH and PSMA-617-NH_2 from Huayi Isotopes Co. Deuterated solvents for NMR spectra from Deutero. Silica gel 60 F254 coated aluminum plates from Merck were used for thin layer chromatography. NMR measurements were performed on an Avance III 600 spectrometer (600 MHz, 5mm TCI CryoProbe sample head with z-Gradient and ATM and SampleXPress Lite 16 sample changer) from Bruker. The LC/MS measurements were performed on an Agilent Technologies 1220

Infinity LC system coupled to an Agilent Technologies 6130B Single Quadrupole LC/MS system. Semi-preparative HPLC purification was performed on a 7000 series Hitachi LaChrom using a semi-preparative LiChrospher 100 RP18 EC (250 x 10 mm) 5 µ column.

Organic Synthesis

MMAE.VC.SA

MMAE.VC (20 mg, 0.018 mmol) was dissolved in 0.5 M phosphate buffer pH 7 (500 µL) and DMSO (500 µL). 3,4-Diethoxycyclobut-3-ene-1,2-dione (5 mg, 4 µL, 0.027 mmol) was added and stirred for 8 days. Every second day 0.5 eq of 3,4-Diethoxycyclobut-3-ene-1,2-dione were added. The solvent was removed via lyophilisation and the product was used in the next step without purification.

MS (ESI^+): 236.0 ($[M+H]^+/2$), calculated for $C_{64}H_{98}N_{10}O_{15}$: 1246.72 $[M]^+$.

MMAE.VC.SA.617

MMAE.VC.SA (20 mg, 0.016 mmol) and PSMA-617-NH_2 (10 mg, 0.016 mmol) were dissolved in ethanol (3 mL). Triethylamine (50 µL) was added and the reaction mixture was stirred for 6 days. The solvent was removed under reduced pressure. MMAE.VC.SA.617 was obtained as white powder (14.2 mg, 43%) after HPLC purification (LiChrospher 100 RP18 EC (250 x 10 mm) 5 µ, flow rate: 5 mL/min, H_2O/MeCN + 0.1% TFA, 45% to 55% MeCN in 20 min, t_R = 9.0 min).

MS (ESI^+): 929.0 ($[M+H]^+/2$), calculated for $C_{95}H_{137}N_{15}O_{23}$: 1857.22 $[M]^+$.

^{1}H NMR (600 MHz, EtOD-d_6) δ [ppm] = 7.77 (dd, *J* = 19.3, 9.2 Hz, 2H), 7.69 (d, *J* = 31.8 Hz, 3H), 7.41 (t, *J* = 7.9 Hz, 5H), 7.30 (dt, *J* = 15.4, 7.4 Hz, 3H), 7.24 – 7.15 (m, 1H), 5.18 (dt, *J* = 28.3, 15.2 Hz, 1H), 5.07 (d, *J* = 11.7 Hz, 1H), 4.93 (d, *J* = 31.6 Hz, 1H), 4.32 – 4.04 (m, 4H), 3.93 – 3.87 (m, 1H), 3.84 (s, 1H), 3.70 (s, 3H), 3.45 (d, *J* = 14.1 Hz, 2H), 3.41 – 3.26 (m, 9H), 3.23 (s, 1H), 3.11 (d, *J* = 15.3 Hz, 3H), 2.96 (td, *J* = 18.7, 7.0 Hz, 3H), 2.52 (s, 1H), 2.34 – 2.15 (m, 3H), 2.06 (s, 1H), 2.01 – 1.77 (m, 2H), 1.75 – 1.27 (m, 12H), 1.27 – 1.16 (m, 6H), 1.08 – 0.69 (m, 28H).

***In vitro* binding affinity**

LNCaP prostate cancer cells (purchased from Sigma-Aldrich) were cultured in RPMI 1640 (Thermo Fisher Scientific) supplemented with 10% fetal bovine serum (Thermo Fisher Scientific), 100 µg/ml streptomycin, and 100 units/ml penicillin at 37°C in 5% CO_2.

LNCaP cells were incubated for 45 min with different concentrations of the MMAE-conjugates in the presence of 0.75 nM [^{68}Ga]Ga-PSMA-10. Free radioactivity was removed by several washing steps with ice-cold PBS. Probes were measured in a γ-counter (2480 WIZARD^2 Automatic Gamma Counter, PerkinElmer). Obtained data were analyzed in GraphPad Prism 9 using nonlinear regression.

CellTiter-Blue® Viability Assay

10^4 cells per well were seeded in a 96-well plate for 24 h prior to incubation with increasing concentrations of either MMAE (0.1 nM to 0.5 µM) or MMAE.VC.SA.617 (2.5 nM to 10 µM). Subsequently 20 µL of CellTiter-Blue® Reagent were added in each well and incubated for 2 h at 37°C. For blocking studies, 2.5 nmol of PMPA was added to each well prior to incubation with SMDC. Fluorescence ($560_{Ex}/590_{Em}$) was recorded using a Tecan Spark multimode reader.

Immunofluorescence studies

2000 cells/well were seeded in Nunc® Lab-Tek® II - CC2™ Chamber Slide™ (Sigma Aldrich) and incubated with the test compounds at 37 °C for 24 h. After fixation with 4% PFA, cells were permeabilized with 0.5% Triton X-100 for 15 min at room temperature. Cells were then washed several times with PBS and blocked with 3% BSA in PBS for 1 h at room temperature. α-tubulin staining was performed by incubating the cells with alpha-Tubulin Antibody, Alexa Fluor® 488 conjugate (B-5-1-2) (ThermoFisher Scientific) at a final concentration of 2 µg/mL for 3h at room temperature. Counterstaining with DAPI was carried out with ProLong™ Gold Antifade Mountant with DAPI (ThermoFisher Scientific) according to the manufacturer's protocol. Cells were visualized using a fluorescence microscope (Keyence BZ-8000) at 20x.

Cathepsin B cleavage assay

Cathepsin B from human liver (Sigma Aldrich) was activated by incubation at room temperature with 30 mM dithiothreitol DTT and 15 mM EDTA at pH 5.5. Subsequently, 2.5 µM of the activated cathepsin B was added to 25 µM of MMAE.VC.SA.617 and incubated at 37 °C. Aliquots were taken at different time points. The enzymatic activity of cathepsin B was blocked by adding 1 µL of E-64 (1 mM) in each vial. Samples were analyzed using an Agilent Technologies 1220 Infinity LC system coupled to an Agilent Technologies 6130B Single Quadrupole LC/MS system.

Animal studies

Animals used for the biodistribution studies were obtained from the breeding facilities of the Institute of Biosciences and Applications, NCSR "Demokritos". Our experimental animal facility is registered according to the Greek Presidential Decree 56/2013 (Reg. Number: EL 25 BIO 022), in accordance to the European Directive 2010/63 which is harmonized with national legislation, on the protection of

animals used for scientific purposes. All applicable national guidelines for the care and use of animals were followed. The study protocol was approved by the Department of Agriculture and Veterinary Service of the Prefecture of Athens.

Toxicology study in healthy NOD-SCID mice

Prior to the therapeutic efficacy study in LNCaP tumour-bearing mice, a toxicology study is carried on healthy NOD-SCID mice to determine the tolerable dose of the single drug MMAE. Nine NOD-SCID mice were divided into 3 groups and received a single dose of MMAE. Group A received 0.1 mg (54 nmol)/kg body weight, Group B received 0.5 mg (270 nmol)/kg body weight while Group C received 1 mg (540 nmol)/kg body weight. Mice injected with 1 mg/kg MMAE had to be euthanized 5 days post-injection due to massive body-weight loss.

Therapeutic efficacy study in LNCaP tumour-bearing NOD-SCID mice

A therapeutic efficacy study of the MMAE.VC.SA.617 vs MMAE was performed in six groups of LNCaP tumour-bearing NOD/SCID mice, two of which acted as reference groups while an additional group acted as the control group. LNCaP cells were cultured in RPMI-1640 medium of pH 7.4, supplemented with 10% FBS, 100 U/mL of penicillin, 100 μg/mL of streptomycin, 2 mM glutamine, 10 mM HEPES and 1 mM sodium pyruvate. Cell cultures were maintained in 75 cm^2 flasks, grown at 37°C in 5% CO_2 in a humidified atmosphere and the medium was changed approximately every 72 hours (doubling time is about 40 hrs). Cells in exponential phase of growth were harvested by a 10 min treatment with a 0.05% trypsin–0.02% EDTA solution and neutralized with medium containing serum immediately. Cultures at passages 8–10 were used for the experiments. For the LNCaP xenograft development, cells were suspended in 100 μL in RPMI-1640 medium (supplemented as described above) and 100 μL Matrigel (ratio 1:1) (1×10^6 cells/200 μL) and maintained on ice until the inoculation. All equipment (syringes and needles) was chilled on ice prior to use in tumour cell inoculation. The mice were subcutaneously inoculated on the left shoulder with the LNCaP cells. The tumour-bearing animals were ready for experimentation approximately 14 days after cell inoculation.

The six groups of experimentation were as follows:

Group A: MMAE 0.1 mg/kg mouse body weight (reference group A)

Group B: MMAE 0.5 mg/kg mouse body weight (reference group B)

Group C: MMAE.VC.SA.617, 0.1 mg/kg mouse body weight

Group D: MMAE.VC.SA.617, 0.5 mg/kg mouse body weight

Group E: MMAE.VC.SA.617, 1 mg/kg mouse body weight

Group F: Mice injected with 0.9% NaCl (Control group)

All groups of mice were intravenously injected twice a week, for the first 5 doses of MMAE, MMAE.VC.SA.617 or saline, and then an additional 3 doses once a week, resulting in a total of 8 doses over a period of 7 weeks. Body weight and tumour volume were assessed on each day of i.v. injection, and every 3-4 days after the end of treatment administration, to 52 days after the initiation of the therapeutic efficacy study.

Acknowledgment

The authors thank the Max Planck Graduate Center Mainz (MPGC) for supporting Tilmann Grus. The authors gratefully acknowledge X.X. for supporting X.X.

The authors gratefully acknowledge X.X. as well as X.X. for the provision of equipment required for cytotoxicity studies. The authors thank X.X. for excellent technical assistance.

References

(1) Krementz, E. T.; Kokame, G. M.; Iglesias, F. Current Status of Chemotherapy of Cancer. *Postgrad. Med.* **1964**, *35* (4), 384–394.

(2) Brockman, R. W. Mechanisms of Resistance to Anticancer Agents. *Adv. Cancer Res.* **1963**, *7* (C), 129–234.

(3) Nissim, A.; Chernajovsky, Y. Historical Development of Monoclonal Antibody Therapeutics. In *Therapeutic Antibodies. Handbook of Experimental Pharmacology, vol. 181*.; Chernajovsky, Y., Nissim, A., Eds.; Springer: Berlin, Heidelberg, 2008; Vol.181, pp. 3–18.

(4) Firer, M. A.; Gellerman, G. Targeted Drug Delivery for Cancer Therapy: The Other Side of Antibodies. *J. Hematol. Oncol.* **2012**, *5*, 70.

(5) Govindan, S. V.; Goldenberg, D. M. Designing Immunoconjugates for Cancer Therapy. *Expert Opin. Biol. Ther.* **2012**, *12* (7), 873–890.

(6) Vázquez-Rey, M.; Lang, D. A. Aggregates in Monoclonal Antibody Manufacturing Processes. *Biotechnol. Bioeng.* **2011**, *108* (7), 1494–1508.

(7) Hedrich, W. D.; Fandy, T. E.; Ashour, H. M.; Wang, H.; Hassan, H. E. Antibody–Drug Conjugates: Pharmacokinetic/Pharmacodynamic Modeling, Preclinical Characterization, Clinical Studies, and Lessons Learned. *Clin. Pharmacokinet.* **2018**, *57* (6), 687–703.

(8) Prostate cancer statistics, World Cancer Research Fund International. Available online: https://www.wcrf.org/dietandcancer/prostate-cancer-statistics/ (accessed on 30th of December 2021).

(9) Barsouk, A.; Padala, S. A.; Vakiti, A.; Mohammed, A.; Saginala, K.; Thandra, K. C.; Rawla, P.; Barsouk, A. Epidemiology, Staging and Management of Prostate Cancer. *Med. Sci.* **2020**, *8* (3), 28.

(10) Chang, S. S.; Heston, W. D. W. The Clinical Role of Prostate-Specific Membrane Antigen (PSMA). *Urol. Oncol.* **2002**, *7* (1), 7–12.

(11) Ghosh, A.; Heston, W. D. W. Tumor Target Prostate Specific Membrane Antigen (PSMA) and Its Regulation in Prostate Cancer. *J. Cell. Biochem.* **2004**, *91* (3), 528–539.

(12) Perner, S.; Hofer, M. D.; Kim, R.; Shah, R. B.; Li, H.; Möller, P.; Hautmann, R. E.; Gschwend, J. E.; Kuefer, R.; Rubin, M. A. Prostate-Specific Membrane Antigen Expression as a Predictor of Prostate Cancer Progression. *Hum. Pathol.* **2007**, *38* (5), 696–701.

(13) Donin, N. M.; Reiter, R. E. Why Targeting PSMA Is a Game Changer in the Management of Prostate Cancer. *J. Nucl. Med.* **2018**, *59* (2), 177–182.

(14) Silver, D. A.; Pellicer, I.; Fair, W. R.; Heston, W. D. W.; Cordon-Cardo, C. Prostate-Specific Membrane Antigen Expression in Normal and Mailgant Human Tissues. *Clin. Cancer Rersearch* **1997**, *3* (1), 81–85.

(15) Bräuer, A.; Grubert, L. S.; Roll, W.; Schrader, A. J.; Schäfers, M.; Bögemann, M.; Rahbar, K. ^{177}Lu-PSMA-617 Radioligand Therapy and Outcome in Patients with Metastasized Castration-Resistant Prostate Cancer. *Eur. J. Nucl. Med. Mol. Imaging* **2017**, *44* (10), 1663–1670.

(16) Kularatne, S. A.; Wang, K.; Santhapuram, H. K. R.; Low, P. S. Prostate-Specific Membrane Antigen Targeted Imaging and Therapy of Prostate Cancer Using a PSMA Inhibitor as a Homing Ligand. *Mol. Pharm.* **2009**, *6* (3), 780–789.

(17) von Eyben, F. E.; Picchio, M.; von Eyben, R.; Rhee, H.; Bauman, G. ^{68}Ga-Labeled Prostate-Specific Membrane Antigen Ligand Positron Emission Tomography/Computed Tomography for Prostate Cancer: A Systematic Review and Meta-Analysis. *Eur. Urol. Focus* **2018**, *4* (5), 686–693.

(18) Eissa, A.; Elsherbiny, A.; Coelho, R. F.; Rassweiler, J.; Davis, J. W.; Porpiglia, F.; Patel, V. R.; Prandini, N.; Micali, S.; Sighinolfi, Ma. C.; Puliatti, S.; Rocco, B.; Bianchi, G. The Role of ^{68}Ga-PSMA PET/CT Scan in Biochemical Recurrence after Primary Treatment for Prostate Cancer: A Systematic Review of the Literature. *Minerva Urol Nefrol.* **2018**, *70* (5), 462–478.

(19) Petrylak, D. P.; Vogelzang, N. J.; Chatta, G. S.; Fleming, M. T.; Smith, D. C.; Appleman, L. J.; Hussain, A.; Modiano, M.; Singh, P.; Tagawa, S. T.; Gore, I.; McClay, E. F.; Mega, A. E.; Sartor, A. O.; Somer, B. G.; Wadlow, R. C.; Shore, N. D.; Stambler, N.; DiPippo, V. A.; Israel, R. J. A Phase 2 Study of Prostate Specific Membrane Antigen Antibody Drug Conjugate (PSMA ADC) in Patients (Pts) with Progressive Metastatic Castration-Resistant Prostate Cancer (MCRPC) Following Abiraterone and/or Enzalutamide (Abi/Enz). *J. Clin. Oncol.* **2015**, *33* (7_suppl), 144–144.

(20) Milowsky, M. I.; Galsky, M. D.; Morris, M. J.; Crona, D. J.; George, D. J.; Dreicer, R.; Tse, K.; Petruck, J.; Webb, I. J.; Bander, N. H.; Nanus, D. M.; Scher, H. I. Phase 1/2 Multiple Ascending Dose Trial of the Prostate-Specific Membrane Antigen (PSMA)-Targeted Antibody Drug Conjugate MLN2704 in Metastatic Castration-Resistant Prostate Cancer. *Urol. Oncol.* **2016**, *34* (12), 530.e15-530.e21.

(21) Niaz, M. O.; Sun, M.; Ramirez-Fort, M. K.; Niaz, M. J. Prostate-Specific Membrane Antigen Based

Antibody-Drug Conjugates for Metastatic Castration-Resistance Prostate Cancer. *Cureus* **2020**, *12* (2), e7147.

(22) Boinapally, S.; Ahn, H.-H.; Cheng, B.; Brummet, M.; Nam, H.; Gabrielson, K. L.; Banerjee, S. R.; Minn, I.; Pomper, M. G.; Morgan, R. H. A Prostate-Specific Membrane Antigen (PSMA)-Targeted Prodrug with a Favorable in Vivo Toxicity Profile. *Sci. Reports* **2021**, *11*, 7114.

(23) Lv, Q.; Yang, J.; Zhang, R.; Yang, Z.; Yang, Z.; Wang, Y.; Xu, Y.; He, Z. Prostate-Specific Membrane Antigen Targeted Therapy of Prostate Cancer Using a DUPA-Paclitaxel Conjugate. *Mol. Pharm.* **2018**, *15* (5), 1842–1852.

(24) Leamon, C. P.; Reddy, J. A.; Bloomfeld, A.; Dorton, R.; Nelson, M.; Vetzel, M.; Kleindl, P.; Hahn, S.; Wang, K.; Vlahov, I. R. Prostate-Specific Membrane Antigen-Specific Antitumor Activity of a Self-Immolative Tubulysin Conjugate. *Bioconjug. Chem.* **2019**, *30* (6), 1805–1813.

(25) Wang, X.; Shirke, A.; Walker, E.; Sun, R.; Ramamurthy, G.; Wang, J.; Shan, L.; Mangadlao, J.; Dong, Z.; Li, J.; Wang, Z.; Schluchter, M.; Luo, D.; Wang, Y.; Stauffer, S.; Brady-Kalnay, S.; Hoimes, C.; Lee, Z.; Basilion, J. P. Small Molecule-Based Prodrug Targeting Prostate Specific Membrane Antigen for the Treatment of Prostate Cancer. *Cancers.* **2021**, *13* (3), 417.

(26) Li, C.; Zhang, C.; Li, Z.; Samineni, D.; Lu, D.; Wang, B.; Chen, S.-C.; Zhang, R.; Agarwal, P.; Fine, B. M.; Girish, S. Clinical Pharmacology of Vc-MMAE Antibody–Drug Conjugates in Cancer Patients: Learning from Eight First-in-Human Phase 1 Studies. *MAbs* **2020**, *12* (1), 1699768.

(27) Sinha, A. A.; Morgan, J. L.; Buss, R. J.; Ewing, S. L.; Fernandes, E. T.; Le, C.; Wilson, M. J. Cathepsin B Expression Is Similar in African-American and Caucasian Prostate Cancer Patients. *Anticancer Res.* **2007**, *27* (5A), 3135–3141.

(28) Gondi, C. S.; Rao, J. S. Cathepsin B as a Cancer Target. *Expert Opin. Ther. Targets* **2013**, *17* (3), 281–291.

(29) Wurm, F. R.; Klok, H. A. Be Squared: Expanding the Horizon of Squaric Acid-Mediated Conjugations. *Chem. Soc. Rev.* **2013**, *42* (21), 8220–8236.

(30) Huppertsberg, A.; Kaps, L.; Zhong, Z.; Schmitt, S.; Stickdorn, J.; Deswarte, K.; Combes, F.; Czysch, C.; Vrieze, J. De; Kasmi, S.; Choteschovsky, N.; Klefenz, A.; Medina-Montano, C.; Winterwerber, P.; Chen, C.; Bros, M.; Lienenklaus, S.; Sanders, N. N.; Koynov, K.; Schuppan, D.; Lambrecht, B. N.; David, S. A.; Geest, B. G. De; Nuhn, L. Squaric Ester-Based, PH-Degradable Nanogels: Modular Nanocarriers for Safe, Systemic Administration of Toll-like Receptor 7/8 Agonistic Immune Modulators. *J. Am. Chem. Soc.* **2021**, *143* (26), 9872–9883.

(31) Grus, T.; Lahnif, H.; Klasen, B.; Moon, E.-S.; Greifenstein, L.; Roesch, F. Squaric Acid-Based Radiopharmaceuticals for Tumor Imaging and Therapy. *Bioconjug. Chem.* **2021**, *32* (7), 1223–1231.

(32) Akaiwa, M.; Dugal-Tessier, J.; Mendelson, B. A. Antibody-Drug Conjugate Payloads; Study of Auristatin Derivatives. *Chem. Pharm. Bull. (Tokyo).* **2020**, *68* (3), 201–211.

(33) Chen, R.; Chen, B. Brentuximab Vedotin for Relapsed or Refractory Hodgkin's Lymphoma. *Drug Des. Devel. Ther.* **2015**, *9*, 1729–1733.

(34) Dragovich, P. S.; Pillow, T. H.; Blake, R. A.; Sadowsky, J. D.; Adaligil, E.; Adhikari, P.; Bhakta, S.;

Blaquiere, N.; Chen, J.; Dela Cruz-Chuh, J.; Gascoigne, K. E.; Hartman, S. J.; He, M.; Kaufman, S.; Kleinheinz, T.; Kozak, K. R.; Liu, L.; Liu, L.; Liu, Q.; Lu, Y.; Meng, F.; Mulvihill, M. M.; O'Donohue, A.; Rowntree, R. K.; Staben, L. R.; Staben, S. T.; Wai, J.; Wang, J.; Wei, B.; Wilson, C.; Xin, J.; Xu, Z.; Yao, H.; Zhang, D.; Zhang, H.; Zhou, H.; Zhu, X. Antibody-Mediated Delivery of Chimeric BRD4 Degraders. Part 1: Exploration of Antibody Linker, Payload Loading, and Payload Molecular Properties. *J. Med. Chem.* **2021**, *64* (5), 2534–2575.

(35) Su, Z.; Xiao, D.; Xie, F.; Liu, L.; Wang, Y.; Fan, S.; Zhou, X.; Li, S. Antibody–Drug Conjugates: Recent Advances in Linker Chemistry. *Acta Pharm. Sin. B* **2021**, *11* (12), 3889–3907.

(36) Bargh, J. D.; Isidro-Llobet, A.; Parker, J. S.; Spring, D. R. Cleavable Linkers in Antibody-Drug Conjugates. *Chem. Soc. Rev.* **2019**, *48* (16), 4361–4374.

(37) Fernández, P. L.; Farré, X.; Nadal, A.; Fernández, E.; Peiró, N.; Sloane, B. F.; Shi, G. P.; Chapman, H. A.; Campo, E.; Cardesa, A. Expression of Cathepsins B and S in the Progression of Prostate Carcinoma. *Int. J. Cancer* **2001**, *95* (1), 51–55.

4.4 Project D: PSMA inhibitor structure optimisation

Comparison of the binding affinity of squaramide containing lysine-urea-glutamate- and glutamate-urea-glutamate-based PSMA inhibitors

Tilmann Grus, X.X., X.X. and X.X.

In preparation for submission

Summary

The most common PSMA radiopharmaceuticals such as PSMA-617, PSMA-I&T, PSMA-11 and PSMA-1007 have one thing in common. All of these compounds contain a KuE (lysine-urea-glutamate) unit as PSMA target vector. [1] Nevertheless, studies of Hillier et al. and Robu et al. indicate that the exchange of KuE against K-EuE (lysine-glutamate-urea-glutamate) leads to better pharmacokinetic properties.[2,3]

The aim of this study is to synthesize squaric acid containing KuE and K-EuE based PSMA radiopharmaceuticals and compare them first regarding the influence of the target vector on binding affinity and second regarding the influence of the conjugated chelator on the binding affinity. For comparison, compounds carrying the targeting unit of PSMA-617 were also evaluated.

In the first step the unconjugated targeting units SAME.KuE, SAME.K-EuE and 617.KuE were tested for their PSMA *in vitro* binding affinity. Among the three structures, SAME.K-EuE showed the highest affinity, but all three targeting units displayed IC_{50} values in the same area. (17.2 ± 5.2 nM for SAME.K-EuE, 35.9 ± 2.6 nM for SAME.KuE and 21.5 ± 1.9 nM for 617.KuE)

In the second part of the study the three targeting units were conjugated to the three chelators DATA^{5m}, AAZTA^{5} and DO2AGA. The resulting nine compounds were also evaluated regarding their PSMA binding. In contrast to the findings with the unconjugated targeting units, the SA.K-EuE containing compounds showed by far the worst affinities (between 178 nM and 407 nM). All other compounds of with the units SA.KuE and 617.KuE showed values in the two-digit nanomolar range (between 12.7 nM and 92.1 nM). Defined influences of the chelators could not be find. Influences seems to be dependent on the exact combination of chelator and targeting unit.

The literature findings that K-EuE is superior to KuE could not be reproduced with the here designed squaric acid containing compounds. It was shown that the conjugation of a chelator leads to a decrease of affinity. Thus, in future studies, a longer spacer unit between chelator and squaramide could reduce influences of the chelator moiety on binding behavior.

Author contributions

T. Grus, X.X. and X.X. planned the study. **T. Grus** performed organic synthesis. X.X. participated in organic synthesis under the supervision of **T. Grus**. X.X. was in charge of the LNCaP cells and the *in vitro* binding affinity. The obtained data were interpreted by **T. Grus**. **T.Grus** wrote the manuscript. X.X. supervised the project.

References of the summary

(1) Kopka, K.; Benešová, M.; Bařinka, C.; Haberkorn, U.; Babich, J. Glu-Ureido-Based Inhibitors of Prostate-Specific Membrane Antigen: Lessons Learned during the Development of a Novel Class of Low-Molecular-Weight Theranostic Radiotracers. *J. Nucl. Med.* **2017**, *58* (Suppl 2), 17S-26S.

(2) Hillier, S. M.; Maresca, K. P.; Lu, G.; Merkin, R. D.; Marquis, J. C.; Zimmerman, C. N.; Eckelman, W. C.; Joyal, J. L.; Babich, J. W. ^{99m}Tc-Labeled Small-Molecule Inhibitors of Prostate-Specific Membrane Antigen for Molecular Imaging of Prostate Cancer. *J. Nucl. Med.* **2013**, *54* (8), 1369–1376.

(3) Robu, S.; Schmidt, A.; Eiber, M.; Schottelius, M.; Günther, T.; Hooshyar Yousefi, B.; Schwaiger, M.; Wester, H. J. Synthesis and Preclinical Evaluation of Novel ^{18}F-Labeled Glu-Urea-Glu-Based PSMA Inhibitors for Prostate Cancer Imaging: A Comparison with ^{18}F-DCFPyl and ^{18}F-PSMA-1007. *EJNMMI Res.* **2018**, *8*, 30.

Abstract

Background: The prostate-specific membrane antigene (PSMA) is a membrane bound receptor and offers a potential target for early diagnosis and therapy of prostate cancer, since it is highly over expressed in prostate cancer. The binding pocket and the active site of PSMA is well discovered and thus, the development of well-fitting PSMA inhibitors is possible. In recent years, urea-based targeting vectors were developed and today most of PSMA radiopharmaceuticals used in clinic applications are urea-based inhibitors. The most prominent representative of this class of inhibitors are KuE (lysine-urea-glutamate) inhibitors. Recent studies indicated that the use of K-EuE (lysine-glutamate-urea-glutamate) inhibitors leads to higher affinities of the PSMA radiopharmaceuticals. In this study, we designed K-EuE and KuE based inhibitors, conjugated them to different chelators via squaric acid, evaluated them regarding PSMA binding affinity, and compared all compounds among each other. For comparative purposes, we also replaced the squaric acid linking moiety against the linking moiety of PSMA-617, one of the most potent and most used PSMA radiopharmaceuticals.

Methods: Three PSMA inhibitors and nine chelator containing PSMA radiopharmaceuticals were synthesized. The two hybrid chelators DATA^{5m} and AAZTA^{5} as well as the DOTA derivative DO2AGA were used as chelator moieties. The affinity towards PSMA (IC_{50} value) of every compound was determined in an *in vitro* competitive radioligand binding assay. The assay was performed in PSMA-positive LNCaP cells and [^{68}Ga]Ga-PSMA-10 was used as reference. The affinities were compared.

Results: IC_{50} values of 12.7 ± 1.7 to 407.1 ± 19.2 nM were found for the 12 synthesized compounds. The inhibitors without a conjugated chelator showed affinities in the range of 17.2 ± 5.2 nM to 35.9 ± 2.6 nM. The conjugation of a radiolabelling moiety to SA.K-EuE led to a significant decrease in affinity (affinity values between 178.2 ± 42.7 nM and 407.1 ± 19.2 nM). The influence of the chelators on the other two targeting units depends on the corresponding combination, as no further trends were identified. Increases, decreases and no influence on the affinity were found here.

Conclusion: The findings of other studies indicte that EuE is superior to KuE could not be reproduced. In this study all EuE-based compounds showed a significant lower affinity than the corresponding KuE analogues. In addition, it depends on the chelator whether squaric acid-based KuE target vectors, yields better affinities than KuE target vectors, which are conjugated to the linker unit of the highly potent PSMA-617.

Keywords: PSMA, KuE, EuE, K-EuE, prostate cancer, squaric acid, squaramide

Introduction

In 2020, prostate cancer (PCa) was second most diagnosed cancer and one of the leading death causes among men worldwide.[1] Thus, there is a high interest in the development of novel diagnostics, enabling an early diagnosis and an early start of therapy, as well as the development of effective treatment applications. With the discovery of the prostate-specific membrane antigens (PSMA), the development of novel small molecule based radiotracer become possible. These PSMA inhibitors bind to the PSMA receptor and are internalised, which enables their usage in imaging and radionuclide therapy of prostate cancer.[2,3] The expression of PSMA on the cell surface is very low under normal physiologic conditions in the prostate but increases drastically (up to a factor of 1000) in prostate cancer cells and PSMA is also present in its metastases. This fact makes PSMA to an interesting prostate cancer biomarker.[4] The reason of this upregulation, as well as the physiological function in the prostate remains unclear.[5,6]

PSMA is a membrane bound receptor molecule, which is also known as glutamate carboxypeptidase II, is a membrane bound zinc dependent protease and has a size of about 100 kDa.[7] It is composed of 750 amino acids, which are mainly found in the extracellular area.[8]

The PSMA binding pocket has been very well studied, which allows adjustment of radiopharmaceuticals for optimal binding affinity. One important area of the binding pocket is a glutamate binding pocket in position S1‘ to the active site of PSMA. As the name already implies, this area has a high affinity towards glutamate and glutamate-like structures. Potent inhibitors have a glutamate moiety that binds in this area, as even the exchange of glutamate to the glutamate-like aspartate causes a significant reduction in affinity.[8–10] The active site is located next to this binding area. It consists of two zinc ions, which are responsible for the enzymatic cleavage. For this reason, the radiotracer has to contain in this position a unit which binds to the zinc but can’t be cleaved by it. The so-called entrance funnel represents the largest part of the binding pocket and is not very selective. Thus, a variety of different chemical structures can be included here. Nevertheless, there are some areas inside the funnel which, when addressed with the right units, lead to an increase in affinity. One of these areas is near to the active site. The so-called arginine patch is defined by arginine side chains and thus prefers negatively charged groups. For this reason, a lot of inhibitors contain negatively charged units, such as carboxyl groups, in direct vicinity to the zinc-binding unit.[8,9] An area which enables π-interactions is located near to the entrance lit of the binding pocket. The use of aromatic units in the correct position of the inhibitor allows interactions with this area of the binding pocket which increases the affinity of the inhibitor.[8,11]

The first developed PSMA inhibitors were inhibitors with a phosphonate unit.[10] Phosphonates are suitable as PSMA inhibitors, since they can coordinate the zinc ions in the active site, but are not cleavable. However, because of the difficulties in phosphonate synthesis, they have not been established and other units with the same properties were searched and the phosphonates were replaced by urea derivatives.[12] Today, the most common PSMA radiopharmaceuticals consist of urea-based inhibitors (figure 1).[9] All compounds show a similar inhibitor structure, in which the N-terminus of glutamate is conjugated to the N-terminus of another amino acid through a urea unit. The C-terminus of the second amino acid provides a negatively charged group, which can interact with the arginine patch. The side chain can be used for further functionalisation. The most common amino acids used here are lysine and glutamate. If the glutamate is conjugated to lysine via urea, it is named KuE (lysine-urea-glutamate) based inhibitor.[9,13] If the conjugation is carried out with another glutamate, it is called EuE (glutamate-urea-glutamate) based inhibitor.[13–15] Also known is the functionalisation of one glutamate of EuE with a lysine. Here, due to the additional C-terminus of lysine (K-EuE), the interaction with the arginine patch is increased which can also interact with the arginine patch and can lead for example to a better affinity or rapid clearance properties combined with high tumour binding.[15,16]

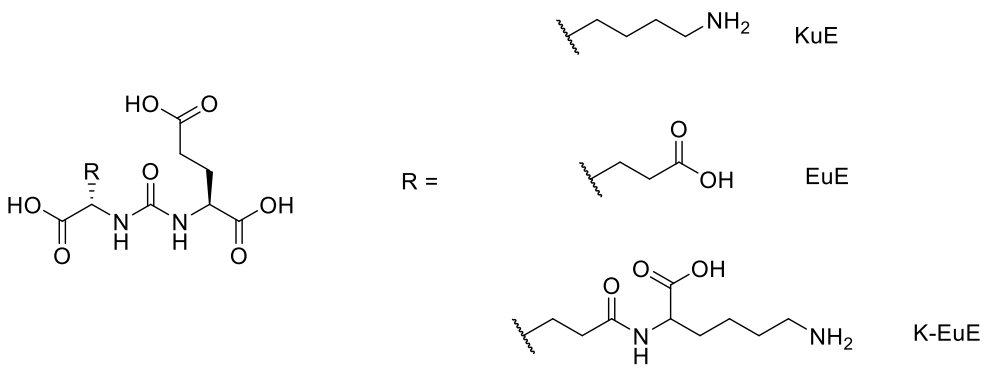

Figure 1: Glutamate-urea-based PSMA inhibitors.

Among the most prominent urea-based PSMA radiopharmaceuticals are [^{68}Ga]Ga/[^{177}Lu]-PSMA-617, [^{68}Ga]Ga-PSMA-11 or [^{68}Ga]Ga/[^{177}Lu]Lu-PSMA-I&T. All these include a KuE unit as inhibitor.[9,17–20] Nevertheless, EuE-based PSMA radiopharmaceuticals are also found in clinical applications. The technetium-99m labelled ligand MIP-1404 was the first PSMA ^{99m}Tc-labelled inhibitor who was evaluated in clinical studies with promising results and PCa lesion detection rates in patients with PSA values of more than 2 ng/mL, which are comparable to [^{68}Ga]Ga-PSMA-11.[2,21]

The PSMA inhibitor is normally connected to the radiolabelling moiety via a linker system. This linker provides space between the inhibitor and the radiolabelling unit and prevents the influence of each

other. In addition, the linker can carry additional structure features for an increased pharmacokinetic such as an increased affinity towards PSMA due to structures which interact with the binding pocket.

The general number of possible linker structures for radiopharmaceuticals is large, but the linker must be adapted to the required conditions. One interesting linking molecule is squaric acid (SA). In the life sciences it is established, for example, as coupling agent for e.g. peptide, protein or carbohydrate conjugates or as bioisoster in drug development.[22,23] Our group recently introduced the first application of squaric acid in the field of radiopharmacy as linking unit of chelators and targeting vectors.[24] Besides the functionalisation of a chelator unit with monoclonal antibodies[25,26] or the fibroblast activation protein inhibitor (FAPi)[27–30], also squaric acid conjugated KuE inhibitors were presented.[31–33] An interesting result of these studies of squaric acid conjugated KuE derivatives is that the squaric acid seems to have improved kidney clearance kinetics in contrast to PSMA ligands such as PSMA-11.[31,33] Due to its aromatic character, if it is in the right position of the PSMA inhibitor, it can contribute to an increased affinity.

As already mentioned, some studies indicate some advantages of K-EuE-based inhibitors over KuE-based inhibitors.[15,16] In this study, we synthesized several K-EuE and KuE-based inhibitors, conjugated them to different chelators via squaric acid. We evaluated and compared them systematically regarding their potential of *in vitro* binding of PSMA. To compare the suitability of the sqauric acid unit as potential linking unit for a PSMA radiopharmaceutical, we compared SA.KuE and SA.K-EuE based inhibitors with inhibitors containing the PSMA-617 linker unit.

In this study, we used three different chelators. The hybrid chelator DATA^{5m} (figure 2A) enables fast gallium-68 labelling under mild conditions.[34,35] AAZTA^{5} (figure 2B) is also a hybrid chelator but in contrast to DATA^{5m}, AAZTA^{5} can be labelled with diagnostic radionuclides (e.g. gallium-68 or scandium-44) as well as with therapeutic nuclides (e.g. lutetium-177).[36] The chelator DO2AGA (figure 2C) is a derivative of the DOTAGA chelator. Like AAZTA^{5} it can be labelled with diagnostic nuclides as well as with therapeutic nuclides.[17,37] Both chelators are therefore suitable for theranostic approaches. One amine of the DO2AGA scaffold is functionalised with an amine function instead of a carboxyl group which is normally found on this position in DOTA or DOTAGA derivatives. This functionalisation can be used to functionalise the chelator with other target vectors in further studies.

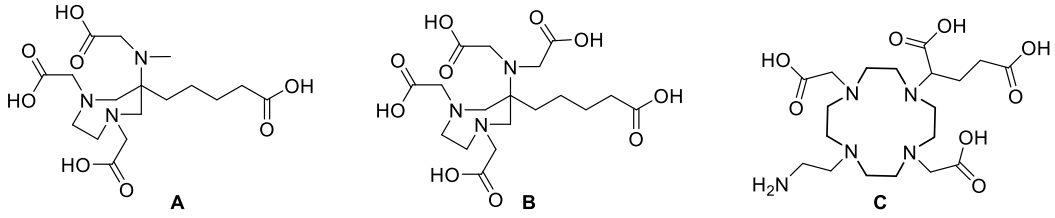

Figure 2: Structure of the chelators used in this study. A: DATA^{5m}; B: AAZTA^{5}; C: DO2AGA.

Results

In this study we synthesised 12 different compounds and sorted them into four sets (figure 3). The sorting was based on the containing chelator moiety. Set A contains the targeting units without a chelator (**1**-**3**). Set B includes the DATA^{5m} conjugated target vectors (**4**-**6**), set C the AAZTA^{5} bound compounds (**7**-**9**) and set D the DO2AGA conjugated compounds (**10**-**12**).

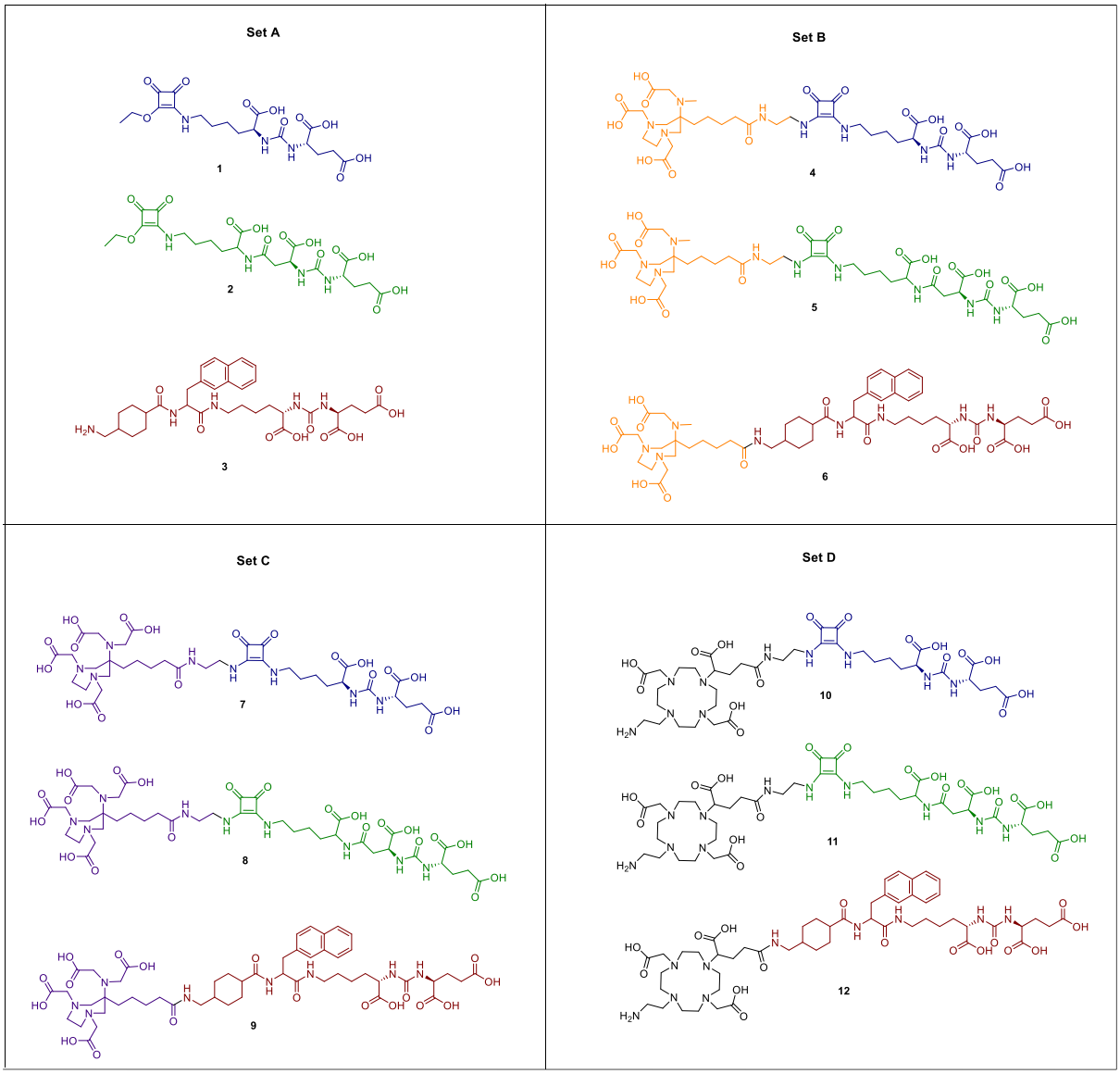

Figure 3: Compounds analysed in this study. The division of the compounds into the sets is based on the used chelator moiety. A: no chelator; B: DATA^{5m}; C. AAZTA^{5}; D: DO2AGA. Colour-code for the structure units: blue: SAME.KuE; green: SAME.K-EuE; red: 617.KuE; orange: DATA^{5m}; purple: AAZTA^{5}; black: DO2AGA.

Both, the target vectors (**1**-**3**) and the chelator moieties were synthesized individually and then conjugated to each other.

The synthesis of SAME.KuE is already described by Lahnif et al.[33] and the synthesis of 617.KuE was carried out according to the protocol of Benešová et al.[20,38] . Therefore, only the synthesis of SAME.K-EuE will be described below (figure 4).

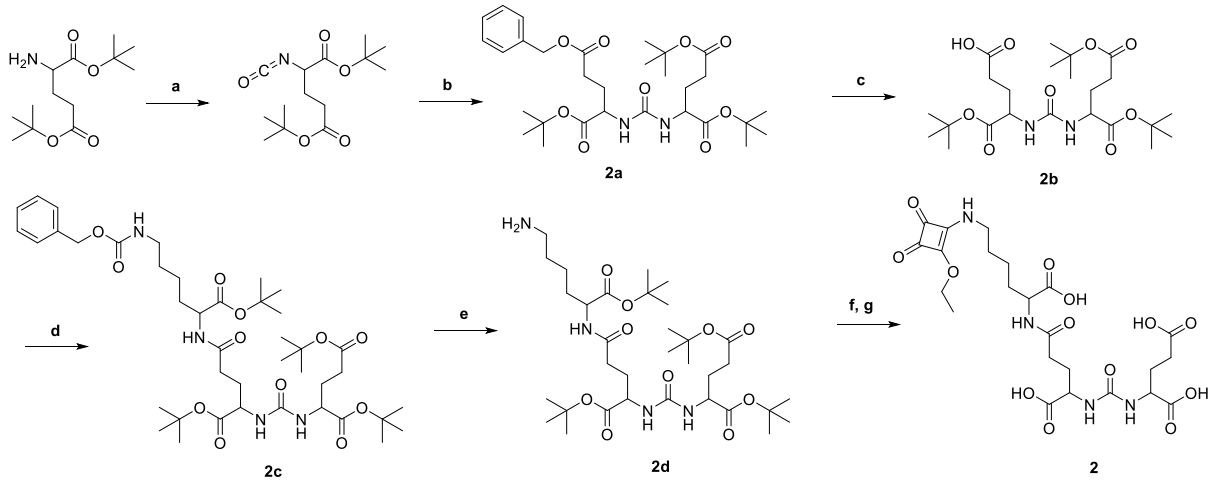

Figure 4: Synthesis scheme of SAME.K-EuE. a) triphosgene, L-glutamic acid di-*tert*-butyl ester hydrochloride, DIPEA, DCM, 1.5 h, 0°C-RT; b) L-glutamic acid α-*tert*-butyl-γ-benzyl ester hydrochloride, DIPEA, DCM, overnight, RT, 62%; c) Pd/C, H_2, MeOH, overnight, RT, 90%; d) N(*ε*)-benzoyloxycarbonyl-L-lysine *tert*-butyl ester hydrochloride, HATU, HOBt, DIPEA, MeCN, overnight, RT, 73%; e)) Pd/C, H_2, EtOH, overnight, RT, 94%; f) 3,4-Diethoxy-3-cyclobutene-1,2-dione, 0.5 M phosphate buffer pH 7, 2 d, RT, 86%; g) DCM / TFA (2:1), 4 days, RT, 38%.

The target vector SAME.K-EuE was carried out in a 7 step synthesis with an overall yield of 13%. L-glutamic acid di-*tert*-butyl ester hydrochloride was treated with triphosgene and DIPEA to form *in situ* an isocyanate. The amino function of L-glutamic acid α-*tert*-butyl-γ-benzyl ester hydrochloride formed with the isocyanate a urea unit and the protected EuE unit was formed. To functionalize the EuE unit with a lysine, the orthogonal benzyl protecting group was removed by hydrogenation. The lysine unit with the benzyl protected side chain was introduced using a standard amide coupling reaction with HATU and HOBt as reagent. After reductive deprotection of the side chain amine, squaric acid was added to the molecule via an asymmetrical amidation at a pH value of 7. Thus, the squaric acid is introduced as squaramide. To get the operational target vector **2**, the remaining protecting groups were cleaved from the molecule under acidic conditions and the compound was HPLC purified.

The synthesis of DATA^{5m} and AAZTA^{5} is already described in literature.[25,39,40] In the following, the synthesis of the chelator DO2AGA is described (figure 5).

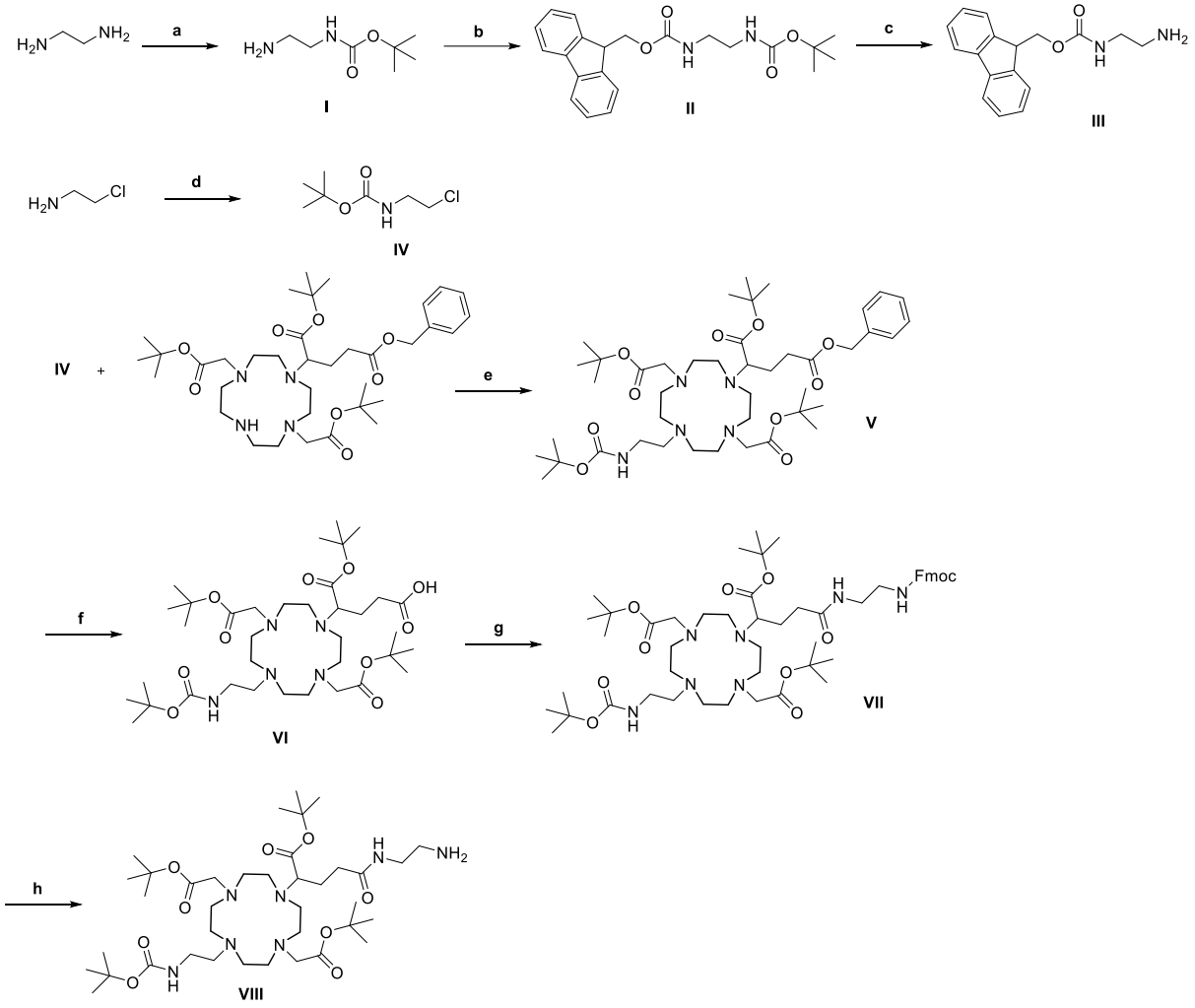

Figure 5: Synthesis scheme of DO2AGA. a) Ethylenediamine, di-*tert*-butyl dicarbonate, chloroform, 16 h, 0°C- RT, 65%; b) (fluorenylmethoxy)carbonyl chloride, pyridine, DCM, 2 h, RT, 74%; c) DCM / TFA, 16 h, RT, 97%; d) 2-chloroethylamine hydrochloride, di-*tert*-butyl dicarbonate, DCM, 16 h, RT, 79%; e) **IV**, DO2A(*t*Bu)-GABz, K_2CO_3, MeCN, 90 °C, 16 h, 90%; f) Pd/C, H_2, MeOH, over night, RT, 89%; g) **III**, HATU, HOBt, DIPEA, MeCN, 16 h, RT, 93%; h) DCM, Triethylamine, 20 min, RT, 85%.

The synthesis of DO2AGA was performed in an 8-step synthesis with an overall yield of 23%. In the first step of the secondary amine of DO2A(*t*Bu)-GABz was functionalisied with a Boc protected ethylamine (**IV**) via nucleophilic substitution. The benzyl protecting group of compound **V** was removed by hydrogenation. Product **VI** was directly used for conjugation to the resin bound 617.KuE linker. For squaric acid conjugation, however, a terminal amine is necessary, so compound **VI** was functionalised with an ethylenediamine bridge. One amine of the ethylenediamine unit was previously protected an Fmoc protecting group (**III**). For this one amine of ethylenediamine was first protected with a Boc-protecting group and then the protection of the second amine with the Fmoc group was carried out. Afterwards, the Boc-protecting group was removed under acidic conditions. A direct protection of only one amine with Fmoc is not possible and the indirect rout via the Boc group is necessary. The functionalisation of **VI** with **III** was carried out with a standard amide formation reaction using HATU

and HOBt as coupling reagent. Afterwards, the Fmoc group of compound **VII** was removed under basic conditions and compound **VIII** was ready for squaric acid conjugation.

The conjugation of the squaric acid moieties SAME.XuE (X = K (**1**) and X = K-E (**2**)) with the amine function of the chelators were all performed as asymmetric amidation under basic conditions. Figure 6A shows the general reaction scheme for this type of conjugation. In terms of the syntheses of the hybrid chelator containing compounds (**4**-**9**) the chelators were first functionalised with an ethylendiamine bridge to provide a terminal amine for the sqauric acid conjugation. The chelators were then deprotected and conjugated to squaric acid via an asymmetric amidation. In terms of the DO2AGA conjugation (figure 6B), compound **VIII** was conjugated to the still *tert*-butyl protected SAME.XuE target vectors, followed by a complete acidic deprotection of the compounds. The used solvent depends on the compound. Here organic solvents as well as aqueous solutions can be considered. While the conjugation of the already deprotected DATA^{5m} and AAZTA^{5} was carried out in aqueous phosphate buffer with a pH value of 9, the conjugation of the *tert*-butyl protected DO2AGA was carried out in an organic solvent (ethylene diamine or dichloromethane) and an organic base (triethylamine) was added to provide basic conditions.

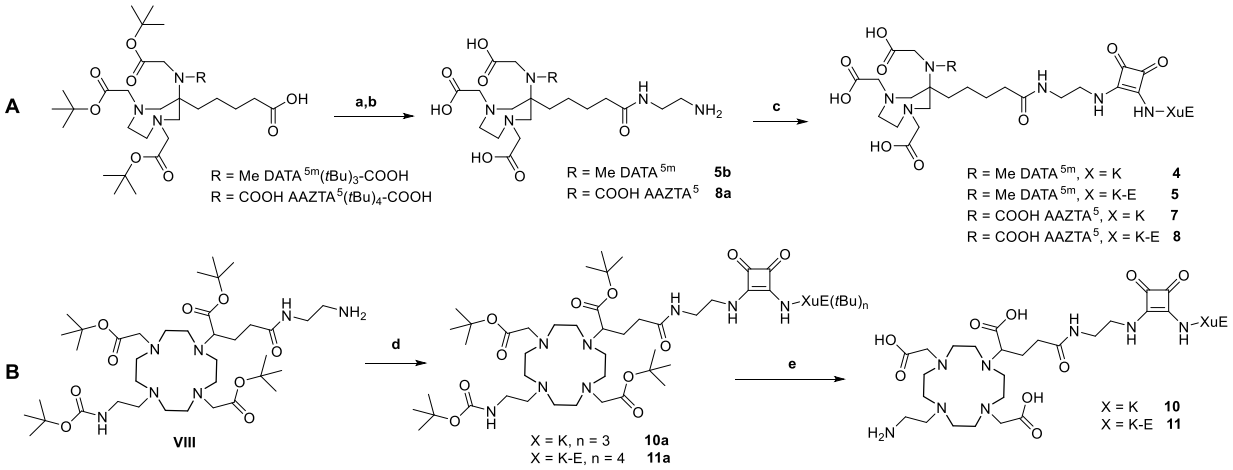

Figure 6: General conjugation strategies for asymmetric amidation of SAME.XuE (X = K (**1**) and X = K-E (**2**)) with A) hybrid chelators DATA^{5m} and AAZTA^{5} and B) DO2AGA. a) *Tert*-butyl (2-aminoethyl)carbamate, HATU, DIPEA, MeCN, RT; b) DCM /TFA, RT; c) SAME.XuE, 0.5 M phosphate buffer (pH 9), RT; d) SAME.XuE, DCM or ethyl acetate, triethylamine; e) DCM / TFA, RT.

The final synthesis of **6**, **9** and **12** was carried out using a standard solid phase peptide synthesis reaction. The free carboxyl groups of the *tert*-butyl protected chelators DATA^{5m}(*t*Bu)$_3$-COOH, AAZTA^{5}(*t*Bu)$_4$-COOH and DO2A(*t*Bu)$_3$(NHBoc)-GA-COOH (**VI**) were coupled to the free amino function of the resin bound 617.KuE unit using HATU and HOBt as reagents. A schematic overview of this reaction pathway is shown in figure 7. The final compounds **6**, **9**, **12** were cleaved of the resin and deprotected under acidic conditions and were obtained after a final HPLC purification.

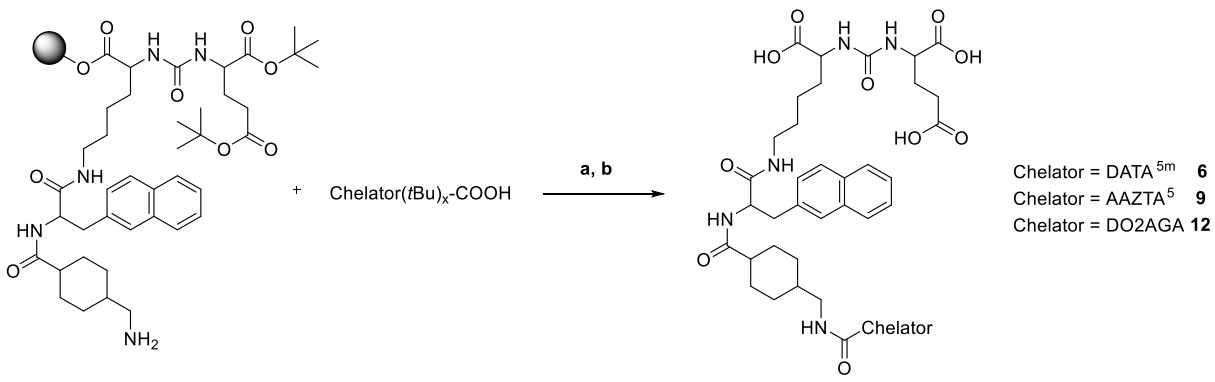

Figure 7: Conjugation of the chelators to the targeting unit 617.KuE. a) HATU, HOBt, DIPEA, DMF, RT; b) DCM / TFA, RT.

The *in vitro* binding affinities of the synthesized compounds were determined in a competitive radioligand binding assay. PSMA-positive LNCaP cells were incubated with different amounts of the compounds **1**-**12** and with a known concentration of [^{68}Ga]Ga-PSMA-10. The IC_{50} values were determined and the results are shown in table 1.

Table 1: IC_{50} values of the evaluated compounds. * Data taken from Lahnif et al.[33].

Compound	**IC_{50} (nM) ± SD (n = 3)**
1 (SAME.KuE)	35.9 ± 2.6
2 (SAME.K-EuE)	17.2 ± 5.2
3 (617.KuE)	21.5 ± 1.9
4 (DATA^{5m}.SA.KuE)*	51.1 ± 5.5
5 (DATA^{5m}.SA.K-EuE)	386.2 ± 81.0
6 (DATA^{5m}.617.KuE)	92.1 ± 11.7
7 (AAZTA^{5}.SA.KuE)*	52.1 ± 4.0
8 (AAZTA^{5}.SA.K-EuE)	178.2 ± 42.7
9 (AAZTA^{5}.617.KuE))	12.7 ± 1.7
10 (DO2AGA.SA.KuE)	20.2 ± 3.5
11 (DO2AGA.SA.K-EuE)	407.1 ± 19.2
12 (DO2AGA.617.KuE)	20.2 ± 2.6

Discussion

To compare the two squaric acid-based urea-glutamate PSMA targeting vectors SA.KuE and SA.K-EuE, we conjugated them to three different chelator moieties and evaluated the *in vivo* binding affinity towards PSMA in a competitive radioligand binding assay. We also integrated the linker and targeting vector structure of PSMA-617 in our study to compare the binding potential of our squaric acid-based

targeting vectors to the binding potential of the targeting structure of literature known reference compound PSMA-617. We divided the successful synthesized compounds **1**-**12** into four sets. The division was based on the conjugated chelator moieties. The affinities of the compounds were compared. A graphical comparison is shown in figure 8.

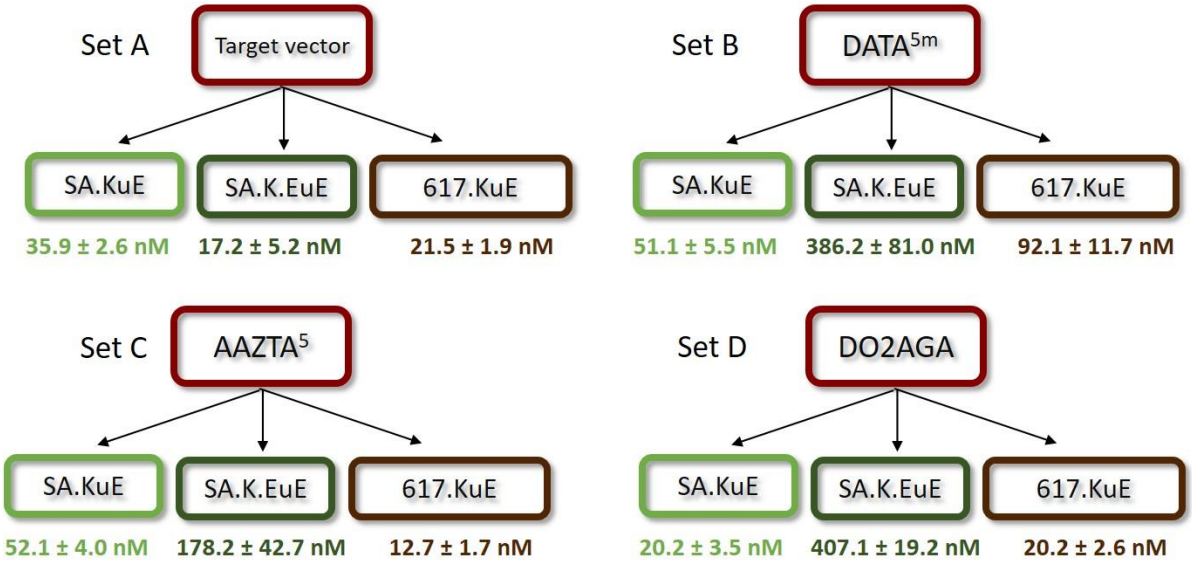

Figure 8: Graphical comparison of the IC_{50} values of all tested compounds.

If the individual IC_{50} values of the target vectors with each other in set A are compared, it is apparent that the EuE-based compound (**2**) shows the best affinity with a value of 17.2 ± 5.2 nM. However, the target vector 617.KuE (**3**) only showed a slightly lower affinity (21.5 ± 1.9 nM), which lied within the error range of the value of **2**. With an IC_{50} value of 35.9 ± 2.6 nM SA.KuE (**1**) showed the lower affinity of the three target units. It was 2-fold lower than the affinity of **2**.

The comparison of the compounds inside the sets B, C and D showed that the conjugation of a chelator can have a high influence on the binding affinity. While SA.K-EuE showed the best affinity without chelator (compound **2**), the attachment of a labelling unit led to a significant decrease in affinity. This can be seen all three sets. The IC_{50} value droped dramatically if a chelator was added to SA.K-EuE and ranked only in ranges between 178.2 ± 42.7 nM (compound **8**) and 407.1 ± 19.2 nM (Compound **11**). The chelator seems to have an important negative influence on the conformation that SA.K-EuE can form in the binding pocket. Such a consistent influence of the chelator cannot be observed with the other two targeting units SA.KuE and 617.KuE. While in set B, **4** (51.1 ± 5.5 nM) showed a nearly 2-fold higher affinity than **6** (92.1 ± 11.7 nM), in set C, **9** (12.7 ± 1.7 nM) showed a significant better affinity than **7** (52.1 ± 4.0 nM) and in set D **10** and **12** have the same affinity (20.2 ± 3.5 nM and 20.2 ± 2.6 nM, respectively). Thus, with the two targeting vectors SA.KuE and 617.KuE, no general positive or negative influence can be determined and it depends on the chelator which provides the better affinity.

In general, it cannot be said that the conjugation of a chelator leads to a general decrease or increase in affinity. Whether the chelator has positive or negative influences seems to depend on the targeting vector/chelator combination. While DATA^{5m} seems to lead to a decrease of affinity in general, the addition of AAZTA^{5} to SA.KuE (**7**) leads to a decrease and the addition to 617.KuE (**9**) leads to an increase in affinity. Since both units contain a KuE unit, the AAZTA^{5} chelator seems to have an influence on the linker arrangement in the PSMA binding pocket. It is notable that there is such a difference in the effect of DATA^{5m} and AAZTA^{5}, since both chelators only vary in one structural element. In terms of the DO2AGA compounds, the chelator shows a positive (compound **10**) or no significant influence (compound **12**) on the IC_{50} value, while the affinity of the SA.K-EuE conjugated to DO2AGA (**11**) displayed the lowest affinity among all tested compunds.

A general statement as to whether squaric acid-based KuE variants are better than the 617.KuE cannot be made due to the differences in the results.

The superiority of EuE-based PSMA inhibitors over KuE-based PSMA inhibitors, as shown by other studies[15,16], could not be confirmed by this study and rather showed the better suitability of KuE-based targeting vectors, independent of the linker structure.

It is possible that a negative influence of the celator can be reduced by adding longer linking units such as alkyl chains between the chelator and the target vector. Thus, the chelator could be in a higher distance to the binding unit and thus have less influence on the binding inside the pocket. This needs to be further evaluated.

Conclusion

In summary, nine different potential PSMA radiopharmaceuticals were designed, synthesized and their binding affinity towards PSMA was compared. The design based on three different chelators and three different PSMA inhibitor structures (set B to D). For comparison purposes the targeting units without chelator moiety were also evaluated (set A). The results show that the radiolabelling moieties have a certain influence on binding affinity. While SA.K-EuE showed without a labelling moiety the best IC_{50} value, the addition of a chelator led to a drastically decrease of affinity. For the other two targeting vector units, the influence of the chelator moiety is dependent on the chelator/targeting unit combination. Here an improvement or a decline as well as no influence can occur.

The high influence of the chelator has to be considered in the development of novel chelator conjugated PSMA inhibitors. Nevertheless, the design of the targeting unit (in combination with a

potent linker unit) is mainly responsible for the binding potential of the PSMA inhibitor, since a low affinity of the linker/targeting unit cannot be balanced by a chelator.

The published fact[15,16] that EuE-based compounds are superior to KuE-based compounds could not be confirmed in this study.

Materials and Methods

Chemicals were obtained from AcrosOrganics, AlfaAesar, Fluka, Fisher Scientific, Iris Biotech, Merck, Sigma-Aldrich, TCI and VWR. Dry solvents were purchased from VWR, Merck, AlfaAesar and AcrosOrganics. Deuterated solvents were purchased from Deutero. DO2A(*t*Bu)-GABz was obtained from ChrioBlock GmbH. All chemicals were used without further purification. Silica gel 60 F254 coated aluminium plates from Merck were used for thin layer chromatography and evaluated by fluorescence extinction at λ=254 nm or potassium permanganate staining. An Avance III HD 300 spectrometer (300 MHz, 5mm BBFO sample head with z-gradient and ATM and BACS 60 sample changer), an Avance II 400 spectrometer (400 MHz, 5mm BBFO sample head with z-Gradient and ATM and SampleXPress 60 sample changer) and an Avance III 600 spectrometer (600 MHz, 5mm TCI CryoProbe sample head with z-Gradient and ATM and SampleXPress Lite 16 sample changer) from Bruker were used for NMR measurements. Agilent Technologies 1220 Infinity LC system coupled to an Agilent Technologies 6130B Single Quadrupole LC/MS system were used for LC/MS analysis and a 7000 series Hitachi LaChrom HPLC were used for HPLC purification.

Synthesis of SAME.KuE (1, glutamate-urea-lysine-squaric acid ethylester)

The synthesis of SAME.KuE was carried out as described by Lahnif et al.[33]

Synthesis of EuE-K.SAME (2, glutamate-urea-glutamate-lysine-squaric aicd ethylester)

*2-[3-(3-benzyloxycarbonyl-1-tert-butoxycarbonyl-propyl)-ureido]-pentanedioic acid di-tert-butyl ester (**2a**)*

Triphosgene (300 mg, 0.001 mol) was dissolved in dichloromethane (6 mL). L-glutamic acid di-*tert*-butyl ester hydrochloride (920 mg, 0.0031 mol) and DIPEA (1.05 mL, 801 mg, 0.0062 mol) were dissolved in dichloromethane (10 mL) and added dropwise to the triphosgene solution over a period of 60 min at 0 °C. The solution was stirred for 15 min at 0 °C and for additional 30 min at room temperature. L-glutamic acid alpha-*tert* butyl-gamma-benzyl ester hydrochloride (1.02 g, 0.0031 mol) and DIPEA (1.05 mL, 801 mg, 0.0062 mol) were dissolved in dichloromethane (5 mL) and added to the

solution. It was stirred overnight and the solvent was removed under reduced pressure. The crude product was dissolved in ethyl acetate (20 mL) and washed with 1M $NaHCO_3$ solution (3 x 20 mL) and brine (3 x 20 mL). Ethyl acetate was dried over magnesium sulfate and removed under removed pressure. The final product **2a** was obtained after column purification (hexane / ethyl acetate, 3:1 + 3% triethylamine; R_f = 0.38) as yellow oil (1.12 g, 0.002 mol, 62%).

^{1}H-NMR (400 MHz, $CDCl_3$) δ [ppm] = 7.54 – 7.17 (m, 5H), 5.25 – 4.99 (m, 4H), 4.35 (dtd, J = 20.4, 8.0, 4.9 Hz, 2H), 4.12 (q, J = 7.1 Hz, 1H), 2.53 – 2.36 (m, 2H), 2.34 – 2.09 (m, 2H), 1.99 – 1.79 (m, 2H), 1.48 - 1.36 (m, 27H).

MS (ESI$^+$): 579.3 $[M+H]^+$, calculated for $C_{30}H_{46}N_2O_9$: 578.32 $[M]^+$.

*2-[3-(1-tert-butoxycarbonyl-propyl)-ureido]-pentanedioic acid di-tert-butyl ester (**2b**)*

Product **2a** (1.12 g, 0.002 mol) was dissolved in methanol (10 mL) and palladium on activated carbon (20 mg) was added. The solution was stirred overnight with hydrogen. Palladium on activated carbon was filtered over celite and the methanol was removed under reduced pressure. Product **2b** was used without further purification and obtained as colorless oil (0.92 g, 0.0018 mol, 90%).

MS (ESI$^+$): 489.3 $[M+H]^+$, calculated for $C_{23}H_{40}N_2O_9$: 488.27 $[M]^+$.

*tetra-tert-butyl (9S,14S,18S)-3,11,16-trioxo-1-phenyl-2-oxa-4,10,15,17-tetraazaicosane-9,14,18,20-tetracarboxylate (**2c**)*

Product **2b** (320 mg, 0.655 mmol), HATU (374 mg, 0.98 mmol), HOBt (266 mg, 1,97 mmol) and DIPEA (335 µL, 255 mg, 1.31 mmol) were dissolved in acetonitrile (5 mL). *N*(ε)-benzoyloxycarbonyl-L-lysine tert-butyl ester hydrochloride (489 mg, 1.31 mmol) was added. The solution was stirred overnight. The solvent was removed under reduced pressure and the crude product was purified by column chromatography (hexane / ethyl acetate, 1:1; R_f = 0.22) The product (**2c**) was obtained as yellow oil (361 mg, 0.48 mmol, 73%)

^{1}H-NMR (400 MHz, $CDCl_3$) δ [ppm] =.7.40 – 7.29 (m, 5H), 7.24 (s, 1H), 5.92 (d, *J* = 8.6 Hz, 1H), 5.19 (d, *J* = 9.0 Hz, 1H), 5.08 (s, 2H), 5.00 (s, 1H), 4.48 (td, *J* = 9.5, 5.4 Hz, 1H), 4.35 (ddd, *J* = 9.1, 7.6, 4.6 Hz, 1H), 4.21 (td, *J* = 9.1, 4.5 Hz, 1H), 3.18 (q, *J* = 6.5 Hz, 2H), 2.40 – 1.62 (m, 7H), 1.44 (dd, *J* = 10.4, 5.2 Hz, 37H), 1.25 (t, *J* = 7.2 Hz, 1H).

MS (ESI$^+$): 807.5 $[M+H]^+$, 829.4 $[M+Na]^+$, calculated for $C_{41}H_{66}N_4O_{12}$: 806.47 $[M]^+$.

*tetra-tert-butyl (5S,10S,14S)-1-amino-7,12-dioxo-6,11,13-triazaheptadecane-5,10,14,17-tetracarboxylate (**2d**)*

Product **2c** (361 mg, 0.48 mmol), was dissolved in ethanol (40 mL) and palladium on activated carbon (60 mg) was added. The solution was stirred with hydrogen overnight. The product was filtered over celite and the ethanol was removed under reduced pressure. The product was used without further purification. Product **2d** was obtained as yellow oil (301 mg, 0.45 mmol, 94%).

MS (ESI$^+$): 673.4 $[M+H]^+$, 695.4 $[M+Na]^+$, calculated for $C_{33}H_{60}N_4O_{10}$: 672.43 $[M]^+$.

*tetra-tert-butyl (5S,10S,14S)-1-amino(3-ethoxy-3-cyclobutene-1,2-dione)-7,12-dioxo-6,11,13-triazaheptadecane-5,10,14,17-tetracarboxylate (**2e**)*

Product **2d** (300 mg, 0.45 mmol) was dissolved in 0.5 M phosphate buffer pH 7 (10 mL). 3,4-Diethoxy-3-cyclobutene-1,2-dione (198 µL, 228 mg, 1.34 mmol) was added and the pH was adjusted to 7. Ethyl acetate (3 mL) was added and the solution was stirred for 2 days. The solvent was removed under reduced pressure and the product **2e** (304.5 mg, 0.38 mmol, 86%) was obtained as yellow oil after column chromatography (Cyclohexan / ethyl acetate, 3:1 to 1:2).

^{1}H-NMR (400 MHz, $CDCl_3$) δ [ppm] =.5.33 (s, 1H), 4.76 (q, *J* = 7.5, 7.0 Hz, 2H), 4.42 (s, 2H), 4.12 (q, *J* = 7.1 Hz, 2H), 3.43 (s, 2H), 2.41 – 2.09 (m, 2H), 2.04 (s, 3H), 1.67 – 1.54 (m, 2H), 1.50 – 1.37 (m, 36H), 1.25 (t, *J* = 7.1 Hz, 3H).

MS (ESI$^+$): 797.4 $[M+H]^+$, 819.4 $[M+Na]^+$, calculated for $C_{39}H_{64}N_4O_{13}$: 796.45 $[M]^+$.

*5S,10S,14S-1-amino(3-ethoxy-3-cyclobutene-1,2-dione)-7,12-dioxo-6,11,13-triazaheptadecane-5,10,14,17-tetracarboxylate (**EuE-K.SAME,2**)*

Product **2e** (50 mg, 0.063 mmol) was dissolved in dichloromethane (100 µL) and trifluoroacetic acid (50 µL) and stirred for one day. Additional trifluoroacetic acid was added (100 µL) and stirred for another three days. The solvent was removed under reduced pressure. Half of the batch size was used for further experiments without purification, the other half was purified via HPLC (Phenomenex Luna C18 (250 x 10 mm) 10 µm; 5 mL/min; water/acetonitrile + 0.1% TFA; 15% acetonitrile to 50% acetonitrile in 20min, R_t = 7.0 min). The final product **2** was obtained as white power (6.8 mg, 0.012 mmol, 38%).

MS (ESI$^+$): 573.3 $[M+H]^+$, calculated for $C_{23}H_{32}N_4O_{13}$: 572.20 $[M]^+$.

Synthesis of 617.KuE (3)

The synthesis of the target vector KuE conjugated to the PSMA-617 linking unit was performed as described by Benešová et al.[20,38]

Synthesis of the DO2AGA chelator

*Tert-butyl(2-aminoethyl)carbamate (**I**)*

Ethylenediamine (5.41 mL, 4.86 g, 0.081 mol) was dissolved in chloroform (40 mL). Di-*tert*-butyl dicarbonate (2.3 mL, 2.2 g, 0.01 mol) was dissolved in chloroform (20 mL) and added to the solution dropwise at atemperature of 0 °C and over a period of one hour. The Solution was stirred for 16 hours. Water (20 mL) was added and the organic phase was washed with water (3 x 20 mL) and brine (3 x 20 mL). The chloroform was dried with magnesium sulfate and the solvent was removed under reduced pressure. The product **I** was obtained as colourless oil (938 mg, 6.5 mmol, 65%).

^{1}H-NMR (400 MHz, $CDCl_3$) δ [ppm] = 4.95 (s, 1H), 3.16 (q, *J* = 5.8 Hz, 2H), 2.79 (q, *J* = 6.2 Hz, 2H), 1.43 (d, *J* = 3.1 Hz, 9H).

*(9H-fluorene-9-yl)methyl-tert-butyl-ethane-1,2-diyldicarbamate (**II**)*

Product **I** (938 mg, 6.5 mmol) was dissolved in dichlormethane (5 mL) and stirred for 30 min. Pyridine (572 µL, 562 mg, 7.1 mmol) and (fluorenylmethoxy)carbonyl chloride (1.84 g, 7.1 mmol) were added. The solution was stirred for 2 hours at room temperature. The solvent was removed under reduced pressure. The product **II** was obtained as colourless solid (1.84 g, 4.8 mmol, 74%) after column chromatography (dicloromethane / methanol, 100:1; R_f = 0.2).

^{1}H-NMR (300 MHz, $CDCl_3$) δ [ppm] = 7.79 (dt, *J* = 7.6, 0.9 Hz, 2H), 7.61 (dd, *J* = 7.5, 1.2 Hz, 2H), 7.42 (ddd, *J* = 8.5, 7.5, 1.4 Hz, 2H), 7.38 – 7.26 (m, 2H), 5.29 (d, *J* = 18.1 Hz, 1H), 4.43 (d, *J* = 6.9 Hz, 2H), 4.24 (d, *J* = 6.9 Hz, 1H), 3.30 (s, 4H), 1.47 (s, 9H).

MS (ESI$^+$): 283.1 [M+H-Boc]$^+$, calculated for $C_{22}H_{26}N_2O_4$: 382.19 [M]$^+$.

*(9H-fluorene-9-yl)methyl-(2-aminoethyl)carbamate (**III**)*

Product **II** (1 g, 2.6 mmol) was dissolved in dichloromethane. Trifluoracetic acid (5 mL) was added and stirref for 16 hours at room temperature. The solvent was removed under reduced pressure and the product **III** (716 mg, 2.5 mmol, 97%) was used without further purification.

^{1}H-NMR (400 MHz, MeOD) δ [ppm] = 7.75 (d, *J* = 7.7 Hz, 2H), 7.64 – 7.54 (m, 2H), 7.39 – 7.31 (m, 2H), 7.26 (td, *J* = 7.4, 1.2 Hz, 2H), 4.17 (t, *J* = 6.6 Hz, 1H), 3.33 (t, *J* = 5.9 Hz, 2H), 3.26 (p, *J* = 1.6 Hz, 2H), 2.98 (t, *J* = 5.9 Hz, 2H).

MS (ESI$^+$): 283.2 $[M+H]^+$, calculated for $C_{17}H_{18}N_2O_2$: 282.14 $[M]^+$.

*Tert-butyl-N-(2-chloroethyl)carbamate (**IV**)*

2-Chloroethylamine hydrochloride (1 g, 8.6 mmol) was dissolved in dichloromethane (10 mL) and cooled to 0 °C. Di-*tert*-butyl dicarbonate (1.8 mL, 1.84 g, 8.6 mmol) was added dropwise. The solution was stirred for 16 hours and washed with water (3 x 20 mL) and brine (3 x 20 mL). The organic solvent was removed under reduced pressure. Product **IV** (1.22 g, 6.7 mmol, 79%) was obtained as colourless oil and used without further purification.

^{1}H-NMR (300 MHz, $CDCl_3$) δ [ppm] = 4.95 (s, 1H), 3.59 (t, *J* = 5.6 Hz, 2H), 3.46 (t, *J* = 5.1 Hz, 2H), 1.44 (s, 9H).

5-benzyl-1-tert-butyl-2-(4,10-bis(2-(tert-butoxy)-2-oxoethyl)-7-(2-((tert-butoxycarbonyl)amino)ethyl)-1,4,7,10-tetraazacyclododecane-1-yl)pentanedioate (*DO2A(tBu)$_3$(NHBoc)-GABz, **V**)*

Compound **IV** (344 mg, 1.9 mmol), DO2A(*t*Bu)-GABz (517 mg, 0.76 mmol) and potassium carbonate (191 mg, 1.4 mmol) were dissolved in dry acetonitrile (10 mL) and stirred for 16 hours at 90 °C. The carbonate was filtered off and the solvent was removed under reduced pressure. The crude product was purified by column chromatography (hexane / ethyl acetate + 3% triethylamine, 1:1; R_f = 0.4). The product **V** (565 mg, 0.69 mmol, 90%) was obtained as yellow oil.

MS (ESI$^+$): 821.2 $[M+H]^+$, 410.9 ½$[M+H]^+$, calculated for $C_{43}H_{73}N5O_{10}$: 819.54 $[M]^+$.

*4-(4,10-bis(2-(tert-butoxy)-2-oxoethyl)-7-(2-((tert-butoxycarbonyl)amino)ethyl)-1,4,7,10-tetraaza-cyclododecane-1-yl)-5-(tert-butoxy)-5-oxopentanoic acid (DO2A(tBu)$_3$(NHBoc)-GA, **VI**)*

Product **V** (565 mg, 0.769 mmol), was dissolved in methanol (3 mL) and palladium on activated carbon (40 mg) was added. The solution was stirred with Hydrogen over night. After filtration over celite and removing the solvent under reduced pressure, the product was used without further purification. Product **VI** was obtained as colourless oil (450 mg, 0.62 mmol, 89%).

MS (ESI$^+$): 730.5 $[M+H]^+$, 752.4 $[M+Na]^+$, calculated for $C_{36}H_{67}N_5O_{10}$: 729.49 $[M]^+$.

*Di-tert-butyl 2,2'-(4-(1-(9H-fluoren-9-yl)-14,14-dimethyl-3,8,12-trioxo-2,13-dioxa-4,7-diazapentadecane-11-yl)-10-(2-((tert-butoxycarbonyl)amino)ethyl)-1,4,7,10-tetraazacyclododecane-1,7-diyl)diacetate (DO2A(tBu)$_3$(NHBoc)-GA(N-Fmoc-ethylenediamine), **VII**)*

Product **VI** (180 mg, 0.25 mmol), HATU (144 mg, 0.37 mmol) DIPEA (128 µL, 98 mg, 0.75 mmol) and HOBt (51 mg, 0.37 mmol) were dissolved in acetonitrile (2 mL) and stirred for 30 min at room temperature. Compound **III** (139 mg, 0.49 mmol) was added and the solution was stirred for 16 hours at room temperature. The solvent was removed under reduced pressure and the product **VII** (231 mg, 0.23 mmol, 93%) was obtained after column chromatography (dichloromethane / methanol + 3% triethylamine, 100:1; R_f = 0.04).

MS (ESI$^+$): 497.9 ½$[M+H]^+$, calculated for $C_{53}H_{83}N_7O_{11}$: 993.62 $[M]^+$.

*Di-tert-butyl 2,2'-(4-(5-((2-aminoethyl)amino)-1-(tert-butoxy)-1,5-dioxopentane-2-yl)-10-(2-((tert-butoxycarbonyl)amino)ethyl)-1,4,7,10-tetraazacyclododecane-1,7-diyl)diacetate (DO2A(tBu)$_3$(NHBoc)-GA(ethylenediamine), **VIII**)*

Product **VII** (231 mg, 0.23 mmol) was dissolved in dichloromethane (3 mL). The solution was stirred for 20 min with triethylamine (255 µL, 180 mg, 0.18 mmol). The solvent and the triethylamine were removed under reduced pressure and Product **VIII** (148 mg, 0.19 mmol, 85%) was obtained as colourless oil and used without further purification.

MS (ESI$^+$): 772.5 $[M+H]^+$, 795.5 $[M+Na]^+$, 386.9 ½$[M+H]^+$, calculated for $C_{38}H_{73}N_7O_9$: 771.55 $[M]^+$.

General procedure of the conjugation of chelator and target vector

Squaric acid-based conjugation (**4**, **5**, **7**, **8**, **10**, **11**)

The synthesis of DATA^{5m}-SA.KuE (**4**) can be found at Lahnif et al.[33] and the synthesis of AAZTA^{5}.SA.KuE (**7**) can be found at Greifenstein et al.[32] and these syntheses are therefore not discussed here.

*DATA^{5m}.SA.K-EuE (**5**)*

DATA^{5m}(*t*Bu)$_3$-COOH was synthesized according to Farkas et al.[39] and Lahnif et al.[33]

(5a) DATA^{5m}(*t*Bu)$_3$-COOH (100 mg, 0.17 mmol) was dissolved in dry acetonitrile (2 mL). HATU (65.4 mg, 0.17 mmol) and DIPEA (87 µL, 66 mg, 0.51 mmol) were added and stirred for 15 min. *Tert*-butyl(2-aminoethyl)carbamate (40 µL, 41 mg, 0.26 mmol) was added and stirred for an additional hour at room temperature. The solvent was removed under reduced pressure. The product **5a** (139 mg, 0.19 mmol) was obtained after column chromatography (chloroform / methanol + 1% triethylamine, 19:1; R_f = 0.24) as yellow oil.

^{1}H-NMR (400 MHz, DMSO-d_6) δ [ppm] = 7.77 (s, 1H), 6.77 (s, 1H), 3.23 (s, 6H), 3.05 - 2.94 (dt, *J* = 6.4 Hz, 2H), 2.59 -2.54 (m, 8H), 2.17 (s, 3H), 2.06 - 2.02 (t, *J* = 8.0 Hz, 2H), 1.44 - 1.38 (m, 4H), 1.20 (s, 36H).

MS (ESI$^+$): 714.5 $[M+H]^+$, calculated for $C_{36}H_{67}N_5O_9$: 713.49 $[M]^+$.

(5b) Product **5a** (139 mg, 0.19 mmol) was dissolved in dichloromethane (500 µL) and trifluoroacetic acid (500 µL) was added and stirred for 5 days. Additional trifluoroacetic acid (250 µL) was added and stirred for additional two days. The solvent was removed under reduced pressure and the product **5b** (220 mg, 0.49 mmol) was obtained as brown oil and used without further purification.

MS (ESI$^+$): 446.2 $[M+H]^+$, calculated for $C_{19}H_{35}N_5O_9$: 445.25 $[M]^+$.

Product **5b** (220 mg, 0.49 mmol) and EuE-K.SAME (**2**, 205 mg, 0.36 mmol) were dissolved in phosphate buffer (0.5 M, pH 9, 2 mL). The pH value was adjusted with 1 M NaOH solution and 1 M HCl solution. The solution was stirred over night. The solvent was removed by lyophilisation. The product **5** was purified by semi-preparative HPLC purification (column: Phenomex Luna C18 (250 x 10 mm) 10 µ, flow rate: 5 mL/min, H_2O/MeCN + 0.1% TFA, 30% MeCN to 40% MeCN in 20 min, t_R = 6.1 min) and obtained as colourless solid (26 mg, 0.03 mmol, 8%).

MS (ESI$^+$): 972.4 $[M+H]^+$, calculated for $C_{40}H_{61}N_9O_{19}$: 971.41 $[M]^+$.

*AAZTA^5.SA.K-EuE (**8**)*

AAZTA^5(*t*Bu)$_4$(NHBoc) was synthesized as described by Greifenstein et al.[32]

(8a) AAZTA^5(*t*Bu)$_4$(NHBoc) (5.5 mg, 0.0062 mmol) was dissolved in dichloromethane (500 µL) and trifluoroacetic acid (500 µL) was added and stirred for six days. Additional trifluoroacetic acid was added after two and six days. The solvent was removed under reduced pressure and the product **8a** was used without further purification.

MS (ESI$^+$): 490.2 $[M+H]^+$, calculated for $C_{20}H_{35}N_5O_9$: 489.24 $[M]^+$.

Product **8a** and EuE-K.SAME (**2**, 2.6 mg, 0.0062 mmol) were dissolved in phosphate buffer (0.5 M, pH 9, 450 µL) and stirred for 19 days. The pH value was adjusted every day with 1m NaOH solution and 1 M HCl solution. Additional EuE-K.SAME (**2**, 2.6 mg, 0.0062 mmol) was added after 10 days. The solvent was removed by lyophilisation and purified by semi-preparative HPLC purification (column: LiChrospher 100 RP18 EC (250 x 10 mm) 5 µ, flow rate: 5 mL/min, H_2O/MeCN + 0.1% TFA, 10% MeCN to 15% MeCN in 20 min, t_R = 9.6 min) The product **8** (0.43 mg, 0.00042 mmol, 7%) was obtained as colourless solid.

MS (ESI$^+$): 1016.3 $[M+H]^+$, 508.8 ½$[M+H]^+$, calculated for $C_{41}H_{61}N_9O_{21}$: 1015.40 $[M]^+$.

*DO2AGA.SA.KuE (**10**)*

(**10a**) Product **VIII** (82 mg, 0.11 mmol), EuK.SAME (**1**, 65 mg, 0.11 mmol) and DIPEA (100 µL) were dissolved in ethanol (2 mL). The solution was stirred over night. The solvent was removed under removed pressure and Product **10a** (114 mg, 0.085 mmol, 77%) was obtained as brown oil after column chromatography (ethyl acetate / methanol, 15:1 to 15:1; R_f = 0.25 (ethyl acetate / methanol, 10:1))

MS (ESI$^+$): 669.5 ½$[M+H]^+$, calculated for $C_{66}H_{116}N_{10}O_{18}$: 1336.85 $[M]^+$.

(**10**) Product **10a** was dissolved in dichloromethane (2.5 mL) and trifluoroacetic acid (400 µL). The mixture was stirred for two days. After one day, trifluoroacetic acid (400 µL) was added. The product (**10**, 4.7 mg, 0.0052 mmol, 7%) was obtained as a yellow powder after semi-preparative HPLC

purification (column: Phenomex Luna C18 (250 x 10 mm) 10 µ, flow rate: 5 mL/min, H_2O/MeCN + 0.1% TFA, 8% MeCN to 10% MeCN in 20 min, t_R = 7.6 min).

MS (ESI$^+$): 901.3 $[M+H]^+$, 451.3 ½$[M+H]^+$, calculated for $C_{37}H_{60}N_{10}O_{16}$: 900.42 $[M]^+$.

*DO2AGA.SA.K-EuE (**11**)*

Product **VIII** (10 mg, 0.013 mmol), EuE-K.SAME (**2**, 15.5 mg, 0.019 mmol) and triethylamine (10 µL) were dissolved in ethyl acetate (100 µL) and stirred over night. The solvent and triethylamine were removed under reduced pressure (Product **11a**). The residue was dissolved in dichloromethane (400 µL) and trifluoroacetic acid (10 µL) was added. The mixture was stirred for 5 days. Every day trifluoroacetic acid was added. The crude product was purified by semi-preparative HPLC purification (column: Phenomex Luna C18 (250 x 10 mm) 10 µ, flow rate: 5 mL/min, H_2O/MeCN + 0.1% TFA, 8% MeCN to 10% MeCN in 20 min, t_R = 9.0 min). The product **11** (1.1 mg, 0.0011 mmol, 8.5%) was obtained as colourless solid.

MS (ESI$^+$): 1030.4 $[M+H]^+$, 515.8 ½$[M+H]^+$, calculated for $C_{42}H_{67}N_{11}O_{19}$: 1029.46 $[M]^+$.

Conjugation to 617.KuE (**6**, **9**, **12**)

The synthesis of the resin bound target vector KuE conjugated to the PSMA-617 linking unit (resin bound 617.KuE) was performed as described by Benešová et al.[20,38]

The synthesis of AAZTA^5.617.KuE (**9**) is already described by Sinnes et al.[41] and thus are not discussed here.

*DATA^{5m}.617.KuE (**6**)*

DATA^{5m}(tBu)$_3$-COOH (52 mg, 0.09 mmol), HATU (33 mg, 0.09 mmol), HOBt (26 mg, 0.26 mmol) and DIPEA (45 µL, 34 mg, 0.26 mmol) were dissolved in DMF (2 mL) and stirred for 20 min. The resin bound 617.KuE (65 mg, 0.06 mmol) was added and stirred for two days. The solution was filtered and the resin was washed with dichloromethane. To the resin trifluoroacetic acid (2 mL) was added and stirred for 20 min. The resin was filtered off and the procedure was repeated two times. The trifluoracetic acid solutions were combined and trifluoroacetic acid was removed under reduced pressure. Product **6** (1.42 mg, 0.0014 mol, 2%) was obtained after HPLC purification (column: Phenomex Luna C18 (250 x 10 mm) 10 µ, flow rate: 5 mL/min, H_2O/MeCN + 0.1% TFA, 30% MeCN to 40% MeCN in 20 min, t_R = 5.9 min)

MS (ESI$^+$): 1041.4 $[M+H]^+$, 521.3 ½$[M+H]^+$, calculated for $C_{50}H_{72}N_8O_{16}$: 1040.51 $[M]^+$.

*DO2AGA.617.KuE (**12**)*

Product **VI** (500 mg, 0.69 mmol), HATU (259 mg, 0.69 mmol), HOBt (269 mg, 1.99 mmol) and DIPEA (229 µL, 257 mg, 1.99 mmol) were dissolved in DMF (16 mL) and stirred for 20 min at room temperature. The resin bound 617.KuE (498 mg, 0.46 mmol) was added and the mixture was stirred for four days at room temperature. The resin was filtered off and washed with dichloromethane. To the resin trifluoroacetic acid (3 mL) was added and stirred for 20 min. The resin was filtered off and the procedure was repeated two times. The trifluoracetic acid solutions were combined and trifluoroacetic acid was removed under reduced pressure. Product **12** (6.52 mg, 0.0059 mol, 1%) was obtained as colourless solid after HPLC purification (column: LiChrospher 100 RP18 EC (250 x 10 mm) 5 µ, flow rate: 5 mL/min, H_2O/MeCN + 0.1% TFA, 20% MeCN to 30% MeCN in 20 min, t_R = 15.2 min).

MS (ESI$^+$): 1100.5 $[M+H]^+$, 550.3 ½$[M+H]^+$, calculated for $C_{52}H_{78}N_{10}O_{16}$: 1098.56 $[M]^+$.

***In vitro* binding affinity studies**

The cell cultivation was performed as described by Lahnif et al.[33] According to the cell cultivation protocol by Lahnif et al.[33], the LNCaP cells (Sigma Aldrich) were cultured in RPMI 1640 medium (Thermo Fisher Scientific). 10% fetal bovine serum (Thermo Fisher Scientific), 100 µg/mL streptomycin and 100 units/mL penicillin were added to the cells and medium and incubated at 37 °C in 5% CO_2. Cells were harvested using a solution of 0.05% trypsin and 0.02% EDTA. The cells were neutralized before further experiments using serum-containing medium.

The affinity studies were performed according to a protocol of Benešová et al.[20] Here 10^5 LNCaP cells were incubated with a solution of 0.75 nM of the radiolabelled reference compound [^{68}Ga]Ga-PSMA-10 and 12 different concentrations of the compound (**1**-**12**) to be analysed. The cells were incubated for 45 min at room temperature. After the incubation ice-cold PBS was used to wash the cells and the cell-bound activity was measured. For measurement, a γ-counter (2480 WIZARD^2 Automatic Gamma Counter, PerkinElmer) was used and data were analysed using nonlinear regression in GraphPad Prism 9.

Acknowledgement

The authors acknowledge and thank Max Planck Graduate Center Mainz (MPGC) for supporting Tilmann Grus. The authors thank X.X. for supporting X.X.

References

(1) Sung, H.; Ferlay, J.; Siegel, R. L.; Laversanne, M.; Soerjomataram, I.; Jemal, A.; Bray, F. Global Cancer Statistics 2020: GLOBOCAN Estimates of Incidence and Mortality Worldwide for 36 Cancers in 185 Countries. *CA. Cancer J. Clin.* **2021**, *71* (3), 209–249.

(2) Rahbar, K.; Afshar-Oromieh, A.; Jadvar, H.; Ahmadzadehfar, H. PSMA Theranostics: Current Status and Future Directions. *Mol. Imaging* **2018**, *17*, 1536012118776068.

(3) Czarniecki, M.; Mena, E.; Lindenberg, L.; Cacko, M.; Harmon, S.; Radtke, J. P.; Giesel, F.; Turkbey, B.; Choyke, P. L. Keeping up with the Prostate-Specific Membrane Antigens (PSMAs): An Introduction to a New Class of Positron Emission Tomography (PET) Imaging Agents. *Transl. Androl. Urol.* **2018**, *7* (5), 831–843.

(4) Donin, N. M.; Reiter, R. E. Why Targeting PSMA Is a Game Changer in the Management of Prostate Cancer. *J. Nucl. Med.* **2018**, *59* (2), 177–182.

(5) Kularatne, S. A.; Wang, K.; Santhapuram, H. K. R.; Low, P. S. Prostate-Specific Membrane Antigen Targeted Imaging and Therapy of Prostate Cancer Using a PSMA Inhibitor as a Homing Ligand. *Mol. Pharm.* **2009**, *6* (3), 780–789.

(6) Barinka, C.; Rojas, C.; Slusher, B.; Pomper, M. Glutamate Carboxypeptidase II in Diagnosis and Treatment of Neurologic Disorders and Prostate Cancer. *Curr Med Chem.* **2012**, *19* (6), 856–870.

(7) Czerwińska, M.; Bilewicz, A.; Kruszewski, M.; Wegierek-Ciuk, A.; Lankoff, A. Targeted Radionuclide Therapy of Prostate Cancer-from Basic Research to Clinical Perspectives. *Molecules* **2020**, *25* (7), 1743.

(8) Pavlicek, J.; Ptacek, J.; Barinka, C. Glutamate Carboxypeptidase II: An Overview of Structural Studies and Their Importance for Structure-Based Drug Design and Deciphering the Reaction Mechanism of the Enzyme. *Curr. Med. Chem.* **2012**, *19* (9), 1300–1309.

(9) Kopka, K.; Benešová, M.; Bařinka, C.; Haberkorn, U.; Babich, J. Glu-Ureido-Based Inhibitors of Prostate-Specific Membrane Antigen: Lessons Learned during the Development of a Novel Class of Low-Molecular-Weight Theranostic Radiotracers. *J. Nucl. Med.* **2017**, *58* (Suppl 2), 17S-26S.

(10) Jackson, P. F.; Cole, D. C.; Slusher, B. S.; Stetz, S. L.; Ross, L. E.; Donzanti, B. A.; Trainor, D. A. Design, Synthesis, and Biological Activity of a Potent Inhibitor of the Neuropeptidase N-Acetylated α-Linked Acidic Dipeptidase. *J. Med. Chem*. **1996**, *39* (2), 619–622.

(11) Zhang, A. X.; Murelli, R. P.; Barinka, C.; Michel, J.; Cocleaza, A.; Jorgensen, W. L.; Lubkowski, J.; Spiegel, D. A. A Remote Arene-Binding Site on Prostate Specific Membrane Antigen Revealed by Antibody-Recruiting Small Molecules. *J. Am. Chem. Soc.* **2010**, *132* (36), 12711–12716.

(12) Kozikowski, A. P.; Nan, F.; Conti, P.; Zhang, J.; Ramadan, E.; Bzdega, T.; Wroblewska, B.; Neale, J. H.; Pshenichkin, S.; Wroblewski, J. T. Design of Remarkably Simple, yet Potent Urea-Based Inhibitors of Glutamate Carboxypeptidase II (NAALADase). *J. Med. Chem* **2001**, *44* (3), 298–301.

(13) Mosayebnia, M.; Rezaeianpour, S.; Rikhtechi, P.; Hajimahdi, Z.; Beiki, D.; Kobarfard, F.; Sabzevari, O.; Amini, M.; Abdi, K.; Shahhosseini, S. Novel and Efficient Method for Solid Phase Synthesis of Urea-Containing Peptides Targeting Prostate Specific Membrane Antigen (PSMA) in Comparison with Current Methods. *Iran. J. Pharm. Res.* **2018**, *17* (3), 917–926.

(14) Kularatne, S. A.; Zhou, Z.; Yang, J.; Post, C. B.; Low, P. S. Design, Synthesis, and Preclinical Evaluation of Prostate-Specific Membrane Antigen Targeted ^{99m}Tc-Radioimaging Agents. *Mol. Pharm.* **2009**, *6* (3), 790–800.

(15) Hillier, S. M.; Maresca, K. P.; Lu, G.; Merkin, R. D.; Marquis, J. C.; Zimmerman, C. N.; Eckelman, W. C.; Joyal, J. L.; Babich, J. W. ^{99m}Tc-Labeled Small-Molecule Inhibitors of Prostate-Specific Membrane Antigen for Molecular Imaging of Prostate Cancer. *J. Nucl. Med.* **2013**, *54* (8), 1369–1376.

(16) Robu, S.; Schmidt, A.; Eiber, M.; Schottelius, M.; Günther, T.; Hooshyar Yousefi, B.; Schwaiger, M.; Wester, H. J. Synthesis and Preclinical Evaluation of Novel ^{18}F-Labeled Glu-Urea-Glu-Based PSMA Inhibitors for Prostate Cancer Imaging: A Comparison with ^{18}F-DCFPyl and ^{18}F-PSMA-1007. *EJNMMI Res.* **2018**, *8*, 30.

(17) Weineisen, M.; Schottelius, M.; Simecek, J.; Baum, R. P.; Yildiz, A.; Beykan, S.; Kulkarni, H. R.; Lassmann, M.; Klette, I.; Eiber, M.; Schwaiger, M.; Wester, H. J. ^{68}Ga-and ^{177}Lu-Labeled PSMA i and T: Optimization of a PSMA-Targeted Theranostic Concept and First Proof-of-Concept Human Studies. *J. Nucl. Med.* **2015**, *56* (8), 1169–1176.

(18) Eder, M.; Schäfer, M.; Bauder-Wüst, U.; Hull, W. E.; Wängler, C.; Mier, W.; Haberkorn, U.; Eisenhut, M. ^{68}Ga-Complex Lipophilicity and the Targeting Property of a Urea-Based PSMA Inhibitor for PET Imaging. *Bioconjug. Chem.* **2012**, *23* (4), 688–697.

(19) Afshar-Oromieh, A.; Holland-Letz, T.; Giesel, F. L.; Kratochwil, C.; Mier, W.; Haufe, S.; Debus, N.; Eder, M.; Eisenhut, M.; Schäfer, M.; Neels, O.; Hohenfellner, M.; Kopka, K.; Kauczor, H. U.; Debus, J.; Haberkorn, U. Diagnostic Performance of ^{68}Ga-PSMA-11 (HBED-CC) PET/CT in Patients with Recurrent Prostate Cancer: Evaluation in 1007 Patients. *Eur. J. Nucl. Med. Mol. Imaging* **2017**, *44* (8), 1258–1268.

(20) Benešová, M.; Schäfer, M.; Bauder-Wüst, U.; Afshar-Oromieh, A.; Kratochwil, C.; Mier, W.; Haberkorn, U.; Kopka, K.; Eder, M. Preclinical Evaluation of a Tailor-Made DOTA-Conjugated PSMA Inhibitor with Optimized Linker Moiety for Imaging and Endoradiotherapy of Prostate Cancer. *J. Nucl. Med.* **2015**, *56* (6), 914–920.

(21) Schmidkonz, C.; Hollweg, C.; Beck, M.; Reinfelder, J.; Goetz, T. I.; Sanders, J. C.; Schmidt, D.; Prante, O.; Bäuerle, T.; Cavallaro, A.; Uder, M.; Wullich, B.; Goebell, P.; Kuwert, T.; Ritt, P. ^{99m}Tc-MIP-1404-SPECT/CT for the Detection of PSMA-Positive Lesions in 225 Patients with Biochemical Recurrence of Prostate Cancer. *Prostate* **2018**, *78* (1), 54–63.

(22) Wurm, F. R.; Klok, H. A. Be Squared: Expanding the Horizon of Squaric Acid-Mediated Conjugations. *Chem. Soc. Rev.* **2013**, *42* (21), 8220–8236.

(23) Agnew-Francis, K. A.; Williams, C. M. Squaramides as Bioisosteres in Contemporary Drug Design. *Chem. Rev.* **2020**, *120* (20), 11616–11650.

(24) Grus, T.; Lahnif, H.; Klasen, B.; Moon, E.-S.; Greifenstein, L.; Roesch, F. Squaric Acid-Based Radiopharmaceuticals for Tumor Imaging and Therapy. *Bioconjug. Chem.* **2021**, *32* (7), 1223–1231.

(25) Klasen, B.; Moon, E. S.; Rösch, F. AAZTA^5-Squaramide Ester Competing with DOTA-, DTPA- and CHX-A-DTPA-Analogues: Promising Tool for ^{177}Lu-Labeling of Monoclonal Antibodies under Mild Conditions. *Nucl. Med. Biol.* **2021**, *96–97*, 80–93.

(26) Klasen, B.; Lemcke, D.; Mindt, T. L.; Gasser, G.; Rösch, F. Development and in Vitro Evaluation of New Bifunctional ^{89}Zr-Chelators Based on the 6-Amino-1,4-Diazepane Scaffold for Immuno-PET Applications. *Nucl. Med. Biol.* **2021**, *102–103*, 12–23.

(27) Moon, E. S.; Elvas, F.; Vliegen, G.; De Lombaerde, S.; Vangstel, C.; De Bruycker, S.; Bracke, A.; Eppard, E.; Greifenstein, L.; Klasen, B.; Kramer, V.; Staelens, S.; De Meester, I.; Van Der Veken, P.; Roesch, F. Targeting Fibroblast Activation Protein (FAP): Next Generation PET Radiotracers Using Squaramide Coupled Bifunctional DOTA and DATA^{5m} Chelators. *EJNMMI Radiopharm Chem.* **2020**, *5*, 19.

(28) Moon, E. S.; Rymenant, Y. Van; Battan, S.; Loose, J. De; Bracke, A.; Van Der Veken, P.; De Meester, I.; Rösch, F. In Vitro Evaluation of the Squaramide-Conjugated Fibroblast Activation Protein Inhibitor-Based Agents AAZTA^5.SA.FAPi and DOTA.SA.FAPi. *moleules* **2021**, *26* (12), 3482.

(29) Ballal, S.; Yadav, M. P.; Kramer, V.; Moon, E. S.; Roesch, F.; Tripathi, M. A Theranostic Approach of [^{68}Ga]Ga-DOTA.SA.FAPi PET/CT-Guided [^{177}Lu]Lu-DOTA.SA.FAPi Radionuclide Therapy in an End-Stage Breast Cancer Patient : New Frontier in Targeted Radionuclide Therapy. *Eur. J. Nucl. Med. Mol. Imaging* **2021**, *48* (3), 942–944.

(30) Kreppel, B.; Gaertner, F. C.; Marinova, M.; Attenberger, U.; Meisenheimer, M.; Toma, M.; Kristiansen, G.; Feldmann, G.; Moon, E. S.; Roesch, F.; Van Der Veken, P.; Essler, M. [^{68}Ga]Ga-DATA^{5m}.SA.FAPi PET/CT: Specific Tracer-Uptake in Focal Nodular Hyperplasia and Potential Role in Liver Tumor Imaging. *Nuklearmedizin* **2020**, *59* (05), 287–389.

(31) Greifenstein, L.; Engelbogen, N.; Lahnif, H.; Sinnes, J.-P.; Bergmann, R.; Bachmann, M.; Rösch, F. Synthesis, Labeling and Preclinical Evaluation of a Squaric Acid Containing PSMA-inhibitor Labeled with ^{68}Ga – a Comparison with PSMA-11 and PSMA-617. *ChemMedChem* **2020**, *15* (8), 695–704.

(32) Greifenstein, L.; Grus, T.; Nagel, J.; Sinnes, J. P.; Rösch, F. Synthesis and Labeling of a Squaric Acid Containing PSMA-Inhibitor Coupled to AAZTA^5 for Versatile Labeling with ^{44}Sc, ^{64}Cu, ^{68}Ga and ^{177}Lu. *Appl. Radiat. Isot.* **2020**, *156*, 108867.

(33) Lahnif, H.; Grus, T.; Pektor, S.; Greifenstein, L.; Schreckenberger, M.; Rösch, F. Hybrid Chelator-Based PSMA Radiopharmaceuticals: Translational Approach. *Molecules* **2021**, *26* (21), 6332.

(34) Seemann, J.; Waldron, B.; Parker, D.; Roesch, F. DATATOC: A Novel Conjugate for Kit-Type ^{68}Ga Labelling of TOC at Ambient Temperature. *EJNMMI Radiopharm. Chem.* **2017**, *1*, 4.

(35) Seemann, J.; Waldron, B. P.; Roesch, F.; Parker, D. Approaching “kit-Type” Labelling with ^{68}Ga: The DATA Chelators. *ChemMedChem* **2015**, *10* (6), 1019–1026.

(36) Sinnes, J.; Nagel, J.; Rösch, F. AAZTA^5/AAZTA^5-TOC: Synthesis and Radiochemical Evaluation with ^{68}Ga, ^{44}Sc and ^{177}Lu. *EJNMMI Radiopharm Chem.* **2019**, *4*, 18.

(37) Fakiri, M. El; Geis, N. M.; Ayada, N.; Eder, M.; Eder, A. C. PSMA-Targeting Radiopharmaceuticals for Prostate Cancer Therapy: Recent Developments and Future Perspectives. *Cancers.* **2021**, *13* (16), 3967.

(38) Benešová, M.; Bauder-Wüst, U.; Schäfer, M.; Klika, K. D.; Mier, W.; Haberkorn, U.; Kopka, K.; Eder, M. Linker Modification Strategies to Control the Prostate-Specific Membrane Antigen (PSMA)-Targeting and Pharmacokinetic Properties of DOTA-Conjugated PSMA Inhibitors. *J. Med. Chem.* **2016**, *59* (5), 1761–1775.

(39) Farkas, E.; Nagel, J.; Waldron, B. P.; Parker, D.; Tóth, I.; Brücher, E.; Rösch, F.; Baranyai, Z. Equilibrium, Kinetic and Structural Properties of Gallium(III) and Some Divalent Metal Complexes Formed with the New DATA^m and DATA^{5m} Ligands. *Chem. Eur. J.* **2017**, *23* (43),

10358–10371.

(40) Greifenstein, L.; Späth, D.; Sinnes, J. P.; Grus, T.; Rösch, F. Mild and Efficient ^{64}Cu Labeling of Perhydro-1, 4-Diazepine Derivatives for Potential Use with Large Peptides, Proteins and Antibodies. *Radiochim. Acta* **2020**, *108* (7), 555–563.

(41) Sinnes, J. P.; Bauder-Wüst, U.; Schäfer, M.; Moon, E. S.; Kopka, K.; Rösch, F. ^{68}Ga, ^{44}Sc and ^{177}Lu-Labeled AAZTA^{5}-PSMA-617: Synthesis, Radiolabeling, Stability and Cell Binding Compared to DOTA-PSMA-617 Analogues. *EJNMMI Radiopharm. Chem.* **2020**, *5*, 28.

5. Conclusion

The aim of this project was the development, improvement and application of urea-glutamate-based PSMA inhibitors for the diagnosis and therapy of prostate cancer. This dissertation also attempts to provide solutions to the remaining problems and issues in the field of PSMA inhibitor-based imaging and therapy of prostate cancer. These problems include the search for compounds with high PSMA affinity and no enrichment in other tissues like salivary glands, enableing higher tomour doses or the search for suitable drug delivery systems for a targeted drug delivery directly to the PCa cells. Other addressed problems are the efficient therapy of PCa related bone metastases and the development of kit-labelable compounds.

This work presents alternatives to already existing and literature-known PSMA radiopharmaceuticals, evaluates them regarding synthesis, radiolabelling, *in vitro* and *in vivo* behaviour and compares them with reference compounds known in literature. For this purpose different chelators were conjugated to various urea-based PSMA inhibitors via linking units (project A and D). Novel PSMA ligands have been developed and evaluated in this work of which some compounds have been found with similar or even better properties in comparison to common used PSMA ligands. For example, [^{68}Ga]Ga-DATA^{5m}.SA.KuE showed better pharmacokinetic properties regarding kidney clearance in comparison to [^{68}Ga]Ga-PSMA-11, which is used in clinical routine.

Furthermore, this work presents novel approaches to addressing known problems, such as the heterogeneous expression of PSMA in PCa related bone metastases (project B). If PCa related bone metastases show a low or even no expression of PSMA, a treatment with the highly potent [^{177}Lu]Lu-PSMA-617 is difficult or not possible. To overcome this problem, a PSMA inhibitor was combined with a bisphosphonate targeting vector. This compound combine the enrichment mechanism of [^{177}Lu]Lu-PSMA-617 with the enrichment mechanism of bisphosphonates which are accumulated in regions with high bone metabolism as found in bone metastases.

This work also uses the already known concept of drug delivery and presents two approaches that make this principle possible for application in prostate cancer treatment (project C). Here, liposomes are functionalized with a PSMA targeting vector to enable a targeted transport of the liposomes to the cancer cells. Furthermore, an approach for targeted transport of a cytotoxic agent bound to a PSMA inhibitor is described.

A widely used linker in this work is squaric acid. Squaric acid is commonly used in a lot of different conjugation approaches in chemistry[1] but gains little attention in radiopharmacy. First squaric acid containing PSMA-radiopharmaceuticals were introduced by Engelbogen and Greifenstein.[2–5] A large

part of this dissertation deals with the evaluation and further development of squaric acid-based PSMA inhibitors and their application.

All in all, novel PSMA radiopharmaceuticals with improved properties and novel PSMA inhibitor containing approaches to overcome known problems are presented, which could lead to an improved diagnosis and therapy of prostate cancer. The preclinical investigations of some subprojects are completed and the next step is the translation into clinic.

In the following, the results of all individual projects are shortly summarised.

5.1 Project A: Hybrid chelator conjugated PSMA inhibitors

The aim of this project was the synthesis of hybrid chelator conjugated KuE inhibitors. The hybrid chelator DATA^{5m} was mainly used in this project. DATA^{5m} shows optimal labelling conditions with gallium-68. This radiometal is one of the most important PET nuclides. It is known that the radiolabelling of DATA^{5m} with gallium-68 provides fast kinetics at mild conditions and stabile complexes, making it interesting for potential kit-type like applications.[6,7]

In the publication *Hybrid chelator-based PSMA-radiopharmaceuticals: translational approach*[8] the synthesis of DATA^{5m}.SA.KuE is described. Here, the actual PSMA inhibitor KuE was linked via a squaramide linker to the DATA^{5m} chelator. The use of squaric acid as linking unit and coupling reagent enables not only a simplified syntheses due to the selectivity towards amines, the synthesis at mild conditions and the pH controlled asymmetric amidation, it also allows a synthesis without side products.[5] Squaric acid can also interact with the PSMA binding pocket due to its aromatic character and have a positive influence on the binding affinity of the molecule. The quantitative radiolabelling of DATA^{5m}.SA.KuE with gallium-68 was possible at mild conditions and the complex showed a high stability over 2 hours in PBS as well as in human serum.

The *in vitro* and *in vivo* evaluation of DATA^{5m}.SA.KuE was done along AAZTA^{5}.SA.KuE. This compound was synthesized and radiolabelled with scandium-44 and lutetium-177 in a previous work.[5] The hybrid chelator AAZTA^{5}, in contrast to DATA^{5m} allows the radiolabelling of diagnostic as well as therapeutic radionuclides. Both compounds were evaluated regarding *in vitro* binding affinity and internalisation ratio and compared with the reference compound PSMA-11. Although both DATA^{5m}.SA.KuE and AAZTA^{5}.SA.KuE displayed a 2-fold lower affinity than PSMA-11 (51.1 ± 5.5 nM and 52.1 ± 4.0 nM vs. 26.2 ± 2.4 nM), a similar internalisation ratio was found for all compounds ([^{68}Ga]Ga-DATA^{5m}.SA.KuE = 6.6 ± 0.6%, [^{44}Sc]Sc-AAZTA^{5}.SA.KuE = 4.8% and [^{68}Ga]Ga-PSMA-11 = 5.2%). *In vivo* studies in PSMA-positive LNCaP tumour bearing Balb/c nude mice showed a similar tumour uptake of all compounds.

Notable was the significant lower kidney uptake of the SA.KuE-based compounds (between 13.63 ± 6.81% ID/g and 22.70 ± 0.90% ID/g) in contrast to [^{68}Ga]Ga-PSMA-11 (73.69 ± 18.77% ID/g). This showed that the SA.KuE compounds have a fast renal excretion and a tumour accumulation, which does not underperform [^{68}Ga]Ga-PSMA-11. Thus, [^{68}Ga]Ga-DATA^{5m}.SA.KuE is an interesting novel compound for PET imaging and the pair of [^{44}Sc]Sc-AAZTA^{5}.SA.KuE and [^{177}Lu]Lu-AAZTA^{5}.SA.KuE are promising candidates for future theranostic applications. Here, further studies are necessary to verify these first results of this promising study.

In the manuscript *[^{68}Ga]Ga-DATA^{5m}-PSMA-617 as novel diagnostic kit-based counterpart for [^{177}Lu]Lu-PSMA-617* the DOTA chelator of PSMA-617 is replaced by the chelator DATA^{5m} to develop a PSMA radiopharmaceutical which can be labelled fast and under mild conditions in a kit-labelling like approach. The compound carries the highly potent target vector and linking unit of the well-known PSMA-617. Applied in kit applications, a diagnostic counterpart to the therapeutic [^{177}Lu]Lu-PSMA-617 with the same pharmacophore unit and thus same pharmacokinetic properties could be made available for clinical routine.

The pharmacophore unit of PSMA-617 was synthesized on a resin and conjugated to DATA^{5m}. Radiochemical evaluation showed an efficient labelling of DATA^{5m}-PSMA-617 with gallium-68 under mild conditions and with fast reaction times. Quantitative yields were obtained after already three minutes. The labelled compound also showed a high purity of > 99% after the labelling, thus no further purification was necessary. This is an important aspect for the suitability for a use in kit labelling. The complex was also stable in human serum, NaCl and PBS for at least 90 min. It was not possible to reproduce the radiolabelling results of the thesis of J-P. Sinnes.[9] This could be due to a different generator system and setting.

In vitro PSMA affinity studies showed that DATA^{5m}-PSMA-617 (92.1 ± 11.7 nM) showed a lower affinity than PSMA-11 (26.2 ± 2.4 nM) and (DOTA)-PSMA-617 (15.9 ± 5.1 nM). DATA^{5m}-PSMA-617 and (DOTA)-PSMA-617 only vary in the chelator, thus the DATA^{5m} chelator seems to have a high influence towards the PSMA affinity. It is in accordance to previous studies. The comparison of the affinity DOTAGA.SA.KuE (17.6 ± 5.1 nM)[3] and DATA^{5m}.SA.KuE (51.1 ± 5.5 nM)[8] also showed a significant lower affinity of DATA^{5m}. J-P. Sinnes found a similar affinity of PSMA-617 in comparison to the DATA^{5m} containing compound (21.5 ± 1.15 nM).[9] This result was not found in the present study and can be due to differences in the implementation protocol and handling of the assay. J-P. Sinnes just conducted initial labelling and affinity experiments. Thus, comparison of the other and more detailed results of the present study is not possible.

In the present study, we also investigated the lipophilicity of the two compounds. The lipophilicity of DATA^{5m}-PSMA-617 was higher than the lipophilicity of PSMA-617. The different lipophilicity could led to different binding conditions in the PSMA binding pocket and thus may led to the found differences in binding affinity. The DATA^{5m} chelator seemed to have an influence on the conformation of the pharmacophore unit inside the binding pocket. Thus, in further studies a spacer, such as an alkyl chain, could be introduced between DATA^{5m} and the targeting unit. This introduction of a spacer could lead to a longer distance between both units and thus could reduce the influence of the chelator. Additionally, units, such as PEG groups that have an influence on lipophilicity could be added to the DATA^{5m} compound to adjust the lipophilicity.

All the findings indicate that the novel compound is a promising diagnostic counterpart to [^{177}Lu]Lu-PSMA-617. Further *in vivo* examinations are necessary to evaluate the *in vivo* behaviour of [^{68}Ga]Ga-DATA^{5m}-PSMA-617. In cooperation with the radiochemical studies laboratory, INRASTES NCSR "Demokritos" in Athens, Greece such animal studies are ongoing. *Ex vivo* biodistribution studies are being conducted to compare the tumour accumulation of [^{68}Ga]Ga-DATA^{5m}-PSMA-617 and [^{68}Ga]Ga-PSMA-617. Unfortunately, at the time of submission of this dissertation, the studies have not been finished and no results can be shown.

5.2 Project B: Prostate cancer and related bone metastases

Since most men with late stage prostate cancer will develop bone metastases, it is a crucial aspect to find potent treatment methods to treat both, the primary tumour as well as the bone metastases.[10] Unfortunately, the PSMA expression in PCa related bone metastases can vary.[11,12] In nuclear medicine, [^{177}Lu]Lu-PSMA-617 is a highly potent PSMA radiopharmaceutical, which shows very good results in the therapy of prostate cancer.[13] But, if the formed bone metastases show no or only low PSMA expression, a therapy with [^{177}Lu]Lu-PSMA-617 is challenging.[14] Novel strategies for treatment of heterogeneous bone metastases with low PSMA expression are to be found.

In the manuscript *DOTA conjugate of bisphosphonate and PSMA-inhibitor: A promising combination for therapy of prostate cancer related bone metastases* a novel compound is presented which can address this problem. The novel compound DOTA-L-Lys(SA.Pam)-PSMA-617 consists of three structural elements. These are the PSMA inhibitor structure of PSMA-617 for targeting of PSMA and third generation bisphosphonate SA.Pam, which can bind to HAP, the mineral structure of bones. HAP is exposed in areas of high bone metabolism, as it is also found at bone metastases. The bisphosphonate pamidronate (Pam) is conjugated to the rest of the molecule via a squaramide, which also shows a

positive influence on the HAP binding of Pam. The third essential structure element is a DOTA chelator, which enables the radiolabelling of the compound with nuclides like lutetium-177.

After successful synthesis, radiolabelling properties were evaluated. The compound displayed radiochemical yields of over 90% with lutetitium-177 in five minutes and the complex was stable in PBS, NaCl and human serum for at least 14 days. The lipophilicity of the novel compound was comparable to the lipophilicity of [^{177}Lu]Lu-PSMA-617. In the next step, the binding to HAP was evaluated in a HAP binding assay. The binding of the novel ^{177}Lu-labelled compound was compared to the HAP binding of [^{177}Lu]Lu-PSMA-617 and free lutetium-177. With a binding of over 98%, [^{177}Lu]Lu-DOTA-L-Lys(SA.Pam)-PSMA-617 showed a very strong affinity towards HAP. This HAP affinity is comparable to the binding of free lutetium-177 (99.89 ± 0.02%), which is known for a high HAP affinity. [^{177}Lu]Lu-PSMA-617 showed no binding to the crystalline HAP structure (1.20 ± 0.30%). This is as expected, since [^{177}Lu]Lu-PSMA-617 has no structural element that have HAP affinity and thus [^{177}Lu]Lu-PSMA-617 can only accumulate in bone metastases with PSMA expression. The same experiment with prior blocking of HAP with another bisphosphonate showed that the binding of [^{177}Lu]Lu-DOTA-L-Lys(SA.Pam)-PSMA-617 and free lutetium-177 is a selective HAP binding and no significant unselective binding occurred, since the two probes determined only a very low binding in the blocking studies. In comparison to other literature-known bisphosphonate compounds, [^{177}Lu]Lu-DOTA-L-Lys(SA.Pam)-PSMA-617 exhibited a very high HAP affinity.

The binding affinity (K_i value) of the novel heterodimeric compound, determined in an *in vitro* competitive binding assay, was lower than the affinity of PSMA-617 (K_i values: 52.6 ± 3.5 nM vs. 6.9 ± 1.3 nM; IC_{50} values: 64.4 ± 4.3 nM vs. 15.9 ± 5.1 nM). Additionally, the SA.Pam unit seems to have an influence on the affinity, since the affinity of the precursor molecule without the SA.Pam unit had a more than twice as high K_i value (19.7 ± 3.3 nM; IC_{50}: 24.1 ± 4.1 nM) than the final SA.Pam containing compound.

The tumour and bone accumulation were determined in LNCaP tumour-bearing mice to evaluate the *in vivo* potential of the novel compound. The compound demonstrated a tumour uptake of 4.2 ±0.7% ID/g which is lower than the literature tumour uptake of [^{177}Lu]Lu-PSMA-617 (11.2 ± 4.17% ID/g).[15] This reflects differences in the K_i values with a better PSMA binding of [^{177}Lu]Lu-PSMA-617. This differences can also be due to differences in the assay, since the compared tumour uptake value of [^{177}Lu]Lu-PSMA-617 is taken from literature. [^{177}Lu]Lu-PSMA-617 showed no HAP binding and consequently, no bone uptake was observed and thus, this compound did not accumulate in bone metastases without PSMA expression. In contrast to that, [^{177}Lu]Lu-DOTA-L-Lys(SA.Pam)-PSMA-617 showed a bone uptake of 3.4 ± 0.4% ID/g, which is comparable to other literature-known bisphosphonates, such as [^{177}Lu]Lu-DOTA^{ZOL}.[16] This showed that,

in contrast to [^{177}Lu]Lu-PSMA-617, the novel compound have the possibility for accumulate via both mechanisms in bone metastases. The significantly higher kidney uptake of the novel compound in contrast to [^{177}Lu]Lu-DOTA^{ZOL} can be explained with the physiological existence of PSMA in the kidneys.

Although the PSMA affinity and tumour accumulation of [^{177}Lu]Lu-PSMA-617 are higher than [^{177}Lu]Lu-DOTA-L-Lys(SA.Pam)-PSMA-617, the novel compound is a potential candidate for future therapy of PCa related bone metastases. It demonstrated favourable properties for the therapy of bone metastases using two independent targeting mechanisms and could contribute to the care of patients with PCa related bone metastases. This is especially the case, if PSMA expression is too low for a successful therapy with known PSMA radiopharmaceuticals or unclear PSMA level. In future the findings of this initial study needs to be further investigated by additional investigations. Additionally, since DOTA can also be radiolabelled with other radionuclides than lutetium-177, the radiolabelling of the compound with diagnostic nuclides can be investigated, enabling a theranostic approach.

5.3 Project C: PSMA inhibitor conjugated drug delivery systems

A frequently used concept in oncology is the use of drug delivery systems for a targeted transport of a drug to its place of effect. There are different ways to realise such a drug delivery system. A drug, in particular a cytotoxic drug, can be covalently bound to a cleavable linker and a targeting vector (SMDC). The targeting vector is responsible for specific transport and the drug is realised by cleavage of the linker by special conditions in the area of interest.[17] Another approach is the inclusion of the drug in nanoparticles such as liposomes.[18] This systems have some advantages over a systemic application of a cytostatic drug. Since the drug can only effect the targeted area or tissue, side effects are reduced and bioavailability of drugs can be increased by this concepts too.[19] The difference of both delivery systems is the size and the ratio of target vector and transported drug. While a SMDC contains one drug molecule and one targeting unit, a liposome can contain a certain number of drug molecules and more than one targeting units. A schematic comparison is shown in figure 24.

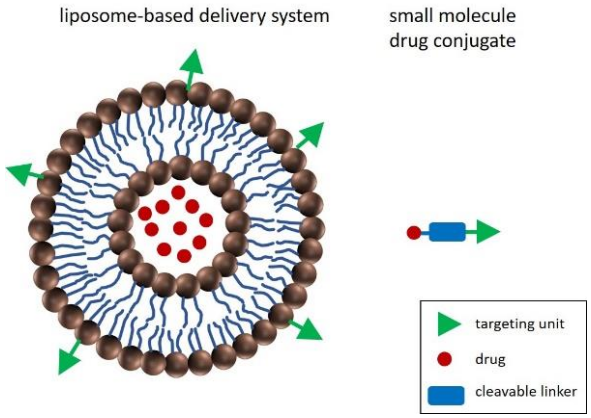

Figure 24: Schematic comparison of a liposme-based drug delivery system and a small molecule durg delivery system (Figure not true to scale). SMDC carries one drug and one targeting vector. In liposome-based delivery systems, the numbers of targeting vectors and transported drug can vary, depending on preparation.

In the manuscript *^{18}F-labeled, PSMA-specific liposomes: promising and PET-traceable tool for future targeted drug delivery in the treatment of prostate cancer,* a proof-of-principle study for the application of drug-loaded liposomes for the targeted transport to prostate cancer cells were demonstrated. The aim was to synthesize liposomes out of hyperbranched polyglycerols with hydrophobic alkyl chain anchors (BisHD-*hb*PG) block copolymers, which are functionalised with a PSMA inhibitor for the targeted delivery and with an ^{18}F-label to evaluate the behaviour of the novel PSMA inhibitor liposome in PET measurements *in vivo*. The radiolabelling and liposome formation of the PSMA inhibitor containing liposome should be compared with a liposome without a PSMA inhibitor. For the synthesis of the PSMA inhibitor carrying polymer, the BisHD-*hb*PG polymer which carries alkyne groups (provided by the group of Prof. Frey, Uni Mainz) were functionalized with previous synthesized PSMA targeting vector azide.SA.KuE in a CuAAC reaction. After purification via spin filtration the PSMA inhibitor containing polymer as well as the PSMA inhibitor free polymers were functionalised with [^{18}F]F-TEG-azide via CuAAC for PET imaging. The radiochemical yield of the PSMA inhibitor caring polymer (73% RCY) was comparable to the radiochemical yield of the free polymer (81%). Afterwards liposome formation was carried out in an aqueous solution via a thin film hydration method. For liposome stabilisation, DOPC and cholesterol were added. Liposomes which are obtained by this method have different sizes. To obtain only one-sized liposomes, an extrusion mechanism was used, in which the liposomes were passed through different-sized membranes. After a fractionated size exclusion chromatography to remove smaller unwanted components such as unassembled polymers, the purified ^{18}F-labelled liposomes were obtained. The KuE.SA functionalised liposomes were obtained in a RCY of 25% and the non-functionalised liposomes with a RCY of 14%.

Important to consider is that the pharmacokinetic properties of a liposome is dependent on the size. Sizes of 100 to 200 nm showed the best pharmacokinetic properties with the lowest enrichment in

tissues such as liver.[20,21] With sizes of 199.1 nm of the KuE containing liposome and 157.5 nm of the non-functionalised liposome, the sizes of the evaluated liposomes were favourable and enable a good transport of the potential payload of the liposomes. In this study it was shown that liposomes with a PSMA targeting unit can be synthesized and radiolabelled with fluorine-18 for PET *in vivo* evaluation of the liposome behaviour. These liposomes enable a drug delivery approach targeted towards PCa cancer cells.

In future studies, the *in vivo* behaviour of the KuE-containing liposomes should be evaluated in PSMA positive tumour-bearing mice via PET and should be compared to the PSMA inhibitor free liposomes. Furthermore, in additional studies the incorporation of drugs into the liposomes have to be evaluated and the therapeutic effect should be tested *in vivo*.

The manuscript *Old drug, new delivery strategy: MMAE repacked* deals with the development of a small molecule drug delivery system. In such systems, a targeting vector is responsible for targeted drug delivery. The drug is covalently bound to the targeting vector via a cleavable linker, which is cleaved in the tumour cell by defined conditions and the drug is released by this mechanism. In this study, the compound design of MMAE.VC.SA.617 should combine several structural features. The targeting and linker unit of PSMA-617 is used as targeting unit, since it shows high affinity towards PSMA. It is conjugated via a squaramide which should introduce increased pharmacokinetic properties as found in previous studies (project A). The cytotoxic drug MMAE is conjugated to the squaramide through the enzymatic cleavable linker valine-citrulline, which is responsible for drug release in the prostate cancer cell.

After the successful synthesis of MMAE.VC.SA.617, the compound was evaluated regarding its binding affinity towards PSMA. In comparison to PSMA-617, the affinity of the drug conjugate was nine times lower (21.5 ± 1.9 nM for PSMA-617 and 188.6 ± 24.7 nM for MMAE.VC.SA.617). This extreme difference can only be explained by a high influence of the parts of the molecule which are not involved in PSMA binding. The PSMA-617 binding motive is designed to address all affinity increasing binding areas in the binding pocket. The additional DOTA chelator seems to have no significant influence. The situation is different for MMAE.VC.SA.617. It has a big molecule part with a high molecule mass which is not involved in PSMA binding and could have a steric influence. For example a steric hindrance of MMAE or the cleavable linker could prevent the binding of naphthyl unit to the aromatic binding area of PSMA, leading to a significant decrease in affinity. Introduction of a long spacer unit between the cleavable linker and the targeting unit, such as an alkyl chain, could result in the non-binding part being outside the pocket and having no influence on the affinity.

The cytotoxicity of the novel drug delivery system was evaluated *in vitro* via a CellTiter-Blue® assay using PSMA positive LNCaP cells. MMAE.VC.SA.617 showed with an IC_{50} value of 33.0 ± 4.9 nM a lower cytotoxicity than the free MMAE (0.23 ± 0.06 nM). This could be due to differences in the uptake mechanism of both compounds. A PSMA blocking study with PMPA showed that blocked PSMA led to a decreased cytotoxicity. This proved that the compound is indeed mainly taken up via PSMA internalization and confirmed the suitability of our novel compound as PSMA driven drug delivery system. A blocking of cathepsin B, also led to a decrease in affinity (84.4 ± 0.1 nM), showing that the release of MMAE is based on the cleavage of the valine-citrulline linker by cathepsin B. This was also verified in a cathepsin B cleavage assay. The addition of cathepsin B to a solution of MMAE.VC.SA.617 led to an increasing amount of free MMAE in the probe over the time. Complete release was reached after 20 min.

Subsequent *in vivo* studies showed that the application of MMAE.VC.SA.617 can inhibit tumour growth. During the complete time of the study no further increase of the wight of the tumour was observed. Furthermore, comparisons with free MMAE, showed that the novel compound has a higher tolerance *in vivo*, since nearly all mice in one MMAE comparative study (0.5 mg MMAE/kg) died, while all mice of the equivalent MMAE.VC.SA.617 group (3.35 mg MMAE.VC.SA.617/kg, equivalent to 0.5 mg MMAE/kg) survived.

The studies showed that MMAE.VC.SA.617 is a promising candidate for small molecule drug delivery of MMAE. Further optimizations of the structure as discussed above could lead to an increased binding affinity. Higher affinities could lead to more PSMA bound compound and thus a higher internalization ratio. Thus, more MMAE.VC.SA.617 would be present in the cell and could be cleaved by cathepsin B, increasing the cytotoxicity.

5.4 Project D: PSMA inhibitor structure optimisation

In project D, the manuscript C*omparison of the binding affinity of squaramide containing lysine-urea-glutamate- and glutamate-urea-glutamate-based PSMA inhibitors* is about the comparison of the binding affinities of novel urea-based PSMA inhibitors to identify possible potent PSMA target vector/chelator conjugates. KuE is the most used PSMA inhibitor right now, but studies indicating that the exchange of the lysine residue against another glutamate unit and its functionalization with a lysine leads to better pharmacological properties.[22,23] Based on these studies squaric acid conjugated K-EuE was compared to SAME.KuE. As reference, the well-known and established targeting vector and linking unit of PSMA-617 was also included in this study.

First, the binding affinities of the targeting vectors were evaluated. Here, it was shown that SAME.K-EuE has the highest affinity (17.2 ± 5.2 nM) among all three targeting units. 617.KuE showed a similar affinity with an IC_{50} value of 21.5 ± 1.9 nM. SAME.KuE has the lowest affinity (35.9 ± 2.6 nM). To make the target vectors usable in radiopharmacy, functionalisation with chelators were performed. Three different chelators were chosen for evaluation containing the two hybrid chelators $DATA^{5m}$ and $AAZTA^{5}$ as well as the DOTA derivative DO2AGA.

The comparison of the affinity of all chelator-conjugated compounds displayed the drastically decrease of the affinity, if a chelator is added to SAME.K-EuE. This conjugation led to a decrease from 17.2 ± 5.2 nM (only targeting unit) to IC_{50} values between 178 nM and 407 nM. The chelator seems to have a highly negative effect on the conformation of the SA.K-EuE in the binding pocket. The affinity of the best SA.K-EuE-based conjugate was almost twice as low as the affinity of the worst 617.KuE-based compound ($DATA^{5m}$.617.KuE) and even 3.5-fold lower than the SA.KuE derivative ($AAZTA^{5}$.SA.KuE) with the lowest IC_{50} value. The studies indicating that "K-EuE is better than KuE" could not be verified, at least not for squaric acid-based chelator conjugates. One option to improve the PSMA binding affinity could be to add a spacer between the chelator and the squaramide. This could lead to a less steric influence of the chelator.

Concerning the compounds with the targeting units SA.KuE and 617.KuE, a clear statement of influence of the chelator cannot be made. It was not possible to identify if one of both targeting units is superior to the other. While the $DATA^{5m}$.SA.KuE conjugate showed a better affinity than $DATA^{5m}$.617.KuE, it was differently observed for the $AAZTA^{5}$ conjugates. Here, the $AAZTA^{5}$-617.KuE variant showed a better affinity than the $AAZTA^{5}$.SA.KuE version and no differences were observed with the corresponding DO2AGA derivatives. All these results show that a clear classification of the chelator towards affinity influence is not possible. The influence seems to be dependent on the combination of each moiety. As for the SA.K-EuE derivatives, all compounds could be synthesized with a longer alkyl chain to get a distance between chelator and binding pocket to be sure that the influence of the often bulky chelator is minimal. Then, the impact of a covalent modification of the targeting moiety and the resulting conformation in the binding pocket can be evaluated without influences of bulky residues in new binding affinity studies.

5.5 References in the conclusion

(1) Wurm, F. R.; Klok, H. A. Be Squared: Expanding the Horizon of Squaric Acid-Mediated Conjugations. *Chem. Soc. Rev.* **2013**, *42* (21), 8220–8236.

(2) Engelbogen, N. Quadratsäurediester Als Brücke Zwischen Chelatoren Und Biomolekülen in Der Radiopharmazie : Synthese Und Evaluierung von Radiopharmaka Zur Diagnose von

Leberfibrose Sowie Zur Diagnose Und Therapie von Tumorerkrankungen. *Dissertation. - Johannes Gutenberg-Universität Mainz* **2017**.

(3) Greifenstein, L.; Engelbogen, N.; Lahnif, H.; Sinnes, J.-P.; Bergmann, R.; Bachmann, M.; Rösch, F. Synthesis, Labeling and Preclinical Evaluation of a Squaric Acid Containing PSMA Inhibitor Labeled with ^{68}Ga: A Comparison with PSMA-11 and PSMA-617. *ChemMedChem* **2020**, *15* (8), 695–704.

(4) Greifenstein, L. Synthesis, Radiolabeling and in Vitro and in Vivo Evaluation of Different Chelator Systems with ^{44}Sc, ^{64}Cu, ^{68}Ga and ^{177}Lu. *Dissertation. - Johannes Gutenberg-Universität Mainz* **2019**.

(5) Greifenstein, L.; Grus, T.; Nagel, J.; Sinnes, J. P.; Rösch, F. Synthesis and Labeling of a Squaric Acid Containing PSMA-Inhibitor Coupled to AAZTA^5 for Versatile Labeling with ^{44}Sc, ^{64}Cu, ^{68}Ga and ^{177}Lu. *Appl. Radiat. Isot.* **2020**, *156*, 108867.

(6) Seemann, J.; Waldron, B.; Parker, D.; Roesch, F. DATATOC: A Novel Conjugate for Kit-Type ^{68}Ga Labelling of TOC at Ambient Temperature. *EJNMMI Radiopharm. Chem.* **2017**, *1*, 4.

(7) Seemann, J.; Waldron, B. P.; Roesch, F.; Parker, D. Approaching "kit-Type" Labelling with ^{68}Ga: The DATA Chelators. *ChemMedChem* **2015**, *10* (6), 1019–1026.

(8) Lahnif, H.; Grus, T.; Pektor, S.; Greifenstein, L.; Schreckenberger, M.; Rösch, F. Hybrid Chelator-Based PSMA Radiopharmaceuticals: Translational Approach. *Molecules* **2021**, *26* (21), 6332.

(9) Sinnes, J.-P. Synthese Und Radiochemische Evaluierung von Chelatoren Für Milde Markierungen Mit ^{68}Ga, ^{44}Sc Und ^{177}Lu Sowie in Vitro- Und in Vivo- Evaluierung von Deren TOC- Und PSMA-Derivaten. *Dissertation. - Johannes Gutenberg-University Mainz* **2018**.

(10) Thomas, T. S.; Pachynski, R. K. Treatment of Advanced Prostate Cancer. *Mo. Med.* **2018**, *115* (2), 156–161.

(11) Hyväkkä, A.; Virtanen, V.; Kemppainen, J.; Grönroos, T. J.; Minn, H.; Sundvall, M. More than Meets the Eye: Scientific Rationale behind Molecular Imaging and Therapeutic Targeting of Prostate-Specific Membrane Antigen (PSMA) in Metastatic Prostate Cancer and Beyond. *Cancers.* **2021**, *13* (9), 2244.

(12) Ravi Kumar, A. S.; Hofman, M. S. Mechanistic Insights for Optimizing PSMA Radioligand Therapy. *Clin. Cancer Res.* **2020**, *26* (12), 2774–2776.

(13) Sartor, O.; de Bono, J.; Chi, K. N.; Fizazi, K.; Herrmann, K.; Rahbar, K.; Tagawa, S. T.; Nordquist, L. T.; Vaishampayan, N.; El-Haddad, G.; Park, C. H.; Beer, T. M.; Armour, A.; Pérez-Contreras, W. J.; DeSilvio, M.; Kpamegan, E.; Gericke, G.; Messmann, R. A.; Morris, M. J.; Krause, B. J. Lutetium-177–PSMA-617 for Metastatic Castration-Resistant Prostate Cancer. *N. Engl. J. Med.* **2021**, *385* (12), 1091–1103.

(14) Ahmadzadehfar, H.; Matern, R.; Baum, R. P.; Seifert, R.; Kessel, K.; Bögemann, M.; Kratochwil, C.; Rathke, H.; Ilhan, H.; Svirydenka, H.; Sathekge, M.; Kabasakal, L.; Yordanova, A.; Garcia-Perez, F. O.; Kairemo, K.; Maharaj, M.; Paez, D.; Virgolini, I.; Rahbar, K. The Impact of the Extent of the Bone Involvement on Overall Survival and Toxicity in MCRPC Patients Receiving [^{177}Lu]Lu-PSMA-617: A WARMTH Multicentre Study. *Eur. J. Nucl. Med. Mol. Imaging* **2021**, *48* (12), 4067–4076.

(15) Benešová, M.; Schäfer, M.; Bauder-Wüst, U.; Afshar-Oromieh, A.; Kratochwil, C.; Mier, W.; Haberkorn, U.; Kopka, K.; Eder, M. Preclinical Evaluation of a Tailor-Made DOTA-Conjugated PSMA Inhibitor with Optimized Linker Moiety for Imaging and Endoradiotherapy of Prostate Cancer. *J. Nucl. Med.* **2015**, *56* (6), 914–920.

(16) Meckel, M.; Bergmann, R.; Miederer, M.; Roesch, F. Bone Targeting Compounds for Radiotherapy and Imaging: *Me(III)-DOTA Conjugates of Bisphosphonic Acid, Pamidronic Acid and Zoledronic Acid. *EJNMMI Radiopharm. Chem.* **2017**, *1*, 14.

(17) Wang, X.; Shirke, A.; Walker, E.; Sun, R.; Ramamurthy, G.; Wang, J.; Shan, L.; Mangadlao, J.; Dong, Z.; Li, J.; Wang, Z.; Schluchter, M.; Luo, D.; Wang, Y.; Stauffer, S.; Brady-Kalnay, S.; Hoimes, C.; Lee, Z.; Basilion, J. P. Small Molecule-Based Prodrug Targeting Prostate Specific Membrane Antigen for the Treatment of Prostate Cancer. *Cancers.* **2021**, *13* (3), 417.

(18) Sercombe, L.; Veerati, T.; Moheimani, F.; Wu, S. Y.; Sood, A. K.; Hua, S. Advances and Challenges of Liposome Assisted Drug Delivery. *Front. Pharmacol.* **2015**, *6* (DEC), 286.

(19) Yan, L.; Shen, J.; Wang, J.; Yang, X.; Dong, S.; Lu, S. Nanoparticle-Based Drug Delivery System: A Patient-Friendly Chemotherapy for Oncology. *Dose-Response* **2020**, *18* (3), 1559325820936161.

(20) Ernsting, M. J.; Murakami, M.; Roy, A.; Li, S.-D. Factors Controlling the Pharmacokinetics, Biodistribution and Intratumoral Penetration of Nanoparticles. *J Control Release* **2013**, *172* (3), 782–794.

(21) Liu, D.; Mori, A.; Huang, L. Role of Liposome Size and RES Blockade in Controlling Biodistribution and Tumor Uptake of GM1-Containing Liposomes. *BBA - Biomembr.* **1992**, *1104* (1), 95–101.

(22) Hillier, S. M.; Maresca, K. P.; Lu, G.; Merkin, R. D.; Marquis, J. C.; Zimmerman, C. N.; Eckelman, W. C.; Joyal, J. L.; Babich, J. W. ^{99m}Tc-Labeled Small-Molecule Inhibitors of Prostate-Specific Membrane Antigen for Molecular Imaging of Prostate Cancer. *J. Nucl. Med.* **2013**, *54* (8), 1369–1376.

(23) Robu, S.; Schmidt, A.; Eiber, M.; Schottelius, M.; Günther, T.; Hooshyar Yousefi, B.; Schwaiger, M.; Wester, H. J. Synthesis and Preclinical Evaluation of Novel ^{18}F-Labeled Glu-Urea-Glu-Based PSMA Inhibitors for Prostate Cancer Imaging: A Comparison with ^{18}F-DCFPyl and ^{18}F-PSMA-1007. *EJNMMI Res.* **2018**, *8*, 30.

6. Appendix

6.1 List of abbreviations

%ID/g	Percent injected dose per gramm
^{18}F-TEG	2-(2-[^{18}F]fluoroethoxy)ethoxy) ethane
2-PMPA	2-phosponomethyl pentanedioic acid
a	years
AAZTA	1,4-bis (carboxymethyl)-6-[bis (carboxymethyl)]amino-6-methylperhydro-1,4-diazepine
AAZTA^5	1,4-bis-(carboxylmethyl)-6-[bis-(carboxymethyl)-amino-6-pentanoic-acid]-perhydro-1,4-diazepine
ACN	Acetonitrile
ADC	antibody drug conjugate
Amc	aminomethylcyclohexane
Arg	arginine
AROP	anionic ring opening polymerization
A_s	specific activity
Asn	asparagine
Asp	aspartate
ATP	adenosine triphosphate
BFC	bifunctional chelator
BGO	bismuth germanate
BisHD-*hb*PG	hyperbranched polyglycerols with hydrophobic alkyl chain anchors
BisHD-OH	1,2-bis-*n*-hexadecyl glyceryl ether
BisOD-OH	1,2-bis-*n*-octadecyl glyceryl ether
Boc	*tert*-butyloxycarbonyl protecting group
BPAPD	4-{[(bis–phosphonopropyl) carbomoyl]methyl}-7,10-bis-(carboxy-methyl)-1,4,7,10-tetraazacyclododec-1-yl)-acetic acid
Bq	Bequerel
Bq/g	Bequerel per gramm
c.a.	carrier-added
c.f.	carrier-free
CAF	cancer associated fibroblast
CAR	Chelator-to-antibody-ratio
cpm	counts per minute
CT	computed tomography
CuAAC	copper(I)-catalysed huisgen 1,3-dipolar cycloaddition
d	days
DAPI	4’,6-diamidino-2-phenylindole
DATA^{5m}	1,4-bis(carboxymethyl)-6-pentanoic acid[amino(methyl) carboxymethyl] perhydro-1,4-diazepine
DATA^{m}	1,4-bis(carboxymethyl)-6-[amino(methyl) carboxymethyl]methylperhydro-1,4-diazepine
DC	dendritic cell
DCM	dichloromethane
DFG	Deutsche Forschungsgemeinschaft
DFO	deferoxamine B
DIPEA	*N*,*N*-Diisopropylethylamine
DLS	Dynamic light scattering
DMF	Dimethylformamide
DMSO	Dimethyl sulfoxide
DNA	Deoxyribonucleic acid
DOPC	1,2-dioleoyl-sn-glycero-3-phosphocholine
DOTA	1,4,7,10-tetraazacyclo-dodecane-1,4,7,10-tetraacetic acid
DOTAGA	1,4,7,10-tetraazacyclododececane-1-glutaric acid-4,7,10-triacetic acid
DOTAM	1,4,7,10-Tetrakis(carbamoylmethyl)-1,4,7,10-tetraazacyclododecane
DPP	dipeptidyl peptidase
DTPA	diethylenetriaminepentaacetic acid
E	energy
E	glutamate
EC	electron capture
EDTA	Ethylenediaminetetraacetic acid
EDTMP	ethylenediaminetetramethylene phosphonic acid
EEGE	ethoxyethyl glycidyl ether
ERT	endoradiotherapy
ESI	Electrospray ionization

e.g.	for example
EtOH	ethanol
EuE	glutamate-urea-glutamate
FAP	fibroblast activation protein
FAPi	fibroblast activation protein inhibitor
FDA	U.S. Food and Drug Administration
[^{18}F]FDG	2-deoxy-2-[^{18}F]fluoro-D-glucose
FFPS	farnesyl pyrophosphate synthase
Fmoc	fluorenylmethoxycarbonyl protecting group
FOLH1	folate hydrolase 1
g	gramm
GCPII	glutamate carboxypeptidase II
Glu	glutamate
GSH	glutathion
GSO	gadolinium orthosilicate
h	hours
HAP	hydroxyapatite
HATU	1-[Bis(dimethylamino)methylene]-1H-1,2,3-triazolo[4,5-b]pyridinium 3-oxide hexafluorophosphate
HBED	*N,N*'-Di(2-hydroxybenzyl)ethylenediamine-*N,N'*-diacetic acid
HBED-CC	*N,N'*-bis-[2-hydroxy-5-(carboxyethyl)benzyl] ethylenediamine-*N,N'*-diacetic acid
hbPG	hyperbranched polyglycerols
HBTU	2-(1*H*-benzotriazol-1-yl)-1,1,3,3-tetramethyluronium hexafluorophosphate
HEPES	4-(2-hydroxyethyl)-1-piperazineethanesulfonic acid
His	histidine
HMDP	hydroxymethylenediphosphonate
HOBt	Hydroxybenzotriazole
HPLC	high performance liquid chromatography
HS	human serum
HSQC	heteronuclear single quantum coherence
INRATES	Institute of Nuclear & Radiological Sciences and Technology, Energy & Safety
i.v.	intravenous
IC_{50}	half maximal inhibitory concentration

K	lysine
kDa	kilodalton
K-EuE	lysine-glutamate-urea-glutamate
K_i	inhibitory constant
KuE	lysine-urea-glutamate
LC/MS	liquid chromatography / mass spectroscopy
LET	linear energy transfer
Leu	leucine
LNCaP	Lymph Node Carcinoma of the Prostate
$logD_{7.4}$	distribution coefficient in water and organic solvent at pH 7.4
LOR	line of response
LSO	lutetium oxyorthosilicate
Lys	lysine
mAb	monoclonal antibody
mCrPC	Metastatic castration-resistant prostate cancer
MDP	methylenediphosphonate
MeCN	Acetonitrile
MeOH	methanol
mg	milligramm
min	minutes
MMAE	monomethyl auristatin E
M_n	molecular weight
mPEG	methoxy PEG
MPGC	Max Planck Graduate Center Mainz
MPS	mononuclear phagocyte system
MRI	magnetic resonance imaging
MWCO	Molecular weight cut-off
n	Neutron
n.c.a.	no-carrier-added
NAAG	*N*-acetyl-aspartyl-glutamate
NAALDase	*N*-acetyl-L-aspartyl-L-glutamate peptidase
NHS	N-hydroxysuccinimide
NMP	*N*-methylpyrrolidone
NMR	nuclear magnetic resonance
NODAGA	1,4,7-triazacyclononane,1-glutaric acid-4,7-acetic acid
NOTA	1,4,7-triazacyclononane-1,4,7-triacetic acid
p	Proton
p.i.	post injection
PABC	*p*-amino benzyloxycarbonyl
Pam	pamidronate
PBS	phosphate-buffered saline

PCa	Prostate cancer
PEG	Polyethylene glycol
PET	positon emission tomography
Phe	phenylalanine
PMDETA	N,N,N',N'',N''-Pentamethyldiethylentriamine
PREP	prolyl oligopeptidase
Ps	Positronium
PSA	prostate specific antigen
PSMA	prostate-specific membrane antigen
PSMAi	prostate-specific membrane antigen inhibitor
QMA	quaternary methyl ammonium
RCY	radiochemical yield
R_f	retention factor
RT	room temperature
s	seconds
SA	squaric acid
SADE	squaric acid diester
SAME	squaric acid monoester
SD	standard deviation
SEC	size exclusion chromatography
SFB	Sonderforschungsbereich
SMA	slow monomer addition
SMDC	small molecule drug conjugate
S_N2	second order nucleophilic substitution
SPAAC	strain-promoted-alkyne-azide-cycloaddition
SPECT	single-photon emission computed tomography
SUL	standardized uptake value (SUV) normalized by lean body mass
SUV	standardized uptake value

$t_{1/2}$	half-life time
T_C	transition temperature
TFA	Trifluoroacetic acid
TLC	thin layer chormatography
t_R	retention time
TRAM	(1,4,7-triazonane-1,4,7-triyl)tris(methylene))tris((1-amino-15-oxo-4,7,10-trioxa-14-azaheptadecan-17-yl)phosphinic acid
TransMed	Mainz Research School of Translational Biomedicine
TRAP	(1,4,7-triazonane-1,4,7-triyl)tris(methylene))tris((1-amino-15-oxo-4,7,10-trioxa-14-azaheptadecan-17-yl)phosphinic acid
TRIGA	Training, Research, Isotopes, General Atomic
Trp	tryptophane
TV	targeting vector
Tyr	tyrosine
VC	valine-citrulline
V_h	hydrodynamic volume
WARMTH	World Association of Radiopharmaceutical and Molecular Therapy
Zol	zoledronate

6.2 List of publications

6.3 Acknowledgment

6.4 Eidesstattliche Erklärung

Die vorliegende Arbeit wurde unter der Betreuung von X.X. in der Zeit von September 2018 bis Januar 2022 am Institut für Kernchemie / Department Chemie- Standort TRIGA der Johannes Gutenberg-Universität Mainz angefertigt.

Hiermit erkläre ich, Tilmann Grus, dass die vorliegende Disseration von mir selbstständig verfasst wurde und alle schriftlichen und elektronischen Quellen sowie andere Hilfsmittel angegeben habe.

„I hereby declare that I wrote the dissertation submitted without any unauthorized external assistance and used only sources acknowledged in the work. All textual passages which are appropriated verbatim or paraphrased from published and unpublished texts as well as all information obtained from oral sources are duly indicated and listed in accordance with bibliographical rules. In carrying out this research, I complied with the rules of standard scientific practice as formulated in the statutes of Johannes Gutenberg-University Mainz to insure standard scientific practice."

Mainz, 27th of January 2022

Tilmann Grus

6.5. Curriculum Vitae